Studies on Macrocyclic Complexes

by

Christian Radek

Thesis presented for the Degree of
Doctor of Philosophy
The University of Edinburgh
1995

Der Herbst des Einsamen

Der dunkle Herbst kehrt ein voll Frucht und Fülle,
Vergilbter Glanz von schönen Sommertagen.
Ein reines Blau tritt aus verfallener Hülle;
Der Flug der Vögel tönt von alten Sagen.
Gekeltert ist der Wein, die milde Stille
Erfüllt von leiser Antwort dunkler Fragen.

Und hier und dort ein Kreuz auf ödem Hügel;
Im roten Wald verliert sich eine Herde.
Die Wolke wandert übern Weiherspiegel;
Es ruht des Landmanns ruhige Geberde.
Sehr leise rührt des Abends blauer Flügel
Ein Dach von dürrem Stroh, die schwarze Erde.

Bald nisten Sterne in des Müden Brauen;
In kühlen Stuben kehrt ein still Bescheiden
Und Engel treten leise aus den blauen
Augen der Liebenden, die sanfter leiden.
Es rauscht das Rohr; anfällt ein knöchern Grauen,
Wenn schwarz der Tau tropft von den kahlen Weiden.

Georg Trakl (1887 - 1914)

The work described in this thesis is dedicated to the memory of Uli and my grandparents without whom this work would not have been possible.

ACKNOWLEDGEMENTS

I would like to thank Martin Schröder for giving me the opportunity to undertake the work presented in this thesis in his research group. I am indebted to him for his support, encouragement, enthusiasm and friendship throughout the course of this work.

My thanks also go to Sandy Blake, Bob Gould and Simon Parsons for their invaluable help with the intricacies of X-ray crystallography. My thanks include Steve Harris who did his fourth year project with Sandy Blake for solving and refining the structure of [21]aneS_2O_5.

Further thanks go to John Millar, Heather Grant, David Reed and Wesley Kerr for recording NMR-spectra, Alan Taylor and Elizabeth Stevenson for running FAB- and EI-mass spectra, Lorna Eades for performing microanalytical measurements and Jeremy Rawson for running ESR spectra. My thanks also include Dr.J.G.Fitton (Department of Geology) for running X-ray fluorescence spectra.

I would like to acknowledge the support, encouragement, advice and friendship of a range of people over the last four years namely Prof. Brian Johnson, Prof. Karl Wieghardt, Lisa Martin, Helen Baxter, Bob Baxter and Thomas Weyhermüller, the members of Prof. Schröder's research group and the inorganic section in particular Andy Atkins, Phil Bailey, Armando Marin-Beccera, Daniel Black, Rhona Crofts, Jon Danks, Therese Donlevy, Paul Dyson, Ian Fallis, Rachel Grimditch, Broer de Groot, Malcolm Halcrow, Vito Lippolis, Colin Pulham, Gill Reid, Heiko Richtzenhain, Steve Ross, Otto Smékal and Martin Sullivan.

For essential financial support I would like to thank first of all my grandparents. Additionally I would like to thank my uncle Uli, my mother, Prof. B.FG.Johnson and Martin Schröder. My thanks also go to the British Crystallographic Association (BCA) for a grant which enabled me to participate at the Intensive Course in X-Ray Crystallography, The University of Edinburgh, Senatus Postgraduate Studies Committee for a financial contribution to my studies, and The University of Edinburgh Student Accommodation Service for offering me the position of a senior resident in a student house over a period of two years.

I would also like to express my gratitude for the use of laboratory facilities and computer resources at The University of Edinburgh and the use of online database facilities of the S.E.R.C. at Daresbury.

ABSTRACT

The work described in this thesis deals with the co-ordination chemistry of the macrocyclic ligands:

[9]aneS_3 ..... (1,4,7-trithiacyclononane)
[12]aneS_4 ..... (1,4,7,10-tetrathiacyclododecane)
[14]aneS_4 ..... (1,5,8,12-tetrathiacyclotetradecane)
[16]aneS_4 ..... (1,5,9,13-tetrathiahexadecane)
[15]aneS_5 ..... (1,4,7,10,13-pentathiacyclopentadecane)
[18]aneS_6 ..... (1,4,7,10,13,16-hexathiacyclooctadecane)
[24]aneS_8 ..... (1,4,7,10,13,16,19,22-octathiacyclotetraeicosane)
[15]aneS_2O_3 ..... (1,4,7-trioxa-10,13-dithiacyclopentadecane)
[18]aneS_2O_4 ..... (1,4,7,10-tetraoxa-13,16-dithiacyclooctadecane)
benzo[18]aneS_2O_4 .... (4,7,10,13-tetraoxa-1,16-dithia[16]-*o*-cyclophane)
[21]aneS_2O_5 ..... (1,4,7,10,13-pentaoxa-16,19-dithiacycloheneicosane)
[18]aneS_3O_3 ..... (1,4,7-trioxa-10,13,16-trithiacyclooctadecane)
[20]aneS_3O_3 ..... (1,4,7-trioxa-10,14,18-trithiacycloeicosane)

The synthesis of [18]aneS_2O_4, [18]aneS_3O_3 benzo[18]aneS_2O_4 and [20]aneS_3O_3, the single crystal X-ray structures of [15]aneS_2O_3, [18]aneS_2O_4 and ([21]aneS_2O_5)1·½H_2O, and molecular mechanics calculations on [18]aneS_2O_4 are described. ([21]aneS_2O_5)·1½H_2O is the first example of a neutral molecule binding to a mixed O/S-donor ionophore with H-bonding to the hard polyether binding site.

Studies of Ru(II) and Pd(II) complexes with these ligands were initiate in order to establish the fundamental co-ordination chemistry between mixed O/S-donor ionophores and to establish the potential of these complexes to be used in the development of a metal mixed O/S-donor macrocyclic host guest chemistry. [$RuCl_2PPh_3$([15]aneS_2O_3)] and [RuCl(PPh_3)([15]aneS_2O_3)$_2$]PF_6 were prepared by the reaction of [15]aneS_2O_3 with [$RuCl_2$(PPh_3)$_3$]. The role of [$RuCl_2PPh_3$([15]aneS_2O_3)] as a potential intermediate in the formation of the two isomers of [RuCl(PPh_3)([15]aneS_2O_3)$_2$]PF_6 is discussed. The reaction of [18]aneS_2O_4 with [$RuCl_2$(PPh_3)$_3$] afforded [RuCl(PPh_3)([18]aneS_2O_4)$_2$]PF_6. [Ru([18]aneS_2O_4)$_3$](PF_6)$_2$ was prepared by the reaction of [18]aneS_2O_4 and '$RuCl_3$·xH_2O' in the presence of potassium oxalate as a reducing agent.

Reactions of $[18]aneS_2O_4$ with $[Ru_2Cl_4(\eta^6\text{-}C_6H_6)_2]$ and $[RuCl(PPh_3)_2(\eta^5\text{-}C_5H_5)]$ afforded the organometallic species $[RuCl(\eta^6\text{-}C_6H_6)([18]aneS_2O_4)]PF_6$, $[RuCl(\eta^6\text{-}C_6H_6)([18]aneS_2O_4)]BPh_4$ and $[Ru(\eta^5\text{-}C_5H_5)(PPh_3)([18]aneS_2O_4)]PF_6$. The single crystal X-ray structures of all compounds prepared are described. In all cases the macrocyclic ligands co-ordinate to the Ru(II) ion in an *exo* bidentate manner.

$[PdCl_2([18]aneS_2O_4)]$ and $[Pd([18]aneS_2O_4)_2](PF_6)_2$ were prepared by reaction of $PdCl_2$ with $[18]aneS_2O_4$. The reaction of $[18]aneS_3O_3$ and $[20]aneS_3O_3$ with $PdCl_2$ afforded $[Pd([18]aneS_3O_3)_2](PF_6)_2$. and $[PdCl([20]aneS_3O_3)]BPh_4$, the single crystal X-ray structures of which we describe. The Pd(II) ion adopts in the first three cases an *exo* co-ordination mode whereas in case of $[PdCl([20]aneS_3O_3)]BPh_4$ *endo* co-ordination is present. Mixed O/S-donor macrocyclic complexes containing *exo* co-ordinated Ru(II) and Pd(II) ions are unsuitable candidates as hosts for other cations or neutral molecules due to steric and conformational reasons. $[20]aneS_3O_3$ has been identified as a potential candidate for further investigation and development.

The complexes $[Tl([15]aneS_2O_3)_2]PF_6$, $[Tl([18]aneS_2O_4)]PF_6$ and $[Tl(benzo[18]aneS_2O_4)]PF_6$ were prepared by the reaction of $TlPF_6$ with $[15]aneS_2O_3$, $[18]aneS_2O_4$ and $benzo[18]aneS_2O_4$ respectively. The characterisation of these compounds is described. Similarities between spectroscopic results for these compounds compared with Ag(I) complexes (see below) suggest in-cavity co-ordination of the Tl(I) ions within the macrocycle.

Reactions of $[18]aneS_2O_4$ with $AgNO_3/NH_4PF_6$ and $AgClO_4$ afforded the two complexes $[Ag_2([18]aneS_2O_4)_2](PF_6)_2$ and $[Ag_4([18]aneS_2O_4)_4](ClO_4)_4$. The single crystal X-ray structures of the products show Ag-atoms co-ordinated within the macrocyclic cavities with a range of Ag-S and Ag-O bonds. The structures of both compounds exhibit a series of thioether bridges between Ag(I) ions and $[Ag_4([18]aneS_2O_4)_4](ClO_4)_4$ shows an unusual cyclic 4-membered Ag_2S_2 moiety. NMR studies, however, suggest the presence of mononuclear species in solution. The features found in the single crystal X-ray structures are therefore confined to the solid state and the degree of oligomerisation is dependent on the nature of the counterion.

$[Ag([18]aneS_6)]I_7$ and $[Ag([18]aneS_6)]I_3$ were prepared by the reaction of $[Ag([18]aneS_6)]BF_4$ with I_2 in MeCN. The single crystal X-ray structure of $[Ag([18]aneS_6)]I_7$ shows a novel 3-dimensional polymeric polyiodide $(I_7^-)_n$, which forms a cubane structure around the cation whereas $[Ag([18]aneS_6)]I_3$ shows a sheet-like structure. No AgI precipitation was observed in either reaction underlining the inertness of the $[Ag([18]aneS_6)]^+$ cation under these conditions. The ability of cationic metal macrocyclic complexes to not only stabilise but to template extended anionic species is discussed.

The reaction of I_2 with S-donor macrocycles in CH_2Cl_2 afforded I_2 thioether charge transfer complexes. Solid state studies on $([9]aneS_3)_2(I_2)_4$, $([12]aneS_4)I_2$, $([14]aneS_4)I_2$, $([16]aneS_4)I_2$ $([16]aneS_4)(I_2)_4$, $([15]aneS_5)(I_2)_5$, $([18]aneS_6)I_2$, $([18]aneS_6)(I_2)_4$, $([24]aneS_8)I_2$ and $([24]aneS_8)(I_2)_4$ are described. These structures can be broadly divided into two groups. I_2 rich compounds show a columnar stacking motif of macrocyclic ligands, and I_2 deficient compounds adopting a layered 1-dimensional chain structures with I_2 molecules bridging between different macrocycles. Solution studies on $[9]aneS_3$ and $[18]aneS_6$ are described.

CHAPTER I

An introduction into the chemistry of macrocyclic compounds is given dealing with a brief historical outline of the key developments. Features special to macrocyclic co-ordination chemistry such as thermodynamic stability and kinetic inertness are emphasised and discussed. Other topics included in this introduction deal with the role of transition metal ions in biological systems, macrocyclic metal complexes in catalysis and applications for macrocyclic ligands in particular covering chemical sensing, solvent extraction and medical applications such as contrast agents for imaging purposes and the development of anti-cancer drugs. The general aims of the project are outlined and discussed.

CHAPTER II

A brief introduction into ligand design and ligand synthesis is given. The synthesis and characterisation of a series of starting materials such as halogenated oligoethylene glycols, thioether and thiols is described. The ionophores [18]aneS_2O_4, benzo[18]aneS_2O_4, [18]aneS_3O_3 and [20]aneS_3O_3 are prepared either *via* high dilution co-condensation, or Cs_2CO_3 mediated cyclisation reactions of a dithiol and a polyether dihalide. The isolation, characterisation and recrystallisation of the products is described. [15]aneS_2O_3 crystallises in the triclinic space group *P*-1 (No. 2), a = 7.2129(24), b = 9.102(3), c = 10.080(4) Å, α = 80.49(3), β = 86.85(3), γ = 74.321(23)°, U = 628 Å^3, Z = 2. The single crystal X-ray structure shows two O-atoms *endo* and one O-atom *exo* oriented. The SCH_2CH_2S moiety adopts an *anti* torsion angle [-165.93(8)°] with the two S-donors in *exo* positions. [18]aneS_2O_4 crystallises in the monoclinic space group *C* 2/*c* (No. 15), a = 15.9074(12), b = 9.5181(8), c = 12.5255(10) Å, β = 124.351(4)°, U = 1566 Å^3, Z = 4. The single crystal X-ray structure shows the molecule on a crystallographic two fold axis. The O-atoms adopt *endo* orientations whereas the S-atoms are *exo*. The two S-atoms are in close contact 3.48 Å with the SCH_2CH_2S moiety adopting a *gauche* conformation. The torsion angle [61.4(5)°] is very similar compared with Pd(II) or Ru(II) complexes where [18]aneS_2O_4 binds as a bidentate chelating ligand. ([21]aneS_2O_5)·1½H_2O crystallises in the monoclinic space group *P* $2_1/n$ (alt. *P* $2_1/c$; No. 14), a = 17.550(12), b = 11.750(8), c = 18.531(9) Å, β = 91.52(4)°, U = 3820 Å^3, Z = 8. The single crystal X-ray structure shows two macrocycles in the asymmetric unit. One H_2O molecule is co-ordinated to two O-atoms *via* H-bridging in each macrocycle. Other H_2O molecules bridge between those co-ordinated H_2O molecules. The conformation of the SCH_2CH_2S moiety [S-C-C-S -174.8(8) and -172.8(4)°] is similar to the one found in [15]aneS_2O_3. The O-atoms adopt *endo* as well as *exo* orientations.

Molecular mechanics calculations on [18]aneS_2O_4 confirm the high flexibility of the macrocycle. The energy minimisation of the single crystal structure based conformation of [18]aneS_2O_4 did not change the conformation. A series of local minima within a small energy band have been identified and whether this ligand should be termed 'pre-organised' for bidentate chelating co-ordination or not is discussed.

CHAPTER III

An introduction dealing with the preparation of Ru(II) starting materials and the co-ordination chemistry of Ru(II) with homoleptic and mixed O/S-donor ionophores is given. The synthesis and characterisation of a series of mixed O/S-donor macrocyclic complexes with Ru(II) is described. Reaction of $[RuCl_2(PPh_3)_3]$ with one molar equivalent of $[15]aneS_2O_3$ affords the complex $[RuCl_2(PPh_3)_2([15]aneS_2O_3)]$; reaction of two equivalents of $[15]aneS_2O_3$ or $[18]aneS_2O_4$ affords the complex cations $[RuCl(PPh_3)([15]aneS_2O_3)_2]^+$ and $[RuCl(PPh_3)([18]aneS_2O_4)_2]^+$ respectively.

The complex $[RuCl_2(PPh_3)_2([15]aneS_2O_3)]\cdot\frac{1}{2}Me_2CO$ crystallises in the triclinic space group P -1 (No. 2), a = 11.3183(19), b = 12.4925(21), c = 18.442(3)Å, α = 101.896(8), β = 100.177(13), γ = 106.669(10)°, U = 2366 Å^3, and Z = 2. The single crystal X-ray structure shows the Ru(II) in an octahedral $Cl_2S_2P_2$ environment [Ru-Cl(1) 2.4447(15), Ru-Cl(2) 2.4154(15), Ru-S(1) 2.4085(15), Ru-S(4) 2.4215(16), Ru-P(1) 2.3775(6) and Ru-P(2) 2.3640(15)Å]. The phosphine ligands are mutually *cis* and occupy with the thioether S-donors of the macrocycle equatorial binding sites whereas in contrast the Cl^- ligands are in apical positions. The reaction pathway and the role of $[RuCl_2(PPh_3)_2([15]aneS_2O_3)]$ as an intermediate in the formation of *cis/trans*-$[RuCl(PPh_3)([15]aneS_2O_3)_2]^+$ is discussed. The complex $[RuCl(PPh_3)([18]aneS_2O_4)]PF_6\cdot\frac{1}{2}EtOH$ crystallises in the triclinic space group P -1 (No. 2), a = 10.674(7), b = 14.487(11), c = 19.241(17)Å, α = 74.88(7), β = 84.34(6), γ = 80.07(6)°, U = 2825 Å^3, and Z = 2. The single crystal X-ray structure shows the Ru(II) in an octahedral ClS_4P environment [Ru-Cl 2.441(6), Ru-P 2.340(5), Ru-S(1) 2.387(5), Ru-S(4) 2.3896(6), Ru-S(1') 2.348(6) and Ru-S(4') 2.438(6) Å]. The Cl^- and PPh_3 ligands adopt in this complex a *cis* configuration in contrast to the reported analogous $[15]aneS_2O_3$ complex. On the other hand ^{31}P-NMR studies show the presence of two geometric isomers in either case. Reaction of '$RuCl_3\cdot xH_2O$' with $[18]aneS_2O_4$ in the presence of potassium oxalate as a reducing agent yields the dicationic complex $[Ru([18]aneS_2O_4)_3]^{2+}$. The complex $[Ru([18]aneS_2O_4)_3](PF_6)_2\cdot H_2O$ crystallises in the trigonal space group R -3 (No. 148), a = 18.6287(17), c = 29.863(5)Å, U = 8975 Å^3, and Z = 6. The single crystal structure X-ray structure shows a highly symmetrical dication $[Ru([18]aneS_2O_4)_3]^{2+}$ with the Ru(II) in an octahedral S_6 environment [Ru-S(1) 2.3864(13) and Ru-S(4) 2.3622(11) Å].

Reactions of [18]aneS$_2$O$_4$ with [Ru$_2$Cl$_4$(η^6-C$_6$H$_6$)$_2$] and [RuCpCl(PPh$_3$)$_2$] afford the complexes [RuCl(η^6-C$_6$H$_6$)([18]aneS$_2$O$_4$)]$^+$ and [RuCp(PPh$_3$)([18]aneS$_2$O$_4$)]$^+$ respectively. The complex [RuCl(η^6-C$_6$H$_6$)([18]aneS$_2$O$_4$)]PF$_6$ crystallises in the orthorhombic space group *P na*2$_1$, *a* = 11.127(4), *b* = 13.348(3), *c* = 16.774(3) Å, *U* = 2491 Å^3, and *Z* = 4. The single crystal X-ray structure shows the Cl$^-$ ligand and [18]aneS$_2$O$_4$, through the thioether S-donors, co-ordinated pseudo octahedrally to the [Ru(η^6-C$_6$H$_6$)] fragment [Ru-Cl 2.416(2), Ru-S(1) 2.382(5) and Ru-S(4) 2.377(5)Å]. The single crystal structure of [RuCl(η^6-C$_6$H$_6$)([18]aneS$_2$O$_4$)]BPh$_4$ which crystallises in the monoclinic space group *P* 2$_1$/*n* (alt. *P* 2$_1$/*c*; No.14), *a* = 18.539(12), *b* = 9.652(7), *c* = 22.335(12) Å, β = 103.84(5), *U* = 3880 Å^3, and *Z* = 4, shows a similar geometry around the Ru(II) ion [Ru-Cl 2.411(6) , Ru-S(1) 2.384(6) and Ru-S(4) 2.369(6)Å]. [Ru(η^5-C$_5$H$_5$)(PPh$_3$)([18]aneS$_2$O$_4$)]PF$_6$ crystallises in the triclinic space group *P* -1 (No. 2), *a* = 11.3023(11), *b* = 12.1200(9), *c* = 14.3983(13) Å, α = 83.393(6), β = 83.274(8), γ = 78.367(7)°, *U* = 1910 Å^3, and *Z* = 2. The single crystal X-ray structure shows the PPh$_3$ ligand and [18]aneS$_2$O$_4$, through the thioether S-donors, co-ordinated to the pseudo octahedral Ru(II) fragment [Ru-P 2.3126(17), Ru-S(1) 2.3793(17) and Ru-S(4) 2.3587(19) Å].

CHAPTER IV

An introduction into the co-ordination chemistry of Pd(II) with homoleptic S- and mixed O/S-donor macrocycles is given. The synthesis and characterisation of *cis*-[PdCl$_2$([18]aneS$_2$O$_4$)], [Pd([18]aneS$_2$O$_4$)$_2$](PF$_6$)$_2$, [Pd([18]aneS$_3$O$_3$)$_2$](PF$_6$)2 and [PdCl([20]aneS$_3$O$_3$)]BPh$_4$ is described. Reaction of PdCl2 with one equivalent of [18]aneS2O4 affords the complex *cis*-[PdCl$_2$([18]aneS$_2$O$_4$)]; addition of a second equivalent affords the *bis* complex cation [Pd([18]aneS$_2$O$_4$)$_2$]$^{2+}$. The complex *cis*-[PdCl$_2$([18]aneS$_2$O$_4$)] crystallises in the monoclinic space group *P* 2$_1$/*n* (alt. *P* 2$_1$/*c*; No. 14), *a* = 8.714(2), *b* = 10.915(3), *c* = 18.787(8) Å, β = 92.04(3)°, *U* = 1785 Å^3 and *Z* = 4. The single crystal structure X-ray structure shows the Pd(II) in a square-planar co-ordination geometry with the Cl$^-$ ligands *cis* to each other [Pd-S(1) 2.776(12), Pd-S(4) 2.2791(12), Pd-Cl(1) 2.3047(15), Pd-Cl(2) 2.3102(12) Å, Cl(1)-Pd-Cl(2) 92.11(5), Cl(1)-Pd-S(1) 176.35(5), Cl(1)-Pd-S(4) 87.75(5), Cl(2)-Pd-S(1) 91.17(4) Cl(2)-Pd-S(4) 179.23(4) and S(1)-Pd-S(4) 89.00(4)°].

The relatively flattened macrocyclic ligand co-ordinates as a bidentate chelating ligand *via* the *exo* oriented S-donor atoms leaving the *endo* oriented O-atoms free. The SCH_2CH_2S moiety adopts a gauche torsion angle [S(1)-C(2)-C(3)-S(4) -58.1(4)°] with the ethylene bridge occupying part of the macrocyclic cavity. $[Pd([18]aneS_2O_4)_2](PF_6)_2$ crystallises in the triclinic space group *P* -1 (No. 2), a = 7.7395(15), b = 11.6179(24), c = 11.8825(24) Å, α = 101.171(12), β = 95.518(15), γ = 103.673(15)°, U = 1003 $Å^3$, Z = 1. The single crystal X-ray structure shows the Pd(II) occupying a crystallographic inversion centre, with square-planar co-ordination by the $[18]aneS_2O_4$ ionophores through the thioether S-donors [Pd-S(1) 2.3217(14), Pd-S(4) 2.3102(13) Å and S(1)-Pd-S(4) 88.71(5)°]. The conformation of the macrocycle is very similar to the one found in *cis*-$[PdCl_2([18]aneS_2O_4)]$ with the O-atoms in *endo* orientations. $[Pd([18]aneS_3O_3)_2]^{2+}$ is prepared by the reaction of $PdCl_2$ with two equivalents of $[18]aneS_2O_4$. $[Pd([18]aneS_3O_3)_2](PF_6)_2$ crystallises in the triclinic space group *P* -1 (No. 2), a = 8.421(8), b = 10.478(8), c = 11.243(11) Å, α = 76.01(7), β = 87.10(8), γ = 84.61(7)°, U = 958 $Å^3$, Z = 1. The single crystal X-ray structure shows the Pd(II) occupying a crystallographic inversion centre, with square-panar co-ordination by the $[18]aneS_3O_3$ ligands via two of the three thioether S-donor atoms [Pd-S(1) 2.3081(22), Pd-(S4) 2.3193(21) Å, S(1)-Pd-S(4) 88.33(8)°]. The structure exhibits some disorder in the polyether/thioether chain which was modelled in two positions with site occupancy factors of 50% each. The third S-donor atom adopts in one of the disordered fragments a long range apical position at the Pd(II) [Pd···S(16) 3.2901(24)Å]. The reaction of $PdCl_2$ with one equivalent of $[20]aneS_3O_3$ affords the monocation $[PdCl([20]aneS_3O_3)]^+$. The proposed structure of this compound which shows inherently different properties compared with other complexes of Pd(II) with mixed O/S-donor ionophores consists of an *endo* square-planar co-ordination of the Pd(II) ion to the macrocyclic ligand.

CHAPTER V

A brief account on the macrocyclic co-ordination chemistry of Tl is given. The synthesis and characterisation of $[Tl([15]aneS_2O_3)_2]PF_6$, $[Tl([18]aneS_2O_4)]PF_6$ and $[Tl(benzo[18]aneS_2O_4)]PF_6$ is described. The reaction of $[15]aneS_2O_3$, $[18]aneS_2O_4$ and $benzo[18]aneS_2O_4$ with $TlPF_6$ in EtOH afforded the complexes $[Tl([15]aneS_2O_3)_2]PF_6$, $[Tl([18]aneS_2O_4)]PF_6$ and $[Tl(benzo[18]aneS_2O_4)]PF_6$ respectively. Similarities in the spectroscopic results for these compounds compared with analogous macrocyclic Ag(I) complexes suggest a similar in-cavity co-ordination of the metal ion to the macrocyclic ligand.

Chapter VI

The co-ordination chemistry of Ag(I) with homoleptic thioether and mixed O/S-donor macrocycles is introduced. The synthesis and characterisation of $[Ag_2([18]aneS_2O_4)_2](PF_6)_2$ and $[Ag_4([18]aneS_2O_4)_4](ClO_4)_4$ are described. Reaction of $AgClO_4$ with one molar equivalent of $[18]aneS_2O_4$ yielded the highly unusual tetranuclear species $[Ag_4([18]aneS_2O_4)_4](ClO_4)_4$ which crystallises in space group $P2_1/c$ (No. 14), a = 10.933(5), b = 23.615(15), c = 14.593(5) Å, β = 101.64(4)°, U = 3690 Å^3 and Z = 2. The single crystal X-ray structure shows each Ag(I) ion co-ordinated within the cavity of a macrocyclic ligand. Each Ag(I) ion shows a series of Ag-S and Ag-O distances [Ag(1)-S(1) 2.612(2), Ag(1)-S(4) 2.640(2), Ag(1)-S(21) 2.6328(15), Ag(1)-O(7) 2.779(3), Ag(1)-O(10) 2.713(3), Ag(1)-O(13) 2.543(3), Ag(1)-O(16) 3.030(3), Ag(2)-S(21) 2.625(2), Ag(2)-S(24) 2.761(2), Ag(2)-O(24') 2.7085(14), Ag(2)-O(27) 3.047(3), Ag(2)-O(30) 2.475(3), Ag(2)-O(33) 2.645(3) and Ag(2)-O(36) 2.787(3)Å] within a wide range making it difficult to describe the co-ordination geometry in simple terms. The tetranuclear cation can be described as two binuclear fragments, which are symmetry related by a crystallographic inversion centre. Each of those binuclear fragments shows a thioether group bridging between the two Ag(I) ions. The bridging between two binuclear fragments consists of a distorted rectangular Ag_2S_2 moiety [Ag(2)···Ag(2') 4.199(2), S(24)···S(24') 3.505(2)Å].

Reaction of $AgNO_3$ with one molar equivalent of $[18]aneS_2O_4$ followed by addition of NH_4PF_6 yielded the binuclear species $[Ag_2([18]aneS_2O_4)_2](PF_6)_2$ which crystallises in space group $P2_1/c$ (No.14), a = 18.1728(2), b = 11.0571(10), c = 20.0893(14)Å, β = 93.327(10)°, U = 4037 Å^3 and Z = 4.

The single crystal X-ray structure shows in analogy to $[Ag_4([18]aneS_2O_4)_4](ClO_4)_4$ two symmetry related binuclear complex cations in close proximity to each other. These two fragments are in contact via two symmetry related thioether S-donor atoms [S(21)···S(21') 3.434(4)Å]. The environment of each Ag(I) ion in $[Ag_2([18]aneS_2O_4)_2](PF_6)_2$ is very similar to the one found in $[Ag_4([18]aneS_2O_4)_4](ClO_4)_4$. Each Ag(I) ion is co-ordinated within the cavity of a macrocycle and shows a range of Ag-S and Ag-O distances [Ag(1)-S(1) 2.698(3), Ag(1)-S(4) 2.556(3), Ag(1)-S(24) 2.521(2), Ag(1)-O(7) 3.371(5), Ag(1)-O(10) 3.097(6), Ag(1)-O(13) 2.564(7), Ag(1)-O(16) 2.712(11), Ag(2)-S(21) 2.555(2), Ag(2)-S(24) 2.706(2), Ag(2)-O(7) 2.661(5), Ag(2)-O(27) 2.873(6), Ag(2)-O(30) 2.458(7), Ag(2)-O(33) 2.649(8) and Ag(2)-O(36) 2.905(8)Å].

^1H- and ^{13}C-NMR solution studies on $[Ag_2([18]aneS_2O_4)_2](PF_6)_2$ and $[Ag_4([18]aneS_2O_4)_4](ClO_4)_4$ suggest that the predominant species in solution are mononuclear symmetrical (two fold axis or mirror plane) species. It has therefore to be concluded that the assembly of mononuclear fragments, $[Ag([18]aneS_2O_4)]^+$ to oligomeric chain structures is a feature of the solid state.

Chapter VII

The reaction of I_2 with $[Ag([18]aneS_6)]BF_4$ in MeCN yielded the blue complexes $[Ag(18ane_6)]I_5$. Recrystallisation of $[Ag(18ane_6)]I_5$ afforded the brown $[Ag([18]aneS_6)]I_3$ and lustrous green complex $[Ag([18]aneS_6)]I_7$. $[Ag([18]aneS_6)]I_3$ crystallises in the monoclinic space group $C\ 2/m$ (No. 12), a = 18.5767(11), b = 11.9188(7), c = 5.2714(5) Å, β = 95.634(9)°, U = 1162 Å^3, Z = 2. The single crystal X-ray structure shows the Ag(I) ion in a distorted octahedral environment [Ag-S_{ap} 2.8007(10) and Ag-S_{eq} 2.7255(7)] within the cavity of the macrocycle. The linear symmetrical $(I_3)^-$ anions [I-I 2.9137(3) Å] are oriented parallel to the longest axis of the $[Ag(18]aneS_6]^+$ cations. $[Ag([18]aneS_6)]I_7$ crystallises in the trigonal space group R -3m (No. 166), a, b, c = 9.458(4) Å, α,β,γ = 103.79(3)°, U = 758 Å^3, Z = 1. The single crystal X-ray structure shows the highly symmetrical $[Ag([18]aneS_6)]^+$ cations [Ag-S = 2.754(2) Å] embedded in a 3-dimensional polyiodide network $[(I_7)^-]_n$ [I-I 2.7519(4) and I$^-$····I 3.3564(15) Å].

The structure of the novel polymeric $[(I_7)^-]_n$ anionic network can best be described as a distorted cubic lattice. Each corner position is occupied by a I^- anion and the edges of each cube are occupied by I_2 molecules. This leads to an overall $I^-\cdots I\text{-}I\cdots I^-$ moiety from one corner to the other along the edges of each cube. One $[Ag([18]aneS_6)]^+$ cation is accommodated within the centre of each cube. A comparison of the geometry of the $[Ag([18]aneS_6)]^+$ cation in $[Ag([18]aneS_6)]I_3$, $[Ag([18]aneS_6)]I_7$ and the reported complex $[Ag([18]aneS_6)]BF_4$ is given. The ability of cationic metal macrocyclic complexes to not only stabilise but to template extended anionic species is discussed.

The reaction of $[9]aneS_3$ with two equivalents of ICl in CH_2Cl_2 afforded a yellow compound with the proposed stoichiometry $[I([9]aneS_3)]ICl_2$. This compound undergoes an unexpected solid state conversion to yield $([9]aneS_3)_2(I_2)_4$. Other I_2-thioether charge-transfer adducts $([12]aneS_4)I_2$, $([14]aneS_4)I_2$, $([16]aneS_4)I_2$ $([16]aneS_4)(I_2)_4$, $([15]aneS_5)(I_2)_5$, $([18]aneS_6)I_2$, $([18]aneS_6)(I_2)_4$, $([24]aneS_8)I_2$ and $([24]aneS_8)(I_2)_4$ were prepared by direct reaction of I_2 with the appropriate homoleptic thioether macrocycle in CH_2Cl_2. The single crystal X-ray structures of these compounds show linear S-I-I and bridging S-I-I-S moieties [S-I 2.74 to 3.64 Å and I-I 2.75 to 2.83 Å]. The electronic structure of these compounds is discussed. The single crystal structures of these compounds exhibit certain features which allows for a broad division into two different groups. I_2 rich compounds show a columnar stacking motif of macrocyclic ligands, and I_2 deficient compounds adopting a layered 1-dimensional chain structures with I_2 molecules bridging between different macrocycles. Solution studies on $[9]aneS_3$ and $[18]aneS_6$ are described.

The reaction of $[18]aneN_2S_4$ with two equivalents of I_2 afforded a yellow microcrystalline precipitate. Reactions of homoleptic thioether macrocycles (L) with two equivalents of ICl in CH_2Cl_2 afforded similar coloured products. The characterisation of these compounds with the proposed stoichiometries $[I([18]aneN_2S_4)]I_3$ and $[I(L)]ICl_2$ are described.

TABLE OF CONTENTS ..... Page

LIST OF FIGURES AND TABLES

CHAPTER I

CHAPTER II

CHAPTER I

General Introduction

1 INTRODUCTION

1.1 History

The co-ordination chemistry of macrocyclic ligands has been extensively studied over the past three decades. Most of this work has been focused on homoleptic N-, O- and S-donor macrocyclic ligands, although more recently some attention has been drawn to homoleptic and mixed donor-macrocycles containing P[1-6]and Se[213].

Macrocyclic compounds had been reported as early as 1934[7-17]. However, no co-ordination of these species to metal ions has been reported. In 1960 Curtis reported the first of a number of pioneering template reactions in the synthesis of a homoleptic N-donor macrocycles (cyclam derivatives)[18-20]. The homoleptic O-donor macrocycle dibenzo[18]aneO_6 was a chance discovery by Pedersen in 1967[21]. Pedersen wanted to prepare the bis-phenol from mono-protected catechol and bis(2-chloroethyl)-ether (**Figure 1.1a**). As a slightly impure sample of the mono-protected catechol was used (it contained some unprotected catechol) a trace (0.4%) of the hexaether (dibenzo[18]aneO_6) was also obtained[22].

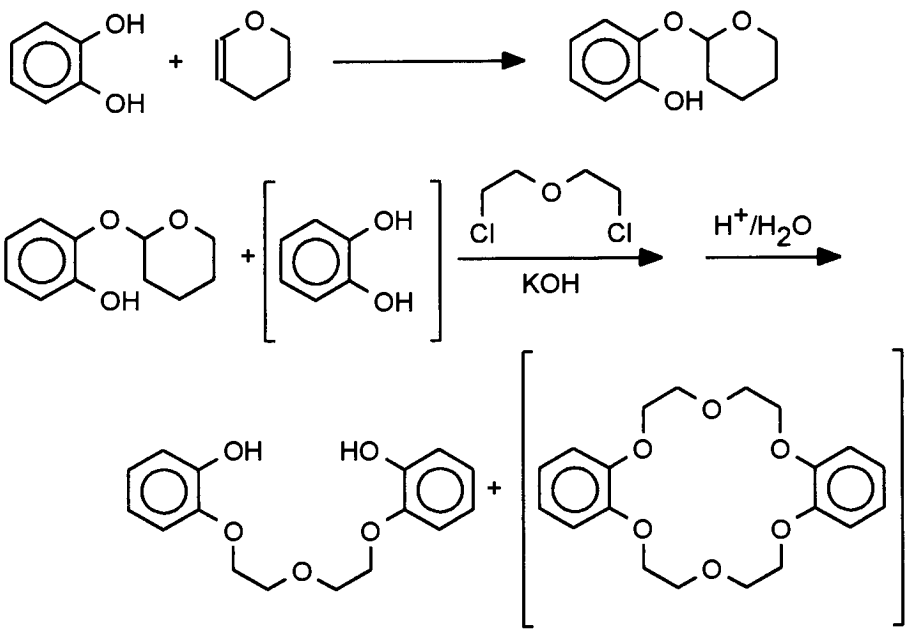

Figure 1.1a Discovery of crown ethers.

The importance of this discovery does not lie in the synthetic procedure but in the way Pedersen recognised the unusual properties of this new material. He noted the good crystallinity and the unusual solubility behaviour. The hexaether was only slightly soluble in MeOH, but on addition of sodium salts, it dissolved surprisingly easily. This, and the fact that with potassium permanganate it could be dissolved in C_6H_6 or $CHCl_3$, prompted him to make this, at the time, bold statement[22]:

> *It seemed clear to me now that sodium ion had fallen into the hole in the centre of the molecule and was held there by the electrostatic attraction between its positive charge and the negative dipolar charge on the six oxygen atoms symmetrically arranged around it in the polyether ring.*
>
> Charles J.Pedersen

This assumption was not made entirely in isolation. Only a short time previously it had been known that certain natural products, so-called ionophores such as *valinomycin* and *nonactin* (**Figure 1.1b**), can enclose alkali metal ions and transport them in biological systems, e.g. through membranes[23-26]. The analogy of natural occurring ionophores to crown ethers is obvious.

Pedersen also suggested the term 'crown' to describe these new macrocyclic compounds[22]. The use of this nomenclature for homoleptic O-donor macrocycles is now widely accepted despite being in some cases ambiguous. Today approximately 5000 different crown compounds, varying in size, molecular flexibility and type and number of donor sites in the ring, are known[27]. From a topological point of view, neutral ligands of this type can be classified into three groups[28,29]: open chain compounds such as classical chelating ligands, known as *podands*, monocyclic systems such as [18]aneO_6 called *coronands*, and oligocyclic (spherical) ligands termed *cryptands*. The work presented in this thesis deals exclusively with coronand-type ligands. The principal macrocyclic ligands discussed in this thesis are depicted in **Appendix 2** with the appropriate abbreviations used throughout this work.

(i)

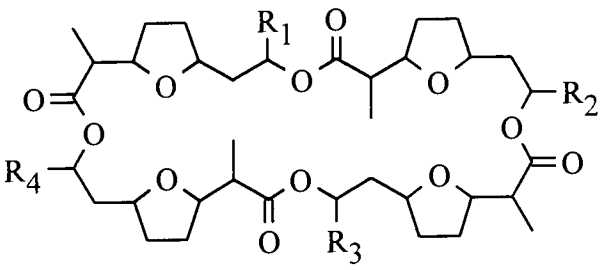

Nonactin	$R_1 = R_2 = R_3 = R_4 = Me$
Monactin	$R_1 = R_2 = R_3 = Me;\ R_4 = Et$
Dinactin	$R_1 = R_2 = Me;\ R_3 = R_4 = Et$
Trinactin	$R_1 = Me;\ R_2 = R_3 = R_4 = Et$
Tetranactin	$R_1 = R_2 = R_3 = R_4 = Et$

(ii)

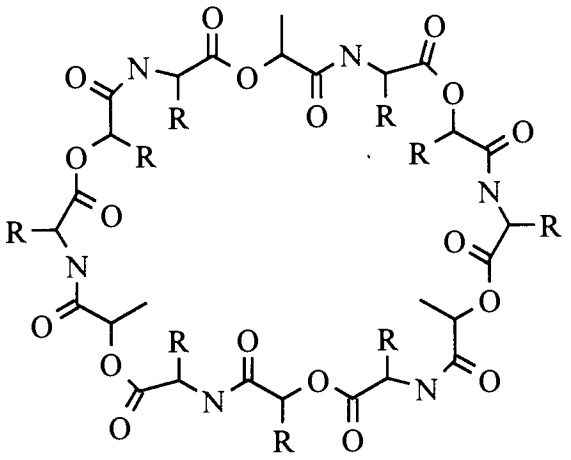

R = ^{i}Pr

Figure 1.1b The natural product ionophores *nonactin* (i) and *valinomycin* (ii).

1.2 Thermodynamics and Kinetics of Macrocyclic Complex Formation

With the discovery of polydentate macrocyclic ligands a new chapter in metal co-ordination chemistry opened. Previously, interest had focused on chelate complexes, an area of study which was initiated in 1893 by Werner[30]. The term 'chelate effect' was first mentioned by Schwarzenbach in 1952[31] and used to describe the enhanced stability constants of chelate complexes in comparison to their mono-dentate analogues.

Much experimental work was carried out to find the thermodynamic origin of this effect[32]. By analogy with the 'chelate effect' a 'macrocyclic effect' was first posited by Margerum in 1969[33] to explain the increased stability of a macrocyclic complex over an open-chain oligochelate analogue and was found to be both kinetic and thermodynamic in origin[34-41]. This enhanced stability has led to a wide interest in macrocyclic chemistry[40-50], since macrocyclic ligands can impose unusual electronic or stereochemical properties on a metal centre[40-44,49,50] and also act as protecting groups to control metal ion reactivity[42,43,46]. The kinetic macrocyclic effect was quantified in a study of the kinetics of formation and dissociation of $[Cu(L_c)]^{2+}$ and $[Cu(L_m)]^{2+}$[35].

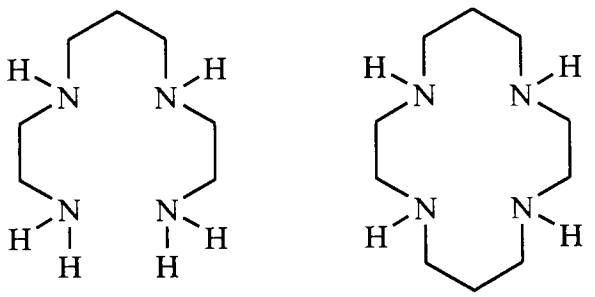

Figure 1.2a The chelating ligand 1,4,8,11-tetraaza-undecane (L_c) and the macrocyclic ligand [14]aneN$_4$ (L_m).

For the reaction

$$Cu^{2+} + L \underset{k_d}{\overset{k_f}{\rightleftharpoons}} [Cu(L)]^{2+}$$

the following rate constants k_f, k_d and stability constants K_s were measured:

	$[Cu(L_c)]^{2+}$	$[Cu(L_m)]^{2+}$
k_f [l·mol^{-1}·s^{-1}]	$8.9 \cdot 10^4$	$5.8 \cdot 10^{-2}$
k_d [s^{-1}]	4.1	$3.6 \cdot 10^{-7}$
$K_s = k_f / k_d$ [l·mol^{-1}]	$2.17 \cdot 10^4$	$1.61 \cdot 10^5$

The conformational flexibility of the open chain chelating ligand means that the complexation and dissociation processes can occur simply by wrapping and un-wrapping of the metal ion (**Figure 1.2b**). Small to medium sized macrocyclic ligands like [14]aneN$_4$ are less flexible and conformational changes induce strain into the relatively rigid macrocyclic framework[34].

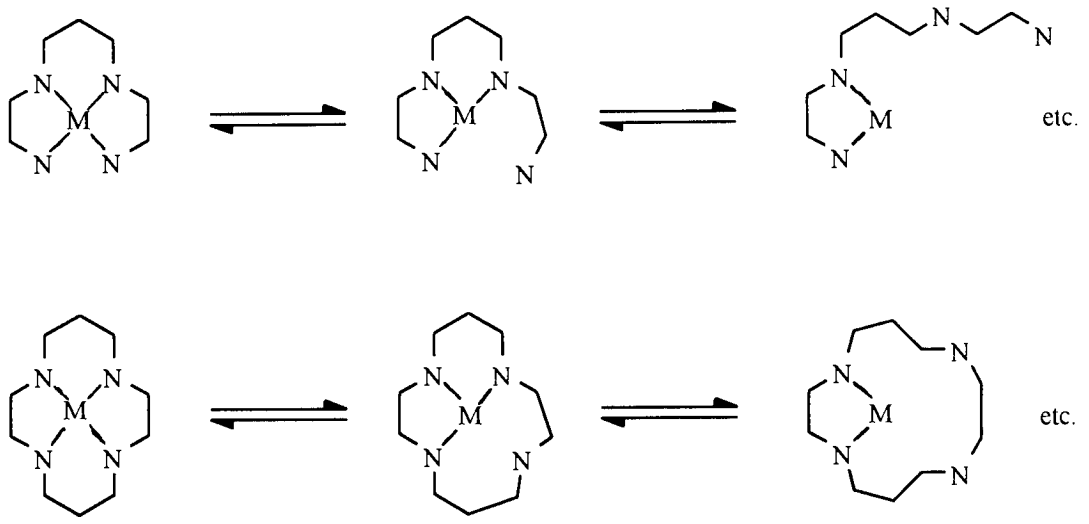

Figure 1.2b Schematic representation of the wrapping mechanism upon complexation and de-complexation reactions for open chain and macrocyclic species (H-atoms omitted).

In practise, the rate of dissociation (k_d) for the macrocyclic system compared to the open-chain species is lowered by more than the rate of complexation (k_f), so that the overall stability constant (K_S) is significantly greater for the macrocyclic complex.

The thermodynamic origins of the macrocyclic effect are still the focus of some controversy. Both entropic and enthalpic considerations are involved, and their relative importance varies between systems.

The entropic component of the macrocyclic effect arises from the relative flexibility of a free open-chain ligand compared to a macrocyclic ligand. The displacement of an open-chain ligand (L_c) by a macrocycle (L_m):

$$[M(L_c)]^{n+} + L_m \longrightarrow L_c + [M(L_m)]^{n+}$$

results in a net gain in configurational entropy, and for this reason it is found that the entropic contribution to such reactions is generally favourable[36,51,52].

The enthalpic term of the macrocyclic effect is mainly derived from the solvation energies of the un-complexed open-chain and macrocyclic ligands, and as such is very dependent on the system under study and on the experimental conditions employed[39]. Early studies on nickel and copper complexes of saturated tetra-aza macrocyclic ligands implied that this enthalpic factor was the dominant contributor to the macrocyclic effect[37,38,10]. However, more recent studies on analogous polythioether complexes have shown that the enthalpic term is diminished in these systems, and the macrocyclic effect is entropically driven[36,52]. This is because of the relatively poor hydrogen bonding between the free ligands and solvent molecules for thioethers, in comparison with the more polar and harder poly-aza species. Consideration of the enthalpic component is further hampered by cavity-size effects, and by ligand pre-organisation energies. A serious mis-match between metal ion and macrocyclic cavity size will diminish the enthalpic contribution since the metal-donor bond(s) will be weakened and the macrocyclic ring strain will be increased. Alternatively, such a mis-match may induce a structural change, such as *trans*- to *cis*-octahedral $[M(N_4)(solvent)_2]^{n+}$, and so causes changes in the observed thermodynamic data[53].

Pre-organisation energy becomes important when the conformation of the free macrocycle is different from that required for in-cavity complexation. This is not generally significant for most tetra-aza ligands[53,54], but becomes important when considering crown thioethers. Most of these adopt exodentate conformations in the un-co-ordinated state[55,56], and must re-arrange to an endodentate form to allow incorporation of a metal ion within the macrocyclic cavity. Such a process amounts to an additional unfavourable enthalpic contribution to the macrocyclic effect.

One notable exception to this is the small-sized macrocyclic ligand 1,4,7-trithiacyclononane ([9]aneS$_3$), which in the solid state adopts a conformation pre-organised for tri-dentate *facial* co-ordination[57]; for this reason [9]aneS$_3$ generally binds to metal centres more strongly than other crown thioethers[42].

1.3 Selectivity of Macrocyclic Complex Formation

The co-ordinative properties of a macrocyclic ligand depend on the nature, number and arrangement of donor atoms, the cavity size and the conformational flexibility (accessibility) of the ligand. Homoleptic O-donor macrocycles (crown-ethers) are known to form very stable complexes with alkali and alkaline earth metal cations, the oxygen donor atoms distributing themselves around the positive charge of the spherical cation. The stability of the complex is dependent primarily upon the 'fit' of the cation within the macrocyclic ring, the ligand forming the most stable complexes with cations whose crystal radius best complements the radius cavity of the ligand[21]. **Table 1.3a** illustrates this phenomenon by comparing hydrophilic cavity diameters of various sized crown-ether ligands with the diameters of the unsolvated alkali metal cations[58].

Cation	Cation diameter (Å)	Crown	Cavity diameter(Å)
Li^+	1.36	[12]aneO$_4$	1.2 - 1.5
Na^+	1.90	[15]aneO$_5$	1.7 - 2.2
K^+	2.66	[18]aneO$_6$	2.6 - 3.2
Cs^+	3.38	[21]aneO$_7$	3.4 - 4.3

Table 1.3a Comparison of alkali metal cation and crown-ether cavity diameters.

In contrast to homoleptic ether macrocyclic ligands, homoleptic thioether macrocycles bind preferably to soft second and third row transition metal ions which exhibit a rigid stereochemistry (e.g. Pd(II) d^8 square planar; Ru(II) d^6 octahedral) depending on their d-configuration and the ligand field strength. The following example illustrates the dominant effect of metal ions over the preferred co-ordination mode of the macrocyclic ligand.

[9]aneS$_3$ has been found by single crystal X-ray diffraction[57] and electron diffraction studies[59] to be pre-organised for *facial*, tridentate co-ordination to a metal ion. Complexes of the composition [M([9]aneS$_3$)$_2$]$^{n+}$ have been particularly well studied[42] and it was found that the ligand shows a remarkable ability to adapt to the conformational requirements of a particular guest-ion. At the same time, however, the inherent preference of the *bis*-[9]aneS$_3$ ligand set for octahedral co-ordination tends to stabilise any metal centre favouring an octahedral geometry, leading to some novel redox behaviour. The metal ions in such octahedral complexes are fully encapsulated by the macrocyclic ligands, and so are protected from attacks by external agents.

Both these properties are exemplified by the series of [Au([9]aneS$_3$)$_2$]$^{+/2+/3+}$ complexes[60,61]. [Au([9]aneS$_3$)$_2$]$^+$ can be prepared by the reaction of [9]aneS$_3$ with [Au(tht)$_2$]$^+$ (tht = tetrahydrothiophene) or [AuCl$_4$]$^-$ under reducing conditions. The single crystal structure of [Au([9]aneS$_3$)$_2$]$^+$ shows a 'tetrahedrally distorted linear' geometry about the Au centre, with one monodentate and one asymmetric *facially* bound [9]aneS$_3$ ligand [Au-S 2.302(6), 2.350(7), 2.733(8), 2.825(8) Å, **Figure 1.3** (i)]. Chemical oxidation of this complex in HClO$_4$ yields the tetragonal [Au([9]aneS$_3$)$_2$]$^{3+}$ [Au-S 2.348(4), 2.354(4), 2.926(4)Å] [**Figure 1.3** (ii)]. Oxidation of the Au(I) complex in HBF$_4$ affords the green paramagnetic species [Au([9]aneS$_3$)$_2$]$^{2+}$, which also adopts a tetragonally Jahn-Teller distorted octahedral stereochemistry [Au-S 2.452(5), 2.462(5), 2.839(5)Å] [**Figure 1.3b** (iii)]. The stabilisation of mononuclear Au(II) is highly unusual; here it is achieved by a combination of the stereochemical preference of [9]aneS$_3$ for tridentate co-ordination with the preference of the thioether donors for a softer metal centre. Similar considerations explain the stabilisation of octahedral d^7 Rh(II), Pd(III) and Pt(III) metal centres by this ligand[62-64,66].

(i) $[Au([9]aneS_3)_2]^+$

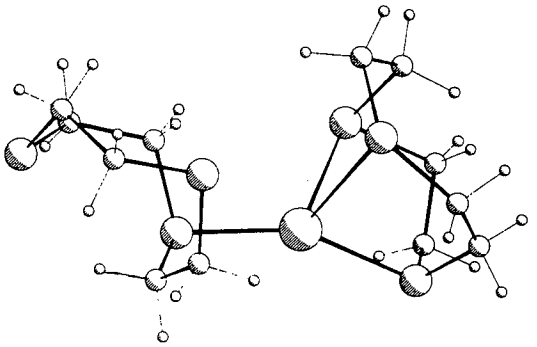

(ii) $[Au([9]aneS_3)_2]^{3+}$

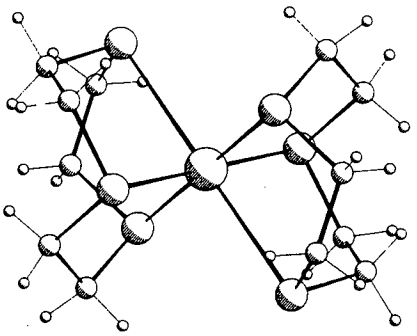

(iii) $[Au([9]aneS_3)_2]^{2+}$

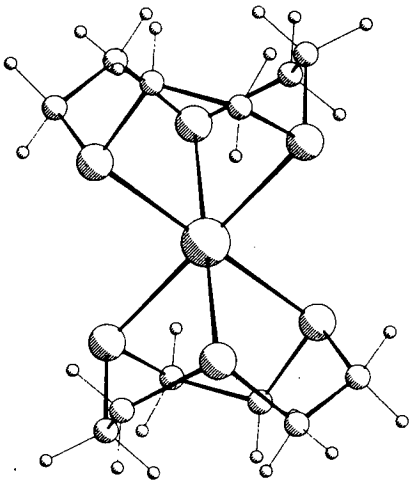

Figure 1.3a Views of the single crystal structures of $[Au([9]aneS_3)_2]^{n+}$.

As mentioned above, the stability of a metal macrocyclic complex does not only depend on the cavity size and preferred stereochemistry. The nature of the donor atoms also needs to be considered. For instance hard alkali and alkaline earth metal ions tend to form stable complexes with hard crown-ethers whereas soft transition metal ions form stable complexes with soft S-donor ionophores. Izatt and co-workers have investigated the thermodynamic parameters for cation-macrocyclic interaction. Thermodynamic data for 260 different macrocyclic ligands have been tabulated and published[67].

In previous studies it was found that successive substitution of O- by S-atoms in [15]aneO_5 and [18]aneO_6 had a dramatic effect on the log K values for metal ions[68]. **Table 1.3b** summarises some of the results obtained for the complexation of Ag(I) and Tl(I) with these ionophores.

Ligand	**Metal/Ligand**	**log*K* for Ag^+**	**log*K* for Tl^+**
[15]aneO_5	1/1	0.94	1.23
[15]aneSO_4	1/1	5.0	0.80
	1/2	2.45	-
[15]aneS_2O_3	1/1	†	<0.6
	1/2	3.31	-
[18]aneO_6	1/1	1.50	2.27
[18]aneS_2O_4	1/1	3.0	1.38
1,10-[18]aneS_2O_4	1/1	4.34	0.94

(† log*K* too large for measurement)

Table 1.3b log*K* values for the reaction of Ag(I) and Tl(I) with mixed O/S-donor ionophores in water[67,68].

It is obvious that in both cases the larger 18-membered macrocycle stabilises the metal ion better than its smaller 15-membered analogue. The stepwise substitution of O- by S-atoms shows an increase in the log*K* values in the case of Ag(I) whereas in case of the Tl(I) cation it decreases. The considerable difference in the log*K* values for the complexes of Ag(I) and Tl(I) with both isomers of [18]aneS_2O_4 (**Table 1.3b**) suggests that the geometry of the free macrocycle and therefore the co-ordination geometry around the metal ion is of importance. However, no structural investigations of Tl(I) and Ag(I) ions with 18-membered mixed O/S-donor ionophores have been reported.

1.4 Metal Complexes in Biological Systems

Metal ions play a pivotal role in biological systems[69-71]. Even though the mechanism of most of the functions of metal ions in physiological systems is still under investigation, it is clear that in particular transition metal ions can perform a number of functions. Some of these processes are highly specific to a certain metal ion, in a specific oxidation state and environment (e.g. Fe(II) in hemoglobin)[72]. In contrast, other processes are much less specific, and it is possible to replace one metal ion by another, although the activity might be reduced [e.g. replacement of Zn(II) by Co(II), Mn(II), Cd(II) in carboxypeptidases][73]. Functions commonly performed by metal ions include the storage and transport of oxygen (iron in myoglobin, hemoglobin[72] and hemerythrin[74,75], enzymatic catalytic processes such as Ni in hydrogenases[76], Fe in cytochrome P_{450}[77] or Zn in carbonic anhydrase[78]. Transition metal ions are also known to act as electron-transfer catalysts (Fe-S clusters in ferredoxins[79], Cu in oxidases[80]) and as free radical initiators (Co in Vitamin B_{12}[81]). Alkali and earth-alkali metal ions on the other hand are heavily involved in certain physiological control and trigger mechanisms. For instance K^+, Ca^{2+} and Mg^{2+} play an important part in maintaining the structure and controlling the function of membranes[82-87].

This introduction can only be fragmentary. Systematic reviews on metal ions in biological systems have been published[69,88,89]. The following three sections give a brief overview of metal ions in biological systems with respect to their ligating environment - *macrocyclic*, *non-macrocyclic* and *cluster*.

1.4.1 Macrocyclic Metal Co-ordination

The most common ligand system for macrocyclic metal co-ordination in metalloenzymes is based on the tetrapyrrole fragment or its partially reduced derivatives. These (see **Figure 1.4.1a**) include the heme iron-porphyrin complexes which can be found in a variety of enzymes[90], the chlorins (found in chlorophylls)[91], the corrins (vitamin B_{12})[81] and the nickeltetrahydroporphinoid complex F_{430}[76].

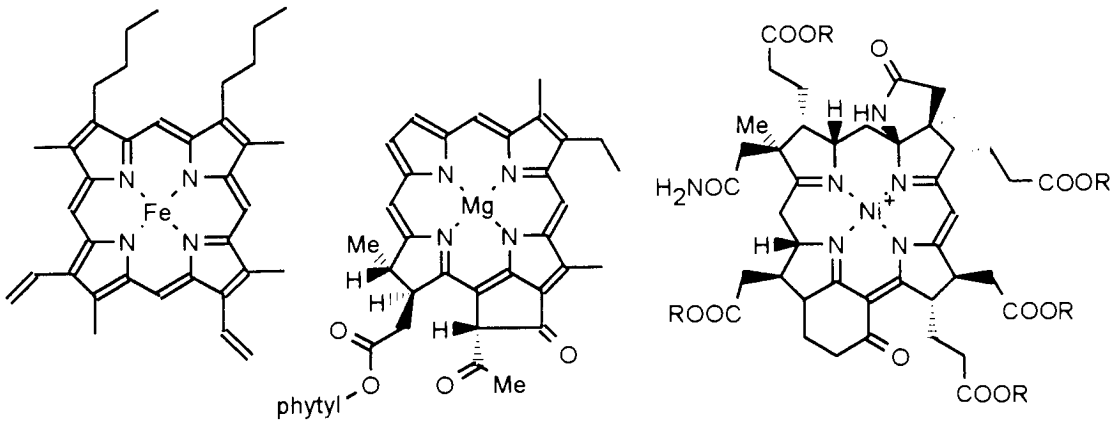

Heme Chlorophyll Ni tetrahydroporphinoid F_{450} complex

Figure 1.4.1a Natural occurring metal macrocyclic complexes in metalloproteins.

The function of the metal ions in these compounds varies between systems, but generally involves a metal-based redox process. The macrocycle provides protection of the metal ion and tunes the metal redox activity. There has been considerable interest in complexes of synthetic porphyrin and phthalocyanin macrocycles (**Figure 1.4.1b**), both as models for the above systems[92] and as novel catalysts in their own right. There are two additional classes of ionophores which play an important part as carriers in biological systems: (i) antibiotics and (ii) siderophores.

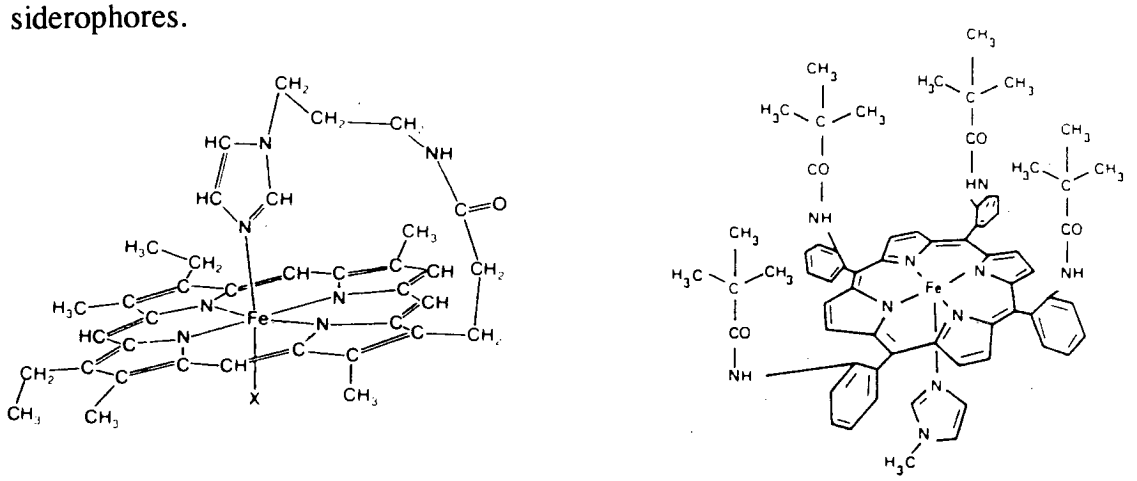

Figure 1.4.1b Model complexes for the O_2 binding site in hemoglobin based on synthetic porphyrin macrocycles.

(i) There are two classes of antibiotic ionophores. One class consists of the channel-forming ionophores, proteins which span the membrane, providing a hydrophilic channel through which cations pass. The second class comprises the carrier ionophores which bind cations prior to transport of the cation-ionophore complex through the membrane. Ionophores are usually peptides (*valinomycin*) (**Figure 1.4.1c**) or esters (*nonactin* and its derivatives) (**Figure 1.4.1d**) containing additional protein linkages and furane units. Measurement of the formation constants of Na^+, K^+ and Cs^+ with *valinomycin* and *nonactin* in aqueous media show a high selectivity for potassium[23]. However, it has been shown that in dry Me_2CO all three cations bind to *nonactin* to the same extent[23]. The metal ion has to be stripped of its hydration shell prior to co-ordination and only in the case of K^+ is this favoured. This emphasises the importance of the hydration energy and in turn the question of ionic size and co-ordination number.

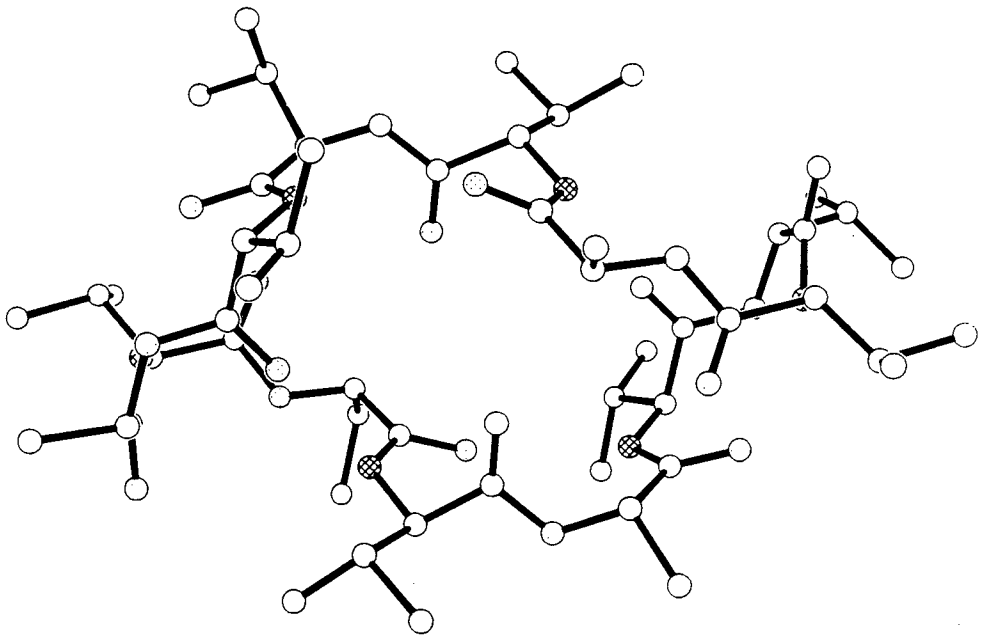

Figure 1.4.1c The single crystal structure of *valinomycin* (compare to **Figure1.1b**)[93].

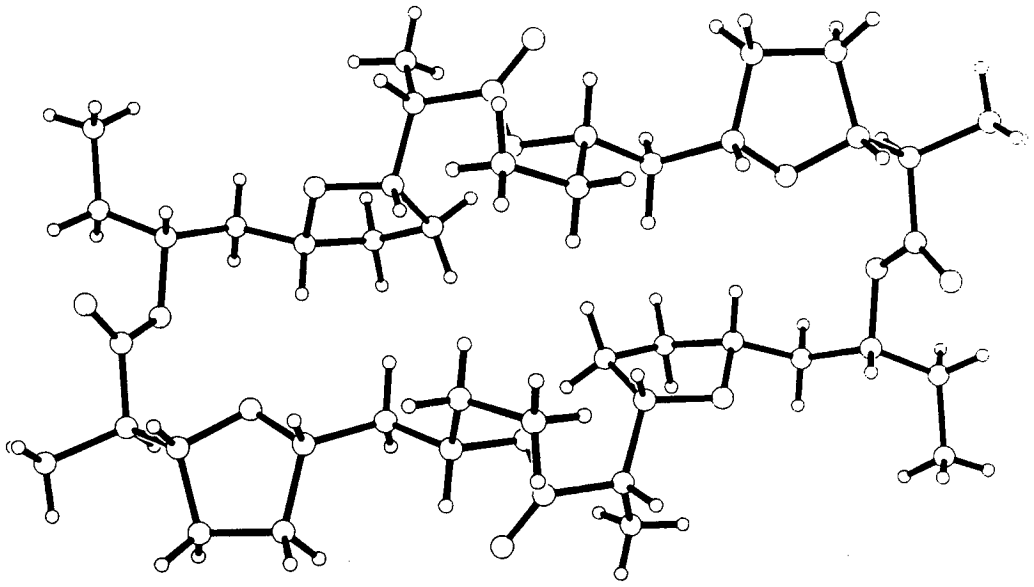

Figure 1.4.1d The single crystal structure of *tetranactin* (compare to **Figure1.1b**)[94].

(ii) Siderophores (Greek for iron bearer)[95] are iron-binding proteins, low-molecular mass compounds with remarkable chemical properties. They are produced by microorganisms to sequester iron from the environment in cases of iron deficiency. The transport of iron in microbes, plants and animals has been reviewed[96]. The first example of a siderophore was discovered in 1911[95,96] but it took about 40 years until its aluminium salt and the metal-free compound could be isolated[97,98] and its chemical properties were investigated[99]. Nevertheless it took a further 30 years until it became obvious that this compound, *mycobactin*, belonged to the siderophores. The siderophore *enterobactin* was first described in 1970. It was isolated from cultures of a*erobacter aerogenes*, e*scherichia coli*[100] and *salmonella typhumurium*[101]. To these bacteria it serves as a ligand for the complexation and transportation of iron and plays a role in their growth. Synthetic and bio-synthetic procedures for enterobactin were published in 1977[102], 1981[103-106]. Even though the siderophores are structurally quite different, they all provide carbonyl- and hydroxy-groups that chelate to the Fe-atom. **Figure 1.4.1e** shows the siderophore *enterobactin* which is based on a macrocyclic framework and the open-chain siderophore *mycobactin*.

(i) *enterobactin*

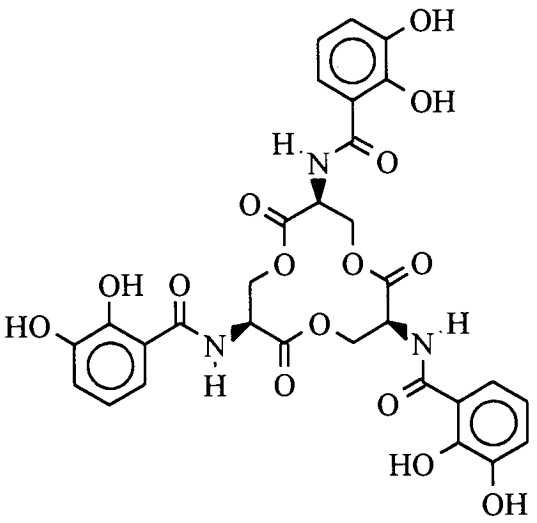

(ii) *mycobactin*

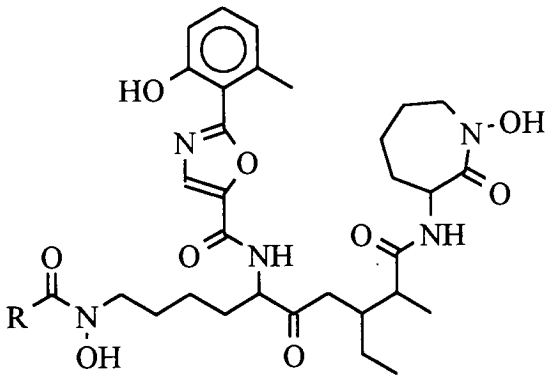

R = C_nH_m with n > 12

Figure 1.4.1e The siderophores *enterobactin* (i) and *mycobactin* (ii).

There has been considerable interest in the chemistry of siderophores on medical grounds. A healthy adult human body contains about 4-5g iron some 65% of this amount is used in the oxygen-transport protein *hemoglobin* and 35% in the iron-storage proteins *ferritin* and *haemosiderin*. The protein *transferrin* promotes the transport of iron thereby maintaining a low level of free iron. Although the human body can regulate the level of free iron, larger amounts of this element are toxic. In addition there is no specific physiological mechanism for the elimination of iron. A healthy human can eliminate a maximum of 1mg of iron per day.

The excess iron in certain diseases (e.g. Cooley's anaemia) threatens especially the heart, liver and pancreas and drugs were sought to selectively complex and excrete it. Siderophores show exceptionally high formation constants for the complexation of Fe. A formation constant of $K_f = 10^{52}$ measured for *enterobactin*,[47,105-110] is the highest ever reported value for an iron complex with a natural compound, although a value seven orders larger has been reported for a synthetic macrobicyclic ligand[105-109].

1.4.2 Non-Macrocyclic Metal Co-ordination

Non-macrocyclic co-ordination sites in metalloenzymes vary considerably in ligand type, co-ordination geometry and nuclearity (several homo- and heterometallic dimeric, and some trimeric, metal centres have been identified). Here the metal atom(s) are co-ordinated directly to amino acid side-chains from the protein; hence a wide range of N-, O- and S-donor ligands are observed, and the (often strained) co-ordination geometry is maintained by the rigid protein backbone[111].

An example is the 'blue' copper site, found in many oxidase enzymes[80]. This has a very distorted, 'flattened' tetrahedral N_2S_2 co-ordination sphere; this strained geometry is adopted to regulate the Cu(II/I) redox couple, and so to facilitate electron transfer. Macrocyclic ligands have received much interest as models for such systems[43,92], since they can be used to impose strained co-ordination geometries on metal ions.

Hemerythrins are O_2 carriers found in some invertebrates. The metalloprotein isolated from *P.gouldii* has a molecular weight of 108,000 and consists of eight subunits, each of which contains two Fe-atoms[75]. The Fe-atoms in hemerythrins are not co-ordinated to porphyrins in contrast to hemoglobin but solely ligated by N/O-donor linkages of amino acids (**Figure 1.4.2a**).

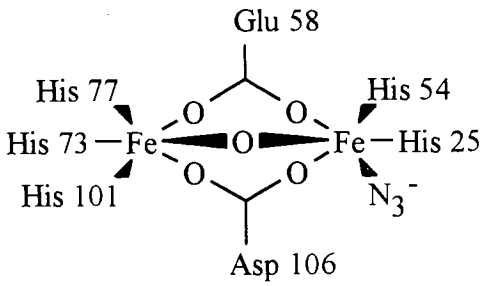

Figure 1.4.2a The active site structure of hemerythrin from an X-ray diffraction study on the azidomet form of *Themiste dyscritum*[112].

The transport of O_2 by hemerythrins involves a two electron oxidation of the two Fe-atoms and co-ordination to the O_2^{2-} anion (**Figure 1.4.2b**). In contrast, the O_2 uptake in hemoglobin is not based on a redox mechanism but on a spin isomerism involving Fe(II). Hemerythrins can be derivatised by addition of additional ligands such as N_3^-, NCS^-, CN^- and F^-. Irreversibly oxidised met-hemerythrins lose their ability to bind O_2.

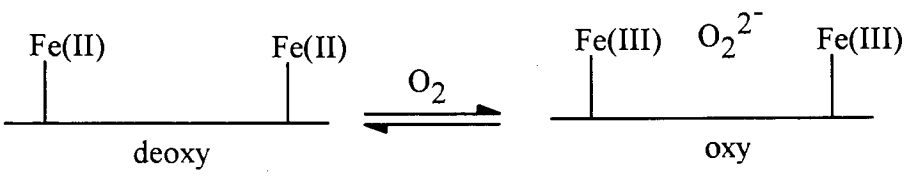

Figure 1.4.2b Schematic representation of the redox processes involved in the reversible binding of O_2 to hemerythrin.

Model complexes for the active site in hemerythrin have been reported. A range of binuclear Fe(III)/Fe(III) complexes $[Fe_2(\mu\text{-}O)(\mu\text{-}O_2CR)_2(HBpz_3)_2]$ (R = H, Me, Ph; $HBpz_3$ = tris-1-pyrazolylborate ion) have been prepared by Lippard and co-workers[113]. (**Figure 1.4.2c**) Wieghardt reported the preparation of two compounds, the Fe(II)/Fe(II) dimer $[Fe_2(\mu\text{-}OH)(\mu\text{-}OAc)_2(Me[9]aneN_3)_2]^+$ and the Fe(III)/Fe(III) dimer $[Fe_2(\mu\text{-}O)(\mu\text{-}OAc)_2(Me[9]aneN_3)_2]^{2+}$ (**Figure 1.4.2d** and **1.4.2e**)[49]. The authors conclude that all three compounds are accurate models for the active site in deoxyhemerythrins and azidomet hemerythrin.

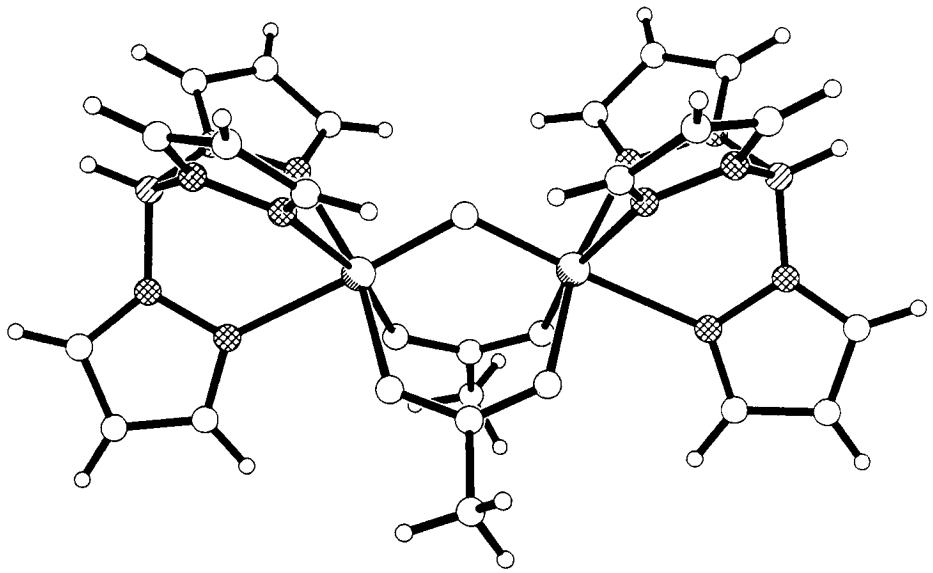

Figure 1.4.2c The single crystal structure of $[Fe_2(\mu\text{-}O)(\mu\text{-}O_2CR)_2(HBpz_3)_2]$[113].

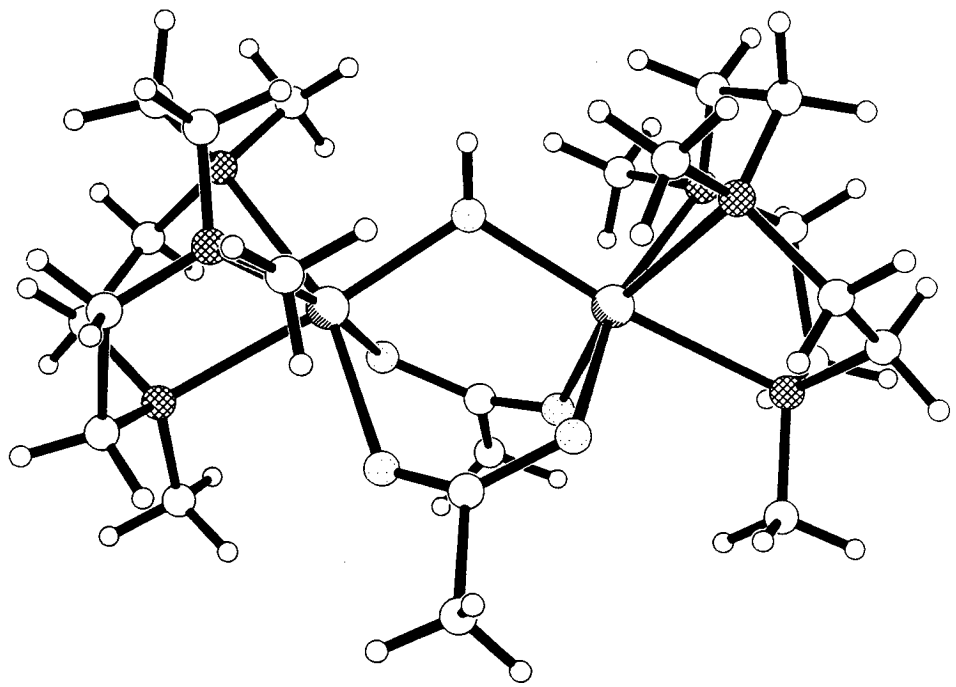

Figure 1.4.2d The single crystal structure of $[Fe_2(\mu\text{-}OH)(\mu\text{-}OAc)_2(Me[9]aneN_3)_2]^{+}$[49].

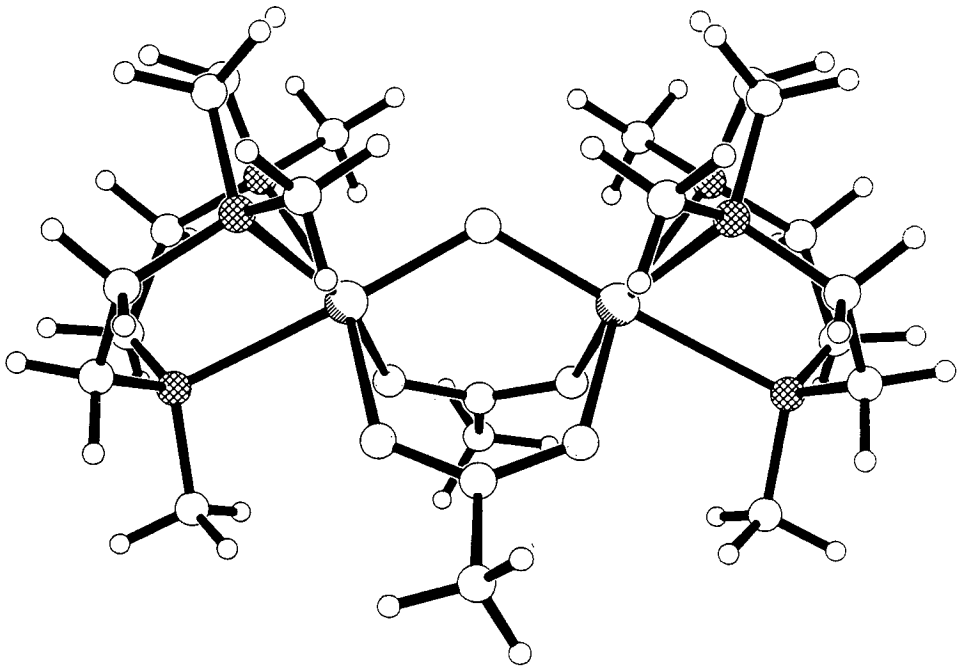

Figure 1.4.2e The single crystal structure of $[Fe_2(\mu\text{-}O)(\mu\text{-}OAc)_2(Me[9]aneN_3)_2]^{2+}$[49].

The two models for hemerythrin reported by Wieghardt illustrate the use of N-donor macrocycles such as [9]aneN$_3$ and its derivatives (Me$_3$[9]aneN$_3$) to mimic three histidin ligands co-ordinated *facially* in an octahedral geometry to a metal centre. Wieghardt and co-workers[50,114-118] have studied a wide range of binuclear complexes with these ligands. These complexes might be suitable model complexes for binuclear sites in metalloproteins such as ribonucleotide reductase (Fe)[119], purple acid phosphatase (Fe)[120-123], catalase (Mn)[124] and photosystem II (Mn)[118]. The role of oxo-bridged iron centres in biology and chemistry has been reviewed[116].

1.4.3 Metal Clusters

Iron-sulphur clusters[78] occur in enzymes that catalyse multiple-electron redox processes. They are often found in conjunction with other metals, such as nickel (in hydrogenases, which catalyse the oxidation of H_2 to $2H^+$) and molybdenum (in nitrogenases, which reduce N_2 to $2NH_3$)[125-127]. Many Fe_4S_4 and Fe_8S_8 proteins have been characterised and show a distorted cubane structure where iron and sulphur atoms occupy alternate corners of the cube. Each iron atom is bonded to three sulphur atoms and vice versa. The cube is linked to the protein backbone by four cystein residues co-ordinated to the iron atoms. The structures of the reduced and oxidised forms of a Fe_4S_4 system have been determined[128] [Carter72]. *Peptococcus aerogenes* ferredoxin is an Fe_8S_8 iron-sulphur protein with a molecular weight of 6000 which contains two Fe_4S_4 cubes separated by 12Å. The structure of this protein has been determined only for the oxidised form[129]. In addition a range of iron-sulphur clusters has been extruded intact from proteins[130-132] or synthetically prepared[65,130,133-135].

The crystal structure of the nitrogenase Mo-Fe protein at 2.7Å resolution from *azetobacter vinelandii* has been reported recently[136,137]. The authors proposed a model for nitrogenase based on their own investigation and on EXAFS studies[138,139] Mössbauer- and ESR-spectroscopy[140]. The proposed clusters are $[Fe_4S_3]$, $[Fe_3MoS_3]$ and $[Fe_4S_4]$[137]. A range of model complexes had been prepared which were termed structural models because they contain the essential components (Fe-, Mo- and S-atoms) but did not show any reactivity towards N_2[141-144].

1.5 Applications

The unique properties of macrocyclic compounds have led to their use in a wide range of applications. This section is meant to outline the wide variety of applications where macrocyclic compounds are of high potential.

1.5.1 Extraction and Transport

The ability of crown ethers to selectively bind cations has been employed to separate mixtures of different cations. Industrially this is achieved by addition of crown ether derivatives to polymeric matrices. When the [18]aneN_2O_4 derivative

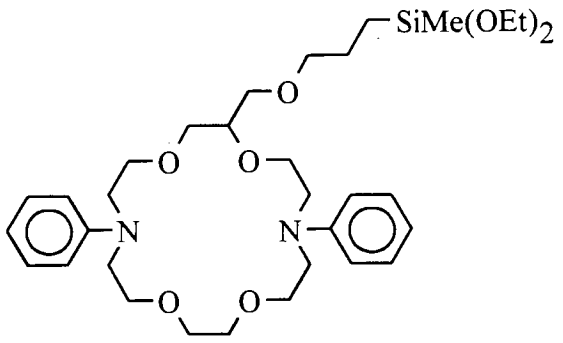

Figure 1.5.1a Silica-bound ionophore for removal of Cu(II), Cd(II) and Ag(I) cations from aqueous media[145,146].

Silica-bound mixed O/S-donor ionophores (**Figure 1.5.1b**) have been studied and it was found that they are able to quantitatively remove trace (20 ppb) amounts Au(III), Pd(II), Ag(I) and Hg(II) ions from acidic aqueous solutions[147].

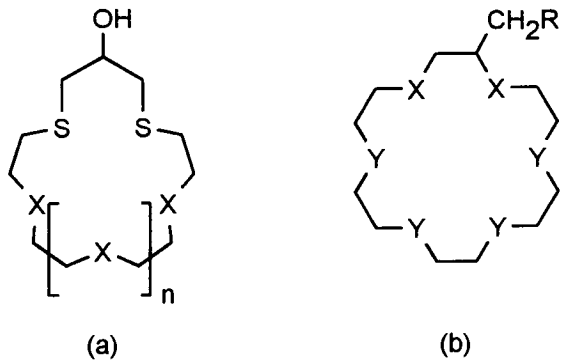

(a) X = O, S; n = 0, 2, 3

(b) X = O, S; Y = S, O; R = $OCH_2CH{=}CH_2$

Figure 1.5.1b Silica-bound mixed O/S donor ionophores for removal of Au(III), Pd(II), Ag(I) and Hg(II) cations from acidic aqueous media.

Chromatographic columns packed with such matrices have been employed for the separation of alkali metal cations[148]. The cations are eluted at different rates according to the stability of the complexes formed. Cations which form the weakest complexes are eluted more quickly than those that form stronger complexes. For example the dibenzo[21]aneO$_7$ derivative shown in **Figure 1.5.1c** separates a mixture of K^+, Na^+ and Li^+ cations. It forms the least stable complex with Li^+ cations which are eluted first and the most stable complex with K^+ cations, which are eluted last.

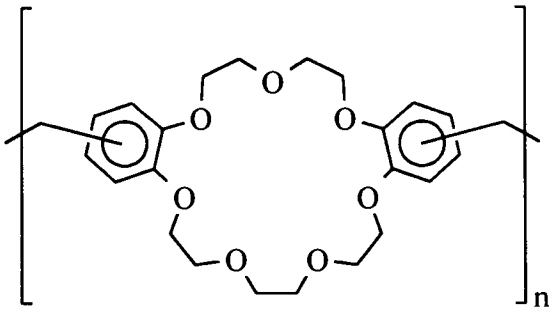

Figure 1.5.1c Dibenzo[21]aneO$_7$ based polymer used in the chromatographic separation of alkali metal ions.

Similar results are obtained for a solution containing equal amounts of Hg(II), Zn(II) and Cd(II) ions. The [18]aneN$_2$O$_4$ ionophore (**Figure 1.5.1a**) forms a very stable complex with Hg(II) cations and it is therefore possible not only to separate Hg(II) cations from Zn(II) and Cd(II) cations but also to enrich Hg(II) cations in the eluent[149].

1.5.2 Medical Applications

The utilisation of macrocyclic ligands in the process of complexation and removal of heavy metal ions from the environment suggests that similar considerations might be of interest in treating heavy metal poisoning. Other potential applications include metal macrocyclic complexes as contrast agents for imaging purposes or cancer treatment. The enhanced inertness over chelating ligands, combined with the possibility to functionalise the macrocyclic framework to make it physiologically acceptable, is of much current interest.

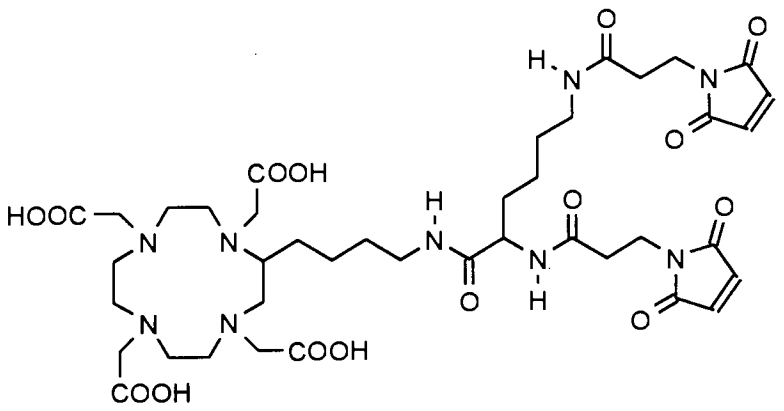

Figure 1.5.2 Macrocyclic ligand used in anti-cancer drug development.

The development of an anti-tumor agent based on the macrocycle [12]aneN_4 is currently under investigation[150-152]. The ligand (**Figure 1.5.2**) forms very stable complexes with In and Y. The complex can be conjugated to the monoclonal antibody B72.3 which recognises a particular antigen TAG72 (found in colorectal, breast and ovarian tumors). The ^{111}In or ^{90}Y radiolabelled species would then deliver irradiation directly to the tumor. Even though the compound showed good tumor localisation and short plasma half life, accumulation of residues in the kidneys poses a problem which may limit the therapeutic use of this particular compound.

1.5.3 Homogenous Catalysis

The design of an effective homogenous metal catalyst involves effective control of the stereochemical and electronic properties of the metal centre. Macrocyclic ligands are ideally suited to fulfill these requirements, and there has been considerable interest in the catalytic properties of synthetic macrocyclic complexes. By analogy with biological systems where metal ions fulfill highly specific functions most attention has been paid to the ability of metalloporphyrins and analogous species to bind and activate small molecular substrates such as CO_2[153-156], CO[157], O_2[158-160], H_2[157,161], N_2[162-164], NO_3^-[165] and C_2H_4[166].

Two processes that have received particular attention are the electrocatalytic reductions of CO_2 and O_2. Several Co and Ni complexes of tetra-aza macrocycles have been shown to reduce CO_2 to CO in aqueous solution[153-155], $[Ni(cyclam)]^{2+}$ has been shown to be a particularly efficient catalyst for this process, whilst avoiding the competing reduction of H_2O to H_2[154]. The cyclam amine H-atoms have been implicated in the mechanism of the process (**Figure 1.5.3a**). In contrast, Ag(II) and Pd(II) porphyrin complexes reduce CO_2 to $C_2O_4^{2-}$ under similar conditions[156].

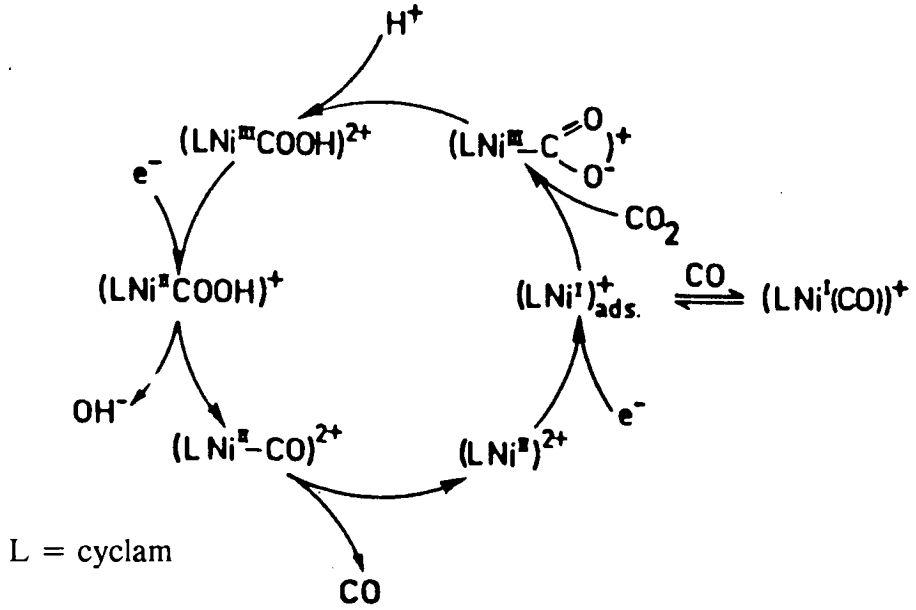

Figure 1.5.3a Proposed mechanism for the electroreduction of CO_2 to CO by $[Ni(cyclam)]^{2+}$ (taken from ref. 154).

The reduction of O_2 to H_2O has potential applications in fuel cells[167]. Two metal-porphyrin systems have been shown to be effective catalysts for this process; a di-cobalt co-facial porphyrin dimer[158] and the complex [Ir(OEP)H] adsorbed onto graphite electrodes[159]. Both these reductions are thought to proceed via a dimeric superoxide-bridged intermediate.

The organometallic chemistry of square planar macrocyclic complexes is also of interest[46,168], since the absence of *cis* co-ordination sites in these species means that several common processes, such as α- or β-elimination or insertion reactions, must follow novel mechanisms. An example of this is the photochemical production of methanol and formaldehyde from CO and H_2 using a $[Rh(OEP)]_2$ catalyst[157]. This proceeds by insertion of CO into an Rh-H bond via a free-radical mechanism (**Figure 1.5.3b**)[157,169].

$$[Rh(OEP)]_2 + H_2 \rightleftharpoons 2\,[HRh(OEP)]$$

$$h{\cdot}\nu$$

$$[Rh(OEP)]_2 \rightleftharpoons 2\,[\cdot Rh(OEP)]$$

$$[\cdot Rh(OEP)] + CO \rightleftharpoons [\cdot(OC)Rh(OEP)]$$

$$[\cdot(OC)Rh(OEP)] + [HRh(OEP)] \rightleftharpoons [(OHC)Rh(OEP)] + [\cdot Rh(OEP)]$$

$$+ \text{ termination steps}$$

Figure 1.5.3b Free-radical mechanism for the production of methanol and formaldehyde from CO and H_2 using a $[Rh(OEP)]_2$ catalyst.

Several metal-carbon σ-bonded derivatives have been produced by oxidative additions to low-valent macrocyclic precursors[168,170]; in many cases these can undergo further transformations to species such as carbenes under redox conditions.

1.5.4 Phase Transfer Catalysis

A major problem in organic synthesis occurs when the reactants are not miscible. This is especially difficult for nucleophilic substitution reactions where the substrate is insoluble in water or polar solvents and the nucleophile, which is often an anion, is soluble in water but not in the substrate or other organic solvents. The difficulties can be overcome by using either quaternary ammonium salts, phosphonium salts, crown ethers or other cryptands. The advantage of the use of coronands and cryptands is that they do not require an aqueous phase because the cryptate salts are already soluble in organic solvents. The second important advantage in the use of cryptands is the increase in the nucleophilicity of the anions. There is evidence that free anions and Na^+ and K^+ cations in organic solvents tend to form ion pairs which diminishes the reactivity of the nucleophile. Suitable cryptands have been used to increase greatly the rates of reaction where F^-, Br^-, I^-, OAc^- and CN^- are nucleophiles[171-173].

Although phase transfer catalysis has been most often used for nucleophilic substitutions, it is not confined to these reactions. Any reaction that needs an insoluble anion dissolved in an organic phase can be accelerated by an appropriate phase transfer catalyst[174]. Examples of an oxidation[175], a fluorination[176] and the generation of a dichlorocarben[177] in a two phase system are shown in **Figure 1.5.4.**

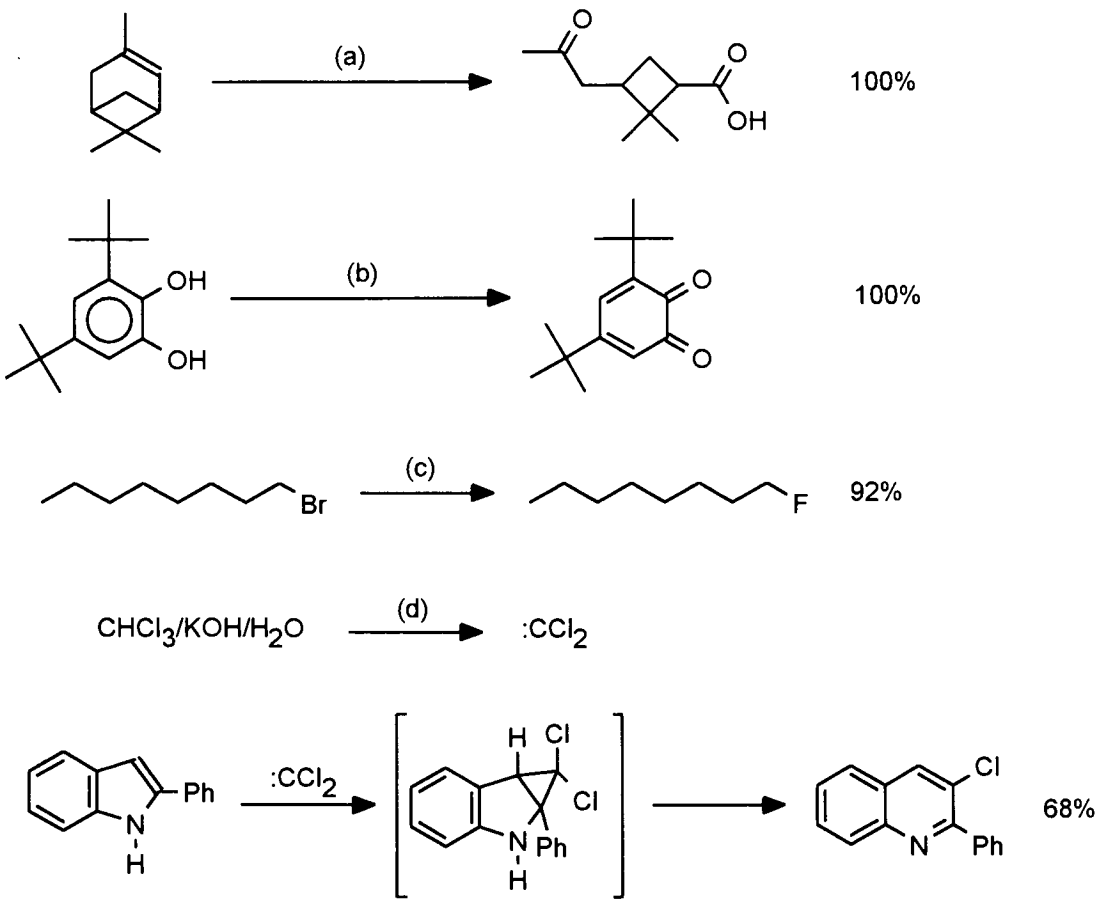

(a) $KMnO_4$/dicyclohexyl[18]aneO_6/C_6H_6
(b) $KMnO_4$/[18]aneO_6/CH_2Cl_2
(c) KF/dibenzo[18]aneO_6/MeCN
(d) dibenzo[18]aneO_6

Figure 1.5.4 Examples of the use of ionophores in organic reactions.

1.5.5 Chemical Sensing - Responsive Macrocyclic Systems

Coupled systems play a vital role in many biological systems, such as oxidative phosphorylation[178,179] and sight[178]. A great deal of recent research has been dedicated to the synthesis of crown-ether derivatives where a responsive group is attached.

The co-ordination chemistry can then be influenced by a physical or chemical stimulus of the responsive centre. The stimulus can be pH[180-182], light[183-189], allosteric[190,191] or electrochemical[192-210]. pH responsive crown-ethers are the oldest class of responsive macrocyclic systems and usually contain one or more carboxylic acid functions attached to the periphery of the crown-ether. These molecules change their cation binding ability in response to the pH of their environment. Fyles[182] has reported lipophilic ionophores with an appended carboxylic acid function (**Figure 1.5.5a**). These macrocycles are able to transport K^+ ions from an alkaline to an acidic medium against a concentration gradient (**Figure 1.5.5b**).

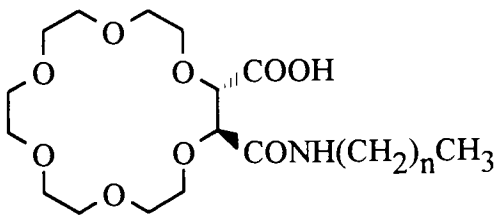

Figure 1.5.5a pH responsive ionophore (n = 7, 13, 17)[182].

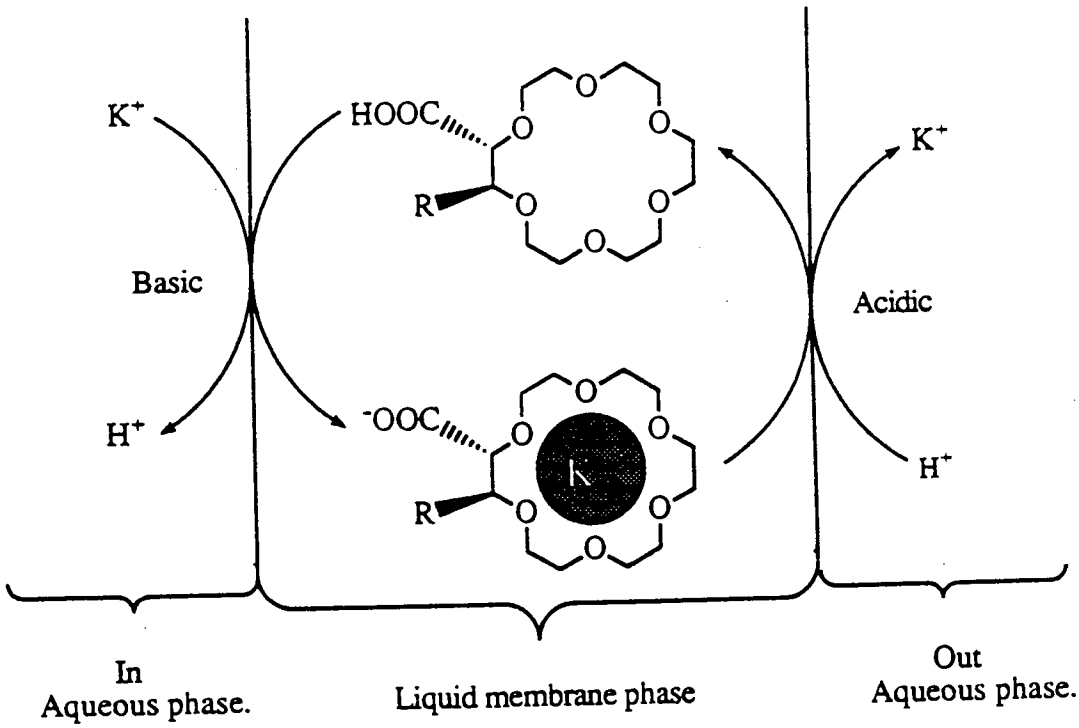

Figure 1.5.5b The active transport of K^+ cations by responsive ionophores.

A photoresponsive *bis*(crown-ether) with a diazo linkage has been reported by Shinkai and co-workers[184-186]. These molecules undergo a photoinduced interconversion from the *trans* (E) isomer to the *cis* (Z) isomer about the diazo linkage (**Figure 1.5.5c**).

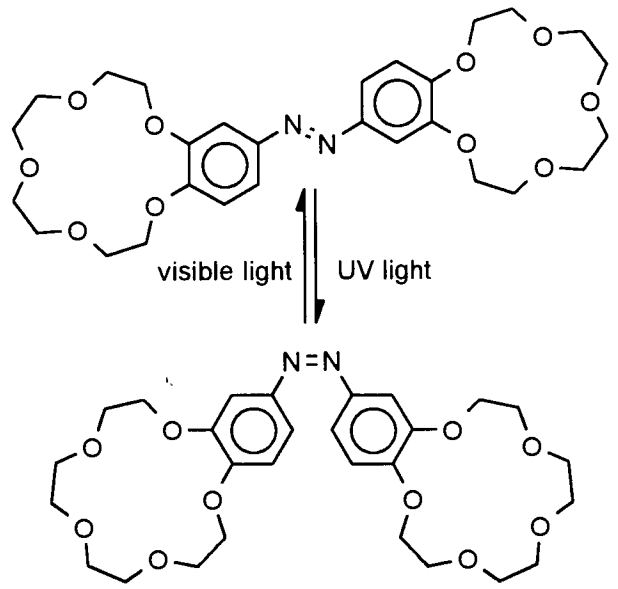

Figure 1.5.5c The *cis* and *trans* isomers of a photoresponsive ionophore.

This results in a marked change in the co-ordination of metal cations. The *trans* (E) isomer extracted sodium cations 5.6 times more efficiently than the *cis* (Z) isomer whereas the *cis* (Z) isomer extracted potassium cations 42.5 times more efficiently than the *trans* (E) isomer[184]. These results suggest the sodium cations are extracted as a 2:1 cation/*trans* (E) complex, whereas K^+ ions are extracted as a 1:1 K^+/*cis* (Z) intramolecular sandwich complex. Shinkai applied this 'photobutterfly crown-ether' to cation transport across a membrane[185,186]. UV light incident upon a solution of the *bis*(crown-ether) in o-dichlorobenzene predominantly produced the *cis* (Z) isomer. The two crown-ether moieties then act co-operatively and form 1:1 intramolecular sandwich complexes with the larger cations (K^+ and Rb^+). Reversion to the *trans* (E) isomer can be accelerated by visible light, which means the two crown-ethers cannot act co-operatively and the alkali metal cations are released into a second phase (**Figure 1.5.5d**). Alternate incidence of UV and visible light was found to accelerate cation transport across membranes when compared to experiments in the absence of light.

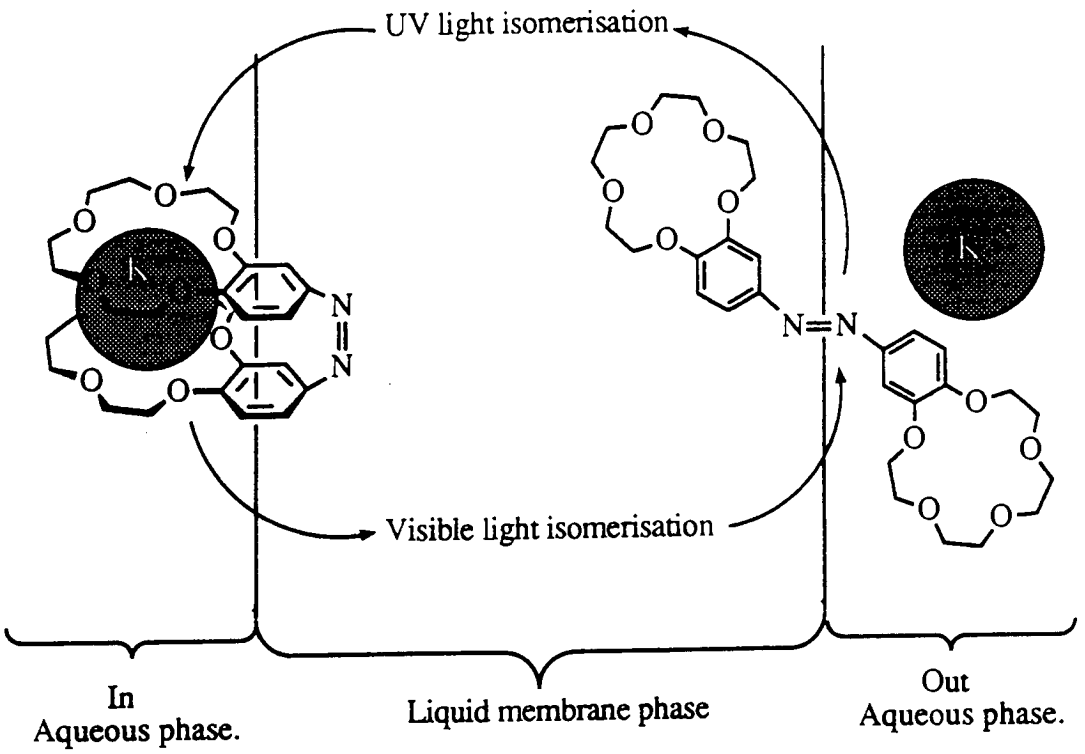

Figure 1.5.5d Transport of K^+ ions accelerated by alternated UV and visible radiation.

By combining ionophores with chromophoric units 'chromoionophores' are created. With these macrocyclic dyes the co-ordination of a cation within the macrocyclic cavity induces a change within the chromophore; resulting in a colour change within the same molecule[189], that in some instances can be detected with the naked eye. Valeur has synthesised a macrocycle linked to the fluorescent dye DFSBO (7-dimethylamino-3-(p-formylstyryl)-1,4-benzoxazin-2-one) **(Figure 1.5.5e)**[188]. The emission band of the fluorescence spectrum showed a marked shift upon addition of alkaline earth metal cations, accompanied by an increase in fluorescence intensity. Li^+ and K^+ ions show a very small change in the spectral parameters of the ligand, indicating selectivity for alkaline earth over alkali metal cations.

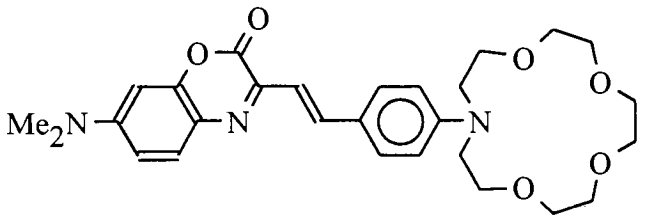

Figure 1.5.5e An ionophore linked to the fluorescent dye DFSBO.

More recently Shinkai reported[183] compounds able to detect enantiomeric differentiation of chiral guests by optically active host molecules, in order to elucidate the absolute configuration of a guest molecule. These systems rely on the fact that the wavelength of reflection for incident light in liquid crystals depends on the pitch of the helical structures in the liquid phase. Thus introduction of complexes of the steroid functionalised ionophore (**Figure 1.5.5f**) with chiral ammonium compounds into cholesteric liquid crystal matrices gave visible wavelength shifts of up to 64 nm.

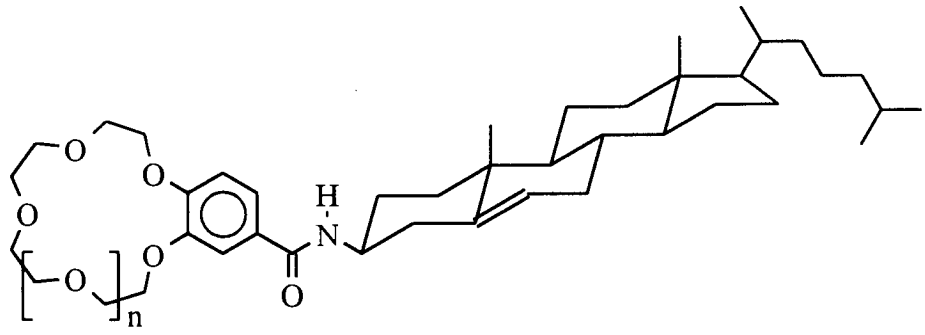

Figure 1.5.5f A steroid functionalised ionophore (n = 1, 2).

Photoresponsive crown ethers have been used in medical applications for chemical analysis. The compounds shown in **Figure 1.5.5g** are used to determine Na^+ and K^+ cation concentrations in blood serum. For example addition of a pre-treated serum into a solution of the benzo[15]aneO_5 derivative followed by measurement of the absorbance at 423 nm gives an accurate Na^+ cation concentration reading over the range 0 to 6 ppm.

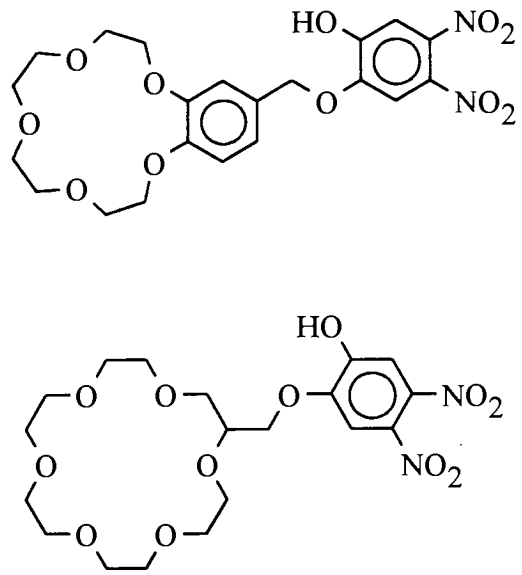

Figure 1.5.5g Photoresponsive ionophores used for chemical analysis of Na^+ cations in the range of 0 - 6 ppm.

The compound shown in **Figure 1.5.5h** produces a characteristic colour change from yellow to red on addition of Li^+ cations. Larger cations such as Na^+ and K^+ show no such colour change under the same conditions[211]. These results were the basis of a method for the determination of Li^+ cation concentration in drugs[212].

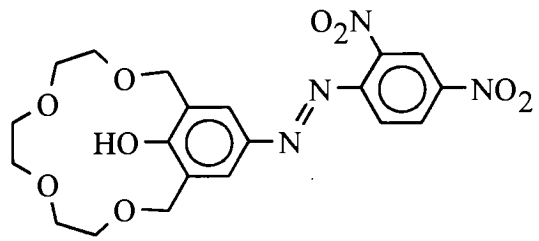

Figure 1.5.5h Photoresponsive crown-ether used for chemical analysis of Li^+ cations.

1.6 Aims of Work

Mixed O/S-donor ionophores such as [15]aneS_2O_3 [**Figure 1.6a** (i)], [18]aneS_2O_4 [**Figure 1.6a** (ii)], [21]aneS_2O_5, [18]aneS_3O_3, [20]aneS_3O_3 and [21]aneS_3O_4 have the potential to bind soft transition metal ions via the S-donor atoms, and hard alkali metal ions or polar organic substrates via the O-donor atoms.

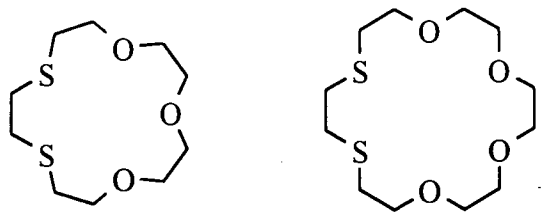

Figure 1.6a (i) [15]aneS_2O_3 and (ii) [18]aneS_2O_4.

Thermodynamical studies by Izatt and co-workers[68,67] have shown that the stability constants of macrocyclic complexes with transition metal ions such as Ag(I) and Hg(II) increases on going from homoleptic O-donor to mixed O/S-donor ionophores [see above (**Table 1.3b**)] and decreases for main group metal ions such as Tl(I) and Pb(II).

In contrast to these extensive studies and reported synthetic procedures for these macrocycles[214-220] only very little preparative work on complexes containing mixed O/S-donor ionophores has been reported. The single crystal structure of $PdCl_2$(1,10[18]aneS_2O_4) (**Figure1.6b**) has been reported in 1974[221] and has been the only example of a complex of a transition metal ion and a mixed O/S-donor macrocycle for about 15 years.

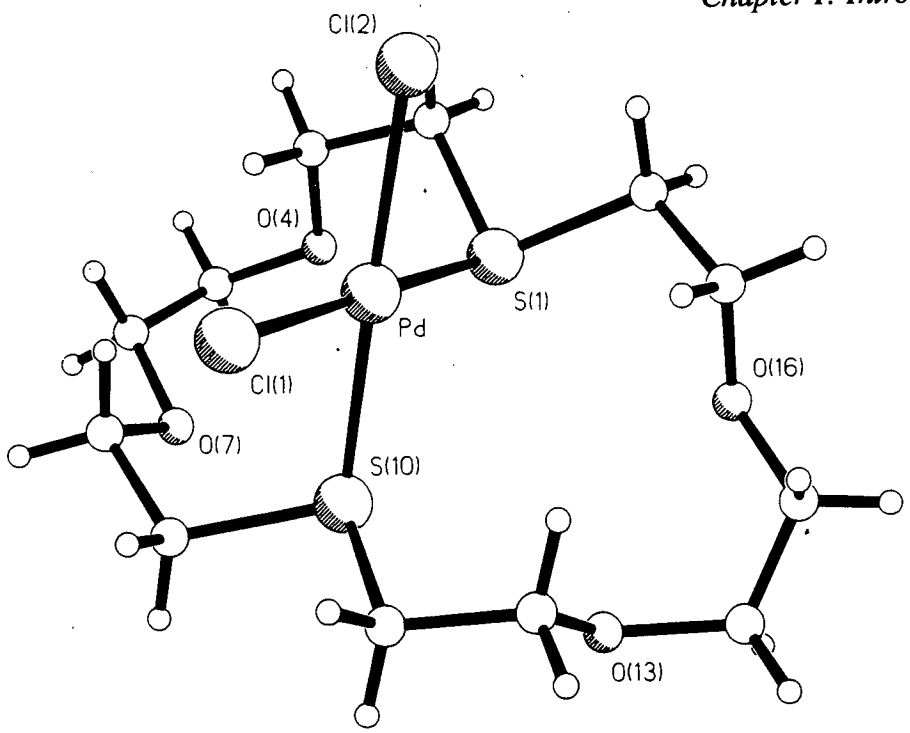

Figure 1.6b The single crystal X-ray structure of $PdCl_2(1,10[18]aneS_2O_4)$[221].

A second structure determination has been mentioned by Izatt and co-workers, however, no crystallographic data have been reported[68,222]. The structure of $[Hg_2Cl_4([18]aneS_2O_4)]$ contains one Hg(II) ion co-ordinated *exo* to the two thioether S-donors of the macrocycle. Two Cl-atoms are associated with this Hg(II) ion while the second Hg(II) ion is bound to two Cl-atoms sharing a third with the first Hg(II) ion[68]. The authors emphasise that the conformation of the ionophore is virtually unchanged compared to the solid state structure of $[18]aneS_2O_4$[68].

Initial work in this area had been initiated roughly 10 years ago in Edinburgh, focusing on the co-ordination chemistry of $[15]aneS_2O_3$ with a series of transition metal ions such as Ru(II), Rh(III), Ir(III), Pd(II), Pt(II) and Ag(I).[223-227] The single crystal structures of a range of complexes have been determined:

$[Pd([15]aneS_2O_4)_2](PF_6)_2$[224,225]	**(Figure1.6c)**
$[RuCl(4\text{-}MeC_6H_4{}^iPr)([15]aneS_2O_3)]BPh_4$[223]	
$[RuCl(PPh_3)([15]aneS_2O_3)_2]PF_6$[225]	**(Figure 1.6d)**
$[RhCp^*([15]aneS_2O_3)Cl]BPh_4$[223]	
$\{[Ag([15]aneS_2O_3)]PF_6\}_n$[226,227]	**(Figure 1.6e)**
$[Ag_2([15]aneS_2O_3)_3](PF_6)_2$[226,227]	**(Figure 1.6f)**

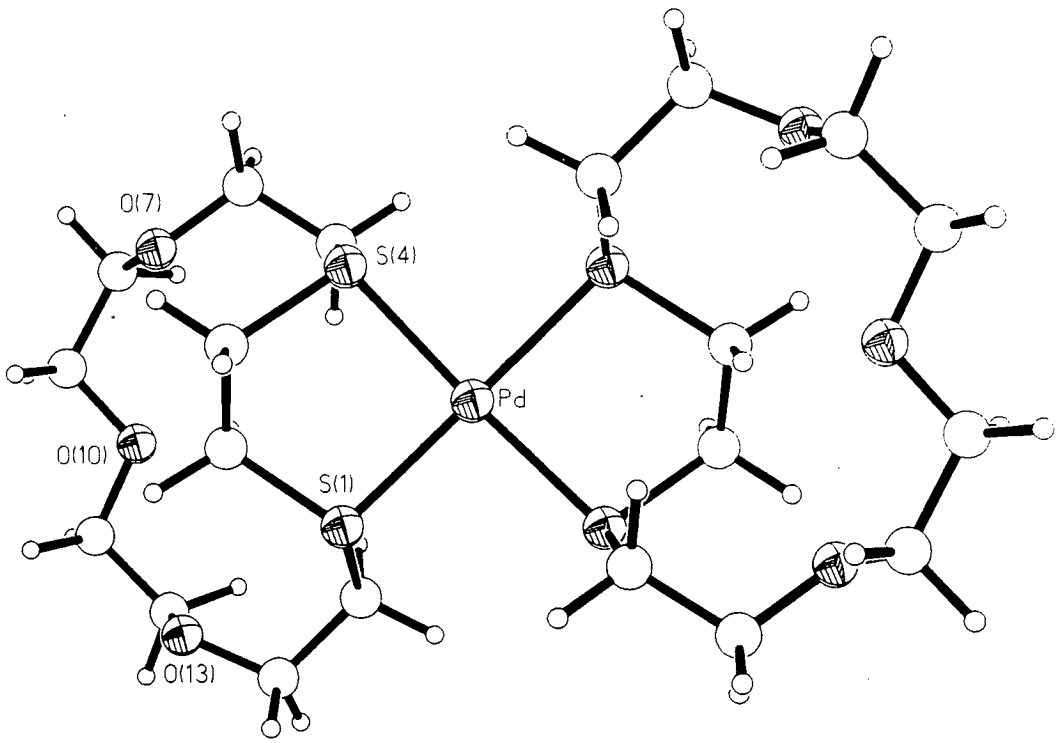

Figure 1.6c The single crystal structure of $[Pd([15]aneS_2O_3)_2](PF_6)_2$.

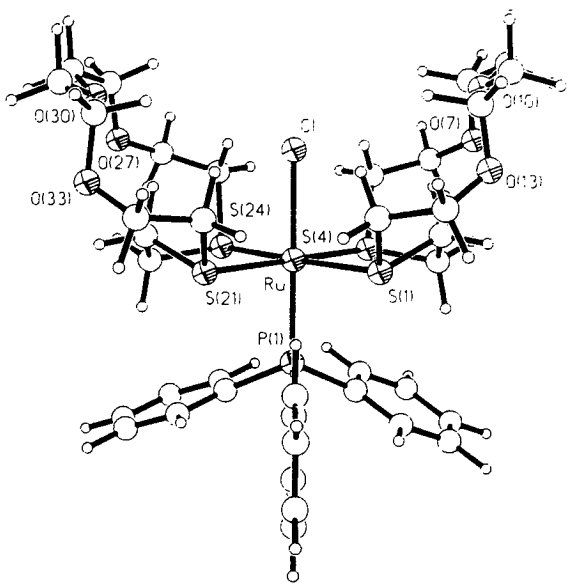

Figure 1.6d The single crystal structure of $[RuCl(PPh_3)([15]aneS_2O_3)_2]PF_6$.

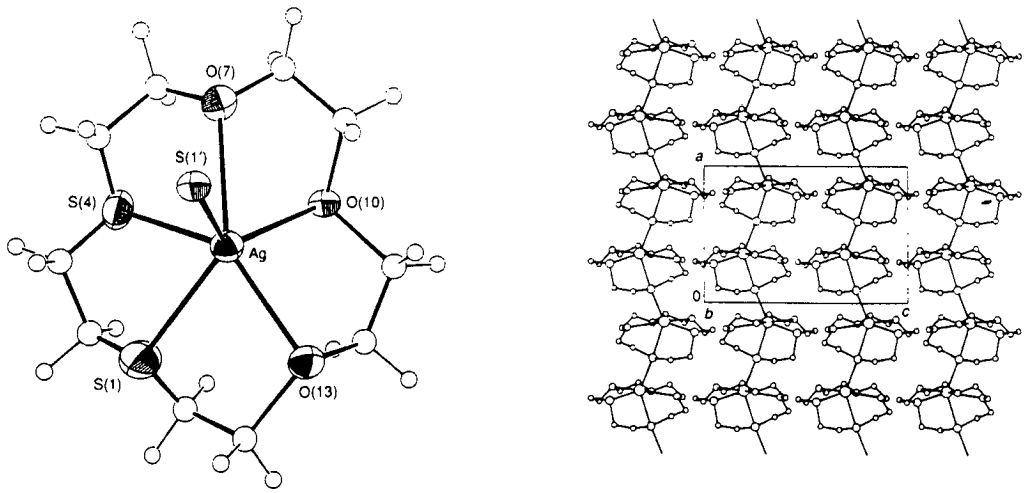

Figure 1.6e The single crystal structure of $\{[Ag([15]aneS_2O_3)]PF_6\}_n$.

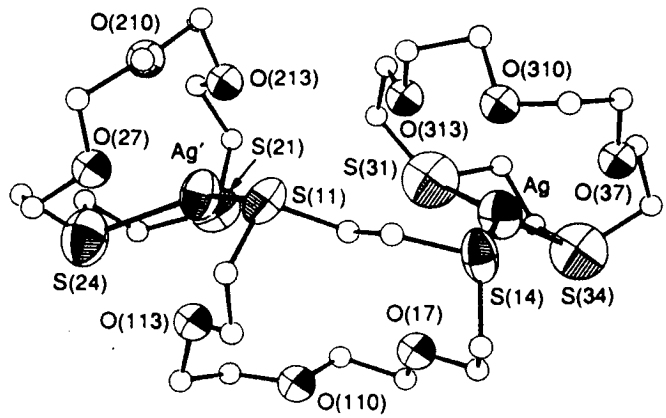

Figure 1.6f The single crystal structure of $[Ag_2([15]aneS_2O_3)_3](PF_6)_2$.

The main conclusions drawn from these studies are, platinum metal ions co-ordinate *exo* to the thioether S-donor atoms leaving the O-donor atoms free for further co-ordination thus establishing one important condition for a host-guest chemistry with these metal macrocyclic complexes. The ethylene bridge between both thioether S-atoms, however, occupies the macrocyclic cavity as a consequence of the chelating binding mode. An in-cavity co-ordination of a potential guest molecule or ion is therefore impossible. The single crystal structure of $[RuCl(PPh_3)([15]aneS_2O_3)_2]^+$ (**Figure 1.6d**) shows two macrocyclic ligands forming a pseudo cavity around the Cl-atom. An enlargement of the macrocyclic ligand and removal of the Cl^- ligand might provide complexes suitable for binding to additional host molecules. We were therefore interested to extend this work towards larger mixed O/S-donor ionophores such as $[18]aneS_2O_4$ and to establish the co-ordination chemistry of this ligand with Ru(II) and Pd(II) ions. It is obvious, that the ethylene bridge between both thioether S-donors will always separate an *exo* co-ordinated metal ion from the macrocyclic cavity. We proposed therefore to investigate means to achieve an in-cavity co-ordination of a platinum metal ion.

Two Ag(I) complexes with $[15]aneS_2O_3$ have been reported[226,227] (**Figures 1.6e** and **1.6f**). It is interesting to note that Izatt and co-workers found evidence for 1:1 and 1:2 Ag(I):$[15]aneS_2O_3$ stoichiometries[68] whereas $\{[Ag([15]aneS_2O_3)]PF_6\}_n$ is of 1:1 and $[Ag_2([15]aneS_2O_3)_3](PF_6)_2$ is of 2:3 stoichiometry. It is even more unexpected that the Ag(I) ion adopts in case of $\{[Ag([15]aneS_2O_3)]PF_6\}_n$ an in-cavity co-ordination mode with an additional Ag-S bond to a neighbouring macrocycle leading to an infinite chain structure, whereas $[Ag_2([15]aneS_2O_3)_3](PF_6)_2$ consists of isolated molecules with each Ag(I) ion co-ordinated *exo* via the S-donor atoms to one macrocyclic ligand and the third bridging between those two Ag(I) ions. We were particularly interested to investigate the co-ordination chemistry of Ag(I) with $[18]aneS_2O_4$ for which Izatt and co-workers found only evidence for a 1:1 stoichiometry[68].

Another topic concerned the co-ordination chemistry of Tl(I) with mixed O/S-donor ionophores. No preparative work has been reported in this area and we were particularly interested to prepare and characterise complexes containing Tl(I) and mixed O/S-donor macrocycles. Izatt and co-workers found that the stability constants of such complexes decreases on going from homoleptic O-donor (crown ethers) to mixed O/S-donor macrocycles. The correlation between the stability constant and the O:S ratio in the macrocyclic ligand indicates some mis-match between the co-ordinative properties of the ligand and the co-ordinative requirements of the metal ion. We were interested whether such a mis-match manifests itself for instance in the single crystal structures of these compounds.

CHAPTER II

Design, Synthesis and Characterisation of Mixed O/S-Donor Ionophores

2.1 INTRODUCTION

The amount of research undertaken in the area of metal macrocyclic chemistry would not have been possible without the development of highly efficient synthetic routes to those ligands. A wide range of reviews dealing with different aspects of macrocyclic chemistry have emerged in recent years[42,44,228-233]. The following section illustrates three different approaches in macrocyclic synthesis using the development of a high yield synthesis for [9]aneS$_3$ as an example.

2.1.1 Macrocyclic Ligand Synthesis

The first report of the synthesis of [9]aneS$_3$ was published by Ochrymowycz and co-workers in 1977[234] in which [9]aneS$_3$ was isolated in 0.04% yield from the reaction of the disodium salt of 2-mercaptoethylsulphide with 1,2-dichloroethane (**Figure 2.1.1a**). Glass and co-workers[235] improved this synthesis by using the $[Me_3N(CH_2Ph)_2NMe_3]^{2+}$-salt instead of the disodium salt of the dithiolate. The reaction was conducted under high dilution conditions and gave a yield of 4.4%. One of the by-products was identified as the 2 + 2 cyclisation product [18]aneS$_6$[236] (**Figure 2.1.1a**) which was obtained in 32% yield.

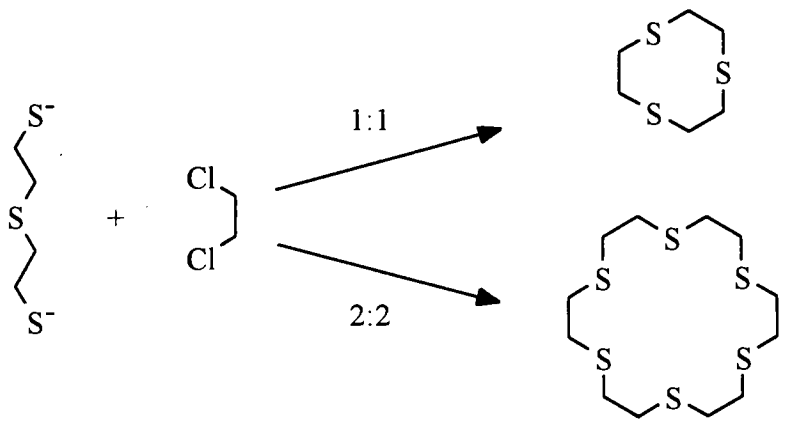

Figure 2.1.1a Synthesis of [9]aneS$_3$ reported by Ochrymowycz[234] and Glass[235].

A high yield template synthesis utilising the $Mo(CO)_3$ fragment was reported in 1984 by Sellmann and Zapf[237,238] (**Figure 2.1.1b**). The use of the template surpresses the formation of polymers and larger macrocycles yielding exclusively the 1 + 1 cyclisation product [9]aneS_3 in more than 60% yield. The $Mo(CO)_3$ fragment has to be removed from the macrocycle but can be recycled and the whole synthesis can be viewed as catalytic in Mo. Contributing factors are the small size and facial co-ordination of the thioether ligand, and the lack of charge on the Mo(0) fragment. The synthesis can therefore be viewed as a template catalysed reaction.

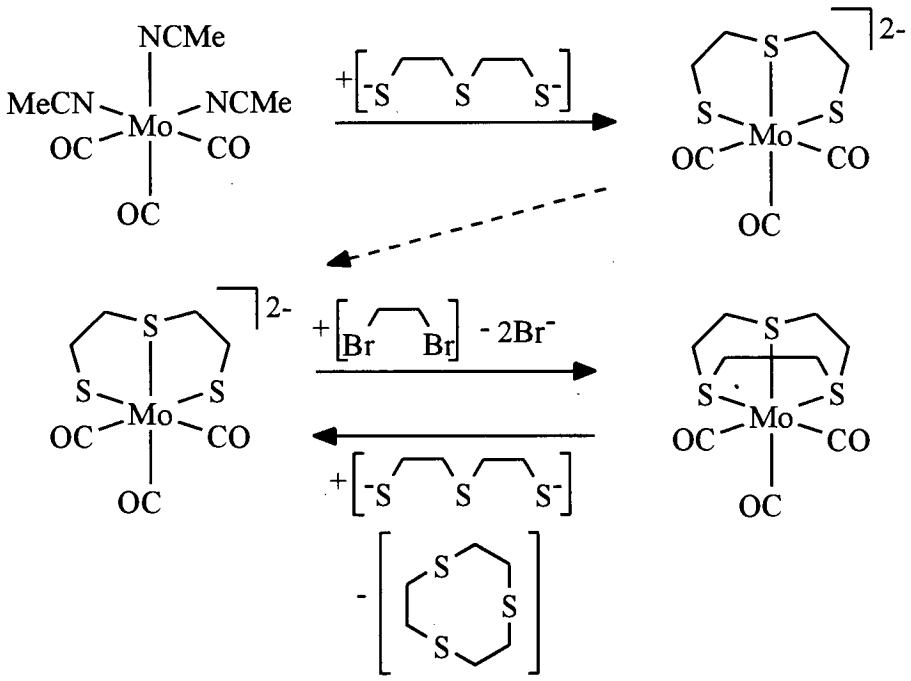

Figure 2.1.1b Template synthesis of [9]aneS_3[237,238].

A large scale synthesis (50% yield) of [9]aneS_3 has been reported by Blower and Cooper[239]. The reaction between 2-mercaptoethylsulphide with 1,2-dibromoethane in DMF is based on the Cs_2CO_3 mediated cyclisation reaction of thioether macrocycles[220,240].

The three different approaches in macrocyclic synthesis highlighted in this example are (i) high dilution synthesis, (ii) template synthesis and (iii) Cs_2CO_3 mediated cyclisation in DMF. Despite these differences all reactions are more or less derived from Williamson's ether synthesis between a halide and an activated $-CH_2X^-$ (X = S, O) anion. Other reactions for instance esterifications[229,241] as the co-condensation step have been reported. In analogy to the first crown-ethers a range of partially unsaturated compounds have been synthesised featuring annelated benzene rings[242], furane, thiophene and pyridine moieties[243].

(i) High dilution synthesis

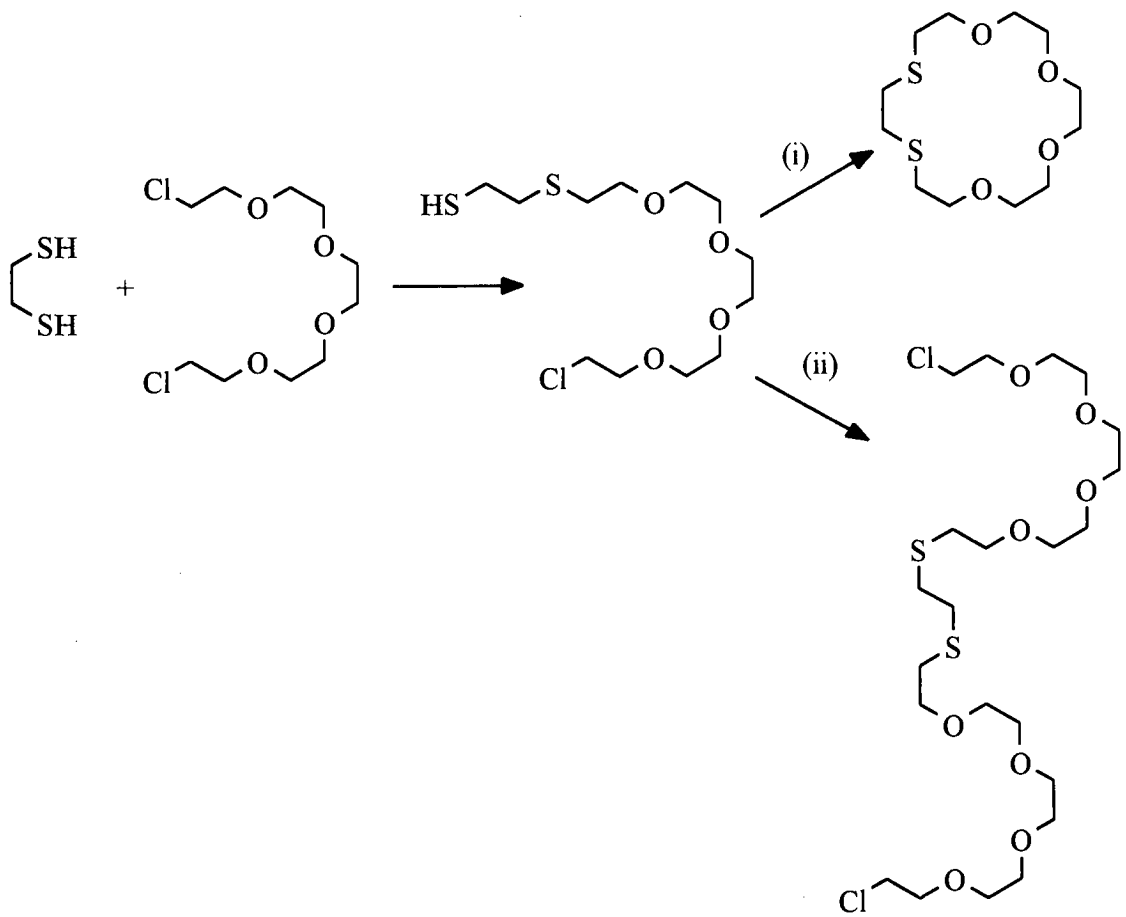

Figure 2.1.1c Reaction pathways in case of (i) high dilution and (ii) low dilution.

The basic principle behind high dilution syntheses is statistical in nature. The initial reaction is a co-condensation of two different molecules (**Figure 2.1.1c**) to yield the precursor for the subsequent cyclisation or polymerisation reaction. The probability of this precursor to undergo cyclisation with itself or polymerisation with a second precursor molecule is very much dependent on the concentration. It is obvious, that high concentration (low dilution) [**Figure 2.1.1c(ii)**] favours polymerisation whereas in contrast low concentration (high dilution) [**Figure 2.1.1c(i)**] favours cyclisation. Early accounts on high dilution techniques are given by Ruggli in 1911[244] and Dann in 1962[245]. Disadvantages of high dilution syntheses are the in general low yields, large amounts of solvents used and prolonged reaction times.

(ii) Template synthesis

The template, usually a metal ion, is thought to hold the reacting fragments in place until the cyclisation is complete. Good examples for confirmed template reactions are for instance the syntheses of [9]aneS_3 (see above), the aza-crown syntheses reported by Curtis (See Chapter I) or the synthesis of catenands. A catena compound consists of two macrocycles intersecting each other with no covalent bond between them. Sauvage and co-workers[246] have reported the synthesis of catenands based around tetrahedral Cu(I) template ions. The importance of alkaline metal ions in the synthesis of crown-ethers has been investigated[247,248]. The strong affinity of crown-ethers for alkaline metal ions strongly suggested that some sort of template effect plays a part in the cyclisation reaction. It should be noted that even though the template enhances the reaction kinetics and shows a high stereoselectivity with regard to the products it is generally not a catalyst in the classical definition. Template ions are usually present in high concentration sometimes exceeding the concentration of the reactants. Additionally the ions do not leave the cavity of the newly formed macrocyclic ligand due to the kinetic effects discussed earlier and have to be often chemically or electrochemically removed.

(iii) Cs_2CO_3 mediated cyclisation in DMF

Thioethers do not show a tendency to co-ordinate to alkaline metal ions and the significance of Cs^+ as a template in these syntheses is rather questionable. There are other hypotheses[249] which try to explain the significant increase in yield of these reactions compared with standard high dilution techniques employing NaOH or KOH.

Even though the cyclisation is usually the yield determining step in a macrocyclic synthesis, the choice of the reactants is quite important. **Figure 2.1.1d** shows some combinations of reactants which would all lead to [18]aneS_2O_4. The decision which combination to use has to be guided by economical considerations, commercial or synthetic availability and hazards involved.

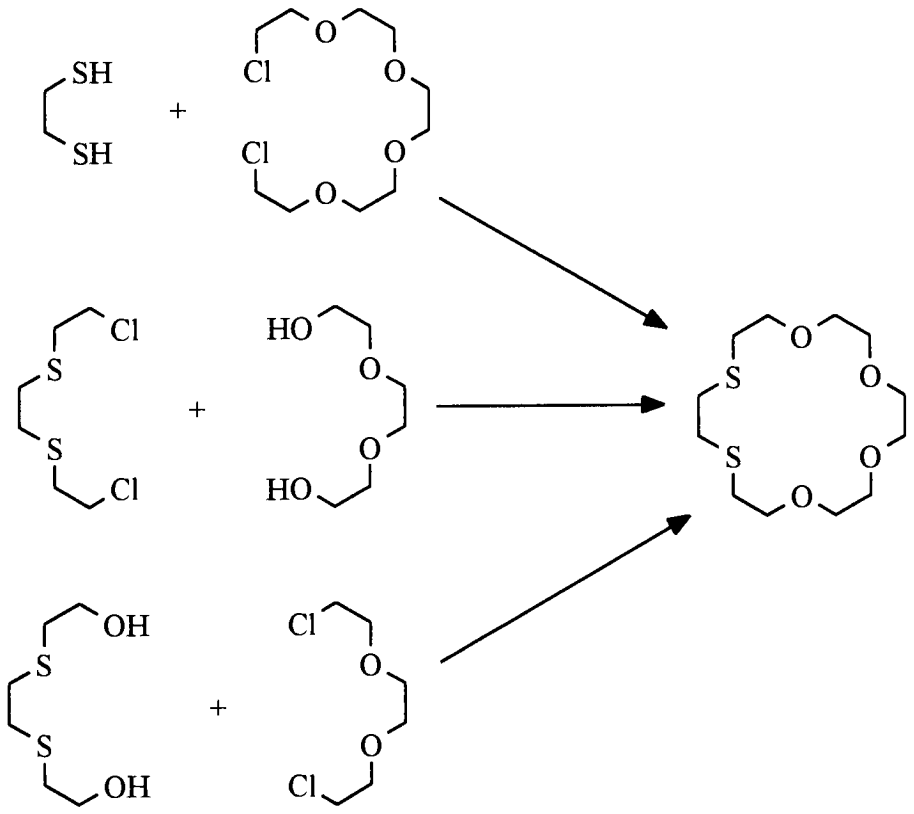

Figure 2.1.1d Combinations of different reactants leading to [18]aneS_2O_4.

In particular the last point has been of some importance with respect to the work presented. Thioether halides are derivatives of first generation chemical warfare agents such as 'S-Lost' (**Figure 2.1.1e**).

S-Lost N-Lost

Figure 2.1.1e First generation chemical warfare agents 'S-Lost' or mustard gas and 'N-Lost'.

Two recent articles dealing in particular with chemical warfare[250,251] mention skin (blistering) and respiratory effects, temporarily blindness, cytotoxic and mutagenic effects by mustard gas. There is also the possibility of life threatening allergic reactions to the substances. Even though handling of these compounds in a modern chemical laboratory should not be a problem, the potentially severe physiological effects of the substances which could be liberated in an accident or while cleaning glassware has lead to the decision not to isolate or use any thioether compounds containing good leaving groups such as halides or tosylates in ligand syntheses during the course of this work.

2.1.2 The Synthesis of Mixed O/S-Donor Ionophores

Numerous reports have been published dealing with synthetic procedures for mixed O/S-donor macrocycles[214-218,220,242,243,245,252-255]. The most convenient and least hazardous (see above) way to prepare mixed O/S-donor ionophores consists of the co-condensation of a dithiol derivative with a bis-halogenated glycol under alkaline high dilution conditions **[Figure 2.1.1c(i)]**. **Table 2.1.2** gives an overview over some of the compounds reported.

Compound		Yield / %	m.p./°C	Reference
[9]aneS$_2$O		6	liquid	214
[9]aneSO$_2$		5	liquid	214
[12]aneS$_3$O		26	89-90	214
1,4[12]aneS$_2$O$_2$		19	20-24	214
1,7[12]aneS$_2$O$_2$		12	liquid	214, 245
[12]aneSO$_3$		14	liquid	214, 245
[15]aneS$_4$O		13	93-95	215
		85	40-42	220
1,4,7[15]aneS$_3$O$_2$		41	43-44	215
1,4,10[15]aneS$_3$O$_2$		5	liquid	215
1,4[15]aneS$_2$O$_3$	†	20	51-52	214
1,7[15]aneS$_2$O$_3$		27	liquid	214
[15]aneSO$_4$		29	liquid	214
1,4,10,13[18]aneS$_4$O$_2$	††	1.7	125	252
		7.3	50	253
1,4,7,10[18]aneS$_2$O$_4$		85	34-36	220
1,4,7[18]aneS$_3$O$_3$	†	11	liquid	215
1,4[18]aneS$_2$O$_4$	†	28	54-56	214, 245
1,7[18]aneS$_2$O$_4$		11	liquid	215
		85	liquid	220
1,10[18]aneS$_2$O$_4$		12	90-91	215
[18]aneSO$_5$		36	liquid	215
1,4,7,10[21]aneS$_4$O$_3$		82	liquid	220
1,4,7[21]aneS$_3$O$_4$	†	11	liquid	215
1,4[21]aneS$_2$O$_5$	†	10	liquid	217
1,7[21]aneS$_2$O$_5$		25	liquid	215
1,4,10,13,19,22[27]aneS$_6$O$_3$		21	123	253

† Compounds used in this work

†† The melting point suggests that he compound is in fact the 1+3 co-condensation product 1,4,10,13,19,22[27]aneS$_6$O$_3$ which has been reported by Black[253].

Table 2.1.2 A selection of reported syntheses for mixed O/S-donor ionophores.

2.1.3 Structural Studies on Macrocyclic Ligands

[9]aneS$_3$, [12]aneS$_4$, [14]aneS$_4$, [16]aneS$_4$, [15]aneS$_5$, [18]aneS$_6$, [15]aneS$_2$O$_3$, 1,10[18]aneS$_2$O$_4$ and [18]aneS$_2$O$_4$ have been studied employing single crystal X-ray diffraction techniques. The aim in determining the structure of a macrocyclic ligand is to understand the processes involved upon co-ordination to a guest molecule (metal ions and neutral molecules). It has already been mentioned that a ligand which does not undergo major conformational changes upon complexation is termed 'pre-organised'.

The drawback of crystallographic studies is that the compounds are studied in the solid state. Complexation reactions on the other hand are in general conducted in a solvent and it is therefore problematic and dangerous to interpolate results obtained from the solid state. Solid state studies have therefore been complemented by electron diffraction studies (see section **2.1.4**) and molecular mechanics calculations (see section **2.1.5**).

Compound	**Conformation**	**Reference**
[9]aneS_3	[333]	256
[12]aneS_4	[3333]	257,258
[14]aneS_4	[3434]	259
[16]aneS_4	[3535]	260
[15]aneS_5	[332133]	257
[18]aneS_6	[1113311133]	257,261,262
[15]aneS_2O_3	[13443]	263, this work
[18]aneS_2O_4	[1111133133]	263, this work

Table 2.1.3 Macrocyclic ligands studied by single crystal X-ray diffraction (For a definition of '[]' nomenclature see ref.264 or section **2.2**).

Table 2.1.3 lists the compounds within the scope of this thesis which have been studied by X-ray diffraction in the solid state. The conformation adopted by [9]aneS_3 in the crystal lattice is [333] in Dale's nomenclature[264] with the S-atoms *endo*-dentate. [9]aneS_3 has been known to adopt a *facial* binding mode in octahedral complexes. The ligand in the [333] conformation can therefore be described pre-organised for facial octahedral co-ordination.
All the other homoleptic thioether macrocycles [12]aneS_4, [14]aneS_4, [16]aneS_4, [15]aneS_5 and [18]aneS_6 adopt conformations with the S-atoms, in general, *exo*-dentate (**Figure 2.1.3**). They can not be termed pre-organised for in cavity co-ordination because they have to undergo conformational changes in order to co-ordinate to square-planar or octahedral metal ions.

(i) [9]aneS_3

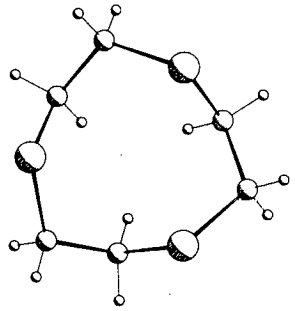

(ii) [12]aneS_4

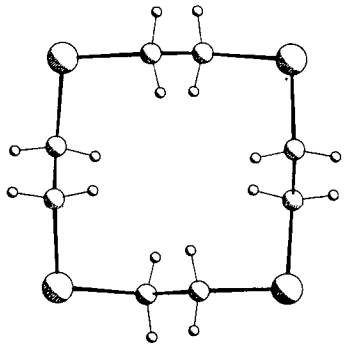

(iii) α-[14]aneS_4

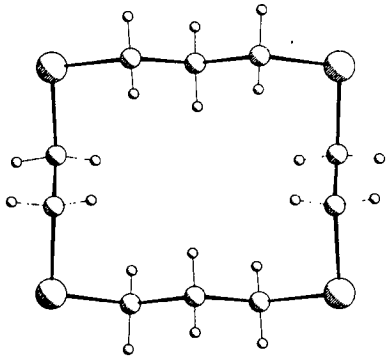

(iv) β-[14]aneS_4

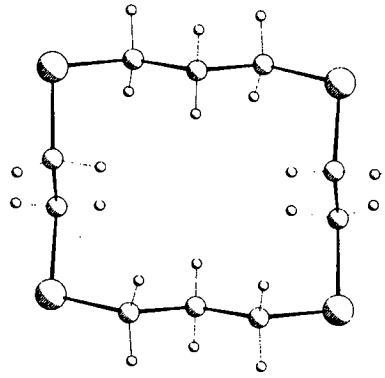

Figure 2.1.3 The solid state structures of (i) [9]aneS_3, (ii) [12]aneS_4, (iii) α-[14]aneS_4 and (iv) β-[14]aneS_4.

It is not uncommon for S-atoms in an C-S-C arrangement to adopt angles smaller than the ideal tetrahedral angle of 109°. The single crystal X-ray structure of [9]aneS_3[256] [**Figure 2.1.3** (i)] illustrates this (C-S-C = 102.8°, C-C-S = 113.0 and 117.0°). These findings have important implications in the refinement of other structures especially in cases where it is necessary to restrain angles in order to model disorder.

2.1.4 Electron Diffraction Studies on Macrocyclic Ligands

The conformation of a vapourised compound does not experience any strain in contrast to solid state studies, where packing forces influence the conformation. A vapourised ligand on the other hand does not present itself as a suitable model for the situation in solution. Gas phase electron diffraction studies combined with molecular mechanics calculations (see section **2.1.5**) are nevertheless a good way to determine the conformation adopted by the macrocycle in the absence of any foreign interaction.

Electron diffraction studies on [9]aneS_3 in the gas phase had been carried out in order to establish whether the ligand adopts a different conformation compared with the solid state[265]. Four models of different symmetry (D_3, C_3, C_2 and C_1) (**Figure 2.1.4**) were fitted to the experimental data. The model which corresponded most closely to the data was not the [333] conformation which was found in the solid state but the C_1 [12222] model.

(i) D_3 model

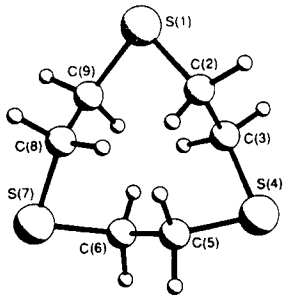

(ii) C_3 model

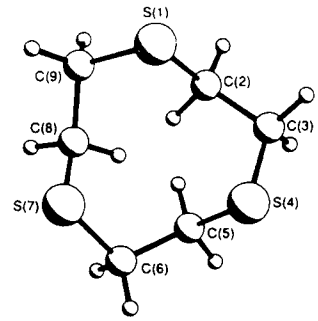

(iii) C_2 model

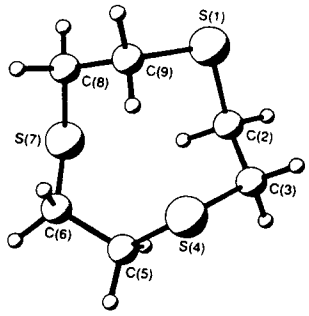

(iv) C_1 model

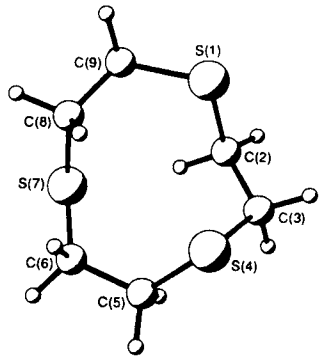

Figure 2.1.4 Models of [9]aneS_3 used in electron diffraction studies.

These results illustrate, how the conformation of a macrocyclic ligand is influenced in the crystal lattice. Even though these results are quite interesting, they do not quantify the extent of the difference in energy. Only the combination of electron diffraction techniques with molecular mechanics can provide quantitative results.

2.1.5 Molecular Mechanics Studies on Macrocyclic Ligands

The structural investigation of [9]aneS$_3$ employing gas phase electron diffraction was joined by molecular mechanics calculations. This was necessary because a range of three-dimensional structures might fit the one-dimensional electron diffraction data[265]. Calculations were carried out on all four models and the best fit model C_3 in the electron diffraction experiment turned out to exhibit also the lowest strain energy. The authors point out that, even though strain energies do not differ very much all conformers are separated by considerable high barriers.

Recent force field studies by Drew and co-workers[266] employing three different search algorithms (Molecular Dynamics, Grid Scan and Random Search) show 13 different conformations of [9]aneS$_3$ within an energy range of 4.53 to 8.52 kcal mol^{-1}. It was found that a [333] conformer compatible with the one present in the solid state has the lowest energy. The one obtained by electron diffraction studies slightly higher in energy (0.31 kcal mol^{-1}). The work presented by the authors focuses in particular on metal complexes with [9]aneS$_3$ and the conformation adopted by the ligand in these complexes. It turned out that the lowest energy conformer is also present in a range of octahedral complexes underlining its pre-organisation for *facial* octahedral co-ordination.

Molecular mechanics calculations have also been conducted on [16]aneS$_4$ in order to investigate the flexibility of the ligand and whether or not a [3535] conformation shows a minimum in strain energy[260,267]. The calculations were conducted on [16]aneS$_4$ and its cyclic hydrocarbon analogue $C_{16}H_{32}$. The [4444] conformer of $C_{16}H_{32}$ and [16]aneS$_4$ with all S-atoms occupying corner positions is according to the calculation the lowest strain energy conformer. However the [3535] conformer of [16]aneS$_4$, which has been found in the solid state is significantly lower in energy compared with $C_{16}H_{32}$ and only 0.7 kcal mol^{-1} higher compared with the [4444] conformer. The authors conclude that energy differences are in general small and suggest that a range of conformers are likely to exist at room temperature. It has also been pointed out that calculated data for $C_{16}H_{32}$ show a discrepancy compared with experimental data.

These few examples show that molecular mechanics calculations combined with other structural studies can enhance the understanding of particular structural features. Concern on the other hand has been expressed by both research groups[265,266] that results obtained using molecular mechanics force field calculations have to be used and interpreted with caution.

2.2 RESULTS AND DISCUSSION

2.2.1 Preparation of Starting Materials

Most starting materials used were commercially available or could be prepared in single step reactions (halogenations). Our initial work focused therefore on optimising these reactions and preparing the mixed O/S-donor ionophore [18]aneS_2O_4. The co-ordinative properties of this ligand described in the next four chapters however triggered our interest to synthesise ligands for which starting materials are not readily available. We were in particular interested to replace the soft thioether binding site in [18]aneS_2O_4 by a flexible tridentate thioether binding site.

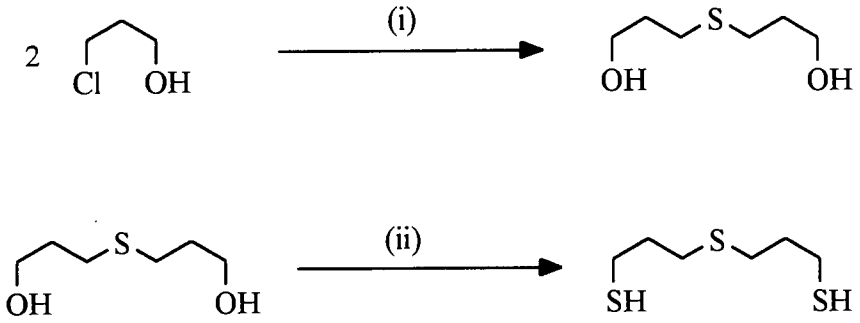

(i) $Na_2S/^nBuOH/\Delta$

(ii) a) conc.$HCl/(NH_2)_2CS/\Delta$, b) $KOH/H_2O/\Delta$, c) HCl/H_2O

Figure 2.2.1a The synthesis of 3-mercaptopropyl sulphide via 3,3'-thiodipropanol.

The reaction of 2 molar equivalents of 2-chloroethanol with 1 molar equivalent of Na_2S in ^nBuOH yielded 3,3'-thiodipropanol in good yield [**Figure 2.2.1a** (i)] The EI mass spectrum shows a basepeak at m/z = 150 which was assigned to the molecular ion $(C_6H_{14}O_2S)^+$. The ^{1}H-NMR spectrum shows four distinct regions. A quintet at 1.41 ppm was assigned to the methylene group in the propylene bridge between the thioether S-atom and the hydroxy-group. ^{1}H resonances at 2.22 ppm (t) and 3.2 - 3.3 ppm lie in sensible regions for thioether- and hydroxy-groups. A broad peak at 3.99 ppm was assigned to the two terminal alcohol functions.

The crude product which was still affected by some impurities such as H_2O was used in the subsequent conversion into a dithiol [**Figure 2.2.1a** (ii)] The conversion was carried out using thiourea in a strong acidic medium (conc. HCl) following the method reported by Buter and Kellogg[268]. The product 3-mercaptopropyl sulphide was obtained as a slightly yellow unpleasantly smelling oil in good yield (64%). The microanalysis is in contrast to the precursor satisfactory and shows good agreement with the stoichiometry $C_6H_{14}S_3$. The ^{1}H-NMR spectrum shows three ^{1}H-resonances assigned to $CH_2S\boldsymbol{H}$ [1.32 ppm (t)] $CH_2C\boldsymbol{H}_2CH_2$ [1.6 - 1.9 ppm (quintet)] and $C\boldsymbol{H}_2S$ [2.5 - 2.7 ppm (multiplet)]. In particular the second methylene group in the propylene bridge is of much interest in macrocyclic ligands. We anticipate that this region might be a useful indicator for the binding mode of the macrocyclic ligand to a metal ion. Co-ordination of a metal-ion via two S-donors in 1,5 position would lead to a six membered ring which is less flexible compared with the non co-ordinated macrocycle thus giving sharper lines and allowing for the deduction of coupling constants (high field spectrometer) used for qualitative conformational analysis.

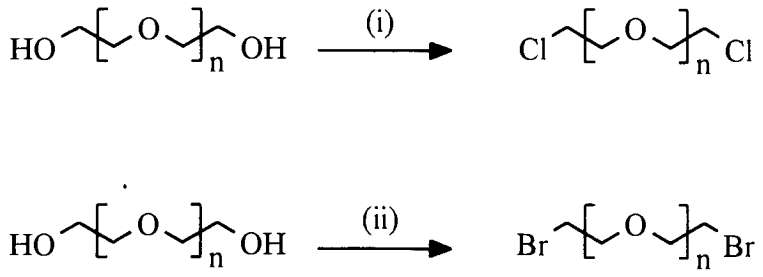

(i) Method 1: a) $SOCl_2/py/C_6H_6/\Delta$, b) $NaHCO_3/H_2O$, c)C_6H_6
Method 2: a) $SOCl_2/py/\Delta$, b) $NaHCO_3/H_2O$, c) Et_2O

(ii) a) PBr_3/py, b) $NaHCO_3/H_2O$, c)CH_2Cl_2

Figure 2.2.1b The halogenation of oligoethylene glycols (n = 3, 4) using $SOCl_2$ and PBr_3.

Halogenation of oligo ethylene glycols was achieved using $SOCl_2$ and PBr_3 as halogenation agents. Oligo ethylene glycols were chlorinated in good yield (~80%) using two methods. The first method [**Figure 2.2.1b** (i)]consisted of the addition of $SOCl_2$ to a hot mixture of the glycol and a small amount of pyridine in benzene. The reaction however did not proceed without difficulties. Solid precipitates which inhibited magnetic stirring and the formation of foam lead to a modified synthesis without any solvent. This step was also taken to decrease the obvious health risks of using benzene as a solvent. Method 2 [**Figure 2.2.1b** (i)] consisted of the slow addition of $SOCl_2$ to the reaction mixture of glycol and pyridine at slightly elevated temperature. This was followed by heating over night and isolation of the product (see experimental section for details). The products of either method were of high purity which could not be further improved for instance by distillation. The purification process could easily be monitored using IR spectroscopy (e.g. absence of OH stretching vibrations). ^{1}H-NMR spectroscopy proved to be unsuitable for assessing purity due to similar ^{1}H chemical shifts of ether- and chloride-functional groups. The EI mass spectrum showed a rich fragmentation pattern but the molecular ion was never observed.

Bromination of oligo ethylene glycols was achieved using PBr_3 [**Figure 2.2.1b** (ii)]. A typical synthesis consisted of the slow addition of PBr_3 to an ice-cold mixture of the glycol and a catalytic amount of pyridine. The reaction mixture which was left in an ice-bath was then allowed to heat up over night to ambient temperature and the product was isolated (see experimental section for details). The yield of this reaction (~50%) is smaller compared with the chlorination reactions. Br^- on the other hand is a better leaving group compared to Cl^- and there is some uncertainty whether the use of brominated oligo ethylene glycols will give larger yields in subsequent macrocyclic syntheses thus rendering this approach economically viable. A practical disadvantage of the bromination reaction is failure of the reaction to start. This happened a couple of times and resulted in a violent exothermic reaction during the isolation procedure and the loss of precious precursors. It seems however that this problem could be overcome by experience.

2.2.2 The Single Crystal Structure of [15]aneS_2O_3

[15]aneS_2O_3 was prepared and characterised prior to this work by Reid[224] according to the method described by Bradshaw and co-workers[214]. Recrystallisation of the slightly yellow waxy material was achieved employing a two phase low temperature diffusion technique. [15]aneS_2O_3 was dissolved in EtOAc and a layer of hexane was added carefully. This arrangement was then placed in a freezer at -25°C. Colourless crystals suitable for X-ray diffraction studies appeared within a week and were collected and dried. This particular method of recrystallisation has been proven to be superior to any other technique (solvent extraction, chromatography, distillation) in the process of purification of dithia mixed O/S donor ionophores.

Single Crystal X-ray diffraction studies of [15]aneS_2O_3 were initiated in order to improve an earlier structure determination[263]. A comparison of bond lengths, angles and torsion angles between this and the reported structure shows only small deviations (**Table 2.2.2**). The e.s.d.s on these values however have been improved by a factor of up to 4 (**Table 2.2.2**). The single crystal structure of [15]aneS_2O_3 (**Figures 2.2.2a** and **2.2.2b**) shows the two S-atoms *exo*-dentate and separated by at least 4.5 Å (the sum of the van der Waals radii for S is 3.6 Å[269]). The torsion angle of the -SCH_2CH_2S- moiety adopts an *anti* angle [166.8(3)°]. Transition metal complexes with this ligand show exo bidentate co-ordination with a torsion angle of the -SCH_2CH_2S- moiety close to 60° [223,224] suggesting a high conformational flexibility of the macrocyclic framework.

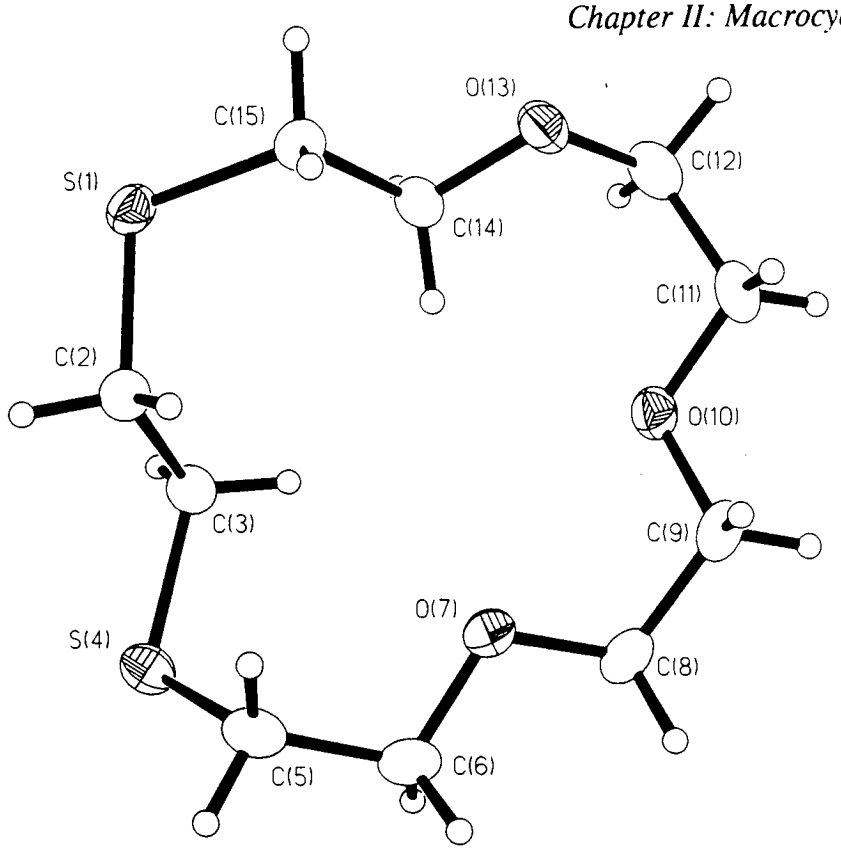

Figure 2.2.2a Single crystal Structure of [15]aneS_2O_3.

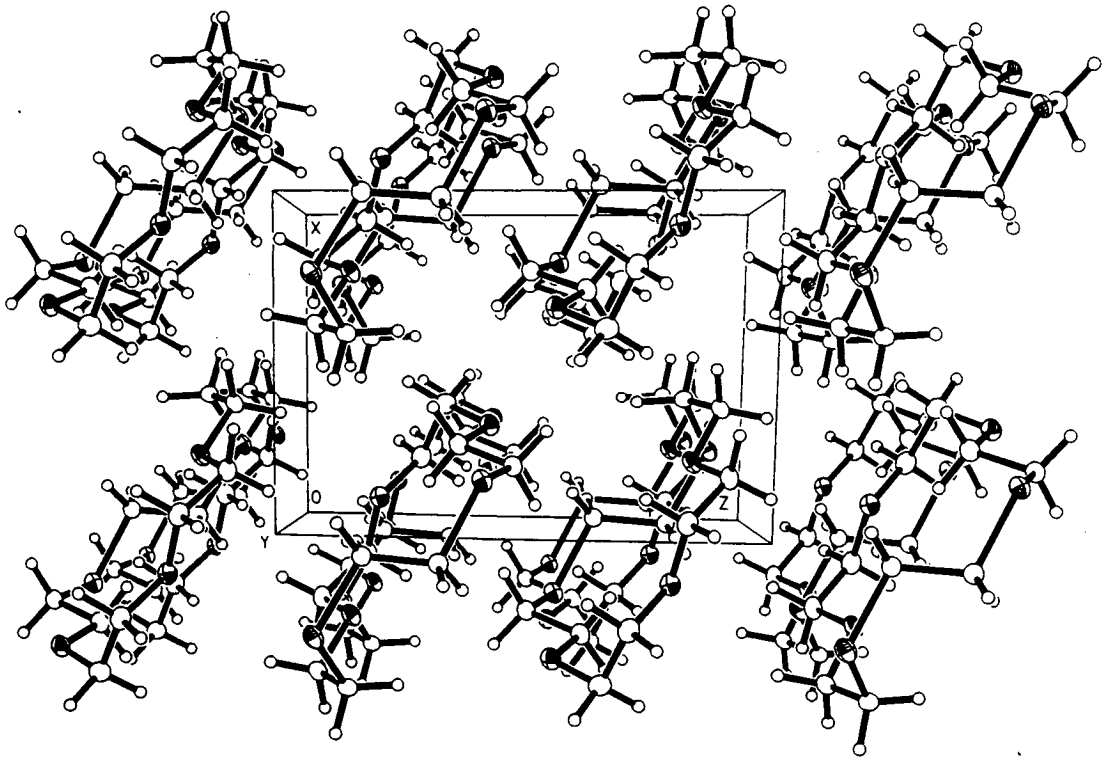

Figure 2.2.2b Packing diagram of [15]aneS_2O_3.

	this work	taken from ref. 263
S(1)-C(2)	1.814(2)	1.810(5)
C(2)-C(3)	1.520(2)	1.507(7)
C(3)-S(4)	1.810(2)	1.802(5)
S(4)-C(5)	1.813(2)	1.798(5)
C(5)-C(6)	1.502(2)	1.504(7)
C(6)-O(7)	1.421(2)	1.417(5)
O(7)-C(8)	1.422(2)	1.427(7)
C(8)-C(9)	1.496(2)	1.489(9)
C(9)-O(10)	1.420(2)	1.405(5)
O(10)-C(11)	1.420(2)	1.427(7)
C(11)-C(12)	1.501(2)	1.500(7)
C(12)-O(13)	1.426(2)	1.426(7)
O(13)-C(14)	1.428(2)	1.416(6)
C(14)-C(15)	1.507(2)	1.514(9)
C(15)-S(1)	1.806(2)	1.801(6)
S(1)-C(2)-C(3)	113.88(11)	112.8(3)
C(2)-C(3)-S(4)	112.49(11)	114.3(3)
C(3)-S(4)-C(5)	103.27(8)	103.1(2)
S(4)-C(5)-C(6)	115.90(11)	113.3(3)
C(5)-C(6)-O(7)	109.86(12)	108.1(4)
C(6)-O(7)-C(8)	111.61(11)	113.3(4)
O(7)-C(8)-C(9)	109.95(12)	113.2(4)
C(8)-C(9)-O(10)	110.00(12)	111.2(4)
C(9)-O(10)-C(11)	111.40(11)	112.3(4)
O(10)-C(11)-C(12)	110.00(13)	109.2(4)
C(11)-C(12)-O(13)	113.14(13)	109.9(5)
C(12)-O(13)-C(14)	113.24(12)	111.8(4)
O(13)-C(14)-C(15)	107.77(12)	109.3(5)
C(14)-C(15)-S(1)	113.12(10)	114.8(4)
C(15)-S(1)-C(2)	102.97(7)	103.2(2)
S(1)-C(2)-C(3)-S(4)	-165.93(8)	-166.8(3)
C(2)-C(3)-S(4)-C(5)	-72.70(12)	-73.2(4)
C(3)-S(4)-C(5)-C(6)	-80.60(13)	-81.9(4)
S(4)-C(5)-C(6)-O(7)	83.07(14)	85.7(5)
C(5)-C(6)-O(7)-C(8)	-175.80(12)	-176.2(4)
C(6)-O(7)-C(8)-C(9)	-165.27(12)	-166.0(5)
O(7)-C(8)-C(9)-O(10)	-58.7(2)	-58.8(6)
C(8)-C(9)-O(10)-C(11)	179.41(12)	-179.9(4)
C(9)-O(10)-C(11)-C(12)	-168.57(12)	-169.3(4)
O(10)-C(11)-C(12)-O(13)	69.1(2)	68.3(6)
C(11)-C(12)-O(13)-C(14)	-87.7(2)	-88.6(5)
C(12)-O(13)-C(14)-C(15)	-179.44(12)	179.5(4)
O(13)-C(14)-C(15)-S(1)	169.94(10)	170.7(3)
C(14)-C(15)-S(1)-C(2)	75.58(12)	77.0(4)
C(15)-S(1)-C(2)-C(3)	-90.14(12)	-89.3(4)

Table 2.2.2 Selected bond lengths(Å), angles(°) and torsion angles (°) with estimated standard deviations for [15]aneS_2O_3.

2.2.3 The Synthesis of [18]aneS_2O_4

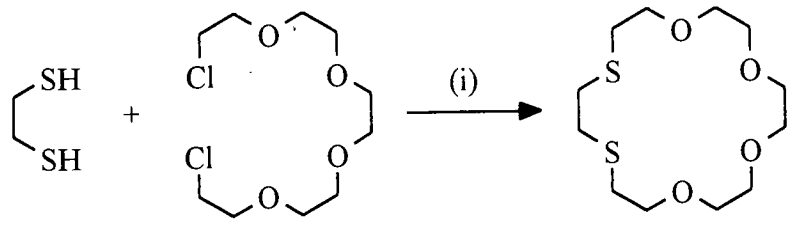

(i) a) EtOH/EtONa/NaOH/Δ, b) HCl/H_2O, c)CH_2Cl_2

Figure 2.2.3a Reaction scheme for the preparation of [18]aneS_2O_4.

[18]aneS_2O_4 was prepared initially according to the method reported by Bradshaw[214] (**Figure 2.2.3a**). The reaction of 1,2-ethanedithiol and dichloro pentaethylene glycol under high dilution conditions afforded [18]aneS_2O_4 in 30% yield (Lit.: 29%). Certain experimental difficulties triggered our interest to improve this synthesis. Both reactants were initially added from two dropping funnels, which caused difficulties in maintaining the addition of equimolar amounts of reactants. The improvised procedure uses only one dropping funnel and both reactants are mixed at ambient temperature in EtOH. Solubility problems were overcome with the addition of a small amount (~10ml) of DMF. This dilute mixture was then added dropwise to the heated and stirred reaction mixture. In contrast to the original procedure which uses pre-dried EtOH we used commercially available glass distilled EtOH (96%). A stoichiometric amount of Na-metal which allows for the water present was added affording a clear solution. This contrasts the heterogeneous reaction mixture of the original procedure where solid NaOH was added to the EtOH. The advantage of this improved synthesis include less time consuming preparations (drying and distillation of EtOH) and the possibility to monitor the progress of the reaction without interference of a solid reactant (NaOH). Isolation of the product follows the original procedure and consists of neutralisation of excess base with HCl, filtration, removal of the solvent under reduced pressure, extraction of the NaCl slurry with CH_2Cl_2, washing with water, drying over anhydrous $MgSO_4$ and evaporation of the CH_2Cl_2. Crystallisation of the initial oily residue was achieved using the low temperature two phase diffusion technique mentioned under **2.2.2**.

The well resolved ^{1}H-NMR spectrum (**Figure 2.2.3b**) is in excellent agreement with the proposed structure. The two triplets at 2.69 ppm and 3.68 ppm

have been assigned to the $-SCH_2CH_2O-$ moiety in the macrocycle. Both show identical *vicinal* coupling constants (^3J = 6.15Hz - assuming the spectrum is first order). Other ^1H resonances include the $-SCH_2CH_2S-$ (s, 4H, 2.85ppm), $-OCH_2CH_2O-$ (s, 8H, 3.61ppm) and another $-OCH_2CH_2O-$ (s, 4H, 3.63ppm) moiety. The ^{13}C-DEPT-NMR spectrum shows six ^{13}C-resonances assigned two $-SCH_2-$ and four $-OCH_2-$ moieties. The presence of only six ^{13}C-resonances for a macrocycle containing 12 C-atoms strongly suggests that the species (one *meso* form or two enantiomeres) in solution adopts a two fold symmetry similar to the solid state structure (see below). Microanalytical and IR spectroscopic results are in good agreement with these findings. A peak at m/z = 296 assigned to $(C_{12}H_{24}S_2O_4)^+$ has been found in the EI mass spectrum.

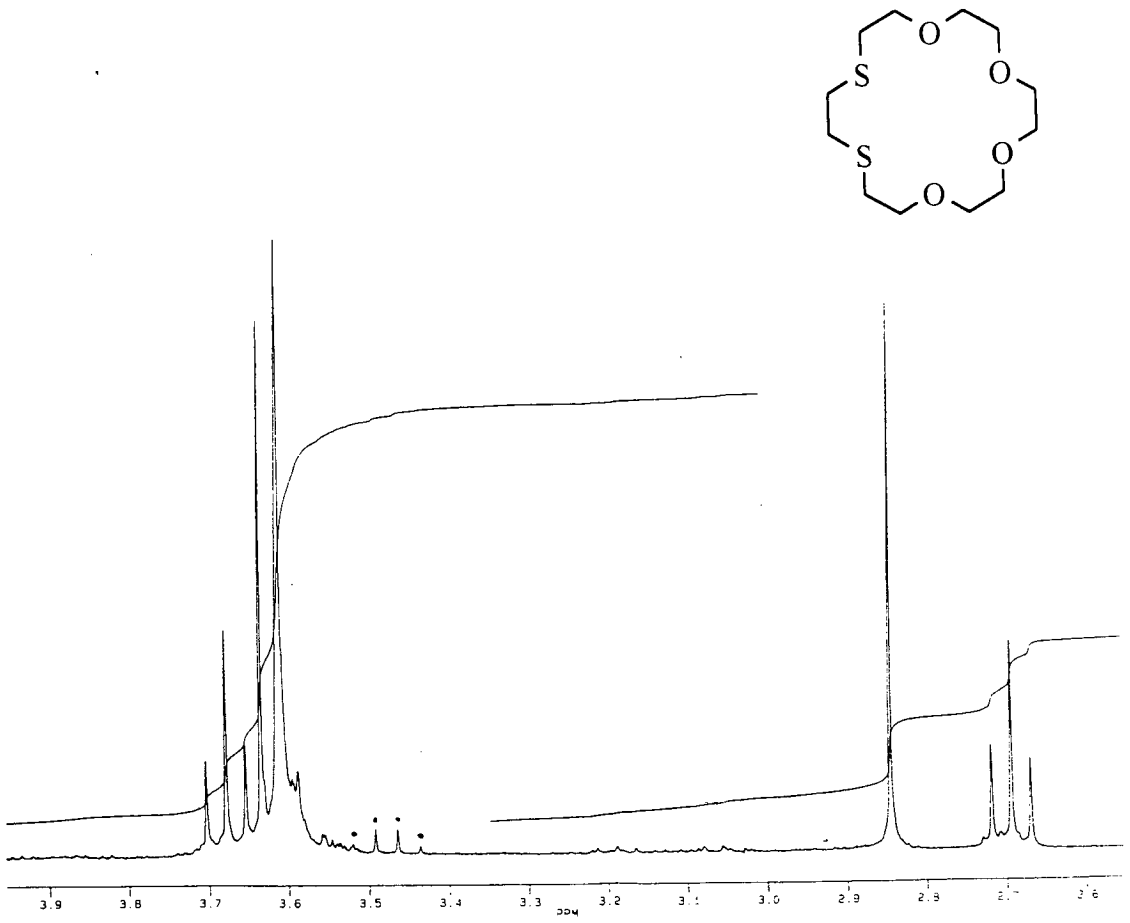

Figure 2.2.3b ^1H-NMR spectrum of [18]aneS_2O_4.

2.2.4 The Single Crystal Structure of [18]aneS_2O_4

Single crystal X-ray diffraction studies on [18]aneS_2O_4 were initiated in order to improve a structure determination reported by Christensen and co-workers[263]. A comparison between this work and the reported structure (**Table 2.2.4**) shows that the magnitude of bond distances, angles and torsion angles are very similar. There is, however, a significant improvement concerning the e.s.d.s at these values by a factor of 2 to 3.

	this work	taken from ref. 263
C(3)-C(3')	1.511 (3)	1.479 (7)
C(3)-S(4)	1.8018 (23)	1.797 (4)
S(4)-C(5)	1.807 (3)	1.772 (7)
C(5)-C(6)	1.492 (4)	1.527 (7)
C(6)-O(7)	1.413 (3)	1.411 (6)
O(7)-C(8)	1.412 (3)	1.421 (6)
C(8)-C(9)	1.485 (4)	1.483 (7)
C(9)-O(10)	1.416 (3)	1.416 (7)
O(10)-C(11)	1.422 (3)	1.419 (5)
C(11)-C(11')	1.484 (4)	1.468 (9)
C(3')-C(3)-S(4)	115.97 (16)	116.2 (4)
C(3)-S(4)-C(5)	104.02 (11)	104.1 (3)
S(4)-C(5)-C(6)	115.43 (18)	116.1 (5)
C(5)-C(6)-O(7)	108.65 (20)	107.0 (3)
C(6)-O(7)-C(8)	113.75 (18)	112.5 (3)
O(7)-C(8)-C(9)	108.74 (21)	108.1 (4)
C(8)-C(9)-O(10)	109.65 (22)	109.6 (6)
C(9)-O(10)-C(11)	111.97 (19)	112.7 (4)
O(10)-C(11)-C(11')	109.98 (21)	110.4 (5)
S(4)-C(3)-C(3')-S(4')	59.96 (21)	61.4 (5)
C(3')-C(3)-S(4)-C(5)	58.77 (19)	57.9 (4)
C(3)-S(4)-C(5)-C(6)	66.79 (21)	68.2 (4)
S(4)-C(5)-C(6)-O(7)	-76.84 (23)	-77.5 (6)
C(5)-C(6)-O(7)-C(8)	166.85 (20)	165.9 (5)
C(6)-O(7)-C(8)-C(9)	-173.73 (20)	-174.2 (6)
O(7)-C(8)-C(9)-O(10)	65.5 (3)	66.3 (7)
C(8)-C(9)-O(10)-C(11)	-179.18 (21)	-179.8 (7)
C(9)-O(10)-C(11)-C(11')	-178.68 (21)	-178.5 (4)
O(10) -C(11)-C(11')-O(10')	-77.8 (3)	-77.9 (6)

[Primed atoms are related to the non-primed atoms by the symmetry operation (-x, y, ½ - z)]

Table 2.2.4 Selected bond lengths (Å), angles (°) and torsion angles (°) with estimated standard deviations for [18]aneS_2O_4.

The single crystal structure of [18]aneS_2O_4 (**Figure 2.2.4a**) shows in sharp contrast to the structure of [15]aneS_2O_3 a *gauche* configuration at the -SCH_2CH_2S- moiety of the macrocycle [61.4(5)°]. Both S-atoms are in *exo*-positions and the O-atoms are *endo*-oriented towards the centre of the macrocyclic cavity. Macrocyclic co-ordination to a potential guest ion is however impossible without major conformational changes because the ethylene bridge between both S-atoms occupies part of the cavity. This ligand has therefore to be termed pre-organised for bidentate chelating co-ordination. Numerous examples of this particular mode of co-ordination have been found during this work with [18]aneS_2O_4. The packing diagram of [18]aneS_2O_4 (**Figure 2.2.4b**) shows no significant intermolecular interactions and no co-crystallisation molecules such as solvents have been found.

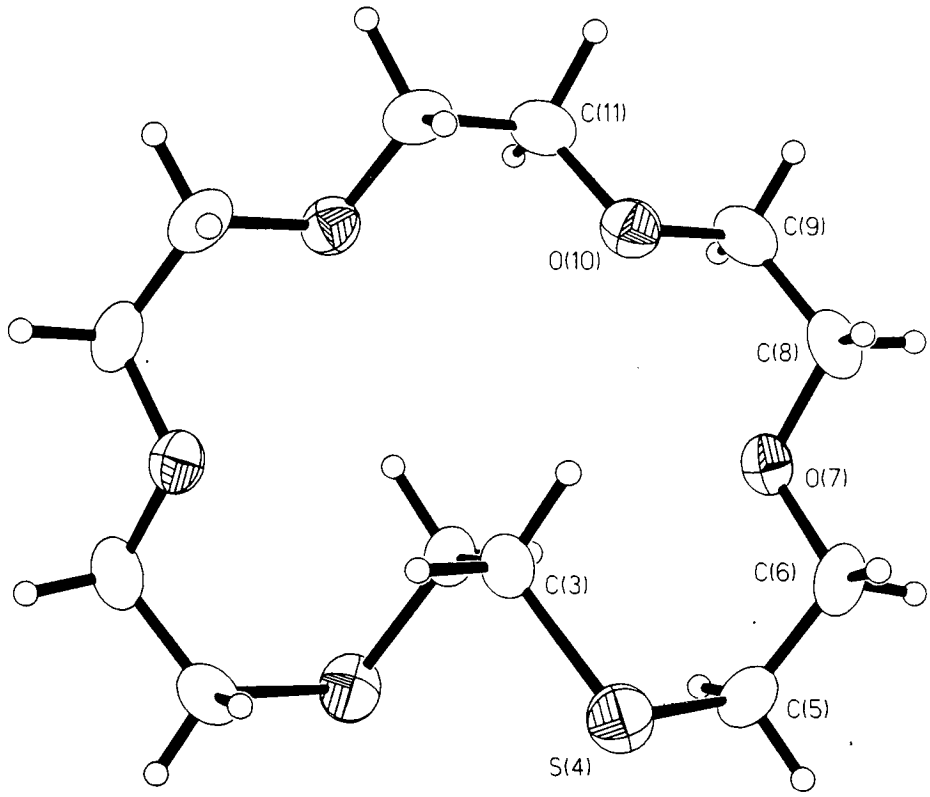

Figure 2.2.4a View of the single crystal structure of [18]aneS_2O_4.

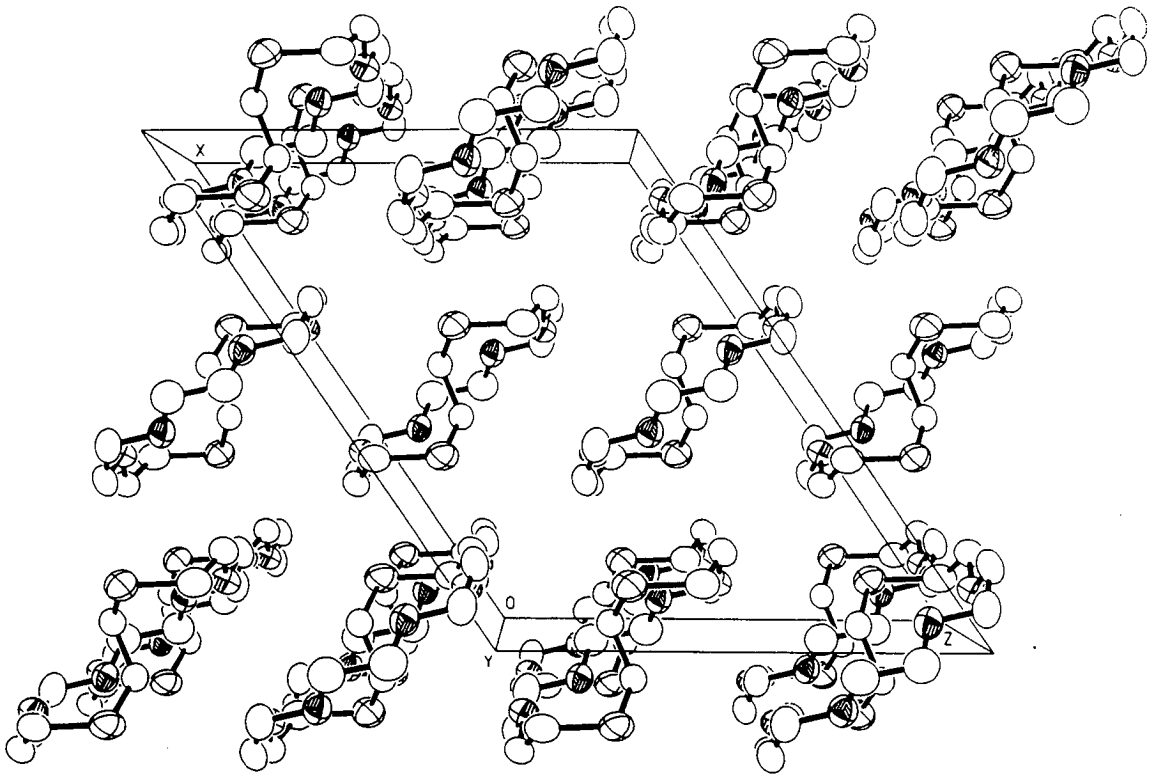

Figure 2.2.4b Packing diagram of [18]aneS_2O_4.

2.2.5 Molecular Mechanics Calculations on [18]aneS_2O_4

It has already been mentioned that one of the ways to describe the conformation of a macrocycle is provided by a scheme developed by Dale[264]. The advantages of this system are that it is widely accepted and easy to use. There are however some disadvantages which makes it rather questionable whether this nomenclature should be used for large macrocyclic ligands or not. The macrocyclic ligand [18]aneS_2O_4 has 18 bonds, 18 angles and 18 torsion angles which define precisely a particular geometry (H-atoms omitted). In order to describe a particular conformation, bond lengths and angles are usually discarded on the grounds that they are very similar in any conformation. However it is not convenient to deal with the remaining (in this particular example 18) torsion angles directly. The scheme devised by Dale is based on three basic rules and provides a convenient way to describe the shape of a particular conformation.

(i) A corner occurs at the junction of any two *gauche* bonds, irrespective of sign, where any torsion angle of $|\alpha| < 90°$ is considered *gauche*.

(ii) A corner exists at the junction of an isolated *gauche* bond and the adjacent bond with the smaller $|\alpha|$.

(iii) When an isolated *gauche* bond contains a two fold axis it has a corner on either side.

A major point of criticism concerns the ambiguity of a particular conformation. The [333] shape of [9]aneS_3 describes two alternative but mutually incompatible geometries (**Figure 2.2.5a**).

Figure 2.2.5a Illustration of the ambiguity of the [333] conformation for [9]aneS_3.

The situation becomes even worse in cases of mixed donor ionophores, mono- or bidentate co-ordination. One way to overcome this problem would be to indicate for instance in the present example that the S-atoms are *exo-* or *endo-*dentate. Another point of criticism is that this system does not allow comparison of parts of structures. It would be quite useful in extended non-trivial systems to compare for instance equivalent moieties independent from others (for instance the polyether chains in [15]aneS_2O_3, [18]aneS_2O_4 and [21]aneS_2O_5).

The major point of criticism however deals with the arbitrary definition of a *gauche-* and an *anti*-angle. The criticism does not focus directly on the value of such an angle, there are certainly reasons why it should be 120° in some or 90° in other cases. The point to mention is that in cases were a *gauche*-angle has *anti*-angles on either side, the corner is determined by the magnitude of the *anti*-angles [Rule (II)].

a) a0-a1-***a2***-a3-a4-a5

a0-a1-a2-a3 = -168°
a2-a3-a4-a5 = 174°

b) a0-a1-a2-***a3***-a4-a5

a0-a1-a2-a3 = 174°
a2-a3-a4-a5 = -168°

Figure 2.2.5b Illustration of the effect of an isolated *gauche* angle (a1-a2-a3-a4) on the overall shape of two nearly identical conformations (see for example section **7.2.12**).

Figure 2.2.5b shows a chain of atoms (a0 to a5) with a1-a2-a3-a4 adopting a *gauche* angle. In the first case (a) the cornering atom would be a2 and in the second case (b) a3. This example illustrates that there will be cases, where a negligible change in the conformation results in two different shapes of roughly the same energy. It also underlines that a change of 18° in the *gauche* region has no effect on the shape. However, a change from 58° to 40° might have severe implications with respect to 1,4-interactions and the energies involved. Using this scheme for large flexible macrocycles will lead to a wide range of different shapes with roughly the same energy and few shapes with a variety of energies. These considerations render this scheme rather useless in particular for the description of large macrocyclic ligands (which do not necessarily adopt a macrocyclic binding mode) such as [18]aneS_2O_4.

A slightly different scheme, which overcomes some of these problems simply lists whether a particular torsion angle is *anti* or *gauche*. The symbol for an *anti* angle is an 'a' and in case of a *gauche* angle the absolute sign of the torsion angle is written. It should be noted that this scheme and the scheme devised by Dale are mutually incompatible because the '+-a' scheme discards absolute values and Dale's scheme discards additionally signs. The results presented below illustrate the superiority of the '+-a' scheme over Dale's scheme (**Table 2.2.5d**)[270].

Molecular mechanics calculations on [18]aneS_2O_4 were initiated in order to confirm the conformational flexibility of the macrocyclic ligand, to analyse changes in the polyether and polythioether region with respect to the overall steric energy and to determine whether the single crystal conformation lies in a global minimum or not.

These calculations were undertaken using MINP[271] and MM3(92)[272] with default parameters. All minimisations were carried out using initial block diagonal followed by full matrix least squares energy minimisation. MINP was used to generate a generic model of [18]aneS_2O_4. The second model used in a conformational stochastic search was taken from the solid state structure of [18]aneS_2O_4 (**Figure 2.2.4a**). Both initial structures were minimised and used as starting points in three conformational stochastic searches (**Table 2.2.5a**).

Model	Pushes	Push width / Å	Conformers	Energy range / kcal mol^{-1}
Generic	50	1.5	48	24.0992 - 36.2687
Crystal	30	2.0	28	23.4998 - 39.5800
Crystal	5	0.5	1	23.4998

Table 2.2.5a Experimental parameters in molecular mechanics calculations.

These studies show, that [18]aneS_2O_4 is able to adopt a large number of different conformations in the limited energy range of 15 kcal mol^{-1}. These studies on the other hand do not give any evidence whether these conformations are populated under standard conditions or could be reached under standard reaction conditions. It is furthermore impossible at this stage to assign pathways for interconversion due to the vast amount of different conformers.

(i) $[RuCl(PPh_3)([18]aneS_2O_4)_2]^+$

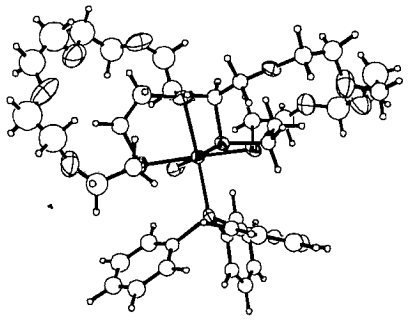

(ii) $[Ru([18]aneS_2O_4)_3]^{2+}$

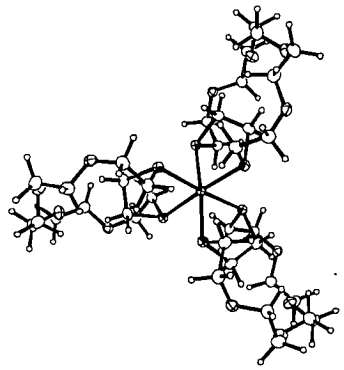

(iii) $[Ag_2([18]aneS_2O_4)_2]^{2+}$

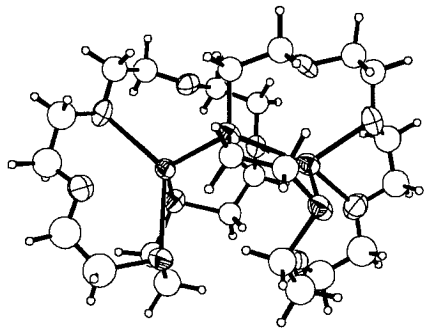

Figure 2.2.5c The single crystal structures of the three complexes which were used to generate input files for molecular mechanics calculations.

The second part of this investigation was therefore initiated in order to establish which major factors actually contribute to the overall steric energy of a conformation. A number of conformations obtained in the stochastic searches were therefore examined more closely. Additional conformations were obtained from three selected complexes. Two input files were taken from $[RuCl(PPh_3)([18]aneS_2O_4)_2]^+$ [RuL_2(1) and (2)] [**Figure 2.2.5c** (i)], $[Ag_2([18]aneS_2O_4)_2]^{2+}$ [Ag_2L_2(1) and (2)] [**Figure 2.2.5c** (ii)] and one from $[Ru([18]aneS_2O_4)_3]^{2+}$ (RuL_3) [**Figure 2.2.5c** (iii)]. Minimisation of the crystal structure based macrocycles lead to 5 different conformers Ag_2L_2(1) and Ag_2L_2(2) converged to the same conformation [**Table 2.2.5b** (7)]. The major contributors to the steric energy are the 1,4-van der Waals energy and the energy from the distortion of angles (Bending). However these contributions are virtually constant in the range from 23.5 to 30.0 kcal mol^{-1}. Only the high energy conformations [**Table 2.2.5b** (10) and (11)] show larger deviations. The dipole-dipole energies exhibit the largest fluctuations within the group of the three major contributors. However their fluctuation does not match the increase in steric energy. It has therefore to be concluded that the gradual increase in steric energy can not be attributed to a single contributor. The inter-relation between the geometric parameters defining a structure makes it impossible to assign a certain energy to a particular geometric feature. For instance the 1,4-van der Waals energy depends not only on the torsion angle but on the bond lengths and angles between the atoms involved.

The third part of this investigation focuses in particular on the difference between metal stripped macrocycles and their minimised conformations. **Table 2.2.5c** illustrates the conformational changes reflected by the torsion angles and the changes in energy upon minimisation. The most obvious feature in this comparison is the huge difference in the compression energy which is probably an artefact of the parameterisation in MM3. It reflects the difference between experimentally (X-ray crystallography) obtained data and idealised treatment by MM3. Bond energies in particular show a big energy response to small distortions of the bond length. The use of the compression energy in a conformational study is therefore not advisable. **Table 2.2.5c** contains therefore additional entries for energy differences between initial and final conformer in particular for 1,4-van der Waals and bending energies. The difference between overall steric energy with and without compression lies in the region 10 to 50 kcal mol^{-1} of which two thirds are roughly contributed by van der Waals interactions and bending.

Conformation	Crystal	(1)	(2)	(3)	(4)	(5)	(6)	(7a)	(7b)	(8)	(9)	(10)	(11)
Source	X-ray	X-ray	st.srch.	st.srch.	st.srch.	$RuL_2(1)$	$RuL_2(2)$	$AgL_2(1)$	$AgL_2(2)$	RuL_3	st.srch.	st.srch.	st.srch.
Compression	-	0.9121	0.9736	0.9670	0.9337	0.8973	1.0755	0.9881	0.9881	1.0890	0.9474	1.4958	1.2266
Bending	-	6.3873	5.8824	7.1832	5.7687	6.1149	6.1111	5.5135	5.5135	7.2626	7.2192	11.4872	14.2104
Bend-Bend	-	-0.0553	-0.0660	-0.0403	-0.0686	-0.0634	-0.0657	-0.0797	-0.0797	-0.0522	-0.0715	0.0738	0.0862
Stretch-Bend	-	0.2914	0.2994	0.3436	0.3334	0.3122	0.3498	0.3123	0.3123	0.4009	0.4043	0.6493	0.5952
Van der Waals energy													
1,4	-	14.4785	14.4005	13.9553	14.8288	14.5551	14.7741	15.0509	15.0509	14.0385	14.6626	14.1393	12.6924
other	-	-0.7985	-0.0299	0.6174	-0.1570	-0.4673	-0.8715	-1.6063	-1.6063	-0.3106	-0.3217	2.1052	2.2222
Torsional	-	-1.2686	-1.0104	-0.3584	-1.3795	-0.1264	2.6447	0.7504	0.7504	2.1577	0.8969	4.9507	5.4852
Torsion-Stretch	-	-0.0586	-0.1005	-0.1340	-0.0866	-0.0707	-0.2012	-0.1710	-0.1710	-0.1830	-0.0586	-0.4261	-0.2247
Dipole-Dipole	-	3.6115	3.7500	1.7527	4.3574	4.9074	3.9343	7.8023	7.8023	4.4626	7.8712	3.0127	3.2797
Steric energy	-	23.4998	24.0992	24.2865	24.5303	25.2490	27.7510	28.5605	28.5605	28.8655	31.5497	37.4880	39.5734
		0.0000	0.5994	0.7867	1.0305	1.7492	4.2512	5.0607	5.0607	5.3657	8.0499	13.9882	16.0736
Torsion angles / °													
C(18)-S(1)-C(2)-C(3)	58.77	61.8	-68.9	-59.3	59.0	63.3	-71.7	70.3	72.2	78.0	-56.8	65.3	60.4
S(1)-C(2)-C(3)-S(4)	59.96	63.4	175.6	-172.2	-176.5	67.2	-63.6	56.9	56.9	65.4	-47.4	86.0	76.3
C(2)-C(3)-S(4)-C(5)	58.77	61.8	-71.0	-72.4	-179.2	-171.0	-71.7	72.2	70.3	66.3	-61.8	62.4	81.2
C(3)-S(4)-C(5)-C(6)	66.79	64.0	-69.3	-75.5	-60.4	-68.0	-83.3	-171.3	-94.5	77.1	174.2	33.6	61.4
S(4)-C(5)-C(6)-O(7)	-76.84	-77.3	-64.4	-176.3	-49.2	77.7	67.8	66.9	-53.0	-68.3	-64.4	40.0	57.1
C(5)-C(6)-O(7)-C(8)	166.85	174.8	171.3	169.5	-173.8	-173.8	87.1	-170.4	-175.6	-80.4	174.2	168.4	-91.5
C(6)-O(7)-C(8)-C(9)	-173.73	-179.3	63.7	73.7	-175.0	-178.0	-178.9	83.3	-169.4	-180.0	-83.5	149.6	-106.8
O(7)-C(8)-C(9)-O(10)	65.5	69.9	-86.3	-84.9	80.8	-70.6	82.2	65.8	78.6	-71.2	-63.5	-95.7	72.7
C(8)-C(9)-O(10)-C(11)	-179.18	178.3	169.0	-172.6	-174.1	179.4	-167.5	-179.2	-178.8	178.2	-69.9	66.5	51.1
C(9)-O(10)-C(11)-C(12)	-178.68	176.2	179.3	-73.9	-175.8	-178.2	-169.4	173.3	-177.4	-177.2	-168.7	178.6	52.4
O(10)-C(11)-C(12)-O(13)	-77.8	-76.0	64.1	83.9	-66.3	67.5	-67.3	-73.8	-73.8	-73.6	-69.1	-79.5	-163.6
C(11)-C(12)-O(13)-C(14)	-178.68	176.2	-179.0	179.7	-177.8	70.9	-169.4	-177.4	173.3	-173.0	-75.8	-67.7	177.7
C(12)-O(13)-C(14)-C(15)	-179.18	178.3	166.8	75.7	-169.0	171.5	-167.5	-178.8	-179.2	-81.8	-175.7	-60.8	-165.0
O(13)-C(14)-C(15)-O(16)	65.5	69.9	-73.7	-83.3	85.1	69.8	82.2	78.6	65.8	-75.2	-70.7	96.4	71.5
C(14)-C(15)-O(16)-C(17)	-173.73	-179.3	164.6	169.5	-57.2	177.0	-178.9	-169.4	83.3	-171.0	-175.9	176.2	174.6
C(15)-O(16)-C(17)-C(18)	166.85	174.8	-179.6	-177.5	-162.9	173.3	87.1	-175.6	-170.4	-82.0	-177.0	-162.8	-176.1
O(16)-C(17)-C(18)-S(1)	-76.84	-77.3	170.2	177.1	64.1	-79.8	67.8	-53.0	66.9	-66.9	-58.8	-83.9	-87.3
C(17)-C(18)-S(1)-C(2)	66.79	64.0	-70.3	-63.4	54.9	63.5	-83.3	-94.5	-171.3	90.5	170.2	60.2	48.6

Table 2.2.5b Selected conformations of [18]aneS_2O_4 obtained from stochastic searches and crystal structures (Energies are in kcal mol^{-1}; See text for details).

Conformation Source	Crystal L	(1) Minimum	Crystal $RuL_2(1)$	(5) Minimum	Crystal $RuL_2(2)$	(6) Minimum	Crystal $AgL_2(1)$	(7) Minimum	Crystal $AgL_2(2)$	(8) Minimum	Crystal RuL_3	(9) Minimum
Compression	159.6277	0.9121	18.8807	0.8973	14.6407	1.0755	15.8507	0.9881	24.1746	0.9881	11.5765	1.0890
Bending	8.2816	6.3873	24.2053	6.1149	23.8816	6.1111	12.0227	5.5135	9.3741	5.5135	6.1709	7.2626
Bend-Bend	0.0335	-0.0553	0.5236	-0.0634	0.5760	-0.0657	0.1271	-0.0797	0.0722	-0.0797	0.0416	-0.0522
Stretch-Bend	-0.2871	0.2914	-0.6242	0.3122	-0.7086	0.3498	-0.1831	0.3123	-0.1308	0.3123	0.2725	0.4009
Van der Waals energy												
1.4	22.2560	14.4785	23.3715	14.5551	24.5969	14.7741	24.9865	15.0509	20.0876	15.0509	18.9671	14.0385
other	-0.6591	-0.7985	0.4838	-0.4673	3.3946	-0.8715	3.7252	-1.6063	-2.2161	-1.6063	2.1027	-0.3106
Torsional	-0.2264	-1.2686	5.5571	-0.1264	4.6641	2.6447	2.7082	0.7504	2.6828	0.7504	3.2940	2.1577
Torsion-Stretch	0.1086	-0.0586	0.0028	-0.0707	0.1816	-0.2012	0.1360	-0.1710	-0.0024	-0.1710	-0.1944	-0.1830
Dipole-Dipole	3.8751	3.6115	4.4438	4.9074	4.5177	3.9343	8.6201	7.8023	8.9441	7.8023	4.8170	4.4626
Steric energy	193.0098	23.4998	76.8443	25.2490	75.7446	27.7510	67.9935	28.5605	62.9860	28.5605	47.0479	28.8655
Δ (Steric energy)		169.5100		51.5953		47.9936		39.4330		34.4255		18.1824
Δ (Bending)		1.8943		18.0904		17.7705		6.5092		3.8606		-1.0917
Δ (1,4 - van der Waals energy)		7.7775		8.8164		9.8228		9.9356		5.0367		4.9286
Torsion angles / °												
C(18)-S(1)-C(2)-C(3)	58.77	61.8	77.0	63.3	-78.6	-71.7	81.1	72.2	55.9	70.3	80.6	78.0
S(1)-C(2)-C(3)-S(4)	59.96	63.4	59.9	67.2	-55.7	-63.6	53.5	56.9	51.8	56.9	57.5	65.4
C(2)-C(3)-S(4)-C(5)	58.77	61.8	-162.4	-171.0	-75.8	-71.7	61.3	72.2	94.5	70.3	72.6	66.3
C(3)-S(4)-C(5)-C(6)	66.79	64.0	-77.2	-68.0	-73.7	-83.3	175.5	-171.3	-80.1	-94.5	86.4	77.1
S(4)-C(5)-C(6)-O(7)	-76.84	-77.3	67.4	77.7	56.2	67.8	67.3	66.9	-60.3	-53.0	-65.4	-68.3
C(5)-C(6)-O(7)-C(8)	166.85	174.8	-163.1	-173.8	94.0	87.1	-148.3	-170.4	172.5	-175.6	-84.2	-80.4
C(6)-O(7)-C(8)-C(9)	-173.73	-179.3	-178.9	-178.0	-179.9	-178.9	79.3	83.3	-179.2	-169.4	170.0	-180.0
O(7)-C(8)-C(9)-O(10)	65.5	69.9	-48.0	-70.6	80.1	82.2	66.6	65.8	67.3	78.6	-73.6	-71.2
C(8)-C(9)-O(10)-C(11)	-179.18	178.3	149.9	179.4	-158.3	-167.5	-179.1	-179.2	-176.6	-178.8	175.7	178.2
C(9)-O(10)-C(11)-C(12)	-178.68	176.2	157.3	-178.2	-158.9	-169.4	176.1	173.3	-164.6	-177.4	-173.3	-177.2
O(10)-C(11)-C(12)-O(13)	-77.8	-76.0	87.0	67.5	-55.4	-67.3	-74.4	-73.8	-65.0	-73.8	-66.1	-73.6
C(11)-C(12)-O(13)-C(14)	-178.68	176.2	73.1	70.9	-170.6	-169.4	-165.0	-177.4	170.0	173.3	-165.9	-173.0
C(12)-O(13)-C(14)-C(15)	-179.18	178.3	155.5	171.5	163.6	-167.5	175.1	-178.8	-179.3	-179.2	-79.9	-81.8
O(13)-C(14)-C(15)-O(16)	65.5	69.9	73.7	69.8	74.2	82.2	66.2	78.6	61.4	65.8	-74.2	-75.2
C(14)-C(15)-O(16)-C(17)	-173.73	-179.3	-169.6	177.0	-174.0	-178.9	-161.7	-169.4	93.5	83.3	-179.1	-171.0
C(15)-O(16)-C(17)-C(18)	166.85	174.8	172.6	173.3	98.5	87.1	171.9	-175.6	-159.8	-170.4	-83.5	-82.0
O(16)-C(17)-C(18)-S(1)	-76.84	-77.3	-87.1	-79.8	57.7	67.8	-47.7	-53.0	66.9	66.9	-66.3	-66.9
C(17)-C(18)-S(1)-C(2)	66.79	64.0	50.8	63.5	-85.3	-83.3	-94.3	-94.5	-168.0	-171.3	83.4	90.5

Table 2.2.5c Energetic and conformational changes in the minimisation of crystal structure based conformers (Energies are in kcal mol^{-1}; See text for details).

All the compounds examined show more or less conformational changes with changes of *anti-* to *gauche*-torsion angles and *vice versa*. The only exception is the crystal structure based free macrocycle, which apart from minor changes retains the order of *anti-* and *gauche*-angles in the course of energy minimisation. Two other aspects concern the energy minimisation of $RuL_2(2)$ and both Ag_2L_2 compounds. The free ligand exhibits C_2 symmetry in its solid state structure and in the minimised conformation. The two fold axis runs through the mid-points of the C(2)-C(3) and C(11)-C(12) bond. Interestingly $RuL_2(2)$ does not show this but its minimised conformer shows this symmetry feature. The interesting aspect of the Ag-compounds is that two different conformations minimise to the same low energy conformation. This allows for a qualitative estimation of the energy barrier between this and other conformations. The differences in steric energy without compression (see above) lie in the region of 25 to 30 kcal mol^{-1}. Another calculation to estimate this barrier has been the third conformational stochastic search. The small displacement of an atom by 0.5Å was not large enough to change the conformation. All distorted conformers converged back to the initial conformer. The initial energy of the new conformer after the displacement is not rational because bonds are quite dramatically distorted resulting in very high energies indeed. These initial conformers have no chemical meaning. However most of these energies converge quite rapidly within the first ten iterations. The main contributor to the steric energy after ten iterations is the 1,4-van der Waals energy which is roughly 10 kcal mol^{-1} higher compared with the converged conformation. These findings suggest that minima are well defined with respect to energy differences between the minimum itself and the surrounding barriers. A careful estimation suggests that these energies lie in the region 10 to 100 kcal mol^{-1}, however low energy conversion pathways cannot be excluded and would be subject of a more detailed investigation.

Conformation	Steric energy	1.4 - v.d.W. energy	Conformation (+-a)	Conformation (Dale)
L	193.0098	22.2560	++++-aa+aa-aa+aa-+	[1111133133]
(1)	23.4998	14.4785	++++-aa+aa-aa+aa-+	[1111142124]
(2)	24.0992	14.4005	+a+++a-+aa-aa+aaa+	[134343]
(3)	24.2865	13.9553	+a++aa-+a+-a-+aaa+	[34335]
(4)	24.5303	14.8288	+aa--aa+aa-aa+-a++	[144243]
$RuL_2(1)$	76.8443	23.3715	++a-+aa-aa++a+aa-+	[1134324]
(5)	25.2490	14.5551	++a-+aa-aa++a+aa-+	[233424]
$RuL_2(2)$	75.7446	24.5969	++++-aa-aa+aa-aa-+	[111114234]
(6)	27.7510	14.7741	++++--a-aa+aa-aa--+	[111111132123]
$Ag_2L_2(1)$	67.9935	24.9865	+++a+a++aa-aa+aa-a	[1324332]
$Ag_2L_2(2)$	62.9860	20.0876	++a--aa+aa-aa+aa+a	[334242]
(7)	28.5605	15.0509	+++a-aa+aa-aa++a+a	[1323432]
RuL_3	47.0479	18.9671	++++--a-aa-a--a--+	[11111112423]
(8)	28.8655	14.0385	++++--a-aa-a--a--a	[111133233]
(9)	31.5497	14.6626	+++a+a+++a++a+aa+a	[121213242]
(10)	37.4880	14.1393	+++++aaa+a---aaa-+	[111114315]
(11)	39.5734	12.6924	+++++aa+++aaa+aa-+	[1111113144]

Table 2.2.5d Selected conformers in abbreviated representation (Energies are in kcal mol^{-1}; See text for details).

Table 2.2.5d finally summarises some results in a more approachable form. The conformations of the macrocycle are represented by the '+-a' scheme as well as Dale's scheme. The later one is of no use in this context because it does not allow for any comparison or conclusion (see above and compare for instance L and (1), and $Ru_2L(1)$ and (5)). The '+-a' scheme however allows a regional analysis of the different conformations. The first torsion angle to be considered is C-S-C-C, followed by S-C-C-S. It is interesting to note that the S-atom region features mostly *gauche*-conformations with no change of sign in most conformations. The polyether chain on the other hand shows an interesting *gaagaagaagaag* arrangement which falls apart with increasing steric energy. This suggests that the major contribution to the overall steric energy derives from this region. This is supported by the fact that conformational changes in the minimisation process are more likely to occur in the polyether region than in the thioether region which is retained in most cases.

Time and the overall aims of this work do not permit any further investigations at the present moment. It is also questionable whether the outcome of such an investigation would greatly enhance the understanding of these systems.

2.2.6 Characterisation and Single Crystal Structure of [21]aneS_2O_5

[21]aneS_2O_5 was prepared according to the method reported by Bradshaw[217] but not purified prior to this work. Purification and recrystallisation of the dark brown oil was achieved employing the low temperature two phase diffusion technique which gave exceptionally good results with [15]aneS_2O_3 (**2.2.2**) and [18]aneS_2O_4 (**2.2.3**). The compound has been reported as a liquid at room temperature but recrystallisation afforded colourless crystals melting slightly above ambient temperature (~28°C) yielding a colourless oil.

Microanalytical results are in good agreement with the stoichiometry $C_{14}H_{28}S_2O_5 \cdot H_2O$ and the EI mass spectrum shows a peak at m/z = 340 assigned to $(C_{14}H_{28}S_2O_5)^+$. The ^{1}H-NMR spectrum exhibits similar features compared with the 1H-NMR spectrum of [18]aneS_2O_4. Two triplets at 2.58ppm and 3.54ppm have been assigned to the -SCH_2CH_2O- moiety in the macrocycle. The coupling constant (^3J = 6.42Hz) is very similar to the one found for [18]aneS_2O_4 (6.15Hz) suggesting a similar conformation for this region. Other ^{1}H-resonances were assigned to -SCH_2CH_2S- (s, 4H, 2.69ppm), -OCH_2CH_2O- (s, 8H, 3.49ppm) and -OCH_2CH_2O- (s, 8H, 3.51ppm) moieties. The ^{13}C-DEPT-NMR spectrum shows only five -CH_2- resonances assigned to two -SCH_2- and three -OCH_2- moieties. This is not surprising considering the similarity of the chemical environment in the polyether chain and subsequent similarities in chemically shifts.

The single crystal structure of [21]aneS_2O_5 (**Figure 2.2.6a**) contains 1½ H_2O molecules for each macrocycle. Each macrocycle co-ordinates *via* H-bonding to one H_2O molecule (**Figure 2.2.6b**) which is situated slightly below the macrocyclic cavity (**Figure 2.2.6c**). The remaining water molecules bridge between two neighbouring macrocycles *via* H-bonding. This compound is the first example of a neutral guest molecule co-ordinated to a mixed O/S-donor ionophore. It is also the first example of exclusive O-donor co-ordination. All other complexes with mixed O/S-donor ionophores which are discussed in the following chapters exhibit either exclusive S-donor or mixed O/S-donor co-ordination. The -SCH_2CH_2S- moiety is effected by some disorder [s.o.f. for C(2A) and C(2B) 50% each] in one of the two macrocycles indicating some conformational flexibility of this region. Transition metal complexes in which the metal co-ordinates to the S-atoms exhibit disorder in the polyether chain. It might be coincidence and there are not enough data available to draw a conclusion but the common feature of [15]aneS_2O_3 and [21]aneS_2O_5 is the odd numbered macrocycle.

Both exhibit in contrast to the even numbered macrocycle [18]aneS_2O_4 an *anti* torsion angle {166.8(3)° in [15]aneS_2O_3; -174.8(8), -172.8(4) and 158.6(8)° in [21]aneS_2O_5} for the -SCH_2CH_2S- moiety whereas [18]aneS_2O_4 [61.4(5)°] adopts a *gauche* angle.

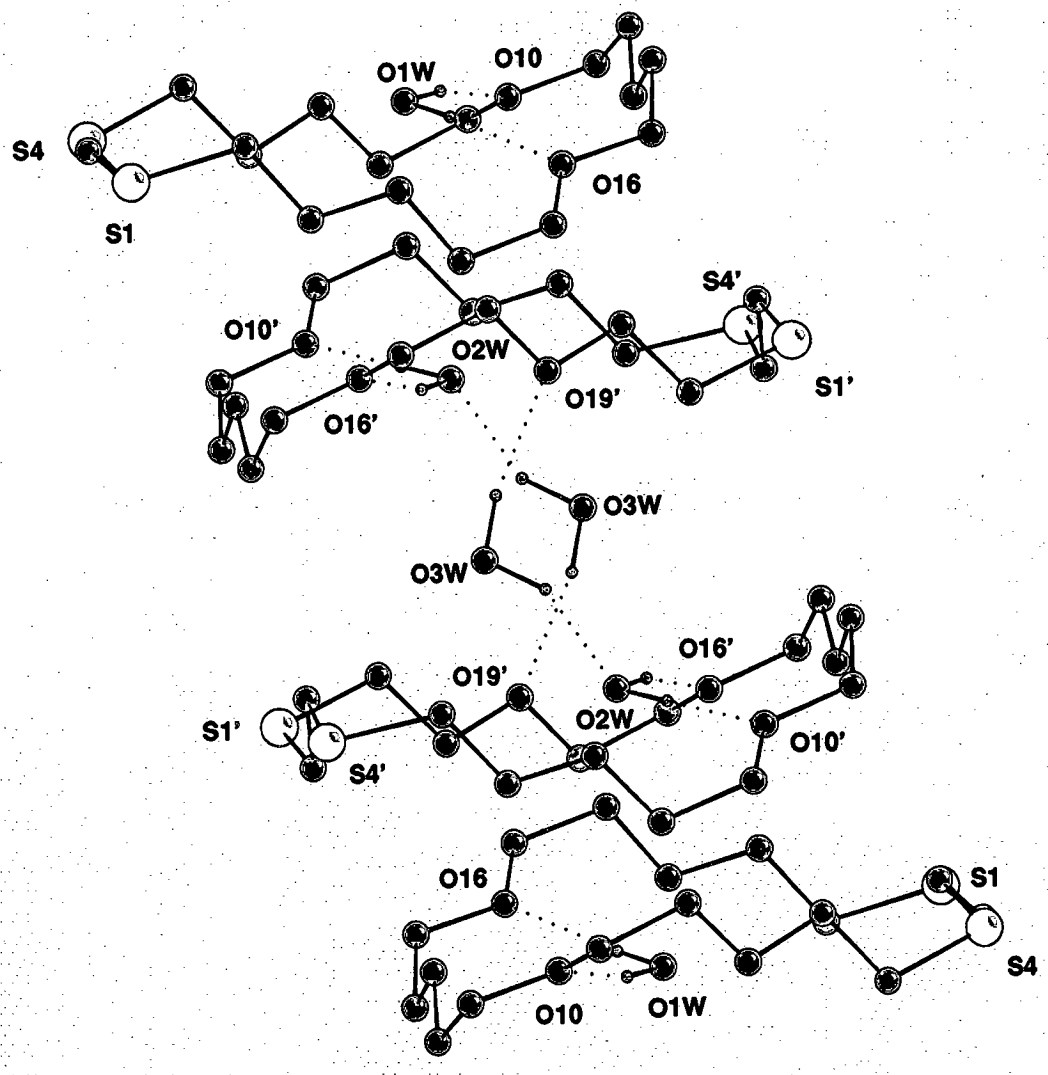

Figure 2.2.6a Packing diagram of [21]aneS_2O_5.

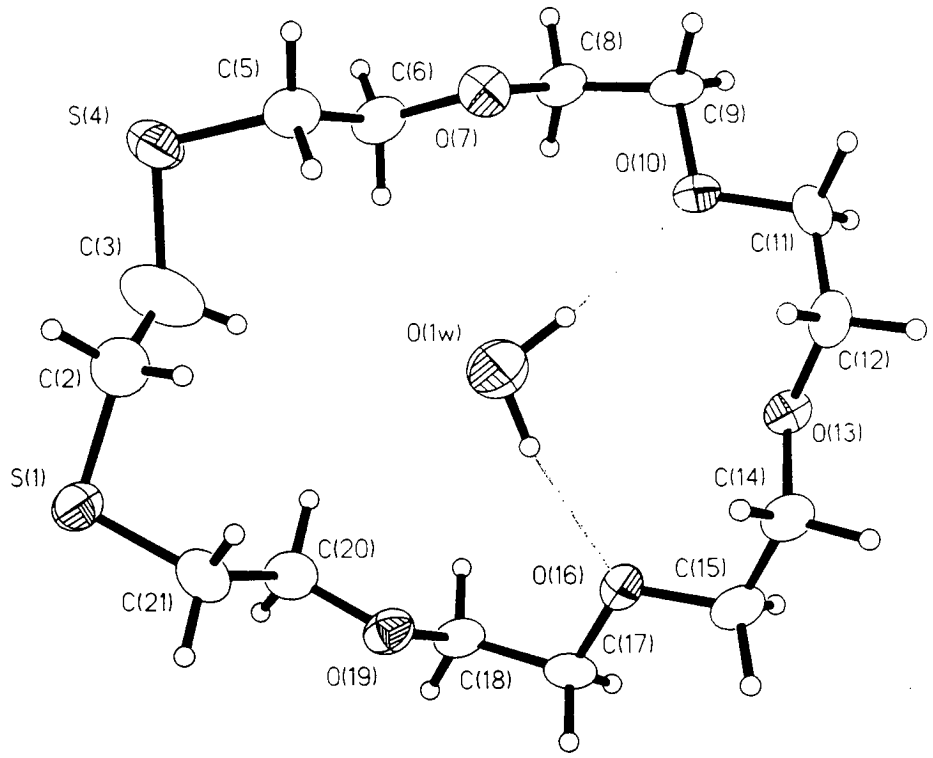

Figure 2.2.6b 'Top view' of the single crystal structure of [21]aneS_2O_5.

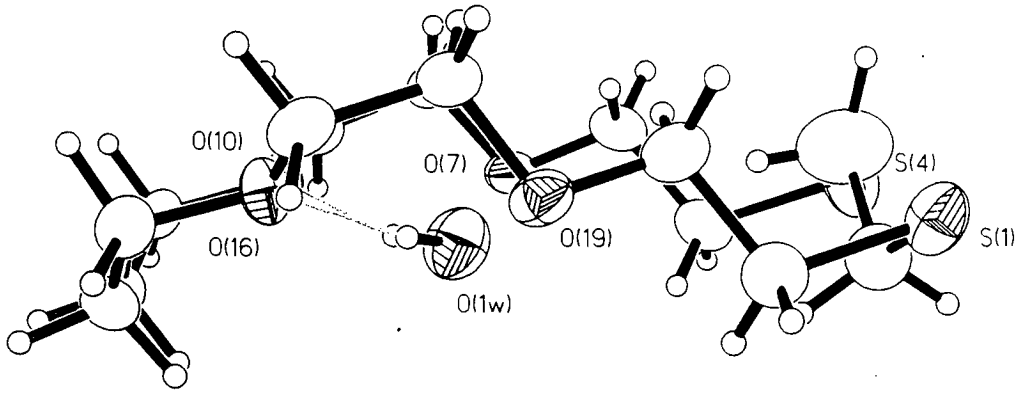

Figure 2.2.6c 'Side view' of the single crystal structure of [21]aneS_2O_5.

Macrocycle 1:		*Macrocycle 2:*	
S(1)-C(2A)-C(3)-S(4)	-174.8(8)	S(1')-C(2')-C(3')-S(4')	-172.8(4)
S(1)-C(2B)-C(3)-S(4)	158.6(8)		
C(2A)-C(3)-S(4)-C(5)	118.8(10)	C(2')-C(3')-S(4')-C(5')	-97.4(6)
C(2B)-C(3)-S(4)-C(5)	90.0(11)		
C(3)-S(4)-C(5)-C(6)	73.7(6)	C(3')-S(4')-C(5')-C(6')	86.7(5)
S(4)-C(5)-C(6)-O(7)	178.9(4)	S(4')-C(5')-C(6')-O(7')	175.8(4)
C(5)-C(6)-O(7)-C(8)	-173.6(5)	C(5')-C(6')-O(7')-C(8')	-170.9(5)
C(6)-O(7)-C(8)-C(9)	-163.6(5)	C(6')-O(7')-C(8')-C(9')	-163.6(5)
O(7)-C(8)-C(9)-O(10)	62.0(7)	O(7')-C(8')-C(9')-O(10')	69.4(7)
C(8)-C(9)-O(10)-C(11)	172.1(5)	C(8')-C(9')-O(10')-C(11')	177.1(6)
C(9)-O(10)-C(11)-C(12)	169.7(5)	C(9')-O(10')-C(11')-C(12')	172.3(6)
O(10)-C(11)-C(12)-O(13)	63.4(7)	O(10')-C(11')-C(12')-O(13')	65.5(7)
C(11)-C(12)-O(13)-C(14)	-172.0(5)	C(11')-C(12')-O(13')-C(14')	-171.2(6)
C(12)-O(13)-C(14)-C(15)	176.7(6)	C(12')-O(13')-C(14')-C(15')	174.2(5)
O(13)-C(14)-C(15)-O(16)	-69.7(7)	O(13')-C(14')-C(15')-O(16')	-68.2(7)
C(14)-C(15)-O(16)-C(17)	-171.8(5)	C(14')-C(15')-O(16')-C(17')	-161.4(5)
C(15)-O(16)-C(17)-C(18)	-174.1(5)	C(15')-O(16')-C(17')-C(18')	-177.4(5)
O(16)-C(17)-C(18)-O(19)	-66.6(7)	O(16')-C(17')-C(18')-O(19')	-64.1(7)
C(17)-C(18)-O(19)-C(20)	166.8(5)	C(17')-C(18')-O(19')-C(20')	165.7(5)
C(18)-O(19)-C(20)-C(21)	175.0(5)	C(18')-O(19')-C(20')-C(21')	172.6(5)
O(19)-C(20)-C(21)-S(1)	-179.2(4)	O(19')-C(20')-C(21')-S(1')	-175.8(4)
C(20)-C(21)-S(1)-C(2A)	-90.6(7)	C(20')-C(21')-S(1')-C(2')	-77.9(5)
C(20)-C(21)-S(1)-C(2B)	-93.9(6)		
C(21)-S(1)-C(2A)-C(3)	72.6(14)	C(21')-S(1')-C(2')-C(3')	-85.2(7)
C(21)-S(1)-C(2B)-C(3)	105.3(13)		

Table 2.2.6 Torsion angles (°) with estimated standard deviations for [21]aneS_2O_5 (Note: C(2A) and C(2B) have a mutual s.o.f.s of 0.5 each).

2.2.7 The Synthesis of benzo[18]aneS_2O_4

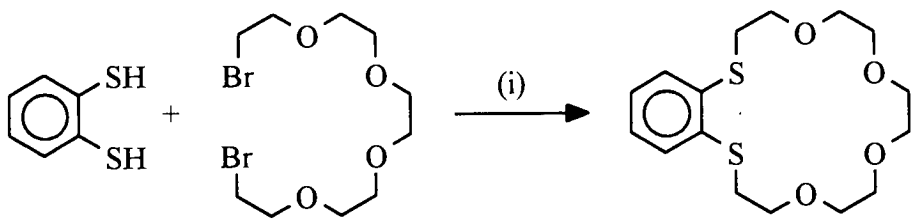

(i) a) $CsCO_3$/DMF/Δ, b) CH_2Cl_2

Figure 2.2.7 Reaction scheme for the preparation of benzo[18]aneS_2O_4.

Benzo[18]aneS_2O_4 was prepared using a Cs_2CO_3 mediated cyclisation reaction in DMF (**Figure 2.2.7**). 1,2-Benzenedithiol and dibromo pentaethylene glycol were dissolved in DMF (600 dm^3) and slowly added to a suspension of Cs_2CO_3 in DMF (1l). The reaction mixture was kept at 70-80°C and stirred for 48 hours. Isolation of the product consisted of the removal of DMF under reduced pressure, extraction with CH_2Cl_2, washing with water, drying over anhydrous $MgSO_4$ and evaporation of the solvent. Characterisation of the initial crude product was less than satisfactorily. A reaction conducted with $TlPF_6$ (see **Chapter V**), afforded however excellent microanalytical and spectroscopic results, confirming the successful synthesis of this ligand. The general problem with Cs_2CO_3 mediated cyclisation reactions is the quantitative removal of DMF. Excessive washing with water on one hand contaminates the sample and on the other hand may diminish the yield.

2.2.8 The Synthesis of [18]aneS_3O_3

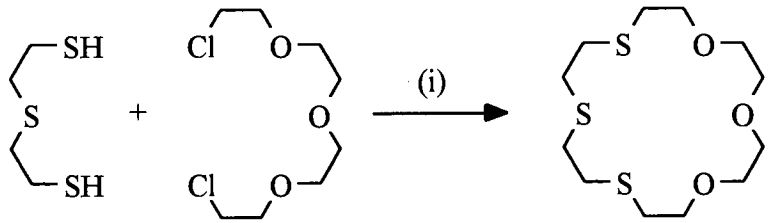

(i) a) EtOH/NaOH/Δ, b) HCl/H_2O, c) CH_2Cl_2

Figure 2.2.8 Reaction scheme for the preparation of [18]aneS_3O_3.

[18]aneS_3O_3 was prepared by the co-condensation of 2-mercaptoethyl sulphide and dichloro-tetraethylene glycol in a mixture of EtOH and solid NaOH (**Figure 2.2.8**). A major problem during this synthesis was that the mixture of the reactants separated into two layers and the addition of equimolar amounts of each reactant could not be maintained throughout the reaction. This problem has been solved by the addition of a small amount of DMF in subsequent ligand syntheses (see **2.2.3**). Isolation of the crude product, which seemed to be severely affected by polymeric by-products followed the route given earlier. Purification employing column chromatography has not been successful due to difficulties to identify a suitable solvent system.

The successful synthesis and characterisation of $[Pd([18]aneS_3O_3)](PF_6)_2$ (see **Chapter IV**) proved however the successful preparation of $[18]aneS_3O_3$. Further evidence was found in the EI mass spectrum which shows a peak at m/z = 312 assigned to $(C_{12}H_{24}S_3O_3)^+$. The ^{1}H-NMR spectrum which was still affected with some impurities shows two distinct regions assigned to $-SCH_2-$ (2.6-3.0 ppm) and $-OCH_2-$ (3.5-3.8 ppm) moieties in the macrocycle. The ^{13}C-DEPT-NMR spectrum shows six ^{13}C resonances assigned to $-SCH_2-$ (31.5, 32.1 and 32.8 ppm) and $-OCH_2-$ (70.5, 70.7 and 72.2 ppm). The same arguments given for $[18]aneS_2O_4$ apply with respect to the most likely species in solution (two-fold symmetry).

2.2.9 The Synthesis of $[20]aneS_3O_3$

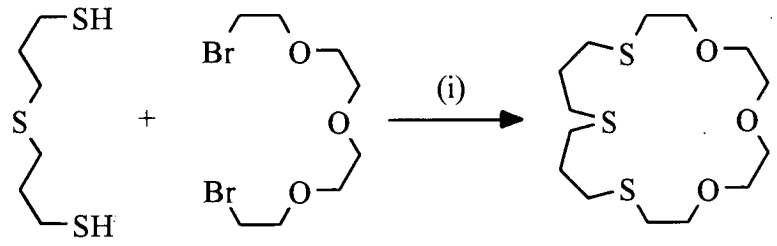

(i) a) EtOH/EtONa/NaOH/Δ, b) HCl/H_2O, c) CH_2Cl_2

Figure 2.2.9 Reaction scheme for the preparation of $[20]aneS_3O_3$.

$[20]aneS_3O_3$ was prepared by the co-condensation of 3-mercaptopropyl sulphide with dibromo tetraethylene glycol under high dilution conditions following the improved procedure given for the synthesis of $[18]aneS_2O_4$ (**Figure 2.2.9**). The crude product was obtained in good yield and the major impurities have been identified as EtOH and CH_2Cl_2 in the ^{1}H-NMR spectrum. The ^{1}H-NMR spectrum shows apart from signals for EtOH (t, 1.08ppm; quartet 3.40ppm) and CH_2Cl_2 (s, 5.21ppm) three complicated (probably 2nd order) regions assigned to $-CH_2-$ (1.7-1.8 ppm), $-SCH_2-$ (2.45-2.65 ppm) and $-OCH_2-$ (3.4-3.7ppm). An assignment of peaks in these regions has so far been impossible and further characterisation have to be postponed until the purity of the compound has significantly improved.

2.3 CONCLUSION

The synthesis of a range of mixed O/S-donor ionophores has been described and viable pathways to other mixed O/S-donor ionophores have been identified. Purification of macrocycles containing the 1,4-dithia moiety such as [15]aneS_2O_3, [18]aneS_2O_4 and [21]aneS_2O_5 has been achieved using a low temperature two phase diffusion technique which proved to be superior to other techniques. The single crystal structures of [15]aneS_2O_3, [18]aneS_2O_4 and [21]aneS_2O_5 have subsequently been determined or re-determined in order to improve previous structure determinations. [21]aneS_2O_5 which was isolated as a sesquihydrate is the first example of a complex between a mixed O/S-donor ionophore and a neutral guest molecule (H_2O).

Molecular mechanics calculations on [18]aneS_2O_4 lead to many different conformations within an energy range of less than 20 kcal mol^{-1}. This is in good agreement with the results described in the following chapters where [18]aneS_2O_4 adopts *exo* and *endo* co-ordination modes in a range of complexes with metal ions. These results confirm the high flexibility of the macrocyclic ligand. The solid state conformation of [18]aneS_2O_4 has been termed pre-organised for bidentate chelating co-ordination. The term pre-organised is in this case of little relevance because its conformation in solution is not known. The solid state conformation of [15]aneS_2O_3 is in contrast not pre-organised for bidentate chelating co-ordination and must undergo a conformational change in order to *exo* co-ordinate to a metal ion.

2.4 EXPERIMENTAL SECTION

2.4.1 The Synthesis of 3,3'-Thiodipropanol

Na_2S (120.2 g, 0.5 mol) and NaOH (2 g, 0.05 mol) were slowly dissolved under heating in ^{n}BuOH (200 cm^3). The reaction apparatus was purged throughout the reaction with N_2. 2-Chloroethanol (94.54 g, 1 mol) was added dropwise to the hot reaction mixture. The mixture was kept refluxing for an additional 18 hours after addition was completed. The cold reaction mixture was filtered to remove solid NaCl which precipitated and the solvent was removed under reduced pressure. The residue, was treated with MeOH/H_2O (1:1 v/v) and afforded after removal of the solvents a slightly green residue which was still affected by impurities (see Microanalysis). The crude product was used without further purification in the synthesis of 3-mercaptopropyl sulphide.

Microanalysis for ($C_6H_{14}O_2S$; Mol.wt. = 150.24 g mol^{-1})

	%C	%H
Calculated	47.96	9.39
Found	40.88	9.15

EI mass spectrum:

Fragment:	m/z (calc.)	m/z (found)
$(C_6H_{14}O_2S)^+$	150	150 (basepeak)

IR spectrum (KBr disc): 3365vs, 2940s, 2880s, 1650w, 1425m, 1260w, 1210w, 1150w1085s, 1050s, 880m, 630w, 520w, 440w and 415w cm^{-1}.

^{1}H-NMR spectrum ($CDCl_3$; 297K; 200.13 MHz)

δ 1.41 ppm	(quintet, 4H)	$CH_2C\boldsymbol{H}_2CH2$.
δ 2.22 ppm	(t, 4H)	$C\boldsymbol{H}_2S$.
δ 3.2 - 3.3ppm	(m, 8H)	$C\boldsymbol{H}_2OH$.
δ 3.99 ppm	(s, broad, 2H)	$CH_2O\boldsymbol{H}$.

2.4.2 The Synthesis of 3-Mercaptopropyl Sulphide

(30.05 g, 0.2 mol) was placed in a 1l round bottom flask equipped with a stirrer, condenser and N_2 inlet. The flask was purged with N_2 for the whole time of the reaction. Concentrated hydrochloric acid (106 cm^3) and thiourea (30.46 g, 0.4 mol) were added and the reaction mixture was heated up and refluxed for 12 hours. Ice cold KOH solution (75 g in 400 cm^3 H_2O) was then carefully added to the cooled reaction mixture (ice bath) and again refluxed for 3 hours. The product formed as a yellow oily layer on top of the aqueous reaction mixture and was quantitatively extracted using CH_2Cl_2. The combined CH_2Cl_2 portions were dried over anhydrous $MgSO_4$. Evaporation of the solvent yielded a slightly yellow unpleasantly smelling oil which was characterised. Yield: 23.5 g, 0.13 mol, 64 %

Microanalysis for ($C_6H_{14}S_3$; Mol.wt. = 182.36 g mol^{-1})

	%C	%H
Calculated	39.52	7.74
Found	40.54	7.50

EI mass spectrum:

Fragment:	m/z (calc.)	m/z (found)
$(C_6H_{14}S_3)^+$	182	182

IR spectrum (Film between KBr plates): 2920s, 2850w, 2550w, 1430m, 1345w, 1295w, 1260m, 1210w, 1140w, 1055m, 875w, 840w and 695w cm^{-1}.

^{1}H-NMR spectrum ($CDCl_3$; 297K; 200.13MHz)

δ 1.32 ppm	(t, 2 H)	CH_2SH.
δ 1.6 - 1.9 ppm	(quintet, 4 H)	$CH_2CH_2CH_2$.
δ 2.5 - 2.7 ppm	(m, 8 H)	CH_2S.

2.4.3 General Procedure for the Conversion of Primary Alcohols (Glycols) into Chlorides

Method 1:

The glycol (0.05 mol) and pyridine (0.11 mol) were dissolved in benzene (60 cm^3) and placed in a three neck round bottom flask. The flask, equipped with a condenser, gas inlet and dropping funnel was purged with nitrogen and heated. $SOCl_2$ (0.12 mol) was added dropwise over 20 min to the stirred refluxing mixture. The reaction mixture was kept refluxing over night (18h) during which time the colour changed from slightly yellow to brown. The reaction mixture was allowed to cool down to ambient temperature and slightly acidic water (10 cm^3) was added and a two phase system formed. The top layer containing the product was isolated and the bottom layer, a red oily liquid, was extracted twice with benzene (25 cm^3). The combined benzene solutions were carefully washed with saturated aqueous $NaHCO_3$ solution, washed with water, dried over $MgSO_4$ and the solvent removed under reduced pressure. The product, a slightly coloured liquid, was of high purity (^{1}H-NMR and IR spectroscopy) and distillation did not improve its quality.

Method 2:

The glycol (0.05 mol) and pyridine (0.11 mol) were placed in a three neck round bottom flask equipped with a condenser, gas inlet and dropping funnel. The flask was purged with N_2 and heated to about 40°C. $SOCl_2$ (0.12 mol) was then added dropwise over a period of 2 hours to the stirred reaction mixture. The reaction mixture was then heated up to 80°C and kept at that temperature for 24 hours. Diluted HCl was then added carefully to the cool reaction mixture to give a slightly acidic solution. This aqueous solution was then extracted 5 times with Et_2O (50 cm^3 each). The combined Et_2O portions were carefully washed with saturated aqueous $NaHCO_3$ solution, washed with water, dried over anhydrous MgSO4 and evaporated. The product was similar to method 1 of high purity and further purification was unnecessary. Both methods were used with a series of oligoethylene glycols and gave excellent yields in the range 75 to 85%.

Product:	$Cl(C_2H_4)(O(C_2H_4))_3Cl$ $C_8H_{16}O_3Cl_2$	$Cl(C_2H_4)(O(C_2H_4))_4Cl$ $C_{10}H_{20}O_4Cl_2$
Mol.wt.	231.12 $gmol^{-1}$	275.17 $gmol^{-1}$
Microanalysis:		
Calculated		43.6 %C 7.33%H
Found		43.1 %C 7.21%H
EI mass spectrum:		
Fragment		$(C_{10}H_{20}O_4Cl_2)^+$ found: m/z = 275 calc.: m/z = 275
IR spectrum	2895vs, 2745w, 1945w, 1630w,	2870s, 1455m, 1440w, 1350m,
(Film between	1450m, 1430m, 1350m, 1300m,	1300m, 1255w, 1200w, 1115vs,
940w		
KBr plates)	1255m, 1200m, 1130vs, 970w,	840w, 735m, 700w and 665m cm^{-1}
	935m, 885w, 830w, 745m, 665m,	
	530w and 485w cm^{-1}.	
^{1}H-NMR		($CDCl_3$; 297 K; 200.130 MHz)
		3.56 - 3.75 ppm (m, 20H)

Table 2.4.3 Analytical and spectroscopic data for chlorination products of oligoethylene glycols.

2.4.4 General Procedure for the Conversion of Primary Alcohols (Glycols) into Bromides

The glycol (0.5 mol) and pyridine (5g) were placed in a three neck round bottom flask. The flask was cooled in crushed ice and purged with N_2. PBr_3 (0.4 mol) was then added dropwise to the stirred glycol. The ice was allowed to thaw over night and diluted HCl was carefully added to destroy any unreacted PBr_3. The two phase system was then extracted with three portions of CH_2Cl_2. The combined solutions were washed with saturated aqueous $NaHCO_3$ solution and water. The solvent was removed under reduced pressure after drying over anhydrous $MgSO_4$. The product a slightly coloured liquid was of high purity (^{1}H-NMR and IR spectroscopy) and further purification was unnecessary. This procedure gives in general satisfactory results (typical yields are 45 to 55%), however, failure of the reaction to start results in a large amount of PBr_3 being present in the flask. Addition of water might than result in a violent exothermic reaction.

Product:	$Br(C_2H_4)(O(C_2H_4))_3Br$	$Br(C_2H_4)(O(C_2H_4))_4Br$
	$C_8H_{16}O_3Br_2$	$C_{10}H_{20}O_4Br_2$
Mol.wt.	320.02 $gmol^{-1}$	364.07 $gmol^{-1}$
Microanalysis:		
Calculated	30.03 %C; 5.04 %H	
Found	28.58 %C; 5.03 %H	
IR spectrum (Film between KBr plates)	2870s, 1460m, 1420m, 1350m, 1280s, 1230m, 1185m, 1115vs, 875w, 755w, 665m, 570m and 465w cm^{-1}.	2970s, 1455m, 1350m, 1250s, 1115vs, 975s, 840w and 571w cm^{-1}.
^{1}H-NMR	($CDCl_3$; 297K; 200.130MHz) 3.33 - 3.73 ppm (m, 16H)	
^{13}C-NMR	($CDCl_3$; 298 K; 90.558 MHz; DEPT)	
-CH_2Br	30.52 ppm	
-CH_2O-	71.03, 70.49, 70.36 ppm	

Table 2.4.4 Analytical and spectroscopic data for bromination products of oligoethylene glycols.

2.4.5 The Synthesis of [18]aneS_2O_4

The following procedure is typical. EtOH (1l, 96%) was placed in a 2l three neck round bottom flask, equipped with a magnetic stirring bar, a condenser and a gas inlet. The flask was purged with N_2 and Na-metal (60g, 2.6 mol) was added in small pieces over 12 hours.

The EtOH/EtONa/NaOH solution was then heated up to 90°C and a mixture of both reactants [1,14-dichloro-3,6,9,12-tetraoxatetradecane (13.76 g 0.05 mol) and 1,2-ethanedithiol (4.71 g 0.05 mol) dissolved in EtOH/DMF (250 cm^3, 24:1 v/v)] was added dropwise over a period of 18 hours. The clear solution became slowly opaque and a precipitate formed (NaCl) allowing to monitor the progress of the reaction. The solution was kept hot for additional 24 hours and was then allowed to cool to ambient temperature. Diluted HCl was added to neutralise excess of base. The solution was filtered and the EtOH was removed under reduced pressure.
The crude product which contained always DMF and EtOH as impurities was dissolved in CH_2Cl_2 and washed with several portions of water. The progress of purification was monitored using ^{1}H-NMR spectroscopy ($CDCl_3$, 60 MHz). Evaporation of the CH_2Cl_2 afforded a slightly yellow oil. Crystallisation was achieved by dissolving the oil in EtOAc and adding a layer of hexane. Slow diffusion (at -25°C) of hexane into the EtOAc solution afforded large colourless crystals which were isolated and characterised. Yield: 5.2 g, 0.017 mol, 34%

Microanalysis (for $C_{12}H_{24}O_4S_2$; Mol.wt. = 296.44 g mol^{-1})

	%C	%H
Calculated	48.62	8.16
Found	48.71	8.29

EI mass spectrum:

Fragment:	m/z (calc.)	m/z (found)
$(C_{12}H_{24}O_4S_2)^+$	296	296

IR spectrum (KBr disc): 2940w, 2880s, 2840s, 2735w, 2700w, 1985w, 1945w, 1655w, 1450m, 1430m, 1350s, 1275m, 1245m, 1120vs, 1025m, 945m, 890m, 840s, 630w, 525w, 485w and 445w cm^{-1}.

^{1}H-NMR spectrum ($CDCl_3$; 297K; 250.130 MHz)

δ 2.69 ppm (t; 4H) -SC***H***$_2$$CH_2O$- ^3J = 6.15 Hz
δ 2.85 ppm (s; 4H) -SC***H***$_2$$CH_2S$-
δ 3.61 ppm (s; 8H) -OC***H***$_2$$CH_2O$-
δ 3.63 ppm (s; 4H) -OC***H***$_2$$CH_2O$-
δ 3.68 ppm (t; 4H) -OC***H***$_2$$CH_2S$- ^3J = 6.15 Hz

^{13}C-NMR spectrum ($CDCl_3$; 298K; 50.320 MHz; DEPT ¾π)

δ 32.4, 31.0 ppm -***C***H_2S-
δ 70.3, 70.5, 70.6, 72.0 ppm -***C***H_2O-

2.4.6 The Synthesis of benzo[18]aneS_2O_4

Benzo[18]aneS_2O_4 was prepared using a Cs_2CO_3 mediated cyclisation reaction in DMF. 1,2-Benzenedithiol (0.5 g 3.5 mmol) and dibromo pentaethylene glycol (1.28 g, 3.5 mmol) were dissolved in DMF (600 cm^3) and slowly added to a hot suspension of Cs_2CO_3 (1.4 g, 4.2 mmol) in DMF (1l). The reaction mixture was kept at 70-80°C and stirred for 48 hours. Isolation of the product consisted of the removal of DMF under reduced pressure, extraction with three portions of CH_2Cl_2 (50 cm^3 each), washing with water, drying over anhydrous $MgSO_4$ and evaporation of the solvent. The initial product was still badly affected by DMF and further washings with water were required. The estimated yield for this reaction was > 35%. The product showed a colourisation from colourless to bright red over a few days. The red component could however be removed by filtering through silica gel.

Microanalysis for [$C_{16}H_{24}S_2O_4$ (crude); Mol.wt. = 344.48 g mol^{-1}]

	%C	%H
Calculated	55.78	7.02
Found	50.47	6.87

EI mass spectrum:

Fragment:	m/z (calc.)	m/z (found)
$(C_{16}H_{24}S_2O_4)^+$	344	344

IR spectrum (Film between KBr plates):

3050w, 2865s, 1940w, 1570m, 1445s, 1350m, 1295m, 1255m, 1195m, 1115vs, 1040s, 940m, 885w, 840w, 750s and 670 cm^{-1}

^{1}H-NMR spectrum ($CDCl_3$; 297K; 250.130 MHz)

δ 3.06 ppm (t; 4H)	-SCH_2-	^3J = 6.35Hz
δ 3.45-3.70 ppm (s; 20H)	-OCH_2-	
δ 7.00-7.30 ppm (m; 4H)	-SC_6H_4S-	

2.4.7 The Purification and Characterisation of [21]aneS_2O_5

[21]aneS_2O_5 was prepared by Gill Reid prior to this work following the procedure reported by Bradshaw[217]. The crude dark brown product was dissolved in CH_2Cl_2 (100 cm^3) and washed with three portions of water (30 cm^3 each). The solvent was dried over anhydrous $MgSO_4$ and evaporated. The slightly yellow oil was recrystallised using the low temperature two phase diffusion technique used for [15]aneS_2O_3 and [18]aneS_2O_4 (**2.4.5**).

Microanalysis for ($C_{14}H_{28}S_2O_5 \cdot H_2O$; Mol.wt. = 358.53 g mol^{-1})

	%C	%H
Calculated	46.90	8.43
Found	47.09	8.13

EI mass spectrum:

Fragment:	m/z (calc.)	m/z (found)
([21]aneS_2O_5)$^+$	340	340

IR spectrum (KBr disc)

2865s, 1635w, 1450m, 1350m, 1290m, 1250m, 1200w, 1110vs, 1040m, 945m, 840w, 670w.

^{1}H-NMR spectrum ($CDCl_3$; 294K; 360.130 MHz)

δ 2.58 ppm (t, 4H)	-SC***H***$_2$$CH_2O$-	^3J = 6.42 Hz
δ 2.69 ppm (s, 4H)	-SC***H***$_2$$CH_2S$-	
δ 3.49 ppm (s 8H)	-OC***H***$_2$$CH_2O$-	
δ 3.51 ppm (s 8H)	-OC***H***$_2$$CH_2O$-	
δ 3.54 ppm (t, 4H)	-OC***H***$_2$$CH_2S$-	^3J = 6.43 Hz

^{13}C-NMR spectrum ($CDCl_3$; 297K; 62.896 MHz; DEPT ¾π)

δ 30.47 and 31.82 ppm	-***C***H_2S-
δ 69.76, 69.85 and 69.94 ppm	-***C***H_2O-

2.4.8 The Synthesis of [18]aneS_3O_3

2-Mercaptoethyl sulphide (5.56 g, 0.036 mol) and dichloro tetraethylene glycol (8.32 g, 0.036 mol) were dissolved in EtOH (100 cm^3) and placed in a dropping funnel. This mixture was then added to a suspension of NaOH (3.2 g, 0.08 mol) in refluxing EtOH over a period of 16 hours. It became apparent during this time that the solution in the dropping funnel had formed two layers and the addition of equimolar amounts of either reactant was no longer maintained.

The solution was kept refluxing for additional 24 hours and allowed to cool down to ambient temperature. The reaction mixture was neutralised with diluted HCl, filtered and the EtOH removed under reduced pressure. The remaining slurry of NaCl was washed with n-hexane/$CHCl_3$ ($60cm^3$, 5:1 v/v) which afforded after evaporation a yellow oil. The compound was however still affected by some impurities (polymers) and attempts to purify the compound using solvent extraction resulted in general in loss of material.

EI mass spectrum:

Fragment:	m/z (calc.)	m/z (found)
$(C_{12}H_{24}S_3O_3)^+$	312	312

^{1}H-NMR spectrum (CDCl3; 298 K; 200.130 MHz):

δ 2.6 - 3.0 ppm (m; 12H) -C***H***$_2$S-

δ 3.5 - 3.8 ppm (m; 12H) -C***H***$_2$O-

^{13}C-NMR spectrum (CDCl3; 298 K; 50.320 MHz; DEPT ¾π):

δ 31.5, 32.1 and 32.8 ppm -***C***H_2S-

δ 70.5, 70.7 and 72.2 ppm -***C***H_2O-

2.4.9 The Synthesis of [20]aneS_3O_3

EtOH (1l) was placed in a 2l round bottom flask equipped with a mechanical stirrer and purged with N_2. Na-metal (28g, 1.2mol) was added carefully to the stirred EtOH. The clear solution was heated up to 60 to 70°C and a mixture of 3-mercaptopropyl sulphide (3.64 g, 0.02 mol) and dibromo tetraethylene glycol (6.36 g, 0.02 mol) in EtOH/DMF (4:1 v/v) was added slowly over a period of 48 hours. The progress of the reaction could be monitored by the appearance of some cloudiness (precipitation of NaBr). The product was isolated by neutralisation of the strong alkaline solution with diluted hydrochloric acid and evaporation on the rotary evaporator. The remaining NaBr/NaCl slurry was extracted three times with CH_2Cl_2 (50 cm^3 each) and three times with n-hexane (50 cm^3 each). The solvents were evaporated and initial infrared and ^{1}H-NMR spectra were recorded on the crude products to assess purity and success of the synthesis.

Microanalysis for ($C_{14}H_{28}O_3S_3$; Mol.wt. = 340.57 g mol^{-1})

	%C	%H
Calculated	49.37	8.28
Found	42.40	7.39

IR spectrum (Film between KBr plates):

2915s, 2865s, 1445m, 1350m, 1295m, 1250m, 1115vs, 800w, 670w, 570w.

^{1}H-NMR spectrum ($CDCl_3$; 298K; 250.130 MHz)

δ 1.7-1.8 ppm (quintet; 4H) -C***H***$_2$C-

δ 2.45-2.65 ppm (m; 12H) -C***H***$_2$S-

δ 3.4-3.7 ppm (m; 12H) -C***H***$_2$O-

2.4.11 Single Crystal Structure Determinations

The single crystal structures of [15]aneS_2O_3, [18]aneS_2O_4 and ([21]aneS_2O_5)·1½ H_2O have been determined. Selected crystallographic details are summarised in **Table 2.4.11**. The single crystal structure of [15]aneS_2O_3 has been solved and refined by Sandy Blake and the structure of [21]aneS_2O_5 has been solved and refined by Steve Harris a fourth year project student with Sandy Blake and Simon Parsons.

Compound	[15]aneS$_2$O$_3$	[18]aneS$_2$O$_4$	([21]aneS$_2$O$_5$)·1½ H$_2$O
Crystal data			
Formula	$C_{10}H_{20}S_2O_3$	$C_{12}H_{24}S_2O_4$	$C_{14}H_{28}S_2O_5 \cdot 1½\ H_2O$
M / gmol^{-1}	252.40	296.44	340.48
Crystal size / mm	0.37 x 0.42 x 0.54	0.39 x 0.47 x 0.66	0.20 x 0.40 x 0.40
Crystal system	triclinic	monoclinic	monoclinic
Space group	P -1 (No. 2)	C 2/c (No.15)	$P\,2_1/n$ (alt. $P\,2_1/c$ No.14)
a / Å	7.2129 (24)	15.9074 (12)	17.550 (12)
b / Å	9.102 (3)	9.5181 (8)	11.750 (8)
c / Å	10.080 (4)	12.5255 (10)	18.531 (9)
α / °	80.49 (3)	90	90
β / °	86.85 (3)	124.351 (4)	91.52 (4)
γ / °	74.321 (23)	90	90
U / Å^3	628.4	1566	3820.0
Z	2	4	8
D_c / gcm^{-3}	1.334	1.258	1.306
μ / mm^{-1}	0.410	0.344	0.295
F(000)	272	640	1584
T / K	150.0(1)	295	150.0(2)
Reflections at ±ω to refine cell	30	70	30
2θrange / °	28 - 24	30 - 32	26 - 28
Data Collection			
$2\theta_{max}$ / °	50	50	45
Range of h	-8 → 8	-18 → 15	-18 → 18
Range of k	-10 → 10	0 → 11	-1 → 12
Range of l	-1 → 11	0 → 13	0 → 19
Measured reflections	3173	1352	5424
Independent reflections, R_{int}	2173, 0.013	1268	4976, 0.141
Observed reflections	2161 with $F \geq 2\sigma(F)$	998 with $F \geq 2\sigma(F)$	4861 with $F \geq 2\sigma(F)$
ψ scan correction $TF_{max,min}$	0.796, 0.776	-	0.873, 0.716
Solution			
Method	Direct Methods	reported co-ordinates	Direct Methods
using	SHELXS-86	SHELXL-93	SHELXS-86
Refinement			
full matrix least squares on	F^2	F^2	F^2
using	SHELXL-93	SHELXL-93	SHELXL-93
DIFABS max, min	-	-	-
Weighting scheme	0.0344, 0.24	0.0722, 0.64	0.0831, 14.2
Parameters refined	217	84	423
SHELX76 R, R´, S			
SHELXL-93 R1, wR2, S	0.028, 0.067, 1.06	0.039, 0.117, 1.06	0.071, 0.212, 1.08
$(\Delta/\sigma)_{max}$	0.165	0.003	0.620
$\Delta\rho_{max,\ min}$ / eÅ^{-3}	+0.22, -0.22	+0.22, -0.30	+0.52, -0.41

Table 2.4.11 Selected crystallographic data for the single crystal structures of [15]aneS$_2$O$_3$, [18]aneS$_2$O$_4$ and [21]aneS$_2$O$_5$.

CHAPTER III

The Co-ordination Chemistry of Ruthenium(II) with Mixed O/S-Donor Ionophores

3.1 INTRODUCTION

Ru exhibits a range of oxidation states (-II to +VIII), of which Ru(II), Ru(III) and Ru(IV) are the most common. A comprehensive discussion of the chemistry of Ru can be found in the review by Schröder and Stephenson[273]. The chemistry of Ru is by no means trivial which is reflected in the large amount of publications in this area[274,275] and it is beyond the limits of this thesis to cover even a single oxidation state in depth. The following section briefly outlines some of the pathways into the co-ordination chemistry of Ru(II) in particular with respect to compounds prepared in the course of this work.

3.1.1 Entry Points into the Co-ordination Chemistry of Ru(II)

A common entry point into Ru chemistry is '$RuCl_3 \cdot xH_2O$'. The commercially available green compound is a mixture of Ru(III) and Ru(IV) containing a varying amount of water. It is therefore desirable to convert this non stoichiometric compound into well defined starting materials. **Table 3.1.1b** outlines some reactions of '$RuCl_3 \cdot xH_2O$' where the Ru maintains its oxidation state and **Table 3.1.1a** lists reactions where the Ru(III) is reduced to Ru(II).

'RuCl3·xH2O' + CpH (EtOH)	⟶	$Ru(Cp)_2$
'RuCl3·xH2O' + CpH + PPh3 (EtOH)	⟶	$RuCl(Cp)(PPh_3)_2$
'$RuCl_3 \cdot xH_2O$' + di-hydro-arene	⟶	$RuCl(arene)(\mu\text{-}Cl_2)RuCl(arene)$
$[RuCl(arene')]_2(\mu\text{-}Cl_2)$ + arene''	⟶	$[RuCl(arene'')]_2(\mu\text{-}Cl_2)$ + arene'
$[RuCl(arene)]_2(\mu\text{-}Cl_2)$ + NH_4PF_6 (MeCN)	⟶	$[RuCl(arene)(MeCN)_2]PF_6$
'$RuCl_3 \cdot xH_2O$' + PPh_3 (boiling MeOH, N_2)	⟶	$RuCl_2(PPh_3)_3$
'$RuCl_3 \cdot xH_2O$' + PPh_3 (cold MeOH, N_2)	⟶	$RuCl_2(PPh_3)_3 \cdot PPh_3$
'$RuCl_3 \cdot xH_2O$' + DMSO	⟶	$RuCl_2(DMSO)_4$
$RuCl_2(DMSO)_4$ + CO	⟶	$RuCl_2(CO)_2(DMSO)_2$
$RuCl_2(DMSO)_4$ + py	⟶	$RuCl_2(py)_4$
'$RuCl_3 \cdot xH_2O$' + RSC_2H_4SR (MeOH)	⟶	$RuCl_2(RSC_2H_4SR)_2$
'$RuCl_3 \cdot xH_2O$' + NH_3.aq + Zn	⟶	$[Ru(NH_3)_6]Cl_2$

Figure 3.1.1a Selected reactions of '$RuCl_3 \cdot xH_2O$' which involve a reduction from Ru(III) to Ru(II).

'RuCl$_3$·xH$_2$O' + Hacac	⟶	Ru(acac)$_3$
'RuCl$_3$·xH$_2$O' + HBr	⟶	[Ru$_2$Br$_9$]$^{3-}$
'RuCl$_3$·xH$_2$O' + bipy	⟶	Ru(bipy)$_3$
'RuCl$_3$·xH$_2$O' + HCl/KCl	⟶	K$_2$[RuCl$_5$(H$_2$O)]
K$_2$[RuCl$_5$(H$_2$O)] (vacuum, heat)	⟶	K$_3$[Ru$_2$Cl$_9$]
'RuCl$_3$·xH$_2$O' + SMe$_2$	⟶	RuCl$_3$(SMe$_2$)$_3$
'RuCl$_3$·xH$_2$O' + HCO$_2$H/HCl	⟶	[RuCl$_5$(CO)]$^{2-}$

Table 3.1.1b Selected reactions of 'RuCl$_3$·xH$_2$O' maintaining the oxidation state of the Ru(III).

The reaction of 'RuCl$_3$·xH$_2$O' with excess PPh$_3$ in refluxing MeOH[276,277], EtOH[278] or ^{i}PrOH[278] under an inert atmosphere of N$_2$ affords the red-brown compound RuCl$_2$(PPh$_3$)$_3$. The outcome of this reaction depends on the reaction conditions. For instance the reaction of PPh$_3$ with 'RuCl$_3$·xH$_2$O' at room temperature affords Ru(PPh$_3$)$_4$Cl$_2$[276,277], which is better formulated as Ru(PPh$_3$)$_3$Cl$_2$·PPh$_3$ with the fourth PPh$_3$ molecule trapped in the crystal lattice[279,280]. The dissociation pathways of Ru(PPh$_3$)$_3$Cl$_2$ are also very much dependent on the solvents used. Non-polar solvents favour loss of neutral PPh$_3$[276,279-281] whereas in contrast polar solvents favour the loss of Cl$^-$ and the generation of Ru(II) cations[276,279,281]. RuCl$_2$(PPh$_3$)$_3$ is moderately air sensitive while in solution and has to be prepared under an inert atmosphere of N$_2$.

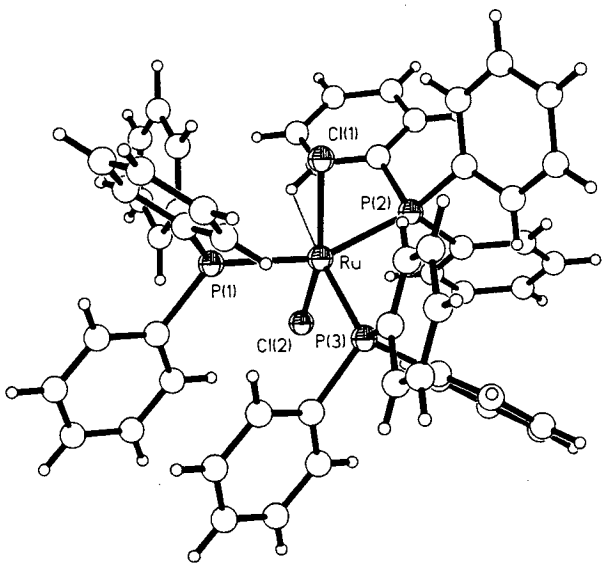

Figure 3.1.1a Single crystal structure of Ru(PPh$_3$)$_3$Cl$_2$[282].

The crystal structure of $Ru(PPh_3)_3Cl_2$ (**Figure 3.1.1a**) has been determined[282] and shows three PPh_3 ligands in *equatorial* and the two Cl-atoms in *apical* positions at the Ru(II) ion. The fourth equatorial binding site is blocked by one of the sterically demanding PPh_3 ligands and formally occupied by an *agostic* H-atom of one of the phenyl rings.

Another group of easily accessible starting compounds are Ru-arene or Ru-cyclopentadienyl complexes. The reaction of '$RuCl_3 \cdot xH_2O$' with 2 equivalents of PPh_3 and freshly distilled CpH under N_2 affords the neutral compound $RuCl(\eta^5\text{-}Cp)(PPh_3)_2$ [**Figure 3.1.1b** (i)][283,284,302]. The cyclopentadienyl-anion co-ordinates *facially* to the octahedral Ru(II) ion. The Cl^- ligand is easily displaced by neutral ligands giving cationic complexes which can be isolated in good yield in particular with large counterions[285,286]. Analogous Cp* complexes of Ru have been prepared[287].

The reaction of cyclohexadiene and its derivatives such as α-phellandrene[288,289] with '$RuCl_3 \cdot xH_2O$' affords neutral bis-chloro bridged Ru-dimers of the general stoichiometry $[(\eta^6\text{-arene})ClRu(\mu\text{-}Cl)_2RuCl(\eta^6\text{-arene})]$ [**Figure 3.1.1b** (ii)][288,290]. These compounds show an exchange of arene ligands at elevated temperatures thus providing an elegant pathway for the synthesis of not readily available Ru-arene complexes such as $[(\eta^6\text{-}C_6Me_6)ClRu(\mu\text{-}Cl)_2RuCl(\eta^6\text{-}C_6Me_6)]$[289]. It has to be emphasised, that these processes also occur under FAB mass spectrometry conditions in the presence of an aromatic matrix and the exchange of arene ligands by 3-NOBA has been observed (see section 3.2).

A substitution of Cl^- ligands by solvent molecules in analogy to Cp-complexes can be achieved by stirring a solution of $[RuCl_2(\eta6\text{-}C_6H_6)]_2$ in MeCN in the presence of $LiBF_4$, NH_4PF_6 or $KAsF_6$[291]. The reaction does not require an inert atmosphere and gives good yields of product in the range 80 to 90%. Two Cl^- ligands are substituted by MeCN molecules at each Ru(II) ion in this reaction leading to monomeric Ru(II) cations - $[RuCl(MeCN)_2(arene)]^+$ (**Figure 3.1.1b** (iii)). These compounds are particular good starting materials for monodentate or bidentate substitution reactions due to the labile monodentate solvent molecules.

(i)$RuCl(\eta^5\text{-}C_5H_5)(PPh_3)_2$

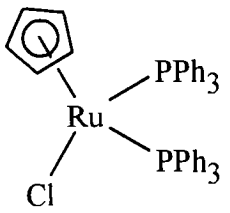

(ii) $[RuCl_2(\eta 6\text{-}C_6H_6)]_2$

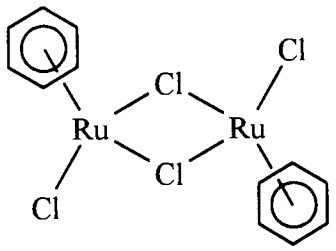

(iii)$[RuCl(\eta 6\text{-}C_6H_6)(MeCN)_2]PF_6$

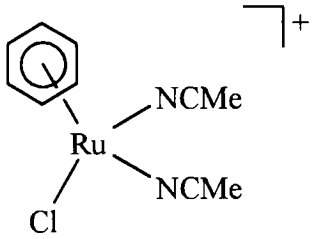

Figure 3.1.1b Structures of starting materials discussed in this section.

3.1.2 Ru Complexes with Homoleptic S-Donor Macrocycles

A wide range of Ru complexes containing homoleptic thioether macrocycles have been reported[42,44]. Research in Edinburgh has shown, that the reaction of $RuCl_2(PPh_3)_3$ with $[9]aneS_3$ affords the yellow complex $RuCl_2(PPh_3)([9]aneS_3)$[42,292]. The single crystal structure has recently been reported and confirms the octahedral Ru(II) ion to be *facially* co-ordinated to the $[9]aneS_3$ ligand [Ru-S = 2.270(2), 2.269(2), 2.356(2)Å], two Cl^- ions [Ru-Cl = 2.456(2), 2.449(2)Å] and the neutral phosphine ligand [Ru-P = 2.345(2)Å][293,294]. The reaction of $RuCl_2(PPh_3)([9]aneS_3)$ with TlPF6 in the presence of a donor ligand (L) has lead to a number of derivatives $RuCl(L)(PPh_3)([9]aneS_3)$ (L = MeCN, PhCN, py, PMe_2Ph, $P(OMe)_2Ph$)[292].

Numerous examples of complexes containing the $[Ru([9]aneS_3)]^{2+}$ fragment have been reported using the same synthetic strategy mentioned above. The reaction of $RuX_2(EPh_3)_3$ (X = Cl; E = P, As; X = Br; E = P) with $[9]aneS_3$ afforded $RuX_2(PPh_3)([9]aneS_3)$ which was than used in substitution reactions leading to species such as $[RuX(L)(EPh_3)([9]aneS_3)]PF_6$ (X = Cl; E = P, As; L = py, PMe_2Ph; X = Br; E = P; L= py, PMe_2Ph)[292]. The reaction of $RuCl_2(PPh_3)([9]aneS_3)$ with $TlPF_6$ in the absence of a donor ligand lead to the binuclear Ru(II) species $[Ru(PPh_3)([9]aneS_3)(\mu\text{-}Cl)]_2(PF_6)_2$ and $[Ru(PPh_3)([9]aneS_3)(\mu\text{-}Cl)_2Tl]_2(PF_6)_2$[295].

(i) space filling plot

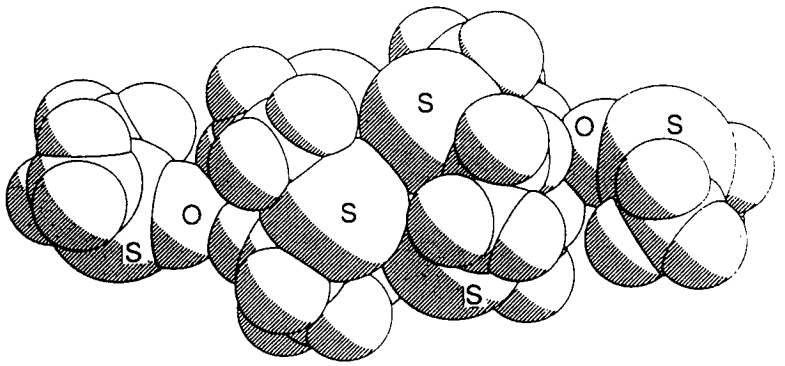

(ii) stick and ball plot

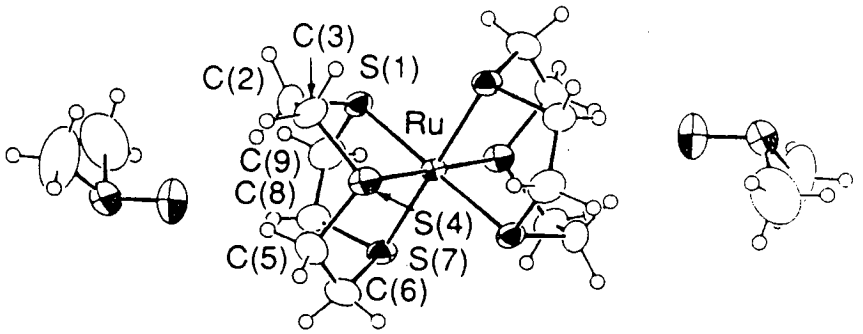

Figure 3.1.2a The single crystal structure of $[Ru([9]aneS_3)_2]^{2+}\cdot 2DMSO$.

The bis-$[9]aneS_3$ sandwich complex of Ru(II) has been prepared by the reaction of '$RuCl_3\cdot xH_2O$' with $[9]aneS_3$ in DMSO. The single crystal structure (**Figure 3.1.2**) shows an octahedral Ru(II) centre with two macrocyclic ligands co-ordinated to opposite faces of the octahedron. Two independent DMSO molecules were found to be present in the crystal lattice[296].

Other complexes of homoleptic thioether macrocycles containing Ru include *cis*-[RuCl(PPh$_3$)([12]aneS$_4$)]$^{+}$[42], *cis*-[RuCl(PPh$_3$)([14]aneS$_4$)]$^{+}$[293] and *cis*-[RuCl$_2$([14]aneS$_4$)][297]. [Ru([18]aneS$_6$)]$^{2+}$[42] has been prepared from 'RuCl$_3$·xH$_2$O' and [18]aneS$_6$ in DMF/MeOH. The single crystal structure shows a *meso*-configuration with a hexadentate binding mode at Ru(II) [Ru-S = 2.3222(23), 2.3326(25), 2.3373(23)Å] (**Figure 3.1.2b**). The analogous complex [Ru([20]aneS$_6$)]$^{2+}$ has been reported[298]. Treatment of 'RuCl$_3$·xH$_2$O' with [14]aneS$_4$ in EtOH affords RuCl$_3$([14]aneS$_4$) which is proposed to involve tridentate [14]aneS$_4$[299]. Reaction of [RuCl$_2$(arene)]$_2$ with [18]aneS$_6$ affords the binuclear complex [Ru$_2$Cl$_2$(arene)$_2$([18]aneS$_6$)]$^{2+}$ in which [18]aneS$_6$ bridges the two Ru atoms adopting a bidentate co-ordination mode[223,300,301].

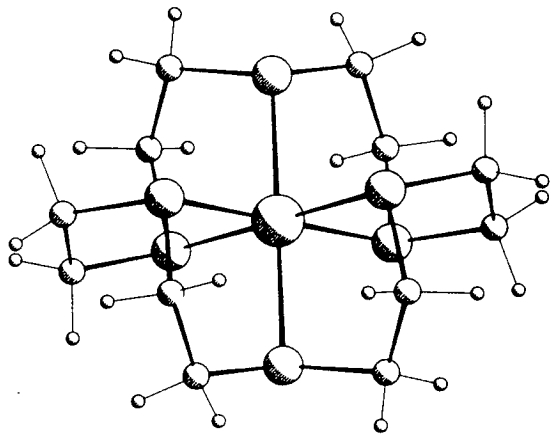

Figure 3.1.2b Single crystal structure of [Ru([18]aneS$_6$)]$^{2+}$.

3.1.3 Ru(II) Complexes with Mixed O/S-Donor Ionophores

Complexes between Ru(II) and [15]aneS$_2$O$_3$ have been prepared by the reaction of (RuCl$_2$(p-arene))$_2$ (arene = C$_6$H$_6$, p-cymene, C$_6$Me$_6$)[223] and RuCl$_2$(PPh$_3$)$_3$[224,225] with [15]aneS$_2$O$_3$. The reaction of [15]aneS$_2$O$_3$ with [RuCl$_2$(arene)]$_2$ (arene = C$_6$H$_6$, p-cymene, C$_6$Me$_6$) in MeOH afforded after addition of NaBPh$_4$ the orange microcrystalline products [RuCl(arene)([15]aneS$_2$O$_3$)]BPh$_4$ in good yield[223].

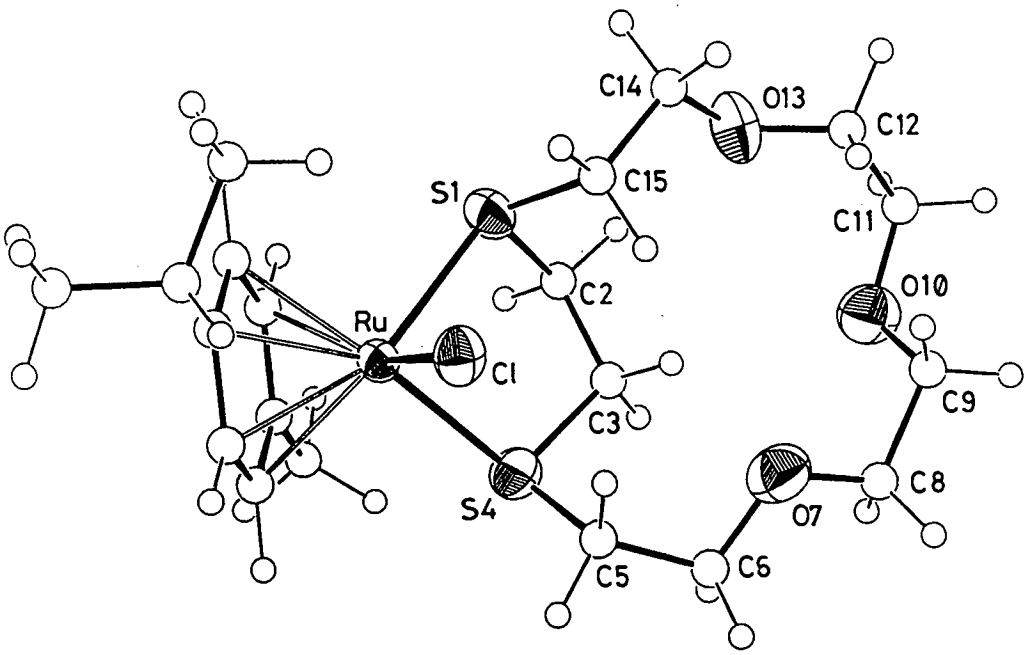

Figure 3.1.3a The single crystal structure of $[RuCl(p\text{-cymene})([15]aneS_2O_3)]^+$.

The single crystal structure of $[RuCl(p\text{-cymene})([15]aneS_2O_3)]^+$ (**Figure 3.1.3a**) shows that the macrocycle adopts a bidentate chelating co-ordination mode. The two S-atoms bind symmetrical *exo*-dentate to the Ru(II) ion [Ru-S = 2.3810(11) and 2.3773(11)Å] which causes the ethylene chain between them to bend away and to occupy most of the cavity. The author points out that the Cl^- ligand in this complex can easily be removed using $TlPF_6$. This is not surprising considering the ease of Cl^- abstraction in Ru-arene complexes using NH_4PF_6 (see above).

trans-$[RuCl(PPh_3)([15]aneS_2O_3)_2]PF_6$ has been prepared by the reaction of $[15]aneS_2O_3$ with $RuCl_2(PPh_3)_3$[224,225]. The single crystal structure (**Figure 3.1.3b**) illustrates that both macrocyclic ligands adopt the same symmetrical chelating binding mode as for instance in $[RuCl(p\text{-cymene})([15]aneS_2O_3)]^+$ [Ru-S = 2.394(3), 2.395(3), 2.390(3) and 2.405(3)Å]. The Cl^- and PPh_3 ligands adopt a *trans*-configuration [Ru-Cl = 2.458(3)Å; Ru-P = 2.319(3)Å] to each other in this structure.

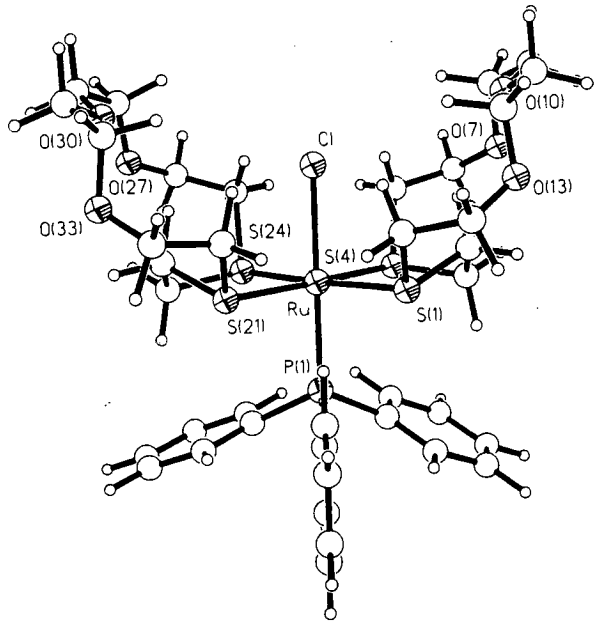

Figure 3.1.3b The single crystal structure of $[RuCl(PPh_3)([15]aneS_2O_3)_2]^+$.

However, the presence of a mixture of *cis*- and *trans*-isomers in the bulk material can not be ruled out. The interesting feature in this compound is the interaction between the flexible macrocycles and the sterically demanding PPh_3 ligand. The macrocycles bend away from the phenyl rings of the PPh_3 ligand forming a partial cavity around the Cl^- ion. The fully reversible Ru(II)/Ru(III) redox couple has been found to lie at $E_{1/2}$ = +0.85V. Addition of Na^+ ions did not exhibit any effect on the electrochemistry. The authors conclude that the positive charge of the complex does not attract a guest cation and that the co-ordinative properties of the macrocyclic ligands are diminished by the presence of the Cl-atom inside the cavity.

It was our aim to investigate the fundamental co-ordination chemistry of $[18]aneS_2O_4$ with Ru(II). We were particular interested to determine whether some of these compounds could be used in the development of chemical sensors. Our general idea of a chemical sensor consists of a receptor site and a responsive centre. The receptor site is formed by the hard polyether binding site in the macrocyclic ligand which should be easily accessible for guest ions or molecules. The responsive centre is the Ru(II) ion. A response can either be a shift of a redox potential or a colour change. We proposed therefore to investigate the electrochemical behaviour and the geometry of complexes prepared using a range of spectroscopic and crystallographic techniques.

3.2 RESULTS AND DISCUSSION

3.2.1 Preparation of Ru(II) Starting Materials

A range of compounds (**Table 3.2.1**) suitable as starting materials were prepared according to literature methods. Experimental data for these complexes can be found in the literature cited and are therefore excluded from this thesis but analytical data of the compounds prepared are included in the experimental section (**3.4**).

Compound:	**Reference:**
$Ru(PPh_3)_3Cl_2$	277
$Ru(\eta^5\text{-}C_5H_5)(PPh_3)_2Cl$	284
$Ru_2(\eta^6\text{-}MeC_6H_4i\text{-}Pr)_2Cl_4$	289
$Ru_2(\eta^6\text{-}C_6H_6)_2Cl_4$	288
$[Ru(\eta^6\text{-}C_6H_6)(MeCN)_2Cl](PF_6)_2$	291

Table 3.2.1 Ru(II) starting compounds prepared in the course of this work.

3.2.2 The Synthesis of $[RuCl(PPh_3)([15]aneS_2O_3)_2]PF_6$

$[RuCl(PPh_3)([15]aneS_2O_3)_2]PF_6$ was prepared according to the method reported by Schröder and co-workers[224,225]. The Ru(II) ion in this complex co-ordinates to two bidentate macrocyclic ligands ($[15]aneS_2O_3$) and two different monodentate ligands (Cl^- and PPh_3). This environment allows the Ru(II) ion to adopt formally three different stereochemistries. A *meso* form consists of the two monodentate ligands co-ordinated *trans* to each other whereas in contrast a *cis* configuration leads to two enantiomers. The single crystal structure of $[RuCl(PPh_3)([15]aneS_2O_3)_2]PF_6$ (**Figure 3.1.3b**)[224,225] shows close resemblance to the *meso* form. We were therefore particularly interested to establish whether the bulk material of the complex contains more than one geometric isomer or not. The ^{31}P-NMR spectrum of $[RuCl(PPh_3)([15]aneS_2O_3)_2]PF_6$ shows indeed two ^{31}P resonances [δ 40.66 and δ 25.89] which were assigned to the two geometric isomers.

3.2.3 The Synthesis of $RuCl_2(PPh_3)_2([15]aneS_2O_3)$

The reaction of $RuCl_2(PPh_3)_3$ with one molar equivalent of $[15]aneS_2O_3$ in MeOH afforded the neutral complex $RuCl_2(PPh_3)_2([15]aneS_2O_3)$. Characterisation of this material was difficult due to solubility problems. The FAB mass spectrum on the other hand shows a range of peaks with the correct isotopic distribution in particular the molecular ion $[^{102}Ru(PPh_3)_2([15]aneS_2O_3)^{35}Cl_2]^+$. The following fragments $[^{102}Ru(PPh_3)_2([15]aneS_2O_3)]^+$ and $[^{102}Ru(PPh_3)([15]aneS_2O_3)^{35}Cl]^+$ were also observed. The ^1H-, ^{13}C- and ^{31}P-NMR spectra in $CDCl_3$ are inconsistent with the presence of a single species in solution. The ^{31}P-NMR spectrum shows at least four different peaks (-4.74, 27.34, 55.80 and 62.92 ppm) of which two were assigned to free PPh_3 (-4.74 ppm) and $[Ru(PPh_3)_2([15]aneS_2O_3)Cl_2]$ (27.34 ppm). The $CDCl_3$ solution of the initial red compound $[Ru(PPh_3)_2([15]aneS_2O_3)Cl_2]$ changed its colour slowly from orange to brown suggesting a reaction in solution. It was impossible to investigate this reaction and to characterise the reaction products in the course of this work. Single crystals could be obtained from the $CDCl_3$ solution and a structure determination is pending.

3.2.4 The Single Crystal Structure of $RuCl_2(PPh_3)_2([15]aneS_2O_3)$

The single crystal structure of $RuCl_2(PPh_3)_2([15]aneS_2O_3)$ (**Figure 3.2.4**) shows the two PPh_3-groups in a *cis* configuration to each other whereas the Cl^- ligands retain *apical* positions as in $RuCl_2(PPh_3)_3$. The macrocycle $[15]aneS_2O_3$ adopts the typical bidentate chelating binding mode found also in $[RuCl(PPh_3)([15]aneS_2O_3)_2]^+$[224,225]. The Ru(II) centre adopts a distorted octahedral environment. The P(1)-Ru-P(2) angle [98.39(5)°] is larger than 90° whereas in contrast the Cl(1)-Ru-Cl(2) [170.48(5)] and S(1)-Ru-S(4) [84.25(5)] angles are smaller than expected in an ideal octahedron.

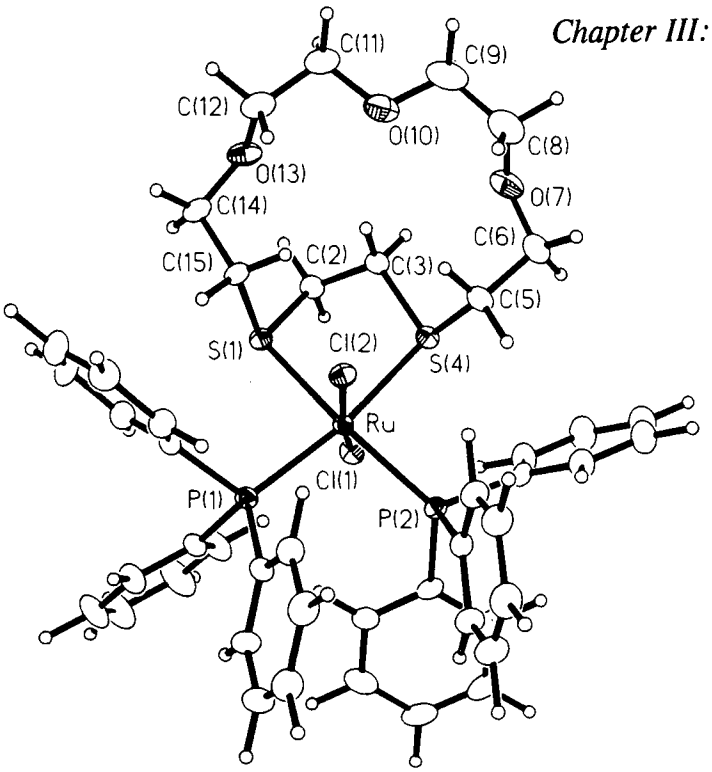

Figure 3.2.4 The single crystal structure of $RuCl_2(PPh_3)_2([15]aneS_2O_3)$.

Ru-Cl(1)	2.4447(15)	Ru-Cl(2)	2.4154(15)
Ru-S(1)	2.4085(15)	Ru-S(4)	2.4215(16)
Ru-P(1)	2.3775(16)	Ru-P(2)	2.3640(15)
P(1)-C(1A1)	1.857(4)	P(2)-C(2A1)	1.850(4)
P(1)-C(1B1)	1.858(4)	P(2)-C(2B1)	1.851(4)
P(1)-C(1C1)	1.875(4)	P(2)-C(2C1)	1.859(4)
Cl(1)-Ru-Cl(2)	170.48(5)	S(1)-Ru-S(4)	84.25(5)
P(1)-Ru-P(2)	98.39(5)		
S(1)-Ru-P(2)	170.13(6)	S(1)-Ru-P(1)	87.60(5)
S(4)-Ru-P(2)	90.06(5)	S(4)-Ru-P(1)	171.41(6)
Cl(1)-Ru-S(1)	84.37(5)	Cl(2)-Ru-S(1)	91.72(5)
Cl(1)-Ru-S(4)	80.88(5)	Cl(2)-Ru-S(4)	90.10(5)
Cl(1)-Ru-P(1)	101.04(5)	Cl(2)-Ru-P(1)	87.43(5)
Cl(1)-Ru-P(2)	86.78(5)	Cl(2)-Ru-P(2)	96.35(5)
Ru-S(1)-C(2)	102.53(19)	Ru-S(4)-C(3)	105.68(20)
Ru-S(1)-C(15)	111.40(19)	Ru-S(4)-C(5)	113.05(22)
S(1)-C(2)-C(3)-S(4)	-57.2(5)	C(9)-O(10)-C(11)-C(12)	-176.9(6)
C(2)-C(3)-S(4)-C(5)	-152.6(4)	O(10)-C(11)-C(12)-O(13)	-74.7(7)
C(3)-S(4)-C(5)-C(6)	-71.7(5)	C(11)-C(12)-O(13)-C(14)	163.5(5)
S(4)-C(5)-C(6)-O(7)	73.9(6)	C(12)-O(13)-C(14)-C(15)	-84.1(6)
C(5)-C(6)-O(7)-C(8)	91.6(7)	O(13)-C(14)-C(15)-S(1)	-95.2(5)
C(6)-O(7)-C(8)-C(9)	-153.5(6)	C(14)-C(15)-S(1)-C(2)	59.3(5)
O(7)-C(8)-C(9)-O(10)	71.2(8)	C(15)-S(1)-C(2)-C(3)	65.2(5)
C(8)-C(9)-O(10)-C(11)	170.0(6)		

Table 3.2.4 Selected bond lengths (Å), angles (°) and torsion angles (°) with estimated standard deviations for $RuCl_2(PPh_3)_2([15]aneS_2O_3)$.

3.2.5 The Synthesis of $[Ru([18]aneS_2O_4)_3](PF_6)_2$

$[Ru([18]aneS_2O_4)_3]^{2+}$ was prepared directly from '$RuCl_3 \cdot xH_2O$' with $[18]aneS_2O_4$ in the presence of $K_2(C_2O_4)$ as a reducing agent. The colour of the reaction mixture changed from initial brown to blue and to green (blue plus yellow) to yellow. Excess of NH_4PF_6 and evaporation of the solvent afforded yellow/green crystalline material. The mixture of yellow and colourless crystals could not be separated even after numerous recrystallisations. Characterisation was therefore limited to FAB mass spectrometry which showed two fragments assigned to $[^{101}Ru([18]aneS_2O_4)_3(PF_6)]^+$ and $[^{101}Ru([18]aneS_2O_4)_2]^+$ with the correct isotopic distribution Problems in reproducing these results indicate the need to convert commercially available '$RuCl_3 \cdot xH_2O$' into complexes of well defined stoichiometry which can be used as starting points into the co-ordination chemistry of Ru(II) and Ru(III).

3.2.6 The Single Crystal Structure of $[Ru([18]aneS_2O_4)_3](PF_6)_2$

A yellow crystal was selected for single crystal X-ray diffraction studies. The single crystal structure of $[Ru([18]aneS_2O_4)_3](PF_6)_2$ (**Figure 3.2.6a**) shows a highly symmetrical dication. Each macrocyclic ligand binds with its two thioether S-donors to the Ru(II) centre [Ru-S 2.3864(13) and 2.3622(11)] in a slightly distorted octahedral co-ordination geometry. The packing diagram (**Figure 3.2.6b**) shows additional solvent molecules (MeOH and H_2O) trapped in the crystal lattice. The solvent molecules lie in special positions above and below each Ru(II) ion and are due to the high symmetry disordered. No relationship between solvent molecules and anions or cations could be identified. It has therefore to be assumed that the solvent molecules occupy small empty cages in the crystal lattice.

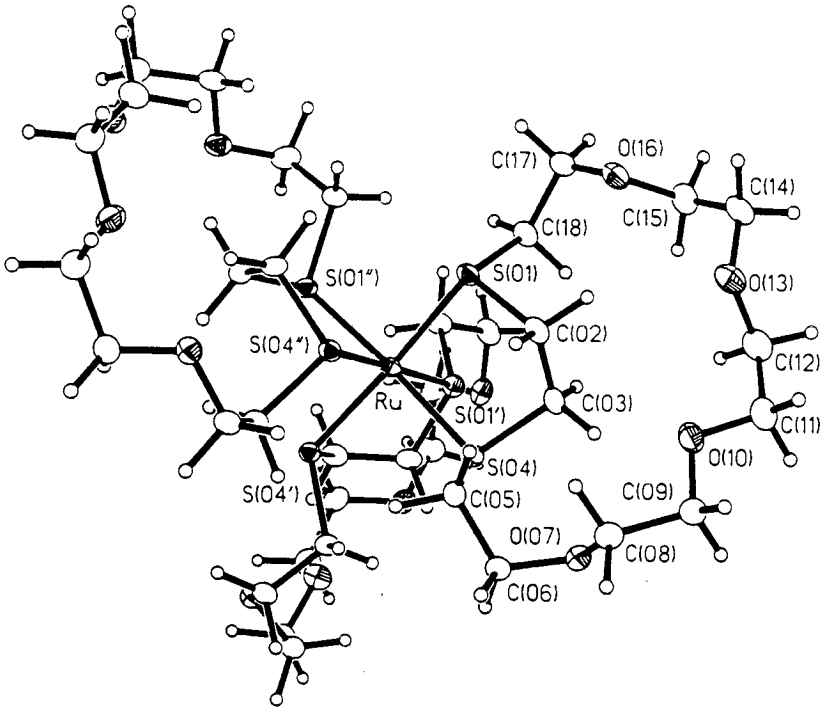

Figure 3.2.6a The single crystal structure of $[Ru([18]aneS_2O_4)_3](PF_6)_2$.

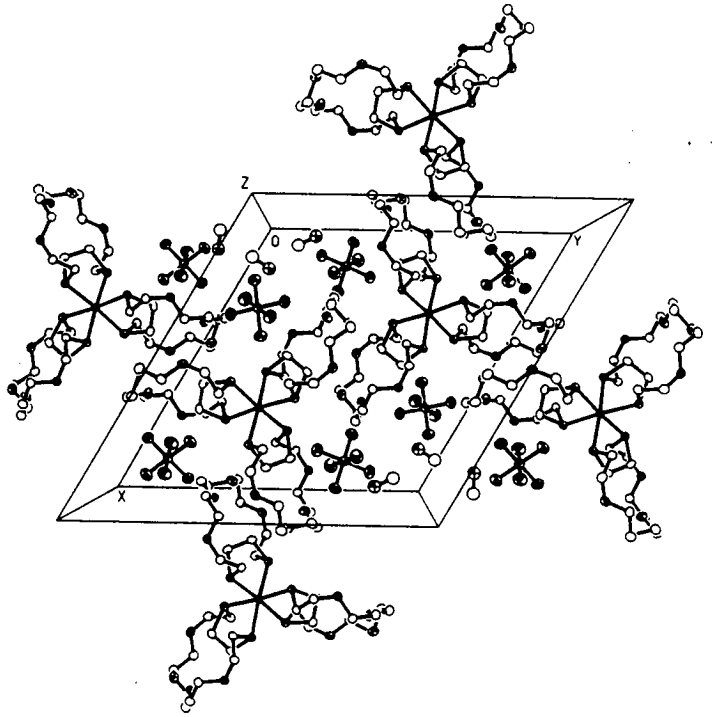

Figure 3.2.6b The packing diagram of $[Ru([18]aneS_2O_4)_3](PF_6)_2$.

Ru-S(1)	2.3864(13)	Ru-S(4)	2.3622(11)
S(1)-Ru-S(4)	87.25(4)	S(1)-Ru-S(1')	96.94(3)
S(1)-Ru-S(4')	175.65(3)	S(4)-Ru-S(4')	94.57(3)
S(1)-Ru-S(4'')	81.33(3)		
Ru-S(1)-C(2)	102.39(16)	Ru-S(4)-C(3)	102.29(16)
Ru-S(1)-C(18)	115.62(17)	Ru-S(4)-C(5)	113.93(15)
S(1)-C(2)-C(3)-C(4)	-57.5(4)	O(10)-C(11)-C(12)-O(13)	66.1(6)
C(2)-C(3)-S(4)-C(5)	-72.6(4)	C(11)-C(12)-O(13)-C(14)	165.9(4)
C(3)-S(4)-C(5)-C(6)	-86.4(3)	C(12)-O(13)-C(14)-C(15)	79.9(6)
S(4)-C(5)-C(6)-O(7)	65.4(4)	O(13)-C(14)-C(15)-O(16)	74.2(5)
C(5)-C(6)-O(7)-C(8)	84.2(5)	C(14)-C(15)-O(16)-C(17)	179.1(4)
C(6)-O(7)-C(8)-C(9)	-170.0(4)	C(15)-O(16)-C(17)-C(18)	83.5(5)
O(7)-C(8)-C(9)-O(10)	73.6(5)	O(16)-C(17)-C(18)-S(1)	66.3(5)
C(8)-C(9)-O(10)-C(11)	-175.7(4)	C(17)-C(18)-S(1)-C(2)	-83.4(4)
C(9)-O(10)-C(11)-C(12)	173.3(4)	C(18)-S(1)-C(2)-C(3)	-80.6(4)

Table 3.2.6 Selected bond lengths(Å), angles (°) and torsion angles (°) with estimated standard deviations for $[Ru([18]aneS_2O_4)_3](PF_6)_2$.

3.2.7 The Synthesis of $[RuCl(PPh_3)([18]aneS_2O_4)_2]PF_6$

$[RuCl(PPh_3)([18]aneS_2O_4)_2]PF_6$ has been prepared by the same route as the $[15]aneS_2O_3$ derivative. The aim in preparing this compound was to investigate the trends identified for $[RuCl(PPh_3)([15]aneS_2O_3)_2]PF_6$ in particular considering the effects of sterically demanding ligands on the conformation of the macrocycles. $[RuCl(PPh_3)([18]aneS_2O_4)_2]PF_6$ was prepared from $RuCl_2(PPh_3)_3$ and $[18]aneS_2O_4$ (1:2 ratio) in refluxing $MeOH/H_2O$ (1:1 v/v) under an inert atmosphere of N_2. It was isolated as a bright yellow microcrystalline powder after addition of NH_4PF_6 to the methanolic solution. Recrystallisation was achieved employing a vapour diffusion technique using EtOH and CH_2Cl_2.

Microanalytical and spectroscopic results are in good agreement with the stoichiometry mentioned above. The FAB mass spectrum shows a peak assigned to the molecular ion $\{[^{101}Ru^{35}Cl(PPh_3)([18]aneS_2O_4)_2]^+\}$ with the correct isotopic distribution at m/z = 991. A series of other fragments were identified, for instance the intensive peak at m/z = 729 assigned to $[^{101}Ru^{35}Cl([18]aneS_2O_4)_2]^+$. The ^{31}P-NMR spectrum shows in analogy to $[RuCl(PPh_3)([15]aneS_2O_3)_2]^+$ two signals (42.9 ppm and 32.2 ppm) assigned to the *cis* and *trans* isomer with respect to the positions of the PPh_3 and Cl^- ligand. The quasi-reversible Ru(II)/Ru(III) redox couple was found to lie at $E_{1/2}$ = +0.837V vs Fc/Fc^+ which is very similar to the fully reversible redox couple for $[RuCl(PPh_3)([15]aneS_2O_3)_2]PF_6$ ($E_{1/2}$ = +0.85V vs Fc/Fc^+)[225].

3.2.8 The Single Crystal Structure of $[RuCl(PPh_3)([18]aneS_2O_4)_2]PF_6$

The single crystal structure of $[RuCl(PPh_3)([18]aneS_2O_4)_2]PF_6$ (**Figure 3.2.8a**) shows in contrast to the *trans* isomer found for the $[15]aneS_2O_3$ derivative the Cl- and PPh_3- ligand *cis* to each other. The structure could therefore be described as a derivative of $[Ru([18]aneS_2O_4)_3]^{2+}$ with one macrocyclic ligand substituted by the two monodentate ligands Cl^- and PPh_3. The Ru(II) centre lies as expected in a slightly distorted octahedral environment. The conformation of either macrocycle is not very well defined. Both macrocycles are affected by disorder and there is no indication for the pre-formation of a host cavity. The packing diagram (**Figure 3.2.8b**) does not give any further indication whether the compound would be able to accommodate guest ions or not.

Ru-Cl(1)	2.441(6)	Ru-P(1)	2.340(5)
Ru-S(1)	2.387(5)	Ru-S(1')	2.348(6)
Ru-S(4)	2.389(6)	Ru-S(4')	2.438(6)
S(1)-Ru-S(4)	84.94(20)	S(1')-Ru-S(4')	86.95(22)
S(1)-Ru-Cl(1)	178.45(21)	S(1')-Ru-Cl(1)	82.94(22)
S(4)-Ru-Cl(1)	94.54(21)	S(4')-Ru-Cl(1)	88.06(22)
S(1)-Ru-P(1)	92.98(19)	S(1')-Ru-P(1)	90.88(21)
S(4)-Ru-P(1)	88.35(20)	S(4')-Ru-P(1)	176.10(22)
Cl(1)-Ru-P(1)	88.47(20)		
1.Macrocycle			
S(1)-C(2)-C(3)-C(4)	-59.9(16)	O(10)-C(11)-C(12)-O(13)	-87.0(37)
C(2)-C(3)-S(4)-C(5)	162.4(14)	C(11)-C(12)-O(13)-C(14)	-73.1(40)
C(3)-S(4)-C(5)-C(6)	77.2(19)	C(12)-O(13)-C(14)-C(15)	-155.5(28)
S(4)-C(5)-C(6)-O(7)	-67.4(23)	O(13)-C(14)-C(15)-O(16)	-73.7(24)
C(5)-C(6)-O(7)-C(8)	163.1(24)	C(14)-C(15)-O(16)-C(17)	169.6(18)
C(6)-O(7)-C(8)-C(9)	178.9(31)	C(15)-O(16)-C(17)-C(18)	-172.6(16)
O(7)-C(8)-C(9)-O(10)	48.0(43)	O(16)-C(17)-C(18)-S(1)	87.1(16)
C(8)-C(9)-O(10)-C(11)	89.6(28)	C(17)-C(18)-S(1)-C(2)	-50.8(16)
C(9)-O(10)-C(11)-C(12)	-157.3(33)	C(18)-S(1)-C(2)-C(3)	-77.0(15)
2.Macrocycle			
S(1')-C(2')-C(3')-C(4')	55.7(21)	O(10')-C(11')-C(12')-O(13')	55.4(49)
C(2')-C(3')-S(4')-C(5')	75.8(20)	C(11')-C(12')-O(13')-C(14')	170.6(43)
C(3')-S(4')-C(5')-C(6')	73.7(27)	C(12')-O(13')-C(14')-C(15')	-163.6(36)
S(4')-C(5')-C(6')-O(7')	-56.2(39)	O(13')-C(14')-C(15')-O(16')	-74.2(45)
C(5')-C(6')-O(7')-C(8')	-94.0(33)	C(14')-C(15')-O(16')-C(17')	174.0(31)
C(6')-O(7')-C(8')-C(9')	179.9(27)	C(15')-O(16')-C(17')-C(18')	-98.5(28)
O(7')-C(8')-C(9')-O(10')	-80.1(30)	O(16')-C(17')-C(18')-S(1')	-57.7(26)
C(8')-C(9')-O(10')-C(11')	158.3(29)	C(17')-C(18')-S(1')-C(2')	-50.8(16)
C(9')-O(10')-C(11')-C(12')	158.9(30)	C(18')-S(1')-C(2')-C(3')	-77.0(15)

Table 3.2.8 Selected bond lengths (Å), angles (°) and torsion angles (°) with estimated standard deviations for $[RuCl(PPh_3)([18]aneS_2O_4)_2]PF_6$.

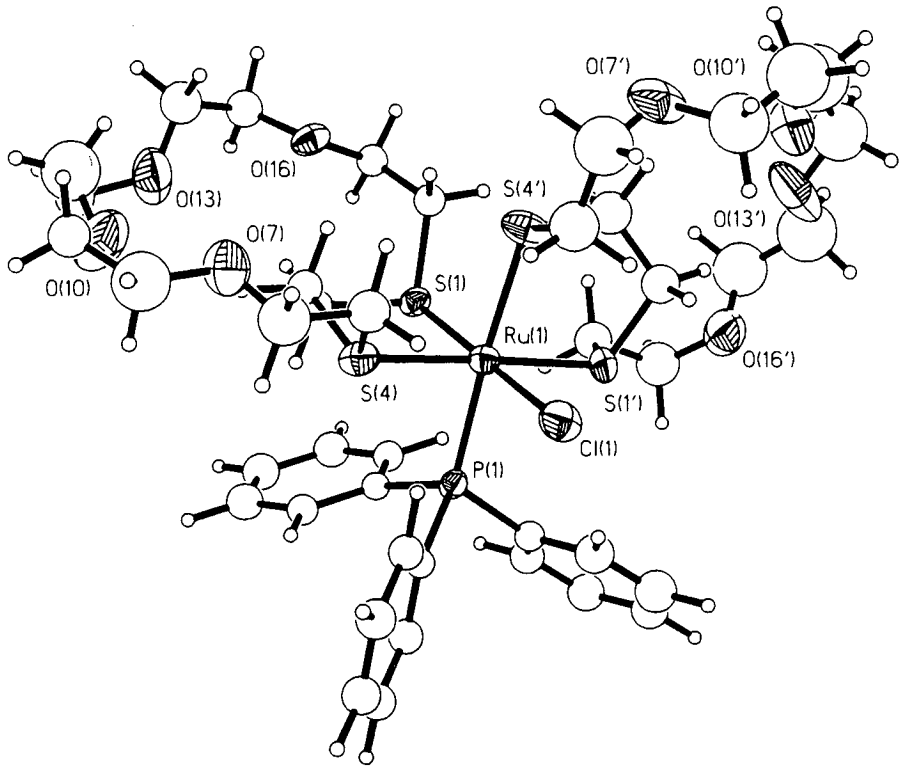

Figure 3.2.8a The single crystal structure of $[RuCl(PPh_3)([18]aneS_2O_4)_2]PF_6$.

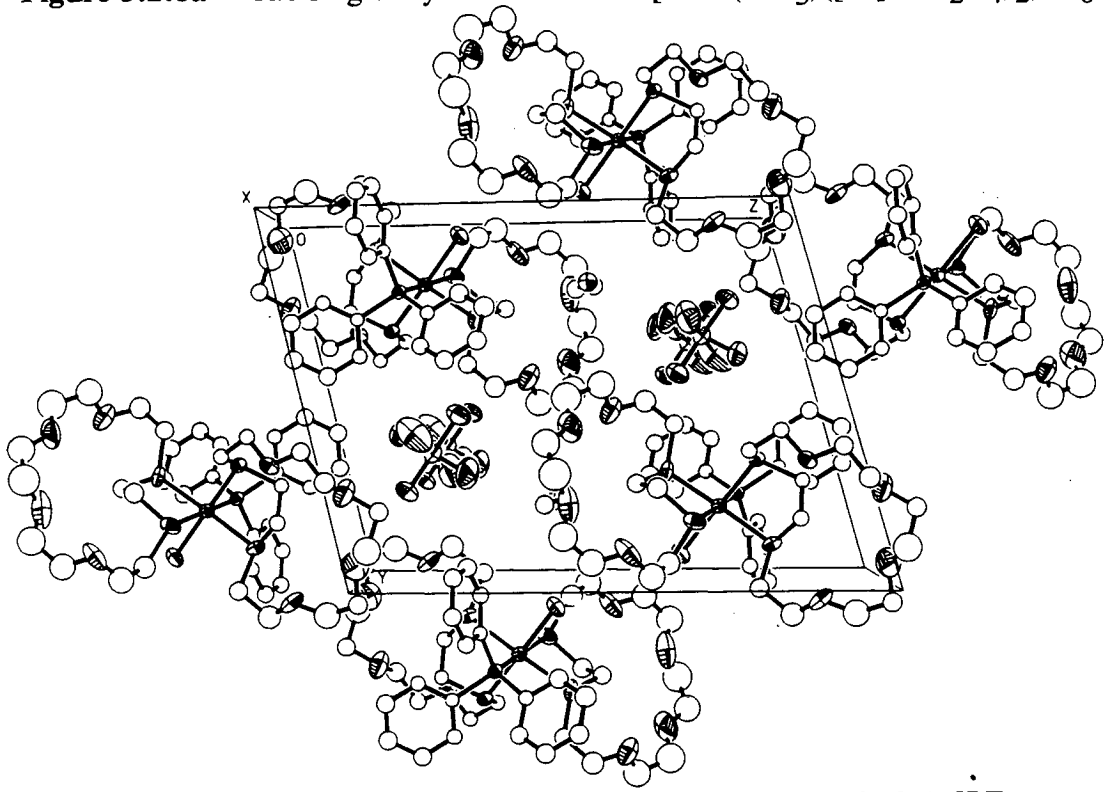

Figure 3.2.8b The packing diagram of $[RuCl(PPh_3)([18]aneS_2O_4)_2]PF_6$.

3.2.9 The Synthesis of $[Ru(\eta^5\text{-}C_5H_5)(PPh_3)([18]aneS_2O_4)]PF_6$

The reaction of $RuCl(\eta^5\text{-}C_5H_5)(PPh_3)_2$ with $[18]aneS_2O_4$ in boiling MeOH under N_2 afforded the complex $[Ru(\eta^5\text{-}C_5H_5)(PPh_3)([18]aneS_2O_4)]PF_6$ in good yield. The stoichiometry was confirmed by microanalysis and FAB mass spectrometry. The molecular ion $[^{101}Ru(\eta^5\text{-}C_5H_5)(PPh_3)([18]aneS_2O_4)]^+$ was found at m/z = 725 with the correct isotopic distribution. The ^{1}H-NMR spectrum shows resonances assigned to the macrocyclic framework in a badly resolved region from 2.75 to 4.10 ppm. The cyclopentadienyl protons were found at 4.53 and the phenyl protons at 7.40 ppm. The absorption maximum in the UV/vis spectrum lies at 364 nm (ε = 2700 dm^3 mol^{-1} cm^{-1}). A quasi reversible Ru(II)/Ru(III) redox couple was found at +0.57V vs Fc/Fc^+.

3.2.10 The Single Crystal Structure of $[Ru(\eta^5\text{-}C_5H_5)(PPh_3)([18]aneS_2O_4)]PF_6$

Single crystals suitable for X-ray diffraction studies were obtained by allowing CH_2Cl_2 vapour to diffuse into a solution of $[Ru(\eta^5\text{-}C_5H_5)(PPh_3)([18]aneS_2O_4)]PF_6$ in EtOH. The single crystal structure of $[Ru(\eta^5\text{-}C_5H_5)(PPh_3)([18]aneS_2O_4)]PF_6$ (**Figure 3.2.10a**) shows the cyclopentadienyl anion *facially* co-ordinated to the Ru(II) ion and the macrocyclic ligand $[18]aneS_2O_4$ adopts the usual bidentate co-ordination mode [Ru-S 2.3793(17) and 2.3587(19)Å]. The ethylene bridge between both *exo* oriented S-donors occupies part of the macrocyclic cavity. An interesting feature concerns the orientation of the O-atoms. The solid state structure of the free macrocycle exhibits an up down up down pattern with respect to the orientation of the O-atoms. In contrast $[Ru(\eta^5\text{-}C_5H_5)(PPh_3)([18]aneS_2O_4)]PF_6$ shows all O-atom pointing more or less in the same direction with respect to the macrocyclic best fit plane. The packing diagram (**Figure 3.2.10b**) does not reveal any reason for this behaviour. It shows nevertheless all molecules in a stacking arrangement with phenyl rings of neighbouring molecules co-planar. It is therefore likely that π-stacking contributes to some degree to the packing in the crystal lattice.

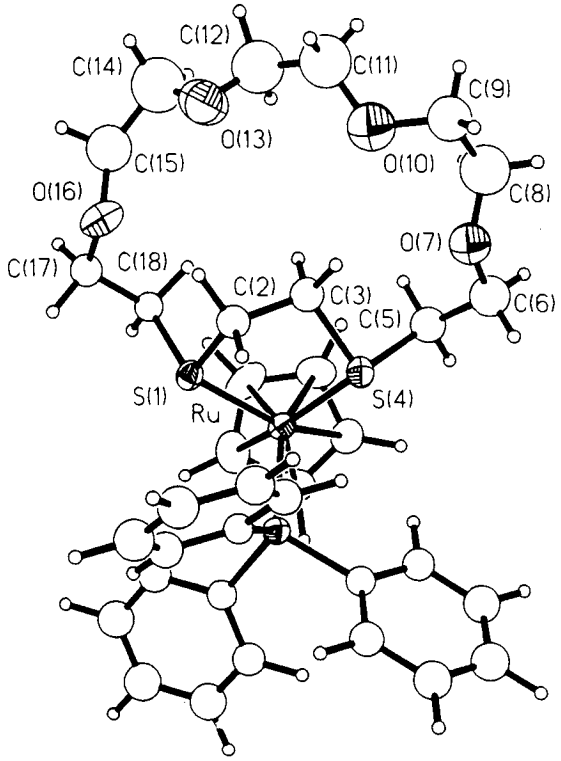

Figure 3.2.10a The single crystal structure of $[Ru(\eta^5\text{-}C_5H_5)(PPh_3)([18]aneS_2O_4)]PF_6$.

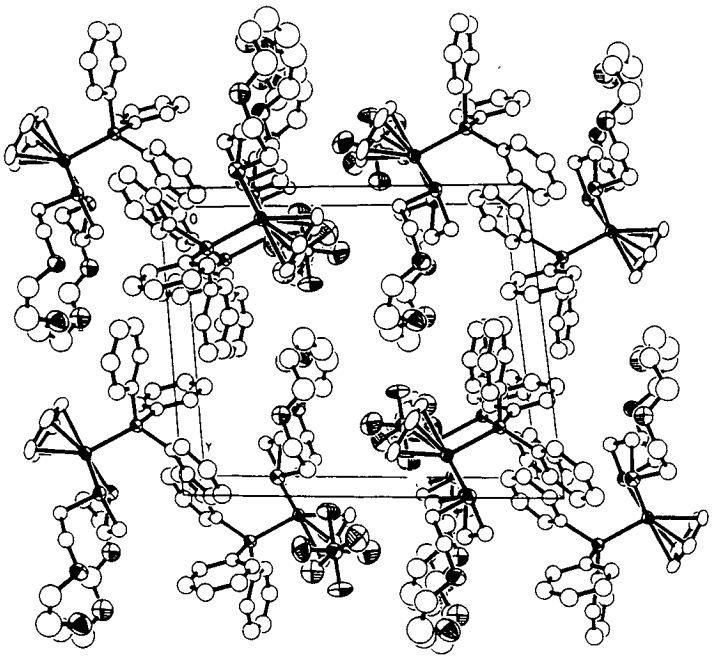

Figure 3.2.10b The packing diagram of $[Ru(\eta^5\text{-}C_5H_5)(PPh_3)([18]aneS_2O_4)]PF_6$.

Ru-C(1CP)	2.206(4)	P(1)-C(1A)	1.833(4)
Ru-C(2CP)	2.186(4)	P(1)-C(1B)	1.841(4)
Ru-C(3CP)	2.203(4)	P(1)-C(1C)	1.840(4)
Ru-C(4CP)	2.235(4)	Ru-S(1)	2.3793(17)
Ru-C(5CP)	2.236(4)	Ru-S(4)	2.3587(19)
Ru-P(1)	2.3126(17)		
S(1)-Ru-S(4)	84.40(6)		
S(1)-Ru-P(1)	90.02(6)	S(4)-Ru-P(1)	92.07(6)
C(18)-S(1)-Ru	106.08(22)	C(3)-S(4)-Ru	102.08(23)
C(2)-S(1)-Ru	109.20(21)	C(5)-S(4)-Ru	110.1(3)
S(1)-C(2)-C(3)-C(4)	55.4(5)	O(10)-C(11)-C(12)-O(13)	-71.6(12)
C(2)-C(3)-S(4)-C(5)	-166.4(5)	C(11)-C(12)-O(13)-C(14)	-173.6(9)
C(3)-S(4)-C(5)-C(6)	-81.5(6)	C(12)-O(13)-C(14)-C(15)	-141.4(9)
S(4)-C(5)-C(6)-O(7)	60.4(8)	O(13)-C(14)-C(15)-O(16)	-0.9(14)
C(5)-C(6)-O(7)-C(8)	102.0(8)	C(14)-C(15)-O(16)-C(17)	146.7(9)
C(6)-O(7)-C(8)-C(9)	-172.1(7)	C(15)-O(16)-C(17)-C(18)	-91.3(7)
O(7)-C(8)-C(9)-O(10)	59.2(11)	O(16)-C(17)-C(18)-S(1)	-76.0(6)
C(8)-C(9)-O(10)-C(11)	120.6(10)	C(17)-C(18)-S(1)-C(2)	70.6(5)
C(9)-O(10)-C(11)-C(12)	-135.4(10)	C(18)-S(1)-C(2)-C(3)	84.4(5)

Table 3.2.10 Selected bond lengths (Å), angles (°) and torsion angles (°) with estimated standard deviations for $[Ru(\eta^5\text{-}C_5H_5)(PPh_3)([18]aneS_2O_4)]PF_6$.

3.2.11 The Synthesis of $[RuCl(\eta^6\text{-}C_6H_6)([18]aneS_2O_4)]X$ (X = PF_6, BPh_4)

The reaction of $[RuCl(C_6H_6)(CH_3CN)_2]PF_6$ with $[18]aneS_2O_4$ afforded the bright orange cation $[RuCl(\eta^6\text{-}C_6H_6)([18]aneS_2O_4)]PF_6$ in good yield. Isolation of the BPh_4^- salt was achieved using $NaBPh_4$. The two compounds were isolated as orange crystals of high purity. Microanalytical and spectroscopic results are in good agreement with each stoichiometry. The ^{13}C-NMR spectra show one peak for the C_6H_6 ligand at 87.6 ppm. Twelve resonances (4 SCH_2 and 8 OCH_2) have been assigned to the macrocyclic framework. The cyclic voltammogram of $[RuCl(\eta^6\text{-}C_6H_6)([18]aneS_2O_4)]PF_6$, shows in contrast to $[Ru(\eta^5\text{-}C_5H_5)(PPh_3)([18]aneS_2O_4)]PF_6$ a single irreversible reduction at -1.476V vs Fc/Fc^+ (at 0.30 Vs^{-1}). The UV/vis spectrum of $[RuCl(\eta^6\text{-}C_6H_6)([18]aneS_2O_4)]PF_6$ shows two absorption bands at 325 nm (ε = 1035 $dm^3\ mol^{-1}\ cm^{-1}$) and 390 nm (ε = 643 $dm^3\ mol^{-1}\ cm^{-1}$).

Solutions of the BPh_4^- salt in $(CH_3)_2CO$ changed colour from yellow to green within a few hours. Evaporation of the solution yielded a conglomerate of green and yellow crystalline material. The infrared spectrum of this green compound is identical to the infrared spectrum of the initial yellow compound. The UV/vis spectrum however shows an additional absorption band at 640nm.

3.2.12 The Single Crystal Structure of $[RuCl(\eta^6\text{-}C_6H_6)([18]aneS_2O_4)]PF_6$

Recrystallisation of $[RuCl(\eta^6\text{-}C_6H_6)([18]aneS_2O_4)]PF_6$ was achieved by allowing a solution in MeCN to evaporate slowly. Data were initially collected at low temperature but the structure showed severe disorder and a second data set was collected at ambient temperature. Nevertheless this structure still showed signs of severe disorder and the whole macrocyclic framework had to be restrained with respect to bond distances and angles.

The single crystal structure shows (**Figure 3.2.12a**) similar features compared with the structure of $[Ru(\eta^5\text{-}C_5H_5)(PPh_3)([18]aneS_2O_4)]PF_6$ The benzene ligand co-ordinates facially to the Ru(II) ion and the macrocycle adopts the typical bidentate chelating binding mode [Ru-S 2.382(5) and 2.377(5)Å]. The last co-ordination site is occupied by the Cl^- ligand [Ru-Cl 2.416(2)Å]. The orientation of the O-atoms follows in contrast to $[Ru(\eta^5\text{-}C_5H_5)(PPh_3)([18]aneS_2O_4)]PF_6$ again an up down up down pattern. The packing diagram (**Figure 3.2.12b**) shows some stacking of the ions but no significant intermolecular interactions could be identified.

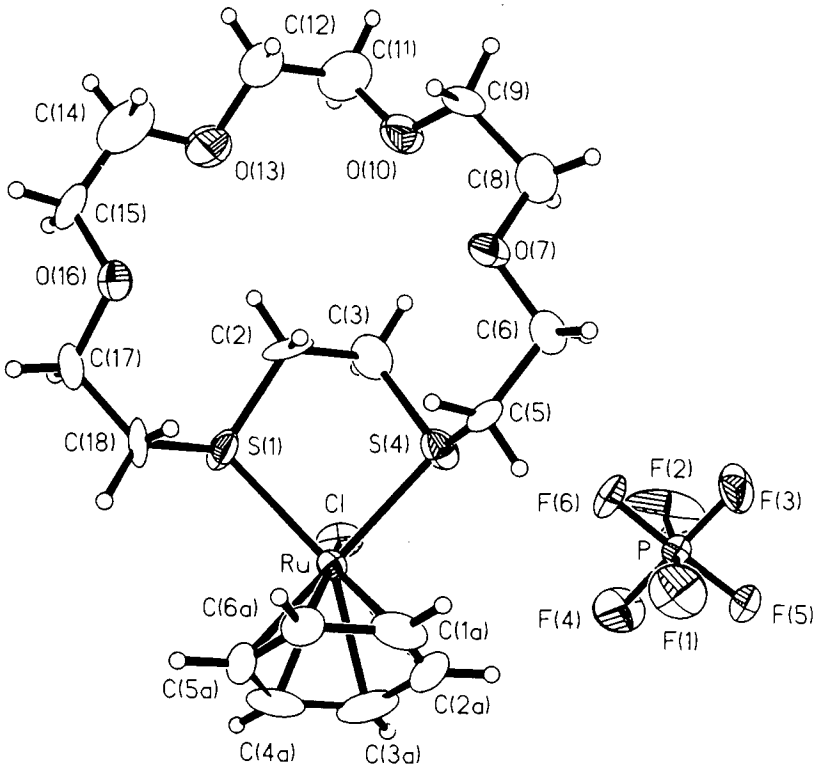

Figure 3.2.12a The single crystal structure of $[RuCl(\eta^6\text{-}C_6H_6)([18]aneS_2O_4)]PF_6$.

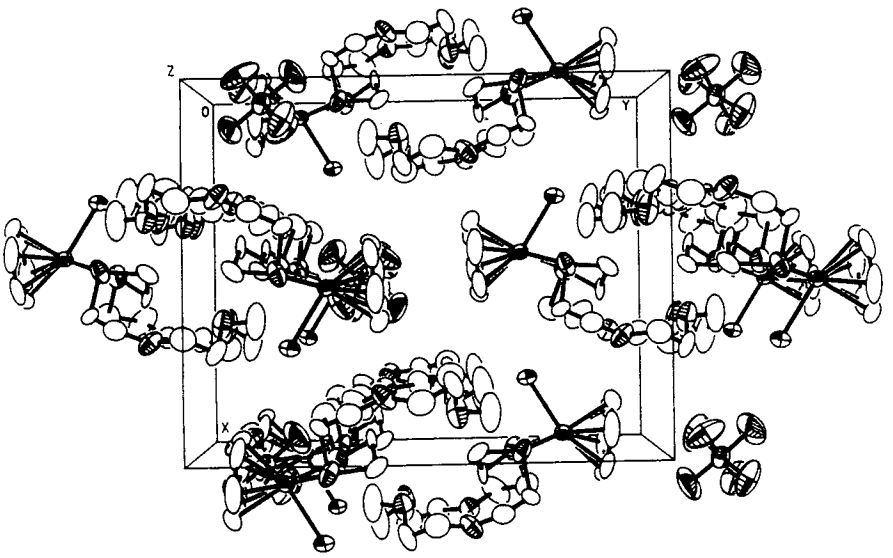

Figure 3.2.12b The packing diagram of $[RuCl(\eta^6\text{-}C_6H_6)([18]aneS_2O_4)]PF_6$.

Ru-C(1A)	2.168(12)	Ru-C(4A)	2.204(12)
Ru-C(2A)	2.181(14)	Ru-C(5A)	2.191(13)
Ru-C(3A)	2.199(11)	Ru-C(6A)	2.173(11)
Ru-S(1)	2.382(5)	Ru-S(4)	2.377(5)
Ru-Cl	2.416(2)		
S(1)-Ru-Cl	82.2(2)	S(4)-Ru-Cl	80.3(2)
S(4)-Ru-S(1)	86.35(13)		
S(1)-C(2)-C(3)-S(4)	-61.8(4)	O(10)-C(11)-C(12)-O(13)	-69.9(25)
C(2)-C(3)-S(4)-C(5)	-70.9(8)	C(11)-C(12)-O(13)-C(14)	178.8(22)
C(3)-S(4)-C(5)-C(6)	-62.8(13)	C(12)-O(13)-C(14)-C(15)	-169.2(22)
S(4)-C(5)-C(6)-O(7)	80.5(18)	O(13)-C(14)-C(15)-O(16)	51.5(35)
C(5)-C(6)-O(7)-C(8)	-151.4(17)	C(14)-C(15)-O(16)-C(17)	-165.4(24)
C(6)-O(7)-C(8)-C(9)	177.1(17)	C(15)-O(16)-C(17)-C(18)	170.5(19)
O(7)-C(8)-C(9)-O(10)	-72.6(20)	O(16)-C(17)-C(18)-S(1)	-74.7(22)
C(8)-C(9)-O(10)-C(11)	-160.5(19)	C(17)-C(18)-S(1)-C(2)	72.5(13)
C(9)-O(10)-C(11)-C(12)	-90.6(25)	C(18)-S(1)-C(2)-C(3)	160.0(7)

Table 3.2.12 Selected bond lengths (Å), angles (°) and torsion angles (°) with estimated standard deviations for $[RuCl(\eta^6\text{-}C_6H_6)([18]aneS_2O_4)]PF_6$.

3.2.13 Single Crystal Structure of $[RuCl(\eta^6\text{-}C_6H_6)([18]aneS_2O_4)]BPh_4$

Single crystal X-ray diffraction studies on the BPh_4^- salt where initiated in order to establish whether the disorder in the PF_6^- salt could be attributed to the size of the counterion. The data set collected at 150K could be solved using DIRDIF and did not cause any problems during refinement. The structure looks (**Figure 3.2.13a**) very similar to the one of the PF_6^- salt. The environment [Ru-S 2.384(6) and 2.368(6)Å; Ru-Cl 2.411(6)Å] at the Ru(II) ion is virtually identical to the one in $[RuCl(\eta^6\text{-}C_6H_6)([18]aneS_2O_4)]PF_6$. The macrocyclic framework however shows significant differences in the absolute values of torsion angles. This is not surprising considering the different ions present in the crystal lattice in either case and of course the effect of disorder on the structure of the PF_6^- salt. The packing diagram (**Figure 3.2.13b**) shows again a stacking arrangement typical for this type of compound.

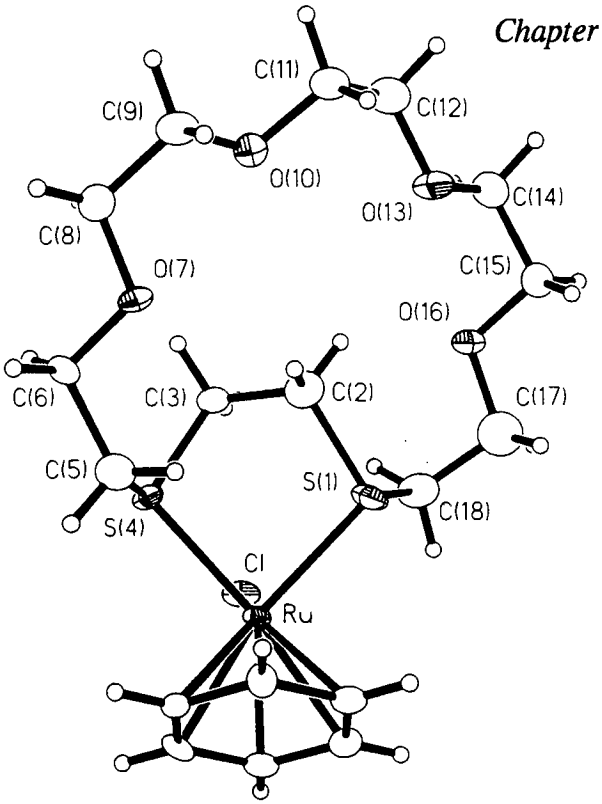

Figure 3.2.13a The single crystal structure of $[RuCl(\eta^6\text{-}C_6H_6)([18]aneS_2O_4)]BPh_4$.

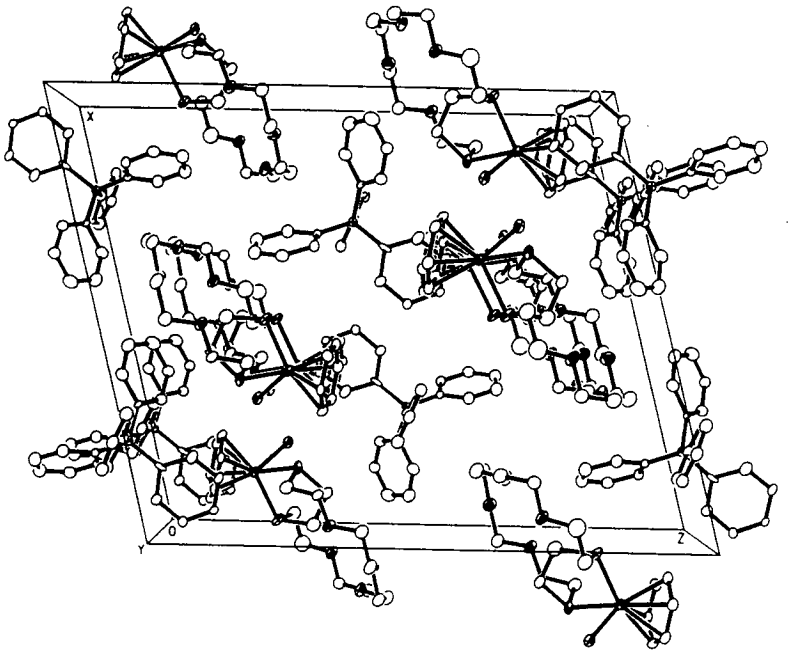

Figure 3.2.13b The packing diagram of $[RuCl(\eta^6\text{-}C_6H_6)([18]aneS_2O_4)]BPh_4$.

Ru-C(1B)	2.204(13)	Ru-C(4B)	2.180(13)
Ru-C(2B)	2.189(13)	Ru-C(5B)	2.195(13)
Ru-C(3B)	2.177(13)	Ru-C(6B)	2.207(13)
Ru-S(1)	2.384(6)	Ru-S(4)	2.368(6)
Ru-Cl	2.411(6)		
S(1)-Ru-Cl	92.1(2)	S(4)-Ru-Cl	82.4(2)
S(4)-Ru-S(1)	85.5(2)		
S(1)-C(2)-C(3)-S(4)	51.3(23)	O(10)-C(11)-C(12)-O(13)	-69.4(27)
C(2)-C(3)-S(4)-C(5)	65.2(20)	C(11)-C(12)-O(13)-C(14)	-175.4(22)
C(3)-S(4)-C(5)-C(6)	54.1(20)	C(12)-O(13)-C(14)-C(15)	177.4(20)
S(4)-C(5)-C(6)-O(7)	-89.7(20)	O(13)-C(14)-C(15)-O(16)	66.2(25)
C(5)-C(6)-O(7)-C(8)	167.5(19)	C(14)-C(15)-O(16)-C(17)	-172.6(21)
C(6)-O(7)-C(8)-C(9)	174.5(20)	C(15)-O(16)-C(17)-C(18)	165.8(22)
O(7)-C(8)-C(9)-O(10)	66.2(26)	O(16)-C(17)-C(18)-S(1)	-77.5(24)
C(8)-C(9)-O(10)-C(11)	-177.5(20)	C(17)-C(18)-S(1)-C(2)	81.0(21)
C(9)-O(10)-C(11)-C(12)	-168.9(21)	C(18)-S(1)-C(2)-C(3)	83.3(21)

Table 3.2.13 Selected bond lengths (Å), angles (°) and torsion angles (°) with estimated standard deviations for $[RuCl(\eta^6\text{-}C_6H_6)([18]aneS_2O_4)]BPh_4$.

3.3 CONCLUSION

The major objective for the investigation of complexes of Ru(II) with mixed O/S donor ionophores in particular $[18]aneS_2O_4$ was to establish whether these novel compounds could be used in further developments of chemical sensors. The successful isolation of a potential intermediate in the formation of $[RuCl(PPh_3)([15]aneS_2O_3)_2]PF_6$ has given some insight in the reaction pathway to the formation of this species. $RuCl_2(PPh_3)_2([15]aneS_2O_3)$ and its derivatives, containing larger macrocyclic ligands, might well be a better choice as a starting material than $RuCl_2(PPh_3)_3$ for the development of a Ru(II) host guest chemistry. It has been suggested[223] that the substitution of the Cl^- ligand in $[RuCl(\eta^6\text{-}C_6H_6)([15]aneS_2O_3)]PF_6$ by bis-functional chain ligands such as hydrazine or ethylenediamine would greatly enhance the co-ordinative properties of this species with respect to guest ion complexation. The compound showed, however, an irreversible reduction which renders it unsuitable for the development of chemical sensors. $[Ru(PPh_3)(\eta^5\text{-}C_5H_5)([15]aneS_2O_3)]PF_6$ on the other hand showed quasi-reversible electrochemical behaviour and future work should therefore focus on Ru(II) complexes containing either a cyclopentadienyl or even better a pentamethylcyclopentadienyl ligand.

A general problem in all complexes studied is the conformation of the macrocycle. The ethylene bridge between both S-donor atoms occupies part of the cavity effectively preventing any further co-ordination to a potential guest ion. Future work should therefore focus on macrocycles containing a tridentate soft donor site. Two general scenarios are possible and we propose that ligands like [18]aneS_3O_3 would co-ordinate either bidentate chelating or *facially* to the octahedral Ru(II) ion. Ligands such as [20]aneS_3O_3 on the other hand would be able to accommodate the Ru(II) ion within the cavity and seem therefore to be the better choice in future investigations.

3.4 EXPERIMENTAL SECTION

3.4.1 The Synthesis of $RuCl_2(PPh_3)_3$

$RuCl_2(PPh_3)_3$ was prepared according to the method reported by Wilkinson and co-workers[277] in very good yield (89%).

Microanalysis (for $C_{54}H_{45}Cl_2P_3Ru$; Mol.wt. = 958.85 $gmol^{-1}$):

	%C	%H
Calculated	67.67	4.73
Found	67.77	4.66

IR spectrum (KBr disc):

3050w, 1480m,1430s, 1315w, 1190w, 1155w, 1120w, 1085m, 1025w, 1000w, 740s, 695vs, 620w, 545m, 520vs, 495m, 455m, 430w and 405w.

FAB mass spectrum (DMF/Glycerol):

Fragment:	m/z (calc.)	m/z (found)	rel.Int.
$[^{102}Ru^{35}Cl(PPh_3)_3]^+$	923	923	0.10
$[^{102}Ru(PPh_3)_3]^+$	888	888	0.10
$[^{102}Ru^{35}Cl(PPh_3)_2]^+$	661	661	0.10
$[^{102}Ru(PPh_3)_2]^+$	626	625	1.00

3.4.2 The Synthesis of $RuCl(\eta^5\text{-}C_5H_5)(PPh_3)_2$

$RuCl(\eta^5\text{-}C_5H_5)(PPh_3)_2$ was prepared according to the method reported by Bruce and co-workers[284] in good yield.

Microanalysis (for $C_{41}H_{35}ClP_2Ru$; Mol.wt. = 726.20 $gmol^{-1}$)

	%C	%H
Calculated	67.8	4.86
Found	67.4	4.83

IR spectrum (KBr disc):

3050w, 1480s, 1430s, 1310w, 1180w, 1160w, 1085s, 1070w, 1030w, 980w, 910w, 855w, 830m, 805m, 750s, 695vs, 620w, 585w, 530s, 520vs and 500s cm^{-1}.

FAB mass spectrum (3-NOBA):

Fragment:	m/z (calc.)	m/z (found)	rel.Int.
$[^{102}Ru^{35}Cl(PPh_3)_2(C_5H_5)]^+$	726	726	0.80
$[^{102}Ru^{35}Cl(PPh_3)(C_5H_5)]^+$	464	464	0.90
$[^{102}Ru(PPh_3)(C_5H_5)]^+$	429	429	1.00

3.4.3 The Synthesis of $Ru_2(\eta^6\text{-}C_6H_6)_2Cl_4$

$[RuCl_2(\eta^6\text{-}C_6H_6)]_2$ was prepared according to the method reported by Bennett and co-workers[288] in very good yield (90%).

IR spectrum (KBr disc):

3075m, 3035m, 2925w, 1430s, 1150w, 975w, 845vs, 670m, 620w and 445w cm^{-1}.

^1H-NMR spectrum (d_6-DMSO; 298K; 80.13 MHz):

δ 5.96 (s, 6H) $C_6\boldsymbol{H}_6$.

3.4.4 The Synthesis of $[Ru(\eta^6\text{-}C_6H_6)(MeCN)_2Cl]PF_6$

$[RuCl(\eta^6\text{-}C_6H_6)(MeCN)_2]PF_6$ was prepared according to the method reported by McCormick and co-workers[291] in good yield (75%).

Microanalysis for ($C_{10}H_{12}ClF_6N_2PRu$; Mol.wt. = 442.61 $gmol^{-1}$)

	%C	%H	%N
Calculated	27.19	2.74	6.34
Found	26.38	2.80	6.38

IR spectrum (KBr disc):

3100s, 3010m, 2945w, 2330m, 2300w, 1510w, 1440m, 1365w, 1035m, 830vs and 560s cm^{-1}.

^{1}H-NMR spectrum (d_3-MeCN; 298K; 360.13MHz)

δ 5.93 (s, 6H) $C_6\boldsymbol{H}_6$

δ 1.95 (s, 6H) $C\boldsymbol{H}_3CN$.

^{13}C-NMR spectrum (d_3-MeCN; 298K; 50.32MHz)

δ 116.70 (s) $CH_3\boldsymbol{C}N$

δ 85.50 (s) $\boldsymbol{C}_6H_6$

δ 0.09 (septet) $\boldsymbol{C}H_3CN$.

3.4.5 The Synthesis of $Ru_2(\eta^6\text{-}MeC_6H_4{}^iPr)_2Cl_4$

$[RuCl_2(\eta^6\text{-}MeC_6H_4{}^iPr)]_2$ was prepared according to the method reported by Bennett and co-workers[289] in good yield (71%).

Microanalysis (for $C_{20}H_{28}Cl_4Ru_2$; Mol.wt. = 612.39 $gmol^{-1}$)

	%C	%H
Calculated	39.2	4.61
Found	39.5	4.71

IR spectrum (KBr disc):

3055m, 3030m, 2960m, 2925m, 2865m, 1635w, 1530w, 1495m, 1470s, 1410w, 1390s, 1360m, 1325w, 1280w, 1200w, 1160w, 1115m, 1095m, 1055vs, 1035s, 1005m, 875s, 805w, 670w, 635w, 570w and 525w cm^{-1}.

FAB mass spectrum (DMF/Glycerol):

Fragment:	m/z (calc.)	m/z (found)
$[^{102}Ru_2{}^{35}Cl_3(C_{10}H_{14})_2]^+$	577	576
$[^{102}Ru_2{}^{35}Cl_2(C_{10}H_{14})_2]^+$	542	542
$[^{102}Ru{}^{35}Cl(C_{10}H_{14})]^+$	271	271

3.4.6 The Synthesis of $Ru(PPh_3)_2([15]aneS_2O_3)Cl_2$

Equimolar amounts of $RuCl_2(PPh_3)_3$ (240 mg, 0.25 mmol) and $[15]aneS_2O_3$ (63 mg, 0.25 mmol) were refluxed in $MeOH/H_2O$ (20 dm^3, 1:1 v/v) for 2 hours affording a yellow cloudy (PPh_3) solution. The solution was allowed to evaporate to dryness yielding red crystals in a light yellow slush. The red material was insoluble in EtOAc, hexane, Et_2O and water and yellow material was removed as complete as possible by successive washings with Et_2O. Crystals still affected by the yellow by-product were manually selected under a microscope and characterised.

IR spectrum (KBr disc):

3055m, 2860m, 1970w, 1655w, 1620m, 1585w, 1575w, 1480s, 1460w, 1430s, 1410m, 1390w, 1365m, 1235w, 1190m, 1170w, 1135s, 1115m, 1075s, 1050w, 1030w, 1000m, 935w, 890w, 845m, 815w, 745s, 695vs, 620w, 560w, 535m, 525vs, 500m, 465w, 435w and 415w cm^{-1}.

FAB mass spectrum (3-NOBA):

Fragment:	m/z (calc.)	m/z (found)	Intensity
$[^{102}Ru(PPh_3)_2([15]aneS_2O_3)^{35}Cl_2]^+$	957	953	0.10
$[^{102}Ru(PPh_3)_2([15]aneS_2O_3)]^+$	625	625	1.00
$[^{102}Ru(PPh_3)([15]aneS_2O_3)^{35}Cl]^+$	651	651	0.80

^1H-NMR spectrum ($CDCl_3$; 298K; 360.13 MHz)

δ 2.5 - 4.3 ppm (m, $[15]aneS_2O_3$, 20H)

δ 7.1 - 7.9 ppm (m, Ph, 30H)

^{13}C-NMR (CDCl3, 297K; 62.90 MHz; DEPT ¾π)

δ 33.01 ppm -S***C***H_2-

δ 70.12 and 70.35 ppm -O***C***H_2-

δ 126.54 to 135.48 ppm -P(***C***$_6H_6)_3$

^{31}P-{^1H}-NMR ($CDCl_3$, 297 K; 101.27 MHz)

δ -4.74 ppm	1.96	free ***P***Ph_3
δ 27.34 ppm	27.46	(Ru-***P***Ph_3)
δ 55.80 ppm	7.30	(not assigned)
δ 62.92 ppm	2.92	(not assigned)

3.4.7 The Synthesis of $[RuCl(PPh_3)([15]aneS_2O_3)_2]PF_6$

$[RuCl(PPh_3)([15]aneS_2O_3)_2]PF_6$ has be synthesised according to the preparation reported by Schröder and co-workers[224,225] in good yield.

IR spectrum (KBr disc):

3040w, 2860m, 1480m, 1455w, 1430m, 1410w, 1360m, 1290m, 1190w, 1130m, 1090m, 1000w, 840vs, 750m, 700vs, 555vs, 530vs and 515m cm^{-1}.

^{31}P-$\{^1H\}$-NMR spectrum ($CDCl_3$; 298K; 145.786 MHz)

δ 25.89, 40.66 (Ru-*P*Ph_3)

UV/vis spectrum (300-800nm; MeCN; 295K):

λ = 400 nm, ε = 490 dm^3 mol^{-1} cm^{-1}

λ = 347 nm, ε = 710 dm^3 mol^{-1} cm^{-1}

3.4.8 The Synthesis of $[Ru([18]aneS_2O_4)_3](PF_6)_2$

'$RuCl_3$' (104 mg; 0.5 mmol) was added to a stirred solution of $[18]aneS_2O_4$ (296 mg; 1.0 mmol) in 25 cm^3 MeOH / H_2O (1:1, v/v) and heated under reflux for 24h during which the colour changed from dark brown over blue to dark green. The hot solution was then treated with $K_2(C_2O_4)$ (92 mg; 0.5 mmol). Stirring continued while the solution was allowed to cool down to ambient temperature over night. The addition of excess NH_4PF_6 to the light green solution finally afforded a yellow solution from which a conglomerate of yellow and colourless crystals precipitated.

FAB mass spectrum (3-NOBA):

Fragment:	m/z (calc.)	m/z (found)	rel. Int.
$[^{101}Ru([18]aneS_2O_4)_3(PF_6)_2]^+$	1280	1288	0.01
$[^{101}Ru([18]aneS_2O_4)_3(PF_6)]^+$	1135	1135	0.6
$[^{101}Ru([18]aneS_2O_4)_3]^+$	990	990	0.2
$[^{101}Ru([18]aneS_2O_4)_2]^+$	694	694	1.0

3.4.9 The Synthesis of $[RuCl(PPh_3)([18]aneS_2O_4)_2]PF_6$

Treatment of $RuCl_2(PPh_3)_3$ (220 mg, 0.23 mmol) with $[18]aneS_2O_4$ (136 mg, 0.56 mmol) in MeOH (25 cm^3) afforded a brown suspension which homogenised upon refluxing for two hours under N_2 to afford a clear yellow solution. Excess NH_4PF_6 was added to the hot solution which was left to cool down to -30°C in the freezer. A yellow solid precipitated and was collected leaving a colourless supernatant liquid.

Yield: 193 mg, 0.17 mmol, 74% based on $RuCl_2(PPh_3)_3$.

Microanalysis (for $C_{42}H_{63}ClF_6O_8P_2RuS_4 \cdot 2H_2O$; Mol.wt. = 1172.68 $gmol^{-1}$)

	%C	%H
Calculated	43.0	5.76
Found	42.7	5.47

FAB mass spectrum (3-NOBA):

Fragment:	m/z (calc.)	m/z (found)	rel.Int.
$[^{101}Ru^{35}Cl(PPh_3)([18]aneS_2O_4)_2]^+$	991	991	0.30
$[^{101}Ru(PPh_3)([18]aneS_2O_4)_2]^+$	956	957	0.05
$[^{101}Ru^{35}Cl([18]aneS_2O_4)_2]^+$	729	729	1.00
$[^{101}Ru([18]aneS_2O_4)_2]^+$	694	695	0.60
$[^{101}Ru([18]aneS_2O_4)]^+$	398	395	0.40

IR spectrum (KBr disc):

3650m, 3475s, 3055w, 2995m, 2875s, 1710w, 1630w, 1480m, 1435s, 1355s, 1300m, 1250m, 1190w, 1120vs, 940w, 840vs, 755w, 670s, 560s, 530s, 515m and 436w cm^{-1}.

^1H-NMR spectrum (d^6-DMSO; 297K; 250.13 MHz)

δ 2.50 - 3.70 ppm (m, 48H) $[18]aneS_2O_4$

δ 7.30 - 7.65 ppm (m, 15H) $-P(C_6\boldsymbol{H}_5)_3$

^{13}C-NMR spectrum (d^6-DMSO; 297K; 62.90 MHz; DEPT ¾π)

δ 30.57, 32.17 and 33.85 ppm ($-S\boldsymbol{C}H_2-$)

δ 68.58, 69.00, 69.02, 69.62, 69.89 and 70.20 ppm ($-O\boldsymbol{C}H_2-$)

δ 127.79, 127.93, 128.21, 128.35, 130.23, 130.54, 134.36 and 134.48 ppm $-P(\boldsymbol{C}_6H_5)_3$

^{31}P-$\{^1H\}$-NMR spectrum (d_6-Me_2CO; 298K; 81.02 MHz)

δ 32.2, 42.9 (Ru-$\boldsymbol{P}Ph_3$)

Cyclic Voltammetry (0.1 mmol dm^{-3} $TBAPF_6$; MeCN; 293K)

$E_{1/2}$ (quasi-reversible Ru(II)/Ru(III) couple) = +0.837V vs Fc/Fc^+.

3.4.10 The Synthesis of $[Ru(\eta^5\text{-}Cp)(PPh_3)([18]aneS_2O_4)]PF_6$

$RuCpCl(PPh_3)_2$ (130 mg, 0.18 mmol) and $[18]aneS_2O_4$ (107 mg, 0.36 mmol) were refluxed in MeOH for three hours under N_2. A yellow precipitate formed after addition of excess NH_4PF_6 which was collected, washed with n-hexane, dried and characterised. Yield: 144mg, 0.16mol, 89%

Microanalysis (for $C_{35}H_{44}F_6O_4P_2RuS_2 \cdot 2H_2O$ Mol.wt. = 905.78 $gmol^{-1}$)

	%C	%H
Calculated	46.4	5.34
Found	46.9	5.05

FAB mass spectrum (3-NOBA):

Fragment:	m/z (calc.)	m/z (found)	rel.Int
$[^{101}Ru(PPh_3)(C_5H_5)([18]aneS_2O_4)]^+$	725	725	1.00
$[^{101}Ru(C_5H_5)([18]aneS_2O_4)]^+$	463	463	0.50

IR spectrum (KBr disc):

3075w, 3050w, 2985w, 2855s, 1480m, 1435s, 1380w, 1355m, 1305m, 1250w, 1200w, 1115s, 1090s, 1010w, 960w, 840vs, 750m, 670s, 560s, 530s, 515s, 495s, 460m, 440w and 405w cm^{-1}.

^1H-NMR spectrum ($CDCl_3$; 298K; 80.13 MHz):

δ 2.75 - 4.10 (m, 24H) $[18]aneS_2O_4$

δ 4.53 (s, 5H) $C_5\boldsymbol{H}_5$

δ 7.40 (m, 15H) $P(C_6\boldsymbol{H}_5)_3$

UV/vis spectrum (300-800nm; MeCN; 295K):

λ = 364 nm, ε = 2700 $dm^3\ mol^{-1}\ cm^{-1}$

Cyclic Voltammetry (0.1 mmol dm^{-3} $TBAPF_6$; MeCN; 293K)

$E_{1/2}$ (quasi-reversible Ru(II)/Ru(III) couple) = +0.570V vs Fc/Fc^+.

3.4.11 The Synthesis of $[RuCl(\eta^6\text{-}C_6H_6)([18]aneS_2O_4)]PF_6$

The reaction of $[RuCl(\eta^6\text{-}C_6H_6)(MeCN)_2]PF_6$ (220 mg, 0.5 mmol) with $[18]aneS_2O_4$ (148 mg, 0.5 mmol) in boiling MeCN (25 dm^3) afforded a yellow solution from which yellow crystals precipitated. The product was isolated and characterised.

Yield: 200 mg, 0.32 mmol, 63%

Microanalysis (for $C_{18}H_{30}ClF_6O_4S_2PRu$; Mol.wt. = 656.05 $gmol^{-1}$)

	%C	%H
Calculated	32.95	4.61
Found	33.09	4.78

FAB mass spectrum (3-NOBA):

Fragment:	m/z (calc.)	m/z (found)
$[^{101}RuCl(C_6H_6)([18]aneS_2O_4)\text{-}H]^+$	510	510

IR spectrum (KBr disc):

3085m, 3000m, 2870s, 1635w, 1475w, 1440m, 1415m, 1355m, 1300m, 1250m, 1200m, 1120vs, 1090s, 1050m, 940m, 840vs, 555s and 520w cm^{-1}.

^1H-NMR spectrum (CD_3CN; 298K; 360.13 MHz)

δ 2.48 ppm (d of d, 4H) -SC***H***$_2$-

δ 2.51 ppm (quartet, 4H) -SC***H***$_2$-

δ 3.0 - 4.0 ppm (m, 16H) -OC***H***$_2$-

δ 5.94 ppm (s, 6H) C_6***H***$_6$

^{13}C-NMR spectrum (CD_3CN; 297K; 50.32 MHz; DEPT ¾π)

δ 32.43, 32.87, 34.48, 37.35 ppm (-S***C***H_2-)

δ 68.30, 68.52, 68.85, 69.07, 69.11, 69.69, 69.85, 69.98 ppm (-O***C***H_2-)

δ 87.57 ppm (***C***6H6)

UV/vis spectrum (250-800nm; MeCN; 295K):

λ = 325 nm, ε = 1035 dm^3 mol^{-1} cm^{-1}

λ = 390 nm, ε = 643 dm^3 mol^{-1} cm^{-1}

Cyclic Voltammetry (0.1 mmol dm^{-3} $TBAPF_6$; MeCN; 293K)

$E_{red.(irreversible)}$[Ru(II)/Ru(I)] =

-1.440V vs Fc/Fc^+ ($0.18Vs^{-1}$)

-1.476V vs Fc/Fc^+ ($0.30Vs^{-1}$)

-1.512V vs Fc/Fc^+ ($1.67Vs^{-1}$)

3.4.12 The Synthesis of $[RuCl(\eta^6\text{-}C_6H_6)([18]aneS_2O_4)]BPh_4$

$[RuCl(\eta^6\text{-}C_6H_6)([18]aneS_2O_4)]BPh_4$ was prepared in according to the preparation given for $[RuCl(\eta^6\text{-}C_6H_6)([18]aneS_2O_4)]PF_6$ but $NaBPh_4$ was added to precipitate the product. The product was recrystallised from $(CH_3)_2CO$ and characterised.

Microanalysis (for $C_{42}H_{50}BClO_4RuS_2$; Mol.wt. = 830.32$gmol^{-1}$)

	%C	%H
Calculated	60.76	6.07
Found	59.80	5.88

FAB mass spectrum (CH_2Cl_2/3-NOBA/MeCN):

Fragment:	m/z (calc.)	m/z (found)	rel.Int.
$[^{101}RuCl(C_6H_6)([18]aneS_2O_4)]^+$	511	511	1.00
$[^{101}Ru(C_6H_6)([18]aneS_2O_4)]^+$	476	476	0.14
$[^{101}RuCl([18]aneS_2O_4)]^+$	433	432	0.07
$[^{101}RuCl(C_6H_6)]^+$	215	215	0.10

IR spectrum (KBr disc):

3050s, 3000s, 2870s, 1580w, 1505w, 1480m, 1430m, 1350s, 1290w, 1245w, 1180w, 1120vs, 1030m, 950m, 895w, 830m, 745s, 710s, 625, 605s, 540w and 480w cm^{-1}.

^{1}H-NMR spectrum ($CDCl_3$; 297K; 250.13 MHz)

δ 2.50 (m, S***C***H_2, 8H)

δ 3.3 - 4.5 (m, O***C***H_2, 16H)

δ 6.62 (s, ***C***$_6H_6$, 6H)

δ 7.21 (t), 7.39 (t), 7.78 (m) (B(C_6***H***$_5)_4$, 20H)

^{13}C-NMR spectrum (CD_3COCD_3; 297K; 62.90 MHz; DEPT ¾π)

δ 32.28, 32.82, 34.32, 37.07 ppm (-S***C***H_2-)

δ 68.33, 68.39, 68.56, 68.98, 69.03, 69.71, 69.89, 70.07 ppm (-O***C***H_2-)

δ 87.62 ppm (***C***$_6H_6$)

δ 135.27, 124.25, 120.51 ppm (B(***C***$_6H_5)_4$)

3.4.13 Single Crystal Structure Determinations

A range of Ru(II) complexes with [15]aneS_2O_3 and [18]aneS_2O_4 complexes were studied using single crystal X-ray diffraction techniques. Most of the structures investigated showed disorder. The regions mostly affected by disorder were counterions and the floppy macrocyclic polyether chain. The disorder was modelled according to the principles outlined in the general procedure (**A.4**). Selected crystallographic details of each structure are tabulated in **Tables 3.4.13a** and **3.4.13b**.

Compound	$RuCl_2(PPh_3)_2$ ([15]aneS_2O_3)	[RuCl(PPh_3) ([18]aneS_2O_4)$_2$]$^+$ PF_6^-	[Ru([18]aneS_2O_4)$_3$]$^{2+}$ 2 PF_6^-
Crystal data			
Formula	$C_{46}H_{50}Cl_2O_3P_2RuS_2 \cdot$ ½ CH_3OCH_3	$C_{86}H_{132}Cl_2F_6O_8P_2$ $RuS_8 \cdot$½ C_2H_5OH	$C_{26}H_{52}F_{12}O_{12}P_2S_6Ru \cdot$ H_2O
M / gmol^{-1}	948.90	1159.60	1394.25
Crystal size / mm	0.08 x 0.27 x 0.35	0.08 x 0.27 x 0.66	0.39 x 0.62 x 0.74
Crystal system	triclinic	triclinic	trigonal
Space group	*P*-1 (No. 2)	*P*-1 (No. 2)	*R*-3 (No. 148)
a / Å	11.3183 (19)	10.674 (7)	18.6287 (17)
b / Å	12.4925 (21)	14.487 (11)	a
c / Å	18.442 (3)	19.241 (17)	29.863 (5)
α / °	101.896 (8)	74.88 (7)	90
β / °	100.177 (13)	84.34 (6)	90
γ / °	106.669 (10)	80.07 (6)	120
U / Å^3	2366	2825	8975
Z	2	2	6
D_c / gcm^{-3}	1.332	1.363	1.548
μ / mm^{-1}	0.626	0.580	0.603
F(000)	980	1202	4356
T / K	298	298	150.0 (1)
Reflections at ±ω to refine cell	22	12 (matrix refined)	28
2θrange / °	23 - 28	20 - 22	30 - 32
Data Collection			
$2\theta_{max}$ / °	45	45	45
Range of h	-12 → 11	-11 → 11	-16 → 19
Range of k	-13 → 13	-14 → 15	-15 → 20
Range of l	0 → 19	0 → 20	0 → 32
Measured reflections	6556	7379	3380
Independent reflections, R_{int}	5602, 0.040	7379	2529, 0.075
Observed reflections	4426 with $F \geq 4\sigma(F)$	3111 with $F \geq 4\sigma(F)$	2280 with $F \geq 6\sigma(F)$
ψ scan correction $TF_{max,min}$	0.9996, 0.8624	-	-
Solution			
Method	Patterson Synthesis	Patterson Synthesis	Patterson Synthesis
using	SHELX76	SHELX76	SHELX76
Refinement			
full matrix least squares on	F	F	F
using	SHELX76	SHELX76	SHELX76
DIFABS max, min	1.088, 0.839	0.594, 1.465	-
Weighting scheme	$3.32 \cdot 10^{-4}$	$2.71 \cdot 10^{-3}$	$3.14 \cdot 10^{-4}$
Parameters refined	458	350	226
SHELX76 R, R´, S	0.038, 0.045, 1.14	0.095, 0.126, 1.27	0.042, 0.064, 1.34
SHELXL-93 R, R´, S			
$(\Delta/\sigma)_{max}$	0.014	0.190	0.004
$\Delta\rho_{max, min}$ / eÅ^{-3}	+0.70, -0.38	+0.92, -0.94	+0.63, -0.49

Table 3.4.13a Selected crystallographic data for the single crystal structures of $RuCl_2(PPh_3)_2([15]aneS_2O_3)$, $[RuCl(PPh_3)([18]aneS_2O_4)_2]PF_6$ and $[Ru([18]aneS_2O_4)_3](PF_6)_2$.

Compound	$[RuCp(PPh_3)([18]aneS_2O_4)]^+ PF_6^-$	$[RuCl(C_6H_6)([18]aneS_2O_4)]^+ PF_6^-$	$[RuCl(C_6H_6)([18]aneS_2O_4)]^+ BPH_4^-$
Crystal data			
Formula	$C_{35}H_{44}F_6O_4P_2RuS_2$	$C_{18}H_{30}ClF_6O_4PRuS_2$	$C_{42}H_{50}BClO_4RuS_2$
M / gmol^{-1}	869.78	656.03	830.27
Crystal size / mm	0.04 x 0.44 x 0.78	0.55 x 0.62 x 0.63	0.27 x 0.35 x 0.35
Crystal system	triclinic	orthorhombic	monoclinic
Space group	*P*-1 (No. 2)	$Pna2_1$ (No. 33)	$P2_1/n$ (alt. $P2_1/c$; No.14)
a / Å	11.3023 (11)	11.127 (4)	18.539 (12)
b / Å	12.1200 (9)	13.348 (3)	9.652 (7)
c / Å	14.3983 (13)	16.774 (3)	22.335 (12)
α / °	83.393 (6)	90	90
β / °	83.274 (8)	90	103.84 (5)
γ / °	78.367 (7)	90	90
U / Å^3	1910	2491	3880
Z	2	4	4
D_c / gcm^{-3}	1.512	1.750	1.421
μ / mm^{-1}	0.653	1.037	0.622
F(000)	892	1328	1728
T / K	298	298	150.0 (1)
Reflections at ±ω to refine cell	26	29	24
2θrange / °	30 - 32	28 - 34	18 - 20
Data Collection			
$2\theta_{max}$ / °	45	45	40
Range of h	-11 → 12	0 → 12	-17 → 17
Range of k	-12 → 13	0 → 14	0 → 9
Range of l	0 → 15	0 → 18	0 → 21
Measured reflections	4981	2214	3888
Independent reflections, R_{int}	4701	1617	3600
Observed reflections	4070 with $F \geq 4\sigma(F)$	1615 with $F \geq 2\sigma(F)$	3536 with $F \geq 4\sigma(F)$
ψ scan correction $TF_{max,min}$	-	0.6214, 0.4939	0.928, 0.759
Solution			
Method	Patterson Synthesis	Patterson Synthesis	
using	SHELX76	SHELX76	DIRDIF
Refinement			
full matrix least squares on	F	F^2	F^2
using	SHELX76	SHELXL-93	SHELXL-93
DIFABS max, min	-	1.044, 0.818	-
Weighting scheme	$7.08 \cdot 10^{-4}$	0.0541, 9.686	0.0001, 420,764
Parameters refined	285	292	396
SHELX76 R, R´, S	0.057, 0.082, 1.27		
SHELXL-93 R1, wR2, S		0.041, 0.107, 1.087	0.127, 0.380, 1.252
$(\Delta/\sigma)_{max}$	0.25	0.09	0.024
$\Delta\rho_{max, min}$ / eÅ^{-3}	+0.79, -0.42	+1.30, -0.50	+2.35, -1.10

Table 3.4.13b Selected crystallographic data for the single crystal structures of $[RuCp(PPh_3)([18]aneS_2O_4)]PF_6$, $[RuCl(C_6H_6)([18]aneS_2O_4)]PF_6$ and $[RuCl(C_6H_6)([18]aneS_2O_4)]BPh_4$.

CHAPTER IV

The Co-ordination Chemistry of Palladium(II) with Mixed O/S-Donor Ionophores

4.1 INTRODUCTION

The most common oxidation state for Pd is +2. In common with other 2nd and 3rd row, d^8 metal ions, the Pd(II) d^8 low spin metal centre prefers a square-planar co-ordination geometry. Additional co-ordination to the Pd(II) centre however does occur in some complexes, often involving a degree of π bonding. The chemistry of Pd has been reviewed[303,304].

Common starting points into the co-ordination chemistry of Pd(II) are the commercially available compounds $(PdCl_2)_n$, $Pd(OAc)_2$ and $[Pd(MeCN)_4]BF_4$[305]. All three compounds adopt a square-planar co-ordination geometry. The crystal structure of $(PdCl_2)_n$[306] consists of an one-dimensional infinite band structures with Cl-bridges. $Pd(OAc)_2$ which should be more precisely written as $[Pd(OAc)_2]_3$ shows isolated trinuclear species. Each Pd(II) ion is co-ordinated to four bridging acetate groups. This trinuclear arrangement has been described as basket shaped[307]. The four monodentate MeCN N-donors co-ordinate in $[Pd(MeCN)_4]BF_4$. square-planar to one Pd(II) ion.

$(PdCl_2)_n$ is only marginally soluble and reaction mixtures need to be refluxed for some time in order to dissolve the solid $(PdCl_2)_n$. $(PdCl_2)_n$ has the advantage that it is not as sensitive to reducing conditions (EtOH, MeOH) compared with the other two compounds. Reactions using $Pd(OAc)_2$ and $[Pd(MeCN)_4](BF_4)_2$ have to be conducted in a non-reducing solvent such as MeCN in order to prevent reduction of Pd(II) to Pd metal.

4.1.1 Pd(II) Complexes with Homoleptic Thioether Macrocycles

The complex $[Pd([9]aneS_3)_2]^{2+}$ has been prepared and structural characterised (**Figure 4.1.1a**)[308,309]. Two S-atoms bind chelating to the square-planar Pd-centre [Pd-S 2.332(3) and 2.311(3)Å] whereas the third S-atom occupies a long range apical site [Pd···S 2.952(4)Å] giving an overall distorted pseudo octahedral co-ordination geometry. The complex reflects the mis-match between preferred square-planar co-ordination geometry of the of Pd(II)-ion and the pre-organisation of the ligand for *facial* co-ordination.

The electrochemical or chemical oxidation of $[Pd([9]aneS_3)_2]^{2+}$ affords the air-stable Pd(III) species $[Pd([9]aneS_3)_2]^{3+}$[42,301,309,311]. The fully reversible Pd(II)/(III) redox couple has been found to be at $E_{1/2}$ = +0.605V vs Fc/Fc^+[309]. This complex illustrates the preference of Pd(III) (d^7 low spin) for an octahedral Jahn-Teller distorted co-ordination geometry [Pd-S_{equ} 2.3558(14) and 2.3692(15)Å; Pd-S_{ap} 2.5448(15)Å] (**Figure 4.1.1a**).

(i) (ii)

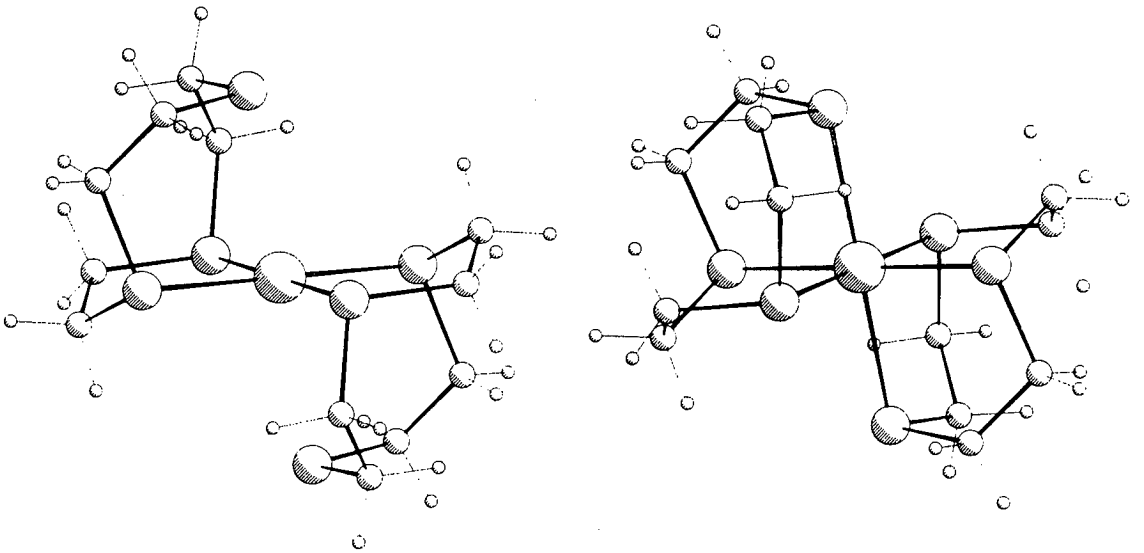

Figure 4.1.1a The single crystal structures of (i) $[Pd([9]aneS_3)_2]^{2+}$ and (ii) $[Pd([9]aneS_3)_2]^{3+}$.

A range of half sandwich complexes[308,311] between $[9]aneS_3$ and Pd(II) have been reported. The Pd(II)-ion adopts in all cases a square-planar co-ordination geometry with the ligand bound bidentate *cisoid* to it. Other examples of Pd-complexes with tridentate homoleptic thioether macrocycles include benzo derivatives of $[11\text{-}14]aneS_3$[312].

Tetrathia ligands such as $[12]aneS_4$, $[14]aneS_4$ and $[16]aneS_4$ match the number of donor sites in square-planar low spin Pd(II). Even though these ligands adopt rectangular shapes in their solid state, they can not be termed 'pre-organised' for square-planar co-ordination because the S-atoms are *exo*-oriented in the free ligand. $[Pd([12]aneS_4)]^{2+}$, $[Pd(14]aneS_4)]^{2+}$ and $[Pd([16]aneS_4)]^{2+}$[42] have been prepared and structural characterised (**Figure 4.1.1b**).

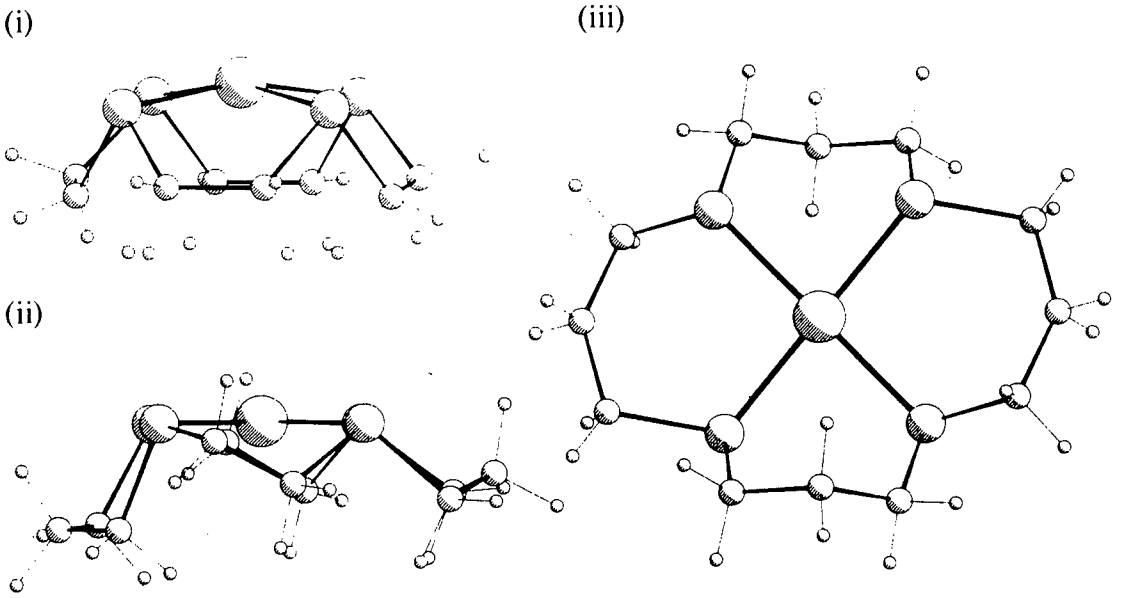

Figure 4.1.1b The single crystal structures of (i) $[Pd([12]aneS_4)]^{2+}$, (ii) $[Pd([14]aneS_4)]^{2+}$ and (iii) $[Pd([16]aneS_4)]^{2+}$.

This series of complexes between Pd(II) and S_4 macrocycles illustrates the effect of the mis-match between the size of the guest ion and the cavity size of the host on the conformation of the macrocycle. $[Pd([16]aneS_4)]^{2+}$ is in this series the least strained complex with the Pd(II) ion fitting well without distortion of the square-planar co-ordination geometry into the macrocyclic cavity. $[Pd([12]aneS_4)]^{2+}$ on the other hand exhibits severe signs of a misfit between the size of the Pd(II) ion and the size of macrocyclic cavity with the Pd(II) ion being displaced by 0.3116Å out of the best fit plane of the four S-donors. The macrocyclic ligand itself shows very unfavourable S-C-C-S *gauche* torsion angles[42]. The situation in $[Pd([14]aneS_4)]^{2+}$ still features a small out of plane displacement (0.0381Å) of the Pd(II) ion but the macrocycle adopts a less strained conformation. One electron reductions of all three complexes yields diamagnetic Pd(I) species which are proposed to be metal-metal bonded dimers[42].

$[Pd([18]aneS_6)]^{2+}$ (**Figure 4.1.1c**) has been prepared by reaction of $(PdCl_2)_n$ with $[18]aneS_6$[313]. The yellow-brown BPh_4^- salt (**Figure 4.1.1c** (i)) shows an S-shaped ligand wrapped around the Pd(II)-ion which is co-ordinated square-planar to four S-donor atoms [Pd-S_{eq} 2.3114(14) and 2.3067(15)Å]. The remaining two S-donors participate in weak interactions with the central Pd(II)-ion, characterised by a particularly long Pd···S_{ap} [3.2730(17)Å] distance.

Interestingly the PF_6^- salt (**Figure 4.1.1c** (ii)) is green in the solid state and shows a different structure compared with the BPh_4^- salt [Pd-S_{eq} 2.3347(18)Å and Pd···S_{ap} 3.0154(25)Å][42]. Another important difference between both structures is that in the PF_6^- salt the methylene chains are mutually eclipsed, whereas in the BPh_4^- salt these chains are staggered.

(i) $[Pd([18]aneS_6)](PF_6)_2$ (ii) $[Pd([18]aneS_6)](BPh_4)_2$

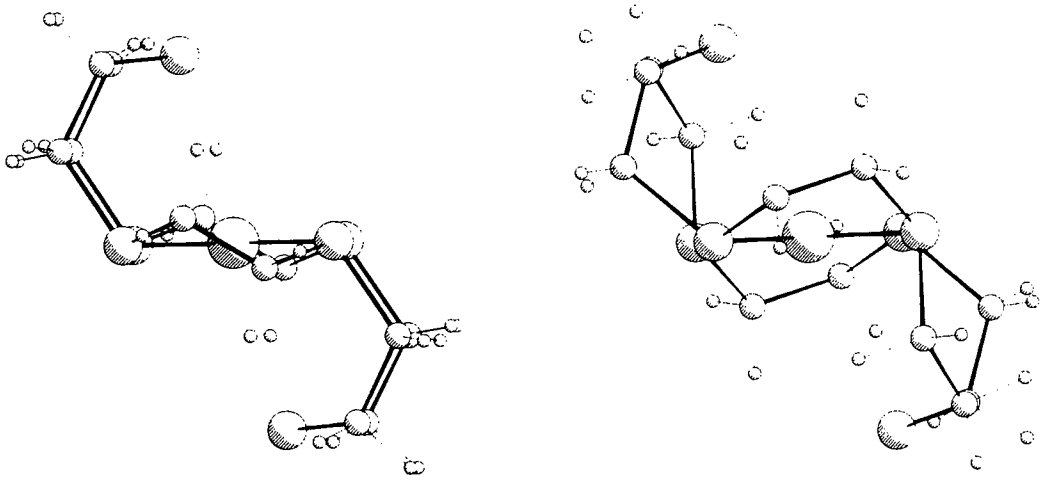

Figure 4.1.1c The single crystal structures of $[Pd([18]aneS_6)]^{2+}$

4.1.2 Pd(II) Complexes with Mixed O/S-Donor Ionophores

Metz and co-workers reported the first complex between a mixed O/S donor ionophore and Pd(II) (**Figure 4.1.2a**)[213]. The single crystal structure of *cis*-$PdCl_2$(1,10-[18]aneS$_2$O$_4$) shows the Pd-atom in a square-planar co-ordination geometry with each Cl-atom [Pd-Cl 2.313(2) and 2.316(2)Å] *trans* to an S-atom [Pd-S 2.302(2) and 2.305(2)Å]. The macrocycle no longer adopts the flat conformation present in its solid state structure but has to wrap around in order to co-ordinate to the Pd-atom in a *cisoid* bidentate binding mode.

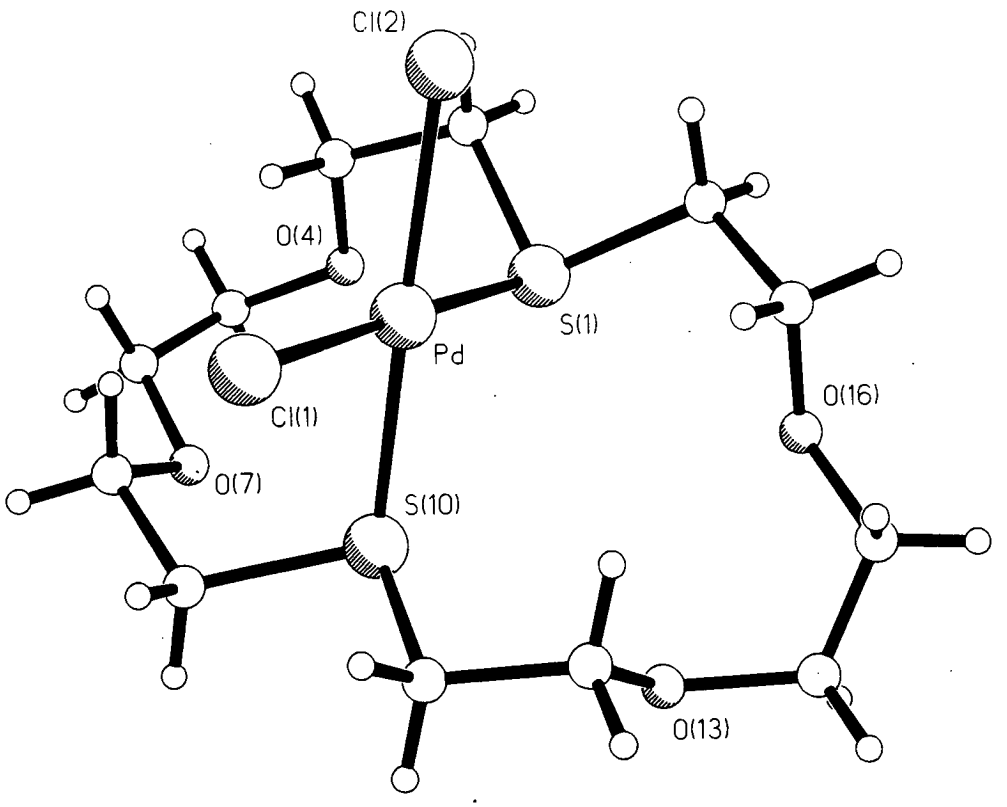

Figure 4.1.2a The single crystal structure of *cis*-$PdCl_2(1,10\text{-}[18]aneS_2O_4)$[221].

Reaction of $(PdCl_2)_n$ with $[15]aneS_2O_3$ in a 1:1 and 1:2 ratio in MeOH yielded the 1:1 product $PdCl_2([15]aneS_2O_3)$ and the 1:2 product $[Pd([15]aneS_2O_3)_2](PF_6)_2$[224,225]. The configuration of Cl- to S-donors in $PdCl_2([15]aneS_2O_3)$ has been assigned to be *transoid* by means of infrared spectroscopy. The single crystal structure of the 1:2 complex shows the Pd(II)-ion occupying a crystallographic inversion centre. The macrocyclic ligand adopts a bidentate symmetrical square-planar co-ordination geometry at the Pd(II) ion [Pd-S 2.3149(10) and 2.3107(10)Å] maintaining a flat conformation with non-interacting *endo*-dentate O-atoms. The ethylene bridge between the two S-atoms bends away from the metal ion to allow for a chelating bidentate co-ordination. The authors point out that $[Pd([15]aneS_2O_3)_2](BPh_4)_2$ can be isolated but decomposition to a black residue occurs readily in solutions of Me_2CO, $MeNO_2$ and MeCN.

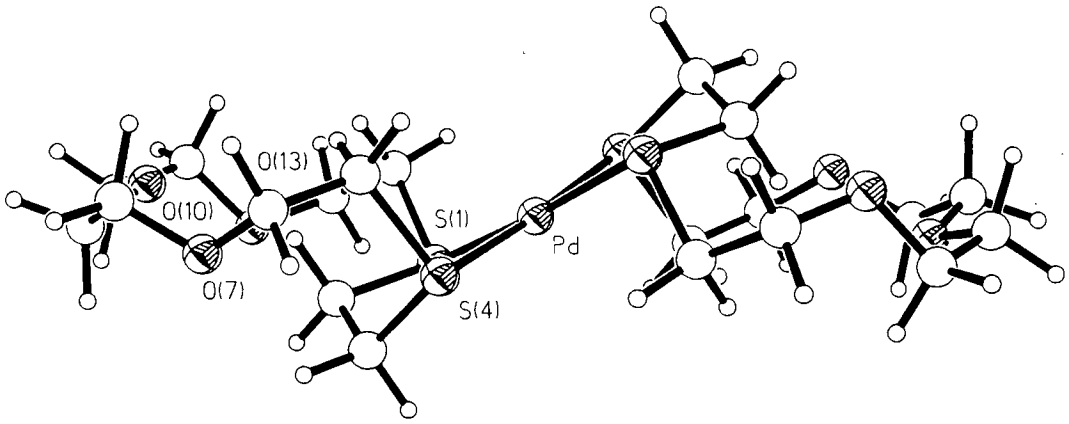

Figure 4.1.2b The single crystal structure of $[Pd([15]aneS_2O_3)_2]^{2+}$ [224,225].

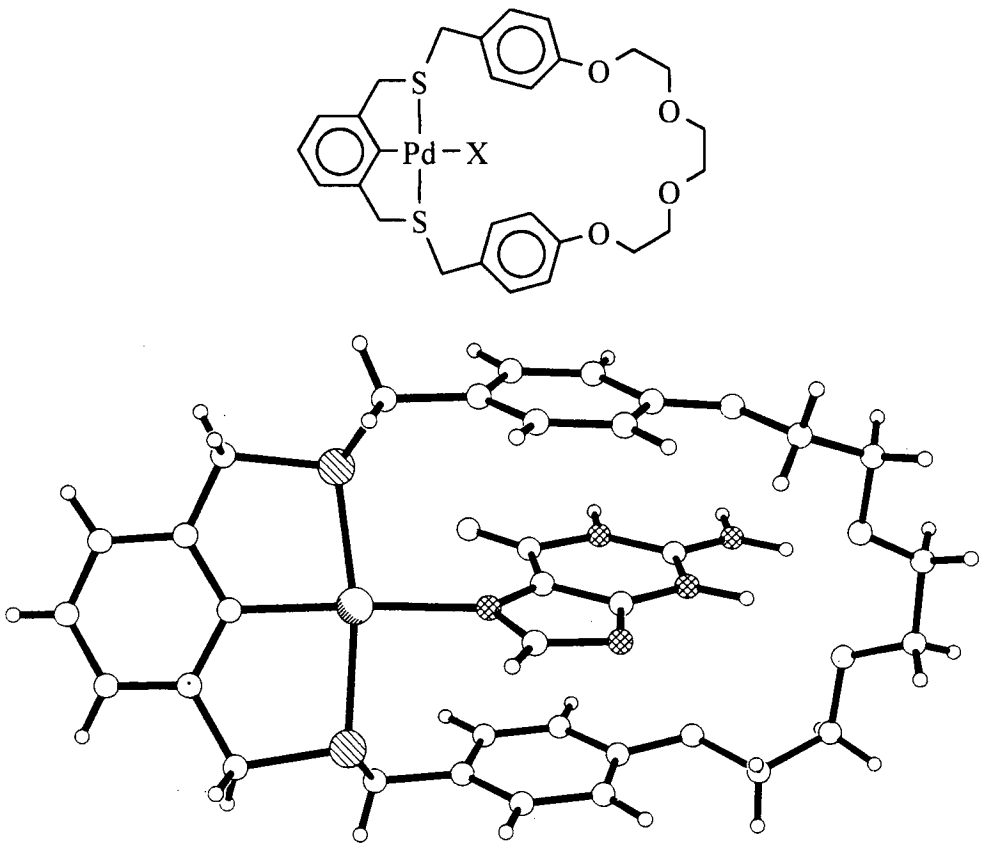

Figure 4.1.2c Mixed O/S-donor receptor molecule and its complex with guanine (X = labile solvent molecule).

Recently Loeb and co-workers[314,315] reported the synthesis of homoleptic S- and mixed O/S-donor macrocycles which simultaneously co-ordinate to a Pd(II) ion, nucleobases or aminopyridines. The compound shown in **Figure 4.1.2c** co-ordinates a Pd(II) ion *transoid* between the two S-atoms. The third co-ordination site binds to a C-atom in the benzene ring leaving the fourth site, which co-ordinates to a labile solvent molecule, free for binding to a guest molecule. The two benzene rings in the polyether chain stabilise the co-ordinated nucleobase via π-stacking. Similar tridentate (NS_2-donor set) ligands containing pyridine instead of benzene moieties and their Rh complexes have been reported by Parker[316,317].

Mixed O/S-donor ionophores such as [18]aneS_2O_4 and the ligand reported by Loeb[314] (**Figure 4.1.2c**) are similar in the sense that both exhibit two different binding sites. It was our aim to establish whether relatively simple mixed O/S-donor ionophores such as [18]aneS_2O_4 are capable of co-ordinating to two different guest ions/molecules at the same time, and to identify certain conditions under which such a bis co-ordination would be possible.

4.2 RESULTS AND DISCUSSION

4.2.1 The Synthesis of $PdCl_2$([18]aneS_2O_4)

The reaction of $(PdCl_2)_n$ with one molar equivalent of [18]aneS_2O_4 in refluxing MeOH/H_2O afforded a yellow solution from which orange crystals precipitated upon cooling. The presence of the ligand in the product was confirmed by infrared and ^{1}H-NMR spectroscopy. The FAB-mass spectrum of the product shows a low intensity peak with the correct isotopic distribution assigned to $[^{106}Pd^{35}Cl_2([18]aneS_2O_4)\text{-}H]^+$. Two additional strong peaks assigned to fragments $[^{106}Pd^{35}Cl([18]aneS_2O_4)]^+$ and $[^{106}Pd([18]aneS_2O_4)]^+$ are also observed. Microanalytical data confirmed the presence of a 1:1 Pd:[18]aneS_2O_4 stoichiometry. Peaks at 340 and 320cm^{-1} in the infrared spectrum were assigned to the Pd-Cl stretching vibration, ν(Pd-Cl), of a *cis*-dichloro complex[225]. This assignment is complicated due to possible Pd-S vibrations. Single crystal X-ray diffraction studies were initiated to confirm the *cisoid* binding in this compound.

4.2.2 The Single Crystal Structure of $PdCl_2([18]aneS_2O_4)$

The single crystal structure of $PdCl_2([18]aneS_2O_4)$ (**Figure 4.2.2a**) shows the Pd(II) ion adopting the expected square-planar co-ordination geometry. The angles around the Pd(II) ion are close to 90° with its largest deviation between the two Cl-atoms [Cl-Pd-Cl = 92.11(5)°]. The Pd-S distances [2.2776(12) and 2.2791(12)Å] are on average 0.038Å shorter compared with the Pd-S distances in $[Pd([18]aneS_2O_4)_2]^{2+}$ (see below) suggesting π-back donation from the Pd(II) ion to the S-atoms with π-donation from the Cl^- to the Pd(II) ion. The macrocyclic ligand binds to the Pd(II) as a bidentate chelate, leaving the O-atoms non-interacting but pointing towards the centre of the cavity. The conformation of the macrocycle [1133343] {a----+aa+aa-aa+aa-+} in this compound is widely unchanged compared with the conformation [1111133133] {++++-aa+aa-aa+aa-+} found in the solid state structure of $[18]aneS_2O_4$. All torsion angles at C-O-C-C are *anti* and *gauche* at O-C-C-O arrangements. The larger deviations can be found in the region directly affected by the binding to the metal in particular the change of a *gauche* to an *anti* angle. The packing diagram of $[PdCl_2([18]aneS_2O_4)]$ (**Figure 4.2.2b**) shows a columnar stacking motif. It is interesting to note that similar environments in particular the macrocyclic polyether chains stack onto each other. Contributing factors are most likely the large size of the $PdCl_2$ moieties and dipole-dipole attraction forces between the planar macrocyclic ligands.

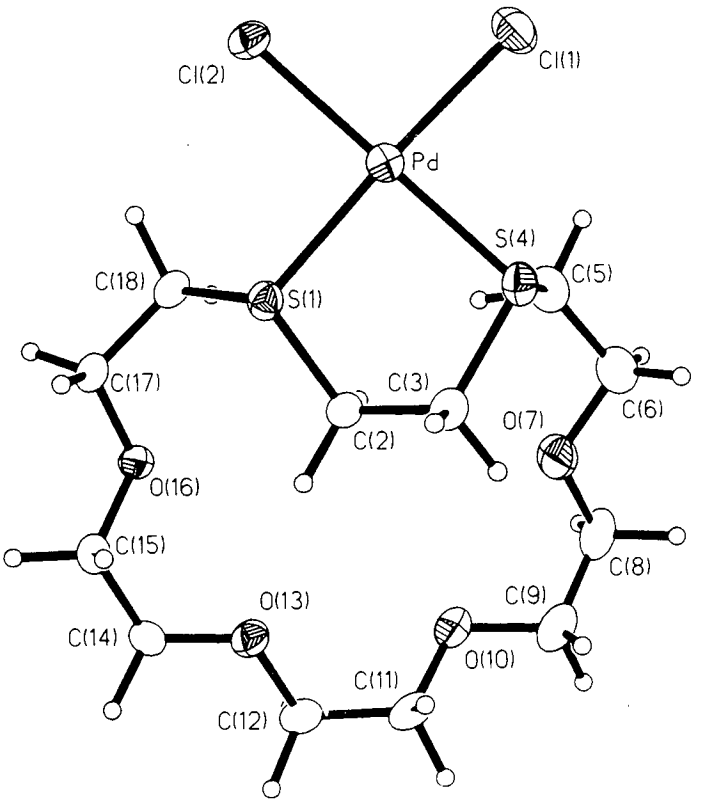

Figure 4.2.2a The single crystal structure of $PdCl_2([18]aneS_2O_4)$.

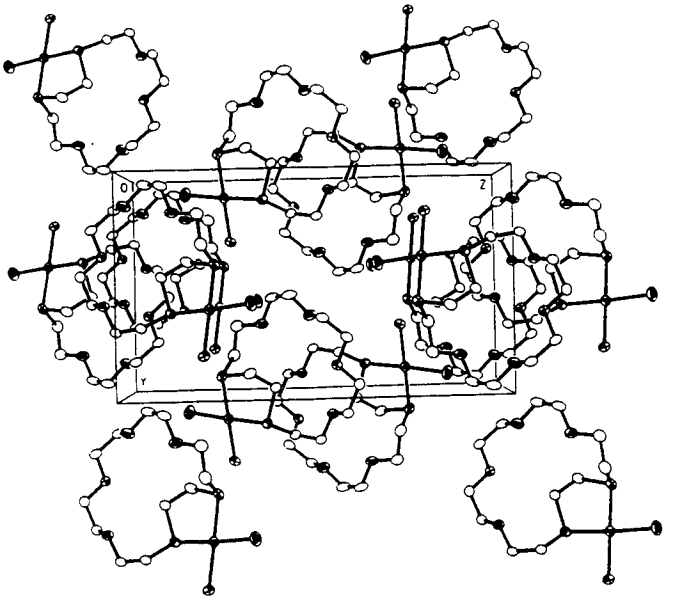

Figure 4.2.2b The packing diagram of $PdCl_2([18]aneS_2O_4)$.

Pd(1)-Cl(1)	2.3047(15)	Pd(1)-S(1)	2.2776(12)
Pd(1)-Cl(2)	2.3102(12)	Pd(1)-S(4)	2.2791(12)
Cl(1)-Pd-Cl(2)	92.11(5)	S(1)-Pd(1)-S(4)	89.00(4)
Cl(1)-Pd-S(1)	176.35(5)	Cl(2)-Pd(1)-S(1)	91.17(4)
Cl(1)-Pd-S(4)	87.75(5)	Cl(2)-Pd(1)-S(4)	179.23(4)
S(1)-C(2)-C(3)-S(4)	-58.1(4)	O(10)-C(11)-C(12)-O(13)	-72.3(5)
C(2)-C(3)-S(4)-C(5)	-68.2(4)	C(11)-C(12)-O(13)-C(14)	177.2(4)
C(3)-S(4)-C(5)-C(6)	-64.2(4)	C(12)-O(13)-C(14)-C(15)	178.9(4)
S(4)-C(5)-C(6)-O(7)	77.2(5)	O(13)-C(14)-C(15)-O(16)	65.7(4)
C(5)-C(6)-O(7)-C(8)	166.0(5)	C(14)-C(15)-O(16)-C(17)	179.9(4)
C(6)-O(7)-C(8)-C(9)	154.4(5)	C(15)-O(16)-C(17)-C(18)	148.1(4)
O(7)-C(8)-C(9)-O(10)	53.8(7)	O(16)-C(17)-C(18)-S(1)	-75.8(4)
C(8)-C(9)-O(10)-C(11)	-163.4(5)	C(17)-C(18)-S(1)-C(2)	74.9(3)
C(9)-O(10)-C(11)-C(12)	-174.3(4)	C(18)-S(1)-C(2)-C(3)	163.8(3)

Table 4.2.2 Selected bond lengths(Å), angles(°) and torsion angles (°) with estimated standard deviations for $PdCl_2([18]aneS_2O_4)$.

4.2.3 The Synthesis of $[Pd([18]aneS_2O_4)_2](PF_6)_2$

$[Pd([18]aneS_2O_4)_2](PF_6)_2$ was prepared following the same procedure as for $PdCl_2([18]aneS_2O_4)$ with a 1:2 Pd:ligand ratio and the addition of excess NH_4PF_6. A yellow microcrystalline powder precipitated out upon cooling and was then isolated and dried. The FAB-mass spectrum of the product shows a molecular ion peak with the correct isotopic distribution corresponding to $[^{106}Pd([18]aneS_2O_4)_2(PF_6)]^+$. The assignment of the compound has been confirmed by IR-spectroscopy and microanalytical data. Attempts to prepare the analogous BPh_4^- salt of the compound failed due to decomposition upon attempted recrystallisation in Me_2CO, MeCN, $MeNO_2$ and DMSO. A similar observation has been made for the analogous complex with $[15]aneS_2O_3$ - $[Pd([15]aneS_2O_3)_2](PF_6)_2$[225] (see section 4.1.2). Single crystals of $[Pd([18]aneS_2O_4)_2](PF_6)_2$ suitable for X-ray diffraction studies were obtained by recrystallisation from $MeNO_2$.

4.2.4 The Single Crystal Structure of $[Pd([18]aneS_2O_4)_2](PF_6)_2$

The single crystal structure of $[Pd([18]aneS_2O_4)_2](PF_6)_2$ (**Figure 4.2.4a**) shows a square-planar geometry [Pd-S = 2.3217(14) and 2.3102(13)Å; S-Pd-S = 88.71(5)°] with the Pd(II) ion occupying a crystallographic inversion centre. The conformation of the macrocycle [1134324]{++a-+aa-aa++a+aa-+} in this compound is very similar to the one in $PdCl_2([18]aneS_2O_4)$ The only difference is the change of an *anti* to a *gauche* angle in the polyether region of the ligand. The region affected by the co-ordination to the Pd(II)-ion is virtually identical to the previous structure.

The packing diagram (**Figure 4.2.4b**) shows isolated dianions and cations in the crystal lattice. No significant intermolecular interactions could be identified. The actual packing is however very similar compared with the one found for $[Pd([18]aneS_3O_3)_2](PF_6)_2$ (see below) which is not surprising because both crystallise in the same space group (*P*-1).

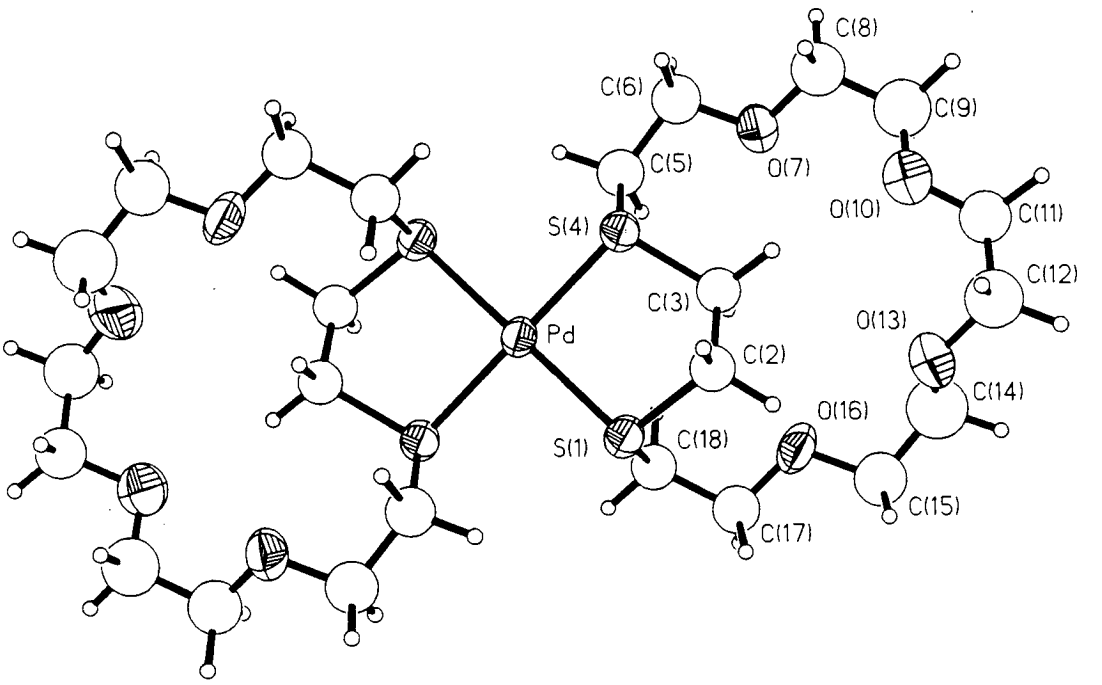

Figure 4.2.4a The single crystal structure of $[Pd([18]aneS_2O_4)_2](PF_6)_2$.

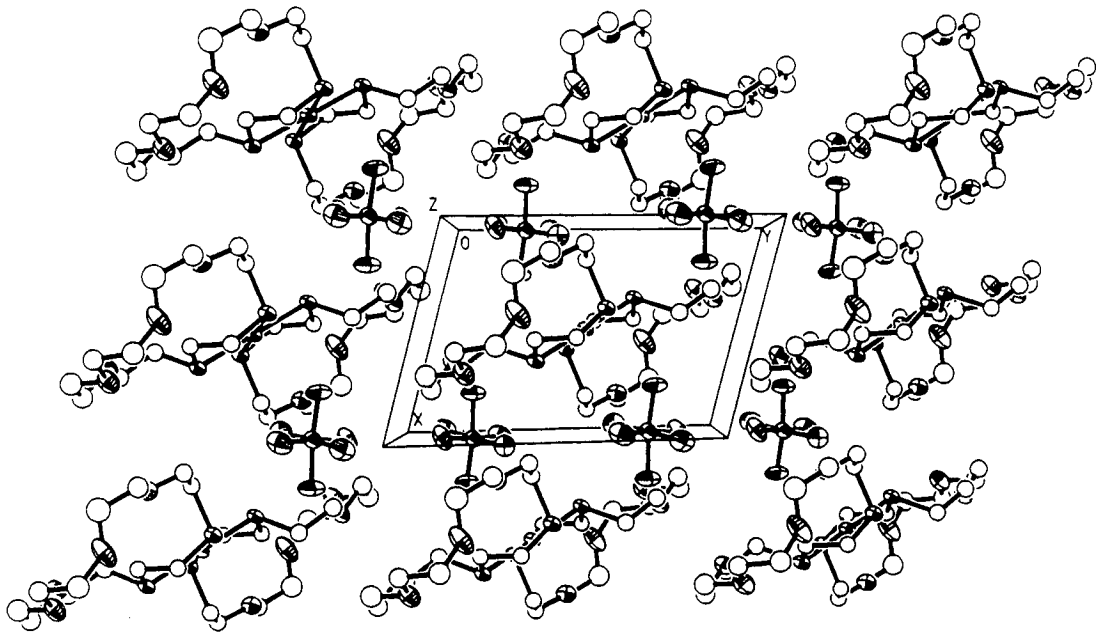

Figure 4.2.4b The packing diagram of $[Pd([18]aneS_2O_4)_2](PF_6)_2$.

Pd-S(1)	2.3217(14)	Pd-S(4)	2.3102(13)
S(1)-Pd-S(4)	88.71(5)	S(1)-Pd(1)-S(1')	91.29(5)
S(1)-C(2)-C(3)-S(4)	59.5(4)	O(10)-C(11)-C(12)-O(13)	75.7(3)
C(2)-C(3)-S(4)-C(5)	-158.7(3)	C(11)-C(12)-O(13)-C(14)	77.6(3)
C(3)-S(4)-C(5)-C(6)	-77.5(4)	C(12)-O(13)-C(14)-C(15)	160.6(4)
S(4)-C(5)-C(6)-O(7)	67.6(5)	O(13)-C(14)-C(15)-O(16)	68.8(6)
C(5)-C(6)-O(7)-C(8)	-161.5(4)	C(14)-C(15)-O(16)-C(17)	-176.9(5)
C(6)-O(7)-C(8)-C(9)	-178.1(5)	C(15)-O(16)-C(17)-C(18)	169.5(4)
O(7)-C(8)-C(9)-O(10)	-63.8(6)	O(16)-C(17)-C(18)-S(1)	-80.9(4)
C(8)-C(9)-O(10)-C(11)	169.0(4)	C(17)-C(18)-S(1)-C(2)	56.4(4)
C(9)-O(10)-C(11)-C(12)	-176.4(3)	C(18)-S(1)-C(2)-C(3)	64.2(4)

(Primed atoms are related to non-primed atoms by the following symmetry operation -x, -y, -z)

Table 4.2.4 Selected bond lengths (Å), angles (°) and torsion angles (°) with estimated standard deviations for $[Pd([18]aneS_2O_4)_2](PF_6)_2$.

4.2.5 The Synthesis of $[Pd([18]aneS_3O_3)_2](PF_6)_2$

The Pd(II) ion in $[Pd([15]aneS_2O_3)_2](PF_6)_2$, $PdCl_2([18]aneS_2O_4)$ and $[Pd([18]aneS_2O_4)_2](PF_6)_2$ co-ordinates *exo* to the macrocyclic ligand. We were on the other hand particularly interested to prepare a mixed O/S donor macrocyclic complex with the Pd(II) ion co-ordinated *endo* within or in close proximity to the cavity in order to study allosteric effects between the Pd(II) ion and a second guest molecule (ion or neutral molecule). We felt at this point that a simple enlargement of the macrocyclic cavity would not yield the desired result of *endo* co-ordination. $[18]aneS_3O_3$ in contrast to $[18]aneS_2O_4$ contains a soft tridentate binding site which seemed to be more promising to force the Pd(II) ion into the cavity.

The reaction of $[18]aneS_3O_3$ with $(PdCl_2)_n$ in refluxing $MeOH/H_2O$ yielded after addition of NH_4PF_6 and removal of the solvent a dark orange resin. Purification was achieved by repeated recrystallisation from Me_2CO. The FAB mass spectrum of the product shows peaks corresponding to $[^{106}Pd([18]aneS_3O_3)_2(PF_6)]^+$ and $[^{106}Pd([18]aneS_3O_3)]^+$ with the correct isotopic distribution. Microanalytical results showed good agreement with the a 1:2 Pd:$[18]aneS_3O_3$ stoichiometry. Single crystal X-ray diffraction studies where initiated to establish the co-ordination geometry in this compound

4.2.6 The Single Crystal Structure of $[Pd([18]aneS_3O_3)_2](PF_6)_2$

$[Pd([18]aneS_3O_3)_2](PF_6)_2$ crystallises in the space group *P*-1 (No. 2) with the Pd(II) ion in a special position (½, ½, ½). Each asymmetric unit contains therefore one $[18]aneS_3O_3$ molecule and the Pd(II) ion with a site occupancy of 50%. The single crystal structure in particular the Pd(II) environment of $[Pd([18]aneS_3O_3)_2](PF_6)_2$ **(Figure 4.2.6a)** is basically similar to the one found in the single crystal structure of $[Pd([18]aneS_2O_4)_2](PF_6)_2$. The Pd(II) ion adopts the typical square-planar S_4 co-ordination geometry [Pd-S_{equ} = 2.3081(22) and 2.3193(21)Å]. The S(1)-Pd-S(4) angle [88.33(8)°] is, similar to $PdCl([18]aneS_2O_4)$ and $[Pd([18]aneS_2O_4)_2](PF_6)_2$, slightly smaller than 90° indicating some strain in the bidentate co-ordination site. The S-C-C-S moiety adopts a *gauche* torsion angle of about 60°. These findings suggest that this situation is generated by a competition of the metal to adopt a square-planar co-ordination geometry and the ligand to minimise its conformational strain.

A major difficulty during refinement of the structure of $[Pd([18]aneS_3O_3)_2](PF_6)_2$ was disorder which affected in particular the environment of the third non co-ordinated S-donor atom. The disorder was modelled in two mutual equivalent positions with site occupancy factors of 50% for each disordered atom. The plot of the contents of the asymmetric unit for each of the two disordered molecules (**Figure 4.2.6b**) shows that S(16) [Pd····$S(16)_{ap}$ 3.2901(24)Å] in contrast to its equivalent S(7) [Pd·····S(7) 4.3744(25)Å] adopts a long range apical position at the Pd(II) ion. The O-atoms even though affected by this disorder [O(7) and O(16)] do not show any interaction with the Pd(II) centre.

Intermolecular (**Figures 4.2.6c** and **4.2.6d**) and intramolecular (**Figure 4.2.6a**) interactions responsible for the disorder could not be identified. It has therefore to be concluded that the disorder found in this structure is statistically random with respect to the distribution within the unit cell and the crystal lattice.

Pd-S(1)	2.3081(22)	Pd-S(4)	2.3193(21)
Pd·····S(16)	3.2901(23)	Pd·····S(7)	4.3744(25)
S(1)-Pd-S(4)	88.33(8)	S(1)-Pd-S(1')	91.67(8)
S(1)-C(2)-C(3)-S(4)	-60.0(7)	O(10)-C(11)-C(12)-O(13)	64.8(11)
C(2)-C(3)-S(4)-C(5)	-65.7(7)	C(11)-C(12)-O(13)-C(14)	-173.9(9)
C(3)-S(4)-C(5)-C(6)	169.5(7)	C(12)-O(13)-C(14)-C(15)	150.4(10)
S(4)-C(5)-C(6)-S(7)	55.3(8)	C(12)-O(13)-C(14)-C(15')	-167.7(9)
S(4)-C(5)-C(6)-O(7)	57.6(10)	O(13)-C(14)-C(15)-O(16)	65.0(17)
C(5)-C(6)-S(7)-C(8)	161.9(7)	O(13)-C(14)-C(15')-S(16)	-67.5(9)
C(5)-C(6)-O(7)-C(8')	172.6(12)	C(14)-C(15)-O(16)-C(17)	173.7(12)
C(6)-S(7)-C(8)-C(9)	79.0(8)	C(14)-C(15')-S(16)-C(17)	-160.9(8)
C(6)-O(7)-C(8')-C(9)	61.2(20)	C(15)-O(16)-C(17)-C(18)	-175.2(11)
S(7)-C(8)-C(9)-O(10)	-78.6(9)	C(15')-S(16)-C(17)-C(18)	-87.3(9)
O(7)-C(8')-C(9)-O(10)	-51.0(16)	O(16)-C(17)-C(18)-S(1)	-76.3(9)
C(8)-C(9)-O(10)-C(11)	-177.4(9)	S(16)-C(17)-C(18)-S(1)	-40.4(11)
C(8')-C(9)-O(10)-C(11)	161.9(9)	C(17)-C(18)-S(1)-C(2)	-55.3(8)
C(9)-O(10)-C(11)-C(12)	-176.7(8)	C(18)-S(1)-C(2)-C(3)	159.9(6)

(Primed atoms are related to non-primed atoms by the following symmetry operation -x, -y, -z)

Table 4.2.6 Selected bond lengths (Å), angles (°) and torsion angles (°) with estimated standard deviations for $[Pd([18]aneS_3O_3)_2](PF_6)_2$.

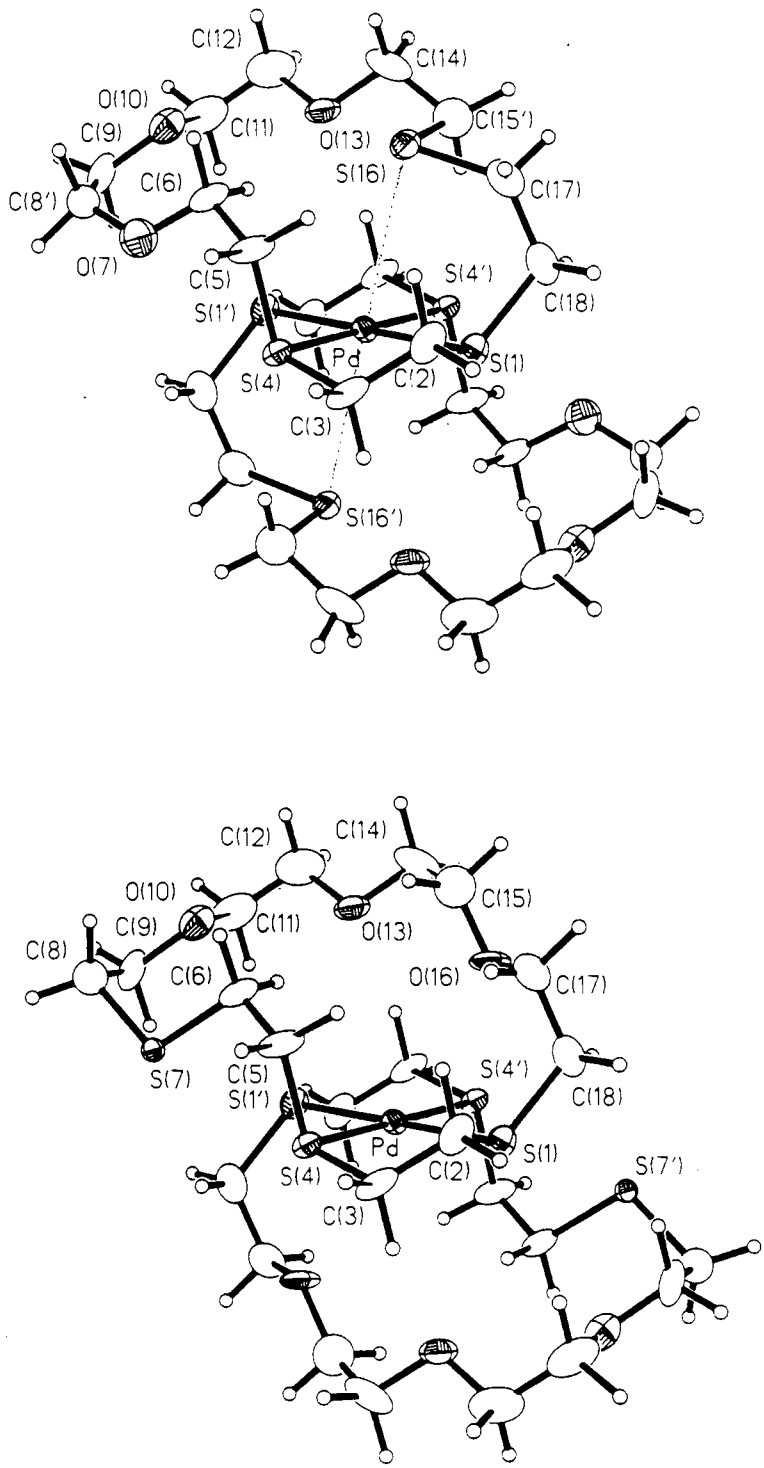

Figure 4.2.6a The two dications found in the single crystal structure of $[Pd([18]aneS_3O_3)_2](PF_6)_2$.

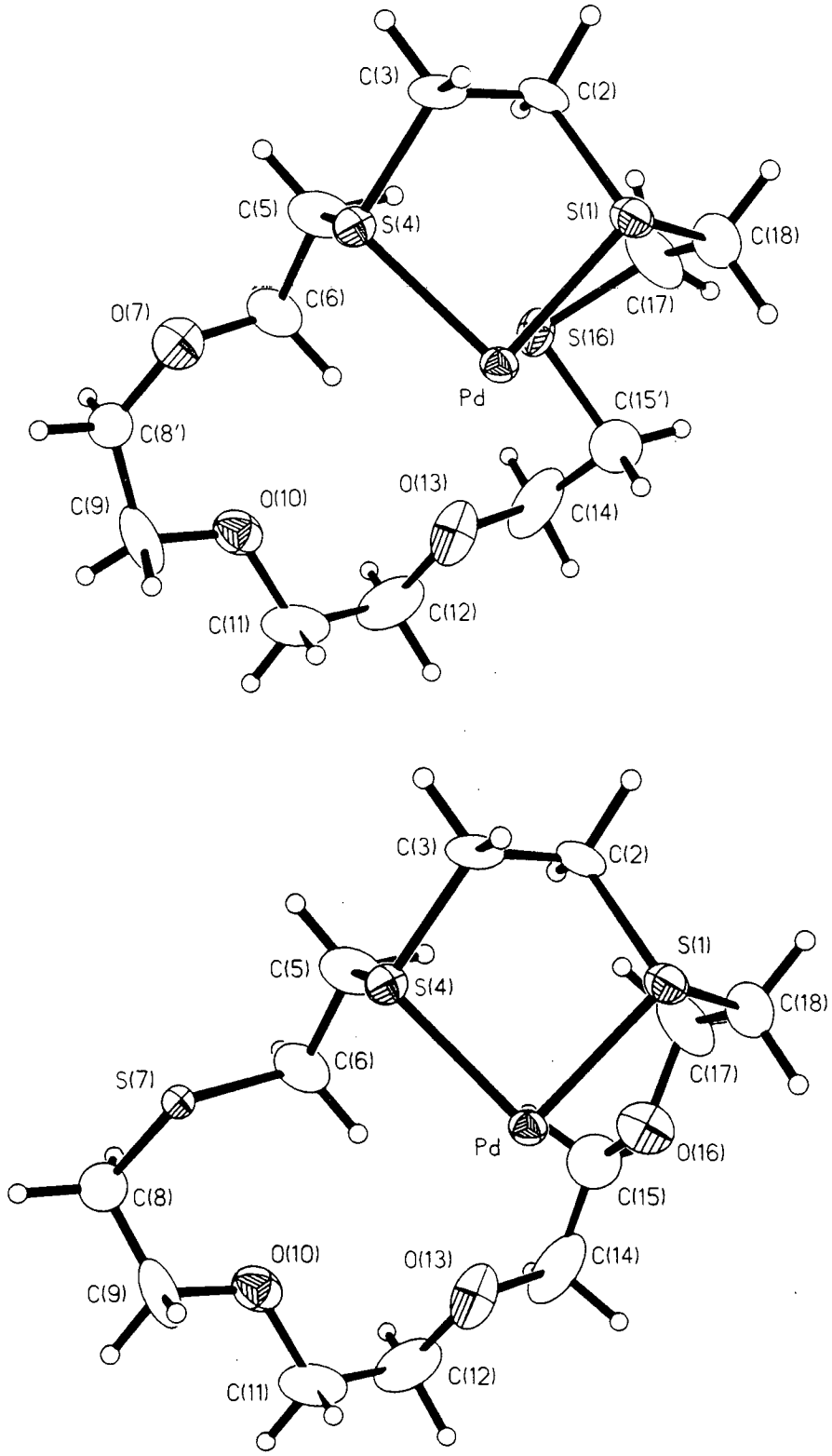

Figure 4.2.6b Plot of the contents of the asymmetric unit for both disordered molecules in $[Pd([18]aneS_3O_3)_2](PF_6)_2$.

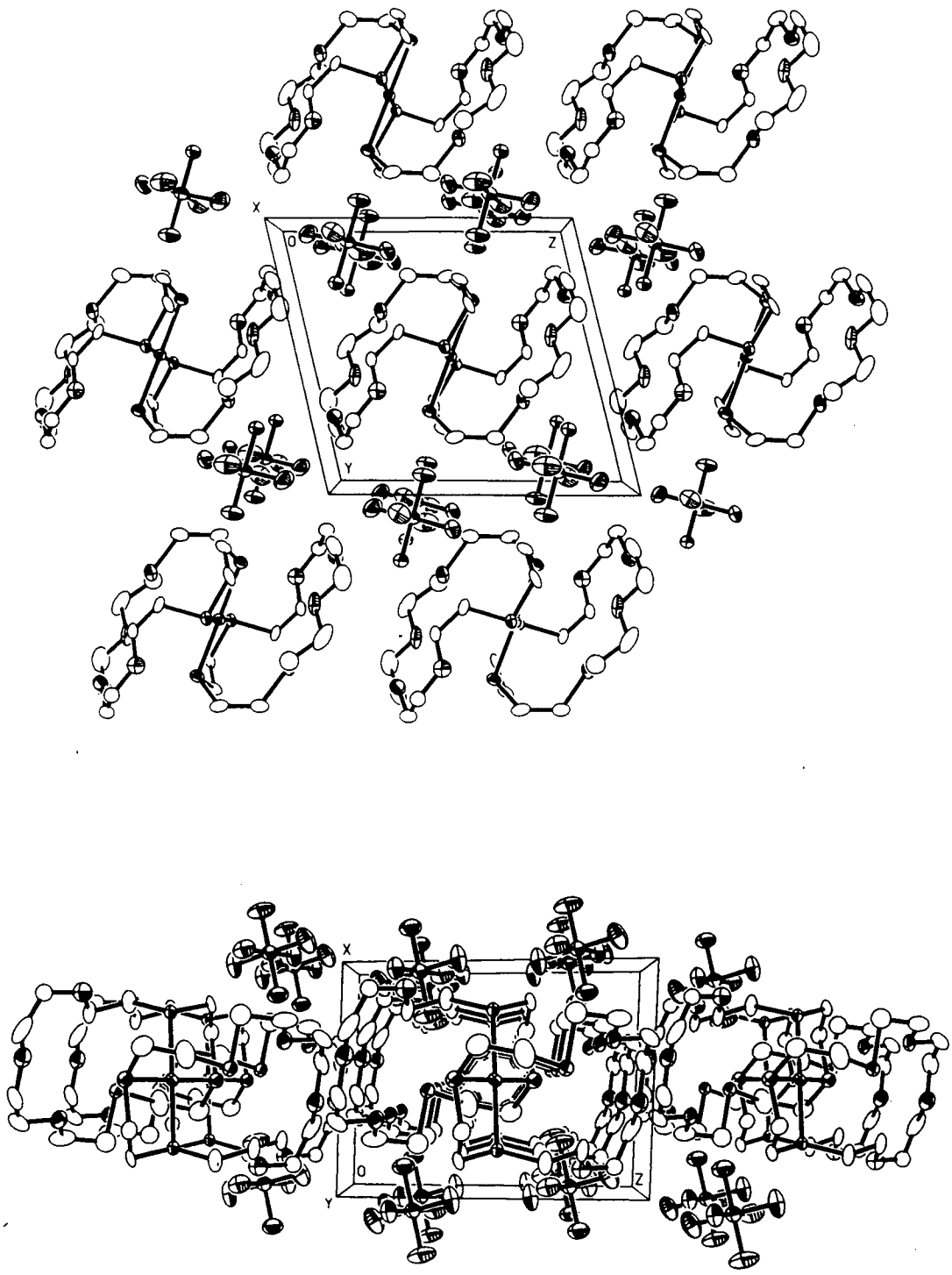

Figure 4.2.6c Packing diagrams of $[Pd([18]aneS_3O_3)_2](PF_6)_2$ showing disordered molecules with apical Pd-S interaction.

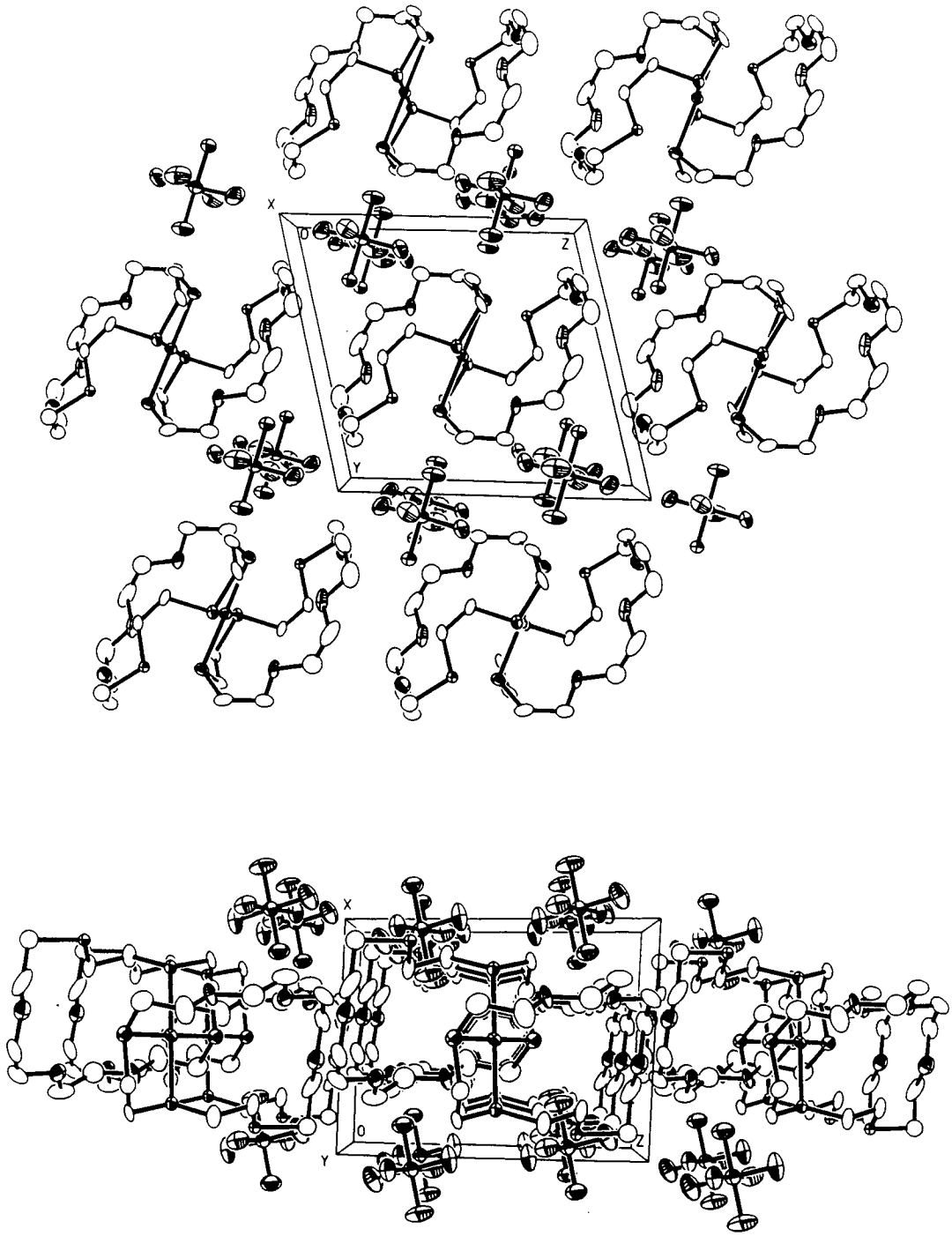

Figure 4.2.6d Packing diagrams of [Pd([18]aneS_3O_3)$_2$](PF_6)$_2$ showing disordered molecules without apical Pd-S interaction.

4.2.7 The Synthesis of $[PdCl([20]aneS_3O_3)]BPh_4$

The macrocyclic ligand $[20]aneS_3O_3$ contains the same donor set compared with $[18]aneS_3O_3$ with the difference of propylene instead of ethylene linkages between the S-donors. We anticipated that such a ligand would be able to co-ordinate with all three S-donors to the Pd(II) ion avoiding any strained geometries. These considerations are based in particular on the results obtained for complexes between Pd and $[12\text{-}16]aneS_4$ macrocycles (see above). In this series the only complex which is completely strain free is the one with $[16]aneS_4$ which contains only propylene bridges.

$[PdCl([20]aneS_3O_3)]BPh_4$ was prepared by reacting $(PdCl_2)_n$ and $[20]aneS_3O_3$ in refluxing $MeOH/H_2O$. Addition of $NaBPh_4$ to the cold reaction mixture afforded an orange microcrystalline product which recrystallised from Me_2CO. The FAB-mass spectrum of the product shows a peak with the correct isotopic distribution assigned to $[PdCl([20]aneS_3O_3)]^+$. The microanalysis is in good agreement with the proposed stoichiometry. Crystals suitable for single crystal X-ray diffraction studies could not be isolated and the actual configuration of the complex has still to be determined.

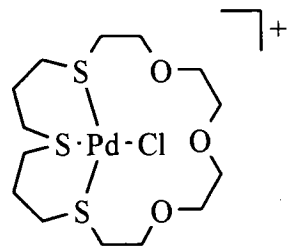

Figure 4.2.7 Proposed structure of $[PdCl([20]aneS_3O_3)]^+$.

The proposed structure shown in **Figure 4.2.7** is primarily based on the microanalytical results and mass spectrometry results. There is however a second argument. All previously prepared complexes between Pd(II) and mixed O/S donor ionophores decomposed rapidly upon recrystallisation when isolated as the BPh_4^- salt to give a black residue[225]. The common feature in all these compounds is the *exo* bidentate co-ordination mode of Pd(II) ion to the macrocyclic ligand ($[15]aneS_2O_3$, $[18]aneS_2O_4$ and $[18]aneS_3O_3$) leaving apical binding sites unprotected. We believe that the observed increased stability of $[PdCl([20]aneS_3O_3)]BPh_4$ is most likely due to a different (*endo* tridentate) co-ordination mode of the Pd(II) ion.

4.3 CONCLUSION

The work described in this chapter identified some important factors for the design of a metal [Pd(II)] macrocyclic host for the co-ordination other metal ions or neutral molecules. The single crystal structures of $PdCl_2([18]aneS_2O_4)$ and $[Pd([18]aneS_2O_4)_2](PF_6)_2$ show clearly that a potential in cavity co-ordination of a guest ion is hindered due to the position of the ethylene bridge between both thioether donors. Substitution of the bidentate ligand $[18]aneS_2O_4$ by the tridentate ligand $[18]aneS_3O_3$ did not lead to the expected complex with the Pd(II) ion co-ordinated inside the macrocyclic cavity but the rigidity of the soft thioether binding site was identified as the cause for this behaviour. The ethylene bridges between the thioether donor-atoms in $[18]aneS_3O_3$ were subsequently substituted by propylene bridges leading to $[20]aneS_3O_3$. $[PdCl([20]aneS_3O_3)]BPh_4$ shows in contrast to all other Pd(II) compounds with mixed O/S-donor ionophores an enhanced stability which strongly suggests the Pd(II) ion adopts a very much different co-ordination geometry in this compound compared with the other complexes studied.

Future work has to confirm the proposed structure of $[PdCl([20]aneS_3O_3)]BPh_4$ which is a potential candidate for further developments. The major objective in such a development has to consist of enlargement of the macrocyclic cavity either by extending the polyether chain or the introduction of aromatic spacers which could stabilise a potential guest molecule via π-stacking.

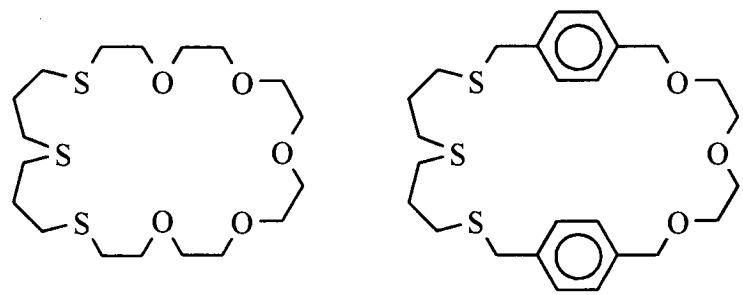

Figure 3.3 Two macrocyclic ligands derived from $[20]aneS_3O_3$ which are potential candidates for the simultaneous co-ordination of metal ions or neutral molecules with a Pd(II).

4.4 EXPERIMENTAL SECTION

4.4.1 The Synthesis of Pd([18]aneS$_2$O$_4$)Cl$_2$

$(PdCl_2)_n$ (40 mg, 0.226 mmol) was added to a solution of [18]aneS$_2$O$_4$ (0.226 mmol, 67 mg) MeOH/H$_2$O (1:1, v/v, 35 cm^3). The reaction mixture was heated under N_2 for 2 hours during which time the colourless solution turned slowly yellow. The solution was filtered while hot to remove metallic Pd and unreacted $PdCl_2$ and was left to cool down to ambient temperature. Orange crystals precipitated from the solution while standing and were collected, dried and characterised. The crystals were suitable for single crystal diffraction studies.

Yield: 55 mg, 0.116 mmol [calc. for $PdCl_2$([18]aneS$_2$O$_4$)], 50%

Microanalysis (for $C_{12}H_{24}Cl_2O_4PdS_2$; Mol.wt. = 473.77 gmol^{-1})

	%C	%H
Calculated	30.4	5.11
Found	30.2	5.14

FAB mass spectrum (3-NOBA):

Fragment:	m/z (calc.)	m/z (found)	rel.Int.
$[^{106}Pd^{35}Cl_2$([18]aneS$_2$O$_4$)]$^+$	473	473	0.04
$[^{106}Pd^{35}Cl$([18]aneS$_2$O$_4$)]$^+$	437	439	1.00
$[^{106}Pd$([18]aneS$_2$O$_4$)]$^+$	402	402	1.00

IR spectrum (KBr disc):

2960m, 2900m, 1480m, 1440m, 1420m, 1400m, 1360m, 1350m, 1340m, 1290m, 1250m, 1180w, 1105s, 1020w, 940m, 920w, 840m, 340w and 320w cm^{-1}.

^{1}H-NMR spectrum (CD_3NO_2; 298K; 200.13 MHz)

δ 3.00 - 4.25 (m, 24H) [18]aneS$_2$O$_4$

4.4.2 The Synthesis of [Pd([18]aneS$_2$O$_4$)$_2$](PF$_6$)$_2$

[Pd([18]aneS$_2$O$_4$)$_2$](PF$_6$)$_2$ was prepared in analogy to PdCl$_2$([18]aneS$_2$O$_4$) using $PdCl_2$ (0.169 mmol, 30 mg) and [18]aneS$_2$O$_4$ (0.338 mmol, 100 mg). Excess NH_4PF_6 was added to the bright yellow solution which had formed after 2 hours refluxing under N_2. The reaction mixture was allowed to cool down to ambient temperature and later transferred to the freezer in order to force precipitation. A yellow powder could be isolated, which was dried and characterise. Recrystallisation, affording crystals suitable for single crystal X-ray diffraction studies, was achieved using $MeNO_2$.

Microanalysis (for $C_{24}H_{48}F_{12}O_8P_2PdS_4$; Mol.wt. = 989.25 $gmol^{-1}$)

	%C	%H
Calculated	29.1	4.89
Found	29.1	4.91

FAB mass spectrum (3-NOBA):

Fragment:	m/z (calc.)	m/z (found)	rel.Int.
$[^{106}Pd([18]aneS_2O_4)_2(PF_6)]^+$	843	843	0.10
$[^{106}Pd([18]aneS_2O_4)_2]^+$	698	697	0.06
$[^{106}Pd([18]aneS_2O_4)]^+$	402	404	1.00

IR spectrum (KBr disc):

3655w, 3510w/br, 2995m, 2955m, 2900s, 1955w, 1630w, 1475m, 1400m, 1355s, 1290m, 1245m, 1195w, 1120vs, 1095s, 1040m, 935m, 920m, 835vs and 560s cm^{-1}.

4.4.3 The Synthesis of $[Pd([18]aneS_3O_3)_2](PF_6)_2$

The reaction between $PdCl_2$ (0.5 mmol, 89 mg), $[18]aneS_3O_3$ (1.0 mmol, 312 mg) and excess NH_4PF_6 in a mixture of MeCN/MeOH (9:1, v/v, 20 cm^3) afforded after two hours refluxing under N_2 and removal of the solvents an orange resin. Successive recrystallisation using MeCN finally afforded crystals suitable for single crystal X-ray diffraction studies, which were characterised.

Microanalysis (for $C_{24}H_{48}F_{12}O_6P_2PdS_6$; Mol.wt. = 1021.38 $gmol^{-1}$)

	%C	%H
Calculated	28.22	4.74
Found	28.61	4.90

FAB mass spectrum (3-NOBA):

Fragment:	m/z (calc.)	m/z (found)	rel. Int.
$[^{106}Pd([18]aneS_3O_3)_2(PF_6)]^+$	875	877	0.15
$[^{106}Pd([18]aneS_3O_3)_2]^+$	730	729	0.20
$[^{106}Pd([18]aneS_3O_3)]^+$	418	418	1.00

UV/vis spectrum (MeCN):

λ_{max} = 295nm (ε_{max} = 18000dm^3 mol^{-1} cm^{-1}).

4.4.4 The Synthesis of [PdCl([20]aneS$_3$O$_3$)]BPh$_4$

$PdCl_2$ (0.5 mmol, 89 mg) and [20]aneS$_3$O$_3$ (0.5 mmol, 170 mg) were heated in MeOH/H_2O (5:1 v/v 12 ml) for two hours under N_2. Addition of excess of $NaBPh_4$ to the cold reaction mixture, removal of the solvent and successive recrystallisation from Me_2CO yielded an orange microcrystalline product, which was characterised.

Yield: 60 mg, 0.075 mmol (calc. for [PdCl([20]aneS$_3$O$_3$)]BPh$_4$), 15%

Microanalysis (for $C_{38}H_{48}BClO_3PdS_3$; Mol.wt. = 801.68 gmol^{-1})

	%C	%H
Calculated	56.93	6.04
Found	56.60	5.92

FAB mass spectrum (3-NOBA):

Fragment:	m/z (calc.)	m/z (found)
[^{106}Pd^{35}Cl([20]aneS$_3$O$_3$)]$^+$	483	483

IR spectrum (KBr disc):

3053m, 2982w, 2920m, 1720w, 1657w, 1579m, 1478m, 1426m, 1351w, 1262m, 1183w, 1110s, 1032m, 904w, 842m, 735vs, 708vs, 620m, 558w, and 464w cm^{-1}.

^{1}H-NMR spectrum ($(CD_3)_2CO$; 297K; 250.13 MHz)

δ 1.9 ppm (m, 4H) $SCH_2C\boldsymbol{H}_2CH_2S$

δ 2.7 ppm (m, 12H) $SC\boldsymbol{H}_2$

δ 3.6 ppm (m, 12H) $OC\boldsymbol{H}_2$

δ 6.7 - 7.8 ppm (m, 20H) [$B(C_6\boldsymbol{H}_5)_4$]$^-$

4.4.5 Single Crystal Structure Determinations

The single crystal X-ray structures of $PdCl_2$([18]aneS$_2$O$_4$), [Pd([18]aneS$_2$O$_4$)$_2$](PF$_6$)$_2$ and [Pd([18]aneS$_3$O$_3$)$_2$](PF$_6$)$_2$ have been solved and refined as outlined in the general procedure for solution and refinement of single crystal X-ray structures (**A.4**). Selected crystallographic details are summarised in **Table 4.4.5**. All three structures exhibited disorder within the macrocyclic ligand. The disorder in [Pd([18]aneS$_3$O$_3$)$_2$](PF$_6$)$_2$ is discussed under section **4.2.6** whereas the minor disorders in the two other structures have been modelled satisfactorily in two alternative positions following general procedures (**A.4**).

Compound	$PdCl_2([18]aneS_2O_4)$	$[Pd([18]aneS_2O_4)_2]^{2+}$ $2\ PF_6^-$	$[Pd([18]aneS_3O_3)_2]^{2+}$ $2\ PF_6^-$
Crystal data			
Formula	$C_{12}H_{24}Cl_2O_4S_2Pd$	$C_{24}H_{48}F_{12}O_8P_2S_4Pd$	$C_{24}H_{48}F_{12}O_6P_2S_6Pd$
M / gmol^{-1}	473.7	989.25	1021.7
Crystal size / mm	0.20 x 0.40 x 1.00	0.12 x 0.19 x 0.82	0.12 x 0.23 x 0.35
Crystal system	monoclinic	triclinic	triclinic
Space group	$P2_1/n$ (alt. $P2_1/c$; No. 14)	P-1 (No. 2)	P-1 (No. 2)
a / Å	8.714(2)	7.7395(15)	8.421(8)
b / Å	10.915(3)	11.6179(24)	10.478(8)
c / Å	18.787(8)	11.8825(24)	11.243(11)
α / °	90	102.171(12)	76.01(7)
β / °	92.04(3)	95.518(15)	87.10(8)
γ / °	90	103.673(15)	84.61(7)
U / Å^3	1785.00	1002.76	958.00
Z	4	1	1
D_c / g cm^{-3}	1.76	1.638	1.770
μ / mm^{-1}	1.56	0.828	0.967
$F(000)$	960	504	520
T / K	295	298	150
Reflections at $\pm\omega$ to refine cell	24	20	11 (matrix refined)
2θ range/°	30 - 32	26 - 29	24 - 26
Data Collection			
$2\theta_{max}$/°	45	45	45
Range of h	$-9 \rightarrow 9$	$-8 \rightarrow 8$	$-10 \rightarrow 9$
Range of k	$0 \rightarrow 11$	$-12 \rightarrow 12$	$-10 \rightarrow 11$
Range of l	$0 \rightarrow 20$	$0 \rightarrow 12$	$0 \rightarrow 12$
Measured reflections	2260	2632	2490
Independent reflections, R_{int}	2260	2632	2336
Observed reflections	2073 with $F \geq 4\sigma(F)$	2306 with $F \geq 4\sigma(F)$	2336 with $F \geq 4\sigma(F)$
ψ scan correction $TF_{max,\ min}$	-	-	-
Solution			
Method	Patterson Synthesis	Patterson Synthesis	Patterson Synthesis
using	SHELX76	SHELX76	SHELX76
Refinement			
full matrix least squares on	F	F	F
using	SHELX76	SHELX76	SHELX76
DIFABS max, min	1.179, 0.874	-	1.162, 0.842
Weighting scheme	$1.20 \cdot 10^{-4}$	$1.93 \cdot 10^{-4}$	$1.214 \cdot 10^{-4}$
Parameters refined	196	210	241
SHELX76 R, R', S	0.028, 0.040, 1.38	0.045, 0.059, 1.22	0.063, 0.083, 1.10
SHELXL93 $R1$, $wR2$, S	-	-	-
$(\Delta/\sigma)_{max}$	0.160	0.100	0.002
$\Delta\rho_{max,\ min}$ / eÅ^{-3}	+0.50, -0.45	+0.65, -0.60	+1.26, -1.11

Table 4.4.5 Selected crystallographic data for the single crystal structures of $PdCl_2([18]aneS_2O_4)$, $[Pd([18]aneS_2O_4)_2](PF_6)_2$ and $[Pd([18]aneS_3O_3)](PF_6)_2$.

CHAPTER V

The Co-ordination Chemistry of Thallium(I) with Mixed O/S-Donor Ionophores

5.1 INTRODUCTION

Tl is one of the elements present in flue dust which is emitted during sulphide roasting for the production of H_2SO_4 and in smelting of Pb and Zn ores. Tl on its own has no major commercial use. Current applications of Tl include semiconductor research and the use of TlBr or TlI in far infrared transparent windows. Tl (as Tl_2SO_4) has been used as a rodenticide. However its lack of taste, smell and colour rendered it too dangerous and it has been banned in many countries[318]. Both, Tl-metal and Tl-salts are extremely toxic[319]. This underlines the importance to be able, even without commercial interest in Tl, to selectively remove it from other elements (Ni, Zn, Cd, In, Ge, Pb, As, Se and Te) in order to protect the environment. The current general extraction process is complicated and involves precipitation of TlCl with HCl and further electrolytic purification. The development of selective ionophores for the complexation of Tl has therefore important environmental implications.

5.1.1 Macrocyclic Chemistry of Tl

The first examples of complexes between Tl and macrocyclic ligands were based on porphyrin derivatives[320-322]. However, none of these compounds has been well characterised which can be attributed in part to the lack of X-ray and spectroscopic techniques (e.g. NMR spectroscopy) during the first half of this century. Naturally occurring Tl has two isotopes ^{203}Tl (29.5%) and ^{205}Tl (70.5%) both of which have the nuclear spin = 1/2. Since Tl(I) and Tl(III) are diamagnetic, Tl-NMR spectroscopy can therefore be used as a probe in Tl chemistry. An example of the usefulness of ^{205}Tl-NMR is provided in a study[323] of the stability of Tl(I) complexes with a range of crown-ethers shown in **Figure 5.1.1a**. The stability constants (K_f) in a variety of non-aqueous solvents were calculated from a plot of ^{205}Tl chemical shift against [ligand] / [Tl(I)] molar ratios. Additionally, a range of Tl(III) complexes with porphyrin derivatives have been prepared and studied employing NMR-techniques[324].

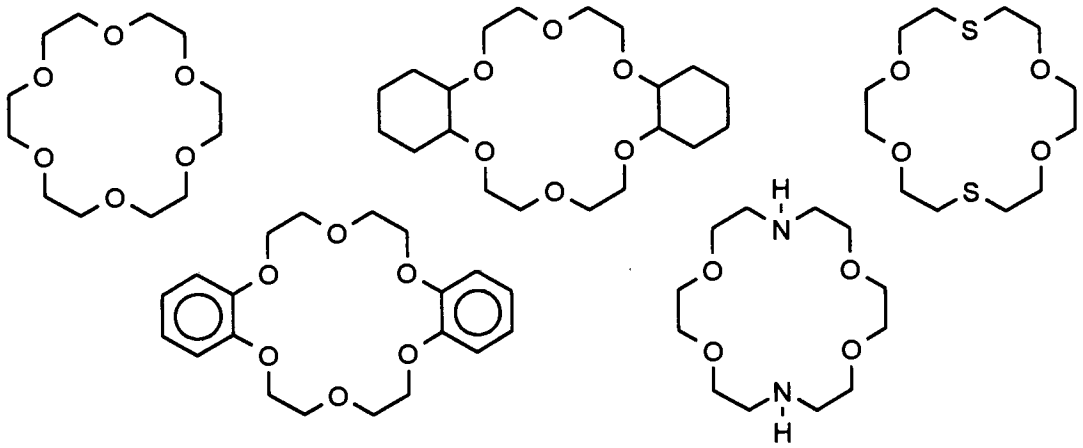

Figure 5.1.1a Macrocyclic ligands used in ^{205}Tl-NMR studies of Tl(I) complexes.

(i) [Tl(OEP)]Cl[325]

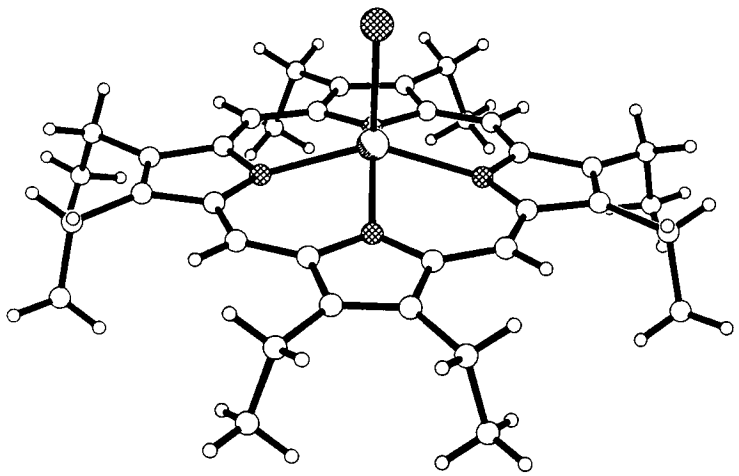

(ii) [Tl(TPP)]Me[326]

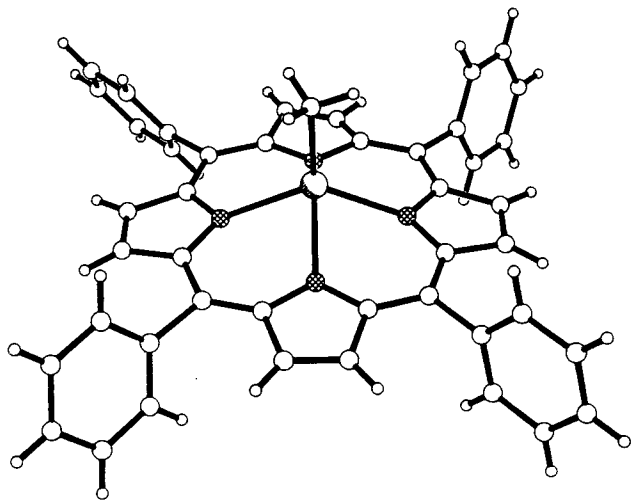

Figure 5.1.1b The single crystal structures of (i) [Tl(OEP)]Cl[325] and (ii) [Tl(TPP)]Me[326] illustrating the mis-match between the cavity size of the porphyrin ligand and the size of Tl(III) ion.

Structural characterisation of the Tl(III) complexes [Tl(OEP)]Cl[325], [Tl(TPP)]Cl[326] and [Tl(TPP)]Me[326] shows that the metal adopts a distorted square pyramidal co-ordination geometry (**Figure 5.1.1b**). **Table 5.1.1** lists values for the out of plane (of the porphyrin) elevation of the Tl(III) ion and the average Tl-N distances.

Compound	**Out of plane elevation / Å**	**Tl-N (average) / Å**	**Reference**
[Tl(OEP)]Cl	0.69	2.212	325
[Tl(TPP)]Cl	0.979	2.29	326
[Tl(TPP)]Me	0.737	2.21	326

Table 5.1.1 Out of plane elevation of the Tl(III)-ion and the average Tl-N bond lengths.

The cavity of the porphyrin ligands is in general too small to accommodate the metal ion within the plane of the N-atoms, and the ligand therefore binds facially to the metal ion. **Table 5.1.1** shows that despite the distorted co-ordination geometry Tl-N distances do not vary. Electrochemical reduction of Tl(III) to Tl(I) increases the radius of the metal ion from 0.95Å to 1.47Å and decreases its charge, making it impossible for the metal to maintain the co-ordination to the rather rigid ligand. These complexes can therefore be considered to be at the limit of their stability or, to put it another way, show a high selectivity towards Tl(III) above Tl(I). It has been found that $[Tl(OEP)]^+$ and $[Tl(TPP)]^+$ undergo demetallation in one electron electrochemical reductions[327].

A range of Tl(I) compounds [Tl(crown-ether)$_2$]X (X = ClO_4^-, SCN^-)[328,329] have been prepared with the ligands depicted in **Figure 5.1.1c**. These complexes were characterised by microanalysis and IR-spectroscopy and have been compared to the analogous K-complexes, [K(crown-ether)$_2$]I[330]. It was found that all four ligands form 1:2 Tl(I):crown-ether complexes with only the larger ligands [18]aneO_6 and its dibenzo derivative forming 1:1 adducts.

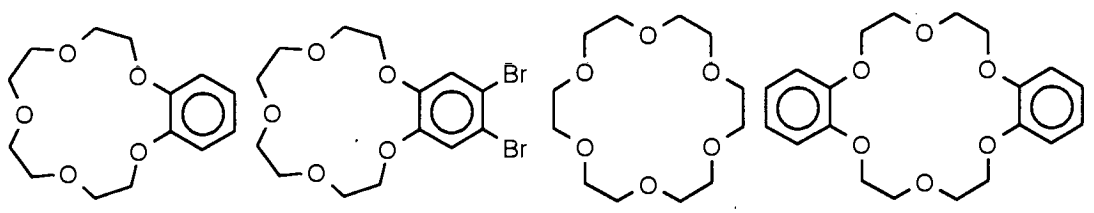

Figure 5.1.1c Crown-ethers used in IR-spectroscopy studies.

Balch and co-workers[331,332] have reported two hetero-binuclear Tl(I) complexes with Pt and Ir shown in **Figure 5.1.1d**. The N-donors of 1,10[18]aneN_2O_4 have been functionalised with the pendant arm -CH_2PPh_2 groups. The Tl(I) ion is in each case co-ordinated to the macrocyclic ligand whereas the platinum metal are co-ordinated *trans* to the two pendant arms. A comparison of the sum (2.96Å) of the formal ionic radii[333] of Tl and N with the Tl···N distance in each compound [Tl···N = 2.975Å(Ir-complex) and 2.995Å(Pt-complex)] indicates no bonding Tl-N interaction. The distances between Tl and the platinum metals [Tl-Pt 2.911(2)Å, Tl-Ir 2.875(1)Å] are suggesting in both cases a true bonding interaction.

(i) $[Tl(crown\text{-}P_2)Ir(CO)Cl]^+$

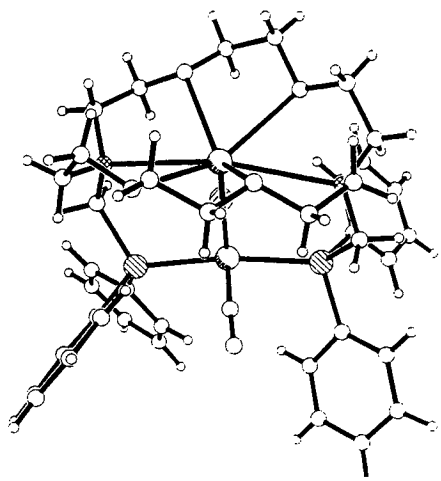

(ii) $[Tl(crown\text{-}P_2)Pt(CN)_2]^+$

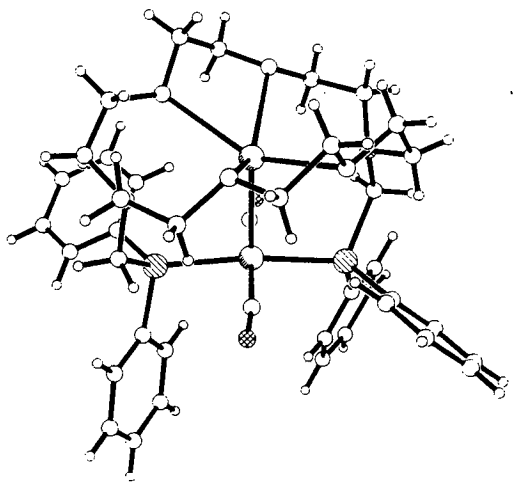

Figure 5.1.1d The single crystal structures of $[Tl(crown\text{-}P_2)Ir(CO)Cl]^+$ and $[Tl(crown\text{-}P_2)Pt(CN)_2]^+$.

It has also been shown that the Tl(I) ion in $[Tl(crown\text{-}P_2)Pt(CN)_2]^+$ can be removed by addition of $[18]aneO_6$. This was determined using ^{31}P-NMR spectroscopy by following the disappearance of $^{203/205}Tl\text{-}^{31}P$ coupling. On the other hand $[Tl(crown\text{-}P_2)Ir(CO)Cl]^+$ undergoes oxidative addition of Cl_2 or I_2, leading to octahedral co-ordination geometries $[ITl(crown\text{-}P_2)Ir(CO)ClI]^+$ and $[ClTl(crown\text{-}P_2)Ir(CO)Cl_2]^+$.

A 1:1 complex between Tl(I) and the cryptate ligand [2.2.2] (**Figure 5.1.1e**) has also been reported[334]. The Tl-N (2.946Å) and Tl-O (avg. 2.960Å) distances show that the ligand adopts a spherical co-ordination geometry around the metal ion (**Figure 5.1.1e**). The Tl-N bond is slightly shorter compared with the previous structure and a comparison of the sum (2.96Å) of the formal ionic radii indicates only marginal covalent character in the Tl-N interaction.

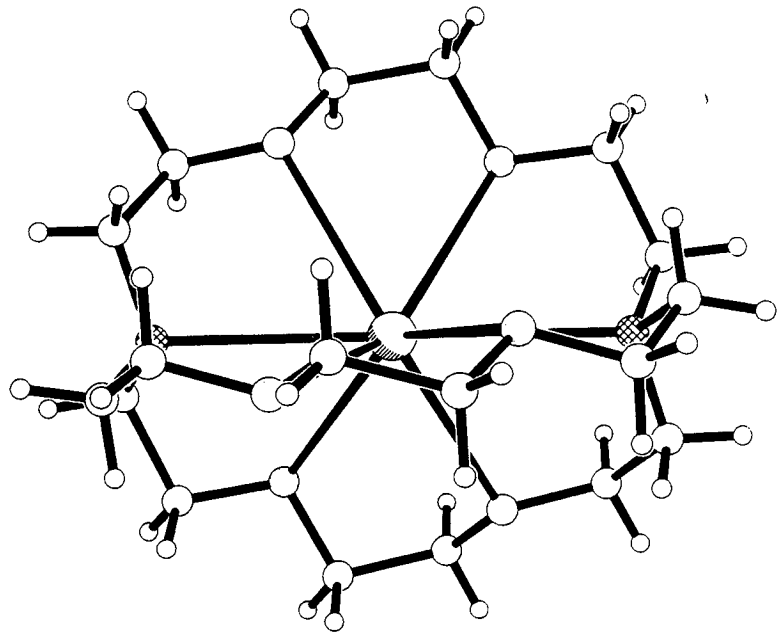

Figure 5.1.1e The Tl(I) complex with the cryptate ligand [2.2.2][334].

Complexes of the composition $Tl([9]aneN_3)X_3$ and $Tl(Me_3[9]aneN_3)X_3$ (X = Cl, Br, I) have been prepared and characterised[335]. However no single crystal X-ray structure determination has been reported but the structure is assumed to be octahedral. The ligands $[9]aneN_3$ and $Me_3[9]aneN_3$ are known to co-ordinate *facially* to metal centres and the complexes show poor solubility in polar solvents which indicates their non-ionic nature. On the other hand a wide range of complexes $TlX_3(N\text{-donor})_3$ (X = Cl, Br; N-donor = py, en, picoline) are known[336]. The single crystal X-ray structure of the neutral complex $TlCl_3(py)_3{\cdot}py$ shows the octahedral species *mer*-$TlCl_3(py)_3$.

The two complexes $[Tl([9]aneN_3)_2](ClO_4)_3$ and $[Tl(Me_3[9]aneN_3)]PF_6$ have been prepared using nitrates instead of chlorides in aqueous media[335]. No high precision structural data are available for $[Tl([9]aneN_3)_2](ClO_4)_3$ due to the bad quality of the crystals[335]. However, the expected sandwich structure with the Tl(III) ion between two ligands has been clearly established with an average Tl-N bond length of 2.48Å.

The single crystal X-ray structure of $[Tl(Me_3[9]aneN_3)]PF_6$ shows the ligand co-ordinated facially to the Tl(I) ion. The Tl-N bond lengths [Tl-N = 2.60(1), 2.59(2) and 2.63(1)Å] are slightly longer compared with $[Tl([9]aneN_3)_2](ClO_4)_3$. It was found in the packing diagram that each $[Tl(Me_3[9]aneN_3)]^+$ cation interacts with three F-atoms from three different PF_6^- anions. The Tl···F distances [Tl···F = 3.23(1), 3.54(2) and 3.27(1)Å] lie between the sum of the ionic radii[333] (2.79Å) and the sum of the van der Waals radii[269] (3.50Å) and were assigned essentially non-bonding with only very weak ionic character. The N-Tl-N angles [N-Tl-N = 68.4°(average)] are very small compared with the expected angle of 90° in an ideal octahedral co-ordination geometry. This is presumably due to some rigidity in the macrocyclic ligand and the size of the Tl(I) ion. It is of interest to note that the F-Tl-F angles [F-Tl-F = 112.2°(average)] are bigger than the ideal 90° angle. The F-atoms show angles close to 90° to 'neighbouring' (excluding those which are on the opposite side of the metal) N-atoms. This gave rise to speculation that a stereochemically active lone-pair of electrons is pointing into the centre of the F_3 face in the TlN_3F_3 distorted octahedron.

The first example of a Tl(I) complex with a homoleptic thioether macrocycle has been isolated by reacting $TlNO_3$ with excess of $[9]aneS_3$ and addition of NH_4PF_6[338,339]. The single crystal structure of $[Tl([9]aneS_3)]^+$ depicted in **Figure 5.1.1f** shows the ligand *facially* co-ordinated to the Tl(I) ion. The Tl-S bond lengths [Tl-S 3.092(3), 3.110(3), 3.114(3)Å] are the longest measured bond lengths in a complex containing $[9]aneS_3$[338,339]. A comparison of the sum (3.34Å) of formal ionic radii[333] for S (1.84Å) and Tl (1.50Å) with these distances suggests that the interaction is at least to some extent covalent. The S-Tl-S angles are very small [S-Tl-S = 66.8°(average)] as a result of the long bond lengths and the small macrocycle. A secondary Tl-S interaction was found in the packing of the complex in the crystal lattice. However, the Tl-S distance is with 3.431(3)Å larger than the sum of the ionic radii indicating non-covalent interaction.

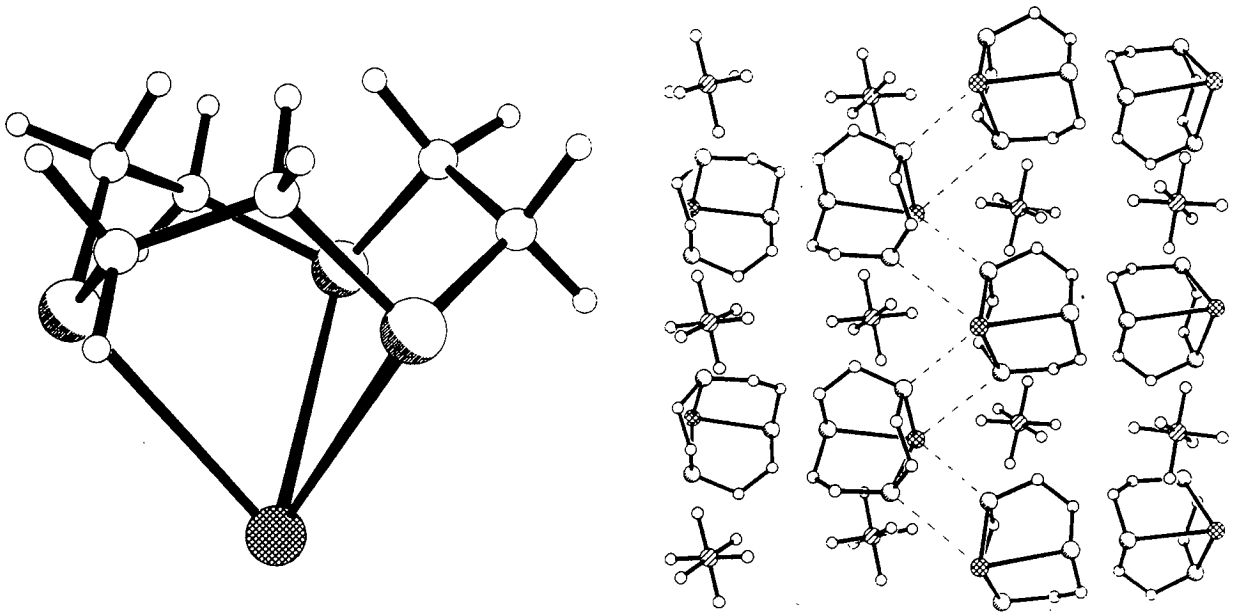

Figure 5.1.1f The single crystal structure of $[Tl([9]aneS_3)]^+$ [338,339].

The single crystal X-ray structures of $[Tl(1,10[18]aneN_2S_4)]PF_6$[337] (**Figure 5.1.1g**) and $[Tl([18]aneS_6)]PF_6$[337] have been reported recently. Tl binds to $1,10[18]aneN_2S_4$ utilising only four of the six donor atoms. The donor set around the Tl(I)-ion is N_2S_2 with long range interactions of the two remaining S-atoms and additional intermolecular Tl···S interactions. The macrocycle adopts a conformation described by the authors as a 'cradle' with the Tl-ion in a distorted square pyramidal co-ordination geometry.

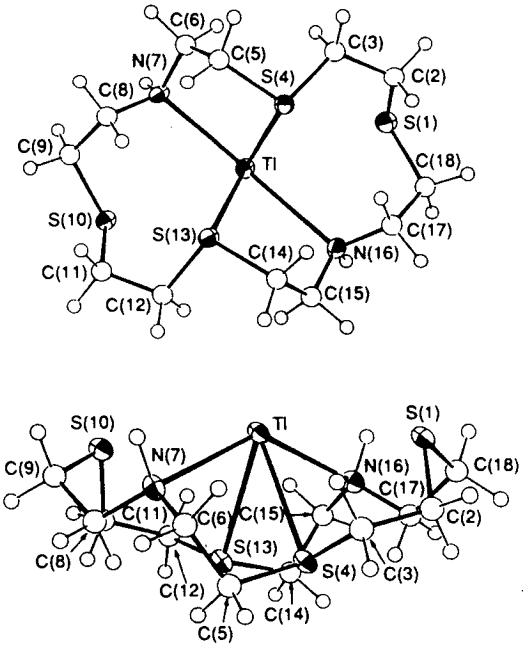

Figure 5.1.1g Single crystal structure of $[Tl(1,10[18]aneN_2S_4)]PF_6$[337].

The single crystal structure of $[Tl([18]aneS_6)]PF_6$ (**Figure 5.1.1h**) exhibits surprisingly a similar co-ordination geometry compared with $[Tl(1,10[18]aneN_2S_4)]PF_6$. The macrocycle adopts again a conformation which can be described as a 'cradle' with the metal atom situated inside. The Tl-ion shows sensible bond lengths to all S-donor atoms with two particular short distances. There have been a range of long intermolecular Tl···S interactions identified in both compounds leading to a quasi polymeric arrangement in the crystal lattice.

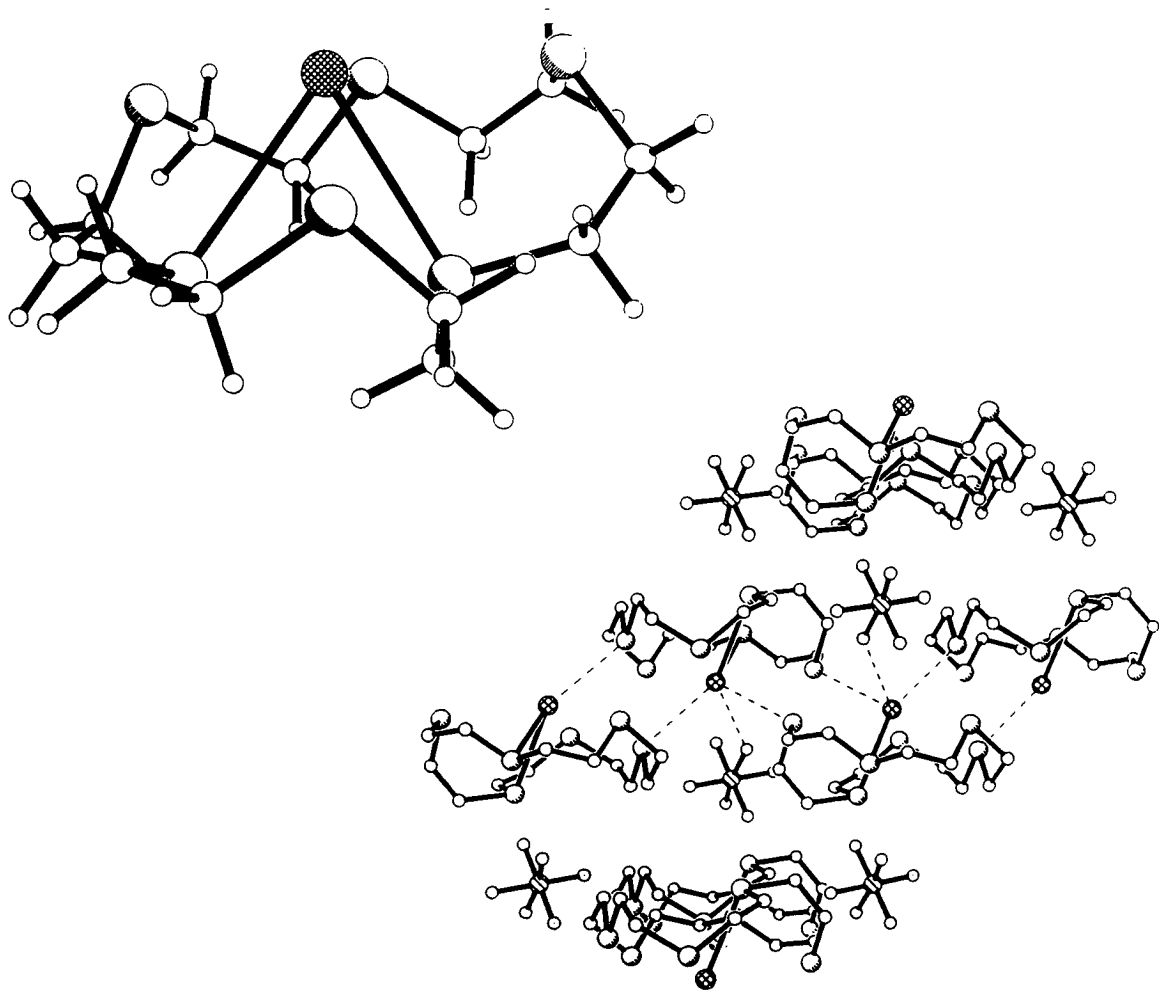

Figure 5.1.1h Single crystal structure of $[Tl([18]aneS_6)]PF_6$.

Tl(I) has been studied in calorimetric titrations of the complexation of metal ions with homoleptic S, O and mixed O/S donor ionophores[68]. Structural investigations have so far focused only on the compounds presented in this introduction but it seems that there might be a possibility to correlate structural properties with stability of the metal macrocyclic complex.

The stepwise substitution of O-donors by S-donors reduces log*K* for the binding of Tl(I) with the macrocycle. This effect is more drastic for 15- compared with 18-membered macrocycles reflecting the size mis-match between host and guest. Differences in log*K* are small for a particular ring size but are nevertheless a good indication for mis-matches between a preferred co-ordination geometry and the flexibility, conformational freedom of the macrocycle. Izatt and co-workers have shown that macrocycles containing two S-donors in 1,4-position have higher log*K* values with Tl(I) compared with other isomers. Macrocycles with the S-donors in 1,4-position have their hard and soft binding sites ideally separated which might be of importance to the oxophillic Tl(I)-ion. It was the aim of this work to investigate to what extent the Tl(I)-ions interact with S- and O-donors in a range of mixed O/S donor ionophores and to structurally characterise the co-ordination geometry around the Tl(I)-ion and the conformation of the macrocycle in particular with respect to other 18-membered macrocycles.

5.2 RESULTS AND DISCUSSION

5.2.1 The Synthesis of [Tl([15]aneS$_2$O$_3$)$_2$]PF$_6$

Treatment of [15]aneS$_2$O$_3$ with TlPF$_6$ in boiling EtOH afforded the colourless complex [Tl([15]aneS$_2$O$_3$)$_2$]PF$_6$. The FAB mass-spectrum (**Figure 5.2.1a**) shows five well resolved fragments which have been identified using their mass and isotopic peak pattern. The base peak at m/z = 457 has been assigned to [^{205}Tl([15]aneS$_2$O$_3$)]$^+$. Two other peaks at m/z = 205 (65%) and 251(5%) have been assigned to ^{205}Tl$^+$ and [([15]aneS$_2$O$_3$)-H]$^+$. Fragments containing more than one macrocyclic ligand have been found at m/z = 710 (7%) and 1060 (35%) and assigned to [^{205}Tl([15]aneS$_2$O$_3$)]$^+$ and [^{205}Tl$_2$([15]aneS$_2$O$_3$)$_2$PF$_6$]$^+$. In particular the last peak is of notable intensity and shows excellent agreement with the simulated isotopic distribution pattern (**Figure 5.2.1a**).

Tl^+

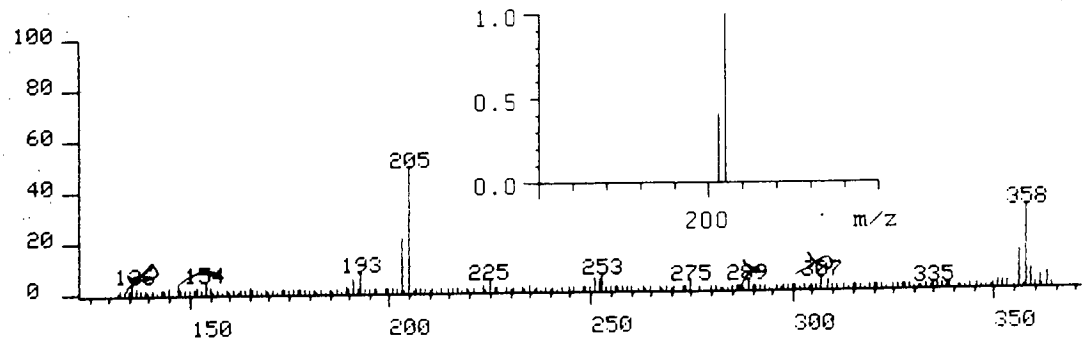

$[Tl([15]aneS_2O_3)]^+$

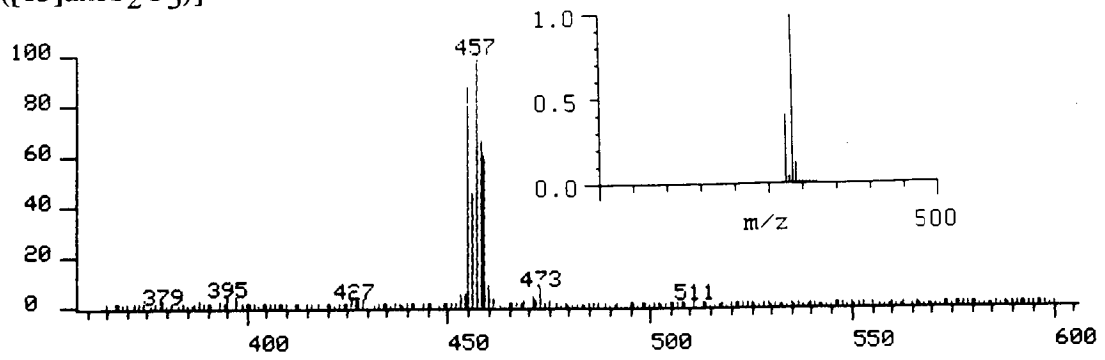

$[Tl([15]aneS_2O_3)_2]^+$

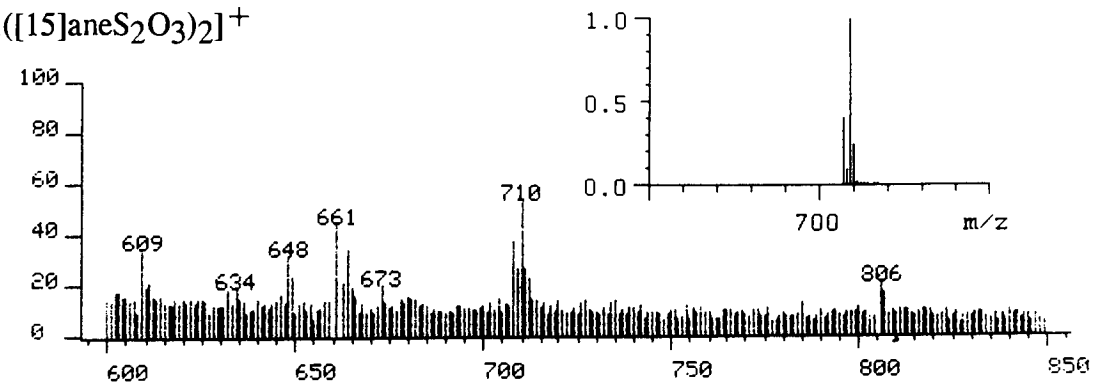

$[Tl_2([15]aneS_2O_3)_2]^+$

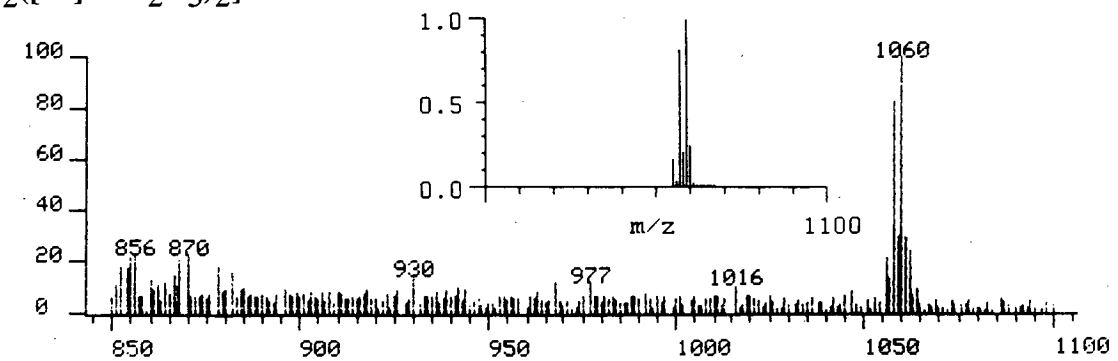

Figure 5.2.1 FAB mass-spectrum (3-NOBA) of $[Tl([15]aneS_2O_3)_2]PF_6$.

The combination of microanalytical together with mass spectroscopic results suggests that the stoichiometry of this compound is of 1:2 Tl(I):[15]aneS_2O_3 composition. The high intensity of a peak assigned to a fragments with more than one Tl(I) ion might suggest that the parent compound is of higher nuclearity. We however feel that this behaviour can also be interpreted as being the result of a polymeric arrangement. The tendency of Tl(I) to form quasi-polymeric arrangements via long range secondary interactions has been mentioned in the introduction to this chapter. We were therefore very interested in obtaining crystalline material suitable for single crystal X-ray diffraction studies. Attempts to obtain suitable crystals for X-ray diffraction failed repeatedly.

5.2.2 The Synthesis of [Tl([18]aneS_2O_4)]PF_6

[Tl([18]aneS_2O_4)]PF_6 has been prepared using the method described in section 5.2.1 using [18]aneS_2O_4 instead of [15]aneS_2O_3. Microanalytical results confirm the composition of the reaction product to be 1:1 Tl(I):[18]aneS_2O_4.

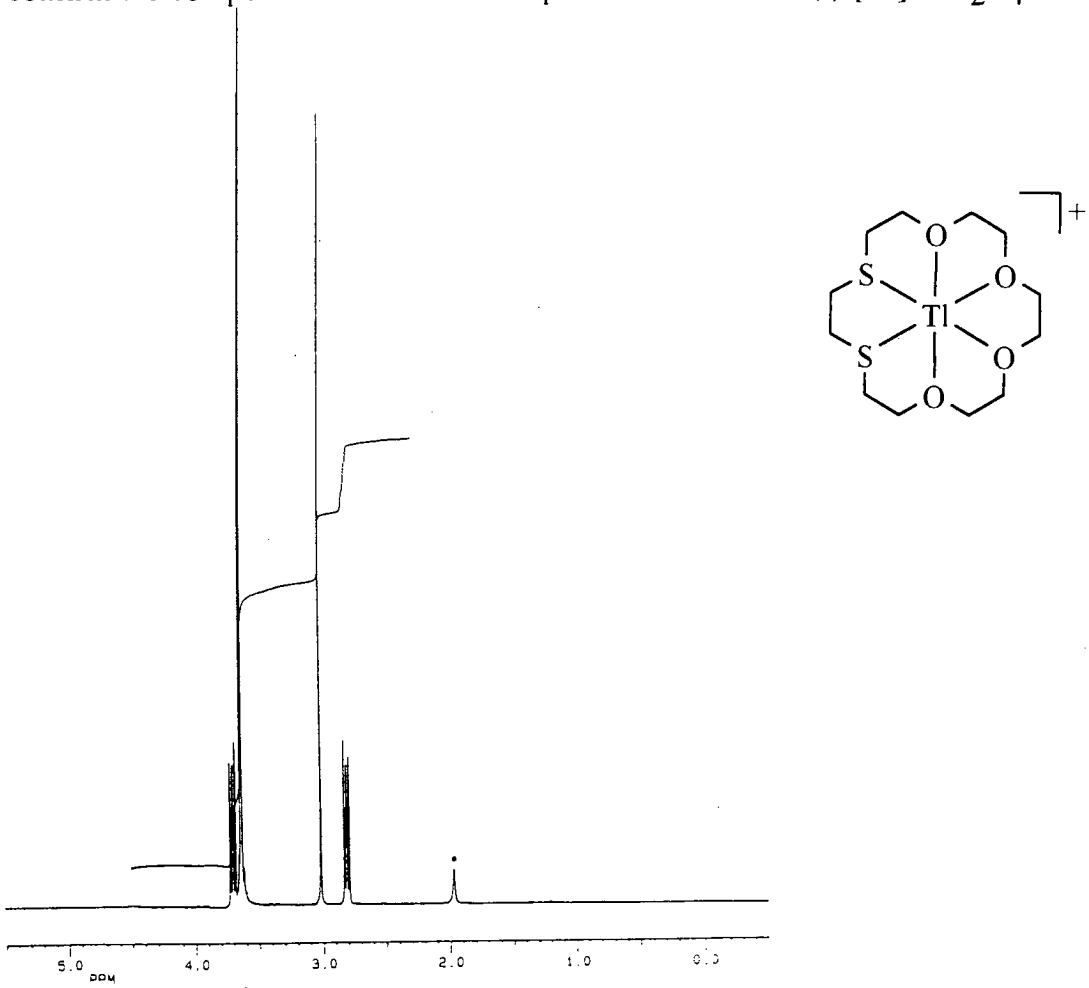

Figure 5.2.2a ^{1}H-NMR ($CDCl_3$; 297K; 250.133 MHz) spectrum of [Tl([18]aneS_2O_4)]PF_6.

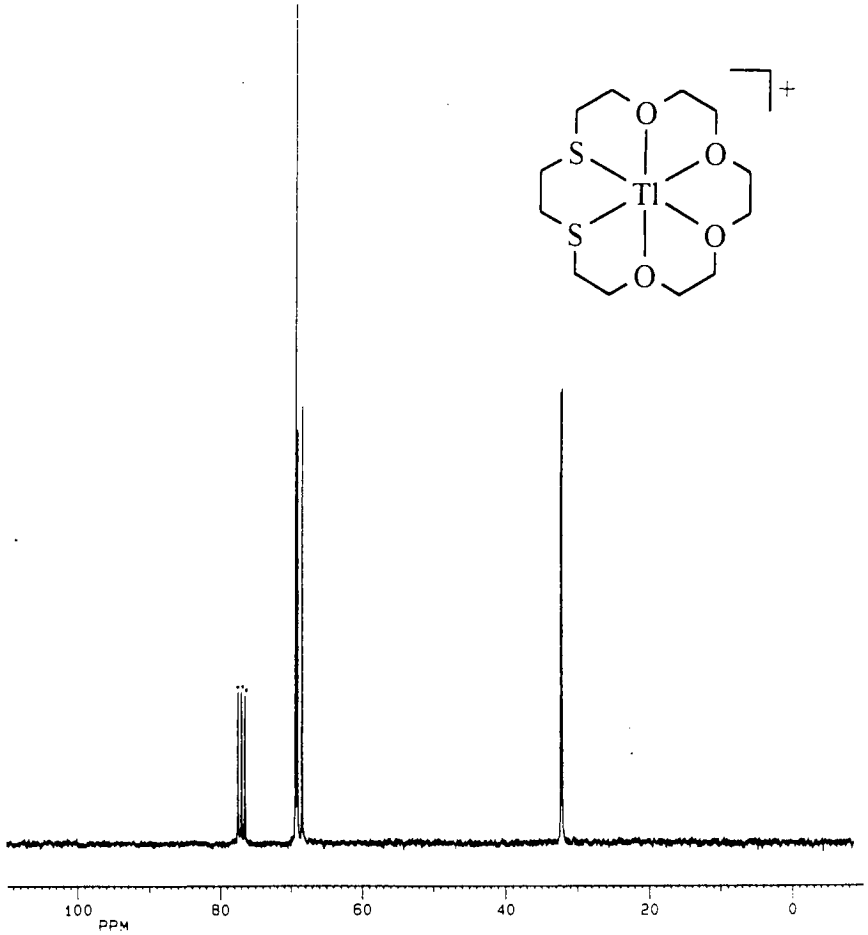

Figure 5.2.2b ^{13}C-NMR ($CDCl_3$; 297K; 62.896 MHz; DEPT ¾ π) spectrum of [Tl([18]aneS_2O_4)]PF_6.

The ^{1}H-NMR (**Figure 5.2.2a**) and the ^{13}C-NMR (**Figure 5.2.2b**) spectra underline the high purity of the products. The ^{13}C-NMR spectrum shows, apart from the solvent ($CDCl_3$), two peaks at high field (32.20 and 31.98 ppm) and three peaks at low field (69.33, 69.04 and 68.39 ppm). Two carbon resonances overlap giving one resonance of double intensity. The chemical shifts are very similar but different to the shifts obtained for the free ligand

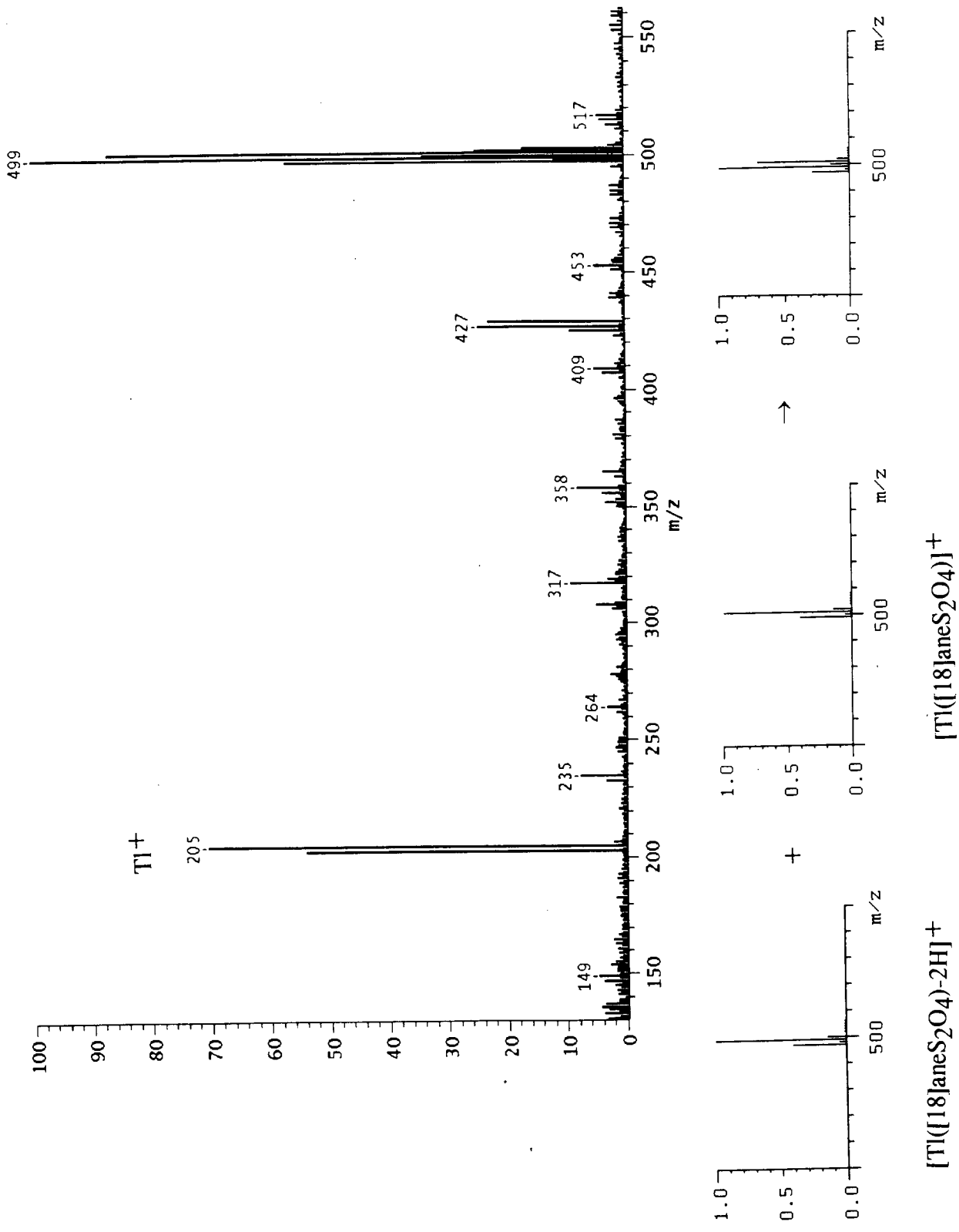

Figure 5.2.2c FAB mass-spectrum (3-NOBA) of $[Tl([18]aneS_2O_4)]PF_6$.

The FAB mass-spectrum of [Tl([18]aneS_2O_4)]PF_6 exhibits a range of features analogous to those of [Tl([15]aneS_2O_3)$_2$]PF_6. The base peak at m/z = 499 has been assigned to the 1:1 Tl(I):[18]aneS_2O_4 fragment, in this case $[^{205}$Tl([18]aneS_2O_4)$]^+$ (m/z = 501). The isotopic distribution of this peak is not consistent with the simulated pattern which is attributed to an overlap of two peaks (m/z =501 and m/z = 499) (**Figure 5.2.2c**). The FAB mass-spectrum of [Tl([18]aneS_2O_4)]PF_6 does not, in contrast to the FAB mass-spectrum of [Tl([15]aneS_2O_3)$_2$]PF_6, show high intensity peaks for fragments of higher nuclearity. The IR-spectrum of [Tl([18]aneS_2O_4)]PF_6 exhibits similar features compared to the IR-spectrum of [Ag_2([18]aneS_2O_4)$_2$]$(PF_6)_2$ (see **Chapter VI**). The most interesting aspect is the position of the C-O stretching vibration, which lies in the free ligand and platinum-metal complexes (see preceding chapters) at about 1120cm^{-1} and in both, the Ag(I) and the Tl (I) compound at 1105cm^{-1}. This is a good indication for the participation of ether O-atoms in the co-ordination to the Tl(I) centre thus suggesting a macrocyclic binding mode to the Tl(I) ion. Proof for this hypothesis can only be obtained by single crystal X-ray diffraction studies but no suitable crystals could be isolated.

5.2.3 The Synthesis of [Tl(benzo[18]aneS_2O_4)]PF_6

[Tl(benzo[18]aneS_2O_4)]PF_6 was prepared using the method described under section 5.2.1 using a crude sample of benzo[18]aneS_2O_4 instead of [15]aneS_2O_3. This is the first complex between benzo[18]aneS_2O_4 and a guest cation. The high success rate of the reaction between mixed O/S-donor ionophores and $TlPF_6$ renders this reaction to be of importance in the initial assessment of a new macrocyclic ligand such as benzo[18]aneS_2O_4. The ligand was prepared on a very small scale due to limitations in starting material and yield. However microanalytical and spectroscopic results show that not only the ligand has been prepared successfully but also the Tl(I) complex. The analysis of microanalytical data, the FAB mass spectrum and the infrared spectrum yielded similar results to the ones obtained for [Tl([18]aneS_2O_4)]PF_6 and were in good agreement with a 1:1 [Tl(I):benzo[18]aneS_2O_4] stoichiometry. A structural investigation of this compound was again hampered by the bad quality of single crystals. However the introduction of rigidity into the macrocyclic framework exemplified by this ligand is of interest, in particular with respect to selectivity, stability and the responsive properties of macrocyclic metal complexes.

5.3 CONCLUSION

The reaction between mixed O/S-donor ionophores and $TlPF_6$ in EtOH afforded colourless microcrystalline compounds. Analytical data show the high purity of the compounds and strongly suggest the presence of a 1:2 (in case of [15]aneS_2O_3) and 1:1 (in case of [18]aneS_2O_4 and benzo[18]aneS_2O_4) Tl : ligand stoichiometry. It is very desirable to undertake a structural investigation in order to establish whether O-atoms do interact with the metal ion, if the macrocycle adopts a macrocyclic or chelating binding mode, and to determine the overall structure in the solid state. $[Tl([15]aneS_2O_3)_2]PF_6$ is very likely to adopt a polymeric or quasi-polymeric motif in the crystal lattice whereas $[Tl([18]aneS_2O_4)]PF_6$ might exist in isolated units or limited oligomeric arrangements comparable to the complexes with Ag(I) (see **Chapter VI**).

5.4 EXPERIMENTAL SECTION

5.4.1 The Synthesis of $[Tl([15]aneS_2O_3)_2]PF_6$

$TlPF_6$ (350 mg, 1.0 mmol) was added to a stirred solution of [15]aneS_2O_3 (250 mg, 1.0 mmol) in EtOH (20 cm^3). The reaction flask was purged with dry nitrogen and the mixture was refluxed for 2 hours. The clear colourless solution was filtered while hot and left standing to cool down to ambient temperature. Needle shaped colourless crystals were collected and recrystallised from MeCN.

Yield: 288mg, 0.34mmol $\{[Tl([15]aneS_2O_3)_2]PF_6\}$, 68% based on [15]ane$S_2O_3$.

Microanalysis (for $C_{20}H_{40}S_4O_6TlPF_6$; Mol.wt. 854.13gmol^{-1})

	%C	%H
calculated	28.12	4.72
found	27.80	4.79

IR spectrum (KBr disc):

2865s, 1655w, 1480m, 1410m, 1360m, 1300m, 1260m, 1120s, 1030m, 1000m, 970w, 910m, 840vs and 560s

FAB mass spectrum (3-NOBA):

Fragment:	m/z (calc.)	m/z (found)	Intensity
$[^{205}Tl_2([15]aneS_2O_3)_2PF_6]^+$	1059	1060	0.35
$[^{205}Tl([15]aneS_2O_3)_2]^+$	709	710	0.07
$[^{205}Tl([15]aneS_2O_3)]^+$	457	457	1.00

^{1}H-NMR spectrum ($CDCl_3$; 297K; 250.133 MHz):

δ 2.77 ppm (t, 4 H) C***H***$_2$S.

δ 2.89 ppm (s, 4 H) C***H***$_2$S.

δ 3.55 - 3.70 ppm (m, 12 H) C***H***$_2$O.

^{13}C-NMR spectrum ($CDCl_3$; 297K; 62.896 MHz; DEPT ¾π):

δ 69.12, 69.00, 68.60 ppm (s, 6 C) ***C***H_2O.

δ 33.32, 32.94 ppm (s, 4 C) ***C***H_2S.

5.4.2 The Synthesis of [Tl([18]aneS_2O_4)]PF_6

[Tl([18]aneS_2O_4)]PF_6 has been prepared following the method described under 5.4.1 using [18]aneS_2O_4 (300 mg, 1.0 mmol) instead of [15]aneS_2O_3. Fern shaped colourless crystals grew upon cooling down over night and were collected, dried and characterised.

Yield: 196 mg, 0.30 mmol {[Tl([18]aneS_2O_4)]PF_6}, 30% based on [18]aneS_2O_4.

Microanalysis (for $C_{12}H_{24}F_6O_4PS_2Tl \cdot H_2O$; Mol.wt. = 663.81 $gmol^{-1}$).

	%C	%H
calculated	21.71	3.95
found	21.87	3.80

IR spectrum (KBr disc):

2920s, 1480m, 1460w, 1420w, 1355m, 1295w, 1270w, 1245w, 1105s, 1030w, 1000w, 980w, 940m, 840vs, 670w, 650w, 625w, 555s.

FAB mass spectrum (3-NOBA):

Fragment:	m/z (calc.)	m/z (found)	Intensity
$[^{205}Tl_2([18]aneS_2O_4)_2PF_6]^+$	1147	1148	0.10
$[^{205}Tl([18]aneS_2O_4)_2]^+$	797	796	0.09
$[^{205}Tl([18]aneS_2O_4)]^+$	501	501	1.00

^{1}H-NMR spectrum ($CDCl_3$; 297K; 250.133 MHz):

δ 2.80 ppm (t, 4 H) C***H***$_2$S.

δ 3.00 ppm (s, 4 H) C***H***$_2$S.

δ 3.64 ppm(m, 16 H) C***H***$_2$O.

^{13}C-NMR spectrum ($CDCl_3$; 297K; 62.896 MHz; DEPT ¾π):

δ 69.33, 69.04, 68.39 ppm (s, 8 C) ***C***H_2O.

δ 32.20, 31.98 ppm (s, 4 C) ***C***H_2S.

5.4.3 The Synthesis of [Tl(benzo[18]aneS$_2$O$_4$)]PF$_6$

[Tl(benzo[18]aneS$_2$O$_4$)]PF$_6$ has been prepared following the method described under 5.4.1. The method was scaled down to 0.4 mmol due to the small amount of crude ligand available. A yield has not been recorded for this reaction.

Microanalysis (for $C_{16}H_{24}F_6O_4PS_2Tl$; Mol.wt. = 693.88 gmol^{-1}).

	%C	%H
calculated	27.70	3.49
found	28.13	3.56

IR spectrum (KBr disc):

2920s, 1630w, 1475m, 1450m, 1420m, 1355m, 1300w, 1250m, 1200w, 1105s, 1075m, 1025m, 975w, 940w, 840vs, 755m, 670w and 555s.

FAB mass spectrum (3-NOBA):

Fragment:	m/z (calc.)	m/z (found)	Intensity
[^{205}Tl(Bz[18]aneS$_2$O$_4$)$_2$(PF$_6$)]$^+$	1243	1243	0.01
[^{205}Tl(Bz[18]aneS$_2$O$_4$)2]$^+$	893	893	0.04
[^{205}Tl(Bz[18]aneS$_2$O$_4$)]$^+$	549	549	1.00

CHAPTER VI

The Co-ordination Chemistry of Silver(I) with Mixed O/S-Donor Ionophores

6.1 INTRODUCTION

6.1.1 Ag(I) Complexes with Homoleptic S-Donor Macrocycles

The first examples of complexes between Ag(I) and homoleptic thioether macrocycles have been reported in 1987 by Cooper[340] and Wieghardt[341]. $[Ag([9]aneS_3)_2]CF_3SO_3$[340] has been prepared by the reaction of two molar equivalents of $[9]aneS_3$ and one molar equivalent of $Ag(CF_3SO_3)$. The single crystal structure of $[Ag([9]aneS_3)_2]^+$ shows a centrosymmetric cation with the Ag(I) ion 'sandwiched' between the two macrocyclic ligands. The six Ag-S distances in the distorted octahedral geometry range from 2.696(2) to 2.753(1)Å. A very similar sandwich type cation has been found in a compound obtained by the reaction of $AgClO_4 \cdot H_2O$ with $[9]aneS_3$ in the ratio 1:1.7[341]. The compound $[Ag_4([9]aneS_3)_5](ClO_4)_4$ contains two different cations: the monomeric $[Ag([9]aneS_3)_2]^+$ **[Figure 6.1.1a(i)]** and a trimeric $[Ag_3([9]aneS_3)_3]^{3+}$ **[Figure 6.1.1a(ii)]**, so that the overall stoichiometry can be formulated as $\{[Ag([9]aneS_3)_2][Ag_3([9]aneS_3)_3]\}(ClO_4)_4$[341]. The co-ordination geometry around the Ag(I) ions in the trimeric cation is highly tetrahedrally distorted. Each Ag(I) ion is bonded to three S-donor atoms of one macrocycle and one S-donor of another. The authors emphasise that this is the first example of a bridging crown thioether. The Ag-S distances are 2.595(4) and 2.613(4)Å to the two non-bridging S-atoms and 2.724(2) and 2.480(2)Å to the bridging thioether.

A similar arrangement of bridging thioether donors between Ag-atoms has been proposed for the Ag(I) complex with 3,6,9-trithiacyclodecanone[342]. Preliminary single crystal X-ray diffraction studies confirmed the presence of a one dimensional polymeric chain structure (**Figure 6.1.1b**).

Complexes between Ag(I) and $[12]aneS_4$, $[14]aneS_4$ and $[16]aneS_4$ have so far not been structurally characterised. In contrast, there are three different single crystal structures **[Figure 6.1.1c (i)-(iii)]** reported for complexes between Ag(I) and $[15]aneS_5$ as a function of the counterion[343].

(i) $[Ag([9]aneS_3)_2]^+$ (ii) $[Ag_3([9]aneS_3)_3]^{3+}$

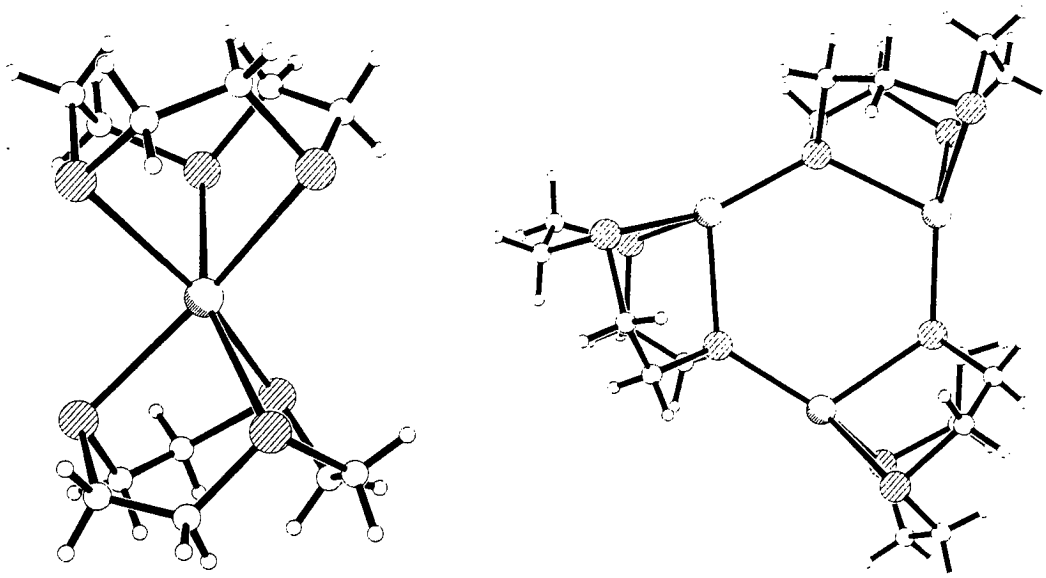

Figure 6.1.1a Plots of the two cations found in the single crystal structure of $[Ag_4([9]aneS_3)_5](ClO_4)_4$[341].

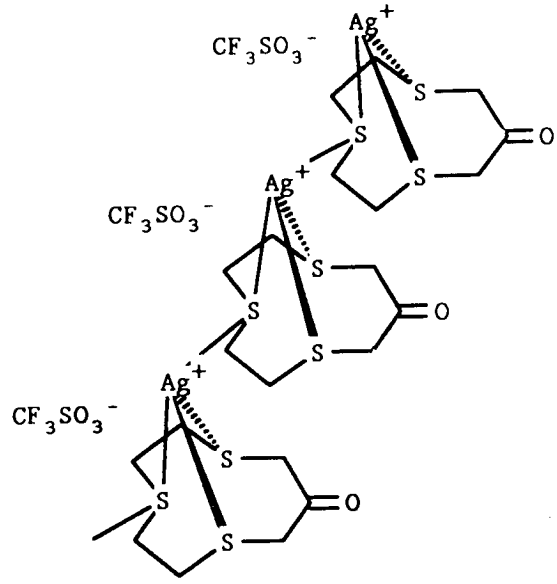

Figure 6.1.1b Proposed structure of [Ag(3,6,9-trithiacyclodecanone)]CF_3SO_3 (taken from ref. 342).

(i) $[Ag_2([15]aneS_5)_2]^{2+}$ [343,344]

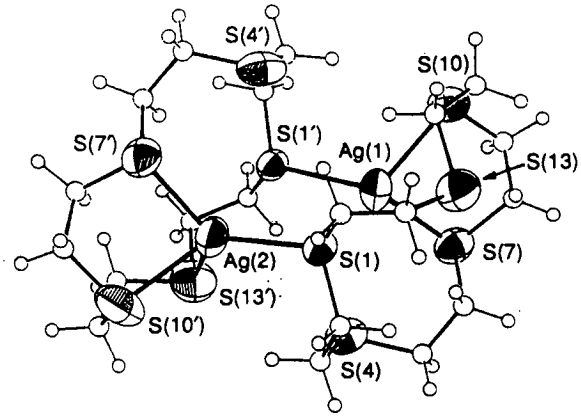

(ii) $[Ag([15]aneS_5)]^{+}$ [343]

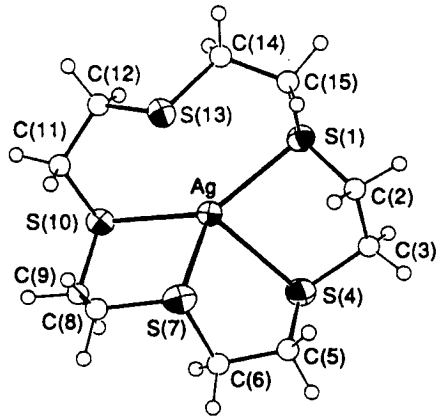

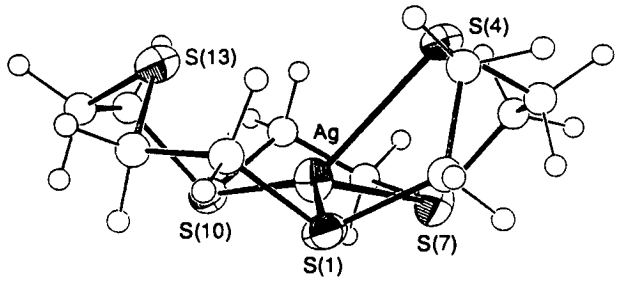

(iii) $\{[Ag([15]aneS_5)]^{+}\}_n$ [343]

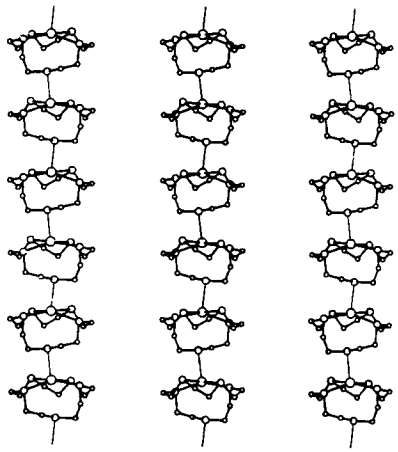

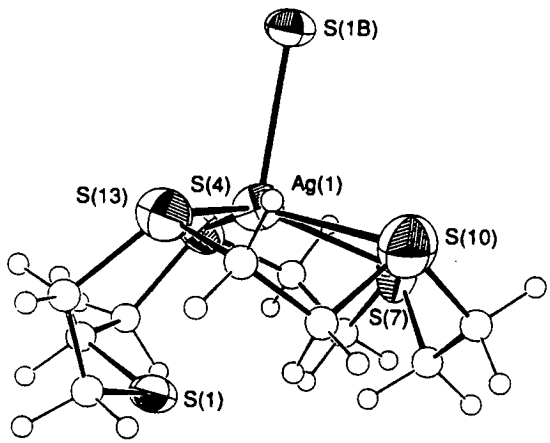

Figure 6.1.1c Plots of the three cations found in solid state structures of Ag(I) complexes with [15]aneS$_5$ [343,344].

The structure of $[Ag_2([15]aneS_5)_2](BPh_4)_2$[343,344] **[Figure 6.1.1c (i)]** consists of a very unusual dimeric cation. One Ag(I) ion shows [3+1] [Ag-S 2.529(3), 2.608(4), 2.537(3) and 2.907(3)Å] thioether co-ordination whereas the other Ag(I) ion shows [4+1] [Ag'-S 2.486(3), 2.558(4), 2.623(5), 2.716(5) and 3.131(3)Å] donation. One S-donor of each macrocyclic ligand bridges asymmetrically between the two metal centres. The single crystal structure of the analogous complex with the perfluorated cation $[B(C_6F_5)_4]^-$ comprises discrete mononuclear cations $[Ag([15]aneS_5)]^+$[343] **[Figure 6.1.1c (ii)]**. The Ag(I) ion exhibits bonding interactions in a very asymmetric [4+1] fashion to all five S-donor atoms [Ag-S 2.4712(19), 2.7262(20), 2.6847(21), 2.5621(19) and 2.8813(19)Å]. The primary S_4 co-ordination geometry is therefore distorted from a pseudo-tetrahedral arrangement by a long range secondary interaction, giving a formally five co-ordinate Ag(I) centre. The PF_6^- salt of the third complex between Ag(I) and $[15]aneS_5$ consists of an infinite one dimensional chain structure[343] **[Figure 6.1.1c (iii)]**. Each Ag(I) ion shows three short [Ag-S 2.659(5), 2.651(6) and 2.564(6)Å] and two long [Ag···S 3.075(7) and 3.219(5)Å] range interactions within the same macrocycle and one short bond to an S-donor [2.742(5)Å] in an adjacent macrocycle. The overall co-ordination geometry could therefore be described octahedrally distorted with a [4+2] S-donor set around each Ag(I) ion.

The Ag(I) complex with the macrocyclic ligand 2,5,7,10-tetrathia[12](2,5)thiophenophane (**Figure 6.1.1d**) has been reported by Lucas and co-workers[345]. The complex has been isolated as the $(ClO_4)^-$ salt and is of 2:2 Ag(I):ligand stoichiometry. It exhibits an interesting Ag_2S_2 bridging arrangement [Ag-S_{bridge} 2.600(2) and 2.995(2)Å; Ag···Ag 4.082(3)Å; Ag-S_{bridge}-Ag 93.45(5)°; S_{bridge}-Ag-S_{bridge} 86.55(5)°] but neither thiophene S-atom is bonded to any Ag(I) ion. Ag-S bond lengths [2.567(2), 2.750(3) and 2.564(2)Å] are similar to those found in saturated homoleptic thioether macrocycles.

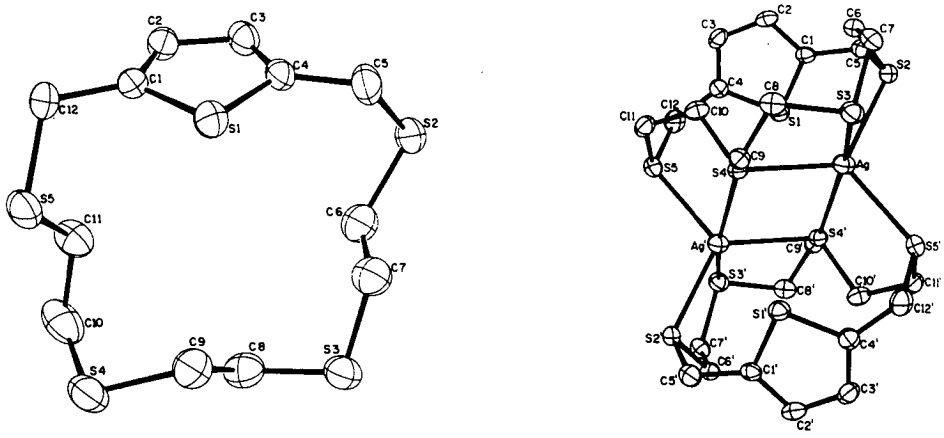

Figure 6.1.1d Structure of the ligand 2,5,7,10-tetrathia[12](2,5)thiophenophane and its complex with Ag(I) (taken from ref. 345).

$[Ag([18]aneS_6)]PF_6$ has been prepared by reaction of $AgNO_3$ and $[18]aneS_6$[346]. The single crystal structure of $[Ag([18]aneS_6)]^+$ (**Figure 6.1.1e**) shows the Ag(I) ion bound to the six thioether donors of $[18]aneS_6$ in a tetragonally compressed stereochemistry [Ag-S = 2.6665(12) and 2.7813(10)Å]. Chemical oxidation of this species has been achieved under strong acidic conditions yielding the blue paramagnetic Ag(II) species $[Ag([18]aneS_6)]^{2+}$. The life span of this species is however very limited at 298K. The presence of a Ag(II) species has been confirmed using ESR spectroscopy of a frozen sample at 77K. The ESR spectrum shows a strong anisotropic signal with g_1 = 2.063, g_2 = 2.028 and g_3 = 2.007. Similar behaviour has been found in other Ag(I) complexes with homoleptic S-donor macrocycles[344,346].

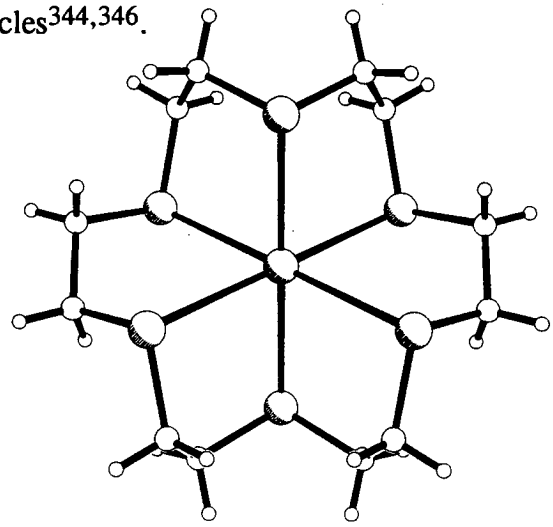

Figure 6.1.1e The single crystal structure of $[Ag([18]aneS_6)]^+$ [346].

Loeb and co-workers reported recently the preparation of a Ag(I) complex with 2,5,8,17,20,23-hexathia[9.9]-*o*-cyclophane (HT[9.9]OC)[347]. Each Ag(I) ion in $[Ag_2(CH_3CN)_2(HT[9.9]OC)](BF_4)_2$ (**Figure 6.1.1f**) co-ordinates to three S-atoms of the macrocycle and one MeCN molecule yielding a distorted NS_3 co-ordination geometry. The Ag-S distances [Ag-S 2.603(4), 2.487(4) and 2.595(4)Å] lie again in the range observed for other thioether macrocyclic complexes.

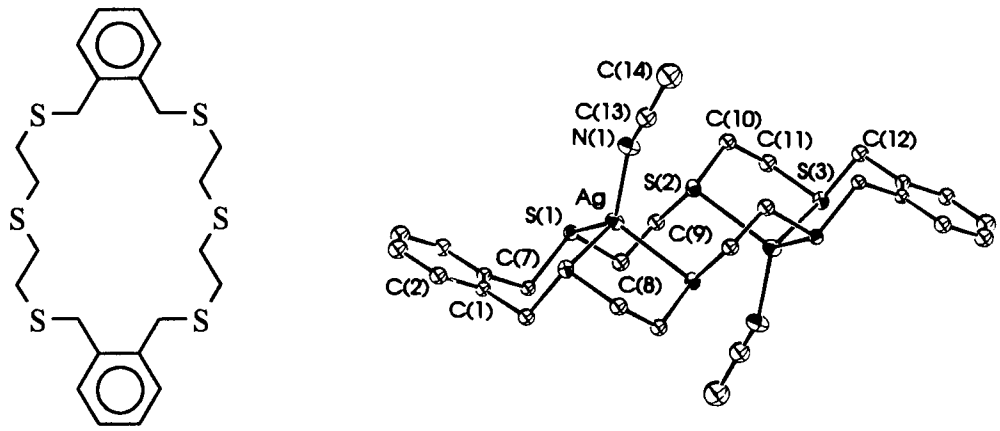

Figure 6.1.1f Structure of HT[9.9]OC and plot of the single crystal structure of $[Ag_2(CH_3CN)_2(HT[9.9]OC)]^{2+}$ [347].

6.1.2 Ag(I) Complexes with Mixed O/S-Donor Ionophores

The only structurally characterised examples of Ag(I) complexes with mixed O/S donor ionophores are $[Ag([15]aneS_2O_3)]^+$ and $[Ag_2([15]aneS_2O_3)_3]^{2+}$ [226,227] (**Figure 6.1.2**).

(i) $[Ag([15]aneS_2O_3)]^+$

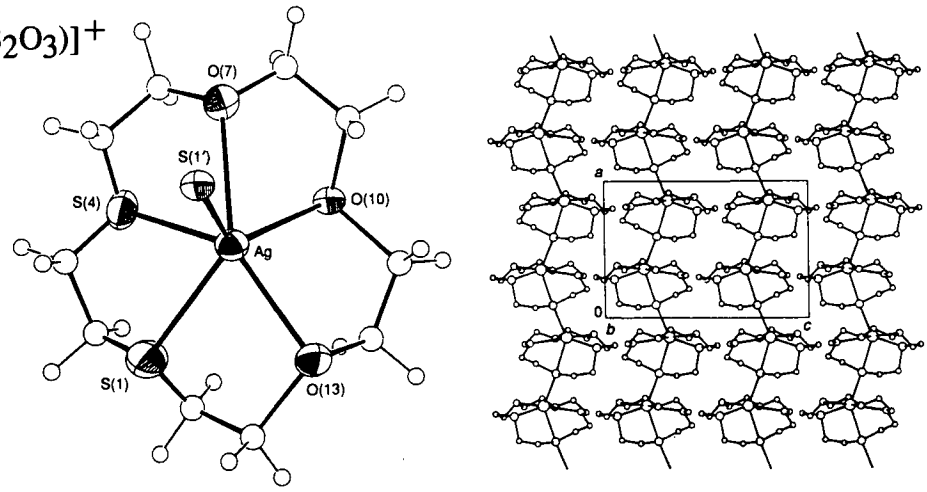

(ii) $[Ag_2([15]aneS_2O_3)_3]^{2+}$

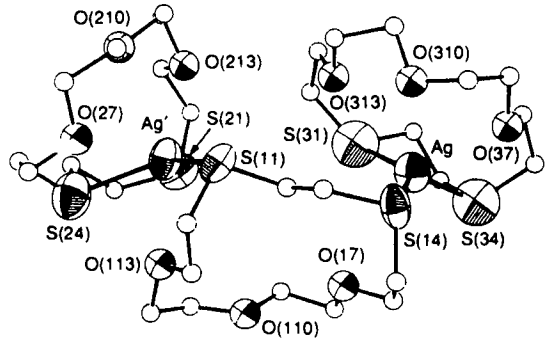

Figure 6.1.2 Plots of the single crystal structures of the cations $[Ag([15]aneS_2O_3)]^+$ and $[Ag_2([15]aneS_2O_3)_3]^{2+}$ [226,227].

$[Ag([15]aneS_2O_3)]^+$ **[Figure 6.1.2 (i)]** is the first example where a mixed O/S donor ionophore actually adopts a macrocyclic binding mode. This is in sharp contrast to all other examples of structurally characterised metal complexes, where $[15]aneS_2O_3$ adopts an *exo* bidentate chelating binding mode[225]. The single crystal structure of $[Ag([15]aneS_2O_3)]^+$ shows a overall polymeric chain structure. Each Ag(I) ion is formally co-ordinated to the two S- and three O-donors in the same macrocycle and a third S-donor in another macrocycle leading to an overall $S_2O_3S_{bridge}$ donor set [Ag-S 2.5401(15), 2.7996(12) and 2.5951(12)Å]. It is however notable that two Ag-O distances [2.667(5) and 2.690(4)Å] are significantly longer compared with the third one [2.492(4)Å] indicating that a more precise description of the actual co-ordination geometry would be of a distorted bicapped tetrahedron.

The highly unusual dication $[Ag_2([15]aneS_2O_3)_3]^{2+}$ has been isolated in attempts to prepare 1:2 Ag(I):ligand complexes[225]. Each Ag(I) ion in this compound is bonded to three thioether S-donors [Ag-S 2.579(18), 2.604(18), 2.540(6), 2.625(8), 2.446(6) and 2.453(5)Å] in a distorted trigonal co-ordination geometry. One of the three macrocyclic ligands acts as a bridging ligand between both Ag(I) ions. The remaining two ligands bind exclusively to each Ag(I) ion and exhibit additional long range Ag···O interactions.

It was our aim to extend this research towards larger mixed O/S donor ionophores. Izatt and co-workers have conducted thermodynamic studies on these compounds and have found only evidence for a 1:1 complex between Ag(I) and $[18]aneS_2O_4$[67,68]. We are particular interested in the structural properties of this compound. Previous work on Ag(I) complexes, as illustrated in this introduction, has shown that structural properties are very much influenced by the nature of the counterion. We propose to investigate the co-ordination chemistry between $[18]aneS_2O_4$ with a range of different counterions and to characterise the products as completely as possible.

6.2 RESULTS AND DISCUSSION

This chapter focuses exclusively on complexes between mixed O/S-donor ionophores and Ag(I). Complexes incorporating homoleptic thioether macrocycles are discussed in **Chapter VII**.

6.2.1 The Synthesis of $[Ag_4([18]aneS_2O_4)_4](ClO_4)_4$

$[Ag_4([18]aneS_2O_4)_4](ClO_4)_4$ was prepared by stirring equimolar amounts of $AgClO_4$ and $[18]aneS_2O_4$ for 24 hours in MeCN. The colourless solution was left to evaporate yielding colourless crystals. Microanalytical results are consistent with a 1:1 stoichiometry. The FAB mass spectrum exhibits two peaks assigned to $[^{107}Ag([18]aneS_2O_4)]^+$ and $[^{107}Ag_2([18]aneS_2O_4)_2(^{35}ClO_4)]^+$ suggesting the presence of at least binuclear species. These assignments are based not only on the mass of the ion but also on the excellent agreement between observed and simulated mass spectrum peak patterns (**Figure 6.2.1a**).

$[^{107}Ag([18]aneS_2O_4)]^+$

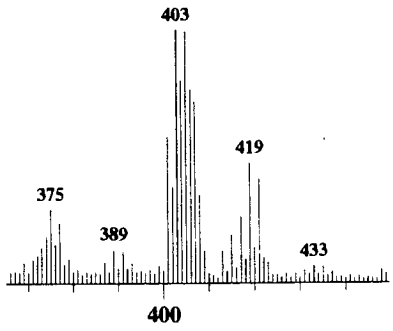

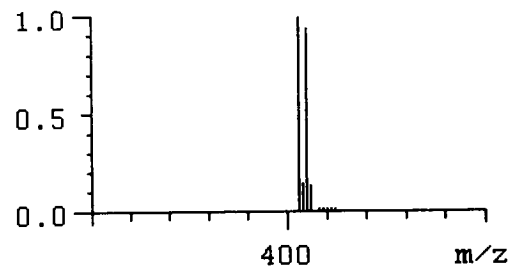

Observed Simulated

$[^{107}Ag_2([18]aneS_2O_4)_2(^{35}ClO_4)]^+$

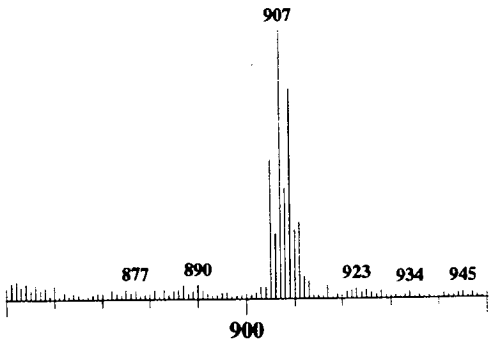

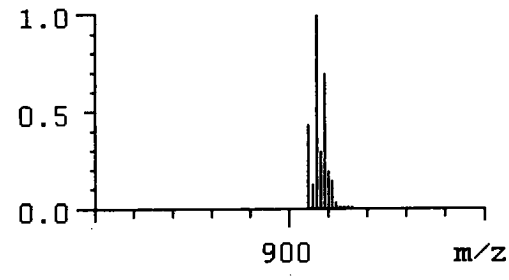

Observed Simulated

Figure 6.2.1a Observed and simulated peak patterns for $[^{107}Ag([18]aneS_2O_4)]^+$ and $[^{107}Ag_2([18]aneS_2O_4)_2(^{35}ClO_4)]^+$.

The ¾π DEPT ^{13}C-NMR spectrum (**Figure 6.2.1b**) shows six resonances at 31.82, 32.22, 67.57, 68.66, 69.97 and 70.10 ppm. This simple pattern implies that the compound is monomeric in solution and dimerisation (see above) or oligomerisation is a feature of the solid state (see below). The presence of only six C resonances for 12 C-atoms in the macrocycle strongly suggests that the macrocycle adopts a rigid two fold symmetry similar to its geometry in the solid state (see **2.2.5**).

The excellent resolved ^{1}H-NMR spectrum allows for an unambiguous assignment of all peaks (**Figure 6.2.1c**). The whole assignment is based on the two triplets which have been assigned to the SCH_2CH_2O region due to their identical shape (apart from being mirrored) and the same coupling constants of $^3J \sim 5.15$ Hz. The coupling constant obtained for the same region in the free macrocycle [18]aneS_2O_4 has been found to be $^3J \sim 6.15$ Hz. The assignment of the two singlets is due to the two fold symmetry of the macrocycle (see above) and the remaining -OCH_2- resonance exhibit the highly symmetrical multiplet between 3.65 to 3.75 ppm.

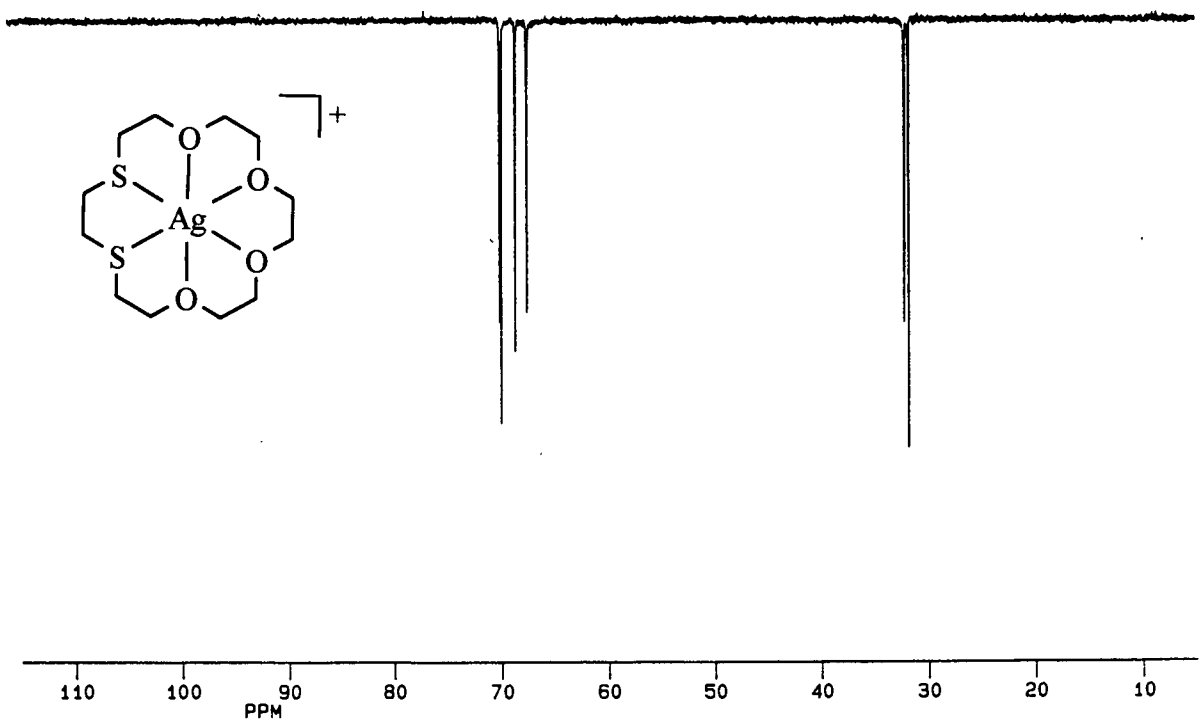

Figure 6.2.1b The ¾π DEPT ^{13}C-NMR spectrum of $[Ag_4([18]aneS_2O_4)_4](ClO_4)_4$ in $CDCl_3$ (297 K; 62.90 MHz).

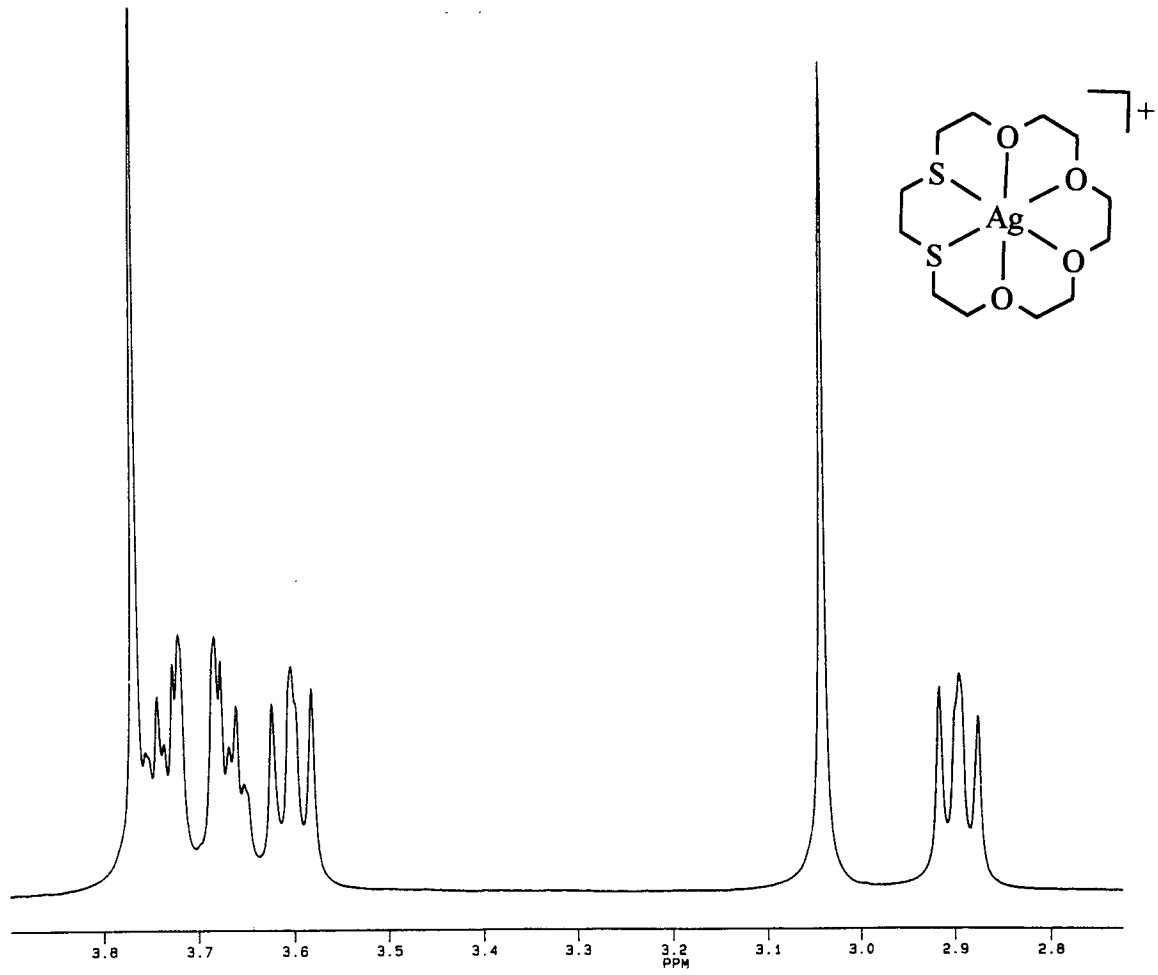

Figure 6.2.1c The ^{1}H-NMR spectrum of $[Ag_4([18]aneS_2O_4)_4](ClO_4)_4$ in $CDCl_3$ (297 K; 250.13 MHz)

6.2.2 The Single Crystal Structure of $[Ag_4([18]aneS_2O_4)_4](ClO_4)_4$

The single crystal structure of $[Ag_4([18]aneS_2O_4)_4](ClO_4)_4$ shows an unusual tetranuclear cation (**Figure 6.2.2a**). One half of the cation is symmetry generated by a crystallographic inversion centre leading to two tetracations in the unit cell. The interesting feature of this compound is the backbone generated by Ag(I) ions and bridging thioether S-donor atoms which forms the skeleton of the cluster. The key building block of this arrangement is the Ag_2S_2 bridging moiety which has been found in a range of Ag(I) complexes with thioketones, thioether and thiols[345,349-354].

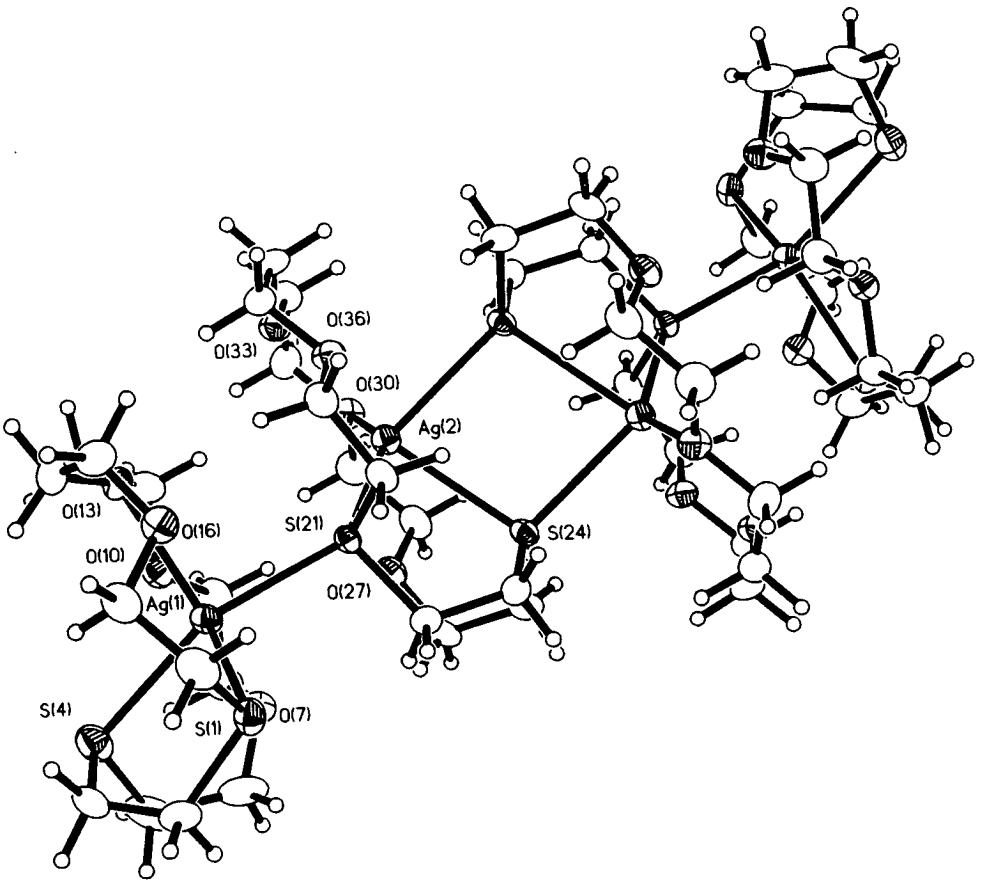

Figure 6.2.2a The single crystal structure of $[Ag_4([18]aneS_2O_4)_4]^{4+}$

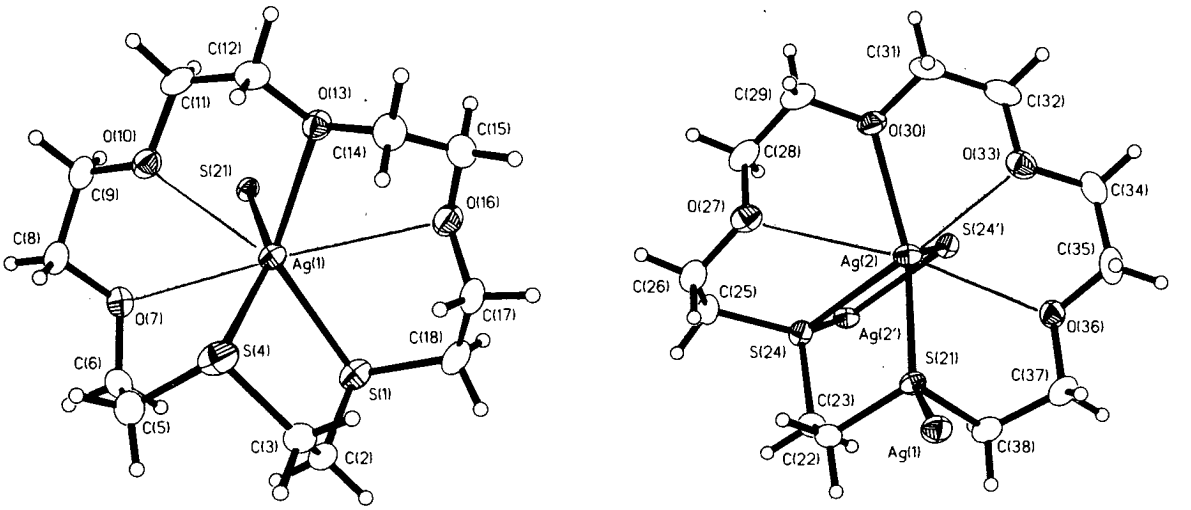

Figure 6.2.2b Best fit plane plot for macrocycle 1 and 2 illustrating the co-ordination geometry around each Ag(I) ion.

The packing diagram (**Figure 6.2.2c**) shows that each tetracation is isolated and does not interact with any of its neighbours. The perchlorate anions occupy spaces between the cations and there is no evidence for any bonding interaction either between different anions or between anions and cations. The size and shape of the thermal ellipsoids of the O-atoms in the $(ClO_4)^-$ anions indicate freedom of rotation around one Cl-O axis.

The co-ordination geometry around each Ag(I) ion is illustrated in **Figure 6.2.2b**. Both Ag(I) ions bind to three S- and one O-atom. The co-ordination geometry does not fit any standard classification but can be in a first approximation described as distorted tetrahedral. The Ag-S distances all lie within a range of 0.15Å, with Ag-O distances in the range from 2.475 to 3.047Å (**Table 6.2.2**). The two shortest Ag-O distances lie within a range of 0.15Å and are therefore considered to be 100% bonding interactions. Four of the remaining six Ag-O distances are about 2.75Å and represent contacts with possible fractional bonding character. The last two O-atoms with distances larger than 3.0Å may be considered to be non interacting. These considerations are supported by the C-O···Ag angles which lie for O(7), O(10), O(33) and O(36) between 102.7 and 118.4°. The angles for O(16) and O(27) deviate on the other hand considerable more from the expected tetrahedral angle of 109°. The co-ordination geometry around each Ag(I) ion can thus be described as a distorted bicapped tetrahedron.

The conformation of each macrocycle is also illustrated in **Figure 6.2.2b**. Both macrocycles exhibit in general the typical *gauche*-angle for O-C-C-O and *anti*-angles for C-O-C-C arrangements. Macrocycle 1 [S(1) to C(18)] exhibits a [1324332] {+++a--a-aa+aa--a--} and macrocycle 2 [S(21) to C(38)] a [12123423] {---+++a+aa-aa+aa-a} conformation (see **Chapter II**).

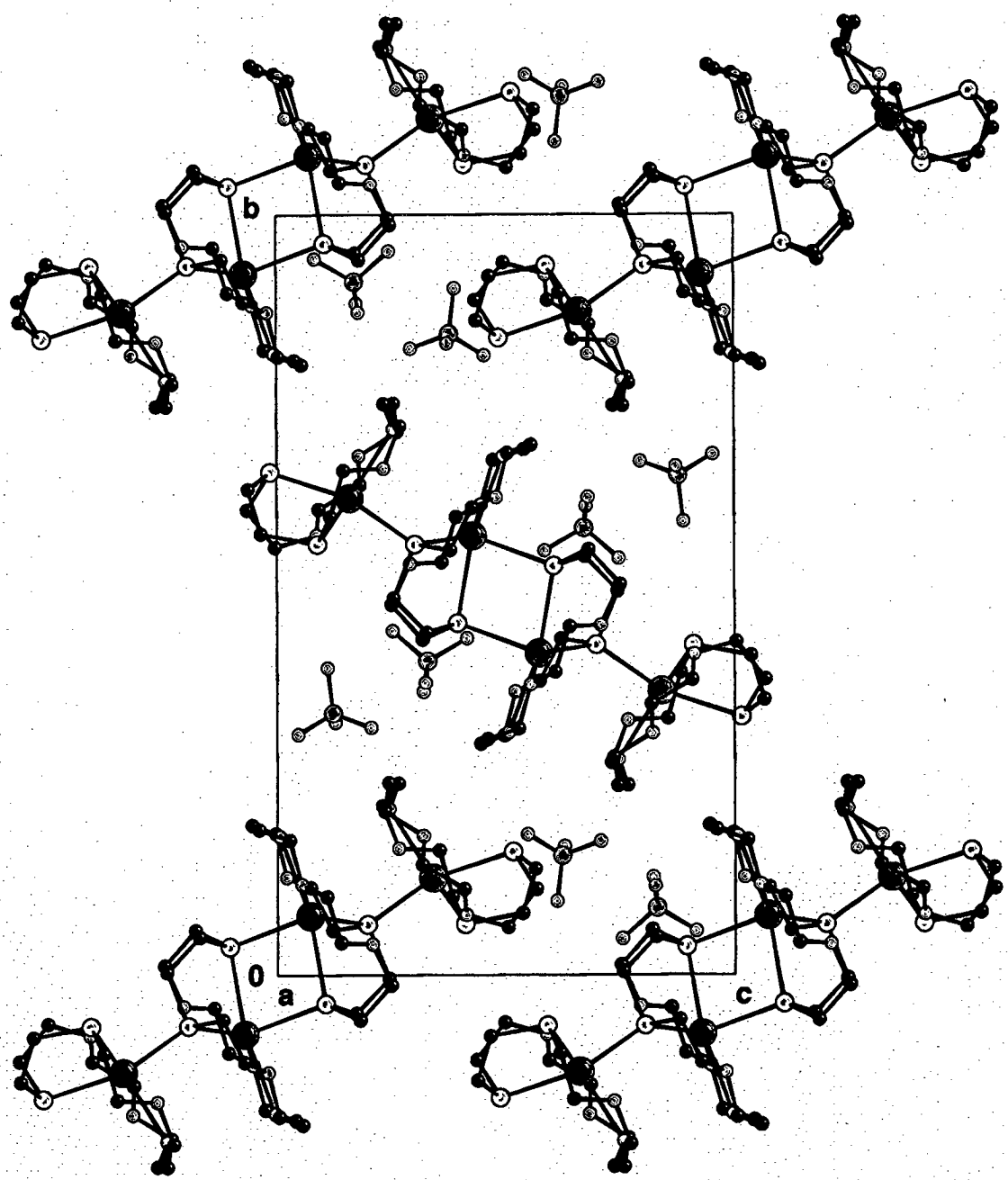

Figure 6.2.2c Packing diagram of $[Ag_4([18]aneS_2O_4)_4](ClO_4)_4$.

Ag(1)-S(1)	2.612(2)	Ag(2)-S(21)	2.625(2)
Ag(1)-S(4)	2.640(2)	Ag(2)-S(24)	2.761(2)
Ag(1)-S(21)	2.6328(15)	Ag(2)-S(24')	2.7085(14)
Ag(1)-O(13)	2.543(3)	Ag(2)-O(30)	2.475(3)
Ag(1)···O(7)	2.779(3)	Ag(2)···O(27)	3.047(3)
Ag(1)···O(10)	2.713(3)	Ag(2)···O(33)	2.645(3)
Ag(1)···O(16)	3.030(3)	Ag(2)···O(36)	2.787(3)
Ag(2)···Ag(2')	4.199(2)	S(24)···S(24')	3.505(2)
Ag(2)-S(21)-Ag(1)	134.66(5)	Ag(2)-S(24)-Ag(2')	100.29(4)

1.Macrocycle		*2.Macrocycle*	
S(1)-C(2)-C(3)-S(4)	57.2(5)	S(21)-C(22)-C(23)-S(24)	-56.0(4)
C(2)-C(3)-S(4)-C(5)	64.8(4)	C(22)-C(23)-S(24)-C(25)	-80.8(4)
C(3)-S(4)-C(5)-C(6)	-99.1(4)	C(23)-S(24)-C(25)-C(26)	85.1(4)
S(4)-C(5)-C(6)-O(7)	-48.9(6)	S(24)-C(25)-C(26)-O(27)	47.1(5)
C(5)-C(6)-O(7)-C(8)	-64.9(5)	C(25)-C(26)-O(27)-C(28)	64.4(5)
C(6)-O(7)-C(8)-C(9)	157.2(4)	C(26)-O(27)-C(28)-C(29)	175.5(4)
O(7)-C(8)-C(9)-O(10)	-64.6(5)	O(27)-C(28)-C(29)-O(30)	69.8(5)
C(8)-C(9)-O(10)-C(11)	178.9(4)	C(28)-C(29)-O(30)-C(31)	-176.6(4)
C(9)-O(10)-C(11)-C(12)	-178.8(4)	C(29)-O(30)-C(31)-C(32)	-172.3(4)
O(10)-C(11)-C(12)-O(13)	67.6(5)	O(30)-C(31)-C(32)-O(33)	-61.4(5)
C(11)-C(12)-O(13)-C(14)	-172.1(4)	C(31)-C(32)-O(33)-C(34)	-178.1(4)
C(12)-O(13)-C(14)-C(15)	-157.8(4)	C(32)-O(33)-C(34)-C(35)	-179.6(4)
O(13)-C(14)-C(15)-O(16)	-56.0(5)	O(33)-C(34)-C(35)-O(37)	60.0(5)
C(14)-C(15)-O(16)-C(17)	-86.6(5)	C(34)-C(35)-O(36)-C(37)	-178.0(4)
C(15)-O(16)-C(17)-C(18)	-178.6(4)	C(35)-O(36)-C(37)-C(38)	161.9(4)
O(16)-C(17)-C(18)-S(1)	-66.9(5)	O(36)-C(37)-C(38)-S(21)	-59.8(4)
C(17)-C18)-S(1)-C(2)	-88.9(4)	C(37)-C(38)-S(21)-C(22)	177.8(3)
C(18)-S(1)-C(2)-C(3)	76.6(4)	C(38)-S(21)-C(22)-C(23)	-65.6(3)

(Primed atoms are symmetry related to their non-primed equivalents by a crystallographic inversion centre; -x, -y, -z.)

Table 6.2.2 Selected bond lengths (Å), interatomic distances (Å), angles (°) and torsion angles (°) with estimated standard deviations for $[Ag_4([18]aneS_2O_4)_4](ClO_4)_4$.

6.2.3 The Synthesis of $[Ag_2([18]aneS_2O_4)_2]X_2$ ($X = PF_6^-, BPh_4^-, CF_3SO_3^-$)

The complexes $[Ag_2([18]aneS_2O_4)_2](PF_6)_2$, $[Ag_2([18]aneS_2O_4)_2](BPh_4)_2$ and $[Ag_2([18]aneS_2O_4)_2](CF_3SO_3)_2$ were prepared by reacting of $AgNO_3$ with $[18]aneS_2O_4$ in refluxing $MeOH/H_2O$. Addition of the appropriate counterion [NH_4PF_6, $NaBPh_4$ or $(^nBu_4N)CF_3SO_3$] followed by evaporation of the solvent afforded the desired products. Recrystallisation gave crystalline material but only the PF_6^- salt yielded crystals suitable for single crystal X-ray diffraction studies. The FAB mass spectrum of each compound exhibited consistently monomeric $[Ag([18]aneS_2O_4)]^+$ and dimeric $[Ag_2([18]aneS_2O_4)_2X]^+$ fragments with the correct isotopic distribution. All compounds were stable and did not exhibit decay on exposure to light. No other stoichiometry could be isolated even though there has been some evidence that species of other composition are generated under mass spectroscopy conditions. The ^{13}C-NMR spectrum of $[Ag_2([18]aneS_2O_4)_2](PF_6)_2$ in CD_3CN (**Figure 6.2.3**) shows six resonances at 30.47, 30.98, 68.17, 68.67, 69.25 and 69.66 ppm. A quantitative comparison with the ^{13}C-NMR spectrum obtained for $[Ag_4([18]aneS_2O_4)_4](ClO_4)_4$ (in $CDCl_3$) is problematic due to different solvents used. However, the presence of only 6 resonances with very similar chemical shifts compared to $[Ag_4([18]aneS_2O_4)_4](ClO_4)_4$ suggests the same mononuclear species to be present in solution (see above). Electrochemical reduction showed only irreversible behaviour followed by de-metallation.

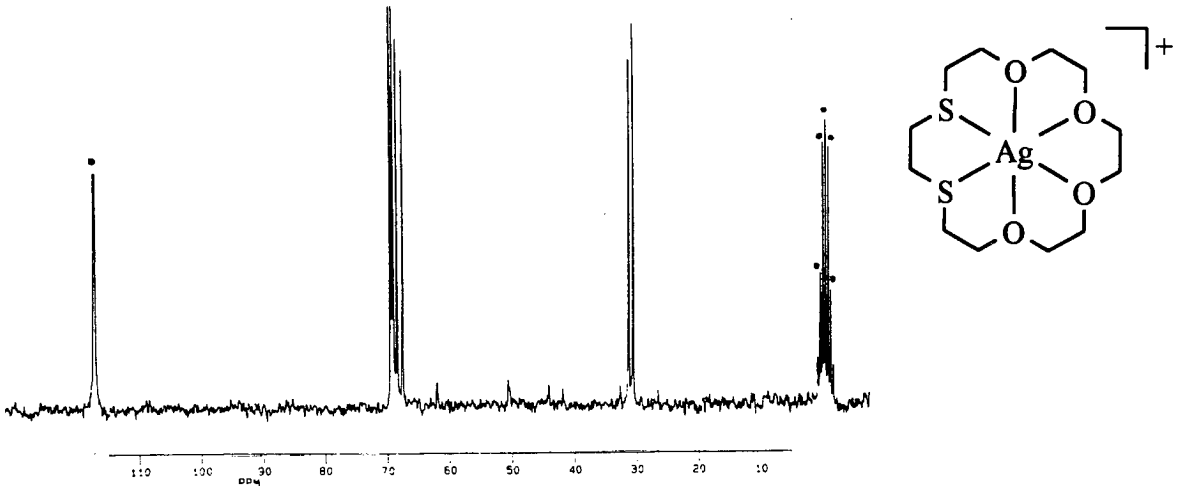

Figure 6.2.3 The ¾π DEPT ^{13}C-NMR spectrum of $[Ag_2([18]aneS_2O_4)_2](PF_6)_2$ in CD_3CN (297 K; 50.32 MHz).

6.2.4 The Single Crystal Structure of $[Ag_2([18]aneS_2O_4)_2](PF_6)_2$

CH_2Cl_2 vapour was allowed to diffuse into a solution of $[Ag_2([18]aneS_2O_4)_2](PF_6)_2$ in EtOH to afford single crystals suitable for X-ray diffraction studies. The single crystal structure of $[Ag_2([18]aneS_2O_4)_2](PF_6)_2$ (**Figure 6.2.4a**) shows a similar configuration to the tetranuclear complex discussed above. Both compounds crystallise in the monoclinic space group $P\,2_1/c$ (No.14). One half of the molecule in $[Ag_4([18]aneS_2O_4)_4](ClO_4)_4$ is symmetry related by a crystallographic inversion centre to the other whereas in contrast the single crystal structure of $[Ag_2([18]aneS_2O_4)_2](PF_6)_2$ shows two symmetry related dications in close proximity (**Figure 6.2.4c**). The backbone of the dication $[Ag_2([18]aneS_2O_4)_2]^{2+}$ consists of a linear 5 membered chain of alternating Ag(I) ions and S-donor atoms. There is again an uncertainty in assigning the co-ordination geometry due to elongated Ag-O distances. **Figure 6.2.4b** illustrates the environment around each Ag(I) ion.

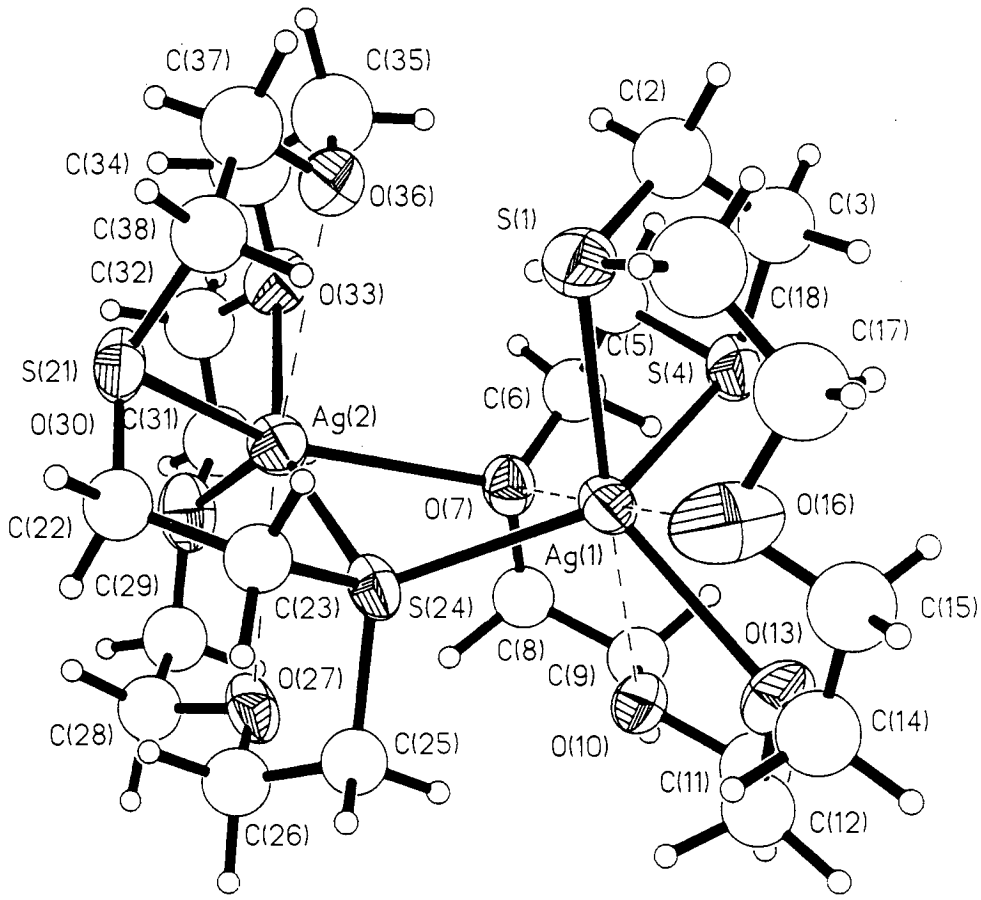

Figure 6.2.4a The single crystal structure of $[Ag_2([18]aneS_2O_4)_2]^{2+}$.

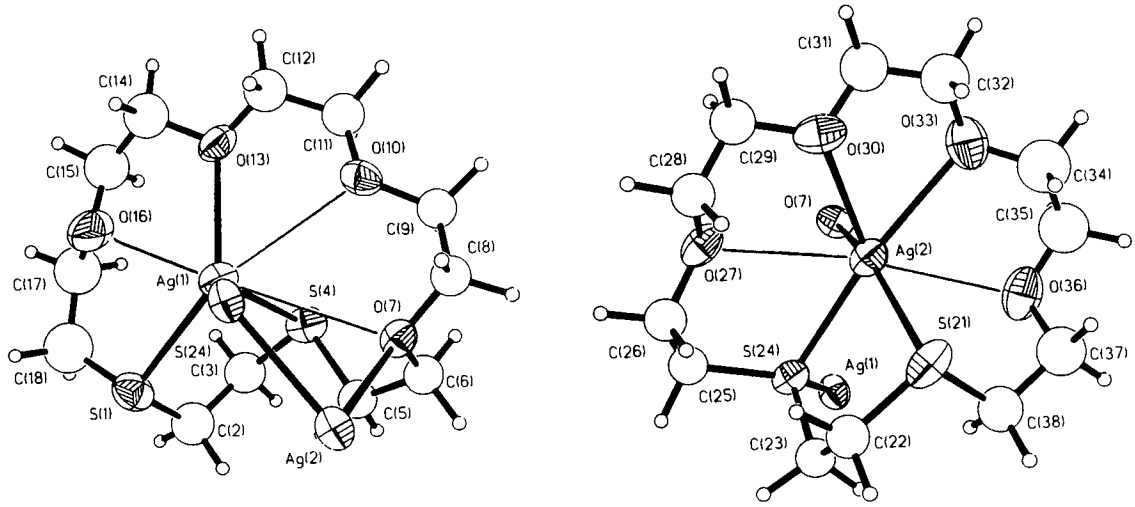

Figure 6.2.4b Best-fit-plane plot for macrocycle 1 and 2 illustrating the co-ordination geometry around each Ag(I) ion.

There are three short Ag-S distances [2.698(3), 2.556(3) and 2.521(2)Å] and one short Ag-O [2.564(7)Å] distance giving to an overall S_3O donor set in a distorted tetrahedral co-ordination geometry. The remaining three Ag-O distances are separated from each other by ~0.3Å. The longest non bonding Ag···O distance [3.371(5)Å] involves O(7) which shows a short distance to Ag(2). O(16) and O(10) are with 2.712(11)Å and 3.097(6)Å assigned to be interactions with partial bonding character, which cap two faces of the primary co-ordination tetrahedron.

The environment around Ag(2) is slightly more complicated. Ag(2) shows usual Ag-S distances [2.555(2) and 2.706(2)Å] to S(21) and S(24). Ag(2)-O(30) is with 2.459(7)Å the shortest Ag-O distance found in either complex. The environment around Ag(2) can therefore be described either as a S_2O- or S_2O_3-environment. The two additional Ag-O bonds are Ag(2)-O(7) [2.661(5)Å] and Ag(2)-O(33) [2.649(8)Å]. The remaining two O-atoms [Ag(2)···O(27) 2.873(6)Å and Ag(2)···O(36) 2.905(8)Å] are considered to be only of fractional bonding character. The co-ordination geometry around Ag(2) can therefore not be described in simple terms.

The conformations of the two macrocycles - [S(1) to C(18)] [1324332] {+++a+a++aa-aa+aa-a} and [S(21) to C(38)] [334242] {++a--aa+aa-aa+aa+a} - in $[Ag_2([18]aneS_2O_4)_2](PF_6)_2$ are not identical to those found for $[Ag_4([18]aneS_2O_4)_4](ClO_4)_4$. Even though Dale's scheme suggests that the 'first' macrocycle in $[Ag_4([18]aneS_2O_4)_4](ClO_4)_4$ and $[Ag_2([18]aneS_2O_4)_2](PF_6)_2$ are identical, the alternative '+-a' scheme shows that there are differences concerning not only the sequence but also the absolute numbers of ±*gauche* and *anti* angles.

Figure 6.2.4c shows two symmetry related dications in close contact. The Ag(2)-S(21) is with 2.555(2)Å short compared with other complexes exhibiting an Ag_2S_2 bridge. The Ag(2)-S(21') distance [4.464Å] on the other hand is far too long to be of any bonding significance. The S(21)···S(21') distance is with 3.434(4)Å shorter than the sum of the van der Waals radii for S (1.85Å; ref. 269). It is however a common feature in macrocyclic thioether ligands that S-S distances are in general less than the sum of the van der Waals radii (see for instance the single crystal structure of $[18]aneS_2O_4$ in **Chapter II**). The close proximity of both dications in the crystal lattice can therefore to be attributed to the packing and not to any positive bonding interaction. The packing diagram of $[Ag_2([18]aneS_2O_4)_2](PF_6)_2$ is shown in **Figure 6.2.4c**.

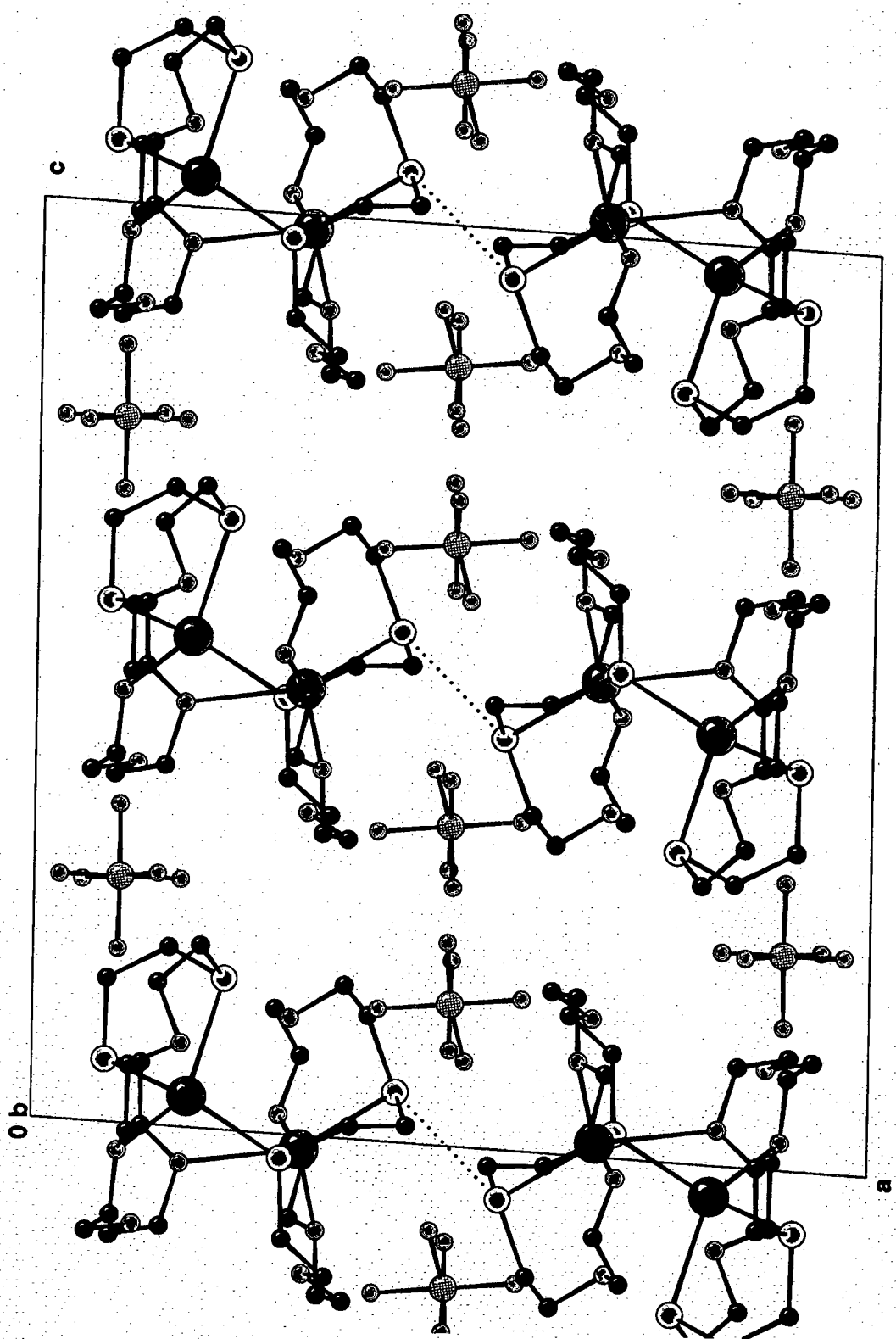

Figure 6.2.4c Packing diagram of $[Ag_2([18]aneS_2O_4)_2](PF_6)_2$.

Ag(1)-S(1)	2.698(3)	Ag(2)-O(7)	2.661(5)
Ag(1)-S(4)	2.556(3)	Ag(2)-S(21)	2.555(2)
Ag(1)-O(7)	3.371(5)	Ag(2)-S(24)	2.706(2)
Ag(1)-O(10)	3.097(6)	Ag(2)-O(27)	2.873(6)
Ag(1)-O(13)	2.564(7)	Ag(2)-O(30)	2.458(7)
Ag(1)-O(16)	2.712(11)	Ag(2)-O(33)	2.649(8)
Ag(1)-S(24)	2.521(2)	Ag(2)-O(36)	2.905(8)
Ag(1)-Ag(2)	4.214(1)	S(1)-S(4)	3.948(4)
S(21)-S(24)	3.438(4)	S(21)-S(21')	3.434(4)

1.Macrocycle		*2.Macrocycle*	
S(1)-C(2)-C(3)-S(4)	53.5(13)	S(21)-C(22)-C(23)-S(24)	-51.8(10)
C(2)-C(3)-S(4)-C(5)	61.3(11)	C(22)-C(23)-S(24)-C(25)	-94.5(8)
C(3)-S(4)-C(5)-C(6)	175.5(8)	C(23)-S(24)-C(25)-C(26)	80.1(8)
S(4)-C(5)-C(6)-O(7)	67.3(10)	S(24)-C(25)-C(26)-O(27)	60.3(10)
C(5)-C(6)-O(7)-C(8)	-148.3(8)	C(25)-C(26)-O(27)-C(28)	-172.5(8)
C(6)-O(7)-C(8)-C(9)	79.3(10)	C(26)-O(27)-C(28)-C(29)	179.2(9)
O(7)-C(8)-C(9)-O(10)	66.6(10)	O(27)-C(28)-C(29)-O(30)	-67.3(11)
C(8)-C(9)-O(10)-C(11)	-179.1(8)	C(28)-C(29)-O(30)-C(31)	176.6(10)
C(9)-O(10)-C(11)-C(12)	176.1(9)	C(29)-O(30)-C(31)-C(32)	164.6(11)
O(10)-C(11)-C(12)-O(13)	-74.4(12)	O(30)-C(31)-C(32)-O(33)	65.0(14)
C(11)-C(12)-O(13)-C(14)	-165.0(10)	C(31)-C(32)-O(33)-C(34)	-170.0(12)
C(12)-O(13)-C(14)-C(15)	175.1(11)	C(32)-O(33)-C(34)-C(35)	179.3(12)
O(13)-C(14)-C(15)-O(16)	66.2(14)	O(33)-C(34)-C(35)-O(37)	-61.4(18)
C(14)-C(15)-O(16)-C(17)	-161.7(14)	C(34)-C(35)-O(36)-C(37)	-93.5(15)
C(15)-O(16)-C(17)-C(18)	171.9(15)	C(35)-O(36)-C(37)-C(38)	159.8(11)
O(16)-C(17)-C(18)-S(1)	-47.7(20)	O(36)-C(37)-C(38)-S(21)	-66.9(12)
C(17)-C18)-S(1)-C(2)	-94.3(15)	C(37)-C(38)-S(21)-C(22)	168.0(9)
C(18)-S(1)-C(2)-C(3)	81.1(11)	C(38)-S(21)-C(22)-C(23)	-55.9(9)

(Primed atoms are symmetry related to their non-primed equivalents by a crystallographic inversion centre; -x, -y, -z.)

Table 6.2.4 Selected bond lengths (Å), interatomic distances (Å), angles (°) and torsion angles (°) with estimated standard deviations for $[Ag_2([18]aneS_2O_4)_2](PF_6)_2$.

6.3 CONCLUSION

This investigation of the co-ordination chemistry of Ag(I) with [18]aneS_2O_4 confirmed the findings by Izatt and co-workers[67,68] that the complex of [18]aneS_2O_4 with Ag(I) in solution and in the solid state is of 1:1 stoichiometry. NMR studies suggested that the species present in solution adopts a two fold symmetry. Solid state studies showed on the other hand oligomerisation of mononuclear $[Ag([18]aneS_2O_4)]^+$ cations to bi- and tetranuclear molecules dependent on the counterion. The substitution of PF_6^- by the slightly smaller counterion ClO_4^- allows two binuclear $[Ag_2([18]aneS_2O_4)_2]^{2+}$ dications to form an overall tetrameric $[Ag_4([18]aneS_2O_4)_4]^{4+}$ tetracation. These findings are in good agreement with similar complexes such as Ag(I) with [15]aneS_5 (see above) and underline that the actual structures of these complexes in the solid state rely predominantly on packing forces rather than stereochemical requirements of the Ag(I) cation. Complexes containing even larger (BPh_4^-) or non-spherical ($CF_3SO_3^-$) counterions were prepared but attempts to obtain crystals suitable for X-ray diffraction studies failed repeatedly.

The co-ordination geometries around Ag(I) ions are of particular interest. Ag(I), as a d^{10} system, does not prefer a particular geometry. However the co-ordination geometries of homoleptic S- and mixed O/S-donor macrocyclic complexes with Ag(I) can in general be described as distorted tetrahedral. The main contributor to the geometry in these cases is not the metal ion but simply the desire of the macrocyclic ligand to minimise the repulsion between donor atoms around the metal centre. This is reflected in almost any case by the [4+n] donor set, where n donor atoms adopt capped positions above a triangular face of the distorted 'tetrahedron'.

6.4 EXPERIMENTAL SECTION

6.4.1 The Synthesis of $[Ag_4([18]aneS_2O_4)_4](ClO_4)_4$

$AgClO_4$ (52 mg, 0.25 mmol) and $[18]aneS_2O_4$ (74 mg, 0.25 mmol) were stirred in MeCN ($20cm^3$) for 24 hours at ambient temperature. Single crystals suitable for structure determination formed by slow evaporation of the solvent.
Yield: 100mg, 0.05 mmol {calc. for $[Ag_4([18]aneS_2O_4)_4](ClO_4)_4$}, 80% based on $[18]aneS_2O_4$.

CAUTION: *Perchlorate salts are often treacherously explosive and although we have been unable to cause this compound to detonate from shock or heating we recommend suitable precautions be taken whenever perchlorates are handled.*

Microanalysis (for $C_{48}H_{96}Ag_4Cl_4O_{32}S_8$; Mol.wt. = 2015.0 $gmol^{-1}$)

	%C	%H
Calculated	28.61	4.80
Found	28.70	4.63

FAB mass spectrum (3-NOBA):

Fragment:	m/z (calc.)	m/z (found)
$[^{107}Ag_2([18]aneS_2O_4)_2(^{35}ClO_4)]^+$	905	907
$[^{107}Ag([18]aneS_2O_4)]^+$	403	403

IR spectrum (KBr disc):

2910s, 2855s, 1635w, 1465m, 1415m, 1355m, 1290w, 1270m, 1250w, 1120s, 1085vs, 1020m, 940m, 900w, 870w, 825w, 785w and 625s.
(the vs peak at 1085 obstructs peaks at 1120 and 1020 which need to be interpreted with appropriate considerations)

^{1}H-NMR spectrum (CD_3Cl; 297 K; 250.13 MHz)

δ 2.90 (t, 4H) SCH_2CH_2O
δ 3.04 (s, 4H) SCH_2CH_2S
δ 3.60 (t, 4H) CH_2O
δ 3.65 - 3.75 (symmetrical m, 8H) CH_2O
δ 3.77 (s, 4H) CH_2O

^{13}C-NMR spectrum (CD_3Cl; 297 K; 62.90 MHz; DEPT ¾π)

δ 31.82, 32.22 (s, 4C) CH_2S
δ 67.57, 68.66, 69.97, 70.10 (s, 8C) CH_2O

6.4.2 The Synthesis of $[Ag_2([18]aneS_2O_4)_2](PF_6)_2$

$AgNO_3$ (68 mg, 0.4 mmol) and $[18]aneS_2O_4$ (119 mg, 0.4 mmol) were stirred in boiling MeOH / H_2O (1/1 v:v 20 cm^3) for three hours. To the hot colourless solution excess of NH_4PF_6 was added and the solution was stirred for additional 15 minutes. After cooling down a white solid precipitated which was isolated and dried. The product was recrystallised from MeOH / H_2O by slow evaporation and single crystals, suitable for structure determination, were obtained.

Microanalysis (for $C_{24}H_{48}Ag_2F_{12}O_8P_2 \cdot H_2O$; Mol.wt. = 1116.56 $gmol^{-1}$)

	%C	%H
Calculated	26.2	4.40
Found	25.8	4.37

FAB mass spectrum (3-NOBA):

Fragment:	m/z (calc.)	m/z (found)
$[^{107}Ag_2([18]aneS_2O_4)_2]^+$	951	951
$[^{107}Ag([18]aneS_2O_4)_2]^+$	699	699
$[^{107}Ag([18]aneS_2O_4)]^+$	403	403

IR spectrum (KBr disc):

3440m/br, 2915s, 2880s, 1920w,1625w, 1475m, 1460w, 1420m,1360m, 1280w, 1270m, 1250w, 1190w, 1105vs, 1030w, 1005w, 970w, 945m, 845vs, 645w, 620w, 560s and 495w cm^{-1}.

^{1}H-NMR spectrum (CD_3CN; 298K; 80.13MHz)

δ 2.1-2.9	(m, 4H)	SCH_2CH_2O
δ 3.00	(s, 4H)	SCH_2CH_2S
δ 3.5 - 3.7	(m, 16H)	CH_2O

^{13}C-NMR spectrum (CD_3CN; 298K; 50.32MHz; DEPT ¾π)

δ 30.98, 30.47 (s, 4C) CH_2S

δ 69.66, 69.25, 68.67, 68.17 (s, 8C) CH_2O

UV/vis spectrum: no absorption in the range 300 to 800 nm (MeCN).

Cyclic Voltammetry (0.1mmol $TBAPF_6$; MeCN; 293K)

$E_{red.(irreversible)}$[Ag(I)/Ag(0)]	1.74V vs Fc/Fc^+ ($0.32Vs^{-1}$)
	1.55V vs Fc/Fc^+ ($0.16Vs^{-1}$)
$E_{demet.}$	-0.036V vs Fc/Fc^+ ($0.32Vs^{-1}$)
	-0.094V vs Fc/Fc^+ ($0.16Vs^{-1}$)

6.4.3 The Synthesis of $[Ag_2([18]aneS_2O_4)_2](BPh_4)_2$

The compound was prepared according to the preparation given under 6.4.2 using $NaBPh_4$ instead of NH_4PF_6.

FAB mass spectrum (3-NOBA):

Fragment:	m/z (calc.)	m/z (found)
$[^{107}Ag_2([18]aneS_2O_4)_2(BPh_4)_2]^+$	1148	1133
$[^{107}Ag_2([18]aneS_2O_4)_2(BPh_4)]^+$	1125	1133
$[^{107}Ag([18]aneS_2O_4)]^+$	403	403

6.4.4 The Synthesis of $[Ag_2([18]aneS_2O_4)_2](CF_3SO_3)_2$

The compound was prepared according to the method described under 6.4.2 using $[^nBu_4N]CF_3SO_3$ instead of NH_4PF_6.

FAB mass spectrum (3-NOBA):

Fragment:	m/z (calc.)	m/z (found)
$[^{107}Ag_2([18]aneS_2O_4)_2(CF_3SO_3)]^+$	955	957
$[^{107}Ag_2([18]aneS_2O_4)_2]^+$	806	811
$[^{107}Ag([18]aneS_2O_4)_2]^+$	699	696
$[^{107}Ag([18]aneS_2O_4)]^+$	403	405

6.4.5 Single Crystal Structure Determinations

Crystallographic data for the single crystal structures of $[Ag_4([18]aneS_2O_4)_4](ClO_4)_4$ and $[Ag_2([18]aneS_2O_4)_2](PF_6)_2$ are summarised in **Table 6.4.5**. The refinement of $[Ag_4([18]aneS_2O_4)_4](ClO_4)_4$ was straightforward with no problems encountered and all non H-atoms have been refined anisotropically. $[Ag_2([18]aneS_2O_4)_2](PF_6)_2$ on the other hand exhibited disorder in one macrocycle and one PF_6^- ion which was modelled satisfactorily (see **A.4**).

Compound	$[Ag_2([18]aneS_2O_4)_2]^{2+}$ $2\,PF_6^-$	$[Ag_4([18]aneS_2O_4)_4]^{4+}$ $4{\cdot}ClO_4^-$
Crystal data		
Formula	$C_{24}H_{48}AgF_{12}O_8P_2S_2$	$C_{48}H_{96}Ag_4Cl_4O_{32}S_8$
M / gmol^{-1}	1098.4	2015.0
Crystal size / mm^3	0.51 x 0.51 x 0.23	0.50 x 0.38 x 0.23
Crystal system	monoclinic	monoclinic
Space group	$P2_1/c$ (No. 14)	$P2_1/c$ (No. 14)
a / Å	18.1728(20)	10.933(5)
b / Å	11.0571(10)	23.615(15)
c / Å	20.0893(14)	14.593(5)
α / °	90	90
β / °	93.327(10)	101.64(4)
γ / °	90	90
U / Å^3	4036.5	3690.0
Z	4	2
D_c / gcm^{-3}	1.807	1.813
μ / mm^{-1}	1.332	1.499
$F(000)$	2208	2048
T / K	298	150.0
Reflections at $\pm\omega$ to refine cell	40	38
2θ range / °	30 - 32	30 - 32
Data Collection		
$2\theta_{max}$ / °	45	45
Range of h	$-9 \rightarrow 9$	$-11 \rightarrow 11$
Range of k	$0 \rightarrow 11$	$-7 \rightarrow 25$
Range of l	$0 \rightarrow 21$	$0 \rightarrow 15$
Measured reflections	6972	7034
Independent reflections, R_{int}	5041, 0.023	4779, 0.044
Observed reflections	4412 with $F \geq 4\sigma(F)$	4051 with $F \geq 4\sigma(F)$
ψ scan correction $TF_{max, min}$	-	0.426, 0.333
Solution		
Method	Patterson Synthesis	Patterson Synthesis
using	SHELX76	SHELXS-86
Refinement on		
full matrix least squares on	F	F^2
using	SHELX76	SHELXL-93
DIFABS max, min	-	-
Weighting scheme	0.000155	0.0449, 4.713
Parameters refined	355	433
SHELX76 R, R', S	0.064, 0.088, 1.31	
SHELXL93 $R1$, $wR2$, S		0.033, 0.128, 1.65
$(\Delta/\sigma)_{max}$	0.41	0.73
$\Delta\rho_{max, min}$ / eÅ^{-3}	+0.90, -0.57	+0.61, -0.66

Table 6.4.5 Selected crystallographic data for the single crystal structures of $[Ag_4([18]aneS_2O_4)_4](ClO_4)_4$ and $[Ag_2([18]aneS_2O_4)_2](PF_6)_2$.

CHAPTER VII

The Co-ordination Chemistry of Iodine in the Oxidation States +I, 0 and -I with Macrocycles and Metal Macrocyclic Complexes

7.1 INTRODUCTION

7.1.1 The Structure of I_2 in the Solid State, in Solution and in Vapour

Elemental I_2 occurs like the other halogens as diatomic molecules in all states of aggregation. Forces between the I_2 molecules are weak due to the non-polar nature of the I_2 molecule, hence the ease of sublimation at room temperature affording violet vapours. The single crystal structure of I_2 as well as the I-I distance in the gas phase [I-I 2.667(2)Å][355] has been determined. There is however a discrepancy between the I-I bond length in I_2 vapour and in the solid state. The single crystal structure of I_2 (at 110K)[356] (**Figure 7.1.1a**) shows that the I-I bond distance [I-I 2.715(6)Å] is significantly longer compared with the one in I_2 vapour.

(i) stacks of sheets

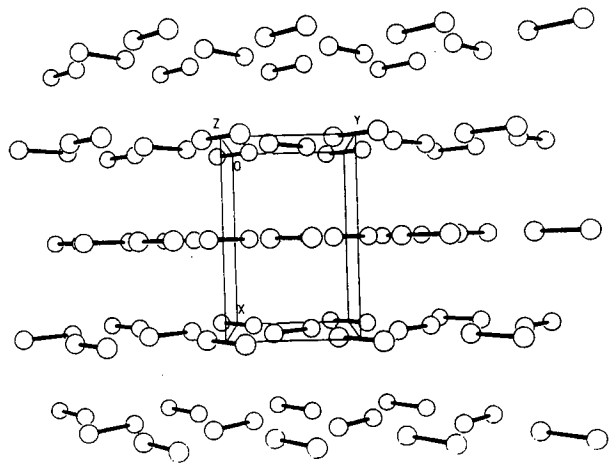

(ii) a single sheet

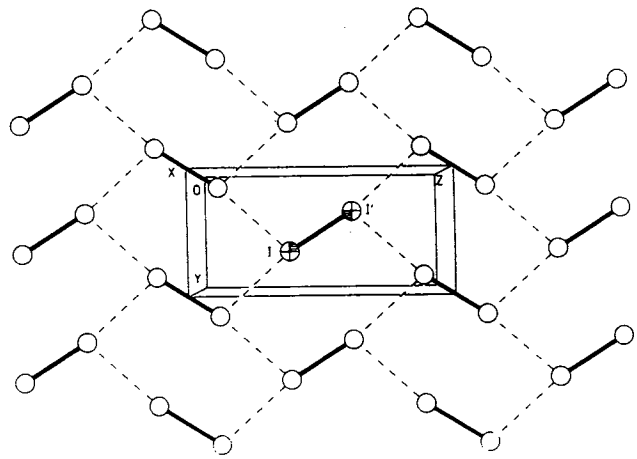

Figure 7.1.1a Packing diagram of I_2.

It is apparent that there are long range interactions between the I_2 molecules [I_2···I_2 3.497(6) and 3.972(7)Å] within a sheet [**Figure 7.1.1a** (ii)]. Since the sum of the van der Waals radii for I_2 (2.1 Å) is 4.2 Å[269], these interactions can therefore be considered partially covalent in nature. The distances between I_2 molecules in different sheets [4.269(6), 4.3317(7) and 4.412(7) Å] are significantly longer compared with the interactions within each sheet [**Figure 7.1.1a** (i)]. The angles between I_2 molecules in each sheet have values close to 90° and 180°.

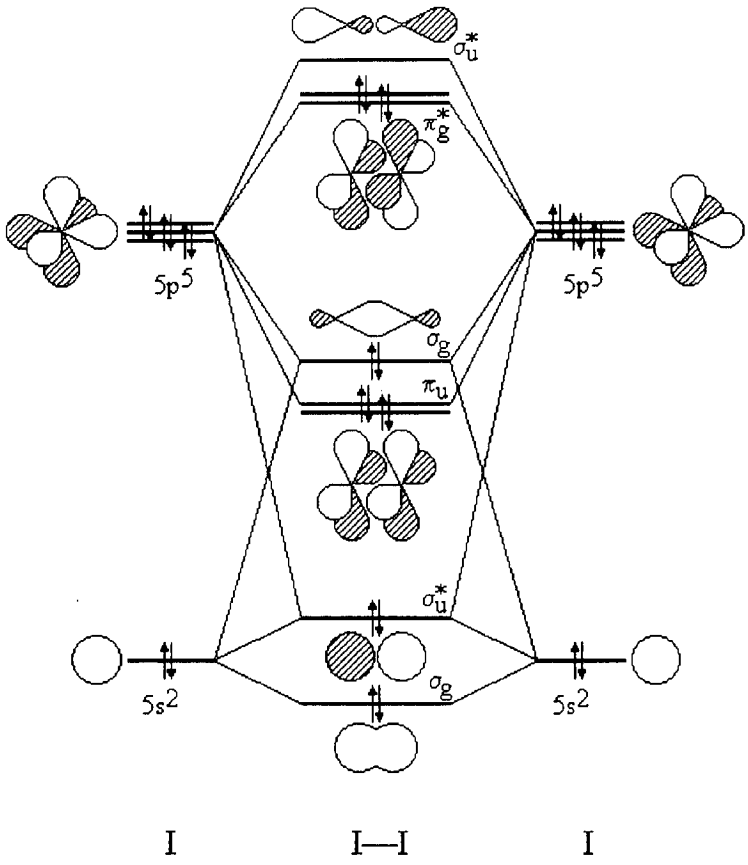

Figure 7.1.1b Qualitative MO-diagram for I_2.

The qualitative MO-diagram of I_2 (**Figure 7.1.1b**) shows that the LUMO is an antibonding σ_u^* orbital which lies along the main axis of the I_2 molecule. The HOMOs are antibonding π_g^* orbitals which lie around the main axis. The I_2 molecule can therefore act either as a σ-acceptor (i) or π-donor (ii). These considerations allow us to understand the geometric and electronic properties in solid I_2, polyiodides and I_2-thioether charge-transfer adducts which all belong into the group of donor-acceptor complexes.

(i) I_2 as a σ-acceptor

The only unoccupied orbital in the I_2 molecule is the antibonding σ_u^* orbital along the main axis of the molecule. The interaction with a donor 'D' such as a heteroatom, I^- or I_2 has therefore to be linear with a D·····I—I angle close to 180°. Deviations from this ideal geometry are most likely due to steric effects of other molecules in the crystal lattice. The donation of electron density into this antibonding orbital lowers the bond order in I_2, increases the bond length and shifts λ_{max} to higher energy (blue shift).

(ii) I_2 as a π-donor

The bonding π_u and antibonding π_g^* orbitals are generated by combination of the wave functions of the p_x and p_y orbitals (assuming the main axis of the molecule lies along the z-axis). The donation of electron density from a π_g^* orbital to an acceptor 'A' such as another I_2 molecule shows therefore an A·····I—I angle close to 90°. The donation of electron density from the antibonding π^*-orbital should decrease the bond length but is superseded by the effect of donation of electron density into the antibonding σ^*-orbital in case of I_2 (see above).

The different colours of I_2 in solution (**Table 7.1.1**) were the subject of much speculation at the beginning of this century. A number of explanations were proposed. Beckmann[357] using cryoscopic methods showed that dissolved I_2 molecules were still diatomic in nature thus discarding ideas of cluster formation. He also suggested that the species in solution are in fact molecular adducts between I_2 and solvent molecules. This hypothesis was confirmed by Lachman[358] who studied the colour of solutions at different temperatures and found that violet solutions turn brown on cooling[359] and brown solutions turn violet on heating. He proposed an equilibrium between free (violet) iodine and iodine adducts (brown).

The modern understanding of this behaviour is that I_2 forms charge-transfer adducts with solvent molecules or other donors present. The actual charge-transfer band ($D \rightarrow I_2$) lies in the UV or vacuum-UV region of the spectrum and is difficult to observe. The band in the visual region has been assigned to an internal transition in the I_2 molecule involving the antibonding LUMO. This is reflected in the increasing blue shift for increasing donor strength of the donor atoms. Reviews covering this area have been published[360,361].

Solvent	**Colour**	**$\lambda_{max.}$ / nm**
Hydrocarbons, CCl_4	violet	520 - 540
Aromatic hydrocarbons	pink-red	490 - 510
Alcohols, amines	brown	450 - 480

Table 7.1.1 Absorbtion ranges of I_2 in different solvents.

7.1.2 Charge Transfer Complexes with N, P, O, S and Se Donors

Group V trialkyl and group VI dialkyl compounds react instantaneously with molecular halogens. The ease of preparation and isolation, the brilliant colours of some of the adducts and their complicated structural features have made these compounds a constant object of study for over a century. The first example of such an adduct has been reported by Husemann in 1863[362]. Even though this first example has been between I_2 and the thioether 1,4-dithiane, a range of compounds of halogens and interhalogens with group V and VI donors have been prepared and structurally characterised. As it can be seen from **Table 7.1.2a**, most compounds studied are adducts between small sized molecules (**Figure 7.1.2a**) and I_2. The most obvious features in the structural investigations include an elongated X-Y (X, Y = I, Br, Cl) bond, the X-D bond is smaller than the sum of the van der Waals radii of the appropriate atoms and the angle D-X-Y is close to 180°. Exceptions to this behaviour usually occur in compounds which have additional I_2 molecules in the crystal lattice and the structure would be better described as extended polyiodides and $(D\text{-}I)^+$ units; for example $(Ph_3P)(I_2)_2$ would be better described as $(Ph_3PI)^+(I_3)^-$ [371].

Compound	X-X(Å)	D-X(Å)	D-X-X(°)	Reference
Nitrogen adducts				
$(Me_3N)I_2$	2.84	2.27	179	363
$(Me_3N)ICl$	2.52	2.30	†	364
(py)ICl	2.54	2.30	†	365
$(C_{12}H_8N_2)I_2$	2.726	2.982	180	366,367
	2.726	3.098	180	
(4-picoline)I_2	2.31	2.83	†	368
$(C_6H_{12}N_4)(Br_2)_2$	2.4	2.3	180	369
Phosphorous adducts				
$(Ph_3P)Br_2$	3.123	2.181	177.16	370
$(Ph_3P)(I_2)_2$	3.551	2.395	156.79	371
$(Ph_3P)_2(I_2)_3$	2.86	2.69	174.6	372,373
$(Ph_3P)_2(I_2)_4$	3.506	2.401	177.4	371
Oxygen adducts				
$(C_4H_8O_2)(ICl)_2$	2.3	2.6	180	374
$(C_4H_8O_2)Br_2$	2.31	2.71	†	375
Thioether adducts				
([9]aneS_3)2$(I_2)_4$	2.754	3.197	176.18	376,377
	2.785	2.870	178.35	
	2.816	2.760	174.86	
	2.799	2.862	177.27	
	2.754	3.054	169.39	
([9]aneS_3)$(I_2)_3$	2.772	2.880	173.5	377
	2.768	2.865	175.1	
	2.751	2.933	174.5	
(1,10-[18]aneS_2O_4)$(I_2)_2$	2.821	2.774	175.24	378
	2.775	2.848	173.47	
	2.810	2.761	178.03	
	2.902	2.654	175.97	
$(C_4H_8S_2)(I_2)_2$	2.77	2.77	176	379
$(C_4H_8S)Br_2$	2.724	2.321	178	380
(Benzylsulphide)I_2	2.819	2.78	178.9	381
Thioketone adducts				
(Ethylenethiourea)$(I_2)_2$	3.147	2.487	177.9	382
(Dithizone)$_2(I_2)_7$	3.215	2.506	179.1	382
(Ethylenethiourea)$_2(I_2)_3$	2.984	2.580	177.5	382
(Ethylenethiourea)I_2	2.987	2.588	178.2	382
(Dithizone)I_2	2.918	2.664	178.4	382
(N-methylthiocaprolactam)I_2	2.888	2.688	176.21	383
Selenium adducts				
$(C_4H_8Se)I_2$	2.914	2.762	179.4	384
$(C_4H_8OSe)I_2$	2.956	2.755	174.8	385
$(C_4H_8OSe)ICl$	2.73	2.630	175.8	386
$(C_4H_8Se_2)(I_2)_2$	2.870	2.829	180.0	379,387

Table 7.1.2a Reported structures of adducts between halogens and group V and VI donors († no value reported).

(i) (4-picoline)I_2

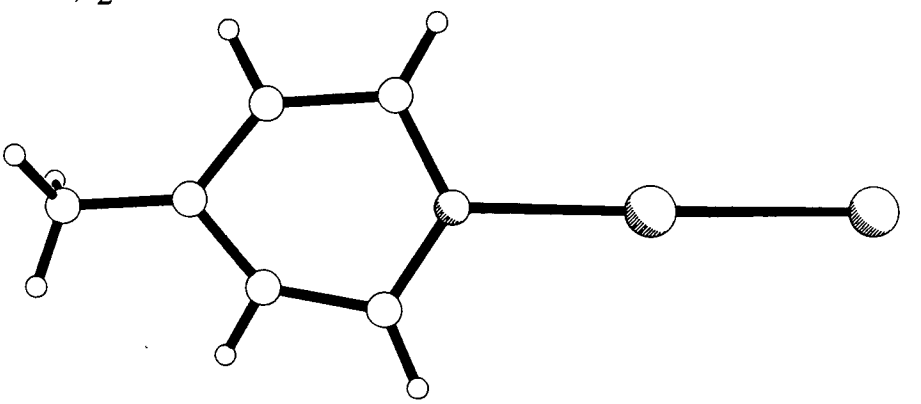

(ii) $[(Bz)_2S]I_2$

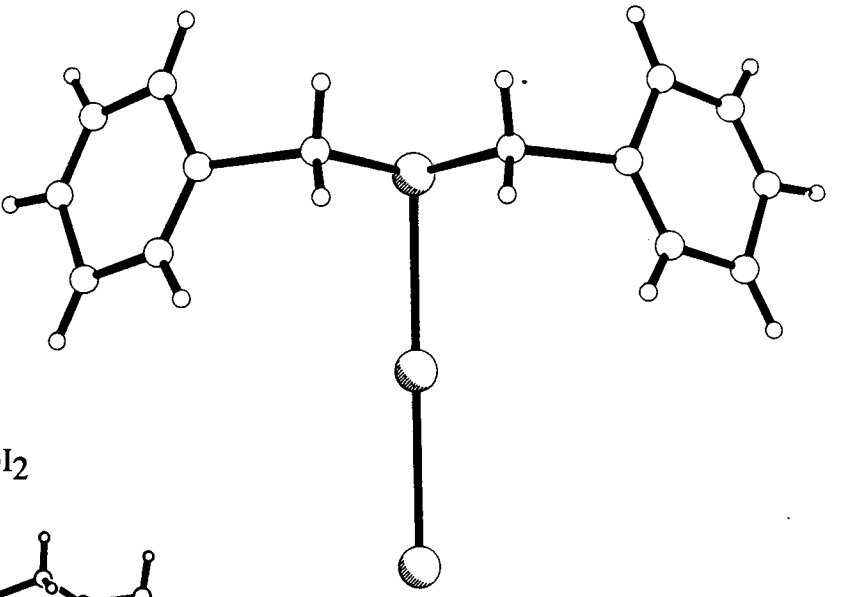

(iii) (1,10[18]aneS_2O_4)I_2

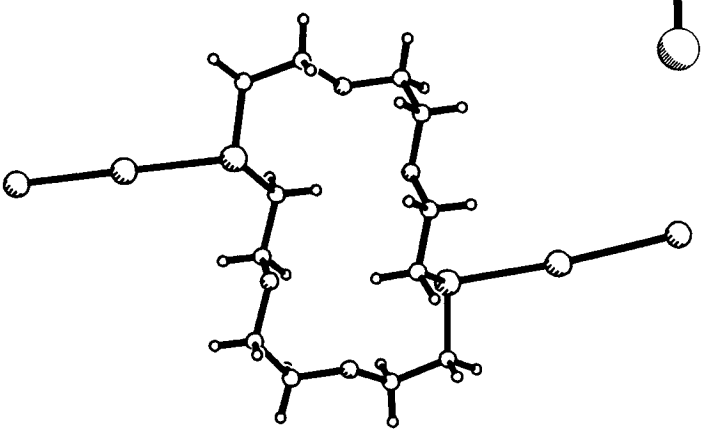

Figure 7.1.2 The single crystal structures of (i) (4-picoline)I_2, (ii) $[(Bz)_2S]I_2$, (iii) (1,10[18]aneS_2O_4)I_2.

Compounds containing I_2 molecules exhibit in general a wide range of contacts. Geometric criteria for σ-donor and π-acceptor interactions have already been discussed (see above). Any other interaction which does not conform to the criteria outlined is most likely a weak dipole-dipole or, in the case of charged species, an electrostatic interaction.

A common way to deal with the variation in the D-I and I-I distances in the structures of I_2 thioether complexes has been reported by Herbstein[382]. A plot of S-I against I-I distances fits a hyperbola. A similar plot will be presented in conjunction with the presentation of the results in this thesis. The boundaries of such a plot are not well defined. One extreme would be the I-I distance in I_2 vapour (i.e. absence of any donor) [I-I(vapour) 2.667(2) Å[355]]. The other extreme would be a covalent bond in a binary S/I_2 compound. Compounds containing covalent S-I bonds are relatively unstable. The report by Gay-Lussac[388] of the direct fusion of the elements has caused some controversy and initiated studies[389-395] to whether or not these elements combine to one or more iodides of sulphur. Despite the failure to isolate binary S/I_2 compounds it has been possible to obtain evidence of their short lived existence. Rao reported the following reaction[396-401] in CCl_4:

$$S_2Cl_2 + 2KI \longrightarrow S_2I_2$$
$$S_2I_2 \longrightarrow \tfrac{1}{4}S_8 + I_2$$

The S_2I_2 which is generated from the reaction of S_2Cl_2 with KI is light sensitive and shows an increasing stability with decreasing temperature and concentration. Spectroscopic studies confirmed the synthesis of S_2I_2[402,403] but no structural data such as S-I bond lengths have been reported. Other examples of compounds containing S-I bonds are listed in **Table 7.1.2b**. These examples contain charged species and charge-transfer adducts but the S-I bond lengths quoted might give an indication of the magnitude of the S-I bond length in S_2I_2. The area of compounds between S and I_2 has been reviewed[404,405].

Compound	S-I (Å)	Reference
$[(S_7I)_2I](SbF_6)_3 \cdot 2AsF_3$	2.108(12), 2.335(7), 2.675(7)	406
$(S_7I)SbF_6$	2.347(6), 2.37(1), 3.384(8)	407
$[I(L^{\dagger})_2]I_7$	2.600(2), 2.634(2)	408
$[I(H_2N)_2CS]I$	2.629	409
$1,4\text{-}C_4H_8S_2 \cdot 2IBr$	2.687(2)	410
$2Ph_3PS \cdot 3I_2$	2.69(2)	372
$(benzylsulfide)_2S \cdot I_2$	2.78	381
$(S_2I_4)(AsF_6)_2$	2.858(6), 3.195(6)	411
$1,4\text{-}C_4H_8S_2 \cdot 2I_2$	2.867(6)	412
$1,4\text{-}C_4H_8S_2 \cdot C_2I_2$	3.27(1)	413
$1,4\text{-}C_4H_8S_2 \cdot CHI_3$	3.32(2)	414
$CHI_3 \cdot 3S_8$	3.500(14)	415
$SbI_3 \cdot 3S_8$	3.602(6)	416
$1,4\text{-}C_4H_8S_2 \cdot 2SbI_3$	3.732(7)	417

($L^{\dagger}$ = N-methylbenzothiazole-2(3*H*)-thione)

Table 7.1.2b S-I bond lengths in reported compounds.

In 1993 McAuliffe and co-workers reported the synthesis and characterisation of a range of adducts between I_2 and phosphines[418]. These compounds have been characterised by microanalysis and studied using ^{31}P-NMR- and Raman-spectroscopy. The authors emphasise that these compounds can be used as starting materials in inorganic syntheses. The reaction of R_3PX_2 (R = alkyl, aryl; X = Br, I) with coarse-grain unactivated metal powders M yielded complexes of the composition $M(PR_3)_nX_y$. Reports of the synthesis and characterisation of such compounds have subsequently appeared {e.g.$[Ni(PPh_3)I_3]$, $[Ni(PPhMe_2)_2Br_2]$[419], $[Mn(PPh_3)_2I_2]$;[420] $[Co(PMe_3)_2I_3]$[421] and $[Mn_2(PMe_3)_3I_5]PMe_3$[422]}.

7.1.3 Polyiodide Compounds

The poor solubility of I_2 in water [0.3 g kg^{-1} (20°C)][423] increases drastically with the addition of KI. I_2 reacts with I^- according with the following equation to the tri-iodide anion I_3^-.

$$I_2 + I^- \longrightarrow I_3^- \qquad K_{(25\,°C)} \approx 698 \pm 10 \text{ (ref. 424)}$$

I_2 reacts in the equation above as a Lewis acid and I^- as a Lewis base. Similar reactions are in general possible between any combination of X_2 and Y^- (X, Y = Cl, Br and I) in aqueous solution[423]. Larger polyhalide anions have been found to be present in other solvents and in the solid state. This area has been reviewed several times[425-428]. The $(I_3)^-$ anion is the only polyiodide species of importance in aqueous solution.

Table 7.1.3a gives an overview of single crystal structures of compounds containing the $(I_3)^-$ anion and its dimension. $(I_3)^-$ anions can be divided into two groups, symmetrical and asymmetrical. Slater has shown that the asymmetric geometry is favoured in cases where the distance between the central I-atom and the terminal I-atoms is large. Slater argued that the occurrence of symmetrical $(I_3)^-$ anions is caused by some 'pressure' of large counter-cations such as $(AsPh_4)^+$ onto the $(I_3)^-$ anion[429].

(i) symmetric triiodide ions

Compound	**I(1)—I(2)**	**I(1)·····I(3)**	**Reference**
$[Mo(diars)_2(CO)Cl]I_3$	2.903	5.806	430
$[Mo(OCl)(MeCN)_4]I_3$	2.914	5.838	431
$[AsPh_4]I_3$	2.92	5.840	432,492
$Eu(ep)_2I_3$	2.925	5.850	433
$[Et_4N]I_3$	2.928	5.856	434
$[(C_5H_4)_2Fe]I_3$	2.93	5.86	435
$KI_3 \cdot KI_5$·valinomycin	2.93	5.86	436
$RbI(I_3)(BiI_6) \cdot 2H_2O$	2.935	5.870	437
KI_3(xanthotoxin)$_2$	2.939	5.878	438
$[Et_4N]I_3$	2.943	5.886	434
$KI \cdot KI_3 \cdot 6$(MeCONHMe)	2.945	5.890	439

(ii) asymmetric triiodide ions

Compound	**I(1)—I(2)**	**I(2)—I(3)**	**Δ**	**I(1)·····I(3)**	**Reference**
$KI_3 \cdot H_2O$	2.925	2.935	0.010	5.860	440
$(BEDT\text{-}TTF)(I_3)(TlI_4)$	2.914	2.916	0.002	5.840	441
$(BEDT\text{-}TTF)(I_3)(I_5)$	2.889	2.932	0.043	5.821	441
$[(L^{\dagger})_2I]I_3$	2.899	2.919	0.020	5.818	408
$[MoCl_4(diars)_2]I_3$	2.890	2.912	0.022	5.812	442
$[C_6H_{12}N_4)_2I]I_3$	2.899	2.931	0.032	5.830	443
$[Et_4N]I_3$	2.912	2.961	0.049	5.873	434
$[W(CO)_4(diars)_2I]I_3$	2.895	2.957	0.062	5.852	444
$[Et_4N]I_3$	2.895	2.981	0.089	5.873	434
$[(C_5H_4)_2Fe]I_3$	2.85	2.97	0.12	5.82	445
$[(C_5H_4)_2Fe]I_3$	2.86	3.00	0.14	5.86	445
CsI_3	2.840	3.042	0.202	5.882	432
RbI_3	2.792	3.016	0.224	5.808	446
$(NH_4)I_3$	2.802	3.114	0.312	5.916	447,448
$(Hpy)_2(I_3)(I_7)^{\dagger\dagger}$	3.124	3.135	0.011	6.259	449

† L = N-methylbenzothiazole-2(3*H*)-selenone
†† polymeric

Table 7.1.3a Dimensions (Å) of reported $(I_3)^-$ anions.

The formation of a $(I_3)^-$ anion from I_2 and I- is schematically shown in **Figure 7.1.3a**. The bond length in I_2 in the absence of interactions with other molecules (i.e. gas phase) is 2.667(2) Å [**Figure 7.1.3a** (a)]. An approaching I^- anion which acts as a donor interacts with the I_2 molecule and induces a dipole along the main axis of the I_2 molecule [**Figure 7.1.3a** (b)]. The electronic features and geometric changes of such a donor-acceptor interaction have already been discussed (see above). The induced dipole attracts the I^- anion even further which results in the formation of the asymmetric [**Figure 7.1.3a** (c)] and symmetric $(I_3)^-$ anion [**Figure 7.1.3a** (d)] depending on the environment in the crystal lattice (see above).

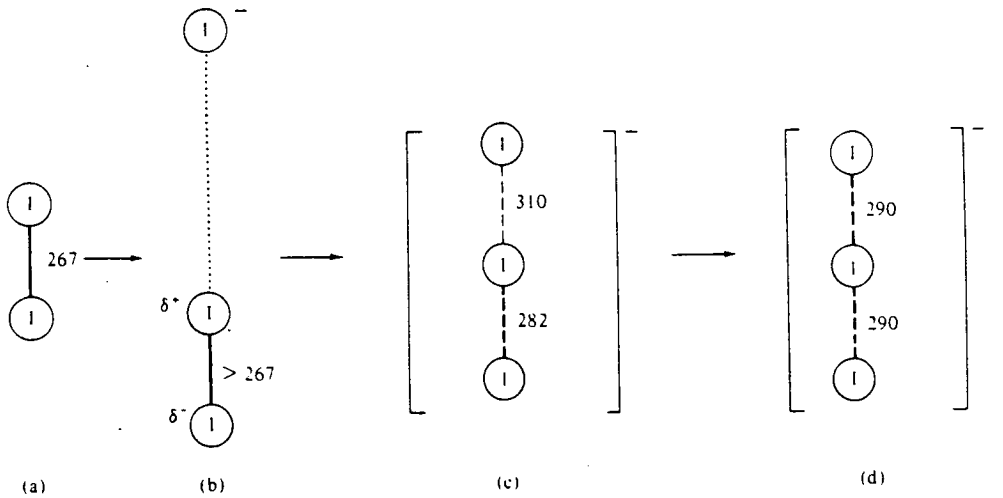

Figure 7.1.3a The formation of $(I_3)^-$ anions from I_2 and I^- (Distances are in pm).

The electronic properties of the $(I_3)^-$ anion can be described in analogy to XeF_2 as four electron three centre bonding[450]. The p_z-orbital of the I-atom in the middle interacts with the p_z-orbital of each terminal I-atom giving an overall linear arrangement (assuming the $(I_3)^-$ anion lies along the z-axis). The linear combination of these three orbitals gives three MOs ψ_b, ψ_n and ψ_a (**Figure 7.1.3b**). The four valence electrons ($I^-5p^2 + I5p1 + I5p1$) fill the bonding ψ_b and the non-bonding ψ_n orbitals leaving the antibonding orbital ψ_a free. The $(I_3)^-$ anion has therefore one single bond (or one bonding MO) over the whole length of the molecule. Similar arguments apply to the $5p_x$ and $5p_y$-orbitals which would lead to $(I_5)^-$ and $(I_7)^-$ polyiodide species.

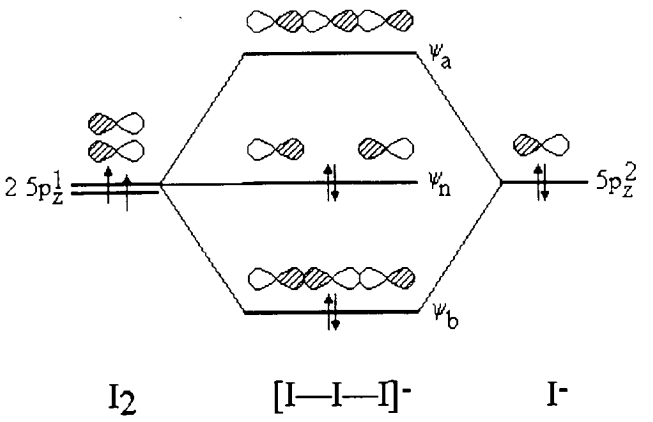

Figure 7.1.3b The MO-diagram of $(I_3)^-$.

A series of polyiodides ranging from $(I_3)^-$ to $(I_{16})^{4-}$ have been reported in single crystal structures (**Table 7.1.3a** and **7.1.3b**). Any polyiodide species is in general assembled from I^-, I_2 and $(I_3)^-$ following the rules outlined above for donor-acceptor complexes. These species in particular extended polyiodides are weakly bonded compounds and dissociate in solution into I^-, I_2 and $(I_3)^-$ or decompose via loss of I_2; their reactions are usually the ones of their components[426].

Polyiodide	Compound	Reference
I_4^{2-}	$(\text{phenacetin})_4(H_2I_4)\cdot 2H_2O$	451
	$[Cu(C_9H_{13}N_5)I_2]\cdot \frac{1}{2}I_2$	452
	$[Cu(NH_3)_4]I_4$	453
	Tl_6PbI_6	454
I_5^-	$(Et_4N)I_5$	455,456
	$[K(\text{valinomycin})]_2(I_5^-)(I_3^-)$	436
	ζ-(BEDT-TTF)$(I_3)(I_5)$	441
	$CaI_{10}\cdot 7H_2O$	457
	$(\text{trimesic acid}\cdot H_2O)_{10}(HI_5)$	458-460
I_7^-	$(Et_4N)I_7$	461
	[(N-methylbenzothiazole-2(3*H*)-thione)$_2$I]I_7	408
	$(Hpy)_2I_{10}$	449
I_8^{2-}	Cs_2I_8	462
	$MgI_8\cdot 6H_2O$	463
I_9^-	$(Me_4N)I_9$	464
I_{14}^{2-}	$(\text{Dithizone})_2(I_2)_7$	465
I_{15}^{3-}	$(SbF_6)(I_5)$	466
I_{16}^{4-}	$(\text{theobromine})_2H_2I_8$	467
	$(C_{10}H_{16}N_2O_2S_3)_2I_{16}$	468

Table 7.1.3b Examples of compounds containing polyiodides.

(i) (phenacetin)$_4$(H_2I_4)·2H_2O[451]

I(1)-I(2)	3.404 Å
I(2)-I(2')	2.774 Å

(ii) Cs_2I_8[462]

I(1)-I(1')	2.83 Å
I(1)-I(2)	3.42 Å
I(2)-I(3)	3.00 Å
I(3)-I(4)	2.84 Å
I(1')-I(1)-I(2)	175°
I(1)-I(2)-I(3)	80°
I(2)-I(3)-I(4)	176°

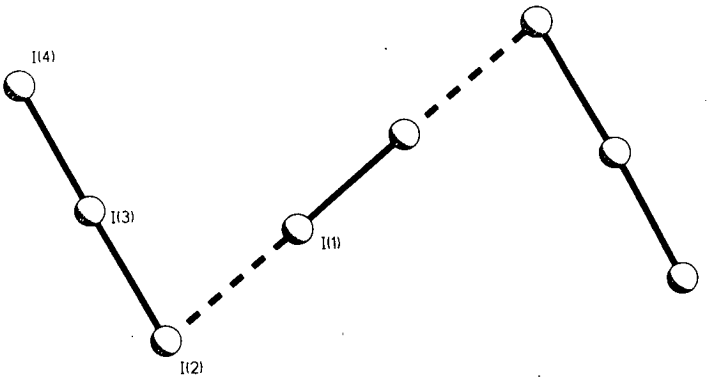

(iii) (Me_4N)I_9[464]

I(1)-I(2)	3.18 Å
I(1)-I(7)	3.43 Å
I(1)-I(8)	3.24 Å
I(2)-I(3)	2.90 Å
I(3)-I(4)	3.24 Å
I(4)-I(5)	2.91 Å
I(6)-I(7)	2.67 Å
I(8)-I(9)	2.67 Å
I(2)-I(1)-I(8)	89°
I(2)-I(1)-I(7)	85°
I(2)-I(3)-I(4)	87°

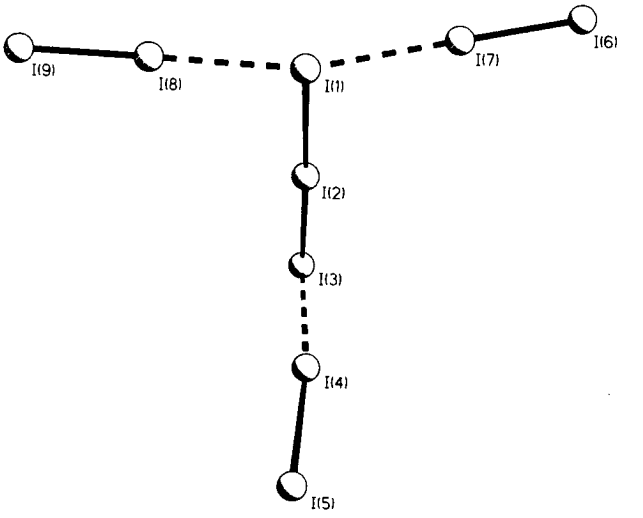

Figure 7.1.3c The structures and dimensions of (i) $(I_4)^{2-}$, (ii) $(I_8)^{2-}$ and (iii) $(I_9)^-$ anions.

(i) $(I_4)^{2-}$

The formation of the $(I_4)^{2-}$ anion can be viewed as the simultaneous interaction of one I_2 molecule with two I^- anions. The linearity of the $I^-\cdots I\text{-}I\cdots I^-$ configuration (**Figure 7.1.3c**) conforms to the rules for donor-acceptor complexes outlined above. **Table 7.1.3c** illustrates again the effect of weak and strong $I_2\cdots I^-$ interactions on the bond length of the I_2 molecule.

Compound	I(1)···I(2)	I(2)-I(3)	I(3)···I(4)	Reference
(phenacetin)$_4$(H_2I_4)·2H_2O	3.404	2.774	3.404	451
[Cu($C_9H_{13}N_5$)I_2]·½I_2	3.35	2.806	3.35	452
[Cu(NH_3)$_4$]I_4	3.34	2.80	3.34	453
Tl_6PbI_6	3.18	3.14	3.18	454

Table 7.1.3c Dimensions (Å) of reported tetraiodide dianions.

(ii) $(I_5)^-$

The interaction of an I^- anion with two I_2 molecules leads formally to the $(I_5)^-$ anion. Two different geometries of the $(I_5)^-$ anion have been reported. The $(I_5)^-$ anion in ζ-(bis(ethylenedithio)tetrathiafulvalene)$(I_3)(I_5)$, $(Et_4N)I_5$ and [K(valinomycin)]$_2(I_5)(I_3)$ is V-shaped with an (I_2)-I-(I_2) angle close to 90°. It is interesting to note that two $(I_5)^-$ anions in [K(valinomycin)]$_2(I_5)(I_3)$ and CaI_{10}·$7H_2O$ show angles smaller than 90° suggesting that the steric repulsion between each side of the anion is small and these small distortions are a packing effect in the crystal lattice. The $(I_5)^-$ anion can be described as an orthogonal (I-I···I···I-I)$^-$ arrangement. The MO-diagram for either side of the anion is similar to the one for $(I_3)^-$. The orthogonality of the anion can be traced back to the two orthogonal $5p^2$-orbitals of the central I-atom. The third $5p^2$-orbital is left free for further interaction with a possible third I_2 molecule to give $(I_7)^-$ (see below). The $(I_5)^-$ anion in (trimesic acid·H_2O)$_{10}(HI_5)$ is linear and forms an infinite chain structure via long range interactions between adjacent $(I_5)^-$ anions [$(I_5)^-$·····$(I_5)^-$ 3.50 Å][458-460]. Marks using Mössbauer- and resonance Raman-spectroscopy has shown that a linear $(I_5)^-$ anion is the major chromophore in the dark blue I_2-starch complex[469]. The colour of $(Et_4N)I_5$ has been described as greyish-green with a metallic shade[455].

Compound	I(1)-I(2)	I(2)-I(3)	I(3)-I(4)	I(4)-I(5)	I(2)-I(3)-I(4)	Ref.
[K(valinomycin)]$_2(I_5^-)(I_3^-)$	2.760	3.080	3.080	2.760	83.8°	436
$(Et_4N)I_5$	2.81	3.17	3.17	2.81	95°	455,456
ζ-(BEDT-TTF)$(I_3)(I_5)$	2.792	3.091	3.087	2.781	92.23°	441
CaI_{10}·$7H_2O$	2.778	3.212	3.156	2.767	91.9°	457
	2.761	3.350	3.098	2.802	85.8°	
(trimesic acid·H_2O)$_{10}(HI_5)$	2.74	3.26	3.26	2.74	linear	458-460

Table 7.1.3d Dimensions (Å) of reported pentaiodide anions.

The single crystal structure of $(Et_4N)I_5$ (**Figure 7.1.3d**) shows that the distance between each terminal I-atom and its nearest neighbour is 3.63 Å. A small distortion of the bond lengths would lead to symmetrical $I^-\cdots I\text{-}I\cdots I^-$ fragments which generate a 2-dimensional polymeric polyiodide network of the stoichiometry $[I(I_2)_2]^-$.

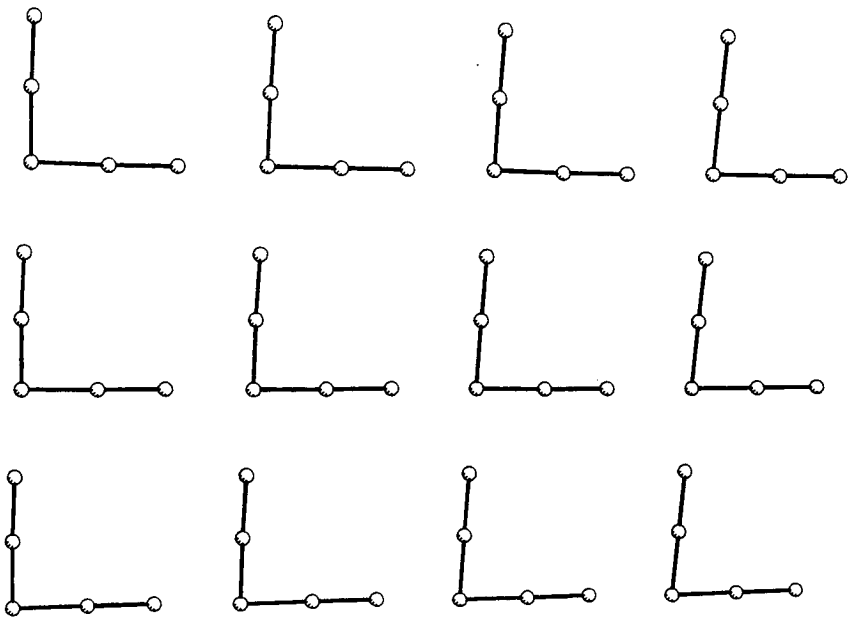

Figure 7.1.3d The arrangement of $(I_5)^-$ anions in the crystal lattice of the single crystal structure of $(Et_4N)I_5$.

(iii) $(I_7)^-$

The preceding pages have illustrated that stoichiometry to structure as well as stoichiometry to property (colour) relationships are rather ambiguous when dealing with polyiodide anions. The three reported structures of the $(I_7)^-$ anions support this view. The single crystal structure of $(Et_4N)I_7$ shows a complicated three dimensional network of symmetrical $(I_3)^-$ anions and I_2 molecules[461] The authors point out that $(I_7)^-$ should be better described as $(I_3)^-\cdot 2I_2$. Recently two examples of $(I_7)^-$ anions were reported by Jacobsen[449] and Devillanova[408]. Even though Devillanova emphasises that this is the first example of an $I^-\cdot 3I_2$ anion, the differences to the structure reported by Jacobson are only marginal (**Table 7.1.3e**).

{I(1)—[I(2,4,6)-I(3,5,7)]$_3$}	$(Hpy)_2I_{10}$	[(N-methylbenzothiazole-2(3*H*)-thione)$_2$I]I_7
Reference:	449	408
I(1)—I(2) (Å)	3.144 (4)	3.260(1)
I(1)—I(4) (Å)	3.144 (4)	3.242 (1)
I(1)—I(6) (Å)	3.324 (16)	3.237 (1)
I(2)-I(3) (Å)	2.787 (5)	2.746 (1)
I(4)-I(5) (Å)	2.787 (5)	2.766 (1)
I(6)-I(7) (Å)	2.759 (9)	2.771 (1)
I(1')—I(7) (Å)	3.545 (13)	3.502 (1)

Table 7.1.3e Dimension of the structures of $[(I_7)^-]_n$ reported by Jacobson[449] and Devillanova[408].

The environment around the 'central' I(1)-atom is distorted orthogonal as a result of the participation of all three 5p orbitals [see above $(I_3)^-$ and $(I_5)^-$]. The $(I_7)^-$ anions can be viewed broadly as isolated species with a long range interaction to a neighbouring $(I_7)^-$ species affording an overall one dimensional chain structure (**Figure 7.1.3e**). The colour of $(Hpy)_2I_{10}$ has been described as black in contrast to lustrous green for [(N-methylbenzothiazole-2(3*H*)-thione)$_2$I]I_7 which is not surprising since $(Hpy)_2I_{10}$ contains not only the $(I_7)^-$ but also the $(I_3)^-$ chromophore in the crystal lattice.

(i) $(Hpy)_2I_{10}$

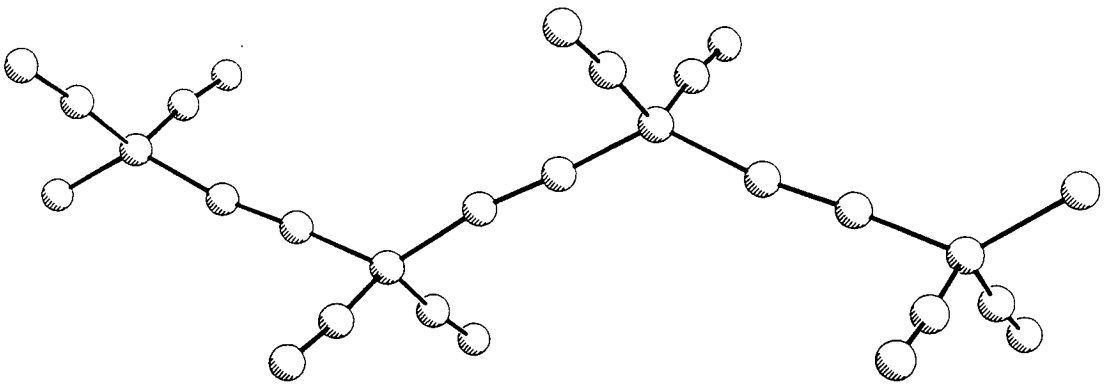

(ii) [(N-methylbenzothiazole-2(3*H*)-thione)$_2$I]I$_7$

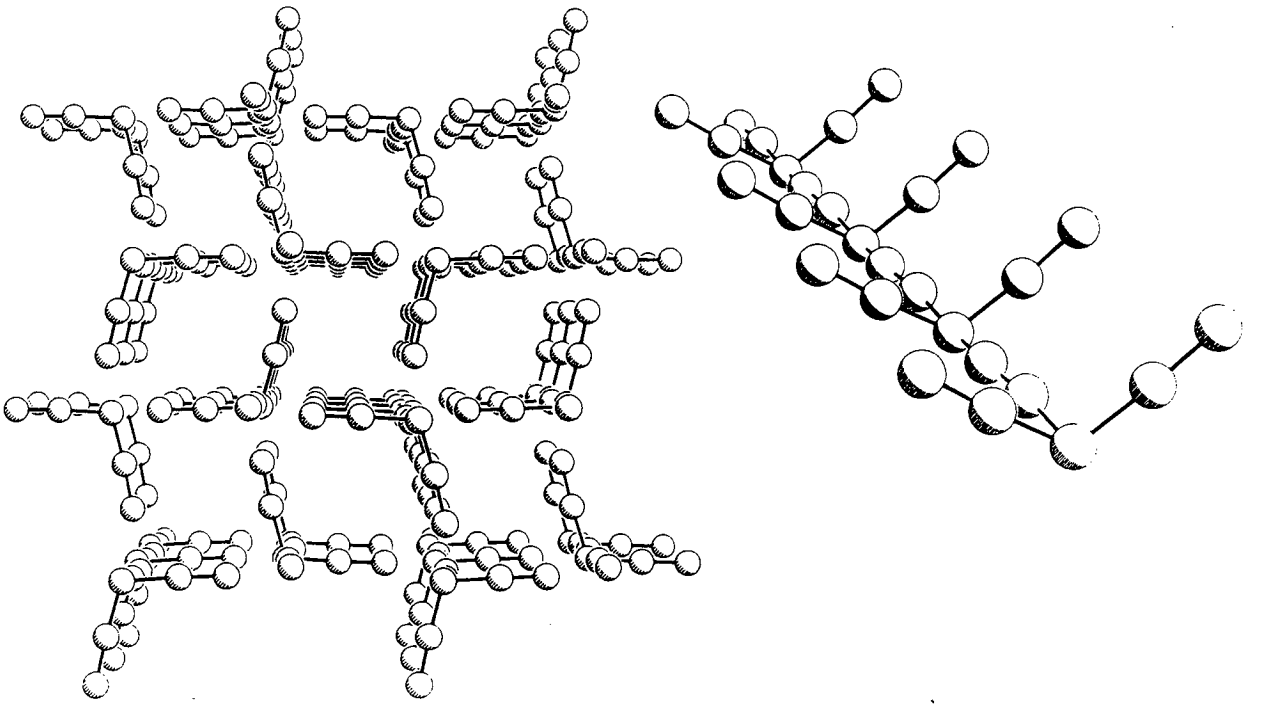

Figure 7.1.3e The structure of the $[(I_7)^-]_n$ species in the single crystal structures of (i) $(Hpy)_2I_{10}$ [449] and (ii) [(N-methylbenzothiazole-2(3*H*)-thione)$_2$I]I$_7$ [408].

7.1.4 The Iodine Monocation I^+

Following the discussion of charge-transfer adducts in the previous sections with a discussion of the iodonium ion might seem slightly discontinuous. However, I^+ is in general prepared by the heterolytic cleavage of the I_2 (or I-X; X = Cl, Br) bond leading to I^- and I^+ ions. It is therefore necessary that the I_2 bond becomes polarised by charge separation during this process:

$$I\text{-}I \longrightarrow [I^{\delta+}\text{—}I^{\delta-}] \longrightarrow I^+ + I^-$$

The effects of the interaction of a donor D with I_2 have already been discussed (see above). These donor-acceptor complexes show a range of features very similar to the ones schematically shown in the polarised I_2 intermediate above. Donor-acceptor complexes of I_2 or already polarised interhalogens are therefore excellent starting points in the synthesis of I^+ complexes:

$$D + I\text{-}I \longrightarrow D^{\delta+}\text{—}I^{\delta+}\text{—}I^{\delta-} \longrightarrow [D\text{-}I]^+ + I^-$$

$$D + I^{\delta+}\text{—}Cl^{\delta-} \longrightarrow [D\text{-}I]^+ + Cl^-$$

Factors, which influence the outcome of such a reaction include first of all the nature and 'strength' of the donor D but also the choice of solvent[470]. For instance the influence of solvent effects on iodine monohalides has been studied by Sharpe[471]. It had already been suggested that the dielectric constant of a given solvent influences the type of reaction which occurs[472,473]. The main reaction of ICl vapour with salicylic acid or phenol is chlorination; in contrast to iodination which predominates in $MeNO_2$. The essential conclusion drawn from those studies is that solvents with a low dielectric constant or the absence of a supporting solvent support homolytic fission which generates radicals whereas solvents with a high dielectric constant support heterolytic fission and the generation of ions.

The second step in the preparation of I^+ consists of the actual cleavage of the polarised bond, stabilising the products and trapping the I^- anions to prevent recombination with the iodonium species. The following examples give a brief overview of reported preparations of iodonium ion complexes.

Marks and co-workers[469] reported a preparation of the blue I_2-amylose complex (see above) by reaction of I_2 vapour with amylose. The I^- necessary for the formation of the $(I_5)^-$ anion is produced by hydrolysis or alcoholysis of I_2. The other product of this reaction, a hypoiodite was assigned in the I_2 Mössbauer spectrum.

The two complexes [(N-methylbenzothiazole-2(3*H*)-thione)$_2$I]I_7 [**Figure 7.2.5b** (ii)] and [(N-methylbenzothiazole-2(3*H*)-selone)$_2$I]I_3 reported by Devillanova[408] were prepared by the reaction of I_2 with N-methylbenzothiazole-2(3*H*)-thione and N-methylbenzothiazole-2(3*H*)-selone in CH_2Cl_2 respectively. The I^+ cation is co-ordinated between two thioketone S- or selenoketone Se-atoms.

A few I_2 charge-transfer and iodonium complexes with N-donor ligands such as py, hmt and 4-picoline have been studied in the solid state. This is in sharp contrast to the vast number of reports on N-donor halogen adducts in solution. These n-σ complexes are probably the most extensive studied species in solution[474]. Bowmaker reported the preparation of (hmt)I_2, [(hmt)$_2$I]I_3 and [(hmt)$_2$I]ClO_4[475]. The reaction of an ethanolic solution of I_2 with a solution of hmt in $CHCl_3$ at 40°C afforded an immediate precipitation of orange crystals of the stoichiometry (hmt)I_2. The product turned slowly brown over a period of several days. The dark brown compound, which can also be prepared by reaction of excess of I_2 with hmt, is of the stoichiometry [(hmt)$_2$I]I_3. [(hmt)$_2$I]ClO_4 has been prepared by the reaction of I_2 with hmt in DMF in the presence of $AgClO_4$ which effectively traps the I^- anions to give AgI which was quantitatively be removed by centrifugation. Similar reactions of other ligands with I_2, Br_2 and ICl have been reported {(py)ICl[365], [(py)$_2$Br]NO_2, [(py)$_2$I]NO_2 [476,477], [(py)$_2$I]X (X = F^-, SF_6^- and SO_3F^-)[478,479], [(py)$_2$I]ClO_4[480], (4-picoline)I_2, [(4-picoline)$_2$I]I_3[481], $[(MeCN)I]^+$ and $[MeCN)_2I]^+$[482,483]} (**Figure 7.1.4a**). The halide substitution in charge transfer-adducts is discussed in ref. 484 and 485.

$$L_N + I_2 \longrightarrow (L_N)I_2 \text{ or } [(L_N)I]^+ + I^- \text{ (fast)}$$

$$2\,(L_N)I_2 \longrightarrow [(L_N)_2I]^+ + (I_3)^- \text{ (slow)}$$

$$2\,L_N + I_2 \longrightarrow (L_N)I_2 \text{ or } [(L_N)I]^+ + I^-$$

$$AgX + [(L_N)I]^+ + I^- \longrightarrow AgI + [(L_N)I]^+ + X^-$$

Figure 7.1.4a Reactions reported for N-donor ligands (L_N) with I_2.

Compound	D	D-I$^+$ / Å	(D-I-D) / °	Reference
$[(hmt)_2I]^+$	N	2.30 (1)	176.5 (4)	443
$[(py)_2I]^+$	N	2.16 (10)	180	486
$[(thiourea)_2I]^+$	S			409
$[(S_7I)_2I]^{3+}$	S	2.675(7)	180	406
[(N-methylbenzothiazole-2(3*H*)-thione)$_2$I]$^+$	S	2.600 (2) 2.634 (2)	174.97 (7)	408
[(N-methylbenzothiazole-2(3*H*)-selone)$_2$I]$^+$	Se	2.800 (1) 2.719 (1)	178.02 (2)	408

Table 7.1.4a Structural properties of reported compounds containing iodonium cations.

Table 7.1.4a gives an overview of structurally characterised iodonium complexes. The single crystal structures of $[I(py)_2]^+$ and $[I(hmt)_2]^+$ (**Figure 7.1.4b**) show similar to $(I_3)^-$ or I_2-D charge-transfer adducts a linear D-I-D arrangement (D = donor). The bonding in iodonium complexes can again be treated as four electron three centre bonding similar to the situation in XeF_2 or $(I_3)^-$. The qualitative MO-diagram shows two sp^2- (py) or sp^3- (hmt or 4-picoline) hybridised lone pair orbitals (ϕ^2 and ϕ'^2) interacting with one $5p^0$ orbital at the I^+ cation. The linear combination of these three orbital gives three MOs (ψ_b, ψ_n and ψ_a) in which the four valence electrons ($5p^0 + \phi^2 + \phi'^2$) are filled in (**Figure 7.1.4c**).

(i) $[(py)_2I]^+$ 486

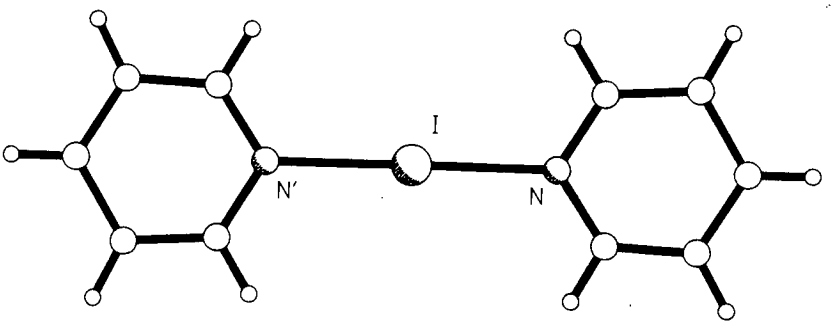

(ii) $[(hmt)_2I]^+$ 443

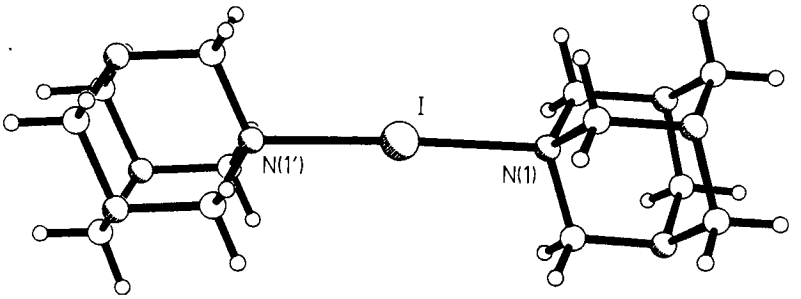

(iii) [(N-methylbenzothiazole-2(3*H*)-thione)$_2$I]$^+$ 408

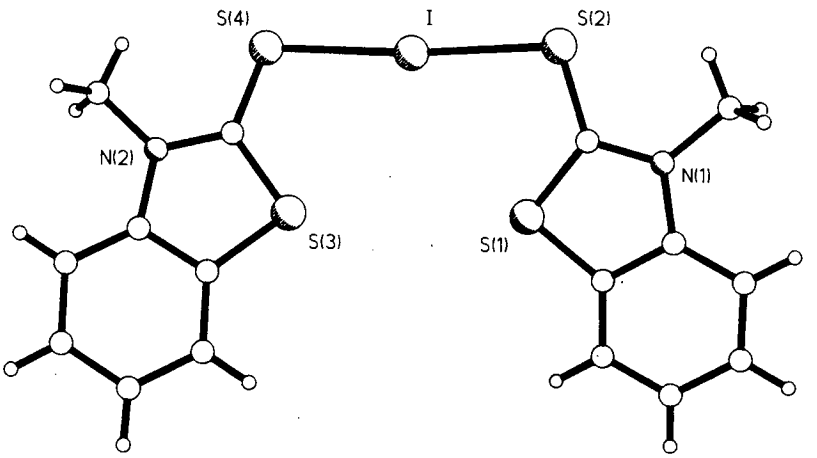

Figure 7.1.4b The single crystal structures of (i) $[I(py)_2]^+$ 486,
(ii) $[I(hmt)_2]^+$ 443 and
(iii) [(N-methylbenzothiazole-2(3*H*)-thione)$_2$I]$^+$ 408.

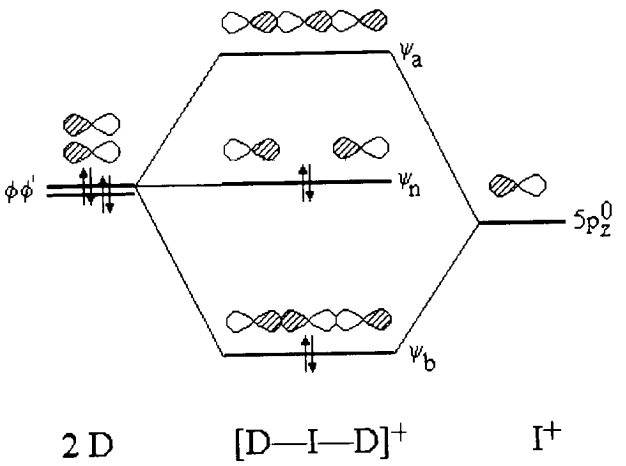

Figure 7.1.4c Qualitative MO-diagram for *bis*(donor)-iodonium complexes.

7.1.5 Aims of Work

This introduction has focused on three different areas of low valent I_2 compounds. We were particularly interested in some aspects of each area outlined below.

(i) Charge-transfer complexes

Previous investigations (see above) have focused in particular on I_2 charge-transfer complexes with small sized mono- or bidentate ligands and I_2. We were interested to investigate the structural properties of I_2 charge-transfer adducts with macrocyclic complexes. Macrocyclic ligands contain in contrast to small mono- or bidentate ligands a large number of donor atoms. They are also more flexible and are able to adopt different co-ordination modes such as *exo* or *endo* depending on the nature of the guest molecule and the reaction conditions (see the preceding chapters). It was our aim to prepare and characterise a range of homoleptic thioether I_2 charge-transfer adducts and to identify features peculiar to a isolated species and trends in a series of complexes.

(ii) Polyiodides

The anion cation relationship in polyiodide compounds has been discussed in case of $(I_3)^-$. Small cations in the crystal lattice give in general asymmetrical $(I_3)^-$ anions whereas in contrast larger cations force the $(I_3)^-$ cation into a symmetrical shape. Metal macrocyclic complexes seem to be ideal reaction partners in the preparation of polyiodide species. As it has already been pointed out, macrocyclic metal cations are chemically relatively inert species, their size varies depending on the actual complex and multiple charged species such as $[Pd([16]aneS_4)]^{2+}$ have been characterised. Our major aim was to establish whether metal macrocyclic polyiodide complexes can be prepared. Long term studies might then focus on the preparation of tailormade polyiodides by identifying a suitable metal macrocyclic complex with respect to shape, charge and size.

(iii) Iodonium complexes

The analogy between two pyridine ligands oriented as found in $[(py)_2I]^+$ and the macrocyclic ligand $[18]aneN_2S_4$ is obvious (**Figure 7.1.5**). We were interested whether the co-ordination of I^+ within the cavity of $[18]aneN_2S_4$ or its dimethylated derivative $Me_2[18]aneN_2S_4$ can be achieved and whether the thioether S-donors are *exo* or *endo* oriented.

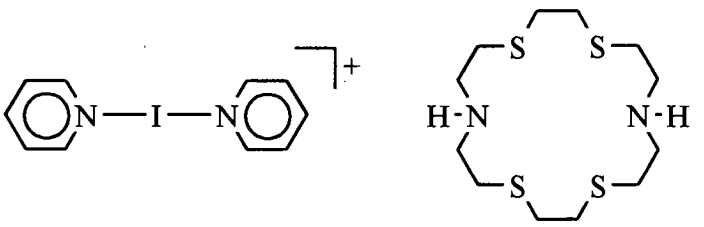

Figure 7.1.5 Comparison between $[(py)_2I]^+$ and $[18]aneN_2S_4$

The co-ordination chemistry of homoleptic thioether macrocycles with metal ions has been studied extensively over the last decade. It was our aim to establish whether homoleptic thioether macrocyclic ligands are able to stabilise non-metal ions such as I^+ and to characterise the complexes as complete as possible.

7.2 RESULTS AND DISCUSSION

7.2.1 The Synthesis of '[Ag([18]aneS$_6$)]I$_5$'

The addition of I_2 dissolved in MeCN to a solution containing [18]aneS$_6$ and $AgBF_4$ in MeCN under N_2 gave a red-brown solution. Immediate evaporation of the solution under reduced pressure yielded a dark blue microcrystalline solid. The initial hypothesis that this compound was a Ag(II) species was discarded on the grounds that the reported $[Ag([18]aneS6)]^{2+}$ complex is highly unstable (see above) and that this compound was ESR silent. The cyclic voltammogram in MeCN reproduced, however, the waves found for $[Ag([18]aneS_6)]^+$ and the FAB mass spectrum showed a peak at m/z = 467/469 with the correct isotopic distribution assigned to $[^{107/109}Ag([18]aneS_6)]^+$.

It seems therefore far more likely that the blue colour is due to a polyiodide species. The only reported blue polyiodide is the linear I_5^- species found in the I_2 amylose (the linear, helical component of starch) complex[469]. We propose therefore that '[Ag([18]aneS$_6$)]I$_5$' contains a similar polyiodide. Recrystallisation of '[Ag([18]aneS$_6$)]I$_5$' to remove any impurities and to obtain crystals suitable for X-ray diffraction studies afforded the two polyiodide complexes [Ag([18]aneS$_6$)]I$_3$ and [Ag([18]aneS$_6$)]I$_7$ (see below).

The reaction pathway to '[Ag([18]aneS$_6$)]I$_5$', [Ag([18]aneS$_6$)]I$_3$ and [Ag([18]aneS$_6$)]I$_7$ is still under investigation. It seems, however, likely that the formation of the anion and cation are independent. The cation is formed simply by the co-ordination of Ag(I) into the cavity of [18]aneS$_6$ leading to the formation of $[Ag([18]aneS_6)]^+$. No precipitation of AgI was observed after the addition of I_2 underlining the inertness of the $[Ag([18]aneS_6)]^+$ complex. The source of I^-, necessary for the formation of any polyiodide species has to be I_2. Disproportionation of I_2 into I^- and I^+ has been found for instance in the gas phase preparation of the I_2 amylose complex mentioned above. The I^+ species has been identified as a hypoiodite employing Mössbauer spectroscopy[469]. The key role of MeCN in the preparation of the initial blue material has been identified since other solvents do not lead to the blue product. Klapötke and co-workers have shown that MeCN stabilises I^+ via 1:1 adduct formation[482,483].

7.2.2 The Synthesis of [Ag([18]aneS$_6$)]I$_3$

Recrystallisation of the proposed [Ag([18]aneS$_6$)]I$_5$ complex in EtOH afforded brown crystals of the stoichiometry [Ag([18]aneS$_6$)]I$_3$. The X-ray fluorescence spectrum (**Figure 7.2.2**) shows peaks assigned to I(K_α), I(K_β), Ag(K_α) and Ag(K_β) confirming the presence of both Ag and I$_2$ in the sample. Microanalytical results are in satisfactorily agreement with the proposed stoichiometry. The FAB mass spectrum shows a peak at m/z = 468 assigned to [$^{107/109}$Ag([18]aneS$_6$)]$^+$ (calc. m/z = 467/469).

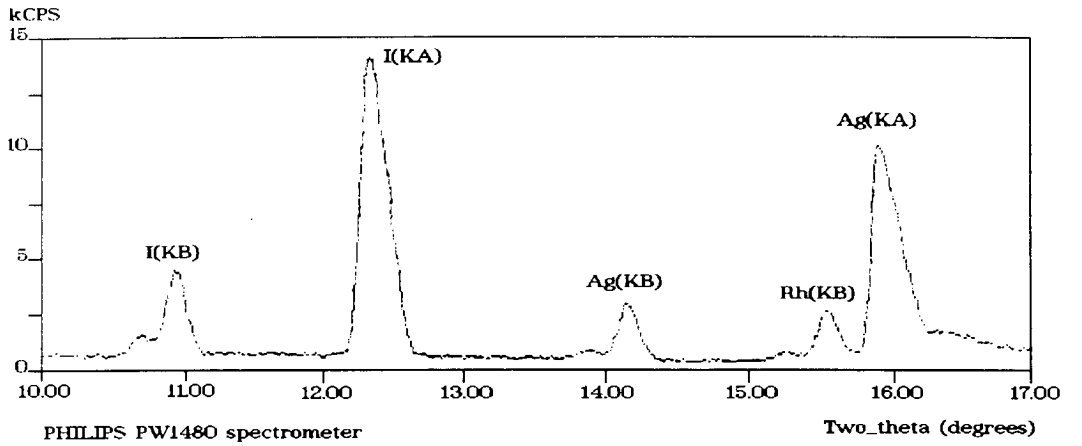

Figure 7.2.2 X-ray fluorescence spectrum of [Ag([18]aneS$_6$)]I$_3$ (Rh X-radiation).

7.2.3 The Single Crystal Structure of [Ag([18]aneS$_6$)]I$_3$

The single crystal structure of [Ag([18]aneS$_6$)]I$_3$ shows independent (I$_3$)$^-$ anions and [Ag([18]aneS$_6$)]$^+$ cations in the crystal lattice (**Figures 7.2.3a** and **7.2.3b**). The (I$_3$)$^-$ ions are symmetrical with an I-I distance of 2.9137(3)Å, fitting well into the series of (I$_3$)$^-$ anions shown in the introduction [**Table 7.1.3a** (i)]. The [Ag([18]aneS$_6$)]$^+$ cation exhibits a distorted octahedral co-ordination geometry. The two apical Ag-S distances [Ag-S(1) 2.8007(10)Å] are significantly longer compared with the other four equatorial Ag-S distances [Ag-S(4) 2.7255(7)Å].

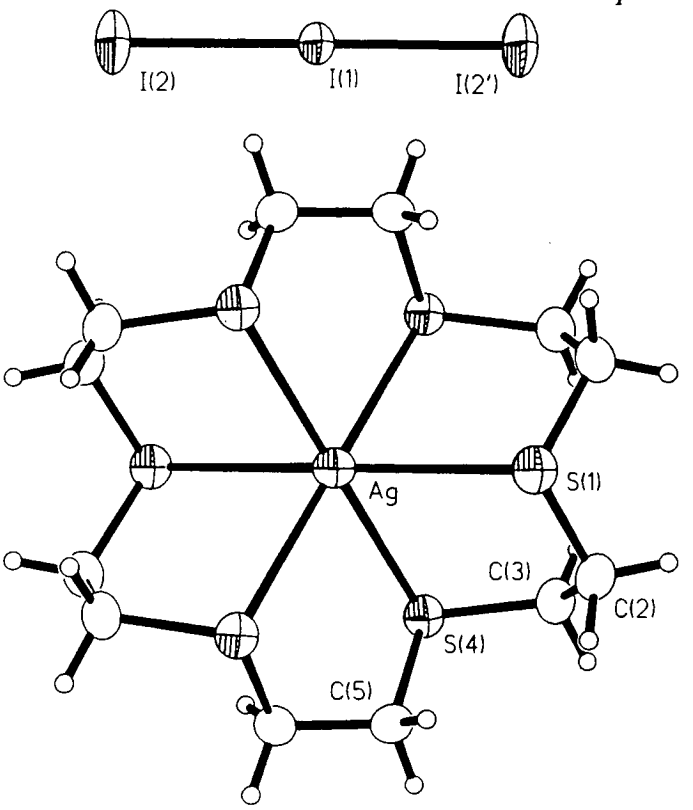

Figure 7.2.3a The single crystal structure of $[Ag([18]aneS_6)]I_3$.

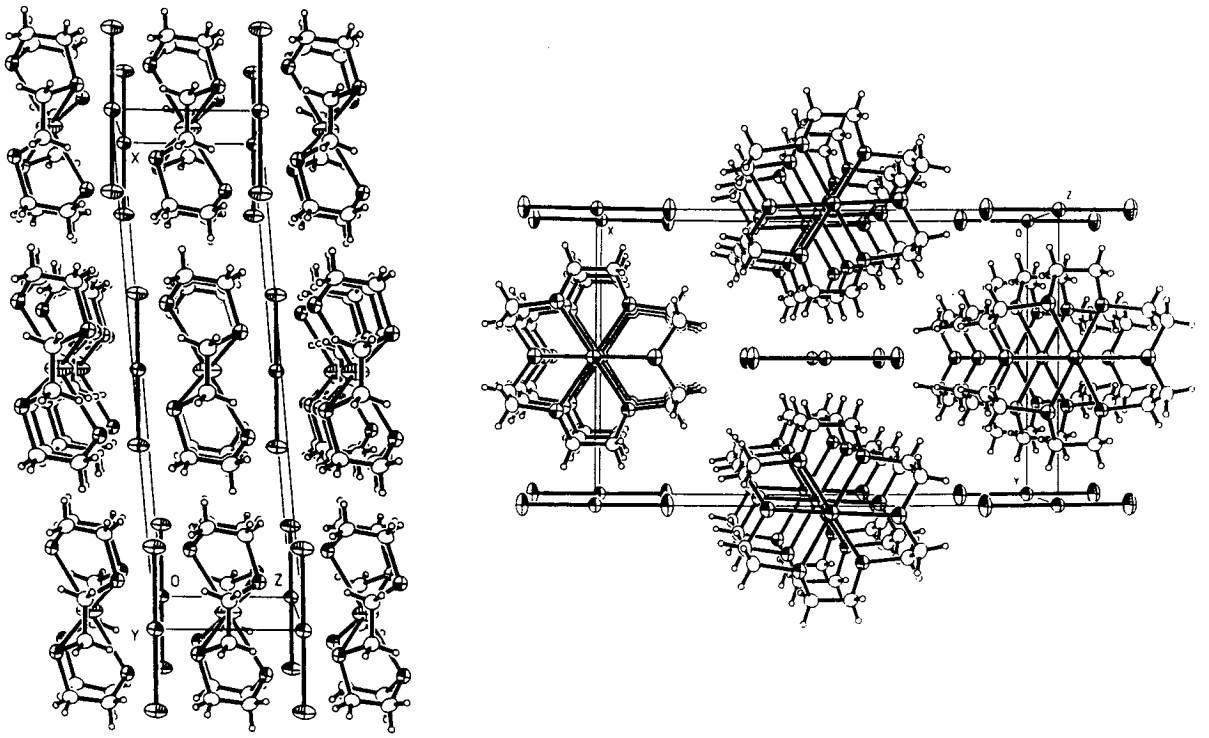

Figure 7.2.3b Packing diagrams in the x-y and x-z plane for $[Ag([18]aneS_6)]I_3$.

The structure (**Figure 7.2.3a**) and packing diagram of $[Ag([18]aneS_6)]I_3$ (**Figure 7.2.3b**) show the $(I_3)^-$ anions aligned parallel to the long S(1)-Ag-S(1') axis in the $[Ag([18]aneS_6)]^+$ cations. This effect of mutual influence between the ions in the crystal lattice is discussed later (**7.2.5**). It should, however, be noted that the co-ordination geometry in $[Ag([18]aneS_6)]^+$ could be described either as *apical* elongated or *equatorial* compressed. The thermal ellipsoids of the two terminal I-atoms [I(2) and I(2')] in the $(I_3)^-$ anion indicate some freedom of motion whereas in contrast the one for the I-atom in the middle [I(1)] does not. This suggests that the anion and the cation are in firm contact and the distortion (*equatorial* compression) of the cation is a direct result of this interaction.

S(1)-Ag	2.8007(10)	S(4)-Ag	2.7255(7)
S(4)-Ag-S(1)	78.40(2)	S(4)-Ag-S(4')	99.68(3)
S(4')-Ag-S(4)	80.32(3)	S(4')-Ag-S(1)	101.60(2)
C(2'')-S(1)-C(2)-C(3)	-80.31(26)	C(3)-S(4)-C(5)-C(5')	162.02(21)
S(1)-C(2)-C(3)-S(4)	-50.6(3)	S(4)-C(5)-C(5')-S(4')	-82.22(19)
C(2)-C(3)-S(4)-C(5)	-59.91(25)		

(Symmetry related atoms are related to their equivalents by the following symmetry operations ' = -x, y, -z+1; '' = x, -y+1, z)

Table 7.2.3 Selected bond lengths (Å), angles (°) and torsion angles (°) with estimated standard deviations for $[Ag([18]aneS_6)]I_3$.

7.2.4 The Synthesis of $[Ag([18]aneS_6)]I_7$

Green lustrous crystals of $[Ag([18]aneS_6)]I_7$ were obtained by the attempted recrystallisation of the proposed $[Ag([18]ane_6)]I_5$ complex in MeCN. Microanalytical results are in satisfactorily agreement with the proposed stoichiometry. The FAB mass spectrum shows a peak at m/z = 469 assigned to $[^{107/109}Ag([18]aneS_6)]^+$ (calc. m/z = 467/469). The compound is, in contrast to $[Ag([18]aneS_6)]I_3$, unstable and liberates I_2 at ambient temperature. However, storage of $[Ag([18]aneS_6)]I_7$ at low temperature (-20 - -28°C) did not give any indication for significant decay.

7.2.5 The Single Crystal Structure of [Ag([18]aneS$_6$)]I$_7$

[Ag([18]aneS$_6$)]I$_7$ crystallises in the space group *R*-3m having less than 5 non H-atoms in the asymmetric unit. The structure shows the isolated cations embedded into a three dimensional polymeric anionic network of composition $(I_7^-)_n$ (**Figure 7.2.5a**). Each I^- anion is surrounded in a distorted octahedral fashion by six I_2 molecules. The overall structure of this polyiodide network in the crystal lattice can best be described as cubic distorted. The eight corners of each cube are occupied by I- anions whereas the edges are occupied by I_2 molecules. Each edge (from corner to corner) in this three dimensional network consists therefore of an $I^-\cdots I—I\cdots I^-$ arrangement. The I_2 distance [2.7519(4)Å] is slightly longer compared with the one in I_2 vapour or solid I_2. The $I^-\cdots I_2$ distance [3.3564(15)Å] is consequently rather long. These findings confirm the presence of a polyiodide species in contrast to isolated I_2 molecules and I^- anions in the crystal lattice. The centre of each cube is occupied by a $[Ag([18]aneS_6)]^+$ cation. The cation is centrosymmetric with all Ag-S distances [2.754(2)Å] of equal length. This is in sharp contrast to the situation in [Ag([18]aneS$_6$)]I$_3$ (see above). The Ag-S distances for [Ag([18]aneS$_6$)]I$_3$, [Ag([18]aneS$_6$)]I$_7$ and the reported structure of [Ag([18]aneS$_6$)]PF$_6$[346] are summarised in **Table 7.2.5a**.

Compound	**$(Ag\text{-}S)_{ap}$**	**$(Ag\text{-}S)_{eq}$**
[Ag([18]aneS$_6$)]PF$_6$	2.697(5)	2.753(4)
[Ag([18]aneS$_6$)]I$_7$	2.754(2)	2.754(2)
[Ag([18]aneS$_6$)]I$_3$	2.8007(10)	2.7255(7)

Table 7.2.5a Ag-S bond lengths in [Ag([18]aneS$_6$)]PF$_6$, [Ag([18]aneS$_6$)]I$_7$ and [Ag([18]aneS$_6$)]I$_3$.

It is interesting to note that on going from [Ag([18]aneS$_6$)]PF$_6$ to [Ag([18]aneS$_6$)]I$_7$ and to [Ag([18]aneS$_6$)]I$_3$ changes the co-ordination geometry of the cation from compressed to centrosymmetric and to elongated. The step from [Ag([18]aneS$_6$)]PF$_6$ to [Ag([18]aneS$_6$)]I$_7$ affects only the apical Ag-S distances whereas the equatorial distances remain unchanged within the estimated standard deviations. The step from [Ag([18]aneS$_6$)]I$_7$ to [Ag([18]aneS$_6$)]I$_3$ on the other hand elongates the cation along the *apical* axis and decreases the *equatorial* Ag-S distances. These three examples illustrate the flexibility of the $[Ag([18]aneS_6)]^+$ cation to adapt to different environments in the crystal lattice.

The effect of a strong anisotropic environment on the geometry of the cation has been discussed already (see above).

Further work in this area has to investigate whether this influence is one-directional from the polyiodide environment or whether there is a mutual influence between metal macrocyclic complexes and polyiodide species. It would be of particular importance to establish whether transition metal macrocyclic complexes with a rigid stereochemistry (uncompleted d-shell) are able to template polyiodide species.

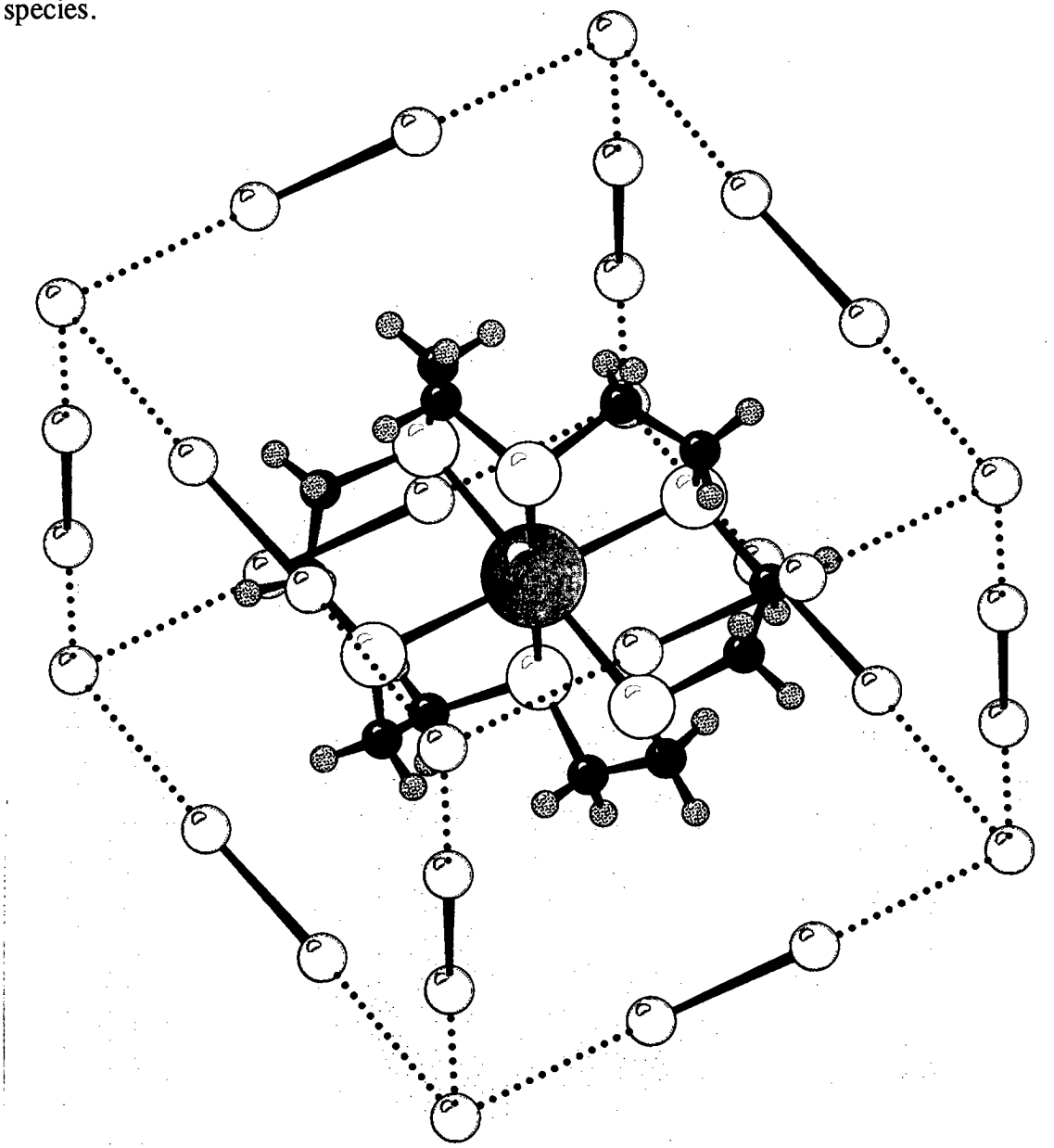

Figure 7.2.5a The unit cell contents of $[Ag([18]aneS_6)]I_7$.

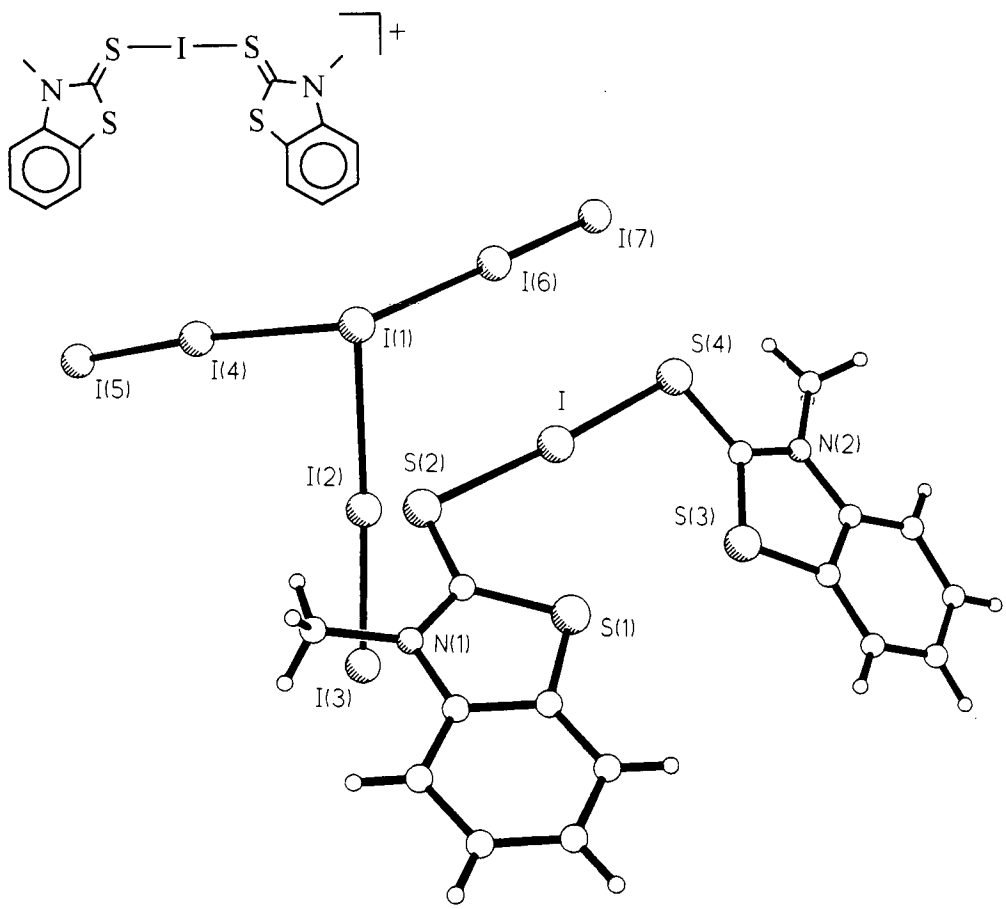

Figure 7.2.5b The structure of the *bis*(N-methylbenzothiazolyl-2-thio)-iodonium cation and the single crystal structure of its $(I_7)^-$ salt[408].

The only other reported example of a structurally related anion of the composition $(I_7)^-$ has been published recently by Devillanova and co-workers[408] (**Figure 7.2.5b**). The major difference to the infinite network of $[(I_7)^-]_n$ in $[Ag([18]aneS_6)]I_7$. is that the structure of $[I(C_8H_7NS_2)_2]I_7$ features individual $(I_7)^-$ anions $[I^-\cdots(I—I)_3]$ in the crystal lattice. The main axes of the three I_2 molecules are oriented similar to the structure of $[Ag([18]aneS_6)]I_7$ orthogonal to each other. A deviation from the ideal orthogonal angle of 90° is probably caused by steric repulsion of the bulky I_2 molecules. The $I^-\cdots I$ distances [3.237(1), 3.260(1), 3.242(1)Å] are slightly shorter compared with $[Ag([18]aneS_6)]I_7$ and the I_2 distances [2.771(1), 2.746(1), 2.766(1) Å] are consequently increased. It is interesting to note that the reported compound $[I(C_8H_7NS_2)_2]I_7$ is also a lustrous green colour.

Ag-S ..... 2.754(2)	
S-Ag-S'' ..... 78.76(4)	S-Ag-S' ..... 101.24(4)
C(2)-S-Ag ..... 103.1(3)	C(18)-S-Ag ..... 101.1(4)
C(2'')-C(2)-S ..... 115.1(5)	C(18')-C(18)-S ..... 112.1(9)
C(2)-S-C(18) ..... 99.1(6)	
S'-C(18')-C(18)-S ..... 71.3(20)	S''-C(2'')-C(2)-S ..... 61.0(16)
C(18')-C(18)-S-C(2) ..... -154.3(14)	C(18)-S-C(2)-C(2'') ..... 61.7(9)

(Symmetry codes (') x-1, z-1, y-1; ('') y-1, x-1, z-1)

Table 7.2.5b Selected bond lengths (Å), angles (°) and and torsion angles (°) with estimated standard deviations for $(Ag(18]aneS_6)I_7$.

7.2.6 The Synthesis of $([9]aneS_3)_2(I_2)_4$

The reaction of one molar equivalent [9]aneS_3 and one molar equivalent ICl in CH_2Cl_2 afforded an orange solution from which a yellow solid precipitated upon addition of a second molar equivalent of ICl. Similar reactions were undertaken with a range of thioether macrocycles and a detailed account on the proposed reaction pathway and analytical data is given below (**7.2.22**) The initial yellow solid obtained from the reaction of [9]aneS_3 with ICl darkened slowly over a period of some months and dark red crystals started to grow on the surface of the yellow material. Microanalytical results, EI mass spectrometry (**Figure 7.2.18**) and single crystal X-ray diffraction studies finally confirmed the composition of the red crystalline material as $([9]aneS_3)_2(I_2)_4$.

7.2.7 The Synthesis of Iodine Charge-Transfer Complexes with Homoleptic S-Donor Macrocycles

Solid charge transfer complexes between I_2 and homoleptic S-donor macrocycles were prepared by slow evaporation of a solution of CH_2Cl_2 containing I_2 and the appropriate ligand. Even though the mixture contained a certain stoichiometry between I_2 and the ligand, the composition of the products was not necessarily the one expected. The compounds deposited on the glass surface in different regions which could be distinguished by the form of deposition (crystalline, microcrystalline or films), the colour intensity and the size and shape of crystals. A typical reaction produced up to four different, well distinguished regions which were collected separately. The characterisation of the products is described in section **7.2.18**.

7.2.8 The Single Crystal Structure of $([9]aneS_3)_2(I_2)_4$

Crystals suitable for single crystal X-ray diffraction studies were obtained from the unexpected solid state transformation of the initial reaction product between $[9]aneS_3$ and ICl. The single crystal structure of $([9]aneS_3)_2(I_2)_4$ (**Figure 7.2.8a**) shows an asymmetric unit containing two macrocyclic ligands and four I_2 molecules. The first macrocycle [S(11) to C(19)] shows co-ordination of one I_2-molecule to each S-atom. One of the I_2 molecules [I(11)-I(21)] bridges between the first and the second macrocycle [S(21)-C(29)] which interacts with the fourth I_2-molecule. Both macrocycles adopt a [333] conformation. Selected bond lengths, angles and torsion angles are tabulated at the end of this section (**Table 7.2.8**).

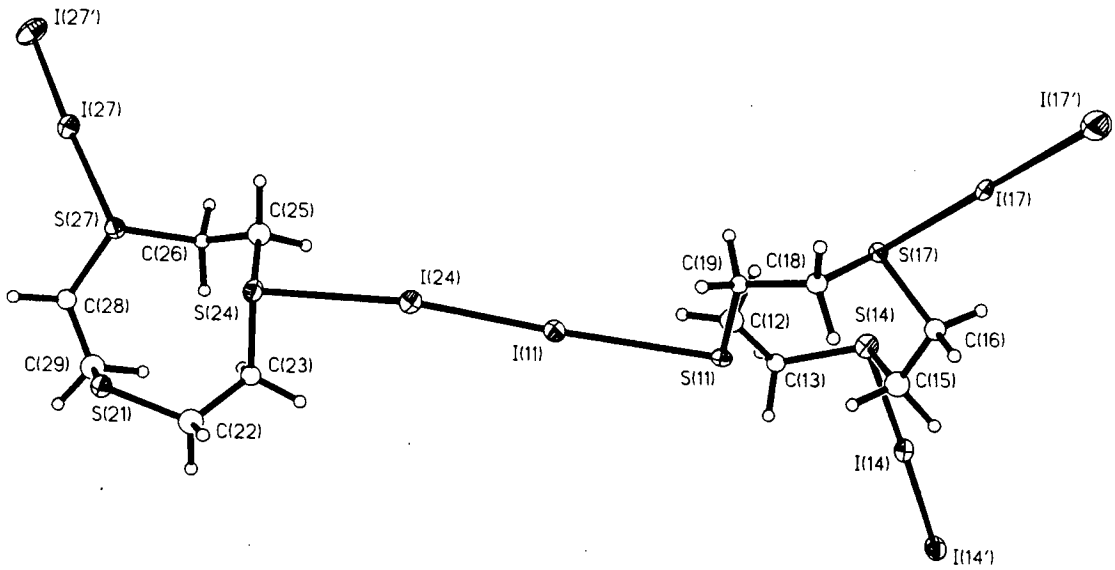

Figure 7.2.8a The single crystal structure of $([9]aneS_3)_2(I_2)_4$.

There are two fundamentally different ways an I_2 molecule can interact with donor atoms. The first one, termed 'terminal' interacts primarily with one S-donor giving an overall S-I-I arrangement. The second type bridges between two S-atoms in different macrocycles. This bridging interaction can be either symmetrical or asymmetrical. S-I distances in S-I-I-S bridges are usually longer compared with terminal arrangements. Asymmetric bridges exhibit differences between the two S-I distances and the angles which are nevertheless close to 180°. These arrangements could therefore also be termed 'terminal with a secondary interaction'.

The bridging found in $([9]aneS_3)_2(I_2)_4$ is asymmetric and is reflected in the two different S-I-I angles [168.39(13) and 176.18(12)°] and S-I distances [2.917(6) and 3.054(6)Å]. The I_2 distance [2.7542(21)Å] is significantly longer compared with the closest distance found in solid I_2.

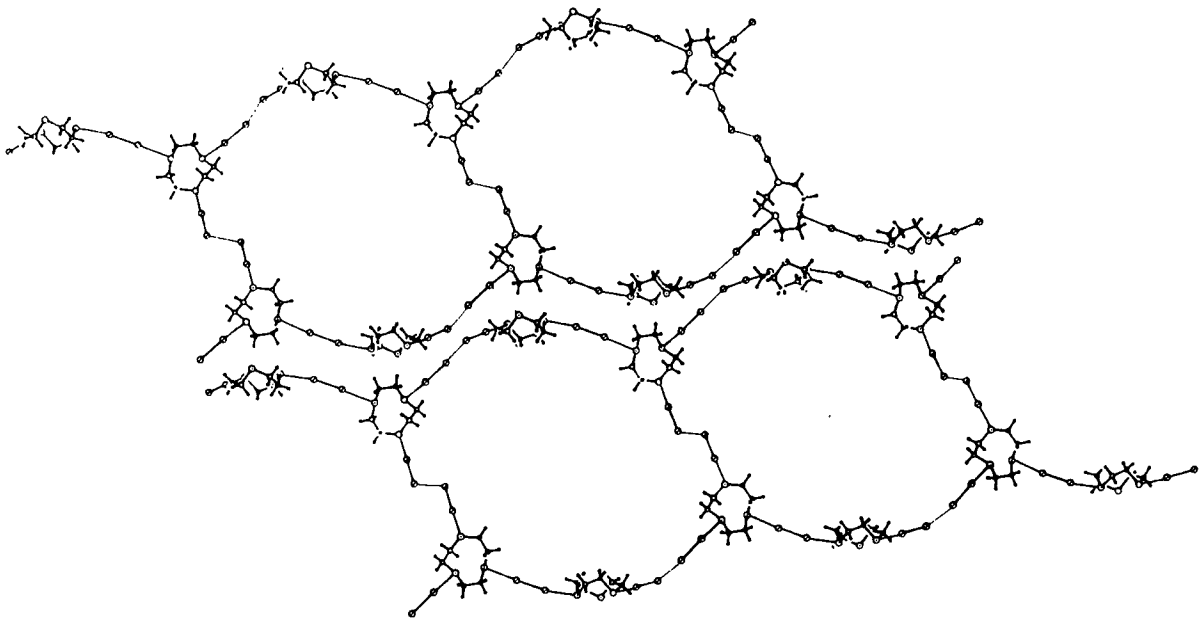

Figure 7.2.8b Packing diagram of $([9]aneS_3)_2(I_2)_4$.

The packing diagram of $([9]aneS_3)_2(I_2)_4$ (**Figure 8.2.6b**) features extended I·····I contacts. These contacts are simply a consequence of the bulky I_2 molecules. Nevertheless the packing adopted by $([9]aneS_3)_2(I_2)_4$ resembles a complicated three dimensional network of stacked bands containing large cyclic arrangements.

I(11)-I(21)	2.7542(21)	I(11)-S(11)	2.917(6)
		I(21)-S(21)	3.054(6)
I(14)-I(14')	2.7846(22)	I(14)-S(14)	2.870(6)
I(17)-I(17')	2.8156(23)	I(17)-S(17)	2.760(6)
I(27')-I(27)	2.7986(23)	I(27)-S(27)	2.862(6)
I(21)-I(11)-S(11)	176.18(12)	I(11)-I(21)-S(21)	168.39(13)
I(14')-I(14)-S(14)	178.35(14)	I(17')-I(17)-S(17)	174.86(14)
I(27')-I(27)-S(27)	177.27(14)		
Macrocycle 1:		Macrocycle 2:	
S(11)-C(12)-C(13)-S(14)	-86.7(18)	S(21)-C(22)-C(23)-S(24)	55.0(22)
C(12)-C(13)-S(14)-C(15)	71.6(18)	C(22)-C(23)-S(24)-C(25)	58.0(20)
C(13)-S(14)-C(15)-C(16)	-123.6(17)	C(23)-S(24)-C(25)-C(26)	-131.9(18)
S(14)-C(15)-C(16)-S(17)	59.5(20)	S(24)-C(25)-C(26)-S(27)	54.7(22)
C(15)-C(16)-S(17)-C(18)	75.3(18)	C(25)-C(26)-S(27)-C(28)	59.0(19)
C(16)-S(17)-C(18)-C(19)	-113.9(16)	C(26)-S(27)-C(28)-C(29)	-132.9(16)
S(17)-C(18)-C(19)-S(11)	77.4(18)	S(27)-C(28)-C(29)-S(21)	55.8(20)
C(18)-C(19)-S(11)-C(12)	-97.5(17)	C(28)-C(29)-S(21)-C(22)	57.8(19)
C(19)-S(11)-C(12)-C(13)	132.2(17)	C(29)-S(21)-C(22)-C(23)	-132.2(17)

Table 7.2.8 Selected bond lengths (Å), angles (°) and torsion angles (°) with estimated standard deviations for $([9]aneS_3)_2(I_2)_4$.

7.2.9 The Single Crystal Structure of $([12]aneS_4)I_2$

The asymmetric unit of $([12]aneS_4)I_2$ (**Figure 7.2.9a**) contains 1½ macrocycles and 3 I-atoms. The second half of the macrocycle and the counterpart of the single I-atom are symmetry related by inversion centres. The structure exhibits therefore two different macrocycles and two different bridging I_2-molecules. Both macrocycles adopt a [3333] conformation which is the same as found in the single crystal structure of the free macrocycle. The bridge within the asymmetric unit is asymmetrical with slightly different S-I distances whereas in contrast the I(7)-I(7') bridge is symmetrical due to the inversion centre. The effects of a stronger and a weaker S-I interaction on the I-I bond distance within the same structure is illustrated in **Figure 7.2.9a** even though the differences are only marginal.

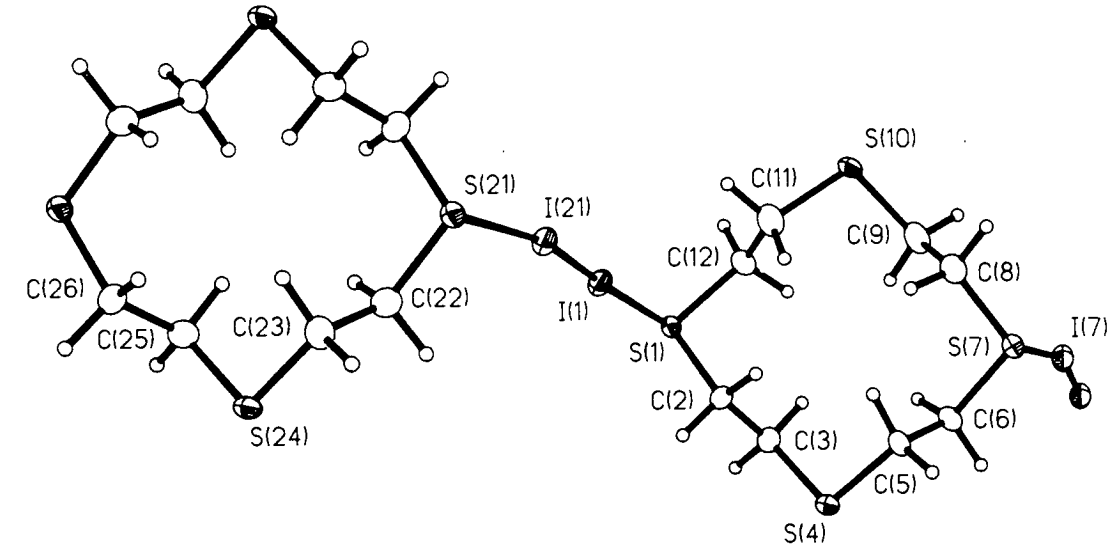

Figure 7.2.9a The single crystal structure of ([12]aneS$_4$)I$_2$.

The packing diagram of ([12]aneS$_4$)I$_2$ (**Figure 7.2.9b**) shows a characteristic stair motif with the macrocyclic ligand [12]aneS$_4$ and I$_2$ forming an alternating infinite chain structure. Interactions between those chains are most likely weak dipole-dipole attraction forces. Similar structures are found in other 1:1 I$_2$-thioether complexes (see below).

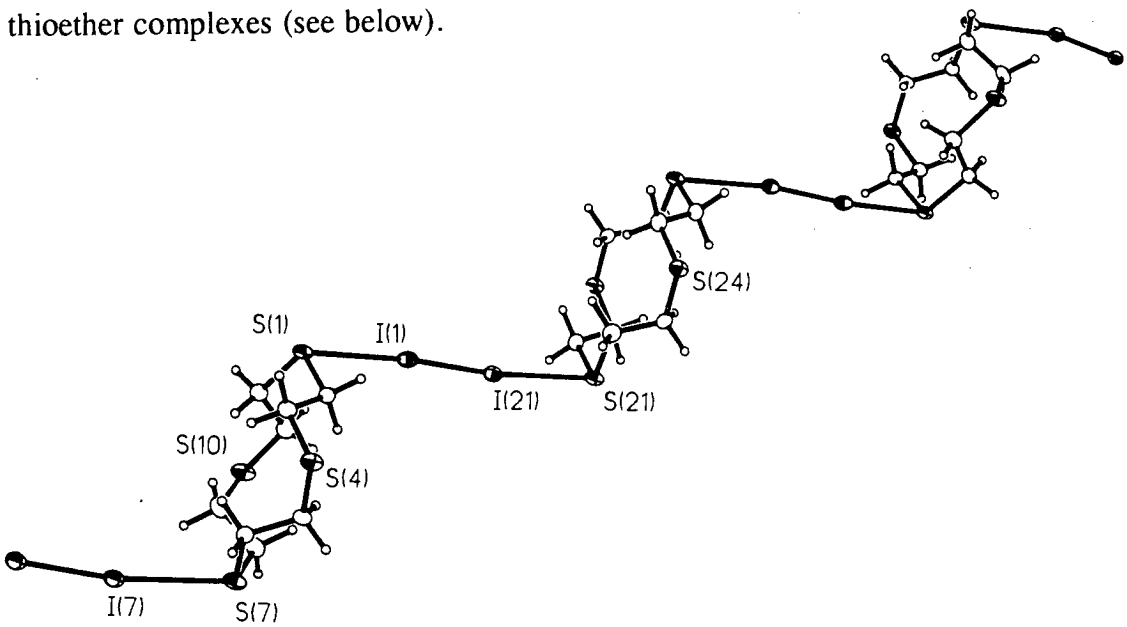

Figure 7.2.9b Packing diagram of ([12]aneS$_4$)I$_2$.

I(7)-I(7')	2.7500(10)	I(7)-S(7)	3.2030(20)
I(21)-I(1)	2.7549(8)	I(1)-S(1)	3.1740(20)
		I(21)-S(21)	3.1480(20)
S(1)-I(1)-I(21)	174.99(4)	S(21)-I(21)-I(1)	170.28(4)
S(7)-I(7)-I(7')	165.00(4)		

Macrocycle 1:		Macrocycle 2:	
C(12)-S(1)-C(2)-C(3)	-72.3(6)	S(21)-C(22)-C(23)-S(24)	172.0(4)
C(2)-S(1)-C(12)-C(11)	-73.7(6)	C(22)-C(23)-S(24)-C(25)	-79.3(6)
S(1)-C(2)-C(3)-S(4)	173.2(4)	C(23)-S(24)-C(25)-C(26)	-82.3(6)
C(2)-C(3)-S(4)-C(5)	-76.0(6)	S(24)-C(25)-C(26)-S(21')	167.0(4)
C(3)-S(4)-C(5)-C(6)	-76.3(6)	C(25-C(26)-C(21')-C(22')	-90.7(6)
S(4)-C(5)-C(6)-S(7)	171.6(4)	C(26)-C(21')-S(22')-C(23')	94.8(6)
C(5)-C(6)-S(7)-C(8)	-60.5(6)		
C(6)-S(7)-C(8)-C(9)	-71.3(7)		
S(7)-C(8)-C(9)-S(10)	173.9(5)		
C(8)-C(9)-S(10)-C(11)	-81.0(7)		
C(9)-S(10)-C(11)-C(12)	-64.4(7)		
S(10)-C(11)-C(12)-S(1)	172.0(4)		

Table 7.2.9 Selected bond lengths (Å), angles (°) and torsion angles (°) with estimated standard deviations for ([12]aneS$_4$)I$_2$.

7.2.10 The Single Crystal Structure of ([14]aneS$_4$)I$_2$

The asymmetric unit in the single crystal structure of ([14]aneS$_4$)I$_2$ (**Figure 7.2.10a**) shows similar features compared with ([12]aneS$_4$)I$_2$. The conformation of the macrocycle [3434] is identical to the one found in the solid state structure of [14]aneS$_4$[259]. One I$_2$ molecule bridges asymmetrically between two S-donor atoms in two different macrocycles [I-S 2.859(3), 3.640(3) and I-I 2.8905(11)Å] leading to an infinite one dimensional chain structure. The packing diagram (**Figure 7.2.10b**) shows that ([14]aneS$_4$)I$_2$ does not adopt the stair motif found in ([12]aneS$_4$)I$_2$ but an 'up down up down' motif with macrocycles aligned parallel to each other.

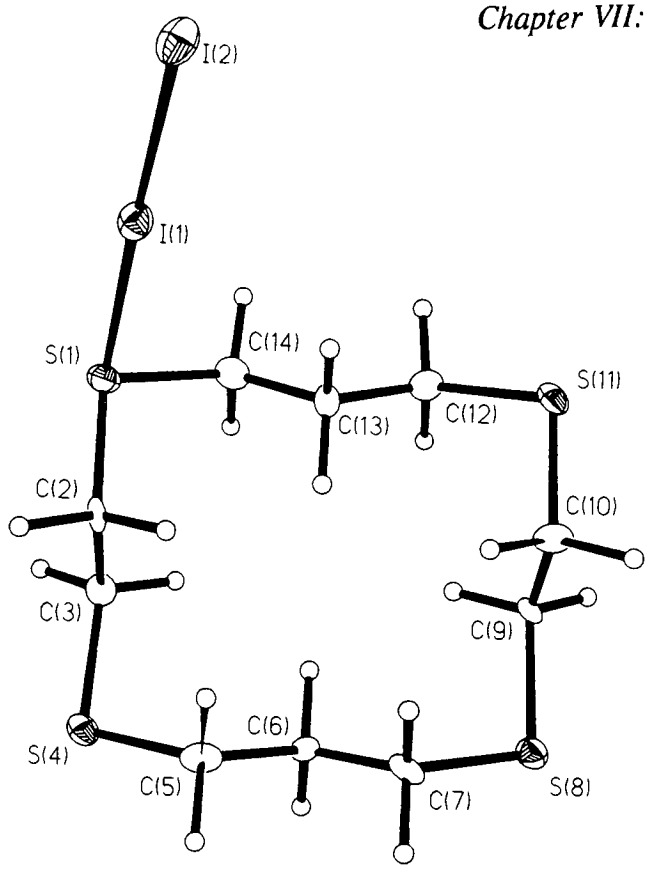

Figure 7.2.10a The single crystal structure of ([14]aneS$_4$)I$_2$.

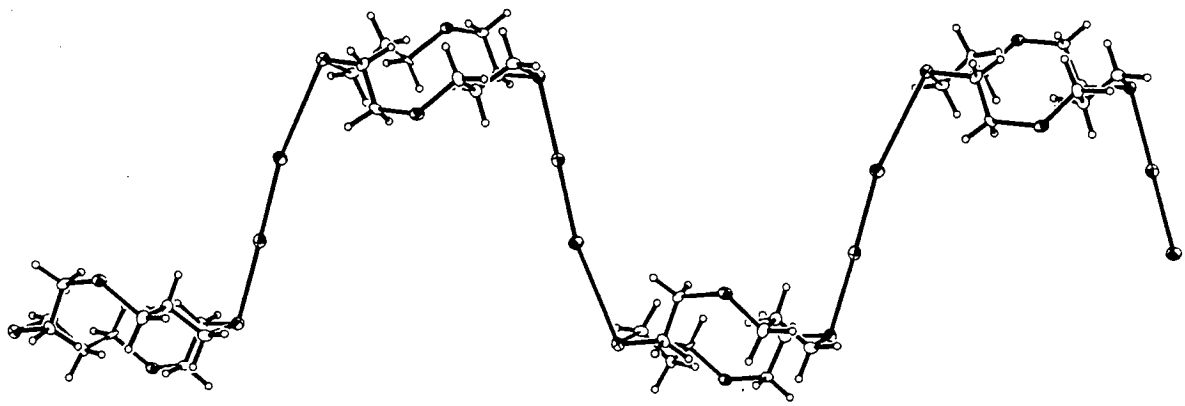

Figure 7.2.10b Packing diagram of ([14]aneS$_4$)I$_2$

I(1)-I(2)	2.8095(11)	I(1)-S(1)	2.859(3)
		I(2)-S(8')	3.640(3)
I(2)-I(1)-S(1)	178.57(7)	I(1)-I(2)-S(8')	168.38(5)
S(1)-C(2)-C(3)-S(4)	-175.2(5)	S(8)-C(9)-C(10)-S(11)	178.6(5)
C(2)-C(3)-S(4)-C(5)	-63.5(8)	C(9)-C(10)-S(11)-C(12)	54.5(9)
C(3)-S(4)-C(5)-C(6)	-67.4(8)	C(10)-S(11)-C(12)-C(13)	61.0(9)
S(4)-C(5)-C(6)-C(7)	177.8(7)	S(11)-C(12)-C(13)-C(14)	172.4(7)
C(5)-C(6)-C(7)-S(8)	-176.8(7)	C(12)-C(13)-C(14)-S(1)	-175.6(7)
C(6)-C(7)-S(8)- C(9)	67.5(8)	C(13)-C(14)-S(1)-C(2)	-55.0(9)
C(7)-S(8)-C(9)-C(10)	69.7(8)	C(14)-S(1)-C(2)-C(3)	-64.8(8)

(Primed atoms are related to the non-primed atom by the symmetry operations x-0.5, y, z+1)

Table 7.2.10 Selected bond lengths (Å), angles (°) and torsion angles (°) with estimated standard deviations for ([14]aneS_4)I_2.

7.2.11 The Single Crystal Structure of ([16]aneS_4)I_2

The single crystal structure of ([16]aneS_4)I_2 (**Figure 7.2.11a**) shows again features typical for 1:1 I_2:thioether adducts. The I_2 molecules bridge symmetrically between two macrocycles [I-I 2.773(12) and S-I 3.114(3)Å] giving an overall one-dimensional chain structure (**Figure 7.2.11b**). The conformation of the macrocycle in ([16]aneS_4)I_2 [3535][260] is however different from the one found in the solid state structure of [16]aneS_4 [224224].

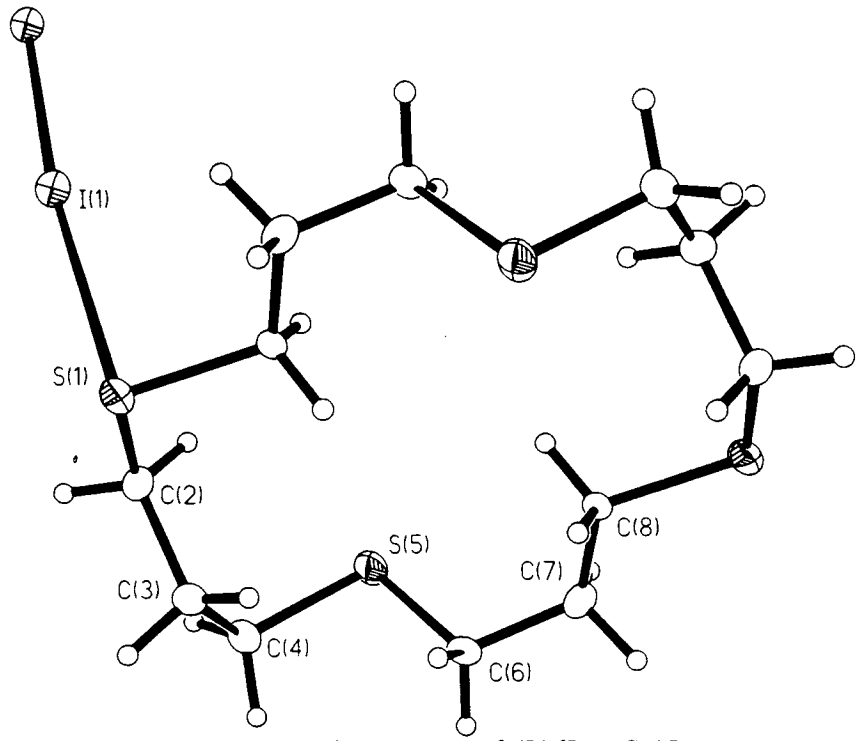

Figure 7.2.11a The single crystal structure of ([16]aneS_4)I_2.

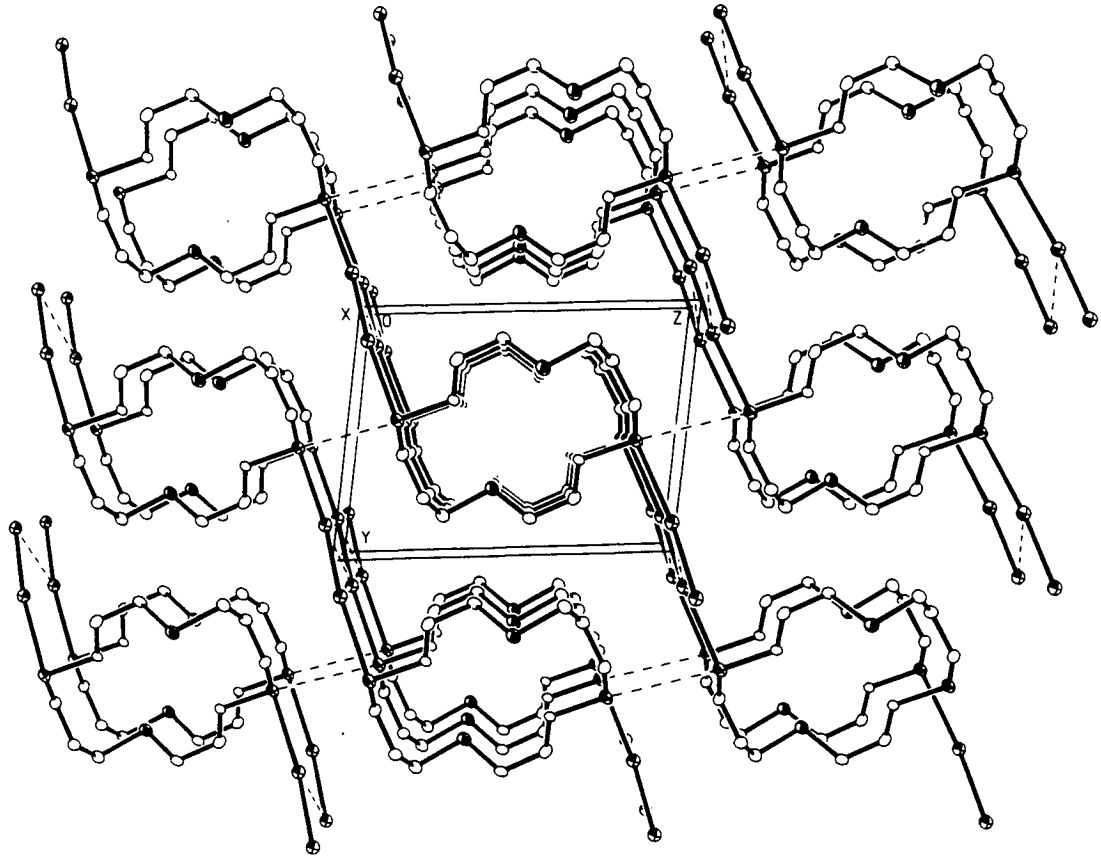

Figure 7.2.11 The packing diagram of ([16]aneS$_4$)I$_2$.

I(1)-I(1')	2.773(12)	S(1)-I(1)	3.114(3)
S(1)-C(2)	1.83(2)	S(5)-C(6)	1.810(15)
C(2)-C(3)	1.51(2)	C(6)-C(7)	1.52(2)
C(3)-C(4)	1.53(2)	C(7)-C(8)	1.52(2)
C(4)-S(5)	1.813(14)	C(8)-S(1'')	1.829(13)
I(1')-I(1)-S(1)	173.02(8)	I(1)-S(1)-C(2)	92.9(6)
		I(1)-S(1)-C(8'')	92.6(5)
C(1)-C(2)-S(3)	114.7(11)	S(5)-C(6)-C(7)	110.9(9)
C(2)-C(3)-C(4)	111.2(12)	C(6)-C(7)-C(8)	111.8(10)
C(3)-C(4)-S(5)	112.3(9)	C(7)-C(8)-S(1'')	110.7(9)
C(4)-S(5)-C(6)	98.7(7)	C(8)-S(1'')-C(2'')	99.4(6)
S(1)-C(2)-C(3)-C(4)	-156.4(9)	S(5)-C(6)-C(7)-C(8)	82.7(12)
C(2)-C(3)-C(4)-S(5)	74.7(13)	C(6)-C(7)-C(8)-S(1'')	173.6(9)
C(3)-C(4)-S(5)-C(6)	81.4(11)	C(7)-C(8)-S(1'')-C(2'')	-165.1(9)
C(4)-S(5)-C(6)-C(7)	-172.0(9)	C(8)-S(1'')-C(2'')-C(3'')	78.6(10)

(Primed and double primed atoms are symmetry related to the non-primed atom by the following symmetry operations '-x,-y,-z; ''+x+1,-y+1,-z+1)

Table 7.2.11 Selected bond lengths (Å), angles (°) and torsion angles (°) with estimated standard deviations for ([16]aneS$_4$)I$_2$.

7.2.12 The Single Crystal Structure of ([16]aneS$_4$)(I$_2$)$_4$

([16]aneS$_4$)(I$_2$)$_4$ is the first example of a macrocyclic thioether charge-transfer adduct where all four S-donor atoms are co-ordinated to I$_2$ molecules. The single crystal structure of ([16]aneS$_4$)(I$_2$)$_4$ (**Figure 7.2.12**) shows all four I$_2$ molecules in *exo* orientation [I-I 2.8108(9), 2.7916(8); I-S 2.7564(21) and 2.8478(23)Å]. One half of the molecule is symmetry related to the other half by a two-fold axis through C(7) and C(15). The conformation of [16]aneS$_4$ in ([16]aneS$_4$)(I$_2$)$_4$ [224224] is identical compared with the conformation in ([16]aneS$_4$)I$_2$ [224224] (see above) and different from the solid state structure of [16]aneS$_4$ [3535][260]. It should be noted that there is a potential danger in using Dale's scheme. The following sequence of torsion angles shows an isolated *gauche* angle:

C(15)-C(16)-S(1)-C(2)..... -166.1(5)°
C(16)-S(1)-C(2)-C(3) .....73.3(6)
S(1)-C(2)-C(3)-C(4)..... 166.4(6)°

A corner should, according to rule (ii) (see **2.2.5**), exist at the adjacent bond with the smaller absolute torsion angle. This gives the [224224] conformation mentioned above. Even though both adjacent torsion angles are different from each other, the difference is only marginal and within the e.s.d.s.. The absolute values of these two torsion angles could therefore be considered identical and following rule (iii) (see **2.2.5**) would give to a different conformation. This example illustrates the potential dangers in using Dale's scheme. The alternative '+-a' scheme however confirms that the conformation of [16]aneS$_4$ is indeed identical {+a++a+aa+a++a+aa} in ([16]aneS$_4$)I$_2$ and ([16]aneS$_4$)(I$_2$)$_4$. The packing diagrams for ([16]aneS$_4$)(I$_2$)$_4$ (**Figure 7.2.12b**) show the macrocycles embedded in a matrix of I$_2$. The macrocyclic ligands adopt a for I$_2$ rich compounds typical columnar stacking motif with extensive I$_2$-I$_2$ contacts.

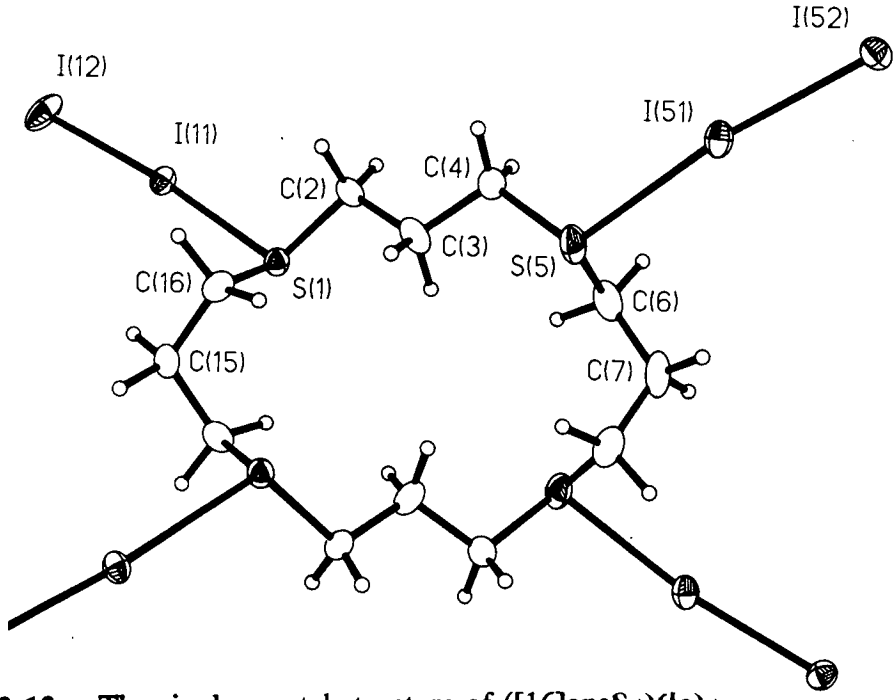

Figure 7.2.12a The single crystal structure of ([16]aneS$_4$)(I$_2$)$_4$.

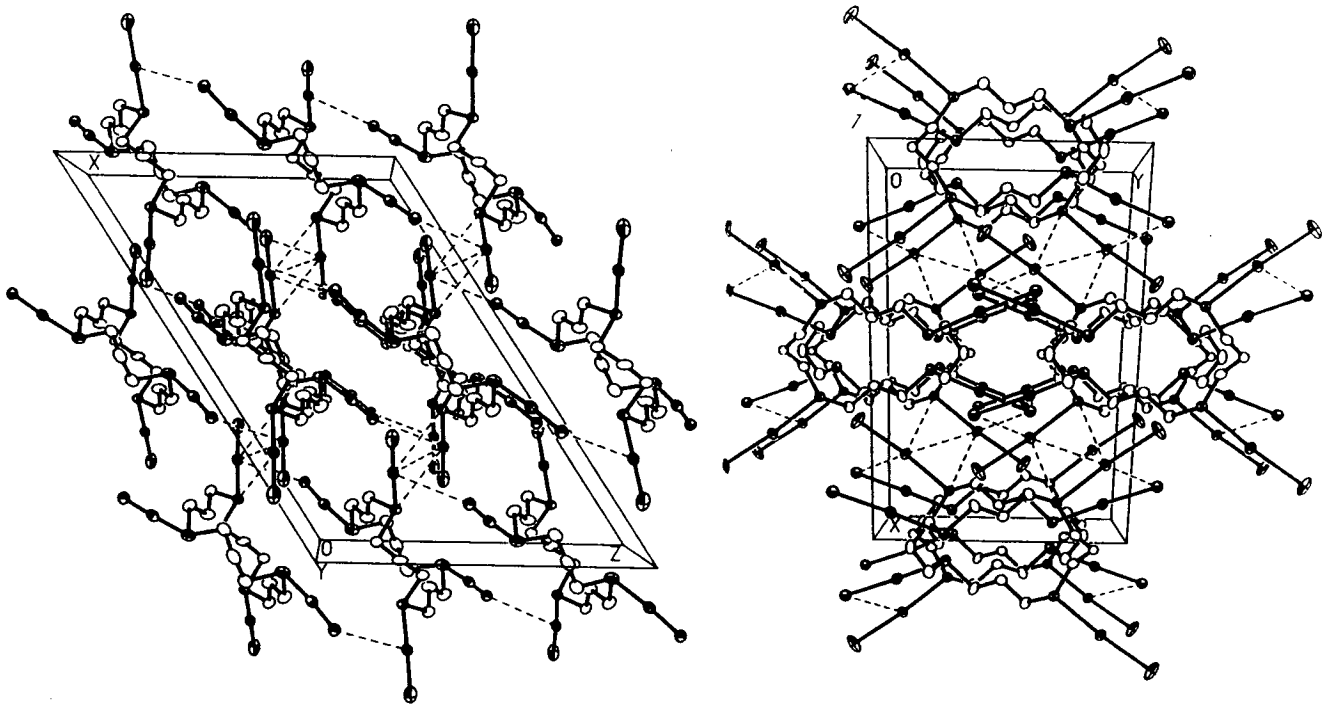

Figure 7.2.12b Packing diagram of ([16]aneS$_4$)(I$_2$)$_4$ in two orientations.

I(11)-I(12)	2.8108(9)	I(11)-S(1)	2.7564(21)
I(51)-I(52)	2.7916(8)	I(51)-S(5)	2.8478(23)
I(12)-I(11)-S(1)	174.74(5)	I(52)-I(51)-S(5)	171.71(5)
C(16')-C(15)-C(16)-S(1)	68.9(7)	C(2)-C(3)-C(4)-S(5)	-177.6(6)
C(15)-C(16)-S(1)-C(2)	-166.1(5)	C(3)-C(4)-S(5)-C(6)	81.8(7)
C(16)-S(1)-C(2)-C(3)	73.3(6)	C(4)-S(5)-C(6)-C(7)	-162.5(6)
S(1)-C(2)-C(3)-C(4)	166.4(6)	S(5)-C(6)-C(7)-C(6')	76.1(7)

(Primed atoms are symmetry related to the non-primed atoms by the following symmetry operation: -x, y, 0.5-z)

Table 7.2.12 Selected bond lengths (Å), angles (°) and torsion angles (°) with estimated standard deviations for ([16]aneS$_4$)(I$_2$)$_4$.

7.2.13 The Single Crystal Structure of ([15]aneS$_5$)(I$_2$)$_3$(I$_2$)$_{0.5}$

The single crystal structure of ([15]aneS$_5$)(I$_2$)$_3$(I$_2$)$_{0.5}$ exhibits certain features, which are unique to this compound and not found in any other single crystal structure of thioether I$_2$ adducts. The environment around I(10) and I(10') (site occupancy of 0.5, both) caused some problems during refinement of the structure. All other I$_2$ molecules in this compound conform to the geometrical properties associated with a Lewis acid-base adduct (see **Table 7.2.13**). The distance between I(10) and I(10') [2.674(3)Å] is however virtually identical to the distance found in I$_2$ vapour. The S(10)-I(10) distance is 2.839(5)Å quite comparable with other S-I distances in this compound and it would therefore be considered to be a significant interaction. A close analysis of the geometry around the S(10)-atom however reveals rather large deviations in the angles compared with other S-atom environments in this compound (see **Table 7.2.13**). It seems to be clear that the directional incompatibility of the lone electron pairs on S(10) and the LUMO on I(10)-I(10') accounts for the short I-I distance.

The structure itself shows further problems with an intense peak (≈12 eÅ^{-3}) near I(10) which has been modelled as partially occupied I-atom. There is no trivial explanation available to account for the situation found in ([15]aneS$_5$)(I$_2$)$_3$(I$_2$)$_{0.5}$. It is on the other hand remarkable that all of these features coincide with an odd numbered macrocycle which also showed rapid decomposition in the reaction with ICl. It seems therefore likely that the packing in the crystal lattice plays an important part in the stability of I$_2$ adducts with [15]aneS$_5$.

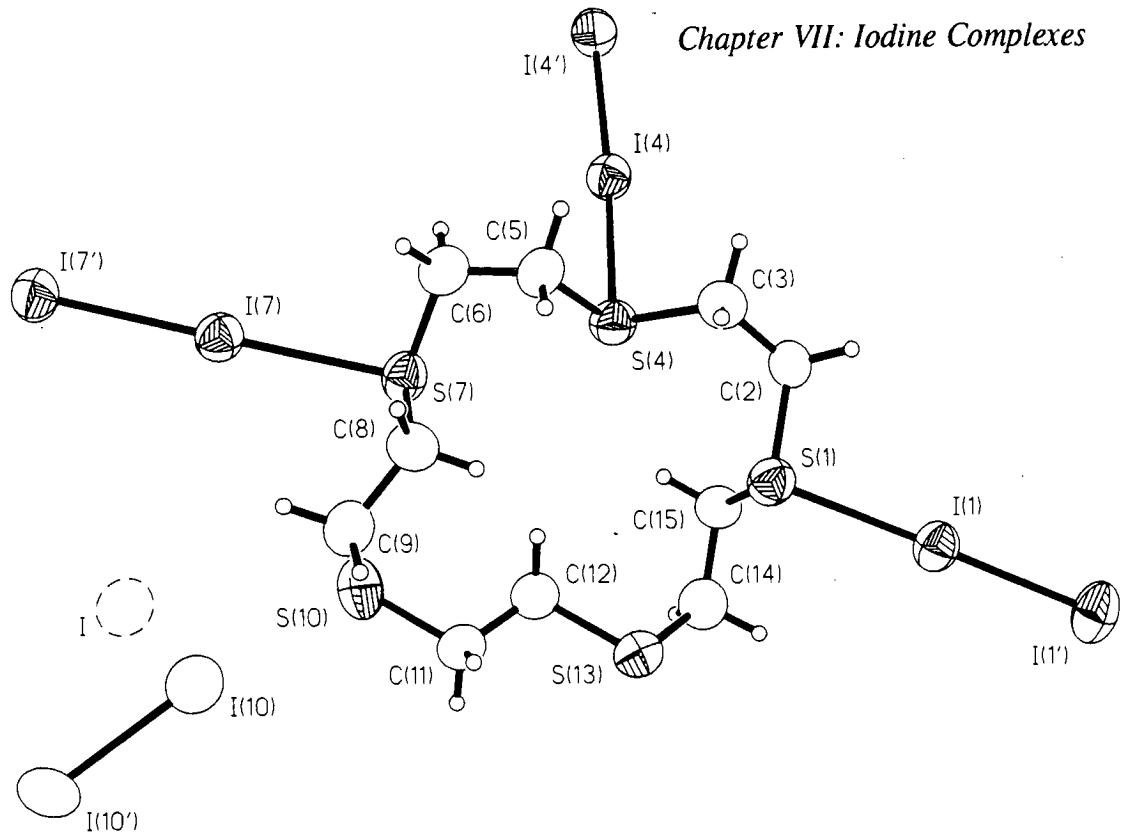

Figure 7.2.13a The single crystal structure of ([15]aneS$_5$)(I$_2$)$_3$(I$_2$)$_{0.5}$ (I(10) and I(10') have mutual s.o.f.s of 0.5 and I has been refined with a s.o.f. of 0.2).

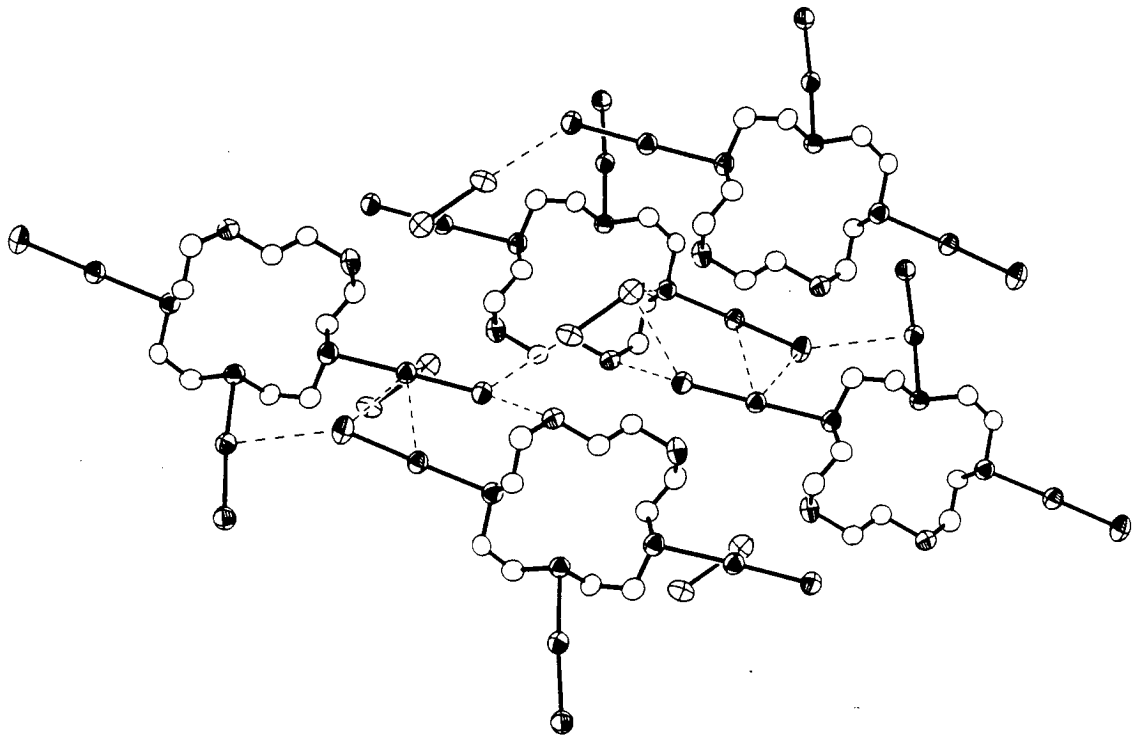

Figure 7.2.13b Packing diagram of ([15]aneS$_5$)(I$_2$)$_3$(I$_2$)$_{0.5}$.

I(1)-I(1')	2.798(2)	I(1)-S(1)	2.797(3)
I(4)-I(4')	2.764(2)	I(4)-S(4)	2.885(4)
I(7)-I(7')	2.779(2)	I(7)-S(7)	2.828(3)
I(10)-I(10')	2.674(3)	I(10)-S(10)	2.839(5)
S(1)-I(1)-I(1')	178.39(8)	S(7)-I(7)-I(7')	178.80(8)
S(4)-I(4)-I(4')	171.12(8)	S(10)-I(10)-I(10')	172.90(13)
C(15)-S(1)-I(1)	96.4(4)	C(2)-S(1)-I(1)	99.9(4)
C(3)-S(4)-I(4)	98.6(5)	C(5)-S(4)-I(4)	94.8(5)
C(6)-S(7)-I(7)	97.3(4)	C(8)-S(7)-I(7)	99.2(5)
C(9)-S(10)-I(10)	99.9(5)	C(11)-S(10)-I(10)	120.2(5)
C(3)-S(4)-C(5)	99.6(6)	C(12)-S(13)-C(14)	101.2(7)
C(6)-S(7)-C(8)	100.9(6)	C(15)-S(1)-C(2)	101.3(6)
C(9)-S(10)-C(11)	102.8(6)		
S(1)-C(2)-C(3)-S(4)	-64.9(11)	C(9)-S(10)-C(11)-C(12)	-92.3(11)
C(2)-C(3)-S(4)-C(5)	161.9(9)	S(10)-C(11)-C(12)-S(13)	173.2(7)
C(3)-S(4)-C(5)-C(6)	174.9(10)	C(11)-C(12)-S(13)-C(14)	161.7(10)
S(4)-C(5)-C(6)-S(7)	53.7(13)	C(12)-S(13)-C(14)-C(15)	62.0(12)
C(5)-C(6)-S(7)-C(8)	59.5(11)	S(13)-C(14)-C(15)-S(1)	57.0(12)
C(6)-S(7)-C(8)-C(9)	156.9(10)	C(14)-C(15)-S(1)-C(2)	176.2(9)
S(7)-C(8)-C(9)-S(10)	51.8(12)	C(15)-S(1)-C(2)-C(3)	101.2(10)
C(8)-C(9)-S(10)-C(11)	73.2(11)		

Table 7.2.13 Selected bond lengths (Å), angles (°) and torsion angles (°) with estimated standard deviations for ([15]aneS$_5$)(I$_2$)$_3$(I$_2$)$_{0.5}$.

7.2.14 The Single Crystal Structure of ([18]aneS$_6$)(I$_2$)$_4$

The single crystal structure of ([18]aneS$_6$)(I$_2$)$_4$ (**Figure 7.2.14**) shows a feature which has not been observed in any of the previous structures. The conformation [3636] of the macrocycle in ([18]aneS$_6$)(I$_2$)$_4$ is much different from the conformation in the solid state structure of [18]aneS$_6$ [1113311133]. The macrocycle adopts a rectangular shape with the typical *anti* torsion angles at all S-C-C-S moieties (**Table 7.2.14**). The difference between ([18]aneS$_6$)(I$_2$)$_4$ and all other structures described so far is that two I$_2$ molecules adopt an *endo* co-ordination mode whereas in contrast the two remaining I$_2$ molecules adopt the typical *exo* co-ordination mode forcing the macrocycle into an S-shape. There is no significant difference in the S-I$_2$ interactions reflected in similar bond lengths [I-I 2.7875(6), 2.8067(7); I-S 2.8379(17) and 2.7921(17)Å] and angles [S-I-I 174.95(4) and 174.43(4)°]. The cause for this unusual behaviour has therefore to be sought in the packing of the compound in the crystal lattice.

The packing diagrams along the y- and z-axis (**Figure 7.2.14b**) show a columnar stacking of the macrocycles onto each other. Other crowded structures such as $([9]aneS_3)_2(I_2)_4$ and $([24]aneS_8)(I_2)_6$ (see below) exhibit similar features. The structure in those case would be described better as macrocyclic ligands embedded in a crystalline matrix of I_2. The weak attraction forces between the I_2 molecules are responsible for instability of the this compound (see for example **7.2.18** and **7.4.7**).

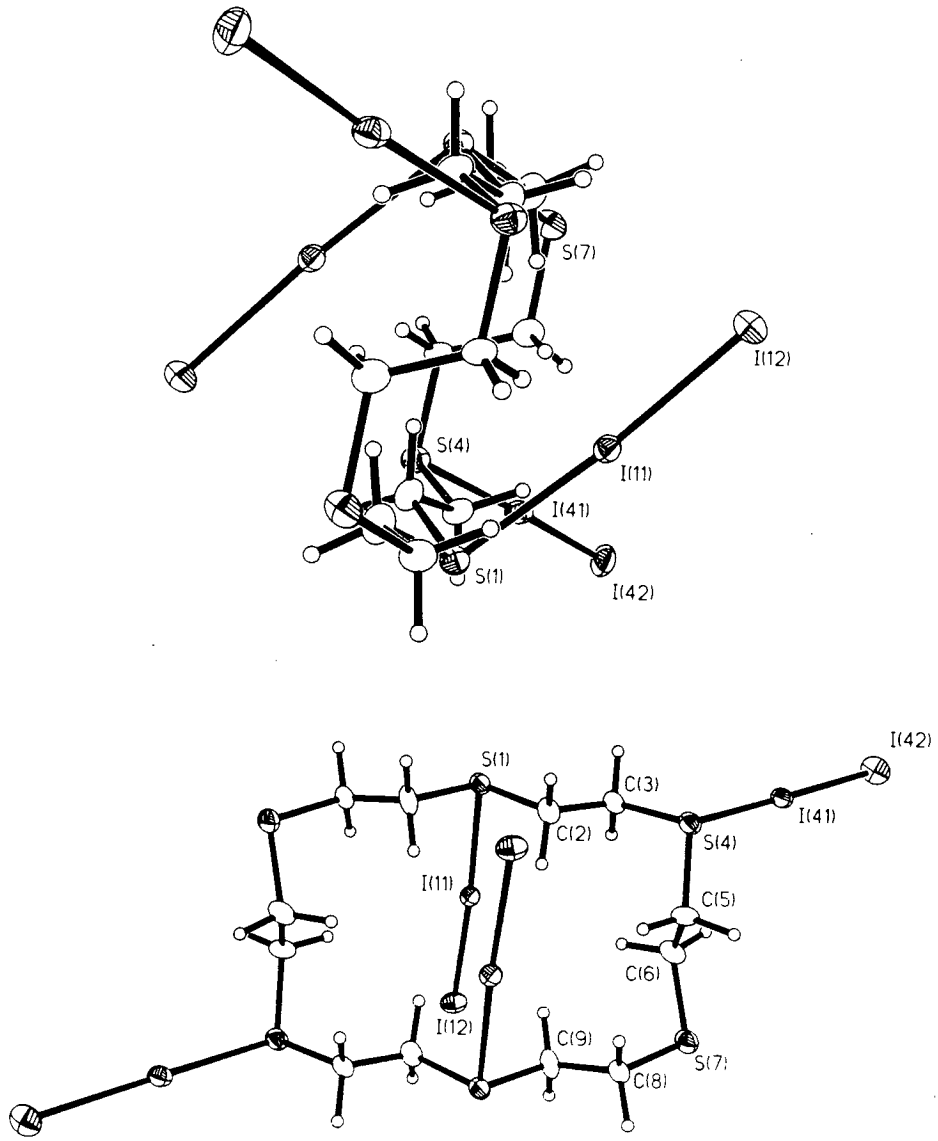

Figure 7.2.14a The single crystal structure of $([18]aneS_6)(I_2)_4$.

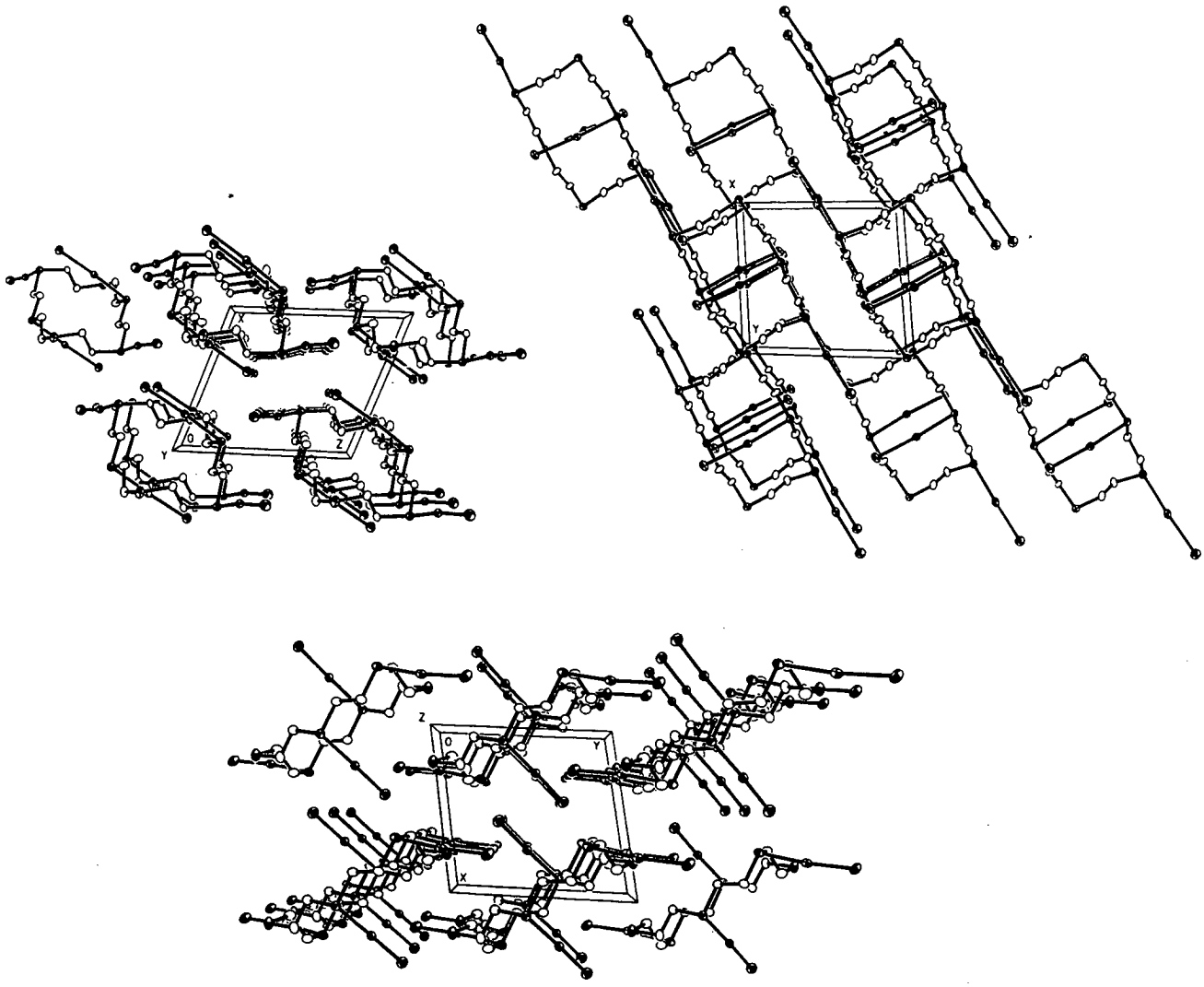

Figure 7.2.14b The packing diagrams of ([18]aneS$_6$)(I$_2$)$_4$ in three different orientations.

I(11)-I(12)	2.7875(6)	I(11)-S(1)	2.8379(17)
I(41)-I(42)	2.8067(7)	I(41)-S(4)	2.7921(17)
I(12)-I(11)-S(1)	174.95(4)	I(42)-I(41)-S(4)	174.43(4)
C(8')-C(9')-S(1)-C(2)	-166.5(5)	S(4)-C(5)-C(6)-S(7)	167.4(4)
C(9')-S(1)-C(2)-C(3)	179.2(5)	C(5)-C(6)-S(7)-C(8)	65.4(5)
S(1)-C(2)-C(3)-S(4)	176.0(3)	C(6)-S(7)-C(8)-C(9)	70.0(5)
C(2)-C(3)-S(4)-C(5)	70.7(5)	S(7)-C(8)-C(9)-S(1')	-175.2(3)
C(3)-S(4)-C(5)-C(6)	51.7(6)		

Table 7.2.14 Selected bond lengths (Å), angles (°) and torsion angles (°) with estimated standard deviations for ([18]aneS6)(I$_2$)$_4$.

7.2.15 The Single Crystal Structure of ([24]aneS$_8$)I$_2$

The single crystal structure of ([24]aneS$_8$)I$_2$ (**Figure 7.2.15a**) shows again the typical stair motif of alternating I$_2$ bridges and macrocycles as found in other 1:1 adducts between I$_2$ and homoleptic thioether macrocycles (**Figure 7.2.15b**). The S-I interaction between symmetrical bridging I$_2$ molecules and S-donors can only be described as weak [I-I 2.755(1)Å; I-S 3.215(2)Å]. It compares however well with the asymmetrical bridging in ([9]aneS$_3$)$_2$(I$_2$)$_4$ [I-I 2.7542(21)Å; I-S 2.917(6), 3.054(6)Å] (see above). The single crystal structure of [24]aneS$_8$ is not known but the conformation of [24]aneS$_8$ in ([24]aneS$_8$)I$_2$ shows features such as *exo* oriented S-atoms and anti S-C-C-S torsion angles commonly found in other thioether macrocycles such as [12]aneS$_4$ [**Figure 2.1.4** (ii)] and [14]aneS$_4$ [**Figure 2.1.4** (iii) and (iv)].

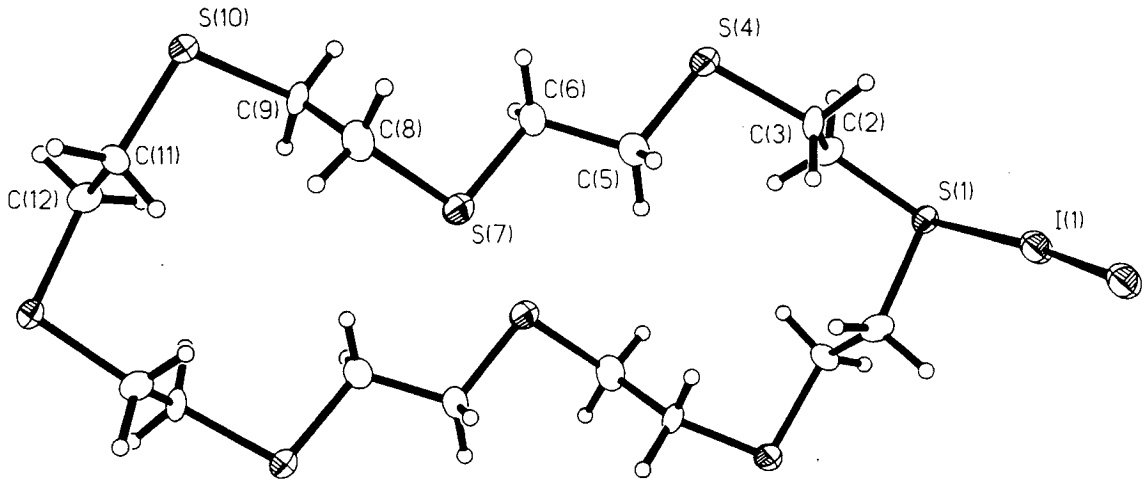

Figure 7.2.15a The single crystal structure of ([24]aneS$_8$)I$_2$.

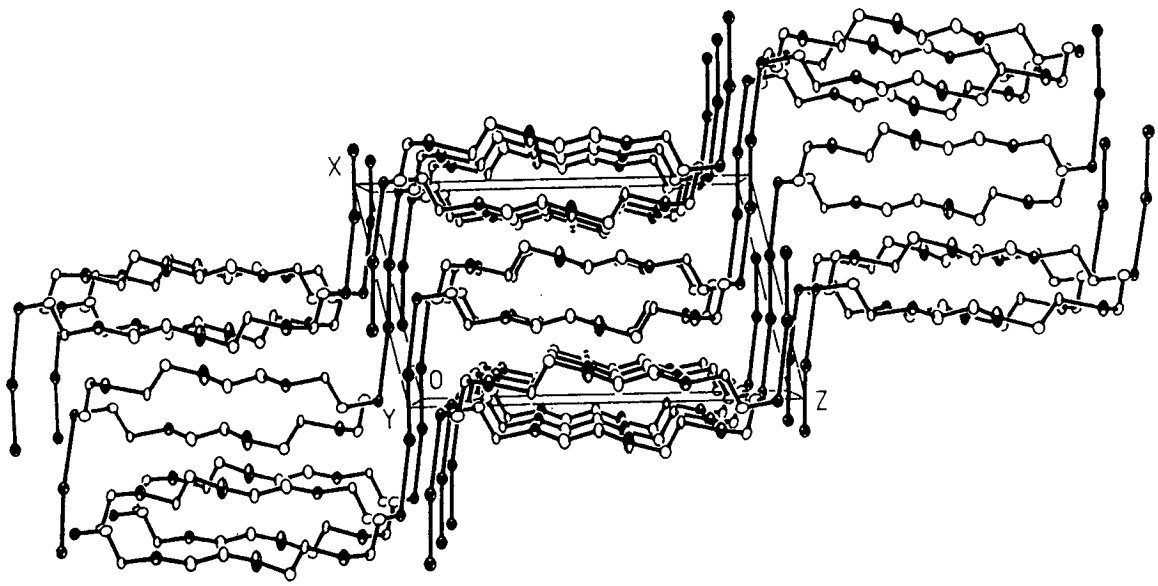

Figure 7.2.15b Packing diagram of ([24]aneS$_8$)I$_2$.

I(1)-I(1'')	2.755(1)	S(1)-I(1)	3.215(2)
I(1'')-I(1)-S(1)	172.75(3)		
S(1)-C(2)-C(3)-S(4)	-174.0(3)	S(7)-C(8)-C(9)-S(10)	168.8(3)
C(2)-C(3)-S(4)-C(5)	105.8(5)	C(8)-C(9)-S(10)-C(11)	-75.9(5)
C(3)-S(4)-C(5)-C(6)	-169.9(5)	C(9)-S(10)-C(11)-C(12)	-78.5(5)
S(4)-C(5)-C(6)-S(7)	-178.7(3)	S(10)-C(11)-C(12)-S(1')	173.0(3)
C(5)-C(6)-S(7)-C(8)	146.1(5)	C(11)-C(12)-S(1')-C(2')	-79.1(5)
C(6)-S(7)-C(8)-C(9)	70.6(5)	C(12)-S(1')-C(2')-C(3')	-86.8(5)

(Primed atoms are symmetry related to the non-primed atoms by the following symmetry operation: 1-x, 2-y, 1-z; Double primed atoms (I'') are equivalent atoms by the symmetry operation: -x, -y, -z)

Table 7.2.15 Selected bond lengths (Å), angles (°) and torsion angles (°) with estimated standard deviations for ([24]aneS$_8$)I$_2$.

7.2.16 The Single Crystal Structure of ([24]aneS$_8$)(I$_2$)$_6$

The single crystal structure of ([24]aneS$_8$)(I$_2$)$_6$ (**Figure 7.2.16a**) shows similar features compared with ([18]aneS$_6$)(I$_2$)$_4$. The compound crystallises in space group $P\ 2_1/c$ (No. 14) and one half of the molecule is symmetry related to the other. Two of the six I$_2$ molecules are co-ordinated *endo* to S-atoms and lie above and below the macrocyclic plane. The other four S-atoms adopt the typical *exo* co-ordination mode found in most of the compounds studied. The conformation of the macrocycle [246246] is similar to the one found in ([24]aneS$_8$)I$_2$ [336336].

([24]aneS$_8$)I$_2$	[336336]	aaaaa|+a-|-a-|-aaaaa|+a-|-a-|-
([24]aneS$_8$)(I$_2$)$_6$	[246246]	aaaa+|+aa-|a+|+aaaa+|+aa-|a++|

Table 7.2.16a Comparison of the conformations in the solid state structures of ([24]aneS$_8$)I$_2$ and ([24]aneS$_8$)(I$_2$)$_6$ (Note: underlined angles denote a S-C-C-S torsion and the '|' indicates a corner in Dale's scheme)

Table 7.2.16a compares both conformations using Dale's and the alternative 'a+-' scheme. Both conformations are defined by 14 *anti* and 10 *gauche* angles. It is interesting to note that all S-C-C-S torsion angles are *anti*. The most likely explanation is that the co-ordination of I$_2$ is rather weak and does not very much interfere with the conformation of the macrocycle. Conformational changes are more likely a result of the packing in crystal lattice. The packing diagram of ([24]aneS$_8$)(I$_2$)$_6$ (**Figure 7.2.16b**) shows extensive contacts between I$_2$ molecules giving the impression that the macrocycle is embedded in a matrix of I$_2$. The packing diagram clearly shows that even though the macrocycles are arranged in columns along the y-axis, they are separated by the two I$_2$ molecules which are *endo* co-ordinated to the macrocycle.

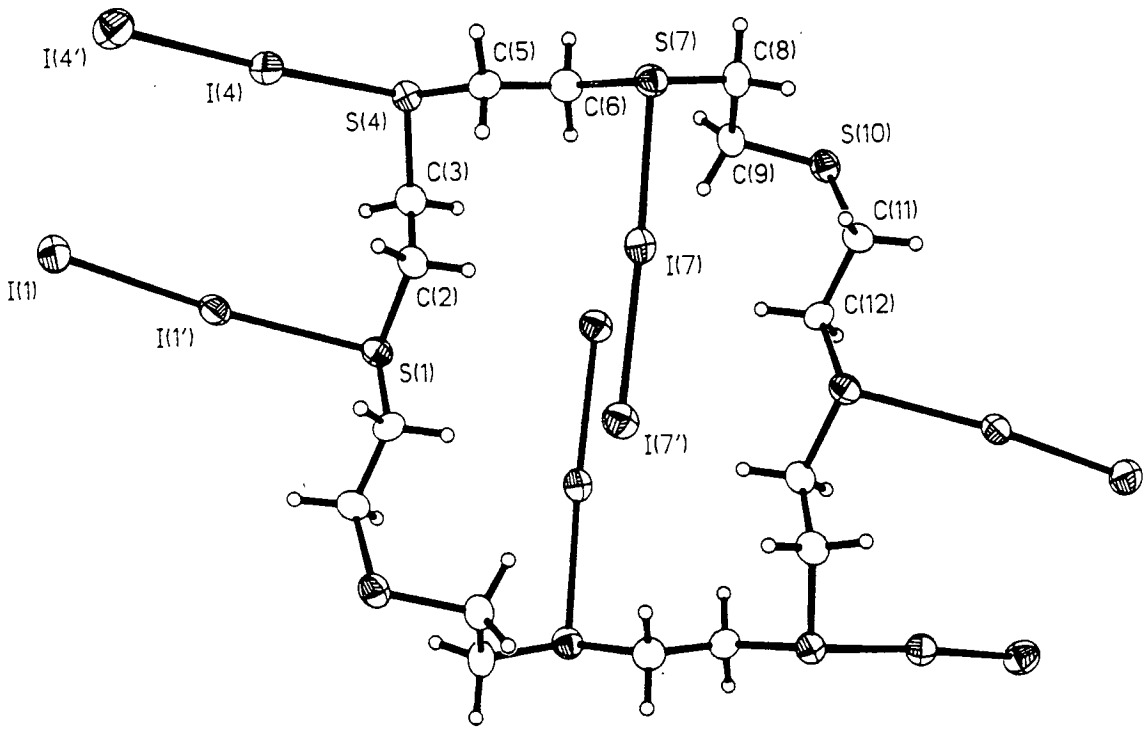

Figure 7.2.16a The single crystal structure of ([24]aneS$_8$)(I$_2$)$_6$.

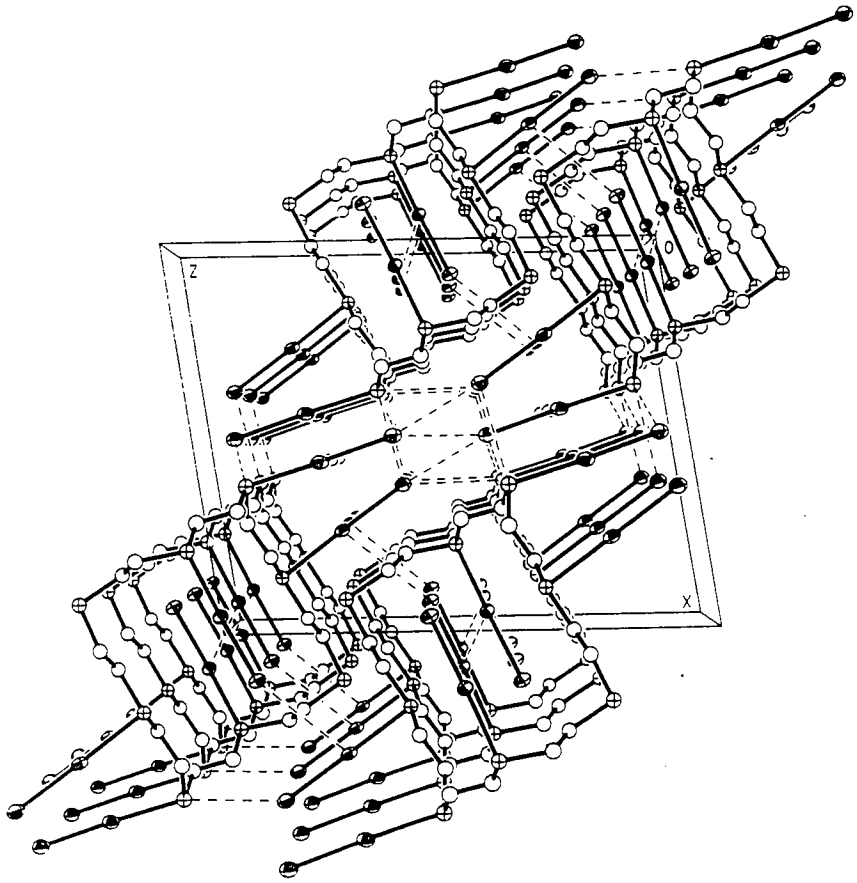

Figure 7.2.16b Packing diagram of ([24]aneS$_8$)(I$_2$)$_6$ in the x-z-plane

I(1)-I(1')	2.7861(8)	I(1)-S(1)	2.8209(21)
I(4)-I(4')	2.7937(8)	I(4)-S(4)	2.8146(22)
I(7)-I(7')	2.8345(8)	I(7)-S(7)	2.7412(22)
I(1')-I(1)-S(1)	170.15(5)	I(7')-I(7)-S(7)	177.24(5)
I(4')-I(4)-S(4)	177.41(5)		
C(12'')-S(1)-C(2)-C(3)	-173.7(6)	C(8)-S(7)-C(6)-C(5)	-178.7(6)
C(11'')-C(12'')-S(1)-C(2)	176.1(6)	C(9)-C(8)-S(7)-C(6)	-46.4(7)
S(4)-C(3)-C(2)-S(1'')	157.3(5)	S(10)-C(9)-C(8)-S(7)	-153.6(4)
C(5)-S(4)-C(3)-C(2)	47.6(7)	C(11)-S(10)-C(9)-C(8)	78.2(6)
C(6)-C(5)-S(4)-C(3)	76.0(7)	C(12)-C(11)-S(10)-C(9)	79.8(6)
S(7)-C(6)-C(5)-S(4)	-176.2(4)	S(1'')-C(12)-C(11)-S(10)	-173.6(4)

(Double primed atoms are symmetry related to the non-primed atoms by the following symmetry operation: -x, 1-y, -z)

Table 7.2.16b Selected bond lengths (Å), angles (°) and torsion angles (°) with estimated standard deviations for ([24]aneS$_8$)(I$_2$)$_6$.

7.2.17 Summary of Structural Results

As it has already been pointed out, there is a close relationship between the I-I and S-I distances. A strong interaction between I_2 and a thioether donor is reflected in a short S-I distance and a long I-I distance and *vice versa* (**Figure 7.2.17**).

Compound	I-I / Å	I-S / Å	Reference
I_2	2.667(2)		355
I_2	2.715(6)		356
([6]aneS_2)(I_2)$_2$	2.787 (2)	2.867 (6)	412
([6]aneS_3)I_2	2.7535 (4)	3.145 (4)	487
(Bz_2S)I_2	2.819 (9)	2.78 (2)	381
(Dithia[3.3.1]propellane)(I_2)$_2$	2.797 (1)	2.852 (2)	488
	2.796 (1)	2.806 (2)	
(Dithia[3.3.2]propellane)(I_2)$_2$	2.794 (1)	2.803 (2)	488
	2.767 (1)	2.902 (2)	
(1,10-[18]aneS_2O_4)$_2$(I_2)$_5$	2.775 (2)	2.848 (3)	378
	2.810 (2)	2.761 (3)	
	2.821 (2)	2.774 (3)	
	2.902 (2)	2.654 (3)	
([9]aneS_3)$_2$(I_2)$_4$	2.8156 (23)	2.760 (6)	this work
	2.7846 (22)	2.870 (6)	
	2.7986 (23)	2.862 (6)	
	2.7542 (21)	3.054 (6)	
	2.7542 (21)	3.197 (6)	
([9]aneS_3)(I_2)$_3$	2.772 (1)	2.880 (3)	377
	2.768 (2)	2.865 (6)	
	2.751 (2)	2.933 (4)	
([12]aneS_4)I_2	2.7500 (10)	3.2030 (20)	this work
	2.7549 (8)	3.1740 (20)	
	2.7549 (8)	3.1480 (20)	
([14]aneS_4)I_2	2.8095 (11)	2.859 (3)	this work
	2.8095 (11)	3.640 (3)	
([16]aneS_4)I_2	2.773 (12)	3.114 (3)	this work
([16]aneS_4)(I_2)$_4$	2.8108 (9)	2.7564 (21)	this work
	2.7916 (8)	2.8578 (23)	
([15]aneS_5)(I_2)$_4$	2.798 (2)	2.797 (3)	this work
	2.764 (2)	2.885 (4)	
	2.779 (2)	2.828 (3)	
	2.674 (3)	2.839 (5)	
([18]aneS_6)(I_2)$_4$	2.7875 (6)	2.8379 (17)	this work
	2.8067 (7)	2.7921 (17)	
([28]aneS_8)I_2	2.755 (1)	3.215 (2)	this work
([24]aneS_8)(I_2)$_6$	2.7861 (8)	2.8209 (21)	this work
	2.7937 (8)	2.8146 (22)	
	2.8345 (8)	2.7412 (22)	

Table 7.2.17a I-I and the corresponding I-S distances for known I_2-thioether adducts.

Table 7.2.17a gives a comprehensive overview over the known I_2-thioether adducts. All I-I distances lie within the range of distances found in solid I_2 (2.715, 3.497 and 3.972Å within a sheet; 4.269, 4.337 and 4.412Å between sheets - see the introduction to this chapter). The shortest S-I distance lies at 2.64Å but no simple binary S/I compounds in contrast to other sulphur halides such as SCl_2 or SBr_2 are known for comparison. A plot of these distances is shown in **Figure 7.2.17**.

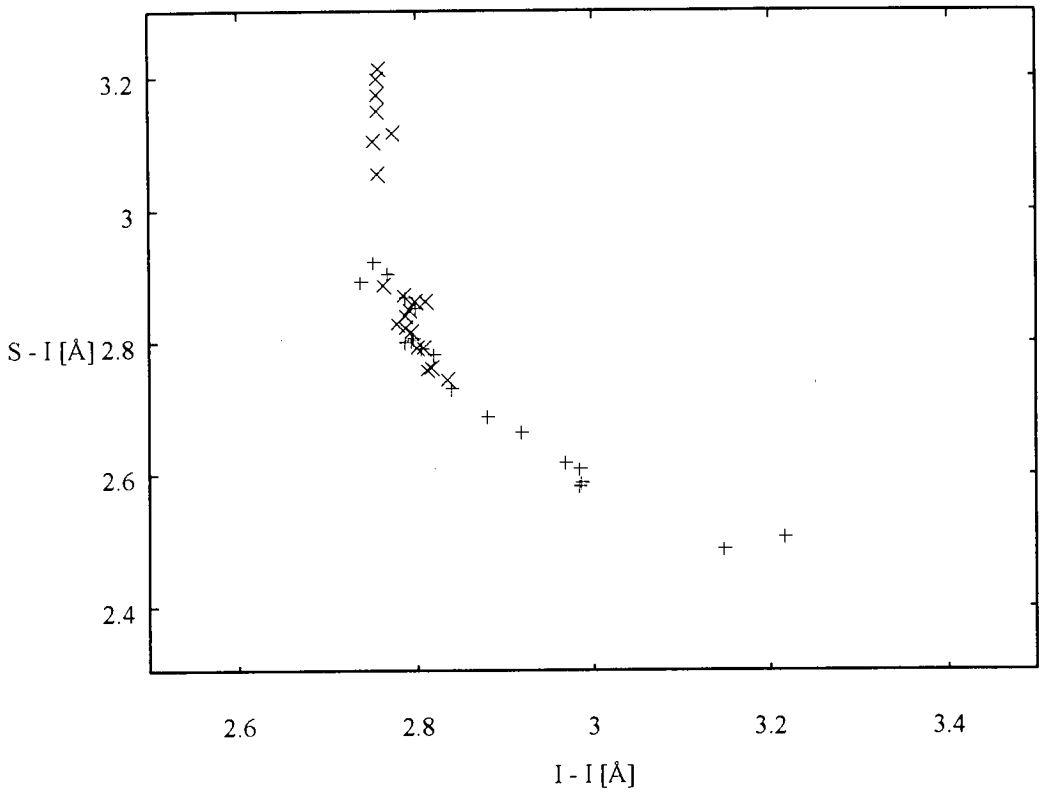

Figure 7.2.17 Plot of the I-I against the I-S distance
(x: present work; +: reported structures).

This plot shows clearly that all data lie on a smooth curve. Small deviations from this curve are due to secondary interactions (for instance I····I interactions) and errors in the distances (error bars for the estimated standard deviations are too small to be printed). It underlines that other interactions apart from the primary S-I interaction are negligible.

One of the by-products in this investigation has been the more accurate determination of the atomic volumes in the crystal lattice. A common way to predict the unit cell contents consists of the multiplication of the number of non-H atoms in the chemical formula of the compound (actually the contents of the asymmetric unit) with an average atomic volume of 18 $Å^3$. The volume of the unit cell divided by this volume should give a value close to Z (the number of independent molecules in the unitcell). It is obvious that 18 $Å^3$ is far too low to be used for compounds containing sterically demanding atoms such as I_2. A more reliable way to account for Z is the use of a linear equation with terms describing the number of C-, S- and I-atoms.

(i) $V_{molecule} = \Sigma(CH_2) \cdot V_C + \Sigma_S \cdot V_S + \Sigma_I \cdot V_I$
(with $V(CH_2) = 23$, $V_S = 24$ and $V_I = 47$ $Å^3$)

(ii) $V_{unitcell} = V_{molecule} \cdot Z$

(i) + (ii) $\Sigma_I = ((V_{unitcell} / Z) - (\Sigma(CH_2) \cdot V_C + \Sigma_S \cdot V_S)) / V_I$

These equations have been successfully used in the prediction of the I_2 contents in a range of compounds during this investigation (**Table 7.2.17b**). Z could also be obtained using information about the space group, the density and the rough composition of the material thus enabling the prediction of the I_2: macrocycle ratio.

Compound	asymmetric unit contents	$V_{calc.}$ [$Å^3$]	V/Z_{found} [$Å^3$]
([9]aneS$_3$)$_2$(I$_2$)$_4$	$C_{12}H_{24}S_6I_4$	608	775
([12]aneS$_4$)I$_2$	$C_{12}H_{24}S_4I_3$	513	548
([14]aneS$_4$)I$_2$	$C_{10}H_{20}S_4I_2$	420	413
([16]aneS$_4$)I$_2$	$C_{12}H_{24}S_4I_2$	466	461
([16]aneS$_4$)(I$_2$)$_4$	$C_{12}H_{24}S_4I_8$	748	763
([18]aneS$_6$)(I$_2$)$_4$	$C_{12}H_{24}S_6I_8$	796	788
([24]aneS$_8$)I$_2$	$C_{16}H_{32}S_8I_2$	654	656
([24]aneS$_8$)(I$_2$)$_6$	$C_{16}H_{32}S_8I_{12}$	1124	1123

Table 7.2.17b Comparison of calculated and observed volumes of the asymmetric unit for compounds studied.

7.2.18 The Characterisation of I_2 Thioether Charge Transfer Complexes

In contrast to the ease in preparation, characterisation of these compounds caused difficulties. Microanalytical results showed in general good agreement with the stoichiometries of compounds with a low I_2 contents such as ([12]aneS_4)I_2 and ([14]aneS_4)I_2. Larger deviations were found in compounds with a high I_2 contents such as ([16]aneS_4)$(I_2)_4$ due to their tendency to slowly liberate I_2. The EI-mass spectrum of I_2 thioether charge transfer complexes features two peaks at m/z = 254 and m/z = 127 assigned to the two cations $(I_2)^+$ and I^+. The molecular ion peak for the macrocyclic ligand was observed in some cases in particular with small macrocycles such as [9]aneS_3 and [14]aneS_4 (**Figure 7.2.18**). A range of other spectroscopic techniques were also evaluated. NMR and IR spectroscopy both gave a good indication for the presence of the macrocyclic ligand. However all the techniques mentioned above proved to be unsuitable for the investigation of the I_2 thioether charge-transfer interaction. Single crystal X-ray diffraction studies seem to be in this context the technique of choice in dealing with these compounds. This investigation was also backed up UV/vis spectrophotometric studies in solution (see below).

(i) $([9]aneS_3)_2(I_2)_4$

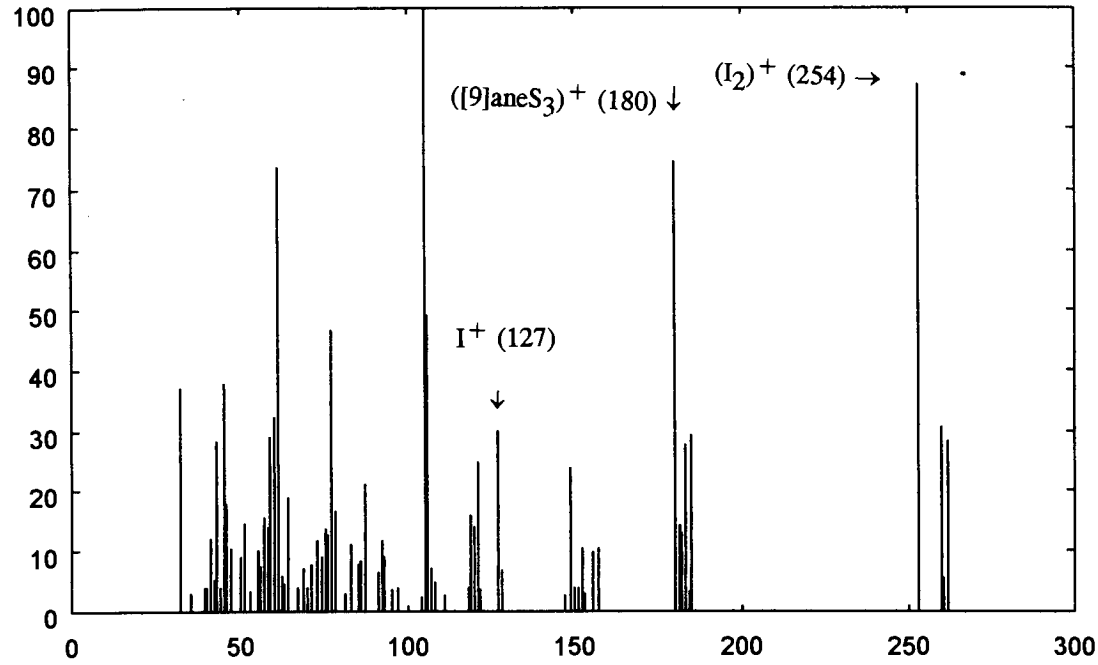

(ii) $([14]aneS_4)I_2$

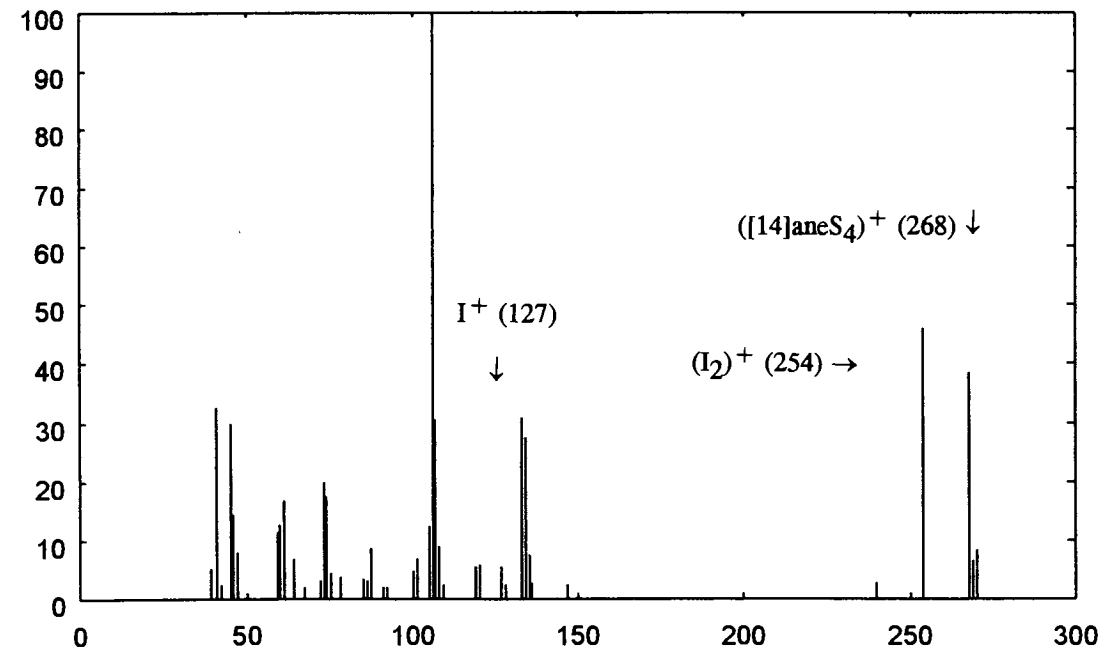

Figure 7.2.18 EI mass spectra of (i) $([9]aneS_3)_2(I_2)_4$ and (ii) $([14]aneS_4)I_2$.

7.4.19 Spectrophotometric Studies in Solution

In order to determine the stoichiometry of the adducts present in solution, Job's method[489,490] of constant concentration variation was employed. Measurements were carried out for [9]aneS$_3$ and [18]aneS$_6$ in CH_2Cl_2.

In a typical experiment equimolar solutions of I_2 and the macrocycle in CH_2Cl_2 were prepared. The mixture to be measured was then made up from different ratios of both solutions thus keeping the overall concentration constant. The absorbance of each mixture was then recorded at the wavelengths (λ_{max}) where the adduct showed an absorption maximum. λ_{max} was in both cases 308 nm indicating that the same chromophore is present in either charge-transfer adduct. The absorption band of I_2 was found at 505 nm. The presence of an ideal equilibrium between both reactants, which is an important condition for this type of measurement, was indicated by an isosbestic point at ~475 nm. The next two pages (**Figures 7.2.19a** and **7.2.19b**) summarise the results obtained in these measurements. A plot of the ligand to I_2 ratio against the absorbance shows a maximum indicating the ratio of ligand to I_2 for the predominant species in solution.

Even though the number of donor atoms in the macrocyclic ligand increases on going from [9]aneS$_3$ to [18]aneS$_6$ the predominant species in solution is of 1:1 (I_2:ligand) stoichiometry in either case. It should however be emphasised that these measurements have been undertaken under high dilution conditions due to large molar absorption coefficients of the compounds involved. It is uncertain whether these results can be extrapolated to concentrated solutions or to other solvents. It would be particularly interesting to establish whether the predominant species in a polar solvent such as MeCN or EtOH would also be of a 1:1 stoichiometry or if not whether there is a tendency to form ionic species in contrast to covalent charge-transfer adducts. The use of polar solvents for this type of measurements causes problems due to the significant reactant solvent interactions which would interfere with the equilibrium between both reactants.

Nevertheless these findings indicate that the structural diversity described in the preceding sections are a unique feature of the solid state. Studies in solution or matrices such as FAB mass spectrometry or NMR spectroscopy have to take into consideration that the compound studied is in fact of 1:1 stoichiometry.

I_2 / [9]aneS_3	A
0 / 10	0.000
1 / 9	0.056
2 / 8	0.097
3 / 7	0.129
4 / 6	0.150
5 / 5	0.164
6 / 4	0.142
7 / 3	0.130
8 / 2	0.103
9 / 1	0.070
10 / 0	0.000

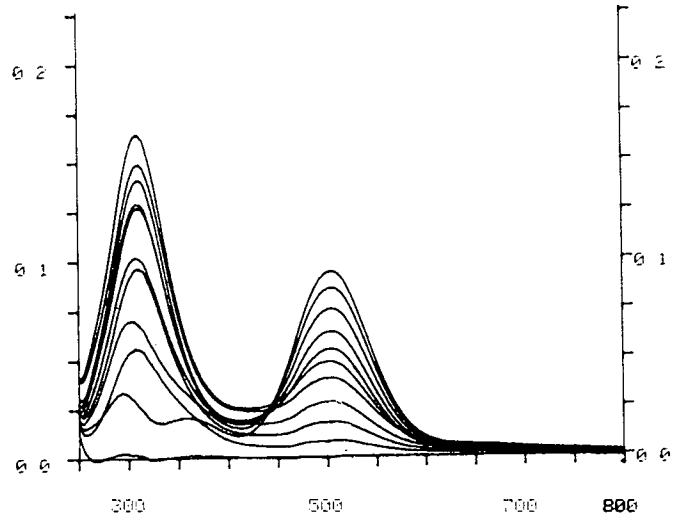

$[I_2]$ = 0.993 mmol l^{-1} in CH_2Cl_2;
$[([9]aneS_3)]$ = 0.993 mmol l^{-1} in CH_2Cl_2;
Path 0.03mm

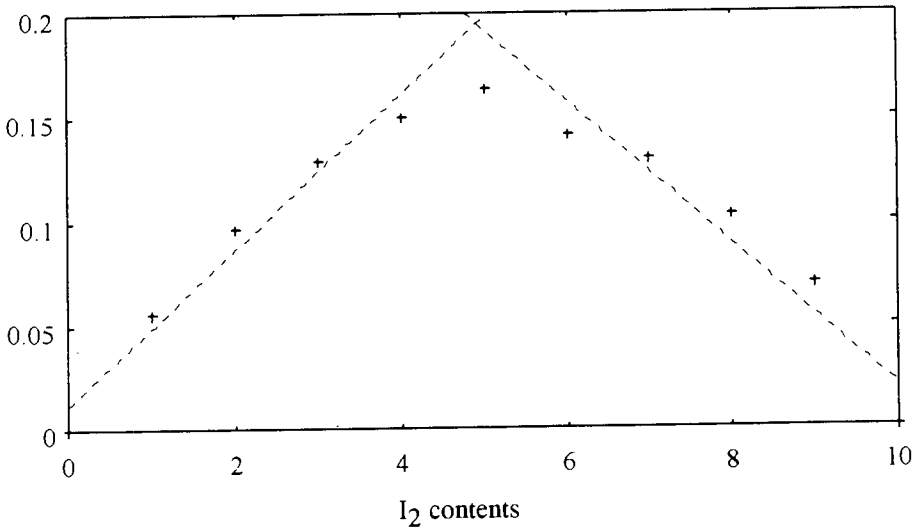

The intersection of the two best fit tangents (0.0118+x·0.0373 and 0.3642-x·0.0344) on the graph lies at a 4.91 / 5.09 $[I_2]/[([9]aneS_3)]$ (i.e. ~ 1 / 1) ratio.

Figure 7.2.19a Table, spectrum and graph of absorbances at 308 ± 3nm for mixtures between I_2 and [9]aneS_3.

I_2 / [18]aneS_6	A
0 / 10	0.000
1 / 9	0.044
2 / 8	0.081
3 / 7	0.114
4 / 6	0.126
5 / 5	0.138
6 / 4	0.130
7 / 3	0.111
8 / 2	0.077
9 / 1	0.043
10 / 0	0.000

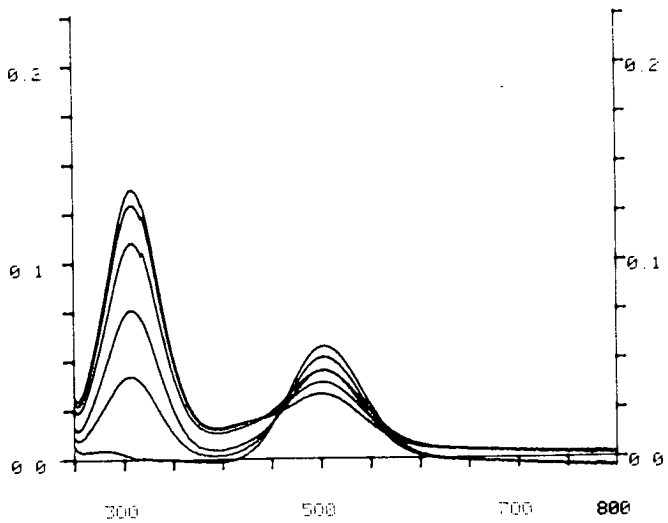

$[I_2]$ = 0.800 mmol l^{-1} in CH_2Cl_2;
$[([18]aneS_6)]$ = 0.800 mmol l^{-1} in CH_2Cl_2;
Path 0.03mm

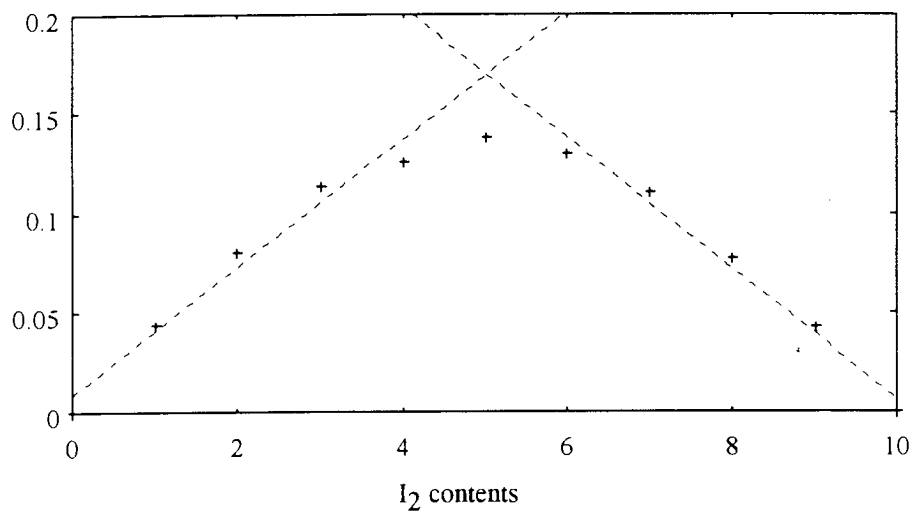

The intersection of the two best fit tangents (0.0086+x·0.0322 and 0.3346-x·0.0328) on the graph lies at a 5.02 / 4.98 $[I_2]/[([18]aneS_6)]$ (i.e. ~ 1 / 1) ratio.

Figure 7.2.19b Table, spectrum and plot of absorbances at 308 ± 3 nm for mixtures between I_2 and [18]aneS_6.

7.2.20 The I^+ Mono-Cation

A number of reactions were undertaken in order to generate and co-ordinate I^+ within the cavity of a macrocyclic ligand. There is some evidence that this has been achieved however no structural data revealing the actual geometry of these species could be obtained.

7.2.21 I_2 as a Source of I^+

Pathways to generate I^+ involving I_2 have been described in the introduction. The underlying principle in these reactions is the heterolytic fission of the I-I bond using halide abstraction agents such as Ag(I)-salts. There are several reasons why this approach is unsuitable for the co-ordination of I^+ into the cavity of a homoleptic thioether ligand. The reaction has to be divided into two steps to avoid competitive co-ordination of Ag^+ and I^+. The initial step involves the generation of I^+ which needs to be stabilised by the solvent while the precipitate of AgI is being quantitatively removed. The second step involves the addition of the macrocyclic ligand and subsequent co-ordination of I^+. This two step scheme avoids competition between I^+ and Ag^+ but it introduces competition between the supporting solvent and the macrocycle. It is vital to remove all Ag(I) quantitatively from the reaction mixture because microanalysis (the molecular weight difference is only 20 g mol^{-1} which is less then the weight of a typical solvent molecule.) and X-ray crystallography (The scattering factors are very similar.) can not distinguish between a Ag- and I-atom. The methods which would without ambiguity confirm the absence of Ag(I) in the product are X-ray fluorescence spectroscopy and mass spectrometry.

The superior alternative to I_2 is ICl. ICl contains already a polarised bond and the reaction with Ag(I) would lead to AgCl which has a lower solubility product compared with AgI. The real advantage of ICl is that it is already a halide abstraction agent which would react with Cl^- to yield $(ICl_2)^-$. It was also decided to investigate whether Friedel Crafts catalysts such as $AlCl_3$, BCl_3 and BF_3 could be used as halide abstraction agents.

7.2.22 ICl as a Source of I^+

The reaction between ICl and homoleptic S-donor macrocycles has been one of the starting points into the chemistry of I^+ with macrocyclic ligands. A typical experiment involved the mixing of equimolar amounts of ICl and the homoleptic S-donor macrocycle in CH_2Cl_2 to yield orange solutions of the adduct between ICl and the S-donor ligand. Further addition of ICl yields a bright yellow precipitate which can be collected and stored over a prolonged period of time without decay. Exceptions are the adducts of [15]aneS_5, which deteriorated rapidly over a few hours giving a black oil, and [9]aneS_3 which underwent an unexpected transformation to yield ([9]aneS_3)$_2$(I_2)$_4$ (see **7.2.6**). The characterisation of the yellow products has not been without difficulties. The infrared spectrum of the reaction product with [9]aneS_3 and [14]aneS_4 showed a series of bands assigned to C-H, C-C and C-S stretching vibrations confirming the presence of the ligand.
The microanalysis of the reaction product with [14]aneS_4 shows also excellent agreement with the stoichiometry ([14]aneS_4)(ICl)$_2$. The FAB mass spectrum of the reaction product with [16]aneS_4 shows a peak at m/z = 423 which could be assigned to a fragment of the composition.[I([16]aneS_4)]$^+$. These results together with the observations during the reactions have lead to a proposed scheme for this reaction (**Figure 7.2.22**).

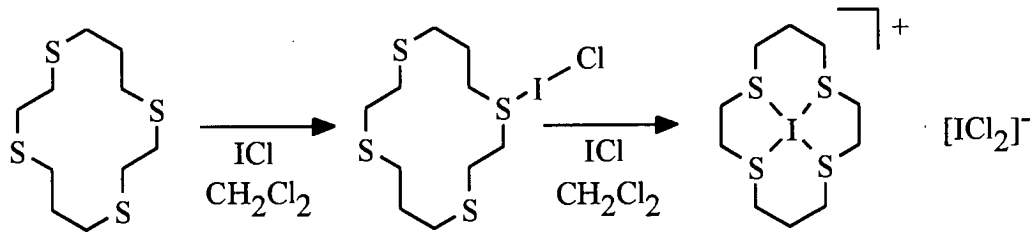

Figure 7.2.22 Proposed reaction scheme for the reaction of ICl with homoleptic S-donor macrocycles.

The initial step is the same as the reaction of I_2 with homoleptic S-donor macrocycles with formation of a charge transfer adduct between ICl and the macrocyclic ligand. The bond distance of the I-Cl molecule increases due to donation of electron density from the lone pair of the S-donor into the antibonding LUMO of the ICl molecule. The addition of a second ICl molecule removes the Cl^- anion affording the cationic iodine macrocyclic complex and $(ICl_2)^-$ which give a microcrystalline precipitate. A similar reaction conducted in MeCN did not yield a precipitate suggesting that indeed an ionic species is formed in this reaction. This observation might be of some importance in the future with respect to anion exchange and crystallisation from solution to yield crystals suitable for X-ray diffraction studies.

The mechanism of the transformation of the initial reaction product of ICl with [9]aneS$_3$ (2:1; ICl:[9]aneS$_3$) which afforded ([9]aneS$_3$)$_2$(I$_2$)$_4$ is still not clear. The second step in the proposed reaction scheme seems to be reversible. It was noted during this reaction that at the end of the addition of one molar equivalent of ICl to the solution of the ligand, a precipitate was formed which redissolved. A second observation was that a solution of ICl in CH_2Cl_2 converts to a solution of I_2 quantitatively in 48 hours. This process was monitored by UV/vis spectroscopy. The conversion of the proposed [I([9]aneS$_3$)]ICl_2 to ([9]aneS$_3$)$_2$(I$_2$)$_4$ is a genuine solid state reaction. No liberation of ICl or I_2 has been observed. The presence of traces of CH_2Cl_2 which might act as a mediator in the conversion can not be excluded. It should be noted that there is a discrepancy between the I_2 contents in ([9]aneS$_3$)$_2$(I$_2$)$_4$ and [I([9]aneS$_3$)]ICl_2. The initial yellow material contains only half the amount of I_2 compared with ([9]aneS$_3$)$_2$(I$_2$)$_4$.

This area of research needs certainly more attention in the future. It would be particularly interesting to establish whether an $(ICl_2)^-$ species is formed using infrared and Raman spectroscopy.

7.2.23 The Reactions of [18]aneN_2S_4 with I_2 and ICl

The reactions of two molar equivalents of I_2 or ICl with [18]aneN_2S_4 in EtOH yielded yellow to orange microcrystalline precipitates similar to the solids obtained from the reaction of ICl and homoleptic S-donor macrocycles in CH_2Cl_2. The products have been isolated but slowly darken on exposure to light until completely black. Both, the initial yellow and the black solid, show good solubility in polar solvents giving orange solutions but are insoluble in non-polar solvents such as CH_2Cl_2, Et_2O and hydrocarbons. These observations are very similar to the ones reported for the preparation of $[I(hmt)_2]^+$ and in sharp contrast to the reactions of I_2 with homoleptic S-donor macrocycles (see above). An indication of the involvement of the N-atoms in the reaction of I_2 with [18]aneN_2S_4 was found in the infrared spectrum. The N-H stretching vibration is shifted by almost 100 cm^{-1} to higher frequency (lower energy) compared with the free ligand. The microanalysis is in good agreement with a stoichiometry of ([18]aneN_2S_4)$(I_2)_2$ but the electron impact mass spectrum (**Figure 7.2.23a**) does not show any peaks which could be assigned to I^+, $(I_2)^+$ or [18]aneN_2S_4. It shows however a fragmentation pattern typical for the macrocyclic ligand. This is in sharp contrast to simple I_2 charge transfer complexes which always show strong peaks assigned to I^+ (m/z = 127) and $(I_2)^+$ (m/z = 254) (see above). These results rule the presence of a simple I_2 charge transfer situation for ([18]aneN_2S_4)$(I_2)_2$ out. We propose therefore that the reaction product between I_2 and [18]aneN_2S_4 is initially an N-donor charge transfer adduct which converts over several days to [I([18]aneN_2S_4)]I_3 which contains an I^+ cation (see above). Attempts to obtain crystals suitable for X-ray diffraction studies failed repeatedly but it would be of much interest to establish the structure of this species.

7.3 CONCLUSION

(i) I_2-thioether charge-transfer complexes

A series of I_2 charge-transfer adducts with homoleptic thioether macrocycles were studied. The geometry of the thioether I_2 donor-acceptor moiety shows the typical features for such an interaction such as linearity and elongation of the I-I bond lengths as a function of the S-I distance. A plot of these I-S against I-I distances combined with reported data gave a smooth graph.

Two distinctively different types of thioether I_2 interactions were identified and termed 'terminal' and 'bridging' thus allowing to divide the complexes studied broadly into two groups. I_2 deficient compounds such as ([12]aneS$_4$)I_2, ([14]aneS$_4$)I_2, ([16]aneS$_4$)I_2 and ([24]aneS$_8$)I_2 show exclusively bridging I_2 moieties between adjacent macrocycles leading to layers of infinite one-dimensional chain structures whereas in contrast I_2 rich compounds such as ([16]aneS$_4$)(I_2)$_4$, ([18]aneS$_6$)(I_2)$_4$ and ([24]aneS$_8$)(I_2)$_6$ show only terminal I_2 molecules giving an overall columnar stacking motif in a matrix of I_2. ([18]aneS$_6$)(I_2)$_4$ and ([24]aneS$_8$)(I_2)$_6$ are the only two examples in this investigation where the I_2 molecules adopt two different *exo* and *endo* co-ordination modes to the macrocycle. The complex ([9]aneS$_3$)$_2$(I_2)$_4$ is the only example which does not fit either category because it shows both terminal and bridging I_2 molecules leading to a complicated three dimensional packing in the crystal lattice.

The general conclusion drawn from these results is that thioether S-donors do not, in contrast to N-donor ligands, cleave the I-I bond to form iodonium complexes. The structural investigation has shown many features (see above) which could not have been obtained with small mono- or bidentate ligands. It would be of interest whether these complexes could be used in reactions with non-activated metal powders similar to the ones reported by McAuliffe[370,418-422,491]:

$$([X]aneS_y)(I_2)_u + M^0 \longrightarrow [M([X]aneS_y)]^{v+} + I^{-}\cdot(I_2)_w$$

Such reactions would be of particular interest in the preparation of polyiodide species (see below).

(ii) Polyiodides

It was our aim to investigate whether large metal macrocyclic cations are able to stabilise polyiodide species in the crystal lattice. The synthesis of '[Ag([18]aneS$_6$)]I$_5$', [Ag([18]aneS$_6$)]I$_3$ and [Ag([18]aneS$_6$)]I$_7$ proved that this is the case. The presence of a symmetrical $(I_3)^-$ anion in the single crystal structure of [Ag([18]aneS$_6$)]I$_3$ is in good agreement with Slater's[492] prediction that large counter-cations force symmetrical $(I_3)^-$ anions (compression). The isolation of the lustrous green compound [Ag([18]aneS$_6$)]I$_7$ which contains the novel highly unusual polymeric $\{(I_7)^-\}_n$ cation supports our view that metal macrocyclic complexes are not only able to stabilise a polyiodide of a certain geometry but also to template this particular geometry. There is some evidence for this in the single crystal structure of [Ag([18]aneS$_6$)]I$_3$ where the main (longest) axes of either ion are aligned parallel.

The initial reaction, which afforded the blue [Ag([18]aneS$_6$)]I$_5$ species was carried out using [Ag([18]aneS$_6$)]BF$_4$ and I$_2$ in MeCN. The I^- anion required for the formation of the polyiodide species had to be generated from I$_2$ by heterolytic cleavage of the I-I bond. We believe that it is highly unlikely that the $[Ag([18]aneS_6)]^+$ cation contributes to this reaction because homoleptic macrocyclic ligands do not cause a cleavage of the I$_2$ bond (see above). The donor capabilities of the co-ordinated macrocycles will even be further diminished by its co-ordination to the Ag(I) ion. We conclude therefore that the solvent (in this case MeCN) is of some importance in this reaction but we cannot exclude the possibility of some sort of catalytic activity of the $[Ag([18]aneS_6)]^+$ cation.

It would be desirable to extend this research area of metal macrocyclic polyiodide species in order to establish the conditions under which polyiodides are formed (influence of the solvent) and which factors (shape, size and charge of the counter-cation) in the solid state influence their geometry.

(iii) Iodonium complexes

The reactions of [18]aneN_2S_4 with I_2 or ICl showed similar features such as precipitation of orange solids and a change of colour from orange to dark brown over several days compared with the preparation of (hmt)I_2 and $[(hmt)_2I]^+$[475]. Spectroscopic and analytical results were in good agreement with the stoichiometry ([18]aneN_2S_4)$(I_2)_2$. The analogy between the preparation of this compound and the synthesis of $[(hmt)_2I]^+$ strongly suggests the presence of a complex containing I^+. A simple co-ordination of the I_2 molecule to thioether S-donors cannot account for the observations such as colour changes. We propose therefore the formula [I([18]aneN_2S_4)]I_3 for this compound.

Unexpectedly the reaction of ICl with homoleptic thioether macrocycles showed also similar features compared to the preparation of (hmt)I_2 and $[(hmt)_2I]^+$. The initial reaction product, an orange microcrystalline solid of the proposed formal stoichiometry '([9]aneS_3)$(ICl)_2$' changes its colour from orange to dark brown over a period of several weeks. from which crystals of the stoichiometry ([9]aneS_3)$_2(I_2)_4$ could be isolated. These examples show that the area of iodonium macrocyclic complexes is by no means trivial. It has to be emphasised that the analogy between *bis*(monodentate) and macrocyclic iodonium complexes is only phenomenological. It is very difficult to judge whether techniques such as halide substitution with Ag(I)-salts which were developed for monodentate N-donor iodonium complexes are applicable in case of macrocyclic ligands or not. For instance it has to be investigated whether Ag^+ competes with I^+ in the co-ordination to the macrocycle.

The overall conclusion is that this area of iodonium macrocyclic chemistry is completely new and the work presented has given some evidence for the successful preparation of macrocyclic I^+ complexes; it also highlights some of the difficulties in dealing with these compounds and further work has to develop techniques to overcome these problems.

7.4 EXPERIMENTAL SECTION

7.4.1 The Synthesis of [Ag([18]aneS$_6$)]I$_5$

[18]aneS$_6$ (90 mg, 0.25 mmol) was dissolved in $CHCl_3$ (3 cm^3) and a solution of $AgBF_4$ (0.25 mmol in 5 cm^3 $MeNO_2$) was added. The clear and colourless solution was then vigorously stirred and a solution of I_2 (0.25 mmol I_2 in 5 cm^3 $CHCl_3$) was added slowly. The colour changed upon addition from colourless, to orange and to violet. A slight cloudiness was removed by passing the solution through a fritted filter funnel (D3). The solvent was removed in vacuo affording a dark blue solid which was collected and characterised. The compound was soluble in polar solvents such as DMF, DMSO, EtOH, $MeNO_2$ affording yellow to brown solutions. A solution in CH_2Cl_2 was purple and the compound was insoluble in Et_2O and hexane.

Microanalysis for ($C_{12}H_{24}AgI_7S_6$; Mol.wt. = 1356.92 gmol^{-1})

	%C	%H
Calculated	10.62	1.78
Found	10.44	2.01

FAB mass spectrum (3-NOBA):

Fragment:	m/z (calc.)	m/z (found)
[$^{107/109}$Ag([18]aneS$_6$)]$^+$	467/469	467/469

IR spectrum (KBr disc):

2920m, 2850w, 1735w, 1700w, 1685w, 1655m, 1635m, 1560w, 1540w, 1460m, 1420m, 1260w, 1085vs and 800w cm^{-1}.

Cyclic Voltammetry (0.1moll^{-1} $TBAPF_6$; MeCN; 293K, scan speed 0.2 V s^{-1})

$E_{red.}$ [irreversible]	-0.39V vs Fc/Fc$^+$	(-0.42 vs Fc/Fc$^+$)[344,346]
$E_{ox.}$ [irreversible]	+0.9V vs Fc/Fc$^+$	(+1.00 vs Fc/Fc$^+$)[344,346]
$E_{demet.}$	-0.03V vs Fc/Fc$^+$	

7.4.2 The Synthesis of [Ag([18]aneS$_6$)]I$_3$

[Ag([18]aneS$_6$)]I$_3$ was isolated by recrystallisation of '[Ag([18]aneS$_6$)]I$_5$' in EtOH. Dark brown crystals were collected from the bottom of the sample vial and characterised.

Microanalysis for ($C_{12}H_{24}AgI_3S_6$; Mol.wt. = 849.30 $gmol^{-1}$)

	%C	%H
Calculated	16.97	2.85
Found	17.34	2.77

FAB mass spectrum (3-NOBA):

Fragment:	m/z (calc.)	m/z (found)
$[^{109}Ag([18]aneS_6)]^+$	469	468

7.4.3 The Synthesis of $[Ag([18]aneS_6)]I_7$

$[Ag([18]aneS_6)]I_7$ was isolated by recrystallisation of '$[Ag([18]aneS_6)]I_5$' in MeCN. Green lustrous crystals were collected from the bottom of the sample vial and characterised.

Microanalysis for ($C_{12}H_{24}AgI_7S_6$; Mol.wt. = 1356.88 $gmol^{-1}$)

	%C	%H
Calculated	10.62	1.78
Found	11.11	1.76

FAB mass spectrum (3-NOBA):

Fragment:	m/z (calc.)	m/z (found)
$[^{109}Ag([18]aneS_6)]^+$	469	469

7.4.4 The Synthesis of $([9]aneS_3)_2(I_2)_4$

$[9]aneS_3$ (45 mg, 0.25 mmol) was dissolved in CH_2Cl_2 (1.0 cm^3) and a solution of ICl (0.156 mol cm^{-3}) in CH_2Cl_2 was added dropwise. The reaction mixture stayed clear during addition of the first molar equivalent of ICl (1.56 ml) but a yellow solid was formed upon further addition. The precipitate was collected, washed with a small portion of cold n-hexane and air dried on the filter funnel. The orange solid was stored in a sample vial for nine months until it became clear that red needle shaped crystals grew from the now dark orange solid. It is notable that no I_2, which would have colourised the white PVC lid of the sample vial, was liberated during this time.

Similar reactions were carried out using $[12]aneS_4$, $[14]aneS_4$, $[16]aneS_4$, $[15]aneS_5$ and $[18]aneS_6$. All gave the characteristic orange precipitate after addition of 2 molar equivalents of ICl in CH_2Cl_2. However, none of them showed any growth of crystalline material upon standing.

[9]aneS$_3$ + 2 ICl

IR spectrum (CsI disc):

2900m, 1655w, 1405vs, 1280s, 1210m, 1150m, 935m, 835m and 670m cm^{-1}.

[14]aneS$_4$ + 2 ICl

Microanalysis for ($C_{10}H_{20}Cl_2I_2S_4$; Mol.wt. = 593.24 gmol^{-1})

	%C	%H
Calculated	20.24	3.40
Found	20.30	3.54

IR spectrum (KBr disc):

2925m, 1425vs, 1270m, 1250w, 1200s, 1135m, 1010m, 725w, 690s and 675m cm^{-1}.

[16]aneS4 + 2 ICl

FAB mass spectrum (3-NOBA):

Fragment:	m/z (calc.)	m/z (found)
[I([16]aneS$_4$)]$^+$	423	423

7.4.5 The Synthesis of Iodine Charge Transfer Complexes containing Homoleptic S-Donor Macrocycles

Solid charge-transfer adducts between thioether macrocycles and I_2 were prepared by allowing a mixture of a solution of I_2 in CH_2Cl_2 and the appropriate thioether macrocycle ([9]aneS$_3$, [12]aneS$_4$, [14]aneS$_4$, [16]aneS$_4$, [15]aneS$_5$, [18]aneS$_6$ and [24]aneS$_8$) dissolved in CH_2Cl_2 (0.1-0.025 mmol macrocycle in 5 cm^3 solvent) to slowly evaporate. The formation of I_2 thioether charge transfer adducts in solution was evident by the colour change from violet (I_2 in CH_2Cl_2) to brown (I_2 thioether adduct). Solid material deposited slowly on the surface of the reaction vessel which was collected and characterised. It has to be emphasised that the material collected does not necessarily contain only one compound. This is reflected in the in part large deviations between 'calculated' and 'found' values in the microanalytical results.

Compound:	M / $gmol^{-1}$	%C calc.	%C found	%H calc.	%H found
$([9]aneS_3)_2(I_2)_4$	1375.88	10.48	11.23	1.76	1.78
$([9]aneS_3)(I_2)_3$	941.79	7.65	7.71	1.28	1.34
$([12]aneS_4)I_2$	494.28	19.44	19.40	3.26	3.30
$([14]aneS_4)I_2$	522.33	23.00	23.00	3.86	3.94
$([16]aneS_4)(I_2)_4$	1311.79	10.99	13.03	1.84	2.18
$([15]aneS_5)I_2$	1214.28	11.87	10.81	1.66	1.76
([18]aneS6)(I2)4	1375.88	10.48	8.14	1.76	1.29
$([24]aneS8)I_2$	734.76	26.15	26.39	4.39	4.49
$([24]aneS8)(I_2)_6$	2003.76	9.59	10.59	1.60	1.70

Table 7.4.5a Microanalytical results for charge transfer adducts of I_2 with homoleptic thioether macrocycles.

EI mass spectroscopic measurements (**Table 7.4.5b**) were dominated in every single case by the presence of peaks at m/z = 254 and m/z = 127 assigned to $(I_2)^+$ and $(I)^+$. The molecular ion peak for the free macrocycle was observed in some cases in particular with small macrocycles {[9]aneS_3 and [14]aneS_4 (**Figure 7.2.18**)} however the overall molecular ion peak of the adduct has never been observed.

Compound	I^+ (m/z = 127)	$(I_2)^+$ (m/z = 254)	Ligand calc.	found
$([9]aneS_3)_2(I_2)_4$	127	254	180	180
$([14]aneS_4)I_2$	127	254	268	268
$([24]aneS_8)(I_2)_6$	127	254	480	-

Table 7.4.5b EI mass spectrometry results for charge transfer adducts of I_2 with homoleptic thioether macrocycles.

7.4.6 The Reactions of I_2 with [18]aneN_2S_4

The reaction of [18]aneN_2S_4 (32.7 mg, 0.1 mmol) with 1 molar equivalents of I_2 (25.4 mg, 0.1 mmol) in EtOH (5 cm^3) afforded an orange solution. Addition of a second molar equivalent of I_2 (25.4 mg, 0.1 mmol) yielded an orange precipitate which was isolated, dried and characterised. The compound darkened slowly when exposed to light until it became black. A reference sample stored in the freezer (at -20 - -25°C) did not show any colour changes at all.

Microanalysis for ($C_{12}H_{26}I_4N_2S_4$; Mol.wt. = 834.22 g mol^{-1})

	%C	%H	%N
Calculated	17.27	3.14	3.36
Found	17.13	3.17	3.50

IR spectrum (KBr disc, Range 3500-2500cm^{-1}):

[18]aneN_2S_4	3235 (υ-NH), 2950, 2910, 2870, 2820 and 2740 cm^{-1}.
[I_4([18]aneN_2S_4)]	3140 (υ-NH), 2880 and 2850 cm^{-1}.

7.4.7 Single Crystal Structure Determinations

Crystallographic details for the single crystal structures described in this chapter are summarised in **Tables 7.4.7a** to **7.4.7d**. A problem common to all thioether I_2 charge-transfer adducts was deterioration or evaporation during data collection at ambient temperature. Data collection on these compounds was therefore undertaken at low temperature (150.0 K) in a stream of dry N_2.

Compound	$[Ag([18]aneS_6)]I_3$	$[Ag([18]aneS_6)]I_7$	$([9]aneS_3)_2(I_2)_4$
Crystal data			
Formula	$C_{12}H_{24}AgS_6I_3$	$C_{12}H_{24}AgI_7S_6$	$C_{12}H_{24}I_8S_6$
M / gmol^{-1}	849.29	1356.84	1375.88
Crystal size / mm	0.16 x 0.16 x 0.38	0.12 x 0.15 x 0.23	0.04 x 0.08 x 0.70
Crystal system	monoclinic	trigonal	triclinic
Space group	*C* 2/*m* (No. 12)	*R* -3*m* (No. 166)	*P* -1 (No. 2)
a / Å	18.5767 (11)	9.458 (4)	8.437 (7)
b / Å	11.9188 (7)	*a*	13.820 (18)
c / Å	5.2714 (5)	*a*	14.752 (10)
α / °	90	103.79 (3)	65.95 (5)
β / °	95.634 (9)	α	89.31 (4)
γ / °	90	α	81.08 (4)
U / Å^3	1161.5	758.0	1549.0
Z	2	1	2
D_c / gcm^{-3}	2.428	2.972	2.949
μ / mm^{-1}	5.389	8.207	8.320
F(000)	796	610	1232
T / K	280	150.0	150.0
Reflections at $\pm\omega$ to refine cell	32	18	20
2θ range / °	29 - 32	30 - 32	25 - 26
Data Collection			
$2\theta_{max}$ / °	50	45	40
Range of h	-22 → 22	-10 → 9	-8 → 8
Range of k	-14 → 14	-10 → 4	-11 → 13
Range of l	-1 → 6	-10 → 9	0 → 14
Measured reflections	2740	1332	2897
Independent reflections, R_{int}	1074, 0.013	383, 0.060	2897
Observed reflections	988 with $F \geq 2\sigma(F)$	380 with $F \geq 2\sigma(F)$	2405 with $F \geq 4\sigma(F)$
ψ scan correction $TF_{max, min}$	0.164, 0.131	0.368, 0.299	0.891, 0.269
Solution			
Method	Patterson Synzhesis	Patterson Synthesis	Direct Methods
using	SHELXS-86	SHELXS-86	SHELXS-86
Refinement			
full matrix least squares on	F^2	F^2	F
using	SHELXL-93	SHELXL-93	SHELX76
DIFABS max, min	-	-	1.390, 0.643
Weighting scheme	0.0181, 2.04		$9.61 \cdot 10^{-4}$
Parameters refined	58	37	177
SHELX76 *R, R´, S*	-	-	0.057, 0.073, 0.85
SHELXL-93 *R1, wR2, S*	0.018, 0.042, 1.081	0.019, 0.039, 1.11	-
$(\Delta/\sigma)_{max}$	0.250	0.000	0.001
$\Delta\rho_{max, min}$ / eÅ^{-3}	+0.44, -0.58	+0.41, -1.07	+2.23, -1.86

Table 7.4.7a Selected crystallographic data for the single crystal structures of $[Ag([18]aneS_6)]I_3$, $[Ag([18]aneS_6)]I_7$ and $([9]aneS_3)_2(I_2)_4$.

Compound	$([12]aneS_4)I_2$	$([14]aneS_4)I_2$	$([16]aneS_4)I_2$
Crystal data			
Formula	$C_{12}H_{24}I_3S_6$	$C_{10}H_{20}I_2S_4$	$C_{12}H_{24}I_2S_4$
M / gmol^{-1}	494.25	522.31	550.39
Crystal size / mm	0.12 x 0.33 x 0.35	0.05 x 0.25 x 0.30	0.04 x 0.15 x 0.31
Crystal system	monoclinic	orthorhombic	triclinic
Space group	$P\,2_1/c$ (No. 14)	$P\,bca$ (No. 61)	P-1 (No. 2)
a / Å	13.882 (4)	9.7030 (11)	5.420 (14)
b / Å	8.550 (3)	17.5093 (17)	8.05 (4)
c / Å	19.653 (6)	19.4450 (23)	10.74 (3)
α / °	90	90	97.4 (3)
β / °	109.44 (3)	90	95.15 (21)
γ / °	90	90	94.9 (3)
U / Å^3	2190	3304	461
Z	4	8	1
D_c / gcm^{-3}	2.249	2.100	1.984
μ / mm^{-1}	4.782	4.232	3.852
F(000)	1404	2000	266
T / K	150.0	150.0	150.0
Reflections at $\pm\omega$ to refine cell	34	47	8 (matrix refined)
2 θrange / °	24 - 26	30 - 32	24 - 26
Data Collection			
$2\theta_{max}$ / °	45	45	45
Range of h	-14 → 14	0 → 10	-5 → 5
Range of k	0 → 9	0 → 18	-8 → 8
Range of l	0 → 21	0 → 20	0 → 11
Measured reflections	3097	3200	1204
Independent reflections, R_{int}	2742	1930, 0.014	1204
Observed reflections	2589 with $F \geq 4\sigma(F)$	1462 with $F \geq 4\sigma(F)$	1053 with $F \geq 2\sigma(F)$
ψ scan correction $TF_{max,\ min}$	0.411, 0.238	0.398, 0.198	0.337, 0.219
Solution			
Method	Direct Methods	Patterson Synthesis	Patterson Synthesis
using	SHELXS-86	SHELX76	SHELXS-86
Refinement			
full matrix least squares on	F	F	F^2
using	SHELX76	SHELX76	SHELXL-93
DIFABS max, min	-	1.245, 0.811	1.236, 0.667
Weighting scheme	$3.63 \cdot 10^{-4}$	$2.06 \cdot 10^{-4}$	0.1647, 1.14
Parameters refined	201	147	82
SHELX76 R, R', S	0.037, 0.056, 1.01	0.037, 0.041, 0.99	-
SHELXL-93 $R1$, $wR2$, S	-	-	0.073, 0.199, 1.09
$(\Delta/\sigma)_{max}$	0.001	0.032	0.051
$\Delta\rho_{max,\ min}$ / eÅ^{-3}	+1.24, -1.37	+0.84, -0.77	+2.93, -1.96

Table 7.4.7b Selected crystallographic data for the single crystal structures of $([12]aneS_4)I_2$, $([14]aneS_4)I_2$ and $([16]aneS_4)I_2$.

Compound	$([16]aneS_4)(I_2)_4$	$([15]aneS_5)(I_2)_3(I_2)_{0.5}$	$([18]aneS_6)(I_2)_4$
Crystal data			
Formula	$C_{12}H_{24}I_8S_4$	$C_{10}H_{20}I_{7.2}S_5$	$C_{12}H_{24}I_8S_6$
M / gmol^{-1}	1311.76	1214.24	1375.88
Crystal size / mm	0.10 x 0.20 x 0.25	0.31 x 0.38 x 0.78	0.05 x 0.12 x 0.15
Crystal system	monoclinic	monoclinic	triclinic
Space group	*C* 2/*c* (No. 15)	*P* 2_1/*c* (No. 14)	*P*-1 (No. 2)
a / Å	21.236 (8)	8.607 (5)	9.123 (3)
b / Å	11.693 (6)	10.100 (4)	9.153 (4)
c / Å	14.771 (6)	33.019 (23)	10.408 (4)
α / °	90	90	82.030 (22)
β / °	123.710 (14)	92.51 (5)	68.352 (17)
γ / °	90	90	77.89 (3)
U / Å^3	3051	2867	788
Z	8	4	1
D_c / gcm^{-3}	2.855	2.813	2.899
μ / mm^{-1}	8.315	8.152	8.178
F(000)	2336	2166	616
T / K	150.0	150.0	150.0
Reflections at ±ω to refine cell	23	40	14
2θ range / °	26 - 32	27 - 32	30 - 32
Data Collection			
$2\theta_{max}$ / °	45	50	50
Range of *h*	-22 → 15	-10 → 10	-9 → 10
Range of *k*	-12 → 0	0 → 12	-10 → 10
Range of *l*	-15 → 15	0 → 39	0 → 12
Measured reflections	2105	5552	2778
Independent reflections, R_{int}	1827	4974, 0.033	2665
Observed reflections	1712 with $F \geq 4\sigma(F)$	4889 with $F \geq 2\sigma(F)$	2450 with $F \geq 4\sigma(F)$
ψ scan correction $TF_{max, min}$	0.906, 0.557		0.648, 0.382
Solution			
Method	Direct Methods	Patterson Synthesis	Direct Methods
using	SHELXS-86	SHELXS-86	SHELXS-86
Refinement			
full matrix least squares on	F	F^2	F
using	SHELX76	SHELXL-93	SHELX76
DIFABS max, min	-	1.126, 0.771	-
Weighting scheme	$0.48 \cdot 10^{-4}$	0.0598, 44.35	$2.83 \cdot 10^{-4}$
Parameters refined	112	218	120
SHELX76 *R, R´, S*	0.027, 0.032, 1.12	-	0.028, 0.039, 1.02
SHELXL-93 *R1, wR2, S*	-	0.052, 0.167, 1.06	-
$(\Delta/\sigma)_{max}$	0.001	0.000	0.002
$\Delta\rho_{max, min}$ / eÅ^{-3}	+1.63, -1.30	+1.86, -1.26	+1.00, -1.06

Table 7.4.7c Selected crystallographic data for the single crystal structures of $([16]aneS_4)(I_2)_4$, $([15]aneS_5)(I_2)_3(I_2)_{0.5}$ and $([18]aneS_6)(I_2)_4$.

Compound	([24]aneS$_8$)I$_2$	([24]aneS$_8$)(I$_2$)$_6$
Crystal data		
Formula	$C_{16}H_{32}I_2S_8$	$C_{16}H_{32}I_{12}S_8$
M / gmol^{-1}	734.76	2006.70
Crystal size / mm	0.16 x 0.39 x 0.43	0.12 x 0.51 x 0.58
Crystal system	monoclinic	monoclinic
Space group	$P2_1/a$ (alt. $P2_1/c$; No. 14)	$P\,2_1/c$ (No. 14)
a / Å	9.547 (5)	14.784 (6)
b / Å	8.599 (6)	8.269 (4)
c / Å	16.367 (12)	18.587 (8)
α / °	90	90
β / °	102.70 (5)	98.73 (3)
γ / °	90	90
U / Å^3	1310.7	2246.0
Z	2	2
D_c / gcm^{-3}	1.861	2.963
μ / mm^{-1}	3.04	8.66
F(000)	724	1784
T / K	150.0	150.0
Reflections at $\pm\omega$ to refine cell	10 (matrix refined)	45
2θ range / °	30 - 32	28 - 32
Data Collection		
$2\theta_{max}$ / °	45	50
Range of h	$-10 \rightarrow 8$	$-17 \rightarrow 17$
Range of k	$0 \rightarrow 9$	$0 \rightarrow 9$
Range of l	$0 \rightarrow 17$	$0 \rightarrow 22$
Measured reflections	1829	4383
Independent reflections, R_{int}	1685	3750, 0.025
Observed reflections	1519 with $F \geq 2\sigma(F)$	3720 with $F \geq 2\sigma(F)$
ψ scan correction $TF_{max,\ min}$	0.400, 0.236	0.523, 0.098
Solution		
Method	Patterson Synthesis	Direct Methods
using	SHELXS-86	SHELXS-86
Refinement		
full matrix least squares on	F^2	F^2
using	SHELXL-93	SHELXL-93
DIFABS max, min	-	1.138, 0.814
Weighting scheme	0.0807, 2.28	0.0617, 21.96
Parameters refined	120	165
SHELX76 R, R', S	-	-
SHELXL-93 $R1$, $wR2$, S	0.038, 0.158, 1.58	0.035, 0.126, 1.30
$(\Delta/\sigma)_{max}$	0.008	0.000
$\Delta\rho_{max,\ min}$ / eÅ^{-3}	+1.14, -1.32	+1.33, -1.04

Table 7.4.7d Selected crystallographic data for the single crystal structures of ([24]aneS$_8$)I$_2$ and ([24]aneS$_8$)(I$_2$)$_6$.

APPENDIX

A.1 Abbreviations

^{31}P-{^{1}H}-NMR ..... proton decoupled ^{31}P-NMR
a..... *anti*
A..... acceptor
Å..... Ångström (1 Å = 100 pm)
acac..... acetylacetonate
AcO ..... acetate
BEDT-TTF..... bis(ethylenedithio)tetrathiafulvalene
^{i}Bu..... *iso*-butyl
^{n}Bu ..... *n*-butyl
Bz..... benzyl
cal..... calorie (1cal = 4.184J)
Cp ..... cyclopentadienyl
Cp* ..... pentamethylcyclopentadienyl
d ..... doublet (NMR)
D..... deuterium (i.e. ^{2}H) or donor
DEPT ..... distortionless enhancement by polarisation transfer
DMF ..... dimethylformamide
DMSO ..... dimethylsulphoxide
EI ..... electron impact or electron ionisation
en ..... diethylenediamine
eq ..... equatorial
e.s.d.(s)..... estimated standard deviation(s)
Et ..... ethyl
FAB ..... fast atom bombardment
Fc/Fc^{+} ..... ferrocene / ferrocenium
g ..... *gauche*
HOMO..... highest occupied molecular orbital
h.s. ..... high spin
IR..... infrared
l.s. ..... low spin
LUMO ..... lowest unoccupied molecular orbital

m ..... medium (IR), multiplet (NMR)
Me ..... methyl
MHz ..... megahertz
MO ..... molecular orbital
Mol.wt. ..... molecular weight
MS ..... mass spectroscopy
NIR ..... near infrared
NMR ..... nuclear magnetic resonance
3-NOBA 3-nitrobenzylalcohol
OEP ..... octaethylporphyrin
ox ..... oxalate
Ph ..... phenyl
ppm ..... parts per million
^{i}Pr ..... *iso*-propyl
py ..... pyridine
s ..... strong (IR), singlet (NMR)
sh ..... shoulder (UV/vis)
s.o.f.(s) ..... site occupancy factor(s)
t ..... triplet (NMR)
hmt ..... hexamethylenetetramine
TBAPF6 ..... tetra(*n*-butyl)ammonium hexafluorophosphate
TTP ..... tetraphenylporphyrin
UV/vis ..... ultraviolet / visible
v.d.W. ..... van der Waals
vs ..... very strong (IR)
v/v ..... volume by volume
w ..... weak (IR)
· ..... Peaks in NMR spectra marked with a black dot are either solvents or impurities.

A.2 Ligands - Nomenclature and Structure

The nomenclature used in this thesis is based closely on the scheme described by Melson[493]. The alternative 'crown' notation which is the widely accepted scheme for naming homoleptic crown-ethers has not been used in order to maintain consistency throughout this thesis.

An abbreviation such as [18]aneS_2O_4 has to be interpreted in the following way. The number in square brackets denotes the ring size, in this case an 18-membered ring. The syllable 'ane' is derived from the corresponding alkane and implies a fully saturated hydrocarbon framework. Heteroatoms are added at the end with subscripts indicating their number as in any usual chemical formula. It should be noted that this scheme is not without ambiguity but it provides an efficient way to identify a certain macrocyclic ligand. The following illustrations (**Figure A.2a to A.2d**) show the ligands mentioned in this thesis and the abbreviations used.

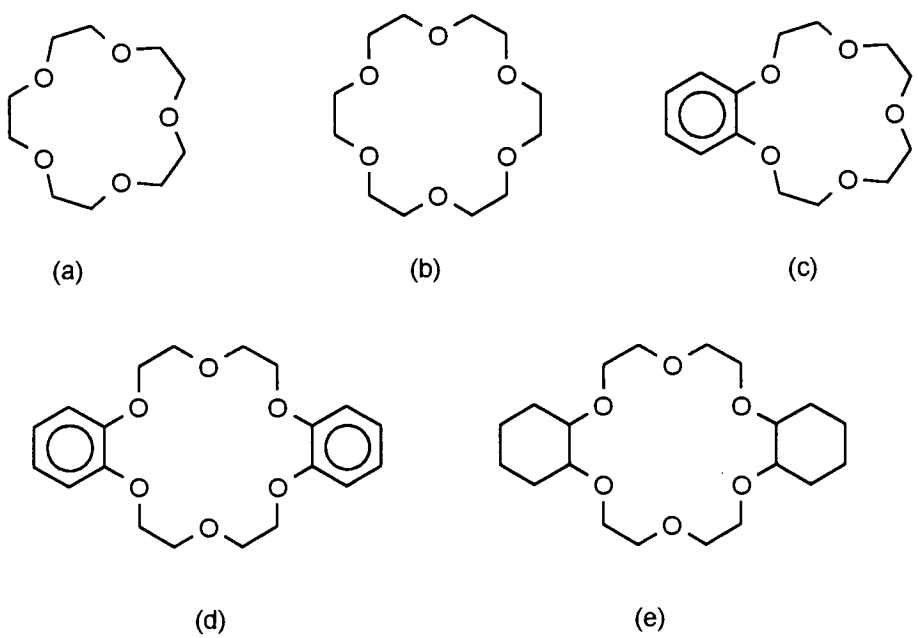

(a) [15]aneO_5, (b) [18]aneO_6, (c) benzo[15]aneO_5, (d) dibenzo[18]aneO_6
(e) dicyclohexano[18]aneO_6

Figure A.2a Crown ether derivatives.

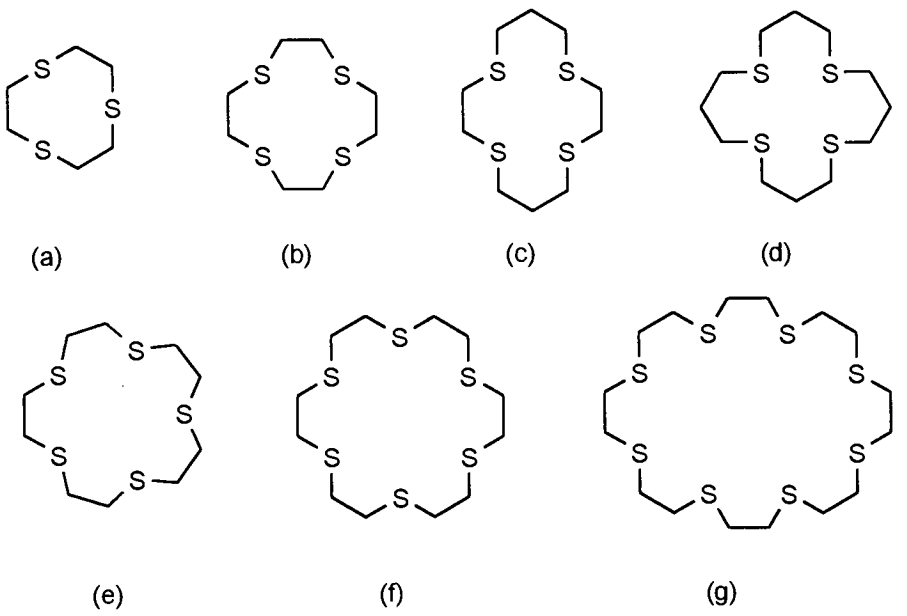

(a) [9]aneS_3, (b) [12]aneS_4, (c) [14]aneS_4, (d) [16]aneS_4, (e) [15]aneS_5, (f) [18]aneS_6, (g) [24]aneS_8

Figure A.2b Homoleptic thioether macrocycles.

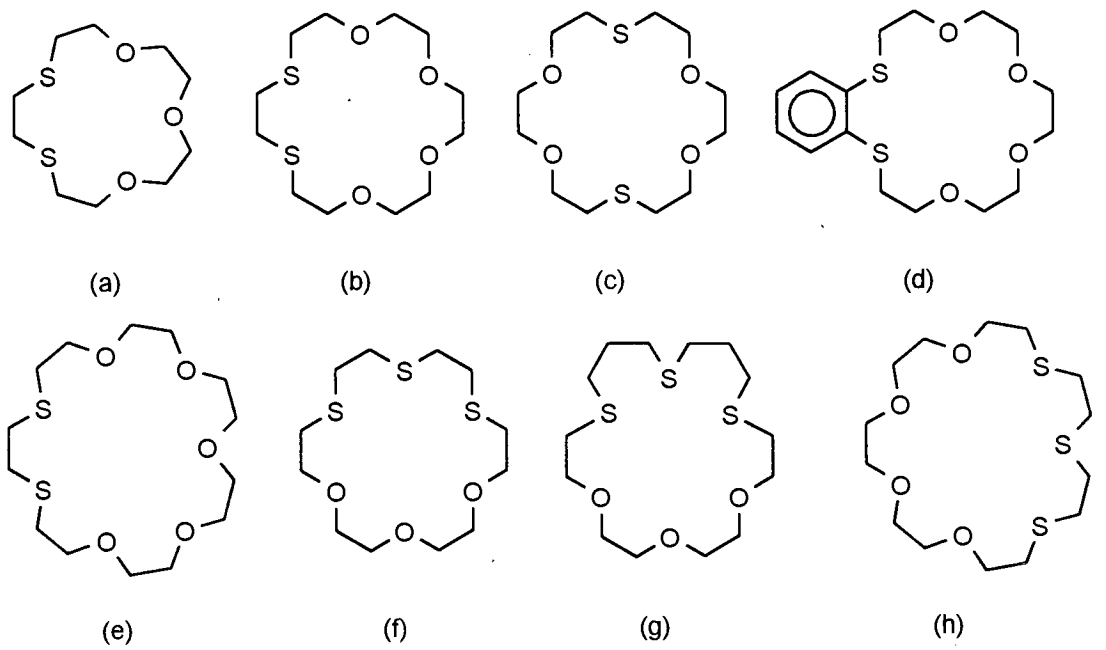

(a) [15]aneS_2O_3, (b) [18]aneS_2O_4, (c) 1,10-[18]aneS_2O_4, (d) benzo[18]aneS_2O_4 (e) [21]aneS_2O_5 (f) [18]aneS_3O_3, (g) [20]aneS_3O_3, (h) [21]aneS_3O_4

Figure A.2c Mixed O/S donor ionophores.

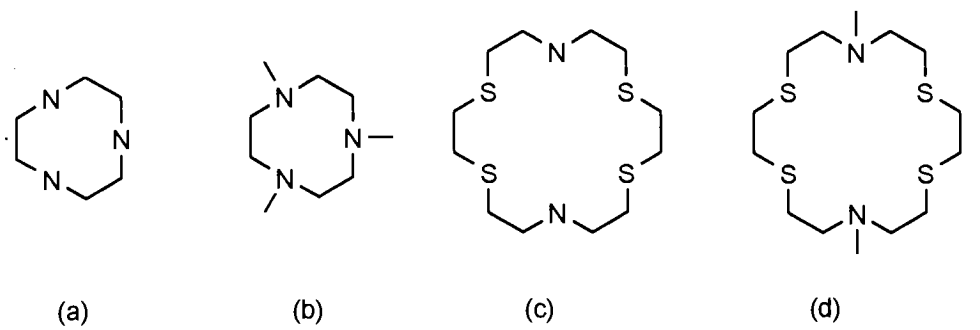

(a) [9]aneN$_3$, (b) Me$_3$[9]aneN$_3$, (c) [18]aneN$_2$S$_4$, (d) Me$_2$[18]aneN$_2$S$_4$

Figure A.2d Macrocycles containing N-donors.

A.3 Materials and Methods

Commercial $RuCl_3$, $PdCl_2$ (*Johnson & Matthey plc*) and $Pd(OAc)_2$ (*Lancaster Synthesis*) were used as supplied. The homoleptic thioether macrocycles ([9]aneS$_3$, [12]aneS$_4$, [14]aneS$_4$, [16]aneS$_4$, [15]aneS$_5$, [18]aneS$_6$, [24]aneS$_8$ and [28]aneS$_8$) (*Aldrich*), the mixed N/S-donor ionophore [18]aneN$_2$S$_4$ (*Lancaster Synthesis*) and standard solvents were used as supplied without further purification. High purity solvents or dry solvents were prepared according to standard laboratory techniques by distillation.

Microanalyses were carried out by The University of Edinburgh microanalytical service. IR spectra were recorded in the range 4000 to 250 cm^{-1} on a Perkin-Elmer 598 infrared spectrometer and in the range 4000 to 400 cm^{-1} on a Perkin Elmer FT-1600 Fourier transform infrared spectrometer. NMR spectra were measured on Joel JNM-PMX60SI 60 (^1H), Joel FX90Q (^{31}P), Bruker WP80 (^1H), WP200 (^1H, ^{13}C, ^{31}P), AC250 (^1H, ^{13}C) and WH 360 (^1H, ^{13}C, ^{31}P) nuclear magnetic resonance spectrometer. The samples were placed in 5 mm NMR tubes containing a deuterated solvent. Mass spectra were acquired using Kratos MS902 (EI-mass spectra; m/z = 0-500) and Kratos 50TC (EI-and FAB-mass spectra; m/z = 0-4000) mass spectrometers. UV/vis spectra were recorded on a Perkin Elmer Lambda 9 UV/vis/NIR spectrophotometer (Path 0.03 to 1.0 cm). X-ray fluorescence measurements were carried out using a Philips PW1480 X-ray fluorescence spectrometer using Rh X-radiation. (Department of Geology, The University of Edinburgh). The samples were measured either in tablets of borax or on a thin plastic film.

Electrochemical measurements were performed on a Bruker E310 Universal Modular Polarograph. All readings were taken using a three-electrode potentiostatic system in MeCN containing 0.1 mol dm^{-3} TBAPF6 as supporting electrolyte. Cyclic voltammetric measurements were carried out using a double Pt-electrode and a Ag/AgCl reference electrode. All potentials were quoted *versus* Fc/Fc^{+}.

A.4 Crystallographic Techniques

This section outlines briefly the instrumentation and general procedures involved in single crystal X-ray structure determination and cites the appropriate references. A comprehensive summary of crystallographic data is summarised at the end of each experimental section. Features such as severe disorder peculiar to a certain structure and deviating largely from the general procedures outlined below are covered in the results and discussion sections. All single crystal X-ray structures apart from [15]aneS_2O_3 and [21]aneS_2O_5 have been solved and refined by the author himself.

(i) Data collection

All crystals were examined prior to data collection using a polarising microscope. Crystals suitable for data collection were mounted on a Stoë Stadi-4 four circle diffractometer. An Oxford Cryosystems low temperature device[494] operating at a 150K was used in cases where sample cooling was required. The radiation used was in all cases graphite-monochromated Mo-K_α X-radiation. Software used in collecting and processing the data include on-line profile-fitting (learnt-profile method)[495] , DIF4 (diffractometer control program)[496], REDU4 (data reduction program)[497] and semi-empirical absorption correction using ψ scans[498].

(ii) Space group determination

Space group determination was carried out by combining Bravais lattice information obtained prior to data collection with an analysis of systematic absences and intensity statistics. Bravais lattice determination utilised DIF4[496] and the other information was derived using programs such as ST4REF[499] and XPREP[500].

(iii) Structure solution

The structures were solved by employing either an automatic direct methods (SHELXS-86[501]) approach or a Patterson synthesis (SHELX76[502] or SHELXS-86[501]). The choice of method took into consideration the expected unitcell contents. Structures containing only a few heavy atoms (transition metals or iodine) were solved using a Patterson synthesis. Direct methods were used in cases of structures without heavy atoms or structures containing a range of heavy atoms (I_2 rich compounds) leading in most cases to a sensible fragment. Development of each structure was achieved by alternating cycles of least squares refinement and difference Fourier synthesis. DIRDIF[503] was used in one case and all non H-atoms were found.

(iv) Refinement

Refinement was carried out using two different software packages. SHELX76[502] which refines against F was used in early stages of this investigation. Refinement against F^2 was carried out using SHELXL-93[504] which became available recently. The weighting scheme, S, R and R' are consequently defined differently for refinement against F and F^2. R for SHELX76 and $R1$ for SHELXL-93 are broadly comparable. Values based on F^2 are in general larger compared with those based on F. A comprehensive discussion of these values and their definition can be found in the program documentation.

Refinement and development of the structure to isotropic convergence was achieved using alternating cycles of least squares refinement and difference Fourier synthesis. Residual peaks near heavy atoms at isotropic convergence justified empirical corrections for absorption using DIFABS[505]. The final stages of refinement included addition of H-atoms in calculated positions and anisotropic refinement of the temperature factors of non H-atoms. Thermal parameters (U_{iso}) for H-atoms were either fixed at a common U_{iso}, refined commonly using a free variable or fixed to 1.2 (CH_2) of the U_{iso} of the appropriate C-atom. Weighting schemes were introduced in the latter stages of refinement (SHELX76) or included throughout (SHELXL-93); extinction correction parameters were refined in appropriate cases.

(v) Dealing with problems

The most common crystallographic problem encountered during this investigation has been disorder. The moieties affected include spherical counterions such as PF_6^- and the flexible polyether chain in macrocycles. In general, the disorder was modelled by including two or more alternative positions with appropriate site occupancies for each affected atom. Thermal parameters were initially refined isotropically. At isotropic convergence H-atoms were added in calculated positions and refined using a riding model. In cases of a large difference between the site occupancies (e.g. 80%/20%) thermal parameters were refined anisotropically for the atoms with a higher occupancy.

Problems closely related to disorder include extreme temperature factors and chemically unrealistic bond lengths and angles. Strongly discrepant bond lengths and angles were restrained to sensible values (C-O 1.42, C-C 1.52, C-S 1.82Å) using free variables. Restrained bond lengths and angles are not tabulated in the results and discussion sections.

(vi) Evaluation of the structure

A refinement was judged to be complete after all necessary parameters had been allowed to refine and their relative shifts in the final cycle were negligible [i.e. $(\Delta/\sigma)_{max} << 1$]. The residuals had to be acceptably low, allowing for the nature of the compound and any residual, uncorrectable effects such as those of absorption, disorder, twinning or crystal quality. ΔF residuals had also to be low, allowing for the nature of the structure, and any significant peak had to lie in reasonable locations such as close to a heavy atom or in a region affected by disorder. The analysis of variance should not have shown bias as a function of reflection intensity, Bragg angle, h, k or l. The refined parameters and their e.s.d.s had to be reasonable, in particular, thermal parameters had to be reasonably low and similar for similar atoms. Derived molecular geometry had to appear chemically sensible and chemically equivalent bonds and angles had to have similar values. An experienced crystallographer was always consulted throughout refinement to advise on or confirm decisions.

Tables of bond lengths, angles, torsion angles, intermolecular distances, fractional co-ordinates, temperature factors and structure factor tables were prepared using CALC[506], SHELX76[502] and SHELXL-93[504]. Molecular plots and packing diagrams were prepared using XP[500], Cameron[507] and WinModel[508].

A.5 Computing

(i) Instrumentation

Crystal structure solutions, refinement and molecular mechanics calculations were accomplished using two mainframe computers of the Edinburgh University Computing Service (EUCS). Both machines, *castle* and *festival*, are Sequent Symmetry 2000/750 systems based on Intel 386 and 486 processors. Each system contains 18 processors, 200 Mbytes of main memory, and approximately 20 Gbytes of disc space. Both systems operate under UNIX. Other computers include Sun Workstations running X and IBM compatible i386/486 personal computers running MS-DOS 5.0 and MS-Windows 3.1.

(ii) Online Databases

Online crystallographic database searches in the CSSR[510] and ICSD[511] databases were conducted using the remote service of the SERC at Daresbury[509]. Online literature database searches were carried out using BIDS[512].

(iii) Mass Spectrum Pattern Simulation - MSPS

The programs *MSPS 2.0* (*MS-DOS*) and *WinMSPS 1.0* (*MS-Windows 3.1*) have been developed by the author parallel to the work presented in this thesis. Both programs have been coded in 'C' using *Borland C++ 3.0*, *Microsoft Visual C++ 1.0* and the *Microsoft Software Developers Toolkit (SDK)*. The purpose of the programs is to generate the mass spectrum peak pattern for a given fragment using a table of isotopic abundancies. *MSPS* has been routinely used to analyse mass spectra during the research presented in this thesis.

(iv) Representation of Crystallographic Data - WinModel

The program *WinModel* (*MS-Windows 3.1*) is a primitive but fast and highly optimised ray-tracing program which converts SHELX-76 and SHELXL-93 files into 256-colour space-filling images. The program has been developed by the author parallel to the work presented in this thesis and is coded in 'C' using *Microsoft Visual C++ 1.0* and the *Microsoft Software Developers Toolkit (SDK)*.

(v) Molecular Mechanics Calculation

Molecular mechanics calculations were carried out using the molecular mechanics software package MM3(92)[272] running on *festival*. Initial generic structures were produced using MINP[271].

A.6 Publications

A.6.1 Paper

1) 'Structural Mis-Matches in Silver and Gold Complexes of Thioether Macrocycles'
A.J.Blake, R.O.Gould, C.Radek, A.Taylor, M.Schröder, in 'The Chemistry of the Copper and Zinc Triads', Eds. A.J.Welch and S.K.Chapman, pp. 95-101, The Royal Society of Chemistry, 1993.

2) 'The Low Temperature X-Ray Structure of Tetra-n-butyl ammonium trifluorosulphate' A.J.Blake, C.Radek, M.Schröder, *Acta Cryst.*, 1651, **C49** (1993).

3) 'The Low Temperature Single X-Ray Structure of Bis-(1,4,7-trithiacyclononane-bis-diiodine) $[([9]aneS_3)_2(I_2)_2]$ ([9]aneS$_3$ = 1,4,7-trithiacyclononane)' A.J.Blake, R.O.Gould, C.Radek, M.Schröder, *J.Chem.Soc., Chem.Commun.*, 1191 (1993).

4) 'The Synthesis and Single Crystal X-Ray Structure of the Tetrameric Silver(I) Complex $\{[Ag_2([18]aneS_2O_4)_2]_2\}(PF_6)_4$ ([18]aneS$_2$O$_4$ = 1,4,7,10-tetraoxa-13,16-dithiacyclooctadecane)' A.J.Blake, R.O.Gould, C.Radek, M.Schröder, *J.Chem.Soc., Chem.Commun.*, 985 (1994).

5) 'The Low Temperature Single Crystal X-Ray Structure of 1,4,7,10,13-pentaoxa-16,19-dithiacycloheneicosane sesquihydrate' A.J.Blake, S. Harris, S.Parsons, C.Radek and M.Schröder, (submitted for publication in *Acta Cryst., Section C*).

6) 'The Synthesis and Single-Crystal X-Ray Structure of the Tetrameric Silver(I) Complex $[Ag_4([18]aneS_2O_4)_4](ClO_4)_4$ ([18]aneS$_2$O$_4$ = 1,4,7,10-tetraoxa-13,16-dithiacyclooctadecane)' Alexander J.Blake, Simon Parsons, Christian Radek and Martin Schröder, (in preparation for publication in *J.Chem.Soc., Chem.Commun.*).

7) 'The Synthesis and Low Temperature Single-Crystal X-Ray Structures of $\{[Ag([18]aneS_6)]I_7\}_n$ and $[Ag([18]aneS_6)]I_3$ ([18]aneS$_6$ = 1,4,7,10,13,16-hexathiacyclooctadecane)' Alexander J.Blake, Robert O.Gould, Simon Parsons, Christian Radek and Martin Schröder, (in preparation for publication in *J.Chem.Soc., Dalton Trans.*).

8) 'The Single Crystal X-Ray Structures of 1,4,7-trioxa-10,13-dithiacyclopentadecane and 1,4,7,10-tetraoxa-13,16-dithiacyclooctadecane' A.J.Blake, C.Radek and M.Schröder, (in preparation for publication in *Acta Cryst., Section C*).

9) 'Di-Iodine Charge Transfer Complexes with Cyclic Thioether Ligands - Part I: Synthesis, Characterisation, Spectroscopic Studies and Single Crystal X-Ray Structures of Small to Medium Sized Cyclic Thioether Ligands' A.J.Blake, F.Christiani, F.Demartin, F.A.Devillanova, A.Garau, R.O.Gould, V.Lippolis, C.Radek and M.Schröder, (in preparation for publication in *J.Chem.Soc., Dalton Trans.*).

10) 'Di-Iodine Charge Transfer Complexes with Cyclic Thioether Ligands - Part II Synthesis, Characterisation, Spectroscopic Studies and Single Crystal X-Ray Structures of Medium to Large Sized Cyclic Thioether Ligands' A.J.Blake, F.Christiani, F.Demartin, F.A.Devillanova, A.Garau, R.O.Gould, V.Lippolis, C.Radek and M.Schröder, (in preparation for publication in *J.Chem.Soc., Dalton Trans.*).

11) 'Ruthenium Complexes of Mixed O/S-Donor Ionophores. The Synthesis and Single Crystal X-Ray Structures of $[RuCl_2(PPh_3)_2([15]aneS_2O_3)]$, [RuCl(PPh3)([18]aneS2O4)]PF6, $[Ru(\eta^5\text{-}C_5H_5)(PPh_3)([18]aneS_2O_4)]PF_6$, $[RuCl(\eta^6\text{-}C_6H_6)([18]aneS_2O_4)]PF_6$ and $[RuCl(\eta^6\text{-}C_6H_6)([18]aneS_2O_4)]BPh_4$ ($[15]aneS_2O_3$ = 1,4,7-trioxa-10,13-dithia-cyclopentadecane; $[18]aneS_2O_4$ = 1,4,7,10-tetraoxa-13,16-dithiacyclopentadecane)' A.J.Blake, R.O.Gould, C.Radek and M.Schröder (in preparation for publication in *J.Chem.Soc., Dalton Trans.*).

12) 'Palladium Complexes of Mixed O/S-Donor Ionophores. The Synthesis and Single Crystal X-Ray Structures of $[PdCl_2([18]aneS_2O_4]$, $[Pd([18]aneS_2O_4)_2](PF_6)_2$ and $[Pd([18]aneS_3O_3)_2](PF_6)_2$ ($[18]aneS_2O_4$ = 1,4,7,10-tetraoxa-13,16-dithiacyclopentadecane; $[18]aneS_3O_3$ = 1,4,7-trioxa-10,13,16-trithiacyclooctadecane)' A.J.Blake, R.O.Gould, C.Radek and M.Schröder (in preparation for publication in *J.Chem.Soc., Dalton Trans.*).

A.6.2 Poster (The author responsible for the poster is underlined)

1) 'The Complexation of Ag(I) with Mixed O/S Donor Ionophores',
A.J.Blake, R.O.Gould, C.Radek, G.Reid, M.Schröder,
1st International Conference of The Copper and Zinc Triads, 1992, Edinburgh, UK.

2) 'Coordination of Platinum Metal Ions by Mixed Donor O/S Macrocycles',
A.J.Blake, R.O.Gould, C.Radek, M.Schröder,
5th International Conference of The Chemistry of The Platinum Group Metals, 1993, St.Andrews, UK.

3) 'Interaction of I_2 with Cyclic Thioethers',
F.Christiani, F.A.Devillanova, A.Garau, F.Isaia, V.Lippolis, G.Verani, F.Demartin, A.J.Blake, R.O.Gould, C.Radek, M.Schröder,
Sintesi e Metodologie Speciali in Chimica Inorganica: Applicazioni a Composti e Materiali Innovativi, 1993, Bressanone, Italy.

4) 'Metal Macrocyclic Complexes as Templates for Polyiodides. The Synthesis and Low Temperature Single Crystal Structures of $\{[Ag([18]aneS_6)]I_7\}_n$ and $[Ag([18]aneS_6)]I_3$ ([18]aneS$_6$ = 1,4,7,10,13,16-hexathiacyclooctadecane)'
A.J.Blake, R.O.Gould, S.Parsons, C.Radek and Martin Schröder
The Royal Society of Chemistry, Autumn Meeting, 1994, Glasgow, UK.

5) 'Charge-Transfer Adducts between I_2 and Homoleptic Thioether Macrocycles
Part I: Small to Medium Sized Macrocycles
The Low Temperature Single Crystal Structures of $([9]aneS_3)_2(I_2)_4$, $([12]aneS_4)I_2$, $([14]aneS_4)I_2$, $([16]aneS_4)I_2$ and $([16]aneS_4)(I_2)_4$'
A.J.Blake, R.O.Gould, C.Radek and M.Schröder
The Royal Society of Chemistry, Autumn Meeting, 1994, Glasgow, UK.

6) 'Charge-Transfer Adducts between I_2 and Homoleptic Thioether Macrocycles
Part II: Medium to Large Sized Macrocycles
The Low Temperature Single Crystal Structures of $[([15]aneS_5)(I_2)_3](I_2)_{0.5}$, $([18]aneS_6)(I_2)_4$, $([24]aneS_8)I_2$ and $([24]aneS_8)(I_2)_6$'
A.J.Blake, R.O.Gould, C.Radek and M.Schröder
The Royal Society of Chemistry, Autumn Meeting, 1994, Glasgow, UK.

A.7 Meetings and Conferences

1988 13th International Symposium on Macrocyclic Chemistry, Hamburg, Germany.

1990 GDCh (Gesellschaft Deutscher Chemiker) - CIC Workshop (Chemie-Information-Computer), Oldenburg, Germany.

1991 14th Annual Irvine Review Lecture, St.Andrews, UK.

1992 1st International Conference of The Copper and Zinc Triads, Edinburgh, UK.

1993 RSC (The Royal Society of Chemistry) - Macrocyclic Chemistry Group Meeting, Oxford, UK

1993 The X-Windows Graphical User Interface, EUCS (Edinburgh University Computing Service), Edinburgh, UK

1993 4th Intensive Course in Structure Analysis, BCA (British Crystallographic Association), Birmingham, UK

1993 Butler Electrochemistry Meeting, Edinburgh, UK

1993 USIC (University of Strathclyde Inorganic Club), Glasgow, UK

1993 5th International Conference of The Chemistry of The Platinum Group Metals, St.Andrews, UK

1994 RSC - Scottish Dalton Meeting, Edinburgh, UK

1994 RSC - Autumn Meeting, Glasgow, UK

1994 BCA - Chemical Crystallography Group, Autumn Meeting, Edinburgh, UK

1991 to 1994 Inorganic and Organic Departmental Colloquia

1991 to 1994 Inorganic Discussion Group Meetings

REFERENCES

1. R.J.Smith, A.K.Powell, N.Barnard, J.R.Dilworth and P.J.Blower, *J.Chem.Soc., Chem.Commun.*, 1993, 54.
2. E.P.Kyba, R.E.Davis, C.W.Hudson, A.M.John, S.B.Brown, M.J.McPhaul, L.-K.Liu and A.C.Glover, *J.Am.Chem.Soc.*, 1981, **103**, 3868.
3. E.P.Kyba, R.E.David, M.A.Fox, C.N.Clubb, S.-T.Liu, G.A.Reitz, V.J.Scheuler and R.P.Kashyap, *Inorg.Chem.*, 1987, **26**, 1647.
4. E.P.Kyba, D.C.Alexander and A.Hohn, *Organometallics*, 1982, **1**, 1619.
5. E.P.Kyba, C.N.Clubb, S.B.Larson, V.J.Scheuler and R.E.Davies, *J.Am.Chem.Soc.*, 1985, **107**, 2141.
6. N.R.Champness, C.S.Frampton, G.Reid and D.A.Tocher, *J.Chem.Soc., Dalton Trans.*, 1994, 3031.
7. K.Ziegler and R.Aurnhammer, *Liebigs Annal. Chem.*, 1934, **513**, 43.
8. A.Lüttringhaus and K.Ziegler, *Liebigs Annal. Chem.*, 1937, **528**, 155.
9. K.Ziegler, A.Lüttringhaus and K.Wolgemuth, *Liebigs Annal. Chem.*, 1937, **528**, 162.
10. A.Lüttringhaus, *Liebigs Annal.Chem.*, 1937, **528**, 181.
11. A.Lüttringhaus, *Liebigs Annal.Chem.*, 1937, **528**, 211.
12. A.Lüttringhaus, *Liebigs Annal.Chem.*, 1937, **528**, 223.
13. A.Lüttringhaus and J.Sichert-Modrow, *Makromol.Chem.*, 1967, **18/19**, 511.
14. D.Vorländer, *Justus Liebigs Ann.Chem.*, 1894, **280**, 167.
15. J.W.Hill and W.H.Carothers, *J.Am.Chem.Soc.*, 1935, **57**, 925.
16. D.G.Stewart, D.Y.Waddan and E.T.Borrows, *British Patent* 23.10.1957, **785**, 229.
17. J.L.Down, J.Lewis, B.Moore, G.Wilkinson, *J.Chem.Soc.*, 1959, 3767.
18. N.F.Curtis, *J.Chem.Soc.*, 1960, 4409.
19. N.F.Curtis and D.A.House, *Chemistry and Industry*, 1961, 1708.
20. N.F.Curtis, Y.M.Curtis and H.K.J.Powell, *J.Chem.Soc.A*, 1966, 1015.
21. C.J.Pedersen, *J.Am.Chem.Soc.*, 1967, **89**, 2495.
22. C.J.Pedersen, *Aldrichim. Acta*, 1971, **4**, 1.
23. R.M.Izatt, D.P.Nelson, J.H.Rytting, B.L.Haymore and J.J.Christensen, *J.Am.Chem.Soc.*, 1971, **93**, 1619.
24. B.C.Pressman, H.J.Harris, W.S.Jagger and J.H.Jonson, *Proc.Nat.Acad.Sci.*, 1967, **58**, 1948.
25. C.Moore and B.C.Pressman, *Biochem.Biophys.Res.Commun.*, 1964, **15**, 562.

26. B.C.Pressman, *Proc.Natl.Acad.Sci.*, 1965, **53**, 1076.
27. G.W.Gokel and S.J.Korzeniowski, eds., 'Macrocyclic Polyether Synthesis', Springer, Berlin, Heidelberg, New York, 1982.
28. E.Weber and F.Vögtle, *Inorg.Chim. Acta*, 1980, **45**, L65.
29. E.Weber and H.P.Josel, *J.Inclus.Phenom.*, 1983, **1**, 79.
30. A.Werner, *Z.Anorg.Allgem.Chem.*, 1893, **3**, 267.
31. G.Schwarzenbach, *Helv.Chim.Acta*, 1952, **35**, 2344.
32. A.E.Martell, in 'Advances in Chemistry Series', ed. R.F.Gould, 72, 62, 1967.
33. D.K.Cabbiness and D.W.Margerum, *J.Am.Chem.Soc.*, 1969, **91**, 6540.
34. D.H.Busch, K.Farmery, V.Goedken, V.Katovic, A.C.Melynk, C.R.Sperati and N.Tokel, *Adv.Chem.Ser.*, 1971, **100**, 44.
35. D.K.Cabbiness and D.W.Margerum, *J.Am.Chem.Soc.*, 1970, **92**, 2151.
36. L.L.Diaddario, L.L.Zimmer, T.E.Jones, L.S.W.L.Sokol, R.B.Cruz, E.L.Yee, L.A.Ochrymowycz and D.B.Rohrabacher, *J.Am.Chem.Soc.*, 1979, **101**, 3511.
37. F.P.Kinz and D.W.Margerum, *Inorg.Chem.*, 1974, **13**, 2491.
38. M.Kodama and E.Kimura, *J.Chem.Soc., Dalton Trans.*, 1976, 2341.
39. J.D.Lamb, R.M.Izatt, J.J.Christensen and D.J.Etough, in 'Coordination Chemistry of Macrocyclic Compounds', pp. 166-169 and refs. therein, ed. G.A.Melson, Plenum, New York, 1979.
40. L.F.Lindoy, 'The Chemistry of Macrocyclic Ligand Compounds', Cambridge University Press, Cambridge, 1989.
41. G.A.Melson ed., 'Coordination Chemistry of Macrocyclic Ligands', Plenum, New York, 1979.
42. A.J.Blake and M.Schröder, *Adv.Inorg.Chem.*, 1990, **35**, 1.
43. D.H.Busch, *Acc.Chem.Res.*, 1978, **11**, 392.
44. S.R.Cooper and S.C.Rawle, *Struct.Bond. (Berlin)*, 1990, **72**, 1.
45. D.J.Cram, *Angew.Chem.Int.Ed.Engl.*, 1988, **27**, 1009.
46. K.M.Kadish and R.Guilard, *Chem.Rev.*, 1988, **88**, 1121.
47. J.-M.Lehn, *Angew.Chem.Int.Ed.Engl.*, 1988, **27**, 89.
48. C.J.Pedersen, *Angew.Chem.Int.Ed.Engl.*, 1988, **27**, 1021.
49. J.R.Hartman, R.L.Rardin, P.Chaudhuri, K.Pohl, K.Wieghardt, B.Nuber, J.Weiss, G.C.Papaefthymiou, R.B.Frankel and S.J.Lippard, *J.Am.Chem.Soc.*, 1987, **109**, 7387.
50. P.Chaudhuri and K.Wieghardt, *Progr.Inorg.Chem.*, 1987, **35**, 329.

51. A.Bianchi, L.Bologni, P.Dapparto, M.Micheloni and P.Paoletti, *Inorg.Chem.*, 1984, **23**, 1201.
52. G.F.Smith and D.W.Margerum, *J.Chem.Soc., Chem.Commun.*, 1975, 807.
53. K.Henrick, P.A.Tasker and L.F.Lindoy, *Prog.Inorg.Chem.*, 1985, **33**, 1.
54. N.F.Curtis, in 'Coordination Chemistry of Macrocyclic Compounds' pp.219 - 301, ed. G.A.Melson, Plenum, New York, 1979.
55. R.E.DeSimone and M.D.Glick, *J.Am.Chem.Soc.*, 1976, **98**, 762.
56. S.C.Rawle, G.A.Admans and S.R.Cooper, *J.Chem.Soc., Dalton.Trans.*, 1988, 93.
57. R.S.Glass, G.S.Wilson and W.N.Setzer, *J.Am.Chem.Soc.*, 1980, **102**, 5068.
58. P.Neumann and F.Vögtle, *Chemiker-Ztg.*, 1973, **97**, 600.
59. R.Blom, D.W.H.Rankin, H.E.Robertson, M.Schröder and A.Taylor, *J.Chem.Soc., Perkin Trans. 2*, 1991, 773.
60. A.J.Blake, J.A.Greig, A.J.Holder, T.I.Hyde, A.Taylor and M.Schröder, *Angew.Chem.Int.Ed.Engl.*, 1990, **29**, 197.
61. A.J.Blake, R.O.Gould, J.A.Greig, A.J.Holder and M.Schröder, *J.Chem.Soc., Chem.Commun.*, 1989, 876.
62. A.J.Blake, R.O.Gould, A.J.Holder, T.I.Hyde, A.J.Lavery, M.O.Odulate and M.Schröder, *J.Chem.Soc., Chem.Commun.*, 1987, 118.
63. A.J.Blake, A.J.Holder, T.I.Hyde and M.Schröder, *J.Chem.Soc., Chem.Commun.*, 1987, 987.
64. S.C.Rawle, R.Yagbasan, K.Prout and S.R.Cooper, *J.Am.Chem.Soc.*, 1991, **113**, 1600.
65 D.Coucouvanis, *Acc.Chem.Res.*, 1991, **24**, 1 and references therein.
66. A.J.Blake, R.O.Gould, A.J.Holder, T.I.Hyde and M.Schröder, *J.Chem.Soc., Dalton Trans.*, 1988, 1861.
67. R.M.Izatt, J.S.Bradshaw, S.A.Nielson, J.D.Lamb, D.Sen and J.J.Christensen, *Chem.Rev.*, 1985, **85**, 271 and references therein.
68. R.M.Izatt, R.E.Terry, A.G.Avondet, J.S.Bradshaw, N.K.Dalley, T.E.Jensen, J.J.Christensen and B.L.Haymore, *Inorg.Chim.Acta*, 1978, **30**, 1.
69. R.W.Hay, 'Bio-Inorganic Chemistry', Horwood, Wiley, Chichester 1984.
70. G.L.Eichhorn Ed., 'Inorganic Biochemistry', Elsevier, Amsterdam.
71. E.Frieden, *J.Chem.Educ.*, 1985, **62**, 917.

72. K.S.Suslick and T.J.Reinert, *J.Chem.Educ.*, 1985, **62**, 974.
73. L.E.Barstow, R.S.Young, E.Yokale, J.J.Sharp, J.C.O'Brien, P.W.Berman and H.A.Harbury, *Proc.Natl.Acad.Sci.U.S.A.*, 1977, **74**, 4248.
74. E.I.Solomon and Y.Zhang, *Acc.Chem.Res.*, 1992, **25**, 343.
75. D.M.Kurtz, D.F.Shriver and I.M.Klotz, *Coord.Chem.Revs.*, 1977, **24**, 145.
76. R.Cammack, *Adv.Inorg.Chem.*, 1988, **32**, 297.
77. F.P.Guengerich and T.L.MacDonald, *Acc.Chem.Res.*, 1984, **9**, 17.
78. S.Lindskog, *Adv.Inorg.Biochem.*, 1982, **4**, 116.
79. T.G.Spiro Ed., 'Iron-Sulfur Proteins', Wiley, New York 1982.
80. A.G.Sykes, *Adv.Inorg.Chem.*, 1990, **36**, 377.
81. J.M.Pratt, *Chem.Soc.Rev.*, 1985, **14**, 161.
82. H.H.Ussing, 'The Alkali Metal Ions in Isolated Systems and Tissues, Handbuch der Experimentellen Pharmakologie', p.1, Springer-Verlag, Berlin 1960.
83. P.Kruhoffer, J.H.Thaysen and N.A.Thorn, 'The Alkali Metal Ions in the Organism, Handbuch der Experimentellen Pharmakologie', p.196, Springer-Verlag, Berlin 1960.
84. P.R.Kernan, 'Cell-Potassium', Butterworths, London, 1965.
85. C.P.Bianchi, 'Cell-Calcium', Butterworths, London 1968.
86. R.J.P.Williams, *Quart.Rev.Chem.Soc.*, 1970, **24**, 331.
87. C.J.Duncan Ed., 'Calcium in Biological Systems', Soc.Exp.Biol.Symp, XXX, 1976.
88. P.M.Harrison Ed., Topics in Molecular and Structural Biology - Metalloproteins,
Part 1: Metal Proteins with Redox Roles, 6, 1985.
Part 2: Metal Proteins with Non-Redox Roles, 7, 1985.
89. M.N.Hughes, 'The Inorganic Chemistry of Biological Processes', John Wiley & Sons, 2nd Ed., 1985.
90. J.M.Rifkind, in 'Inorganic Biochemistry', pp. 832-902, G.L.Eichhorn ed., Elsevier, Amsterdam.
91. J.J.Katz, in 'Inorganic Biochemistry', pp. 1022-1066, G.L.Eichhorn ed., Elsevier, Amsterdam.
92. V.L.Goedken in 'Coordination Chemistry of Macrocyclic Compounds', pp. 603-654, ed. G.A.Melson, Plenum, New York, 1979.
93. I.L.Karle, *J.Am.Chem.Soc.*, 1975, **97**, 4379.

94. Y.Nawata, T.Sakamaki, Y.Iitaka, *Acta Cryst.*, 1974, **30**, 1047.
95. C.E.Lankford, *Crit.Rev.Microbiol.*, 1973, **2**, 273.
96. G.Winkelmann, D.van der Helm and J.B.Neilands, eds.,
'Iron Transport in Microbes, Plants and Animals', VCH Weinheim, 1987.
97. J.B.Neilands, *Annu.Rev.Biochem.*, 1981, **50**, 715.
98. J.Francis. J.Mandinaveitia, H.M.Macturk and G.Snow,
Nature (London), 1949, **163**, 365.
99. A.G.Lockhead, M.O.Burton and R.H.Thexton,
Nature (London), 1952, **170**, 282.
100. J.R.Pollack and J.B.Neilands,
Biochim.Biophys.Res.Commun., 1970, **38**, 989.
101. I.G.O'Brien and F.Gibson, *Biochim.Biophys.Acta*, 1970, **21**, 393.
102. E.J.Corey and S.Bhattacharyya, *Tetrahedron Lett.*, 1977, 3919.
103. W.H.Rastetter, T.J.Erichson and M.C.Venuti,
J.Org.Chem., 1981, **46**, 3579.
104. A.Schanzer and J.Libmann, J.Chem.Soc., Chem.Commun., 1983, 846.
105. Y.Tor, J.Libman, A.Shanzer and S.Lifson,
J.Am.Chem.Soc., 1987, **109**, 6517.
106. K.T.Greenwood and K.R.Luke, *Biochim.Biophys.Acta*, 1980, 614, 183.
105. S.Grammenudi and F.Vögtle,
Angew.Chem.Int.Ed.Engl., 1986, **25**, 1122.
106. S.Grammenudi, M.Franke, F.Vögtle and E.Steckhan,
J.Inclus.Phenom., 1987, **5**, 695.
107. P.Belser, *Chimia*, 1990, **44**, 226.
108. V.Balzani, F.Barigelletti and L.De Cola, *Top.Curr.Chem.*, 1990, **158**, 31.
109. For overview see: C.Seel and F.Vögtle,
Angew. Chem., Int.Ed.Engl., 1992, **31**, 528.
110. J.Jazwinski, J.-M.Lehn, D.Lilienbaum, R.Ziessel, J.Guilhem and C.Pascard,
J.Chem.Soc., Chem.Commun., 1987, 1691.
111. R.J.P.Williams, *J.Mol.Catal.*, 1986, **1** (review issue).
112. R.E.Stenkamp, L.C.Sieker, L.H.Jensen and J.Sanders-Loehr,
Nature, 1981, **291**, 263.
113. W.H.Armstrong, A.Spool, G.C.Papaefthymiou, R.B.Frankel
and S.J.Lippard, *J.Am.Chem.Soc.*, 1984, **106**, 3653.
114. S.Drüeke, K.Wieghardt, B.Nuber, J.Weiss, H.-P. Fleischhauer, S.Gehring
and W.Haase, *J.Am.Chem.Soc.*, 1989, **111**, 8622.

115. S.J.Lippard, *Angew.Chem.*, 1988, **100**, 353.
116. J.R.Hartmann, R.L.Rardin, P.Chaudhuri, K.Pohl, K.Wieghardt, B.Nuber, J.Weiss, G.C.Papaefthymiou, R.B.Frankel and S.J.Lippard, *J.Am.Chem.Soc.*, 1987, **109**, 7387.
117. W.Armstrong, A.Spool, G.C.Papaefthymiou, R.B.Frankel and S.J.Lippard, *J.Am.Chem.Soc.*, 1984, **106**, 3653.
118. K.Wieghardt, *Angew.Chem.*, 1989, **101**, 1179 and references therein.
119. P.Nordlund, B.-M.Sjöberg and H.Eklund, *Nature*, 1990, **345**, 593.
120. J.W.Pyrz, J.T.Sage, P.G.Debrunner and L.Que Jr., *J.Biol.Chem.*, 1986, **261**, 11015.
121. B.A.Averill, J.C.Davis, S.Burman, T.Zirino, J.Sanders-Loehr, T.M.Loehr, J.T.Sage and P.G.Debrunner, *J.Am.Chem.Soc.*, 1987, **109**, 3760.
122. B.C.Antanaitis, T.Strekos and P.Aisen, *J.Biol.Chem.*, 1982, **257**, 3766.
123. R.B.Lauffer, B.C.Antanaitis, P.Aisen and L.Que Jr., *J.Biol.Chem.*, 1983, **258**, 14212.
124. B.K.Vainshtein, W.R.Melik-Adamyan, V.V.Barynin, A.A.Vagin, A.I.Grebenko, *Proc.Int.Symp.Biomol.Struct. Interactions, Suppl.J.Biosci.*, 1985, **8**, 471.
125. W.Newton, J.R.Postgate and C.Rodriguez-Barrueco, eds., 'Recent Developmernts in Nitrogen Fixation', Academic Press, New York, 1977.
126. W.G.Zumft, *Structure and Bonding*, 1976, **29**, 1.
127. R.W.F.Hardy, ed., 'Dinitrogen Fixation', Wiley-Interscience, 1978.
128. S.W.Carter, J.Kraut, S.T.Freer, R.A.Alden, L.C.Sieker, E.Adman and L.H.Jensen, *Proc.Natl.Acad.Sci.U.S.A.*, 1972, **69**, 3526.
129. L.C.Sieker, E.Adman and L.H.Jensen, *Nature*, 1972, **235**, 40.
130. R.H.Holm, *Acc.Chem.Res.*, 1977, **10**, 427.
131. L.Que, R.H.Holm and L.E.Mortensen, *J.Am.Chem.Soc.*, 1975, **97**, 463.
132. W.O.Gillum, L.E.Mortensen, J.S.Chen and R.H.Holm, *J.Am.Chem.Soc.*, 1975, **97**, 463.
133. T.Herskovitz, B.A.Averill, R.H.Holm, J.A.Ibers, W.D.Phillips and J.F.Weiher, *Proc.Natl.Acad.Sci.U.S.A.*, 1972, **69**, 2437.
134. M.A.Bobrik, K.O.Hodgson and R.H.Holm, *Inorg.Chem.*, 1977, **16**, 1851.
135. G.B.Wong, M.A.Bobrik and R.H.Holm, *Inorg.Chem.*, 1977, **16**, 578.
136. J.Kim and D.C.Rees, *Nature*, 1992, **360**, 553.
137. D.Sellmann, *Angew.Chem.Int.Ed.Engl.*, 1993, **32**, 64.

138. S.P.Cramer, K.O.Hodgson, W.O.Gillum and L.E.Mortensen, *J.Am.Chem.Soc.*, 1978, **100**, 3398.
139. S.P.Cramer, W.O.Gillum, K.O.Hodgson, L.E.Mortensen, I.Stiefel, J.R.Chisnell, W.J.Brill and V.K.Shah, *J.Am.Chem.Soc.*, 1978, **100**, 3814.
140. J.Rawlings, V.K.Shah, J.R.Chisnell, W.J.Brill, R.Zimmermann, E.Munck and W.H.Orme-Johnson, *J.Biol.Chem.*, 1978, **253**, 1001.
141. T.E.Wolff, J.M.Berg, C.Warrick, K.O.Hodgson, R.H.Holm and R.B.Frankel, *J.Am.Chem.Soc.*, 1978, **100**, 4630.
142. S.R.Acott, G.Christou, C.D.Garner, T.J.King, F.F.Mabbs and R.M.Miller, *Inorg.Chim.Acta*, 1979, **35**, L337.
143. G.Christou, C.D.Garner, F.E.Mabbs and J.J.King, *J.Chem.Soc., Chem.Commun.*, 1978, 740.
144. G.Christou, C.D.Garner, F.E.Mabbs and J.J.King, *J.Chem.Soc., Chem.Commun.*, 1979, 91.
145. J.S.Bradshaw, K.E.Krakowiak, B.S.Tarbet, R.L.Bruening, R.M.Izatt, *Proc.Int.Macrocyclic Conf.*, 1988.
146. J.S.Bradshaw, R.L.Bruening, K.E.Krakowiak, B.J.Tarbet, M.L.Bruening, R.M.Izatt and J.J.Christensen, *J.Chem.Soc., Chem.Commun.*, 1988, 812.
147. J.S.Bradshaw, K.E.Krakowiak, R.L.Bruening, B.J.Tarbet, P.B.Savage and R.M.Izatt, *J.Heterocyclic Chem.*, 1990, **27**, 347.
148. E.Blasius, K.P.Janzen, W.Adrian, G.Klauthe, R.Lorschneider, P.G.Maurer, B.V.Nguyen-Tien, G.Scholten and J.Stochemer, *Fresenius Z.Anal.Chem.*, 1977, **284**, 377.
149. J.S.Bradshaw, K.E.Krakowiak, R.L.Bruening, B.J.Tarbet, P.B.Savage and R.M.Izatt, *J.Org.Chem.*, 1988, **53**, 3190.
150. D.Parker, R.S.C., UK Macrocyclic Group, 7th Meeting, Oxford 1993
151. J.P.L.Cox, K.J.Jankowski, R.Kataky, D.Parker, N.R.A.Beeley, B.A.Boyce, M.A.W.Eaton, K.Millar, T.A.Millican, A.Harrison and C.Walker, *J.Chem.Soc., Chem.Commun.*, 1989, 797.
152. C.J.Broan, E.Cole, K.J.Jankowski, D.Parker, K.Pulukoddy, B.A.Boyce, N.R.A.Beeley, K.Millar and T.A.Millican, *Synthesis*, 1992, 63.
153. B.Fischer and R.Eisenberg, *J.Am.Chem.Soc.*, 1980, **102**, 7361.
154. M.Beley, J.P.Collin, R.Ruppert and J.-P.Sauvage, *J.Chem.Soc., Chem.Commun.*, 1984, 1315; *J.Am.Chem.Soc.*, 1986, **108**, 7461.

155. D.A.Gangi and R.R.Durand, *J.Chem.Soc., Chem.Commun.*, 1980, 697.
156. J.Y.Becker, B.Vainas, R.Eger and L.Kaufman, *J.Chem.Soc., Chem.Commun.*, 1985, 1471.
157. B.B.Wayland and H.W.Bosch, *J.Chem.Soc., Chem.Commun.*, 1986, 697.
158. Y.le Mest, M.L'Her, J.Courtot-Coupez, J.P.Collman, E.R.Evitt and C.S.Bencosme, *J.Chem.Soc., Chem.Commun.*, 1983, 1286.
159. J.P.Collman and K.Kim, *J.Am.Chem.Soc.*, 1986, **108**, 7847.
160. D.Sazou, C.Araullo-McAdams, B.C.Han, M.M.Franzen and K.M.Kadish, *J.Am.Chem.Soc.*, 1990, **112**, 7879.
161. J.P.Collman, J.E.Hutchison, P.S.Wagenknecht, N.S.Lewis, M.A.Lopez and R.Guilard, *J.Am.Chem.Soc.*, 1990, **112**, 8206.
162. J.P.Collman, J.E.Hutchison, M.A.Lopez, R.Guilard and R.A.Reed, *J.Am.Chem.Soc.*, 1991, **113**, 2794.
163. M.J.Camezind, D.Dolphin and B.R.James, *J.Chem.Soc., Chem.Commun.*, 1986, 1137.
164. T.Yoshida, T.Adachi, M.Kaminaka, T.Ueda and T.Higuchi, *J.Am.Chem.Soc.*, 1988, **110**, 4872.
165. I.Taniguchi, N.Nakashima and K.Yasukouchi, *J.Chem.Soc., Chem.Commun.*, 1986, 1814.
166. J.T.Croves and T.E.Nemo, *J.Am.Chem.Soc.*, 1983, **195**, 5786.
167. J.P.Collman, M.Marrocco, P.Denisevich, C.Koval and F.C.Anson, *J.Electroanal.Chem.*, 1979, **101**, 117.
168. P.J.Brothers and J.P.Collman, *Acc.Chem.Res.*, 1986, **19**, 209.
169. R.S.Paonessa, N.C.Thomas and J.Halpern, *J.Am.Chem.Soc.*, 1985, 107, 4333.
170. T.Yoshida, T.Ueda, T.Adachi, K.Yamamoto and T.Higuchi, *J.Chem.Soc., Chem.Commun.*, 1985, 1137.
171. H.D.Durst, *Tetrahedron Lett.*, 1974, **28**, 2421.
172. C.L.Liotta, H.P.Harris, McDermott, Gonzalez and Smith, *Tetrahedron Lett.*, 1974, **28**, 2417.
173. D.J.Sam and H.E.Simmons, *J.Am.Chem.Soc.*, 1974, **96**, 2252.
174. E.Weber, 'Phase Transfer Catalysts. Properties and Applications', Merck-Schuchardt, Darmstadt, 1987 and references therein.
175. D.J.Sam and H.E.Simmons, *J.Am.Chem.Soc.*, 1972, **94**, 4024.
176. C.L.Liotta and H.P.Harris, *J.Am.Chem.Soc.*, 1974, **96**, 2250.
177. K.W.Kwon, Y.Nishimura, M.Ikeda and Y.Tamura, *Synthesis*, 1976, 249.

178. L.Stryer, 'Biochemistry', 2nd.Ed., Freeman, San Francisco, 1981.
179. E.Racker, *Acc.Chem.Res.*, 1979, **12**, 338.
180. L.A.Frederick, T.Fyles, V.A.Malik-Diemer and D.M.Whitfield, *J.Chem.Soc., Chem.Commun.*, 1980, 1211.
181. L.A.Frederick, T.Fyles, N.P.Gurprasad and D.M.Whitfield, *Can.J.Chem.*, 1981, **59**, 1724.
182. T.Fyles, V.A.Malik-Diemer and D.M.Whitfield, *Can.J.Chem.*, 1981, **59** 1734.
183. T.Nishi, A.Ikeda, T.Matsuda and S.Shinkai, *J.Chem.Soc., Chem.Commun.*, 1991, 339.
184. S.Shinkai, T.Ogawa, Y.Kusano and O.Manabe, *Chem.Lett.*, 1980, 283.
185. S.Shinkai, Y.Kusano and O.Manabe, *J.Am.Chem.Soc.*, 1981, **103**, 111.
186. S.Shinkai, T.Ogawa, Y.Kusano, O.Manabe, K.Kikukawa, T.Goto and T.Matsuda, *J.Am.Chem.Soc.*, 1982, **104**, 1960.
187. S.Shinkai, M.Ishihara, K.Veda and O.Manabe, *J.Chem.Soc., Perkin Trans. 2*, 1985, 511.
188. B.Valeur, S.Fery-Forges, M.T.LeBris and J.P.Guette, *J.Chem.Soc, Chem.Commun.*, 1988, 384.
189. F.Vögtle, *Pure Appl.Chem.*, 1980, **52**, 2405.
190. R.E.Dickerson and I.Geiss, 'Hemoglobin', Benjamin and Cumming, California, 1983.
191. J.Rebek, *Acc.Chem.Res.*, 1984, **17**, 258.
192. T.E.Edmonds, in 'Chemical Sensors', ed. T.E.Edmonts, Blackie, Glasgow, London 1988.
193. J.F.Biernat and T.Wileczewski, *Tetrahedron*, 1980, **36**, 2521.
194. T.Saji and I.Kinoshita, *J.Chem.Soc., Chem.Commun.*, 1986, 716.
195. P.J.Hammond, P.D.Beer, C.Dudman, I.P.Danks and C.D.Hall, *J.Organomet.Chem.*, 1986, **306**, 367.
196. P.J.Hammond, A.P.Bell and C.D.Hall, *J.Chem.Soc., Perkin Trans.1*, 1983, 707.
197. P.D.Beer, J.Elliot, P.J.Hammond, C.Dudman and C.D.Hall, *J.Organomet.Chem.*, 1984, **263**, C7.
198. C.D.Hall, N.W.Sharpe, I.P.Danks and Y.P.Sang, *J.Chem.Soc. Chem.Commun.*, 1989, 419.
199. J.C.Medina, T.T.Goodnow, S.Bott, J.L.Atwood, A.E.Kaifer and G.Gokel, *J.Chem.Soc., Chem.Commun.*, 1991, 290.

200. P.D.Beer, H.Sikanyika and J.F.McAleer, *Inorg.Chem.*, 1990, **29**, 378.
201. P.D.Beer, M.P.Andrews, C.Blackburn, J.F.McAleer and V.D.Patel, *J.Chem.Soc., Chem.Commun.*, 1987, 1122.
202. P.D.Beer, H.Sikanyika, C.Blackburn, J.F.McAleer and M.G.B.Drew, *J.Organomet.Chem.*, 1988, **356**, C19.
203. P.D.Beer, H.Sikanyika, C.Blackburn, J.F.McAleer and M.G.B.Drew, *J.Chem.Soc., Dalton Trans.*, 1990, 3295.
204. P.D.Beer and H.Sikanyika, *Polyhedron*, 1990, **9**, 1091.
205. P.D.Beer and K.Y.Wild, Proc.Int.Macrocyclic Conf., 1991, 106.
206. M.L.H.Green, W.B.Heur and G.C.Saunders, *J.Chem.Soc., Dalton Trans.*, 1990, 3789.
207. J.Granell, M.L.H.Green, V.J.Lowe, S.R.Marder, P.Mountford, G.C.Saunders and N.M.Walker, *J.Chem.Soc., Dalton Trans.*, 1990, 605.
208. P.D.Beer, D.B.Crowe, M.I.Ogden, M.G.B.Drew and B.Main, *J.Chem.Soc., Dalton Trans.*, 1993, 2107.
209. N.D.Lowe and C.D.Garner, *J.Chem.Soc., Dalton Trans.*, 1993, 2197.
210. J.P.Danks, Ph.D. Thesis, University of Oxford, 1993.
211. T.Kaneda, K.Sugihara, H.Kamiya and S.Misuri, *Tetrahedron Lett.*, 1981, **22**, 4407.
212. K.Nakashima, S.Nakatsuji, S.Akiyama, T.Kaneda and S.Misuri, *Chem.Lett.*, 1982, 1781.
213. S.G.Murray and F.R.Hartley, *Chem.Rev.*, 1981, **81**, 365.
214. J.S.Bradshaw, J.Y.Hui, B.L.Haymore, J.J.Christensen and R.M.Izatt, *J.Heterocyclic Chem.*, 1973, **10**, 1.
215. J.S.Bradshaw, J.Y.Hui, J.Y.Chan, B.L.Haymore, J.J.Christensen and R.M.Izatt, *J.Heterocyclic Chem.*, 1974, **11**, 45.
216. J.S.Bradshaw and J.Y.Hui, *J.Heterocyclic Chem.*, 1974, **11**, 649 and references therein.
217. J.S.Bradshaw, R.A.Reeder, M.D.Thompson, E.D.Flanders, R.L.Carruth, R.M.Izatt and J.J.Christensen, *J.Org.Chem.*, 1976, **41**, 134.
218. J.S.Bradshaw and P.E.Stott, *Tetrahedron*, 1980, **36**, 461 and references therein.
219. N.K.Dalley, S.B.Larson, J.S.Smith, K.L.Matheson, R.M.Izatt and J.J.Christensen, *J.Heterocyclic Chem.*, 1981, **18**, 463.
220. J.Buter and R.M.Kellogg, *J.Org.Chem.*, 1981, **46**, 4481.
221. B.Metz, D.Moras and R.Weiss, *J.Inorg.Nucl.Chem.*, 1974, **36**, 785.

222. S.B.Larson, *The Crystal Structures of Several Cyclic Polyethers and their Complexes*', Ph.D. Thesis, Brigham Young University, Provo, Utah 1980.
223. M.N.Bell, Ph.D. Thesis, University of Edinburgh, Scotland 1987.
224. G.Reid, Ph.D. Thesis, University of Edinburgh, Scotland 1989.
225. A.J.Blake, G.Reid and M.Schröder, *J.Chem.Soc., Dalton.Trans.*, 1990, 3849.
226. A.J.Blake, G.Reid and M.Schröder, *J.Chem.Soc., Dalton Trans.*, 1992, 1074.
227. A.J.Blake, R.O.Gould, C.Radek, G.Reid, A.Taylor and M.Schröder 'Structural Mis-Matches in Silver and Gold Complexes of Thioether Macrocycles' in 'The Chemistry of the Copper and Zinc Triads', eds. A.J.Welch and S.K.Chapman, pp. 95-101, The Royal Society of Chemistry, 1993.
228. G.W.Gokel and H.D.Durst, *Synthesis*, 1976, 174.
229. J.S.Bradshaw, G.E.Maas, R.M.Izatt and J.J.Christensen, *Chem.Rev.*, 1979, **79**, 37 and references therein.
230. J.S.Bradshaw and P.E.Stott, *Tetrahedron*, 1980, **36**, 461. and references therein.
231. H.An, J.S.Bradshaw and R.M.Izatt, *Chem.Rev.*, 1992, **92**, 543 and references therein.
232. E.Weber and F.Vögtle, *Liebigs Ann.Chem.*, 1976, 891 and references therein.
233. R.Hoss and F.Vögtle, *Angew.Chem.Int.Ed.Engl.*, 1994, **33**, 375 and references therein.
234. D.Gerber, P.Chongsawangvirod, A.K.Leung and L.A.Ochrymowycz, *J.Org.Chem.*, 1977, **42**, 2644.
235. W.N.Setzer, C.A.Ogle, G.S.Wilson and R.S.Glass, *Inorg.Chem.*, 1983, **22**, 266.
236. A.J.Blake, R.O.Gould, A.J.Lavery and M.Schröder, *Angew.Chem.Int.Ed.Engl.*, 1986, **25**, 274.
237. D.Sellmann and L.Zapf, *Angew.Chem.Int.Ed.Engl.*, 1984, **23**, 807.
238. D.Sellmann and L.Zapf, *J.Organomet.Chem.*, 1985, **289**, 57.
239. P.J.Blower and S.R.Cooper, *Inorg.Chem.*, 1987, **26**, 2009.
240. J.Buter and R.M.Kellogg, *J.Chem.Soc., Chem.Commun.*, 1980, 466.
241. J.S.Bradshaw, M.L.Campbell, L.A.Hassell and J.K.Baxter, *J.Heterocyclic Chem.*, 1979, **16**, 721.

242. C.J.Pedersen, *J.Org.Chem.*, 1971, **36**, 254.
243. G.R.Newkome, J.D.Sauer, J.M.Roper and D.C.Hager, *Chem.Rev.*, 1977, **77**, 513.
244. P.Ruggli, *Ber.d.d.chem.Ges.*, 1911, **44**, 1209.
245. J.R.Dann, P.P.Chiesa and J.W.Gates, *J.Org.Chem.*, 1961, **26**; 1991.
246. C.Dietrich-Buchecker, J.-P.Sauvage and J.-M.Kern, *J.Am.Chem.Soc.*, 1989, **111**, 7791 and references therein.
247. O.I.Asubiojo, J.I.Brauman and R.H.Levin, *J.Am.Chem.Soc.*, 1977, **99**, 7707.
248. M.Ouchi, Y.Inoue, T.Kanzaki and T.Hakushi, *J.Org.Chem.*, 1984, **49**, 1408.
249. D.N.Reinhoudt, F.de Jong, H.P.M.Tomassen, *Tetrahedron Lett.*, 1979, **22**, 2067.
250. L.Leadbeater, *Chemistry in Britain*, 1988, 683.
251. D.Wöhrle and D.Meissner, *Nachr.Chem.Tech.Lab.*, 1989, **37**, 254.
252. J.R.Meadow and E.E.Reid, *J.Am.Chem.Soc.*, 1934, **56**, 2177.
253. D.St.C.Black and I.A.McLean, *Aust.J.Chem.*, 1971, **24**, 1401.
254. J.J.Christensen, D.J.Eatough and R.M.Izatt, *Chem.Rev.*, 1974, **74**, 351.
255. J.S.Bradshaw, K.E.Krakowiak, R.M.Izatt, R.L.Bruening and B.J.Tarbet, *J.Heterocyclic Chem.*, 1990, **27**, 347.
256. R.S.Glass, G.S.Wilson and W.N.Setzer, *J.Am.Chem.Soc.*, 1980, **102**, 5068.
257. R.E.Wolf jr., J.R.Hartman,J.M.E.Storey, B.M.Foxman and S.R.Cooper, *J.Am.Chem.Soc.*, 1987, **109**, 4328.
258. G.H.Robinson and S.A.Sangokoya, *J.Am.Chem.Soc.*, 1988, **110**, 1494.
259. R.E.DeSimone and M.D.Glick, *J.Am.Chem.Soc.*, 1976, **98**, 762.
260. A.J.Blake, R.O.Gould, M.A.Halcrow and M.Schröder, *Acta Cryst.*, 1993, **B49**, 773.
261. J.R.Hartman, R.E.Wolf, B..Foxman and S.R.Cooper *J.Am.Chem.Soc.*, 1983, **105**, 131.
262. P.C.Junk and J.L.Atwood, *Supramol. Chem.*, 1994, **3**, 241.
263. N.K.Dalley, S.B.Larson, J.S.Smith, K.L.Matheson, R.M.Izatt and J.J.Christensen, *J.Heterocyclic Chem.*, 1981, **18**, 463.
264. J.Dale, *Acta Chem.Scand.*, 1973, **27**, 1115.
265. R.Blom, D.W.H.Rankin, H.E.Robertson, M.Schröder and A.Taylor, *J.Chem.Soc., Perkin Trans. 2*, 1991, 773.

266. J.Beech, P.J.Cragg and M.G.B.Drew,
J.Chem.Soc.,Dalton Trans., 1994, 719.
267. M.A.Halcrow, Ph.D.Thesis, University of Edinburgh, 1991.
268. J.Buter and R.M.Kellogg, *Org.Synth.*, 1987, **65**, 150.
269. A.Bondi, *J.Phys.Chem.*, 1964, **68**, 441; for a revision of van der Waals atomic radii see: S.C.Nyburg and C.H.Faerman,
Acta Cryst., 1985, **B41**, 274; D.Kirin, *Acta Cryst.*, 1987, **B43**, 405.
270. The tg± or a+- schemes are not used as frequently as Dale's scheme. See for instance ref. 257 and 261.
271. MINP, J-H.Lii and N.L.Allinger, Q.C.P.E. Program No.543, Quantum Chemical Program Exchange, Indiana University Chemistry Department, Bloomington, Indiana, USA.
272. MM3(92), N.L.Allinger and P.Aped, *J.Am.Chem.Soc.*, 1992, **114**, 1 and references therein.
273. M.Schröder and T.A.Stevenson in 'Comprehensive Coordination Chemistry', ed. G.Wilkinson, Pergamon Press, Oxford, 1987, vol. 4, Chapter 45.
274. M.J.Bruce and M.A.Bennet in 'Comprehensive Organometallic Chemistry', ed. G.Wilkinson, 1982, Pergamon Press, Oxford vol. 4, Chapter 32.
275. E.A.Seddon and K.R.Seddon, 'The Chemistry of Rurthenium', Elsevier, Oxford, 1984.
276. T.A.Stephenson and G.Wilkinson, *J.Inorg.Nucl.Chem.*, 1966, **28**, 915.
277. P.S.Hallman, T.A.Stephenson and G.Wilkinson,
Inorg.Synth., 1970, **12**, 237.
278. R.K.Poddar and U.Agarwala, *Indian J.Chem.*, 1971, **9**, 477.
279. P.W.Armit, A.S.F.Boyd and T.A.Stephenson,
J.Chem.Soc., Dalton Trans., 1975, 1663
280. P.R.Hoffman and K.G.Caulton, *J.Am.Chem.Soc.*, 1975, **97**, 4221.
281. B.R.James and L.D.Markham, *Inorg.Chem.*, 1974, **13**, 97.
282. S.J.La Placa and J.A.Ibers, *Inorg.Chem.*, 1965, **4**, 778.
283. M.I.Bruce and N.J.Windsor, *Aust.J.Chem.*, 1977, **30**, 1601
284. M.I.Bruce, C.Hameister, A.G.Swincer and R.C.Wallis,
Inorg.Synth., 1990, **28**, 270.
285. G.S.Ashby, M.I.Bruce, I.B.Tomkins and R.C.Wallis,
Aust.J.Chem., 1979, **32**, 1003.

286. H.Lehmkuhl, M.Bellenbaum, J.Grundke, H.Mauermann and C.Krüger, *Chem.Ber.*, 1988, **121**, 1719.
287. U.Koelle and J.Kossakowski, *J.Organomet.Chem.*, 1989, **362**, 383 and references therein.
288. M.A.Bennett and A.K.Smith, *J.Chem.Soc., Dalton Trans.*, 1974, 233
289. M.A.Bennett, T.-N.Huang, T.W.Matheson and A.K.Smith, *Inorg.Synth.*, 1982, **21**, 74.
290. R.A.Zelonka and M.C.Baird, *Can.J.Chem.*, 1972, **50**, 3063.
291. F.B.McCormick, D.C.Cox and W.B.Gleason, *Organometallics*, 1993, **12**, 610.
292. R.M.Christie, Ph.D.Thesis, University of Edinburgh, 1989.
293. N.W.Alcock, J.C.Cannadine, G.R.Clarke and A.F.Hill, *J.Chem.Soc., Dalton Trans.*, 1993, 1131.
294. A.F.Hill, N.W.Alcock, J.C.Cannadine and G.R.Clarke, *J.Organomet.Chem.*, 1992, **426**, C40.
295. M.J.Sullivan, Ph.D.Thesis, University of Edinburgh, 1993.
296. M.N.Bell, A.J.Blake, M.Schröder, H.J.Küppers and K.Wieghardt, *Angew.Chem.*, 1987, **99**, 253.
297. T.-F.Lai and C.-K.Poon, *J.Chem.Soc., Dalton Trans.*, 1982, 1465.
298. S.C.Rawle, T.J.Sewell and S.R.Cooper, *Inorg.Chem.*, 1987, **26**, 3769
299. R.Ali, S.J.Higgins and W.Levason, *Inorg.Chim.Acta*, 1984, **84**, 65.
300. M.N.Bell, A.J.Blake, M.Schröder and T.A.Stephenson, *J.Chem.Soc., Chem.Commun.*, 1986, 471.
301. M.Schröder, *Pure Appl.Chem.*, 1988, **60**, 517.
302. M.I.Bruce, C.Hameister, A.G.Swincer and R.C.Wallis, *Inorg.Synth.*, 1982, **21**, 78.
303. F.R.Hartley, 'The Chemistry of Platinum and Palladium', Applied Science Publishers, London, 1973.
304. M.J.Russel, C.F.J.Barnard and A.T.Hutton, *Comprehensive Coordination Chemistry*, Chapter 51, Vol. 5, Pergamon Press, Oxford, 1987.
305. R.B.Thomas and A.Sen, *Inorganic Syntheses*, 1973, **28**, 63.
306. A.F.Wells, 'Structural Inorganic Chemistry', 5th Ed., p.414, Oxford University Press, Oxford, New York, 1993.
307. A.C.Skapski and M.L.Smart, *J.Chem.Soc., Chem.Commun.*, 1970, 658.
308. K.Wieghardt, H.-J.Küppers, E.Raabe and C.Krüger, *Angew.Chem.Int.Ed.Engl.*, 1986, **25**, 1101.

309. A.J.Blake, A.J.Holder, T.I.Hyde, Y.V.Roberts, A.J.Lavery and M.Schröder, *J.Org.Chem.*, 1987, **323**, 261.
310. A.J.Blake, A.J.Holder, T.I.Hyde and M.Schröder, *J.Chem.Soc., Chem.Commun.*, 1987, 987.
311. A.J.Blake, A.J.Holder, Y.V.Roberts and M.Schröder, *Acta Cryst.*, 1988, **C44**, 360.
312. G.R.Giesbrecht, G.S.Hanan, J.E.Kickham and S.J.Loeb, *Inorg. Chem.*, 1992, **31**, 3286.
313. A.J.Blake, R.O.Gould, A.J.Lavery and M.Schröder, *Angew.Chem.Int.Ed.Engl.*, 1986, **25**, 274.
314. J.E.Kickham, S.J.Loeb and S.L.Murphy, *J.Am.Chem.Soc.*, 1993, **115**, 7031.
315. J.E.Kickham and S.J.Loeb, *Inorg.Chem.*, 1994, **33**, 4351.
316. D.Parker, J.-M. Lehn and J.Rimmer, *J.Chem.Soc., Dalton Trans.*, 1985, 1517.
317. G.Ferguson, K.E.Matthes and D.Parker, *J.Chem.Soc., Chem.Commun.*, 1987, 1350.
318. N.N.Greenwood and A.Earnshaw, 'The Chemistry of the Elements', pp. 243-289, Pergamon Press, Oxford, 1985.
319. The Merck Index, Merck & CO., Rahway N.J., 1976.
320. H.Fischer and B.Putzer, *Z.Physiol.Chem.*, 1929, **154**, 39.
321. F.Haurowitz, *Ber.*, 1935, **68**, 1795.
322. P.Rothemund and A.R.Menotti, *J.Am.Chem.Soc.*, 1948, **70**, 1808.
323. Y-C.Lee, J.Allison, A.I.Popov, *Polyhedron*, 1985, **4**, 441.
324. R.J.Abraham, G.H.Barnett and K.M.Smith, *J.Chem.Soc., Perkin Trans. 1*, 1973, 2142.
325. D.L.Cullen, E.F.Meyer and K.M.Smith, *Inorg.Chem.*, 1977, **16**, 1179.
326. K.Henrick, R.W.Mathews and P.A.Tasker, *Inorg.Chem.*, 1977, **16**, 3293.
327. A.Girandeau, A.Lonati, H.J.Callot and M.Gross, *Inorg.Chem.*, 1981, **20**, 769.
328. M.E.Farago, *Inorg.Chim.Acta*, 1977, **23**, 211.
329. N.S.Poonia and M.R.Truter, *J.Chem.Soc.Dalton Trans.*, 1973, 2062.

330. D.G.Parsons, M.R.Truter and J.N.Wingfield,
Inorg.Chim.Acta, 1975, **14**, 45.
331. A.L.Balch and S.P.Rowley, *J.Am.Chem.Soc.*, 1990, **112**, 6139.
332. A.L.Balch, F.Neve and M.M.Olmstead,
J.Am.Chem.Soc., 1991, **113**, 2995.
333. J.E.Huheey, 'Anorganische Chemie', pp. 78-81, de Gruyter, Berlin, 1988.
J.E.Huheey, 'Inorganic Chemistry', p. 73, 3rd Ed., Haper & Row,
New York, 1983.
334. P.D.Moras and R.Weiss, *Acta Cryst.*, 1973, **B29**, 1059.
335. K.Wieghardt, M.Kleine-Boymann, B.Nuber and J.Weiss,
Inorg.Chem., 1986, **25**, 1309.
336. R.A.Walton, *Coord.Chem.Rev.*, 1971, **6**, 1.
337. A.J.Blake, G.Reid and M.Schröder,
J.Chem.Soc., Dalton Trans., 1992, 2987.
338. A.J.Blake, J.A.Greig and M.Schröder,
J.Chem.Soc., Dalton Trans., 1991, 529.
339. J.A.Greig, Ph.D. Thesis, University of Edinburgh, 1991.
340. J.Clarkson, R.Yagbasan, P.J.Blower, S.C.Rawle and S.R.Cooper,
J.Chem.Soc., Chem.Commun., 1987, 950.
341. H.-J.Küppers, K.Wieghardt, Y.-H.Tsay, C.Krüger, B.Nuber and
J.Weiss, Angew.Chem.Int.Ed.Engl., 1987, **26**, 575.
342. J.J.H.Edema, J.Buter, F.S.Schoonbeek, R.M.Kellogg, F.van Bolhuis,
and A.L.Spek, *Inorg.Chem.*, 1994, **33**, 2448.
343. A.J.Blake, D.Collison, R.O.Gould, G.Reid and M.Schröder,
J.Chem.Soc., Dalton Trans., 1993, 521.
344. A.J.Blake, R.O.Gould, G.Reid and M.Schröder,
J.Chem.Soc., Chem.Commun., 1990, 974.
345. C.R.Lucas, S.Liu, M.J.Newlands, J.-P.Charland and E.J.Gabe,
Can.J.Chem., 1990, **68**, 644.
346. A.J.Blake, R.O.Gould, A.J.Holder, T.I.Hyde and M.Schröder,
Polyhedron, 1989, **8**, 513.
347. B.de Groot, S.J.Loeb and G.K.H.Shimizu, *Inorg.Chem.*, 1994, **33**, 2663.
348. A.J.Blake, G.Reid and M.Schröder,
J.Chem.Soc., Dalton Trans., 1990, 3849.
349. M.R.Udupa and B.Krebs, *Inorg.Chim.Acta*, 1973, **7**, 271.

350. B.F.Hoskins, R.Robson, G.A.Williams and J.C.Wilson, *Inorg.Chem.*, 1991, **30**, 4160.
351. A.M.Manotti Lanfredi, F.Ugozzoli, F.Asaro, G.Pellizer, N.Marsich, and A.Camus, *Inorg.Chim.Acta*, 1991, **190**, 71.
352. C.Bonamartini, G.F.Gasparri, M.F.Belicchi and M.Nardelli, *Acta Cryst.*, 1987, **C43**, 407.
353. I.Dance, *Inorg.Chem.*, 1981, **20**, 1487.
354. I.Dance, L.Fitzpatrick, M.Scudder and D.Craig, *J.Chem.Soc., Chem.Commun.*, 1984, 17.
355. I.L.Karle, *J.Chem.Phys.*, 1955, **23**, 1739.
356. F.van Bolhuis, P.B.Koster and T.Migchelsen, *Acta Cryst.*, 1967, **23**, 90.
357. E.Beckmann, *Ann.*, 1909, **367**, 295.
358. A.Lachman., *J.Am.Chem.Soc.*, 1903, **25**, 50.
359. J.Kleinberg and A.W.Davidson, *Chem.Rev.*, 1948, **42**, 601.
360. L.J.Andrews and R.M.Keefer, *Adv.Inorg.Radiochem.*, 1961, **3**, 92 and references therein.
361. R.Foster, 'Organic Charge-Transfer Complexes', Academic Press, London, New York, 1969, and references therein.
362. A.Husemann, *Justus Liebigs Ann.Chem.*, 1863, **126**, 269.
363. K.O.Strømme, *Acta Chem.Scand.*, 1959, **13**, 268.
364. O.Hassèl and H.Hope, *Acta Chem.Scand.*, 1960, **14**, 391.
365. O.Hassel and C.Rømming, *Acta Chem.Scand.*, 1956, **10**, 696.
366. T.Uchida, *Bull.Chem.Soc.Jpn.*, 1967, **40**, 2244.
367. T.Uchida and K.Kimura, *Acta Cryst.*, 1984, **C40**, 139.
368. O.Hassel, O.Rømming and T.Tufte, *Acta Chem.Scand.*, 1961, **15**, 967.
369. O.Hassel and G.Eia, *Acta Chem.Scand.*, 1956, **10**, 139.
370. N.Bricklebank, S.M.Godfrey, A.G.Mackie, C.A.McAuliffe and R.G.Prichard, *J.Chem.Soc., Chem.Commun.*, 1992, 355.
371. F.A.Cotton and P.A.Kibala, *J.Am.Chem.Soc.*, 1987, **109**, 3308.
372. W.W.Schweikert and E.A.Meyers, *J.Phys.Chem.*, 1968, **72**, 1561.
373. J.W.Bransford and E.A.Meyers, *Cryst.Struct.Comm.*, 1987, **7**, 697.
374. O.Hassel and J.Hvoslef, *Acta Chem.Scand.*, 1956, **10**, 138.
375. O.Hassel and C.Rømming, *Acta Chem.Scand.*, 1956, **10**, 696.
376. A.J.Blake, R.O.Gould, C.Radek and M.Schröder, *J.Chem.Soc., Chem.Commun.*, 1993, 1191.

377. F.Christiani, F.A.Devillanova, F.Isaia, V.Lippolis, G.Verani and F.Demartin, *Heteroatom Chem.*, 1993, **4**, 1.
378. A.L.Tipton, M.C.Lonergan, C.L.Stern and D.F.Shriver, *Inorg.Chim.Acta*, 1992, **201**, 23.
379. J.D.McCullough, G.Y.Chao and D.E.Zuccaro, *Acta Cryst.*, 1959, **12**, 815.
380. G.Allegra, G.E.Wilson jr., E.Benedetti, C.Pedone and R.Albert, *J.Am.Chem.Soc.*, 1970, **92**, 4002.
381. C.Rømming, *Acta Chem.Scand.*, 1960, **14**, 2145.
382. F.H.Herbstein and W.Schwotzer, *J.Am.Chem.Soc.*, 1984, **106**, 2367.
383. E.L.Ahlsen and K.O.Strømme, *Acta Chem.Scand.*, 1974, **A28**, 175.
384. H.Hope and J.D.McCullough, *Acta Cryst.*, 1964, **17**, 712.
385. H.Maddox and J.D.McCullough, *Inorg.Chem.*, 1966, **5**, 522.
386. C.Knobler and J.D.McCullough, *Inorg.Chem.* 1968, **7**, 365.
387. G.Y.Chao and J.D.McCullough, *Acta Cryst.*, 1961, **14**, 940.
388. J.L.Gay-Lussac, Ann.Chim.Phys., 1814, **91**, 5.
389. A.Smith and C.M.Carson, *Z.Phys.Chem.*, 1907, **61**, 200.
390. F.Ephraim, *Z.Anorg.Chem.*, 1908, **58**, 338.
391. R.Wright, *J.Chem.Soc.*, 1915, **107**, 1527.
392. M.Amadori, *Gazz.Chim.Ital.*, 1922, **52**, 387.
393. J.Mori, *J.Chem.Soc.Japan*, 1923, **44**, 730.
394. F.Olivari, *Atti Accad.Linc.* [5], 1908, **II 17**, 512.
395. P.S.Varadachari and K.C.Subramaniam, *Proc.Indian Acad.Sci.*, 1936, **A3**, 428.
396. M.R.A.Rao, *Proc.Indian Acad.Sci.*, 1940, **A11**, 162.
397. M.R.A.Rao, *Proc.Indian Acad.Sci.*, 1940, **A11**, 175.
398. M.R.A.Rao, J.Mysore Univ., 1940, **I**, 75; *C.A.*, **35**, 6527.
399. M.R.A.Rao, *Proc.Indian Acad.Sci.*, 1940, **A11**, 185.
400. M.R.A.Rao, *Proc.Indian Acad.Sci.*, 1940, **A11**, 201.
401. M.R.A.Rao, *Proc.Indian Acad.Sci.*, 1940, **A12**, 354.
402. K.Manzel and R.Minkwitz, *Z.anorg.allg.Chem.*, 1978, **441**, 165.
403. G.Vahl and R.Minkwitz, *Z.anorg.allg.Chem.*, 1978, **441**, 217.
404. J.P.Danehy, 'Sulfur in Organic and Inorganic Chemistry', A.Senning, ed, Marcel Dekker, New York, 1971, Chapter 10 - *'The Sulfur-Iodine Bond'*.
405. M.E.Peach, *Int.J.Sulfur Chem.*, 1973, **8**, 151.

406. J.Passmore, G.Sutherland and P.S.White,
J.Chem.Soc., Chem.Commun., 1979, 901.
407. J.Passmore, P.Taylor, T.Whidden and P.S.White,
J.Chem.Soc., Chem.Commun., 1976, 689.
408. F.Demartin, P.Deplano, F.A.Devillanova, F.Isaia, V.Lippolis and G.Verani, *Inorg.Chem.*, 1993, **32**, 3694.
409. G.H.Y.Liu and H.Hope, *Acta Cryst.*, 1972, **28B**, 643.
410. C.Knobler, C.Baker, H.Hope and J.D.McCullough,
Inorg.Chem., 1971, **10**, 697.
411. J.Passmore, G.Sutherland, T.Whidden and P.S.White,
J.Chem.Soc., Chem.Commun., 1980, 289.
412. G.Y.Chao, *Acta Cryst.*, 1960, **13**, 727.
413. O.Holmesland and C.Rømming, *Acta Chem.Scand.*, 1966, **20**, 2601.
414. T.Bjorvatten and O.Hassel, *Acta Chem.Scand.*, 1961, **15**, 1429.
415. T.Bjorvatten, *Acta Chem.Scand.*, 1962, **16**, 749.
416. T.Bjorvatten, O.Hassel and A.Lindheim, *Acta Chem.Scand.*, 1963, **17**, 689.
417. T.Bjorvatten, *Acta Chem.Scand.*, 1966, **20**, 1863.
418. N.Bricklebank, S.M.Godfrey, A.G.Mackie, C.A.McAuliffe,
R.G.Prichard and P.J.Kobryn, *J.Chem.Soc., Dalton Trans.*, 1993, 101.
419. S.M.Godfrey, C.A.McAuliffe and R.G.Pritchard,
J.Chem.Soc., *Dalton Trans.*, 1993, 2875.
420. S.M.Godfrey, C.A.McAuliffe and R.G.Pritchard,
J.Chem.Soc., *Dalton Trans.*, 1993, 371.
421. C.A.McAuliffe, S.M.Godfrey, A.G.Mackie and
R.G.Pritchard, *Angew.Chem. Int.Ed.Engl.*, 1992, **31**, 919.
422. C.A.McAuliffe, S.M.Godfrey, A.G.Mackie and
R.G.Pritchard, *J.Chem.Soc., Chem.Commun.*, 1992, 483.
423. J.E.Huheey, 'Anorganische Chemie', pp.853 - 857, de Gruyter,
Berlin New York, 1985.
424. F.A.Cotton and G.Wilkinson, 'Advanced Inorganic Chemistry',
pp.577 - 579, 5th ed., Wiley, New York, 1988.
425. N.V.Sidgwick, 'Chemical Elements and Their Compounds',
pp.1190 - 1200, Vol.II, Oxford University Press, 1950.
426. E.H.Wiebenga, E.E.Havinga and K.H.Boswijk,
Adv.Inorg.Radiochem., 1961, **3**, 33.
427. R.E.Rundle, *Acta Cryst.*, 1961, **14**, 585.

428. K.F.Tebbe and A.L.Rheingold, 'Polyhalogen Cations and Polyhalide Anions in Homoatomic Rings, Chains and Macromolecules of Main- Group Elements', Elsevier, Amsterdam, 1977.
429. J.C.Slater, Acta Cryst., 1959, **12**, 197.
430. M.G.B.Drew and J.D.Wilkins, *J.Chem.Soc., Dalton Trans.*, 1973, 2664.
431. C.T.Lam, D.L.Lewis and S.J.Lippard, *Inorg.Chem.*,1976, **15**, 989.
432. J.Runsink, S.Swen-Walstra and T.Migchelsen, *Acta Cryst.*, 1972, **B28**, 1331.
433. Y.S.Sohn, A.W.Schlueter, D.N.Hendrickson and M.B.Gray, *Inorg.Chem.*, 1974, **13**, 301.
434. T.Migchelsen and A.Vos, *Acta Cryst.*, 1967, **23**, 796.
435. T.Bernstein and F.H.Herbstein, *Acta Cryst.*, 1968, **B24**, 1640.
436. K.Neupert-Laves and M.Dobler, *Helv.Chim.Acta*, 1975, **58**, 432.
437. F.Lazarini, *Acta Cryst.*, 1977, **B33**, 1957.
438. M.Kapon and F.H.Herbstein, *Nature (London)*, 1974, **249**, 439.
439. K.Toman, J.Honzl and J.Jecný, *Acta Cryst.*, 1965, **18**, 673.
440. R.Thomas and F.H.Moore, *Acta Cryst.*, 1980, **B36**, 2869.
441. M.A.Beno, U.Geiser, K.L.Kostka, H.H.Wang, K.S.Webb, M.A.Firestone, K.D.Carlson, L.Nuñez, M.-H.Whangbo and J.M.Williams, *Inorg. Chem.*, 1987, **26**, 1912.
442. M.G.B.Drew and J.D.Wilkins, *J.Organomet.Chem.*, 1974, **69**, 271.
443. H.Pritzkow, *Acta Cryst.*, 1975, **B31**, 1505.
444. M.G.B.Drew, G.M.Egginton and J.D.Wilkins, *Acta Cryst.*, 1974, **B30**, 1895.
445. J.W.Bats, J.J.de Boer and D.Bright, *Inorg.Chim. Acta*, 1971, **5**, 605.
446. A.J.Finney, Ph.D. thesis, University of Tasmania, 1973.
447. R.C.L.Mooney, *Z.Kristallogr.*, 1935, **90**, 143.
448. K.F.Tebbe, B.Freckmann, M.Hörner, W.Hiller and J.Strähle, *Acta Cryst.*, 1985, **C41**, 660.
449. T.L.Hendixson, M.A.ter Horst and R.A.Jacobson, *Acta Cryst.*, 1991, **C47**, 2141.
450. W.Gabes and M.A.M.Nijman-Meester, *Inorg.Chem.*, 1973, **12**, 589.
451. F.H.Herbstein, M.Kapon and W.Schwotzer, *Helv.Chim.Acta*, 1983, **66**, 35.
452. M.F.Belicci, G.G.Fava and C.Pelizzi, *Acta Cryst.*, 1981, **B37**, 924.

453. E.Dubler and L.Linowsky, *Helv.Chim.Acta*, 1978, **58**, 2604.
454. A.Rabenau, H.Schulz and W.Stoeger, *Naturwissenschaften*, 1976, **63**, 245.
455. J.Broekema, E.E.Havinga and E.H.Wiebenga, *Acta Cryst.*, 1957, **10**, 596.
456. R.J.Hach and R.E.Rundle, *J.Am.Chem.Soc.*, 1951, **73**, 4321.
457. R.Thomas and F.H.Moore, *Acta Cryst.*, 1981, **B37**, 2156.
458. F.H.Herbstein and M.Kapon, *Acta Cryst.*, 1972, **A28**, S74.
459. F.H.Herbstein, M.Kapon and G.M.Reisner, Acta Cryst., 1985, **B41**, 348.
460. F.H.Herbstein, M.Kapon, G.M.Reisner, *Proc.R.Soc.(London) Ser. A*, 1981, **376**, 301.
461. E.E.Havinga and E.H.Wiebenga, *Acta Cryst.*, 1958, **11**, 733.
462. E.E.Havinga, K.H.Boswijk and E.H.Wiebenga, *Acta Cryst.*, 1954, **7**, 487.
463. R.Thomas and F.H.Moore, *Acta Cryst.*, 1981, **B37**, 2153.
464. W.J.James, R.J.Hach, D.French and R.E.Rundle, *Acta Cryst.*, 1955, **8**, 814.
465. F.H.Herbstein and W.Schwotzer, *Angew.Chem.Int.Ed.Engl.*, 1982, **21**, 219.
466. J.Passmore, P.Taylor, T.Whidden and P.S.White, *Can.J.Chem.*, 1979, **57**, 968.
467. F.H.Herbstein and M.Kapon, *Phil.Trans.R.Soc.Lond.*, 1979, **A291**, 199.
468. F.Bigoli, M.A.Pellinghelli, G.Crisponi, P.Deplano and E.F.Trogu, *J.Chem.Soc., Dalton Trans.*, 1985, 1349.
469. R.C.Teitelbaum, SL.Ruby and T.J.Marks, *J.Am.Chem.Soc.*, 1980, **102**, 3322.
470. G.Kortüm and H.Walz, *Zeitschrift für Elektrochemie*, 1953, **57**, 73.
471. F.W.Bennett and A.G.Sharpe, *J.Chem.Soc.*, 1950, 1383.
472. Hughes and Ingold, *J.Chem.Soc.*, 1935, 244.
473. Waters, *J.Chem.Soc.*, 1942, 153.
474. R.S.Mulliken and W.B.Pearson, 'Molecular Complexes', Interscience, New York, 1969, and references therein.
475. G.A.Bowmaker and S.F.Hannan, *Aust.J.Chem.*, 1971, **24**, 2237.
476. H.Carlssohn, Habilitationsschrift, Verlag S.Hirzel, Leipzig, 1932.
477. M.I.Ushakov and W.O.Tchistov, *Ber.dtsch.chem.Ges.*, 1935, **68**, 824.
478. J.Kleinberg, *J.Chem.Edu.*, 1946, **23**, 559.
479. H.Schmidt and H.Meinert, *Angew.Chem.*, 1959, **71**, 126.
480. G.B.Kauffman and K.L.Stevens, *Inorg.Synth.*, 1963, **7**, 169.
481. see ref. 368

482. I.Tornieporth-Oetting, T.Klapötke and J.Passmore, *Z.anorg.allg.Chem.*, 1990, **586**, 93 and references therein.
483. P.K.Gowik and T.M.Klapötke, *J.Chem.Soc., Chem.Commun.*, 1990, 1433.
484. J.B.Lambert, D.H.Johnson, R.G.Keske and C.E.Mixan, *J.Am.Chem.Soc.*, 1972, **94**, 8172.
485. J.Passmore and P.Taylor, *J.Chem.Soc.,Dalton Trans.*, 1976, 804.
486. O.Hassel and H.Hope, *Acta Chem.Scand.*, 1961, **15**, 407.
487. Devillanova - private communication to be published
488. F.H.Herbstein, P.Ashkenazi, M.Kraftory, M.Kapon, G.M.Reisner and D.Ginsburg, *Acta.Cryst.*, 1986, **B42**, 575.
489. P.Job, *Anal.Chim.*, 1928, **9**, 113.
490. P.Job, *Anal.Chim.*, 1936, **17**, 97.
491. H.P.Lane,S.M.Godfrey,C.A.McAuliffe and R.G.Pritchard, *J.Chem.Soc., Dalton Trans.*, 1994, 3249.
492. R.C.L.Mooney Slater, Acta Cryst., 1959, **12**, 187.
493. G.A.Melson, ed, 'Co-ordination Chemistry of Macrocyclic Compounds', pp. 6 - 15, Plenum Press, New York, 1973.
494. J.Cosier and A.M.Glazer, *J.Appl.Cryst.*, 1986, **19**, 105.
495. W.Clegg, *Acta Cryst.*, 1981, **A37**, 22.
496. DIF4 ver.7.09, Stoë & Cie, Darmstadt, Germany, 1990.
497. REDU4 ver. 7.03, Stoë & Cie, Darmstadt, Germany, 1990.
498. A.C.T.North, D.C.Phillips and F.S.Mathews, *Acta Cryst.*, 1968, **A24**, 351.
499. ST4REF, program for reflection statistics, R.O.Gould and D.E.Smith, The University of Edinburgh, 1993.
500. SHELXTL/PC ver. 4.3, Siemens Analytical X-ray Instruments Inc., Madison, Wisconsin, USA, 1992.
501. SHELXS-86, program for crystal structure solution, G.M.Sheldrick, *Acta Cryst.*, 1990, **A46**, 467.
502. SHELX76, program for crystal structure determination, G.M.Sheldrick, University of Cambridge, England, 1976.
503. P.T.Beurskens, G.Admiraal, G.Beurskens, W.P.Bosman, S.Garcia-Granda, R.O.Gould, J.M.M.Smits and C.Smykalla. The DIRDIF program system, Technical Report of the Crystallography Laboratory, University of Nijmegen, The Netherlands, 1992.

504. SHELXL-93, program for crystal structure refinement, G.M.Sheldrick, University of Göttingen, Germany, 1993.
505. DIFABS, program for applying empirical absorption corrections, N.Walker and D.Stuart, *Acta Cryst.*, 1983, **A39**, 158.
506. CALC, program for molecular geometry calculations, R.O.Gould and P.Taylor, The University of Edinburgh, Scotland, 1985.
507. CAMERON, a program for the graphical representation of structural data, L.J.Pearce and D.J.Watkin, Chemical Crystallography Laboratory, University of Oxford, England, 1993.
508. WinModel, program for high resolution molecular graphics, C.Radek The University of Edinburgh, Scotland, 1993.
509. CDS, Chemical Database Services, Daresbury Laboratory, Daresbury, Warrington, England.
510. CSSR, Cambridge Structural Database, over 100,000 entries.
511. ICSD, Inorganic Crystal Structure Database, 35,000 entries.
512. BIDS, Bath Information and Data Services.

REPRINTS OF PUBLICATIONS AND POSTER ABSTRACTS

The Synthesis and Low-temperature Single Crystal X-Ray Structure of the Charge-transfer Complex $([9]aneS_3)_2(I_2)_4$ ([9]aneS$_3$ = 1,4,7-trithiacyclononane)

Alexander J. Blake, Robert O. Gould, Christian Radek and Martin Schröder*

Department of Chemistry, The University of Edinburgh, West Mains Road, Edinburgh, Scotland EH9 3JJ

Reaction of [9]aneS$_3$ (1,4,7-trithiacyclononane) and I_2 in cold CH_2Cl_2 results in the formation of 1 : 1 and 1 : 2 adducts; the single crystal X-ray structure of the 1 : 2 adduct $([9]aneS_3)_2(I_2)_4$ shows an unusual polymeric structure with I_2 bridging [9]aneS$_3$ thioether units.

The complexation of late transition metals by thioether macrocycles has been studied intensively in the last decade.[1,2] Recently, Willey and coworkers have confirmed the ability of thioether crowns to bind to main group cations such as Sb^{III} and Bi^{III}.[3] Our own work has focused on the chemistry of thioether crowns with transition metal ions,[1] and more recently with Ag^{I}, Au^{I} and Tl^{I} centres.[4] We were interested in whether homoleptic thioether crowns might be capable of binding to halogens and inter-halogens such as I_2 and ICl to form charge-transfer complexes. Previous work on iodine-thioether[5] or -thiocarbonyl[6] complexes has shown a wide range of different coordination modes and structures. We report herein the synthesis and structure of an unusual polymeric adduct of I_2 with [9]aneS$_3$.

Addition of I_2 to one molar equiv. of [9]aneS$_3$ in CH_2Cl_2 at 0 °C under N_2 affords a pale-brown solution: further addition of I_2 leads to slight darkening of the solution. The stoichiometry of the I_2:[9]aneS$_3$ charge-transfer complex was determined using Job's method[7] of continuous concentration variation. This was carried out by measuring the variation in the absorption band of the charge-transfer complex at 310 nm as a function of I_2:[9]aneS$_3$ ratio. Although this method does not eliminate the possibility of formation of higher stoichiometries in solution, it does suggest that the main product in CH_2Cl_2 solution is the 1 : 1 species $([9]aneS_3)(I_2)$. Reaction of [9]aneS$_3$ with ICl in a 1 : 1 molar ratio in CH_2Cl_2 likewise affords a brown solution: addition of a further equivalent of ICl affords a yellow precipitate which has the stoichiometry $([9]aneS_3)(ICl)_2$. This yellow product is unstable in MeCN and darkens rapidly to give brown solutions. In the solid state, the complex slowly darkens over a period of weeks with the apparent evolution of ICl and/or I_2.

Red lustrous crystals of the [9]aneS$_3$: I_2 adduct suitable for X-ray diffraction studies were obtained by sublimation. The structure determination† shows (Fig. 1) two [9]aneS$_3$ mol-

† *Crystal data* for: $C_{12}H_{24}I_8S_6$, M = 1375.9, triclinic, space group $P\bar{1}$, a = 8.437(7), b = 13.820(18), c = 14.752(10) Å, α = 65.95(5), β = 89.31(4), γ = 81.06(4)°, V = 1549 Å^3 [from 2θ values of 20 reflections measured at ±ω (2θ = 25–26°, $\bar{\lambda}$ = 0.71073 Å), T = 150.0(1) K], Z = 2, D_c = 2.949 g cm^{-3}, μ(Mo-Kα) = 8.320 mm^{-1}. A red needle (0.04 × 0.08 × 0.70 mm) was mounted in the cold stream of an Oxford Cryosystems low-temperature device (J. Cosier and A. M. Glazer, *J. Appl. Cryst.*, 1986, **19**, 105) on a Stoë Stadi-4 four-circle diffractometer. Data collection using Mo-Kα X-radiation ($\bar{\lambda}$ = 0.71073 Å) and ω scans gave 2897 unique, absorption-corrected reflections (T_{min}, T_{max} = 0.269, 0.891 respectively) to $2\theta_{max}$ = 40°, of which 2405 with $F \geq 4\sigma(F)$ were used in all calculations. Folowing solution by automatic direct methods (SHELXS-86: G. M. Sheldrick, University of Göttingen, Germany 1986), the structure was refined by full-matrix least-squares on F. At isotropic convergence, final corrections (min 0.643, max 1.390) for absorption were applied empirically using DIFABS (N. Walker and D. Stuart, *Acta Crystallogr., Sect. A*, 1983, **39**, 158). Anisotropic thermal parameters were refined for I and S atoms: H atoms were included in fixed, calculated positions with a common U_{iso} of 0.024(12) Å^2 (SHELX-76: G. M. Sheldrick, University of Cambridge, England 1976). At final convergence, R = 0.0573, wR = 0.0730, S = 0.845 for 177 parameters and the final ΔF synthesis showed no feature above 2.2 e Å^{-3}.

Atomic coordinates, bond lengths and angles, and thermal parameters have been deposited at the Cambridge Crystallographic Data Centre. See Notice to Authors, Issue No. 1.

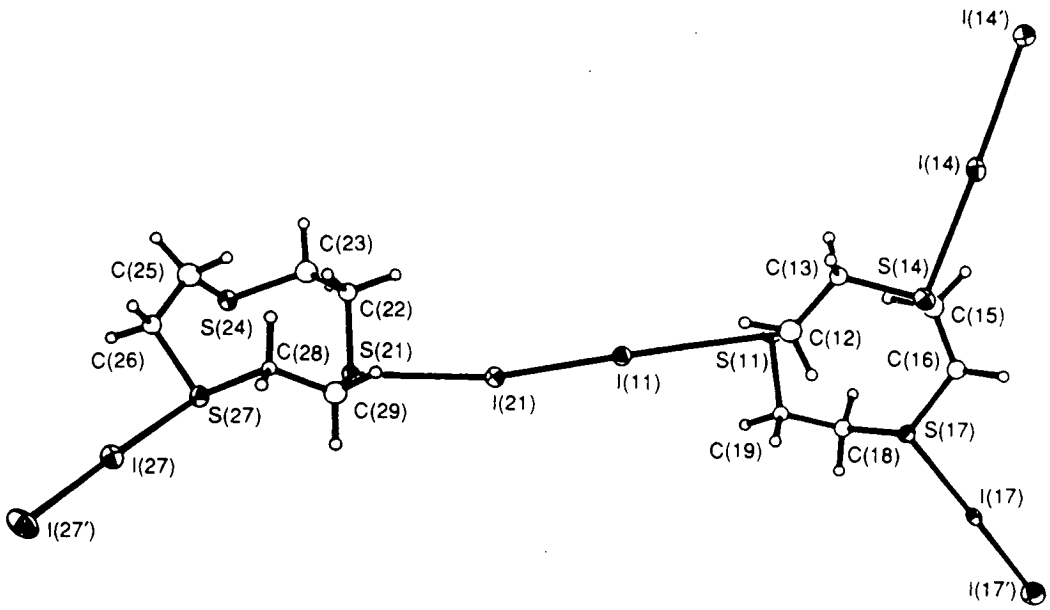

Fig. 1 View of the structure of $([9]aneS_3)_2(I_2)_4$ with numbering scheme adopted

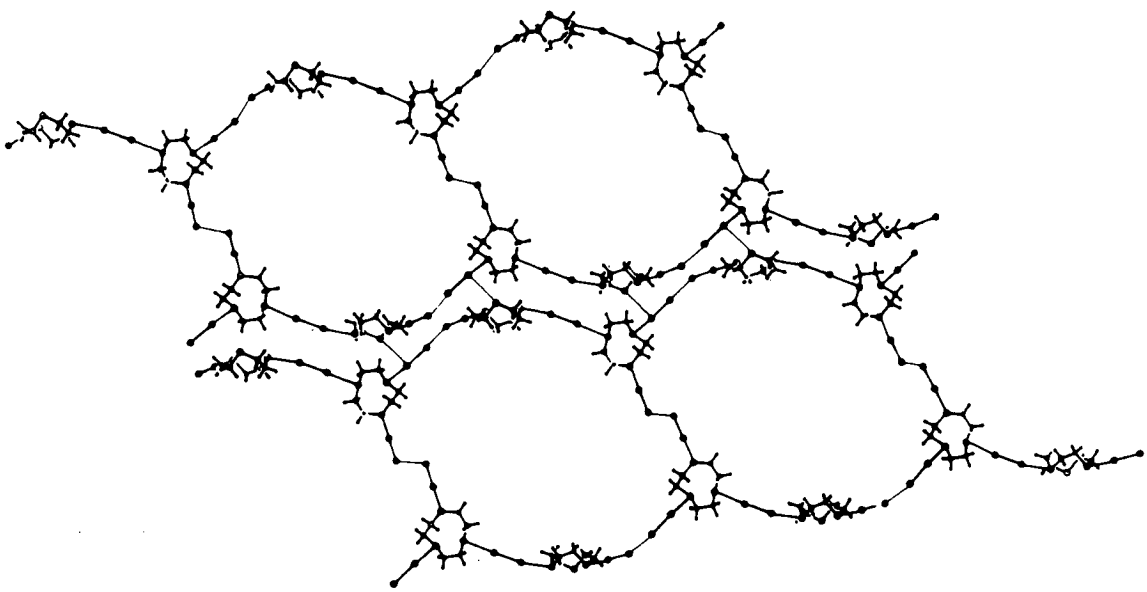

Fig. 2 Packing diagram for $([9]aneS_3)_2(I_2)_4$

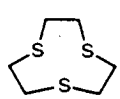

[9]aneS$_3$

ecules linked by a bridging diiodine molecule. The structure is asymmetric: the first macrocycle [S(11)–C(19)] interacts with two terminal I_2 molecules in addition to the bridging molecule; the second [S(21)–C(29)] carries only one terminal I_2 molecule. The two [9]aneS$_3$ moieties also differ markedly in conformation, with the second adopting one similar to the [333] *endo* conformation observed for free [9]aneS$_3$ in the crystal and in the vapour phase:[8] the first ring adopts a different conformation for the region around S(11).

The bond lengths for both bridging [I(11)–I(21) 2.754(2) Å] and terminal [I(14)–I(14') 2.785(2), I(17)–I(17') 2.816(2), I(27)–I(27') 2.799(2) Å] I–I distances are, as expected, significantly longer than the I–I bond length in either the vapour [2.667(2) Å][9] or the solid state at 110 K [2.715(6) Å].[10] The S···I distances involving the I_2 bridge are the longest at 3.197(6) Å [for S(11)–I(11)] and 3.054(6) Å [for S(21)–I(21)]; the S–I distances to terminal diiodine molecules are 2.870(6), 2.760(6) and 2.862(6) Å for S(14)–I(14), S(17)–I(17) and S(27)–I(27) respectively. The variation of I–I *vs.* S–I bond distances fits the curve plotted by Herbstein and Schwotzer[11] in the region of minimum perturbation: that is, long I–I bonds are associated with short S–I bonds and vice versa. The quasi-linear S–I–I angles range from 174.86(14) to 178.35(14)°, with the exception of the I(11)–I(21)–S(21) angle of 168.39(13)°.

As commonly found for structures containing I_2, there are extensive intermolecular contacts, here I···I and S···I. It is noteworthy that the closest S···I intermolecular contacts of

3.721 and 3.751 Å involve the unique, uncoordinated sulfur S(24). The closest I···I contact is one of 3.778(3) Å. The greater non-linearity at I(21) compared with I(11) may be linked to the participation of the former in two relatively short contacts of 4.036(3) and 4.204(3) Å (the van der Waals radius for I is 2.10 Å). Fig. 2 illustrates part of an infinite sheet of $([9]aneS_3)_2(I_2)_4$ molecules formed by these contacts: sheets are cross-linked and offset from one another to form an infinite three-dimensional network of molecules.

Reaction of I_2 and ICl with [12]aneS$_4$, [14]aneS$_4$, [16]aneS$_4$, [15]aneS$_5$ and [18]aneS$_6$ all give similar 1 : 1 and 2 : 1 brown or yellow adducts of varying solubility. Future work is aimed at the solid state characterisation of these materials and the investigation of partially charged species derived from them.

We thank the SERC for support and the Royal Society of Edinburgh and Scottish Office Education Department for a Support Research Fellowship to M. S.

Received, 2nd March 1993; Com. 3/01229H

References

1 A. J. Blake and M. Schröder, *Adv. Inorg. Chem.*, 1990, **35**, 1.
2 S. R. Cooper and S. C. Rawle, *Struct. Bond. (Berlin)*, 1990, **72**, 1.
3 G. R. Willey, M. T. Lakin, M. Ravindran and N. W. Alcock, *J. Chem. Soc., Chem. Commun.*, 1991, 271; G. R. Willey, M. T. Larkin and N. W. Alcock, *J. Chem. Soc., Dalton Trans.*, 1992, 591.
4 *E.g.*: A. J. Blake, D. Collison, R. O. Gould, G. Reid and M. Schröder, *J. Chem. Soc., Dalton Trans.*, 1993, 521; A. J. Blake, J. A. Greig, A. J. Holder, T. I. Hyde, A. Taylor and M. Schröder, *Angew. Chem., Int. Ed. Engl.*, 1989, **29**, 197; A. J. Blake, G. Reid and M. Schröder, *J. Chem. Soc., Dalton Trans.*, 1992, 2987.
5 G. Y. Chao and J. D. McCullough, *Acta Crystallogr.*, 1960, **13**, 727; C. Rømming, *Acta Chem. Scand.*, 1960, **14**, 2145; F. H. Herbstein, P. Ashkenazi, M. Kaftory, M. Kapon, G. M. Reisner and D. Ginsburg, *Acta Crystallogr. Sect. B*, 1986, **42**, 575; A. L. Tipton, M. C. Lonergan, C. L. Stern and D. F. Shriver, *Inorg. Chim. Acta*, 1992, **201**, 23.
6 E. L. Ahlsen and K. O. Strømme, *Acta Chem. Scand., Ser. A*, 1974, **28**, 175; F. Freeman, J. W. Ziller, H. N. Po and M. C. Keindl, *J. Am. Chem. Soc.*, 1988, **110**, 2586; D. Atzei, P. Deplano, E. F. Trogu, F. Bigoli, M. A. Pellinghelli and A. Vacca, *Can. J. Chem.*, 1988, **66**, 1483.
7 P. Job, *Anal. Chim.*, 1928, **9**, 113; 1936, **17**, 97.
8 R. S. Glass, G. S. Wilson and W. N. Setzer, *J. Am. Chem. Soc.*, 1980, **102**, 5068; R. Blom, D. W. H. Rankin, M. Schröder and A. Taylor, *J. Chem. Soc., Perkin Trans. 2*, 1991, 773.
9 I. L. Karle, *J. Chem. Phys.*, 1955, **23**, 1739.
10 F. van Bolhuis, P. B. Koster and T. Migchelsen, *Acta Crystallogr.*, 1967, **23**, 90.
11 E. F. H. Herbstein and W. Schwotzer, *J. Am. Chem. Soc.*, 1984, **106**, 2367.

Acta Cryst. (1993). C**49**, 1652–1654

Tetra(*n*-butyl)ammonium Trifluoromethanesulfonate

ALEXANDER J. BLAKE,* CHRISTIAN RADEK AND MARTIN SCHRÖDER

Department of Chemistry, The University of Edinburgh, West Mains Road, Edinburgh EH9 3JJ, Scotland

(*Received* 21 *October* 1992; *accepted* 10 *February* 1993)

Abstract

The title structure comprises two ion pairs in each asymmetric unit. There are no close contacts between any of the ions. Although the structure determination was carried out at reduced temperature there are large vibration amplitudes for some F atoms and disorder in one of the *n*-butyl chains.

Comment

Trifluoromethanesulfonic acid has been reported in its anhydrous form (Bartmann & Mootz, 1990) and with increasing degrees of hydration (Lundgren & Spencer, 1973; Delaplane, Lundgren & Olovsson, 1975*a*,*b*; Lundgren, 1978*a*,*b*). One series of salts with nonaaqualanthanide(III) cations has been reported (Harrowfield, Kepert, Patrick & White, 1983; Castellano, Machado, Santos & Vicentini, 1985; Chatterjee, Maslen & Watson, 1988). Salts with the cations $[V(H_2O)_6]^{2+}$ (Holt, Larkworthy, Leigh, Povey & Smith, 1989) and $[V(H_2O)_6]^{3+}$ (Cotton, Fair, Lewis, Mott, Ross, Schultz & Williams, 1984) are also known. Although $CF_3SO_3^-$ is a common counteranion for complex metal ions, there are relatively few examples with simple inorganic cations such as oxonium (Lundgren, Olovsson & Tellgren, 1978), ammonium (Brauer & Ganswein, 1975) and seleninyl (Kapoor, Kapoor, Sawyer & Wadhawan, 1988). Salts containing simple alkylammonium cations are even rarer (*e.g.* $CH_3NH_3^+$; Alberts, Noltes, Roelofsen & Spek, 1982).

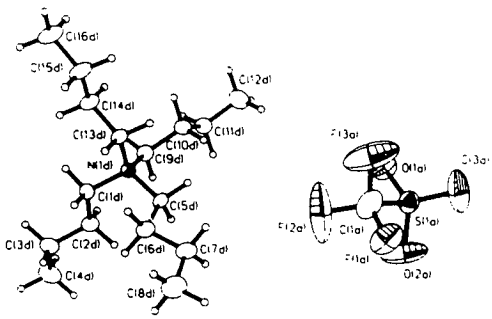

Fig. 1. View of one ion pair showing the labelling of the non-H atoms. Thermal ellipsoids are drawn at the 50% probability level except for H atoms which have artificial radii of 0.10 Å^2 for clarity.

Selected geometric parameters are shown in Table 1. C—C bond lengths are normal; bond angles are in the range 108–112° except for those listed; torsion angles are all in the range 60 ± 10° or 180 ± 10° except those listed.

Experimental

Crystal data

$C_{16}H_{36}N^+.CF_3SO_3^-$
M_r = 391.5
Monoclinic
$P2_1/a$
a = 15.531 (4) Å
b = 18.136 (6) Å
c = 16.895 (4) Å
β = 114.674 (20)°
V = 4324 Å^3
Z = 8
D_x = 1.202 Mg m^{-3}
Mo $K\alpha$ radiation
λ = 0.71073 Å
Cell parameters from 41 reflections
θ = 15–16°
μ = 0.181 mm^{-1}
T = 150.0 K
Block
1.04 × 0.70 × 0.70 mm
Colourless
Crystal source: recrystallization from MeOH/H_2O

Data collection

Stoe Stadi-4 diffractometer
ω–2θ scans
Absorption correction: none
5901 measured reflections
5901 independent reflections
3823 observed reflections [$F>4\sigma(F)$]
θ_{max} = 22.5°
h = −16 → 15
k = 0 → 19
l = 0 → 18
3 standard reflections
frequency: 60 min
intensity variation: 2.5% (isotropic decay)

©1993 International Union of Crystallography
Printed in Great Britain – all rights reserved

Refinement

Refinement on F
Final R = 0.0557
wR = 0.0661
S = 1.342
3823 reflections
450 parameters
Only H-atom U's refined

$w = [\sigma^2(F) + 0.000228F^2]^{-1}$
$(\Delta/\sigma)_{max}$ = 0.001
$\Delta\rho_{max}$ = 0.72 e Å^{-3}
$\Delta\rho_{min}$ = −0.64 e Å^{-3}
Extinction correction: none
Atomic scattering factors from *SHELX*76

Table 1. *Fractional atomic coordinates and equivalent isotropic thermal parameters* (Å^2)

$U_{eq} = \frac{1}{3}\sum_i\sum_j U_{ij}a_i^*a_j^*\mathbf{a}_i.\mathbf{a}_j$.

	x	y	z	U_{eq}
S(1A)	0.06121 (9)	0.16678 (7)	0.87909 (8)	0.0366 (8)
O(1A)	0.02705 (23)	0.20308 (19)	0.79711 (20)	0.0460 (24)
O(2A)	0.15412 (25)	0.1345 (3)	0.9036 (3)	0.087 (4)
O(3A)	0.0511 (4)	0.20292 (22)	0.94757 (25)	0.086 (4)
C(1A)	−0.0101 (4)	0.0853 (3)	0.8614 (3)	0.051 (4)
F(1A)	0.01310 (21)	0.04280 (17)	0.93037 (19)	0.0592 (23)
F(2A)	−0.0150 (4)	0.04515 (23)	0.7973 (3)	0.141 (5)
F(3A)	−0.10146 (25)	0.1062 (3)	0.8413 (3)	0.113 (4)
S(1B)	−0.48274 (8)	0.76989 (7)	0.61336 (7)	0.0336 (8)
O(1B)	−0.56833 (22)	0.73996 (20)	0.61354 (23)	0.053 (3)
O(2B)	−0.47703 (25)	0.76501 (21)	0.53118 (21)	0.056 (3)
O(3B)	−0.39776 (22)	0.75239 (20)	0.68844 (21)	0.0476 (24)
C(1B)	−0.4953 (3)	0.8682 (3)	0.6249 (3)	0.045 (4)
F(1B)	−0.57159 (21)	0.89545 (18)	0.55963 (23)	0.074 (3)
F(2B)	−0.42171 (19)	0.90605 (16)	0.62569 (20)	0.0573 (23)
F(3B)	−0.5008 (3)	0.88472 (21)	0.69887 (24)	0.092 (3)
N(1C)	−0.27582 (23)	0.26923 (19)	0.69270 (21)	0.0260 (23)
C(1C)	−0.2027 (3)	0.23471 (25)	0.6661 (3)	0.030 (3)
C(2C)	−0.2398 (3)	0.2085 (3)	0.5722 (3)	0.034 (3)
C(3C)	−0.1578 (3)	0.1762 (3)	0.5552 (3)	0.040 (3)
C(4C)	−0.1909 (4)	0.1521 (3)	0.4605 (3)	0.047 (4)
C(5C)	−0.2279 (3)	0.28412 (25)	0.79076 (25)	0.026 (3)
C(6C)	−0.1424 (3)	0.3346 (3)	0.8211 (3)	0.029 (3)
C(7C)	−0.1112 (3)	0.3519 (3)	0.9167 (3)	0.042 (4)
C(8C)	−0.0190 (3)	0.3952 (3)	0.9552 (3)	0.046 (4)
C(9C)	−0.3115 (3)	0.34009 (25)	0.6410 (3)	0.030 (3)
C(10C)	−0.3692 (3)	0.39034 (25)	0.6724 (3)	0.033 (3)
C(11C)	−0.4007 (4)	0.4582 (3)	0.6133 (3)	0.045 (4)
C(12C)	−0.4527 (4)	0.5137 (3)	0.6449 (3)	0.055 (4)
C(13C)	−0.3605 (3)	0.21913 (25)	0.6737 (3)	0.029 (3)
C(14C)	−0.3361 (3)	0.1415 (3)	0.7114 (3)	0.042 (4)
C(15C)	−0.4164 (4)	0.0898 (4)	0.6779 (5)	0.090 (6)
C(16)	−0.4933 (6)	0.1133 (5)	0.7088 (6)	0.0500
C(16′)	−0.5232 (5)	0.1085 (8)	0.6440 (9)	0.0500
N(1D)	0.12889 (23)	0.17088 (20)	0.19672 (21)	0.0247 (23)
C(1D)	0.1449 (3)	0.10861 (25)	0.1442 (3)	0.029 (3)
C(2D)	0.2447 (3)	0.1043 (3)	0.1470 (3)	0.035 (3)
C(3D)	0.2542 (3)	0.0330 (3)	0.1042 (3)	0.044 (4)
C(4D)	0.3481 (4)	0.0287 (3)	0.0968 (4)	0.058 (4)
C(5D)	0.1933 (3)	0.1640 (3)	0.29391 (25)	0.027 (3)
C(6D)	0.1967 (3)	0.0886 (3)	0.3334 (3)	0.034 (3)
C(7D)	0.2440 (4)	0.0962 (3)	0.4331 (3)	0.041 (4)
C(8D)	0.2622 (4)	0.0221 (3)	0.4771 (3)	0.061 (4)
C(9D)	0.1504 (3)	0.24393 (24)	0.1648 (3)	0.030 (3)
C(10D)	0.1266 (3)	0.31243 (24)	0.2034 (3)	0.033 (3)
C(11D)	0.1825 (3)	0.3780 (3)	0.1937 (3)	0.038 (3)
C(12D)	0.1581 (4)	0.4494 (3)	0.2260 (4)	0.052 (4)
C(13D)	0.0263 (3)	0.1670 (3)	0.1857 (3)	0.028 (3)
C(14D)	−0.0491 (3)	0.1793 (3)	0.0939 (3)	0.034 (3)
C(15D)	−0.1460 (3)	0.1693 (3)	0.0930 (3)	0.045 (4)
C(16D)	−0.2267 (3)	0.1808 (3)	0.0036 (3)	0.050 (4)

Table 2. *Selected geometric parameters* (Å, °)

S(1A)—O(1A)	1.421 (4)	C(1B)—F(1B)	1.332 (7)
S(1A)—O(2A)	1.448 (5)	C(1B)—F(2B)	1.328 (6)
S(1A)—O(3A)	1.394 (5)	C(1B)—F(3B)	1.322 (7)
S(1A)—C(1A)	1.794 (6)	N(1C)—C(1C)	1.520 (6)
C(1A)—F(1A)	1.317 (7)	N(1C)—C(5C)	1.530 (6)
C(1A)—F(2A)	1.281 (8)	N(1C)—C(9C)	1.522 (6)
C(1A)—F(3A)	1.368 (7)	N(1C)—C(13C)	1.519 (6)
S(1B)—O(1B)	1.437 (4)	N(1D)—C(1D)	1.519 (6)
S(1B)—O(2B)	1.431 (4)	N(1D)—C(5D)	1.530 (6)
S(1B)—O(3B)	1.433 (4)	N(1D)—C(9D)	1.520 (6)
S(1B)—C(1B)	1.812 (6)	N(1D)—C(13D)	1.527 (6)
O(1A)—S(1A)—O(2A)	112.84 (25)	F(1B)—C(1B)—F(2B)	106.3 (4)
O(1A)—S(1A)—O(3A)	117.7 (3)	F(2B)—C(1B)—F(3B)	105.5 (4)
O(1A)—S(1A)—C(1A)	105.38 (25)	N(1C)—C(5C)—C(6C)	115.7 (4)
O(2A)—S(1A)—O(3A)	113.4 (3)	C(6C)—C(7C)—C(8C)	112.8 (4)
O(2A)—S(1A)—C(1A)	100.7 (3)	N(1C)—C(9C)—C(10C)	115.6 (4)
O(3A)—S(1A)—C(1A)	104.5 (3)	N(1C)—C(13C)—C(14C)	114.9 (4)
S(1A)—C(1A)—F(1A)	114.4 (4)	C(13C)—C(14C)—C(15C)	113.9 (5)
S(1A)—C(1A)—F(2A)	115.1 (5)	C(14C)—C(15C)—C(16′)	127.4 (7)
F(1A)—C(1A)—F(3A)	104.7 (5)	N(1D)—C(1D)—C(2D)	115.5 (4)
F(2A)—C(1A)—F(3A)	105.0 (5)	N(1D)—C(5D)—C(6D)	115.7 (4)
O(1B)—S(1B)—O(2B)	114.26 (22)	C(2B)—C(1B)—F(3B)	105.5 (4)
O(1B)—S(1B)—O(3B)	115.18 (22)	C(1C)—N(1C)—C(5C)	107.9 (3)
O(1B)—S(1B)—C(1B)	103.32 (24)	C(1C)—N(1C)—C(13C)	112.3 (3)
O(2B)—S(1B)—O(3B)	115.98 (22)	C(9C)—N(1C)—C(13C)	107.9 (3)
O(2B)—S(1B)—C(1B)	102.60 (24)	N(1C)—C(1C)—C(2C)	115.7 (4)
O(3B)—S(1B)—C(1B)	102.89 (23)	N(1D)—C(9D)—C(10D)	115.5 (4)
S(1B)—C(1B)—F(2B)	112.3 (4)	C(10D)—C(11D)—C(12D)	112.9 (4)
S(1B)—C(1B)—F(3B)	112.2 (4)	N(1D)—C(13D)—C(14D)	116.0 (4)
		C(14D)—C(15D)—C(16D)	113.5 (4)

C(1C)—N(1C)—C(9C)—C(10C)	−167.6 (4)
C(5C)—N(1C)—C(9C)—C(10C)	−48.8 (5)
C(13C)—N(1C)—C(9C)—C(10C)	70.6 (5)
N(1C)—C(13C)—C(14C)—C(15C)	−168.3 (4)
C(13C)—C(14C)—C(15C)—C(16′)	−27.8 (10)
C(1D)—N(1D)—C(5D)—C(6D)	−47.9 (5)
C(9D)—N(1D)—C(5D)—C(6D)	−168.0 (4)
C(13D)—N(1D)—C(5D)—C(6D)	71.0 (5)
N(1D)—C(5D)—C(6D)—C(7D)	−166.5 (4)
N(1D)—C(9D)—C10D)—C(11D)	159.3 (4)

The crystal was cooled in the nitrogen gas stream of an Oxford Cryosystems low-temperature device (Cosier & Glazer, 1986). The structure was solved by automatic direct methods (*SHELXS*86; Sheldrick, 1986) and refined using *SHELX*76 (Sheldrick, 1976). The illustration was prepared using *SHELXTL-PC* (Sheldrick, 1990) and molecular geometry calculations were performed using *CALC* (Gould & Taylor, 1985).

Anisotropic thermal motion was allowed for all non-H atoms except C(16) and C(16′) which constitute a 0.61:0.39 disorder pair. The disorder was modelled by constraining the C(15*C*)—C(16) and C(15*C*)—C(16′) bonds to be 1.55 Å. A common isotropic thermal parameter for H atoms in calculated positions refined to 0.056 (2) Å^2.

We thank the SERC for support.

Lists of structure factors, anisotropic thermal parameters, H-atom coordinates and complete geometry have been deposited with the British Library Document Supply Centre as Supplementary Publication No. SUP 71091 (31 pp.). Copies may be obtained through The Technical Editor, International Union of Crystallography, 5 Abbey Square, Chester CH1 2HU, England. [CIF reference: HA1038]

References

Alberts, A. H., Noltes, J. G., Roelofsen, G. & Spek, A. L. (1982). *Cryst. Struct. Commun.* **11**, 1863–1868.
Bartmann, K. & Mootz, D. (1990). *Acta Cryst.* C**46**, 319–320.
Brauer, G. & Ganswein, B. (1975). *Z. Anorg. Allg. Chem.* **415**, 125–132.
Castellano, E. E., Machado, L. C., Santos, C. O. P. & Vicentini, G. (1985). *Inorg. Chim. Acta*, **110**, 83–86.

Chatterjee, A., Maslen, E. N. & Watson, K. J. (1988). *Acta Cryst.* **B44**, 381–386.
Cosier, J. & Glazer, A. M. (1986). *J. Appl. Cryst.* **19**, 105–107.
Cotton, F. A., Fair, C. K., Lewis, G. E., Mott, G. N., Ross, F. K., Schultz, A. J. & Williams, J.M. (1984). *J. Am. Chem. Soc.* **106**, 5319–5323.
Delaplane, R. G., Lundgren, J. O. & Olovsson, I. (1975*a*). *Acta Cryst.* **B31**, 2202–2207.
Delaplane, R. G., Lundgren, J. O. & Olovsson, I. (1975*b*). *Acta Cryst.* **B31**, 2208–2213.
Gould, R. O. & Taylor, P. (1985). *CALC*. Program for crystallographic calculations. Univ. of Edinburgh, Scotland.
Harrowfield, J. McB., Kepert, D. L., Patrick, J. M. & White, A. H. (1983). *Aust. J. Chem.* **36**, 483–492.
Holt, D. G. L., Larkworthy, L. L., Leigh, G. J., Povey, D. C. & Smith, G. W. (1989). *Polyhedron*, **8**, 1823–1824.
Kapoor, P., Kapoor, R., Sawyer, J. F. & Wadhawan, P. (1988). *Can. J. Chem.* **66**, 2367–2374.
Lundgren, J. O. (1978*a*). *Acta Cryst.* **B34**, 2428–2431.
Lundgren, J. O. (1978*b*). *Acta Cryst.* **B34**, 2432–2435.
Lundgren, J. O., Olovsson, I. & Tellgren, R. (1978). *Acta Cryst.* **B34**, 2945–2947.
Lundgren, J. O. & Spencer, J. B. (1973). *Acta Cryst.* **B29**, 1923–1928.
Sheldrick, G. M. (1976). *SHELX*76. Program for crystal structure determination. Univ. of Cambridge, England.
Sheldrick, G. M. (1986). *SHELXS*86. Program for the solution of crystal structures. Univ. of Göttingen, Germany.
Sheldrick, G. M. (1990). *SHELXTL-PC*. Version 4.2. Siemens Analytical X-ray Instruments Inc., Madison, Wisconsin, USA.

Reprinted from 'The Chemistry of the Copper and Zinc Triads', ed.
A. J. Welch and S. K. Chapman, The Royal Society of Chemistry, Cambridge
© The Royal Society of Chemistry, 1993

Structural Mis-matches in Silver and Gold Complexes of Thioether Macrocycles

A. J. Blake, R. O. Gould, C. Radek, G. Reid, A. Taylor, and M. Schröder*

DEPARTMENT OF CHEMISTRY, THE UNIVERSITY OF EDINBURGH, EDINBURGH EH9 3JJ, UK

1. INTRODUCTION

Macrocyclic ligands are well-known to form complexes that show remarkable thermodynamic stability and kinetic inertness.[1] The macrocyclic ligand can, therefore, be regarded as a protecting group for the metal centre controlling its stereochemical, electronic and redox properties. The introduction of inherent mis-matches between the metal and the donating ligands leads to the formation of strained complexes of unusual stereochemistry, with the resultant co-ordination geometries being a compromise between the preferences of the metal ion and the encapsulating ligand.[2] This has led to the stabilisation of mononuclear d^7 Ni(III),[3] Pd(III)[4] and Pt(III)[5] species such as $[M([9]aneS_3)_2]^{3+}$ and $[M([18]aneS_6)]^{3+}$. Related d^7 Rh(II)[4,6] and Ir(II)[7] have also been reported. We were interested in extending this work to structural and electrochemical studies of silver and gold complexes of thioether crowns.[8-10]

2. SILVER

Homoleptic Thioether Crowns

The structures of $[Ag([9]aneS_3)_2]^-$ [11] and $[Ag([18]aneS_6)]^+$ [8] have been reported previously and show homoleptic thioether co-ordination at octahedral Ag(I) centres. We have undertaken a study of the interaction of Ag(I) with $[15]aneS_5$ since this crown does not have sufficient S-donors to enable simple octahedral geometry at Ag(I). The structure of the $[Ag([15]aneS_5)]^+$ cation is indeed unusual and reflects the mismatch between Ag(I) and $[15]aneS_5$. The solid-state structure of the cation is dependent upon the counter-anion. Thus, the structure of $[Ag([15]aneS_5)]PF_6$ consists of parallel, polymeric chains of $[Ag([15]aneS_5)]^+$ units. The Ag(I) centre is bound to all five S-donors of the crown, Ag-S(1) = 3.219(5), Ag-S = 2.564(6), 2.659(5), 2.651(6), 3.075(7)Å (Figure 1). S(1) interacts with another Ag(I) centre, Ag'-S(1) = 2.742(5)Å, thus linking the $[Ag([15]aneS_5)]^+$ fragments to form the polymer chain. In contrast, the structure of $[Ag([15]aneS_5)]BPh_4$ shows (Figure 2) a dimeric structure in which two Ag(I) centres are bridged by two $[15]aneS_5$ ligands.[12] One Ag(I) is co-ordinated *via* one long and three short Ag-S bonds, while the other has one

long and four short Ag-S contacts. However, $[Ag([15]aneS_5)]B(C_6F_5)_4$ shows (Figure 3) a genuine monomeric structure with five co-ordinate Ag(I), Ag-S = 2.4712(19), 2.5621(19), 2.7262(20), 2.6847(21), 2.8813(19)Å.

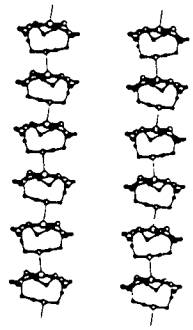

Figure 1

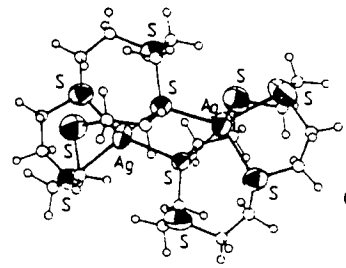

Figure 2

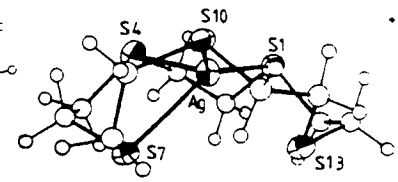

Figure 3

Mixed Oxy-Thioether Crowns

The extraction and transport of Ag(I) and related heavy metal ions across liquid-liquid interfaces and membranes have been achieved using polyether and polythioether cyclic ionophores.[13] The complexation and transport of Ag(I) has focussed particularly on the use of mixed S- and O-donor crowns. The precise mode of co-ordination of these mixed-donor macrocycles to Ag(I) is unknown although 1:1 and 2:1 ligand:Ag complexes involving *exo*-binding of S-donors have been postulated. We were interested in determining the precise mode of co-ordination of the simple mixed O/S macrocycles $[15]aneS_2O_3$ [14,15] and $[18]aneS_2O_4$ (L) to Ag(I).

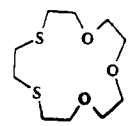

$[15]aneS_2O_3$

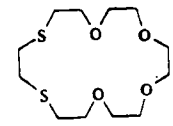

$[18]aneS_2O_4$

Reaction of Ag(I) with one molar equivalent of L affords the expected 1:1 complexes $[Ag(L)]^+$. However, the solid state structure of $[Ag([15]aneS_2O_3)]^+$ shows (Figure 4) a polymeric chain structure with $[Ag([15]aneS_2O_3)]^+$ fragments connected by bridging thioether S-donors. Reaction of Ag(I) salts with $[15]aneS_2O_3$ in ratios of 1:1.5 to 1:3 affords the binuclear species $[Ag_2([15]aneS_2O_3)_3]^{2+}$ (Figure 5). Interestingly, the solid-state structure of $[Ag([18]aneS_2O_4)]^+$ is more complicated than expected and shows a binuclear structure incorporating bridging S-donors. Each $[Ag_2([18]aneS_2O_4)_2]^{2+}$ unit is linked to another *via* a long-range S····S interaction

(3.434Å) to give an overall tetrameric structure of stoichiometry $[Ag_4([18]aneS_2O_4)_4]^{4+}$ (Figure 6).

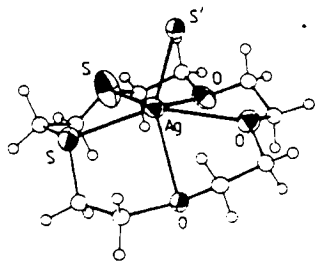

Figure 4

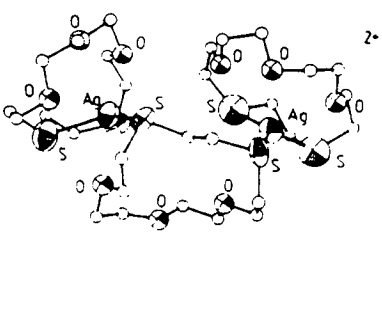

Figure 5

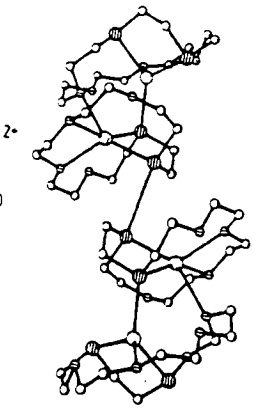

Figure 6

3. GOLD

Au(I) is well known to prefer linear co-ordination; however, treatment of $[Au(tht)_2]^+$ (tht = tetrahydrothiophene) with [9]aneS$_3$, [15]aneS$_5$, [18]aneS$_6$ and Me_2[18]aneN$_2$S$_4$ leads to the formation of complexes exhibiting highly unusual geometries. The single crystal X-ray structure of $[Au([9]aneS_3)_2]^+$ shows (Figure 7) one [9]aneS$_3$ co-ordinated as a monodentate ligand and is therefore relatively labile, Au-S(1') = 2.302(6)Å, while the other [9]aneS$_3$ is bound asymmetrically with one short and two long Au-S distances, Au-S(1) = 2.350(7), Au-S(4) = 2.733(8), Au-S(7) = 2.825(8)Å, <S(1')-Au-S(1) = 153.98(23)°.[10] Thus, the Au(I) centre in $[Au([9]aneS_3)_2]^+$ shows [2+2] S-co-ordination and can therefore be regarded as being in a tetrahedrally-distorted linear environment.[10] The structures of the corresponding Au(II) and Au(III) complexes $[Au([9]aneS_3)_2]^{2+}$ (Figure 8) and $[Au([9]aneS_3)_2]^{3+}$ (Figure 9) reflect the compromise between the facially pre-organised [9]aneS$_3$ crown and the preferred stereochemistries of d^9 and d^8 metal ions.

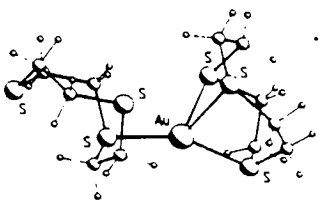

Figure 7

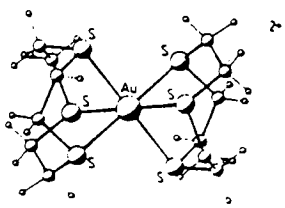

Figure 8

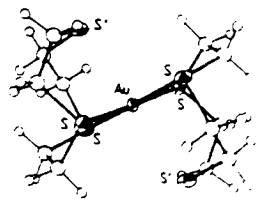

Figure 9

The related complexes $[Au([18]aneS_6)]^+$ (Figure 10) and $[Au(Me_2[18]aneN_2S_4)]^+$ (Figure 11) show similar geometries at Au(I) to those in $[Au([9]aneS_3)_2]^+$ with two short Au-S distances and additional long-range interactions to other donors within the ring. The structure of $[Au([18]aneS_6)]^+$ shows two conformers for the cation in the solid state with Au-S(1) = 2.321(3), Au-S(10) = 2.320(4), Au-S(7) = 2.856(4), Au-S(4) = 2.870(4)Å; for $[Au(Me_2[18]aneN_2S_4)]^+$, Au-S(1) = 2.304(2), Au-S(10) = 2.314(2), Au-S(4) = 2.888(2), Au···S(13) = 3.624(2), Au···N(7) = 3.795(5), Au···N(16) = 3.660(5)Å, <S(1)-Au-S(10) = 177.30(5)°. These complexes, therefore, incorporate large chelate rings that span from 150° to almost 180°.

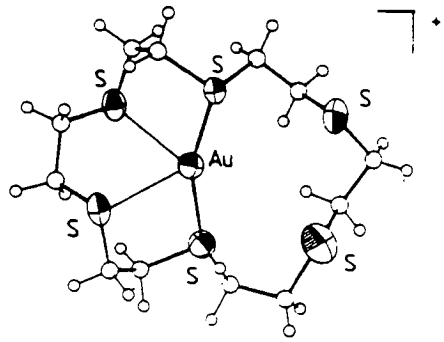

Figure 10

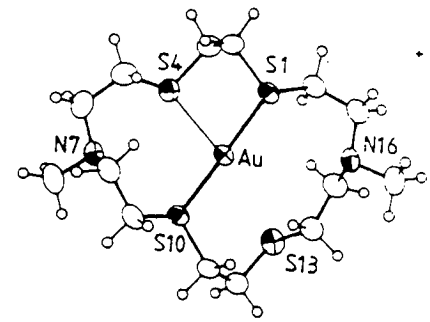

Figure 11

As for the Ag(I) complexes of $[15]aneS_5$, the Au(I) species $[Au([15]aneS_5)]^+$ shows unusual structural features. Encapsulation of Au(I) by $[15]aneS_5$ to give the same structure as that observed in $[Au([18]aneS_6)]^+$ would be unlikely given the inherent strain that would be imposed on the 15-membered ring crown to form a 155° chelate as in Figure 10. The single crystal X-ray structures of $[Au([15]aneS_5)]PF_6$ and $[Au([15]aneS_5)]B(C_6F_5)_4$ both show the cations to be dimeric with Au(I) centres bridging $[15]aneS_5$ crowns in a macrobicyclic structure (Figure 12); in $[Au([15]aneS_5)]PF_6$, for example, Au-S(1) = 2.345(7), Au-S(10') = 2.223(5), Au-S(4) = 2.887(6), Au-S(13) = 2.992(6)Å, S(1)-Au-S(10') = 158.82(22)°.

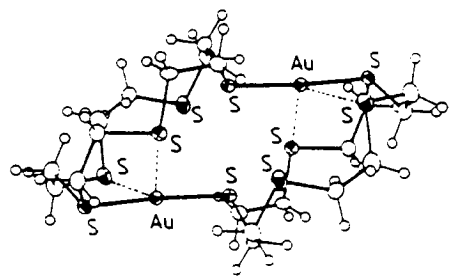

Figure 12

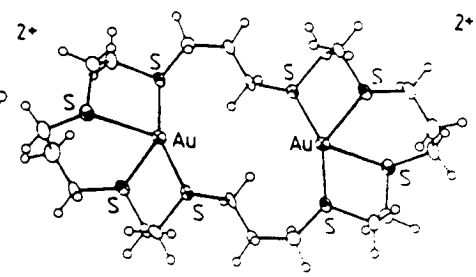

Figure 13

Reaction of two molar equivalents of $[Au(tht)_2]^+$ (tht = tetrahydrothiophene) with one molar equivalent of [24]aneS$_8$ or [28]aneS$_8$ (L) affords the corresponding binuclear complexes $[Au_2(L)]^{2+}$. The analogous binuclear Ag(I) complexes can also be prepared. The single crystal X-ray structure of $[Au_2([28]aneS_8)]^{2+}$ shows (Figure 13) two Au(I) centres complexed tetrahedrally within the octathia macrocycle in a [2+2] manner, Au-S(1) = 2.3301(19), Au-S(11) = 2.3378(18), Au-S(4) = 2.7891(20), Au-S(8) = 2.7629(20), Au···Au = 5.6977(6)Å. The <S(1)-Au-S(11) angle of 155.58(6)° contrasts with the value of 133.39(20)° observed previously for $[Cu_2([28]aneS_8)]^{2+}$ [16] and reflects the preferences of Au(I) for linear and Cu(I) for tetrahedral co-ordination.

The oxidation of $[Au([9]aneS_3)_2]^+$, $[Au([15]aneS_5)]^+$, $[Au([18]aneS_6)]^+$ and $[Au(Me_2[18]aneN_2S_4)]^+$ to form mononuclear Au(II) and Au(III) species has been monitored spectroelectrochemically using *in situ* electronic and esr spectroscopy. Table 1 summarises cyclic voltammetric and coulometric data for these Au(I) thioether complexes.

TABLE 1: **Cyclic Voltammetric[a] and Coulometric Data for Au(I) Thioether Complexes**

Complex	$^1E_{1/2}$	n[b]	$^2E_{1/2}$	n[b]
$[Au([9]aneS_3)_2]^+$	+0.12[i,c]	1	+0.46	1
$[Au([15]aneS_5)]^+$	+0.36	1	+0.54	1
$[Au([18]aneS_6)]^+$	+0.36	1	+0.56	1
$[Au(Me_2[18]aneN_2S_4)]^+$	+0.14	1	+0.43	1
$[Au([18]aneN_2S_4)]^+$	+0.85[i]	2		
$[Au_2([28]aneS_8)]^{2+}$	+0.55[br]	4		
$[Au([16]aneS_4)]^+$	+0.14[br]	2		

i: irreversible; a: measured in MeCN (0.1M ^{n}Bu$_4$NPF$_6$) at 293K at platinum electrodes at a scan rate of 100mV.sec^{-1}. Potentials quoted in V vs Fc/Fc$^+$; b: number of electrons per cation obtained coulometrically at a Pt basket at 243K; br: broad wave with peak-to-peak separation of 200mV.sec^{-1}; c: irreversible wave (E_{pc}) due to slow Au(I) → Au(II) electron-transfer.

The one-electron oxidation products are esr-active and show four-line spectra in solution due to hyperfine coupling to ^{197}Au (I = 3/2, 100%). Interestingly, the complexes of homoleptic thioether crowns that incorporate non-interacting S-donors in the precursor Au(I) species afford the most stable Au(II) species. This reflects the requirement of increasing co-ordination number on going from Au(I) (two co-ordinate) to Au(II) (six co-ordinate, see below). Thus, these precursor Au(I) complexes may be regarded as stereochemically strained in the sense that the extra S-donors destabilise the d^{10} Au(I) configuration and provide a driving force for the formation of mononuclear Au(II). Esr spectroscopic data for the Au(II) complexes in fluid solution are summarised in Table 2. The esr spectra of the Au(II) species in

frozen glass are much more complicated and current work is aimed at simulating and interpreting these spectra to obtain accurate g-values.

TABLE 2: **X-Band Es_1 Spectral Data (293K, $MeNO_2$ solution) for Mononuclear Au(II) Thioether Complexes**

Complex	g_{iso}	A_{iso}
$[Au([9]aneS_3)_2]^{2+}$	2.016	44.3G
$[Au([15]aneS_5)]^{2+}$	2.014	43.3G
$[Au([18]aneS_6)]^{2+}$	2.026	45.5G

ACKNOWLEDGEMENTS

We thank SERC for support, and the Royal Society of Edinburgh and Scottish Office Education Department for a Support Research Fellowship to MS.

REFERENCES

1. *The Chemistry of Macrocyclic Ligand Complexes*, L.F. Lindoy, Cambridge University Press, Cambridge, UK, 1989.
2. A.J. Blake and M. Schröder, *Advances in Inorganic Chemistry*, 1990, **35**, 1; G. Reid and M. Schröder, *Chemical Society Reviews*, 1990, **19**, 239; M. Schröder, *Pure and Applied Chemistry*, 1990, **60**, 517.
3. A.J. Blake, R.O. Gould , M.A. Halcrow, A.J. Holder and M. Schröder, *J. Chem. Soc., Dalton Transactions*, in press; A.J. Holder, PhD Thesis, University of Edinburgh, 1987.
4. A.J. Blake, A.J. Holder, T.I. Hyde and M. Schröder, *J. Chem. Soc., Chem. Commun.*, 1987, 987.
5. A.J. Blake, R.O. Gould, A.J. Holder, T.I. Hyde, M.O. Odulate, A.J. Lavery and M. Schröder, *J. Chem. Soc., Chem. Commun.*, 1987, 118.
6. S.C. Rawle, R. Yagbasan, K. Prout and S.R. Cooper, *J. Am. Chem. Soc.*, 1987, **109**, 6181; A.J. Blake, R.O. Gould, A.J. Holder, T.I. Hyde and M. Schröder, *J. Chem. Soc., Dalton Trans.*, 1988, 1861; S.R. Cooper, S.C. Rawle, R. Yagbasan and D.J. Watkin, *J. Am. Chem. Soc.*, 1991, **113**, 1600.
7. A.J. Blake, R.O. Gould, A.J. Holder, T.I. Hyde and M. Schröder, *J. Chem. Soc., Dalton Trans.*, 1990, 1759.
8. A.J. Blake, R.O. Gould, A.J. Holder, T.I. Hyde and M. Schröder, *Polyhedron*, 1989, **8**, 513 and references therein.
9. A.J. Blake, G. Reid and M. Schröder, *J. Chem. Soc., Dalton Trans.*, 1991, 615.
10. A.J. Blake, R.O. Gould, J.A. Greig, A.J. Holder, T.I. Hyde and M. Schröder, *J. Chem. Soc., Chem. Commun.*, 1989, 876; A.J. Blake, J.A. Greig, A.J. Holder, T.I. Hyde, A. Taylor and M. Schröder, *Angew. Chem.*, 1990, **102**, 203; *Angew. Chem., Int. Ed. Engl.* 1990, **29**, 197 and references therein.
11. H-J. Küppers, K. Wieghardt, Y-H. Tsay, C. Krüger, B. Nuber and J. Weiss, *Angew. Chem.*, 1987, **99**, 583; *Angew. Chem., Int. Ed. Engl.*, 1987, **27**, 575; J. Clarkson, R. Yagbasan, P.J. Blower, S.C. Rawle and S.R. Cooper, *J. Chem. Soc., Chem. Commun.*, 1987, 950.
12. A.J. Blake, R.O Gould, G. Reid and M. Schröder, *J. Chem. Soc., Chem. Commun.*, 1990, 974.

13. R.M. Izatt, L. Eblerhardt, G.A. Clark, R.L. Bruening, J.S. Bradshaw and J.J. Christensen, *Separation Science and Technology*, 1987, **22**, 701 and references therein; E. Sekido, K. Saito, Y. Naganuma and H. Kumazaki, *Analytical Sciences* 1985, **1**, 363; M. Oue, K. Kimura and T. Shono, *Analytica Chimica Acta*, 1987, **194**, 293; K. Chamaya and E. Sekido, *Analytical Sciences*, 1987, **3**, 535; D. Lamb, R.M. Izatt, J.J. Christensen and D.J. Eatough, in *Coordination Chemistry of Macrocyclic Compounds*, Ed G.A. Melson, Plenum Press, 1979, p173 and p158.
14. A.J. Blake, G. Reid and M. Schröder, *J. Chem. Soc., Dalton Transactions*, 1990, 3849.
15. A.J. Blake, G. Reid and M. Schröder, *J. Chem. Soc., Chem. Commun.*, 1992, in press.
16. A.J. Blake, A. Taylor and M. Schröder, *Polyhedron*, 1990, **9**, 2911.

The Synthesis and Single-crystal X-Ray Structure of the Tetranuclear Silver(I) Complex $\{[Ag_2([18]aneS_2O_4)_2]_2\}(PF_6)_4$ ([18]aneS$_2$O$_4$ = 1,4,7,10-tetraoxa-13,16-dithiacyclooctadecane)

Alexander J. Blake, Robert O. Gould, Christian Radek and Martin Schröder*

Department of Chemistry, The University of Edinburgh, West Mains Road, Edinburgh, Scotland, UK EH9 3JJ

Reaction of $AgNO_3$ with [18]aneS$_2$O$_4$ ([18]aneS$_2$O$_4$ = 1,4,7,10-tetraoxa-13,16-dithiacyclooctadecane) affords a 1 : 1 complex, the single-crystal X-ray structure of which confirms the formation of binuclear $[Ag_2([18]aneS_2O_4)_2]^{2+}$ dications; these dications are linked in pairs by a long S···S interaction to give an overall tetranuclear structure.

It has been shown previously that stepwise substitution of S-atoms for the O-atoms in cyclic crown ethers drastically changes the complexation properties of the macrocyclic ligand.[1] Thus, on replacing O-donor atoms with thioether S-atoms, the affinity of crown ionophores for group 1 and 2 metal ions decreases while affinity towards transition-metal complexes increases. This has led to the study of mixed O/S- and homoleptic S-donor ionophores as extraction and transport agents for heavy precious metal ions such as Ag^I.[2] We are currently investigating the structural properties of complexes between d- and p-block metal ions with saturated mixed O/S-donor ionophores[3,4] and are particularly interested in determining the mode(s) of coordination of these extractants with metal ions. We have found that these ligands tend to bind to platinum metal ions[3] in an *exo* manner *via* the thioether S donors, the O donors showing no significant interactions with the metal. There are few reports of complexation of Ag^I by O-donor ether macrocycles[4,5] and we wished to ascertain the extent of Ag–O interactions in large ring S/O donor complexes with Ag^I. We report herein the synthesis and structure of an unusual tetranuclear complex of Ag^I with [18]aneS$_2$O$_4$.

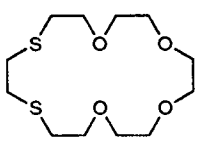

[18]aneS$_2$O$_4$

The reaction of $AgNO_3$ with [18]aneS$_2$O$_4$[6] in a 1 : 1 molar ratio in MeOH–H_2O followed by addition of NH_4PF_6 affords colourless crystals of a product of stoichiometry $[Ag([18]aneS_2O_4)]^+PF_6^-$. Spectroscopic and analytical data are consistent with the formulation of a 1 : 1 Ag^I–[18]aneS$_2$O$_4$ complex. FAB mass spectrometry shows peaks at *m/z* 953 with the correct isotopic distribution assigned to $[Ag_2([18]aneS_2O_4)_2PF_6]^+$ suggesting a dimeric structure in the solid state. Additionally, a peak is observed at *m/z* 1761 with the correct isotopic distribution assigned to a tetranuclear species $\{[Ag_4([18]aneS_2O_4)_4](PF_6)\}^+$. In order to confirm the nature of this product, a single-crystal X-ray structure determination was undertaken.

The single-crystal X-ray structure of the complex shows† (Fig. 1) an unusual dimeric $[Ag_2([18]aneS_2O_4)_2]^{2+}$ cation with Ag(1) bound to two S and one O donors of one macrocycle and to an S donor of another, Ag(1)–S(1) 2.698(3), Ag(1)–S(4) 2.556(3), Ag(1)–O(13) 2.564(7) and Ag(1)–S(24) 2.5214(24) Å, giving an overall tetrahedral geometry at Ag(1). The second metal ion, Ag(2), adopts a different and far more complicated stereochemistry. It is bound to two O and two S donors in one macrocycle and to an O donor of the other, Ag(2)–O(7) 2.661(6), Ag(2)–S(21) 2.555(3), Ag(2)–S(24) 2.7057(24), Ag(2)–O(30) 2.458(7), Ag(2)–O(33) 2.649(9) Å. The overall coordination geometry at Ag(1) and Ag(2) cannot be described in simple terms because the 'free' donor atoms

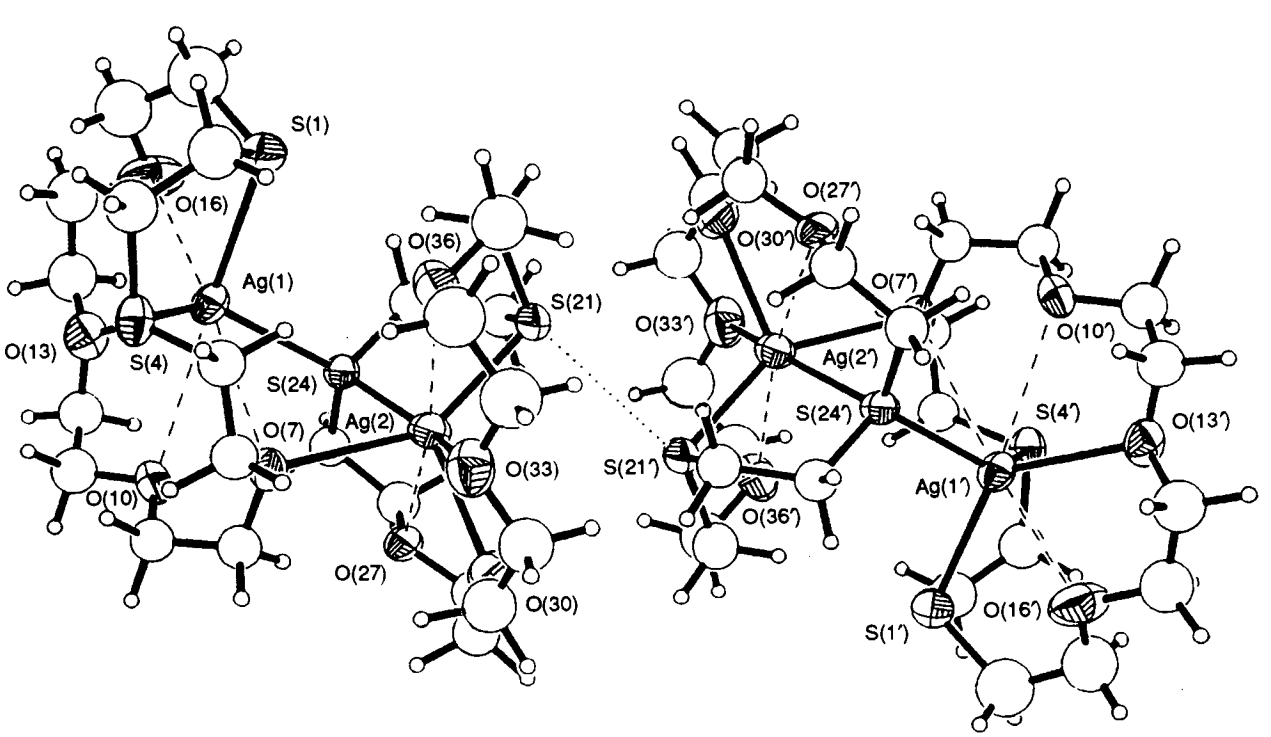

Fig. 1 View of the two $[Ag_2([18]aneS_2O_4)_2]^{2+}$ dications related by inversion through $(\frac{1}{2}, 0, \frac{1}{2})$. Primed atoms are related to unprimed equivalents by the symmetry operation $(1 - x, -y, 1 - z)$. S(21)···S(21') 3.434(4) Å.

show long-range interactions, Ag(1)···O(7) 3.371(5), Ag(1)···O(10) 3.097(6), Ag(1)···O(16) 2.712(11), Ag(2)···O(27) 2.873(6), Ag(2)···O(36) 2.905(8) Å. It is therefore clear that substantial Ag···O interactions are involved in the complexation of Ag^{I}. The Ag(1)···Ag(2) distance is 4.214(1) Å. Interestingly, the metal-free macrocycle [18]aneS_2O_4 adopts a conformation in which the S atoms lie in *exo*-positions with the cavity occupied by the ethylene bridge between the two sulfur atoms.[7] Thus, on complexation to Ag^{I} the conformation of the ligand alters dramatically and this suggests that introduction of stereochemical constraints in the form of bulky or rigid groups might enhance (or at least alter) the selectivity of the macrocycle. The related homoleptic thioether complex $[Ag_2([15]aneS_5)_2]^{2+}$ shows an asymmetrically bridged structure with Ag–S 2.529(3), 2.608(4), 2.558(4), 2.623(5) and 2.716(5) Å; Ag···S(bridge) 2.537(3) and 2.486(3) Å,[8] while $[Ag([18]aneS_6)]^{+}$ shows an octahedral structure with Ag–S 2.6665(12) and 2.7813(10) Å.[9]

However, the most unusual feature of the solid-state structure of $[Ag_2([18]aneS_2O_4)_2]^{2+}$ is the presence of an S···S interaction with a symmetry-related second dication giving an overall tetranuclear structure (Fig. 1). The two dications lie on opposite sides of a crystallographic inversion centre with an S(21)···S(21′) separation of 3.434(4) Å, less than twice the van der Waals radius of sulfur (3.70 Å). S···S interactions in radical cations and sulfonium species have been observed previously in cyclic and noncyclic species,[10] although this is the first example, to our knowledge, of apparent S···S interaction in cyclic crown complexes.

The above results indicate that the complexation and transport of metal ions such as Ag^{+} by mixed thioether/oxy crown ethers is not a simple process. We have now defined the involvement not only of terminal and bridging Ag–S bonding, but of terminal and bridging Ag–O bonding or interactions, and the subsequent formation of oligomer and cluster species *via* long-range S···S interaction. The role of these types of S···S interactions in related systems is under investigation.

We thank the SERC for support, and the Royal Society of Edinburgh and Education Department of the Scottish Office for a Support Fellowship (to M. S.).

Received, 13th December 1993; Com. 3/07346G

Footnote

† *Crystal data* for $C_{24}H_{48}Ag_2O_8S_4^{2+}2PF_6^-$, M = 1098.4, monoclinic, space group $P2_1/c$, a = 18.1728(20), b = 11.0751(10), c = 20.0893(14) Å, β = 93.327(10)°, V = 4036.5 Å^3 [from 2θ values of 40 reflections measured at ±ω (2θ = 30–32°, λ = 0.71073 Å), T = 298 K], Z = 4, D_c = 1.807 g cm^{-3}, μ(Mo-Kα) = 1.332 mm^{-1}. A colourless tablet (0.51 × 0.51 × 0.23 mm) was mounted on a Stoë Stadi-4 four-circle diffractometer. Data collection using Mo-Kα X-radiation, ω–2θ scans and the learnt-profile method (W. Clegg, *Acta Crystallogr., Sect. A*, 1981, **37**, 22) gave 6972 reflections ($2\theta_{max}$ 45°), 5041 unique (R_{int} 0.023), of which 4412 with $F \geq 4\sigma(F)$ were used in all calculations. A Patterson synthesis was used to locate the two silver atoms, from which point the structure was developed by iterative cycles of least-squares refinement and difference Fourier synthesis. The structure was refined by full-matrix least squares (on F) with anisotropic thermal parameters for Ag, S, P, O and fully occupied F atoms. Disorder modelling was required for one PF_6^- group (three orientations for equatorial F atoms) and in the O(16)–C(17)–C(18) region. Outside the disorder region, H atoms were included in fixed, calculated positions (SHELX-76: G. M. Sheldrick, University of Cambridge, 1976). At final convergence, R = 0.0635, R_w = 0.0877, S = 1.307 for 355 parameters and the final ΔF synthesis showed no feature above 0.90 eÅ^{-3}.

Atomic coordinates, bond lengths and angles, and thermal parameters have been deposited at the Cambridge Crystallographic Data Centre. See Information for Authors, Issue No. 1.

References

1 J. J. Christensen, D. J. Eatough and R. M. Izatt, *Chem. Rev.*, 1974, **74**, 351; R. M. Izatt, J. S. Bradshaw, S. A. Nielsen, J. D. Lamb, J. J. Christensen and D. Sen, *Chem. Rev.*, 1985, **85**, 271; R. M. Izatt, R. E. Terry, L. D. Hansen, A. G. Avondet, J. S. Bradshaw, N. K. Dalley, T. E. Jensen, J. J. Christensen and B. L. Haymore, *Inorg. Chim. Acta*, 1978, **30**, 1; R. M. Izatt, D. J. Eatough and J. J. Christensen, *Struct. Bonding (Berlin)*, 1973, **16**, 161; R. M. Izatt, K. Pawlak, J. S. Bradshaw and R. L. Bruening, *Chem. Rev.*, 1991, **91**, 1721.

2 R. M. Izatt, L. Eblerhardt, G. A. Clark, R. L. Bruening, J. S. Bradshaw and J. J. Christensen, *Separation Science and Technology*, 1987, **22**, 701; D. Sevdić and H. Meider, *J. Inorg. Nucl. Chem.*, 1977, **39**, 1403; D. Sevdić, L. Fekete and H. Meider, *J. Inorg. Nucl. Chem.*, 1980, **42**, 885; K. Saito, Y. Masuda and E. Sekido, *Anal. Chim. Acta*, 1983, **151**, 447; E. Sekido, K. Saito, Y. Naganuma and H. Kumazaki, *Anal. Sci.*, 1985, **1**, 363; K. Chayama and E. Sekido, *Anal. Sci.*, 1987, **3**, 535; M. Oue, K. Kimura and T. Shono, *Anal. Chim. Acta*, 1987, **194**, 293.

3 A. J. Blake, G. Reid and M. Schröder, *J. Chem. Soc., Dalton Trans.*, 1990, 3849.

4 A. J. Blake, G. Reid and M. Schröder, *J. Chem. Soc., Chem. Commun.*, 1992, 1074.

5 H. W. Roesky, E. Peymann, J. Schimkowiak, M. Noltemeyer, W. Pinkert and G. M. Sheldrick, *J. Chem. Soc., Chem. Commun.*, 1983, 981; P. G. Jones, T. Gries, H. Grutzmacher, H. W. Roesky, J. Schimkowiak and G. M. Sheldrick, *Angew. Chem., Int. Ed. Engl.*, 1984, **23**, 376; J. S. Bradshaw, C. W. McDaniel, B. D. Skidmore, R. B. Nielsen, B. E. Wilson, N. K. Dalley and R. M. Izatt, *J. Heterocycl. Chem.*, 1987, **24**, 1085; R. Louis, Y. Agnus and R. Weiss, *Acta Crystallogr., Sect. B*, 1977, **33**, 1418; M. Rosser, D. Parker, G. Ferguson, J. F. Gallagher, J. A. K. Howard and D. S. Yufit, *J. Chem. Soc., Chem. Commun.*, 1993, 1267.

6 J. S. Bradshaw, J. Y. Hui, B. L. Haymore, J. J. Christensen and R. M. Izatt, *J. Heterocycl. Chem.*, 1973, **10**, 1.

7 N. K. Dalley, S. B. Larson, J. S. Smith, K. L. Matheson, R. M. Izatt and J. J. Christensen, *J. Heterocycl. Chem.*, 1981, **18**, 463.

8 A. J. Blake, R. O. Gould, G. Reid and M. Schröder, *J. Chem. Soc., Chem. Commun.*, 1990, 974; A. J. Blake, D. Collison, R. O. Gould, G. Reid and M. Schröder, *J. Chem. Soc., Dalton Trans.*, 1993, 521.

9 A. J. Blake, R. O. Gould, A. J. Holder, T. I. Hyde and M. Schröder, *Polyhedron*, 1989, **8**, 513.

10 W. K. Musker, T. L. Wolford and P. B. Roush, *J. Am. Chem. Soc.*, 1978, **100**, 6416, and references therein; K.-D. Asmus, H. A. Gillis and G. G. Teather, *J. Phys. Chem.*, 1978, **82**, 2677, and references therein. See also: R. S. Glass, M. Hojjatie, G. S. Wilson, S. Mahling, M. Göbl and K.-D. Asmus, *J. Am. Chem. Soc.*, 1984, **106**, 5382; R. S. Glass, B. R. Coleman, U. D. G. Prabhu, W. N. Setzer and G. S. Wilson, *J. Org. Chem.*, 1982, **47**, 2761; R. S. Glass, A. Petsom, G. S. Wilson, R. Martinez and E. Juanist, *J. Org. Chem.*, 1986, **51**, 4337; R. S. Glass, M. Hojjatie, A. Petsom, G. S. Wilson, M. Göbl, S. Mahling and K.-D. Asmus, *Phosphorus Sulfur*, 1985, **23**, 143; H. Fujihara, H. Mima, J-J. Chiu and N. Furukawa, *Tetrahedron Lett.*, 1990, **31**, 2307; T. Kataoka, K. Tsutsumi, T. Iwama, H. Shimizu and M. Hori, *Tetrahedron Lett.*, 1990, **31**, 3027, and references therein.

COMPLEXATION OF AG(I) BY MIXED DONOR O/S IONOPHORES

A.J. Blake, R.O. Gould, C. Radek, G. Reid and M. Schröder
Department of Chemistry, West Mains Road, University of Edinburgh, Edinburgh EH9 3JJ

The extraction and transport of Ag(I) and related heavy metal ions across liquid-liquid interfaces and membranes have been achieved using polyether and polythioether cyclic ionophores.[1] The complexation and transport of Ag(I) has focussed particularly on the use of mixed S- and O-donor crowns. The precise mode of co-ordination of these mixed-donor macrocycles to Ag(I) is unknown although 1:1 and 2:1 ligand:Ag complexes involving *exo*-binding of S-donors have been postulated. We were interested in determining the precise mode of co-ordination of the simple mixed O/S macrocycles [15]aneS$_2$O$_3$ [2] and [18]aneS$_2$O$_4$ (L) to Ag(I).

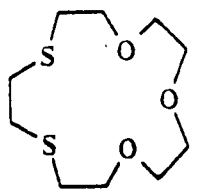

[15]aneS$_2$O$_3$

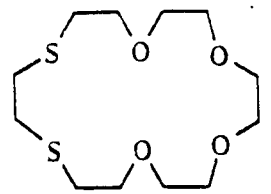

[18]aneS$_2$O$_4$

Reaction of Ag(I) with one molar equivalent of L affords the expected 1:1 complexes [Ag(L)]$^+$. The solid state structure of [Ag([15]aneS$_2$O$_3$)]$^+$ (1) shows, however, a polymeric chain structure with [Ag([15]aneS$_2$O$_3$)]$^+$ fragments connected by bridging thioether S-donors. Likewise, the solid state structure of [Ag([18]aneS$_2$O$_4$)]$^+$ is more complicated than expected and shows a binuclear structure incorporating bridging S-donors. Each [Ag$_2$([18]aneS$_2$O$_4$)$_2$]$^{2+}$ unit, however, is linked to another via a long-range S—S interaction (3.434Å) to give an overall tetrameric structure of stoichiometry [Ag$_4$([18]aneS$_2$O$_4$)$_4$]$^{4+}$ (2).

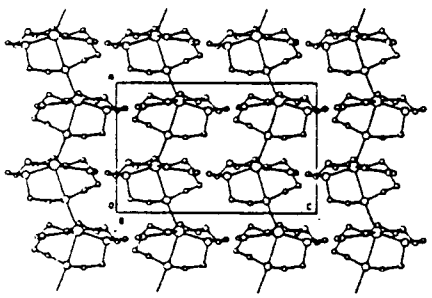

(1)

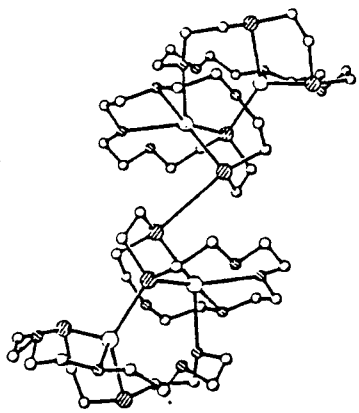

(2)

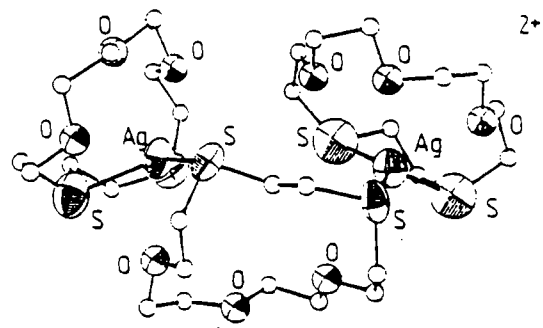

(3)

Attempts to isolate 2:1 ligand:Ag complexes in the solid state have thus far been unsuccessful although these species may well exist in solution. Repeated attempts to prepare [Ag([15]aneS$_2$O$_3$)$_2$]$^+$ leads to the isolation of the binuclear species [Ag$_2$([15]aneS$_2$O$_3$)$_3$]$^{2+}$ which shows approximate trigonal planar AgS$_3$ co-ordination with one [15]aneS$_2$O$_3$ bridging Ag(I) centres (3). The complexes (1) - (3) all show additional long-range interactions with ether O-donors of the macrocycle. These results therefore confirm *endo* Ag—O interactions in these complexes, and suggest that the template synthesis of high nuclearity Ag(I) clusters might be achieved using these types of ionophores.

REFERENCES

1. R.M. Izatt, L. Eblerhardt, G.A. Clark, R.L. Bruening, J.S. Bradshaw and J.J. Christensen, *Separation Science and Technology*, 1987, **22**, 701 and references therein; E. Sekido, K. Saito, Y. Naganuma and H. Kumazaki, *Analytical Sciences* 1985, **1**, 363; M. Oue, K. Kimura and T. Shono, *Analytica Chimica Acta*, 1987, **194**, 293; K. Chamaya and E. Sekido, *Analytical Sciences*, 1987, **3**, 535; D. Lamb, R.M. Izatt, J.J. Christensen and D.J. Eatough, in *Coordination Chemistry of Macrocyclic Compounds*, Ed G.A. Melson, Plenum Press, 1979, p173 and p158.
2. A.J. Blake, G. Reid and M. Schröder, *J. Chem. Soc., Dalton Transactions*, 1990, 3849.

COMPLEXATION OF PLATINUM METAL IONS BY MIXED DONOR O/S MACROCYCLES.

Alexander J.BLAKE, Robert O.GOULD, Christian RADEK and Martin SCHRÖDER
Department of Chemistry, West Mains Road, The University of Edinburgh, Edinburgh, EH9 3JJ

The co-ordination of transition metals with homoleptic thioether macrocycles has been studied extensively over the past decade[1]. We are currently extending our research to investigate the co-ordination chemistry of mixed O/S donor ionophores with platinum group metals[2]. Mixed O/S donor macrocycles offer two different binding sites and afford the possibility of binding both soft and hard metal cations to one ligand. Our aim is to synthesise platinum-group metal complexes with these ligands and monitor the co-ordination of neutral molecules or hard acids (K^+, Cs^+) using a range of spectroscopic and electrochemical methods.

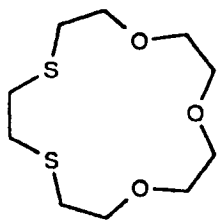

$[15]aneS_2O_3$

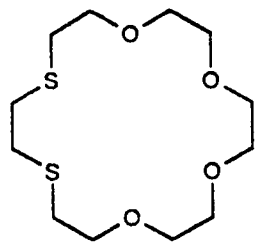

$[18]aneS_2O_4$

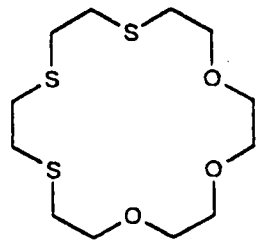

$[18]aneS_3O_3$

The reaction of $PdCl_2$ with one molar equivalent of $[15]aneS_2O_3$ or $[18]aneS_2O_4$ yields the neutral square-planar complexes $PdCl_2([15]aneS_2O_3)$ and $PdCl_2([18]aneS_2O_4)$. The two sulphur atoms are in an *exo*-position and bind to the Pd-ion as a bidentate ligand leaving the cavity metal-free but occupied by the ethylene bridge between the two sulphur atoms. The reaction of two equivalents of ligand with one equivalent $PdCl_2$ removes the two Cl-atoms and forms the 1:2 complexes $[Pd([15]aneS_2O_3)_2]^{2+}$ and $[Pd([18]aneS_2O_4)_2]^{2+}$(I).

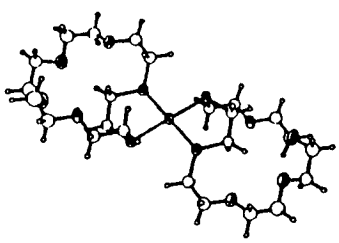

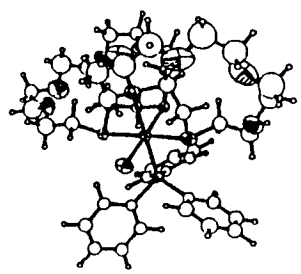

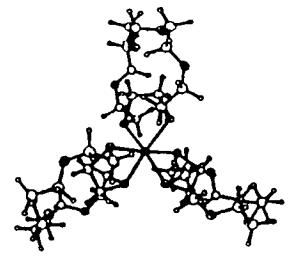

(I) $[Pd([18]aneS_2O_4)_2]^{2+}$ (II) $[RuCl(PPh_3)([18]aneS_2O_4)_2]^{2+}$ $[Ru([18]aneS_2O_4)_3]^{2+}$

The reaction of two equivalents of ligand (L) with one equivalent of $Ru(PPh_3)_3Cl_2$ in boiling MeOH affords octahedral $[RuCl(PPh_3)(L)_2]^{2+}$(II) complexes of different configuration. In the case of the ligand $[15]aneS_2O_3$ the Cl^- and the phosphine ligands are in mutually *trans*-positions whereas in the case of $[18]aneS_2O_4$ they are in mutually *cis*-positions. The bulky phosphine molecule forces the macrocycles to distort out of a flat conformation forming a pocket in which a guest molecule might fit. Despite the structural evidence of the *cis*-complex with $[18]aneS_2O_4$ there is spectroscopic evidence for the *trans* isomer in solution. The complexation of metal ions with $[18]aneS_3O_3$ are also discussed.

REFERENCES

1.) A.J.Blake and M.Schröder, *Adv.Inorg.Chem.*, 1990, **35**, 1 and references therein.
2.) A.J.Blake, G.Reid and M.Schröder, *J.Chem.Soc., Dalton Trans.*, 1990, 3849.

Metal Macrocyclic Complexes as Templates for Polyiodides
The Synthesis and Low Temperature Single Crystal Structures of
$\{[Ag([18]aneS_6)]I_7\}_n$ and $[Ag([18]aneS_6)]I_3$
([18]aneS$_6$ = 1,4,7,10,13,16-hexathiacyclooctadecane).

Alexander J.Blake, Robert O.Gould, Simon Parsons, Christian Radek and Martin Schröder
Department of Chemistry, The University of Edinburgh, West Mains Road,
Edinburgh, Scotland EH9 3JJ

A wide range of polyiodide species have been synthesized over the past decades utilising medium sized to large counter cations such as Cs^{+1}, Me_4N^{+2}, Et_4N^{+3} and $[K(valinomycin)]^{+4}$. We are interested wether metal macrocyclic complexes can be used as template cations in the preparation of polyiodides. $\{[Ag([18]aneS_6)]I_7\}_n$ and $[Ag([18]aneS_6)]I_3$ have been isolated as recrystallisation products of the initially prepared $[Ag([18]aneS_6)]I_5$ complex. The single crystal structure of $\{[Ag([18]aneS_6)]I_7\}_n$ consists of $[Ag([18]aneS_6)]^+$ units embedded in the novel polymeric polyiodide $(I_7^-)_n$. $(I_7^-)_n$ is best described as a distorted (anisotropically compressed) cubic primitive lattice with I^- anions occupying the corners of each cube and I_2 molecules along each vertex effectively bridging between adjacent I^- anions. $[Ag([18]aneS_6)]I_3$ in contrast consists of isolated cations and symmetrical I_3^- anions. Both complexes reflect nicely the kinetical inertness of Ag(I) in the $[Ag([18]aneS_6)]^+$ complex which would otherwise react instantanously with the abundant I^- and I_2.

References

1) H.A.Tasman, K.H.Boswijk, *Acta Cryst.*, 1955, **8**, 59;
E.E.Havinga, K.H.Boswijk and E.H.Wiebenga, *Acta Cryst.*, 1954, **7**, 487.
2) J.Broekema, E.E.Havinga and E.H.Wiebenga, *Acta Cryst.*, 1957, **10**, 596.
3) E.E.Havinga and E.H.Wiebenga, *Acta Cryst.*, 1958, **11**, 733.
4) K.Neupert-Laves and M.Dobler, *Helv.Chim.Acta*, 1975, **58**, 432.

Charge Transfer Adducts between I_2 and Homoleptic Thioether Macrocycles

Part I: Small to Medium Sized Macrocycles
The Low Temperature Single Crystal Structures of $([9]aneS_3)_2(I_2)_4$, $([12]aneS_4)I_2$, $([14]aneS_4)I_2$, $([16]aneS_4)I_2$ and $([16]aneS_4)(I_2)_4$.

Part II: Medium to Large Sized Macrocycles
The Low Temperature Single Crystal Structures of $[([15]aneS_5)(I_2)_3](I_2)_{0.5}$, $([18]aneS_6)(I_2)_4$, $([24]aneS_8)I_2$ and $([24]aneS_8)(I_2)_6$.

Alexander J.Blake, Robert O.Gould, Christian Radek and Martin Schröder
Department of Chemistry, The University of Edinburgh, West Mains Road, Edinburgh, Scotland EH9 3JJ

The adduct formation between I_2 and classical donors (N, O, P, S, Se) has been studied from the beginning of this century. The initial interest in this area at the end of the last century was triggered by the unusual way I_2 colours different solvents[1]. Solid state studies of adducts between small molecules and I_2 have been reported starting in the 50s of this century[2]. However this work was in general confined to small mono- and bi-dentate ligands. We are interested in the structural features of solid state adducts between polydentate homoleptic S-donor macrocycles and I_2. A series of adducts have been prepared and structurally characterised[3]. The different co-ordination modes and structures of these compounds will be discussed and common trends identified. Structural features found in this compounds include *exo* and *endo* co-ordination, terminal and bridging I_2 and a close relationship between S-I and I-I bond lengths.

References

1.) for a historical review see for instance: L.J.Andrews and R.M.Keefer, *Advances in Inorganic and Radiochemistry*, 1961, **3**, 91.

2.) E.g.: G.Y.Chao and J.D.McCullough, *Acta Crystallogr.*, 1960, **13**, 727; C.Rømming, *Acta Chem.Scand.*, 1960, **14**, 2145; F.H.Herbstein, P.Ashkenazi, M.Kraftory, M.Kapon, G.M.Reisner and D.Ginsburg, *Acta.Crystallogr., Sect B*, 1986, **42**, 575; A.L.Tipton, M.C.Lonergan, C.L.Stern and D.F.Shriver, *Inorg.Chim.Acta*, 1992, **201**, 23; E.F.Herbstein and W.Schwotzer, *J.Am.Chem.Soc.*, 1984, **106**, 2367.

3.) A.J.Blake, R.O.Gould, C.Radek and M.Schröder, *J.Chem.Soc., Chem.Commun.*, 1993, 1192.

Complexation of Platinum Metal Ions by Mixed Donor O/S Macrocycles

Alexander J.Blake, Robert O.Gould, Christian Radek and Martin Schröder
Department of Chemistry, The University of Edinburgh, West Mains Road, Edinburgh, Scotland EH9 3JJ

The co-ordination chemistry of transition metal complexes with homoleptic thioether macrocycles has been studied extensively over the past decade[1]. We are currently extending our research to investigate the co-ordination chemistry of mixed O/S donor ionophores with platinum group metals[2]. Mixed O/S donor macrocycles offer two different binding sites and afford the possibility of binding both soft and hard metal cations to one ligand. Our aim is to synthesize platinum-group metal complexes with these ligands and monitor the co-ordination of neutral molecules or hard acids (K^+, Cs^+) using a range of spectroscopic and electrochemical methods. Our results concerning the co-ordination of mixed O/S donor ionophores with Ru(II) and Pd(II) are presented and discussed.

References

1.) A.J.Blake and M.Schröder, *Adv.Inorg.Chem.*, 1990, **35**, 1 and references therein.
2.) A.J.Blake, G.Reid and M.Schröder. *J.Chem.Soc., Dalton Trans.*, 1990, 3849.